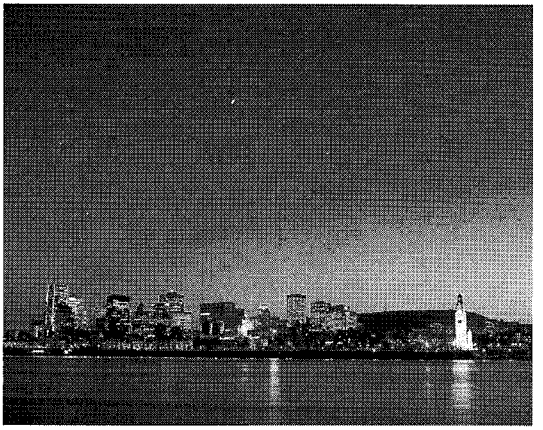

1997 North American Radio Science Meeting

Montreal, Canada July 13-18 1997 The Queen Elizabeth Hotel

Program and Abstracts

International Union of Radio Science

URSI

Union Radio-Scientifique Internationale

COMMITTEES

Steering Committee

Conference Co-Chairmen:	Stan Kubina	Gilles Delisle
Technical Program Chairs	Prakash Bhartia (AP-S)	Lot Shafai (URSI)
Technical Program Vice-Chair (AP-S)	Yahia Antar	
Publications/Publicity	Satish Kashyap	Robert Paknys
Industrial Liaison/Exhibits	Christian Dubé	Raymond Murphy
Local Arrangements	Jean-Jacques Laurin	Benoit Nadeau
Short Courses/Workshops	Amy Pinchuk	Ralph Girard
Special Sessions/Plenary	Martin Fournier	Nizar Sultan
International Liaison/Student Activities	Ke Wu	David Roscoe
URSI Liaison	Ross Stone	
Secretariat	Doris Ruest	Laurier Forget

Technical Program Committee

R. Adve, Y. Antar, P. Bhartia, G. Bridges, G. Brown, K.Chan, S. Chaudhuri, Z. Chen, G. Delisle, N. Herscovici, W. Hoefer, A. Ittipiboon, S. Kashyap, S. Kubina, J.-J. Laurin, M. Lecours, J. Litva, J. Lovetri, A. Martin, D. McNamara, S. Mishra, G. Missout, R. Mongia, G. Morin, R. Murphy, J. Norgard, R. Olsen, R. Paknys, A. Petosa, A. Pinchuk, P. Pramanick, K. Rao, D. Roscoe, T. Sarkar, A. Sebak, L. Shafai, N. Simons, R. Simons, B.P. Sinha, E. Sousa, J.-P. St-Maurice, W. Stone, M. Stuchly, N. Sultan, K. Tapping, M. Thorburn, R. Tomar, D. Wilton, A. Zaghloul.

Canadian National Committee For URSI

Chairman	Gilles Delisle	*Commission D*	Jamal Deen
Past Chairman	Paul H. Wittke	*Commission E*	Amy Pinchuk
Secretary	Ken F. Tapping	*Commission F*	Roderic L. Olsen
Commission A	Gilles Missout	*Commission G/H*	Jean-Pierre St. Maurice
Commission B	Y.M.M. Antar	*Commission J*	Ken F. Tapping
Commission C	Elvino Sousa	*Commission K*	Maria A. Stuchly

Ex officio Members

Int'l Past President of URSI, Ed. V. Jull
1999URSI General Assembly, Keith Balmain
NRC Int'l Affairs, Andreé Bichon

United States National Committee For URSI

Chair	Susan K. Avery	*Commission D*	Robert Mattauch
Vice-Chair	Vacant	*Commission E*	David J. Cohen
Secretary	Gary Brown	*Commission F*	Wolfhard Vogel
Past Chair	David Chang	*Commission G*	Lewis Duncan
Commission A	John D. Norgard	*Commission H*	Umran Inan
Commission B	Donald R. Wilton	*Commission J*	Donald Backer
Commission C	David Thomson	*Commission K*	James C. Lin

Society Representatives

American Astronomical Society, Vacant
American Meteorological Society, Vacant
American Geophysical Union, George Reid (1996)
IEEE-GRSS, Roger Lang (1998)
IEEE-MTT, Arthur A. Oliner (1996)

Members at Large

Albin Gasiewski (1997)
Ronald Pogorzelski (1998)
W. Ross Stone (1997)
Roland T. Tsunoda (1996)
John D. Mathews (1999)
Fritz. Schuermeyer, Fellow (1999)
Edgeworth R. Westwater (1996)
Jill Tarter (1998)

NRC Staff

Director, Donald C. Shapero
Associate Director, Robert L. Riemer

TABLE OF CONTENTS

ROOM	MONDAY AM	MONDAY PM	TUESDAY AM	TUESDAY PM	WEDNESDAY AM	WEDNESDAY PM	THURSDAY AM	THURSDAY PM	FRIDAY AM	FRIDAY PM
Marquette	1 URSI B Discrete Methods	15 URSI B Efficient Methods for Solution & Design	30 URSI B Numerical Methods for Microstrip Antennas	47 URSI B Finite Difference Time Domain	**PLENARY SESSION** **MARQUETTE** **AND** **GRAND SALON**		77 APS/URSI B High Frequency Techniques	93 APS Integral Equation Techniques II	112 URSI B Method of Moments	127 URSI B Mesh Truncation Approaches
Jolliett	2 URSI GH HF Ionospheric Modification	16 URSI G Propagation & Telecommunication I	31 URSI G Radio Studies at High to Very High Latitude I 32 APS/URSI G Propagation & Tele-communication II	48 URSI G Radio Studies at High to Very High Latitude II		62 URSI G Ionospheric Modeling & Lower Latitude Irregularities I 63 URSI B New Materials	78 URSI G D-Region Radio Studies	94 URSI H In Situ Studies of Artificial Waves II	113 URSI GH Electrodynamic Coupling Between Atmospheric Regions II	128 URSI G Ionospheric Tomography
Duluth	3 APS Active Microstrip Antennas I	17 APS Active Microstrip Antennas II 18 APS Adaptive Antennas for Wireless & Mobile Applications	33 APS Microstrip Antenna Analysis	49 APS Special Session Novel Microstrip Antennas & Design Considerations		64 APS Microstrip Arrays	79 APS Special Session Conformal Microstrip Antennas	95 APS Rectangular, Circular & Shorted Microstrip Patch Antennas 96 APS Dual Band & Polariza-tion Characteristics of Microstrip Antennas	114 APS Microstrip Wireless & Mobile Antennas	129 URSI B Microstrip Antennas
MacKenzie	4 APS Efficient CEM Solvers & Periodic Structures	19 APS FDTD Modeling of Structures & Media	34 APS/URSI B Advances in Finite Element Techniques	50 APS Advances in Time Domain Techniques I		65 APS/URSI B Special Session in Memory of Peter P. Silvester	80 APS FDTD: Antenna Modelling	97 APS Time Domain Absorbing Boundary Conditions	115 APS Advances in Time Domain Techniques II	130 APS MOM/Green's Function/Numerical Methods
Galerie 4	5 URSI B Array Antennas	20 APS Mobile Antennas	35 APS Phased Array Antennas	51 APS Adaptive Antennas/ Direction Finding		66 APS Antennas	81 APS Leaky-Wave & Helical Antennas	98 URSI B Antennas	116 APS Integrated Antennas	131 APS Frequency Selective Surfaces
St-Laurent	6 URSI B Reflector & Feed Antennas	21 APS Aperture Antennas	36 APS Special Session Advanced Photonics Technology and Applications to Antennas	52 APS Antenna Design		67 APS Reflector Antennas I	82 APS Reflector Antennas II	99 APS Slot Antennas & Arrays	117 APS Synthesis of Antenna Arrays	132 APS Adaptive Antennas
St-Maurice	7 APS Special Session Interdisciplinary Computational Electromagnetics	22 APS Optimization Methods in EM Design	37 APS Integral Equation Techniques I	53 APS/URSI B Wavelets		68 URSI B Special Session Model Order Reduction for Rapid EM Field Simulation	83 APS Special Session Genetic Algorithms in Electromagnetics	100 APS/URSI B Special Session Frontiers of Mathematical Methods in Electromagnetics	118 APS/URSI B Applications of Neural Networks 119 URSI B Data Representation & Visualization in Scattering	133 APS Active Antennas 134 APS Electromagnetic Education

ROOM	MONDAY AM	MONDAY PM	TUESDAY AM	TUESDAY PM	WEDNESDAY AM	WEDNESDAY PM	THURSDAY AM	THURSDAY PM	FRIDAY AM	FRIDAY PM
Gatineau	8 URSI F Special Session Applications of Rough Surface & Volume Scattering Methods	23 URSI F Special Session Remote Sensing of the Earth's Surface/NASA Scatterometer	38 URSI F Remote Sensing of the Atmosphere	54 URSI F Radar/Rain Gauge Measurements of Precipitation		69 URSI F Mobile Propagation: Models & Measurements	84 URSI F Indoor/Mobile Propagation: Models & Measurements	101 URSI F Satellite-Earth Propagation: Models & Measurements	120 URSI F Special Session Terrestrial Propagation Effects: Models & Measurements	135 URSI B/F/K Volume & Surface Wave Propagation
Bersimis	9 APS Compact Range & Near-Field Measurement Techniques	24 APS Special Antenna Measurement Techniques	39 URSI B Monopoles, Dipoles & Resonators	55 APS Tapered Slot & Leaky Wave Antennas		70 APS Waveguide Component Analysis & Design	85 URSI B Microstrip Lines & Circuits	102 URSI B Guided & Leaky Wave Structures 103 URSI B Characterization of Transient Antennas	121 URSI B Analysis of Guided Wave Structures	136 APS Millimeter Wave Antennas 137 APS Waveguide Discontinuities/Transitions
Peribonca	10 APS Waveguide Electromagnetics	25 URSI B Chiral Media	40 URSI D/A Special Session Packaging & Interconnects 41 APS/URSI B Special Session Radar Polarimetry	56 URSI D/A Special Session Microwave Integrated Circuits for Commercial Applications 57 URSI Student Paper Finalists		71 URSI B Special Session Image Construction from Real Data	86 URSI G Ionospheric Modeling and Low Latitude Irregularities II 87 URSI H In Situ Studies of Artificial Waves I	104 APS Propagation in Mobile Communication	122 URSI C Communications & Signal Processing	138 APS EM Propagation
Richelieu	11 APS Wire Antennas	26 APS/URSI D Microwave, MM-Wave & Optical Devices & Circuit	42 APS/URSI D Space Antennas	58 URSI A Impulse Radar		72 URSI E Spectrum Management Issues:A Perspective on Recent Technical/Economic/ Policy Developments	88 URSI K Electromagnetic Engineering in Medicine & Biology	105 APS/URSI Special Session Radiation Physics	123 URSI B Inverse Problems 124 URSI B Non-Conventional Computational Method	139 URSI B Transient Propagation & Scattering in Dispersive Media
Harricana	12 APS/URSI B RCS Analysis & Measurements	27 URSI B Classical Problems in Electromagnetics	43 APS Electromagnetic Scattering & Diffraction	59 APS Electromagnetic Scattering		73 APS/URSI B Special Session Novel Trends in Electromagnetics	89 APS Imaging & Inverse Scattering 90 APS Electromagnetic Theory/Applications	106 APS/URSI A Measurement Techniques & Material Characterization	125 APS/URSI A Random Media & EM Properties of Materials	140 APS Radar Imaging & Remote Sensing
Chaudière	13 URSI K Hazard Evaluation & Prevention	28 URSI E Electromagnetic Compatibility & Interference (EMC/EMI)	44 URSI E Electromagnetic Noise 45 URSI E Special Session High Power Electromagnetics	60 APS EM Interaction with Biological Structures		74 URSI B Scattering by Periodic Structures	91 APS Scattering by Planar Surfaces	107 APS Electromagnetic Theory	126 URSI J Millimeter/Sub-Millimeter Radio Telescopes and Instrumentation	141 URSI B Scattering by 2 & 3D Dielectric Objects
Matapedia	14 URSI J Very Long Baseline Interferometry: On the Ground & In Space	29 URSI J Instrumentation & Signal Processing Techniques	46 URSI J Aperture Synthesis: Instrumentation & Techniques	61 APS/URSI D Opto-Electronics, Techniques, Devices & Materials		75 URSI B Hybrid Methods	92 URSI B Propagation, Scattering & Radiation in Complex Media	108 URSI J Radio Telescopes for the 21st Century 109 URSI J Natural & Man-Made Disturbances/Effects on Radio Telescopes		
St-Charles						76 URSI A Antennas & EM Field Metrology		110 combined with 113 111 URSI H Auroral Phenomena		

WEDNESDAY **JULY 16**

Plenary Session **Grand Salon/Marquette**

"Our Universe, Our World, Our Technology"
Co-chairs: S.J. Kubina and M. Fournier

08:10	Welcome
08:20	Introduction
08:40	HST – The Half-Way Point, **J. HAYES**, *Space Telescope Science Institute, Baltimore, MD, USA*
09:30	Space Applications in Europe, **R.C. COLLETTE**, *European Space Agency Headquarters, Paris, France*
10:10	Coffee Break
10:30	The International Telecommunications Union, **R.W. JONES**, *International Telecommunications Union, Geneva, Switzerland*
11:10	Radarsat, Status and Development, **J. McNALLY**, *Canadian Space Agency, St. Hubert, QC, Canada*

HST -- The Half-Way Point

Jeffrey Hayes
Space Telescope Science Institute
Baltimore, MD

The Hubble Space Telescope was launched in April 1990 with a great deal of media coverage. When the telescope was subsequently found to suffer from spherical aberration, the project was declared a failure. However, even with the spherical aberration problem, the telescope performed very well and obtained science observations that could not have been otherwise done.

In December 1993, the first in a series of planned servicing missions was flawlessly carried out by the crew of the shuttle *Endeavour*. In the 3 years since that mission, HST has not only performed in a spectacular fashion, but has produced thousands of truly remarkable images, including the very depths of the observable Universe for the Hubble Deep Field project.

Indeed, the astronomical community is poised to answer some of the fundamental questions about the size and age of the Universe we live in, and this is in no small part due to the observations made with HST.

HST is evolving, as we are currently in the middle of commissioning the second generation of scientific instruments (from the second flawless servicing mission that occurred in February 1997). The emphasis of HST is changing from the more typical and familiar optical wavelengths to infra-red wavelengths, and it is both timely and appropriate to look back on the last 6 years of work, to see where they have lead us, and to see where we shall go.

PL2

Space Applications in Europe

René C. Collette
Applications Programmes
European Space Agency Headquarters
Paris, France

A review of European programmes and plans in the fields of Broadcast, Mobile, Multimedia and Broadband Satellite Communications as well as Navigation, Data Relay, Meteorology and Earth Resources.

In particular, in the area of telecommunications, the present developments leading to advanced multimedia and broadband systems will be described, as well as the deployment as of 2000 of the advanced Technology and Data Relay Satellite, ARTEMIS, undertaken in cooperation with Canada.

The contribution of Europe to the present worldwide space navigation infrastructure, GNSS-1, will be highlighted as well as the preparation of the future evolution, GNSS-2.

With respect to Earth Observation, the new generation of Geostationary meteorological satellites as well as the major Envisat LEO System endeavour will be detailed, together with the new polar observation system, a cooperation undertaken with the Eumetsat organisation.

National initiatives, which complete the programmes financed at European level, will also be presented so as to identify the overall spectrum of industrial activities.

Emphasis will be placed on some of the advanced technologies promoted within these systems.

The International Telecommunication Union

Robert W. Jones
Radiocommunication Bureau
International Telecommunication Union
Geneva, Switzerland

The International Telecommunication Union (ITU) is the oldest specialized agency of the United Nations, far older, in fact, than the UN itself. This year, the ITU is marking its 132nd anniversary, having been established as the International Telegraph Union in 1865. The ITU has changed considerably over the past 132 years and today, it is continuing to transform itself to meet the needs of its membership.

The ITU is unique in the sense that while it is first and foremost an intergovernmental organization, it very much is a partnership between the public and private sectors. Indeed, given the explosive growth occurring in the telecommunication sector and the transformations occurring around the world, this partnership is its very strength. And radiocommunications is playing an ever increasing role in the technological evolution which we are witnessing.

This presentation will review briefly the history of the ITU, the recent changes in its structure and functioning and measures being considered to further adapt the ITU to the changing telecommunication environment.

PL4

Radarsat, Status and Development

J. McNally
Canadian Space Agency
St. Hubert, Quebec

The operational status of Radarsat I will be presented, including some of the latest images obtained around the world. The operation of Radarsat I has produced excellent images and data which has been used to manage oil spills, floods, forestry and many other applications. Many countries are using Radarsat data to manage their resources because it is more reliable in time-critical applications since it is not affected by cloud cover.

Plans are well advanced to continue remote sensing using radar satellites and preparations to form a commercial entity using Canadian government support is well underway. Radarsat II will be required to replace Radarsat I early in the next century. The approach to this planning will be discussed.

URSI A **Session 58** **Salon Richelieu**

Impulse Radar
Co-chairs: G. Smith, USA and G. Missout, Canada

13:10 58.1 Mine Detection Using Vee Dipoles in a Short-Pulse Ground Penetrating Radar, **T.P. MONTOYA**, G.S. SMITH, *Georgia Institute of Technology, Atlanta, GA, USA*

13:30 58.2 Impulse Radar for Detection and Classification of Buried Landmines, **H. BRUNZELL**, *Chalmers University of Technology, Göteborg, Sweden*

13:50 58.3 Magnetic Impulse Imaging in Conducting-Heterogeneous Media, **J.E. BRIDGES**, *Interstitial Inc., Park Ridge, IL, USA*

14:10 58.4 Confocal, Synthetic-Impulse, MMW System for Imaging Concealed Dielectric and Metallic Objects, **J.E. BRIDGES**, *Interstitial Inc., Park Ridge, IL, USA*

14:30 58.5 A Comparative Study of UWB Radar Discrimination Schemes in a Noisy Background, **S. PRIMAK**[1], J. LOVETRI[1], S. KASHYAP[2], [1]*University of Western Ontario, London and* [2]*Department of National Defence, DREO, Ottawa, ON, Canada*

14:50 58.6 Ultra-Wideband Imaging Radar System, **F.-C. CHEN**, W.C. CHEW, *University of Illinois at Urbana-Champaign, IL, USA*

15:10 58.7 Ultra-Wideband Transient Backscatter Measurements Through Concrete Walls, **J.F. AURAND**, *Sandia National Laboratories, Albuquerque, NM, USA*

15:30 58.8 Application of Cepstral Analysis to Radar Target Discrimination, G.S. WALLINGA, **E.J. ROTHWELL**, K.M. CHEN, D.P. NYQUIST, *Michigan State University, East Lansing, MI, USA*

15:50 58.9 Effect of Radar-Target Sea-Clutter Interaction on an Enhanced E-Pulse Clutter Cancellation Algorithm, G.S. WALLINGA, A. KIZILAY, **E.J. ROTHWELL**, K.M. CHEN, D.P. NYQUIST, *Michigan State University, East Lansing, MI, USA*

16:10 58.10 Characterization of Off-Boresight Radiation from an Impulse Excited TEM Horn: Experiment Plus Supporting Analyses, W.T. CLARK, III[3], R.L. HUTCHINS[1], J.S.H. SCHOENBERG[2], **J.S. TYO**[2], [1]*BDM International Inc., Albuquerque,* [2]*Phillips Laboratory, Kirtland AFB and* [3]*Voss Scientific Inc., Albuquerque, NM, USA*

16:30 58.11 Time Domain Measurement and Optimisation of Some Simple Antennas, **E.A. ELKHAZMI**, N.J. McEWAN, *University of Bradford, UK*

A58.1

Mine Detection using Vee Dipoles in a Short-Pulse Ground Penetrating Radar

Thomas P. Montoya* **and Glenn S. Smith**
School of Electrical and Computer Engineering
Georgia Institute of Technology
Atlanta, GA 30332-0250

An important problem driving research into ground penetrating radar (GPR) systems is the proliferation of anti-personnel land mines. There are estimated to be about 100 million land mines deployed in 64 countries. Current detection technologies, primarily metal detectors and mechanical probes, are inadequate for dealing with land mines made mostly of ceramics and plastics (low metal content). The small size of many anti-personnel land mines suggests the use of a short pulse for detection.

A short-pulse GPR requires a wideband, directional antenna to radiate the pulse into the ground. We will use Vee dipoles with resistive loading to achieve this objective. For a monostatic GPR; the antenna radiates a pulse, it is reflected from the surface of the ground and the buried target, and the reflected pulse(s) are received by the antenna. Ideally, the received signal should be as large as possible and there should be a minimal voltage reflection at the antenna feed. So that the return from the buried target is not obscured, multiple reflections between the surface of the ground and the antenna as well as reflections internal to the antenna should be minimized. Also, the spot illuminated on the ground should be compact in order that the position of the target can be resolved.

The 3D finite-difference time-domain (FDTD) method was used to evaluate the performance of these antennas in the time domain over a lossy ground. The figure shows the problem geometry: the Vee has arms of length h, an interior angle α, and is at height b above the ground which contains the buried target. The ground is modeled as a simple, lossy dielectric characterized by permittivity ϵ and conductivity σ. Examples of returns from representative problem geometries will be presented.

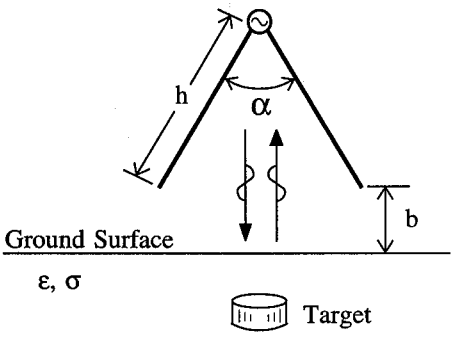

Impulse Radar for Detection and Classification of Buried Landmines.

H. Brunzell
Chalmers University of Technology
Dept. of Applied Electronics
S-412 96 Göteborg
Sweden

January 7, 1997

Abstract

The presence of landmines is a major problem in countries such as Afghanistan, Cambodia, Angola, Somalia and Kuwait. The International Committee of the Red Cross estimates the number of buried landmines around the world to 100 million. Some of the most affected counties are Angola with 9–14 million mines, and Cambodia with 8–10 million. Modern mines are largely constructed of plastics and the explosive is purely dielectric. These mines are practically impossible to detect with metal detectors. A project with the goal to develop a mine detector, able to detect non-metallic mines is carried out at Sweden's Defence Research Establishment (FOA) in Linköping, Sweden. A novel sensor that is able to detect non-metallic objects is the impulse radar. The impulse radar has an extremely large bandwidth, in this case 0.3–3 GHz. The large bandwidth means that information about the target's radar cross section (RCS) can be extracted from the returned signal. The radar cross section depends on the target's shape, material and surface structure. The RCS can thus be used to distinguish between a mine and a stone or a metal fragment from an exploded bomb shell. A complete signal processing chain for classification of buried landmines based on impulse radar measurements has been developed at Chalmers University in close cooperation with FOA. The signal processing chain consists of algorithms for clutter suppression, detection, feature extraction and classification. The algorithms have been evaluated using measured data from an experimental impulse radar system at FOA. This paper will present the main ideas behind the mine detection system, mainly from a signal processing point of view.

A58.3

MAGNETIC IMPULSE IMAGING IN CONDUCTING-HETEROGENEOUS MEDIA*

Jack E. Bridges, Interstitial Inc., 1937 Fenton Lane, Park Ridge, IL 60068

Impulse radar has been considered over the past two decades as a technique not only to detect distant targets, but also to provide additional information on the geometry of the target as well. In the case of radiated pulses, rigorous scattering theory and detailed experiments have demonstrated that, if very short duration radiated pulses are used, the principal scattering centers on complex targets could be resolved.

While not often realized, rigorous scattering theory further disclosed that, in the case where the low-frequency content of a short-duration polarity change of the illuminating field is partially preserved, additional information on the geometry and material of the target can be developed. Developing such low-frequency phenomena may impractical for conventional radar uses, but such responses can be used both to locate and image highly-conducting, nearby targets embedded in heterogeneous, conducting media, such as earth. Such responses can be used to crudely assess the target geometry and to discriminate between different targets..

To illustrate the above, a laboratory-scale, magnetic-impulse system was constructed and tested. A field-excitation drive coil creates a magnetic field that is periodically and rapidly reversed. The time derivative of the rapidly reversed magnetic field induces a unipolar, decaying, eddy-current flow in nearby metallic targets. The eddy currents in the targets decay with time constants much greater than the time for the field reversal. The decay time depends on the target geometry, conductivity and permeability. The output of the receiver coil is blanked when the illuminating field is reversed, thereby isolating the induced decaying magnetic fields from those from the excitation coil. The 3-D location of the scatterer is determined by measuring the divergence of the decaying fields. The targets can be imaged by scanning the coils over the earth's surface . The approximate geometrical features can be developed by analyzing the amplitude responses, decay times and non-linear ferromagnetic behavior.

Tests were conducted to detect metallic gas pipes placed in moist clay [10% water content] that was embedded with metallic debris, such tin cans, large bolts and construction tools. Gas pipes, ranging in 1 to 4 inches in diameter exhibited decay times ranging from 350 to 550 microseconds and were easily resolved from the debris that exhibited time constants of less than 30 microseconds. Assuming the excitation and sensing coils are 0.5 meter diameter, a gas pipe could be detected at depths down to 25 meters.

*This work was partially sponsored by the Gas Research Institute

CONFOCAL, SYNTHETIC-IMPULSE, MMW SYSTEM FOR IMAGING CONCEALED DIELECTRIC AND METALLIC OBJECTS*

Jack E. Bridges, Interstitial Inc., 1937 Fenton Lane, Park Ridge, IL 60068

Current methods to detect concealed weapons being carried by passengers boarding an aircraft are ineffective if the weapons are largely nonmetallic. An impulse radar method, that employed very-short duration, high-peak-power impulses was initially considered as part of an imaging system to detect such targets. However, this option was abandoned in favor of a chirp radar approach, wherein a short duration impulse could be synthesized from a highly-linear swept frequency. Preliminary quasi-optical studies demonstrated that good resolution, in the order of a centimeter, could be realized by a highly focused collection antenna for an operating frequency between 80 to 120 GHz. Experiments demonstrated that good penetration into typical clothing would be possible in this band as well.

A classical plane-wave impulse illumination method coupled with a highly-focused collection-imaging method was abandoned in favor of a confocal illumination and collection method The confocal method offered improved transverse resolution for a given aperture size, suppressed significantly side-lobe responses and exhibited much improved signal-to-noise ratios relative to the plane-wave illumination option. In the case of very thick but translucent clothing, the confocal method could mitigate possible heterogeneity effects in a way similar to that employed in optical confocal microscopes.

To demonstrate the above, a 94 GHz millimeter wave synthetic impulse FM radar was developed to image in 2-D concealed weapons. The focused spot was scanned over the subject by a rotating mirror. The spot was formed by an 0.5 m diameter ellipsoidal reflector, which also served as the collection antenna. A swept frequency bandwidth of 300 MHz provided about 0.5 meter of longitudinal resolution. This was sufficient to isolate system-generated returns, back-scatter returns and side-scatter returns..

Some 3600 tests were conducted using the 2-D imaging equipment. The human subjects carried both concealed weapons or innocuous items, such as belt buckles or glasses. Detection probabilities in excess of 96% with a false alarm rate of about 32% were demonstrated with a throughput of 10 passengers per minute

Detection and false alarms rates might be improved by developing a 3-D display. This might be done by increasing the bandwidth of the synthetic impulse. A 15 GHz swept band could improve the longitudinal resolution to about 1 cm, which is comparable to the 1 cm of transverse resolution.

*This work was partially sponsored by the FAA.

A58.5

A COMPARATIVE STUDY OF UWB RADAR DISCRIMINATION SCHEMES IN A NOISY BACKGROUND

Sergey Primak, Joe LoVetri
Dept. of Electrical Engineering, The University of Western Ontario, London, Ontario, Canada, N6A 5B9

Satish Kashyap
Dept. of National Defence, DREO, 3701 Carling Ave., Ottawa, Ontario, Canada, K1A 0Z4

Radar target identification methods using the time-domain impulse response of a target, so called Ultrawideband (UWB) radar discrimination schemes, have generated considerable interest recently (C.E. Baum, E. Rothwell, K.M. Chen, and D.P. Nyquist, Proc. IEEE, Vol. 79, #10, pp.1481-1492, 1991). The latest investigations utilize the early-time E-pulses (E. J. Rothwell, K.M. Chen, D.P. Nyquist, P. Ilavarasan, J. E. Ross, R. Bebermeyer, and Q. Li, IEEE Trans. AP., Vol. 42, # 9, pp. 1336-1341, 1994) or correlation receiver with Wavelet Transform to reduce the data storage (E. J. Rothwell, K.M. Chen, D.P. Nyquist, J. E. Ross, R. Bebermeyer, IEEE Trans. AP., Vol. 42, # 7, pp. 1033-1042, 1994).

The main effort of the previous research was concentrated on the development of new schemes for discrimination and reducing the amount of data stored for signal processing. For validation it is usual to show that it is possible to discriminate different targets even if White Gaussian Noise (WGN) is added to the impulse response of the target. But such considerations usually involve only one trial for a given Signal-to-Noise Ratio (SNR) and can not be considered as a reliable approach to prove the ability to use a specific scheme. This paper presents a comparative study of a few different receivers in a noisy background emphasizing the quantitative description of errors in discrimination.

As the initial data we use the measured frequency response of a set of 5 cavities of different lengths and cross sections which can be considered as simple models for more sophisticated targets (rockets, for example). The measurements were made for the frequency range 2-18 GHz and many different monostatic angles for each target. This data is used to extract scattering centres and construct the corresponding discriminating E-pulses.

The direct Monte Carlo method is used to simulate the random nature of the radar operation. For each receiving scheme (i.e. different E-pulse schemes and correlation receiver) and fixed SNR we run approximately 10,000 trials and calculate the probability of wrong detection for the given scheme and given target. As a results we obtain the dependence of the probability of wrong detection as function of SNR, true target, and receiving method, thus allowing the comparison of the different schemes. Memory usage is also considered.

Ultra-Wideband Imaging Radar System

FU-CHIARNG CHEN* AND WENG CHO CHEW

ELECTROMAGNETICS LABORATORY
CENTER FOR COMPUTATIONAL ELECTROMAGNETICS
DEPARTMENT OF ELECTRICAL AND COMPUTER ENGINEERING
UNIVERSITY OF ILLINOIS
URBANA, IL 61801

Abstract

It has been a continuing effort to develop an ultra-wideband microwave imaging radar system at the University of Illinois. This paper will describe both the radar system hardware development and the inverse scattering imaging algorithms issues. There are two different radar system platforms, the time-domain pulse system and the frequency-domain stepped-frequency CW system, being investigated at the University of Illinois. The time domain pulse system consists of a Picosecond Pulse Lab (PSPL) 4050B step generator, a PSPL 4050RPH remote pulse head, two PSPL 5210 impulse forming networks, a Hewlett-Packard (HP) 54120B digitizing oscilloscope mainframe, an HP 54121A 20 GHz four-channel test set, a broadband Vivaldi antenna array and two ultra-wideband amplifiers. The frequency-domain stepped-frequency radar system is based on the HP8510 Network Analyzer or the HP8753 Network Analyzer platform. Both systems are automated and controlled by a computer via the IEEE-488 bus. Besides, there are a dual motor system and a two-dimensional positional table for both systems to become a two-dimensional synthetic aperture radar (SAR) system. Both the advantages and disadvantages of these two radar systems will be described. On the inverse scattering imaging issues, two iterative nonlinear reconstructive algorithms, the distorted Born iterative method (DBIM) and the local shape function (LSF) method, are developed to process the measurement data to reconstruct the image of the target object. The DBIM and LSF methods account for multiple scattering effects of the test targets and show a high resolution image reconstruction capability. Besides, wavelet techniques will be applied to denoise the measurement data in order to increase the signal to noise ratio. The combination of the radar system hardware and the inverse scattering imaging algorithms will potentially provide a good platform for microwave imaging radar system.

A58.7

Ultra-Wideband Transient Backscatter Measurements Through Concrete Walls

Dr. John F. Aurand
Sandia National Laboratories
High-Power Electromagnetics Dept. 9323
P.O. Box 5800, MS-1153
Albuquerque, NM 87185-1153

We recently performed a series of experimental measurements of transient electromagnetic backscatter through two different concrete walls. Several different pulse shapes were used for the incident radiation, with frequency content from VHF to 20 GHz. Both walls were 30 cm thick, with 3 layers of reinforcing steel bars inside. For this set of data, the incident wave was linearly polarized with vertical orientation. Corroborating swept-frequency measurements were made with a vector analyzer.

The wideband time-domain system for measuring monostatic backscatter consisted of a very fast pulse generator driving a custom TEM horn antenna (with dielectric aperture lens and uniquely-placed resistive loading) through the loop-through head of a sampling oscilloscope. This offers a straightforward implementation of a radiated-field TDR system, specifically configured to measure the transient monostatic backscatter from scattering objects in the propagation path.

The transient radiated electromagnetic wave (in the main-beam or boresight direction) of the TEM horn is a time derivative of the pulser waveform. Usually, a doublet (or bipolar) radiated waveform was generated by exciting the antenna with an impulse (unipolar) signal. Then, upon reception of the backscattered electromagnetic energy from the wall or layer under test, the same antenna (by the reciprocity theorem) has a replica time-domain response, so that the received voltage waveform measured by the loop-through sampling head is a replica of the backscattered wave. When this time-domain radar system is pointed at a wall, the received signal clearly shows the individual time-resolved reflections from successive discontinuities in the propagation path, including a reflected pulse from the front surface of the wall, then a reflected pulse from the rear surface of the wall, and so forth.

This paper describes the backscatter propagation measurements through the two different walls, along with the experimental procedure for calibrating the time-domain radar system response with flat metal-plate reflectors. We discuss the time-domain scattering features and the derived frequency-domain transfer function, dielectric constant, loss tangent, and attenuation constant of these walls.

This work was supported by the U.S. Dept. of Energy under Contract DE-AC04-94AL85000. Sandia is a multiprogram lab operated by Sandia Corp., a Lockheed Martin Co., for the U.S. DOE.

Application of Cepstral Analysis to Radar Target Discrimination

G.S. Wallinga, E.J. Rothwell*, K.M. Chen and D.P. Nyquist
Department of Electrical Engineering
Michigan State University
East Lansing, MI. 48824

A great deal of effort has been applied to the detection or identification of airborne targets using the scattered return from ultra-wideband radars. One technique used to identify targets is based on the uniqueness of a target's complex frequencies in the late-time transient scattered signal. In general, the scattered return consists of an early-time signal that is aspect angle dependent and a late-time signal which can be modeled as a sum of complex sinusoidal components whose frequencies do not depend on the radar-target geometry. The complex frequencies associated with this signal are unique to each target and can therefore be used to identify a particular target.

One approach to obtaining the late-time target response is to measure the signal return in the frequency domain and transform into the time domain using a fast Fourier transform. Inherent in this process is the need for both magnitude and phase information. If only the magnitude response of the spectrum is available, one must try to construct the time-domain signal using a different technique. For a time sampled causal signal satisfying the minimum phase condition (poles and zeros of its z-transform located inside the unit circle), one can relate the logarithm of the magnitude and the phase through a Hilbert transform integral. An alternative for calculating the minimum phase signal is to use the cepstrum approach. In this approach one attempts to recover the original transient signal using only the spectral magnitude. This method requires one to use both forward and reverse fast fourier transforms, thus requiring considerably shorter computation time than the integral approach.

This paper will attempt to present some of the findings associated with the reconstruction of a late-time signal from different scattering geometries using a minimum-phase cepstral algorithm. A short review of cepstral techniques used in the analysis will be presented as well as some simple examples that may clarify the theory. Several measurements in the frequency domain will be presented. The time-domain reconstruction using both magnitude and phase (ordinary inverse discrete fourier transform) and magnitude only (cepstrum reconstruction) will be compared. Finally a discrimination simulation using E-pulse cancellation will be demonstrated.

A58.9

Effect of Radar-Target Sea-Clutter Interaction on an Enhanced E-pulse Clutter Cancellation Algorithm

G.S. Wallinga, A. Kizilay, E.J. Rothwell*, K.M. Chen and D.P. Nyquist
Department of Electrical Engineering
Michigan State University
East Lansing, MI 48824

An enhanced detection algorithm using a clutter reducing transmit waveform (CRTW) based upon E-pulse cancellation has been devised. A CRTW can be constructed using the measured return from a surface (clutter producer) and the return from an anticipated target. The expected target can be measured in the lab or calculated theoretically. The CRTW produced will maximize the ratio of target to clutter return for some optimal target position within the return's observation window.

Previous research in target detection using the CRTW algorithm concentrated on detection of a target in both a static clutter environment and an evolving sea-surface environment. In both cases the scattered field from a target embedded in sea clutter was obtained by adding the scattered field from the target to the sea-surface clutter. In this case it was quite easy to vary the maximum ratio of target return to clutter return. One shortcoming of this method is that no consideration was given to the electromagnetic interaction caused by multi-path scattering and target/surface current coupling. Since the construction of the CRTW is based upon separate returns from the surface and anticipated target one must ask how well the detection algorithm will work for a target embedded in clutter using an appropriate interaction scattering model.

The purpose of the present study is to demonstrate the effect of the surface-target interaction on the CRTW detection algorithm. A solution for the scattered field from a perfectly conducting cylinder located over a 2-d perfectly conducting surface has been formulated, taking into account the interaction terms. The conducting surface can be of aperiodic finite extent or periodic infinite extent. The size and location of the cylinder above the surface can be varied, causing the interaction term to change. The effect on the detection algorithm will be tested by varying the height of the cylinder above the surface. In addition, the size of the cylinder can be varied to obtain some control over the target to clutter signal ratio. Several simple periodic sea-surface profiles will be used in the testing procedure.

Characterization Of Off-Boresight Radiation From An Impulse Excited TEM Horn: Experiment Plus Supporting Analyses

W. T. Clark III,[3] R. L. Hutchins,[1] J. S. H. Schoenberg,[2] and J. S. Tyo[2] *

[1]BDM International Inc., Albuquerque, NM 87106
[2]Phillips Laboratory, WSQW, Kirtland AFB, NM 87117
[3]Voss Scientific Inc., Albuquerque, NM 87108

Practical applications of antennas and antenna arrays, either narrow band or wide band, require performance data on radiated fields at locations well away from boresight. Some data on off-boresight radiation exist for impulse excited antennas (K. L. Shlager, G. S. Smith and J. G. Maloney, *IEEE Trans. Electromagnetic Comp.* **38** p. 414, August 1996). The purpose of this study was to extend available results on impulse excited TEM horn antennas to include: a sampling of responses as a function of both the azimuth (ϕ) and elevation angles (θ), the influence of adjacent horn elements comprising a horn array, and response differences due to focusing lenses. The primary emphasis or this study was an experimental characterization, however an analytic model is used to provide an approximate summary of results.

Experiments were conducted using one plate of the TEM horn over a 16'x32' ground plane surrounded on three sides by absorbing material. The minimum measured clear time on the ground plane was ~50 ns. The horn plate had a length of 0.73 meters and was inclined 22.7° with respect to the ground plane to produce a characteristic impedance of 93 ohms. The half TEM horn was excited at a ground plane feed through by a pulse generator located beneath the ground plane connected to the feed point by a 50 ohm cable. The pulser produced an approximately rectangular pulse with a peak of 1500 volts, a risetime of about 0.2 nanoseconds and a full width half maximum pulse width of 1.75 nanoseconds. The ratio of the one way transit time on the antenna to the pulse width was 1.39. The electric fields were measured at a distance of 3.05 meters from the horn apex. The electric fields were detected by either an Prodyn AD S110(R) ground plane sensor or a EGG ACD-7C(R) free field sensor. The pulser was operated in a repetitive mode, and the measurements were recorded on a HP 11801B sampling oscilloscope. Measurements of the principal electric field component were obtained over an array of 32 azimuth and elevation points. The baseline horn was conical with a dielectric lens focused at infinity. Measurements were repeated using a flat horn element without a lens, and using two flat adjacent horn elements where one is parasitic and terminated by a 50 ohms load. Some measurements were also repeated at twice the range and with a Prodyn B-60D(R) magnetic field sensor to characterize near field contributions.

Data analyses include: overlays showing comparisons of various cases and plots of waveform parameters such as peak amplitude, waveform energy and median frequency (frequency below which 50% of the available energy lies) versus θ and ϕ. Measurements were compared to an analytic vee wire antenna model that uses a transmission line approximation of the antenna current and a far field radiation prediction based on that current distribution.

Based upon the data, arrays capable of steering up to 30° away from boresight may be contsructed of small-angle, unfocused TEM horns. At an azimuthal steering angle of 30°, the average power is down by 2.5 db and the peak power is down by 5 db relative to the boresight direction. The radiated power falls off more rapidly in elevation, but reasonable steering can be expected at elevation angles that are about half of the horn throat angle. The radiation in the anti-boresight direction, which is dominated by low-frequency content, is down by 11 and 22 db in average and peak power respectively. The inclusion of the focusing lens increases the relative amount of power on boresight, making the "beamwidth" narrower than for the unfocused horn.

A58.11

TIME DOMAIN MEASUREMENT AND OPTIMISATION OF SOME SIMPLE ANTENNAS

E A Elkhazmi and N J McEwan
Department of Electronic and Electrical Engineering,
University of Bradford, UK

While antennas are usually described assuming excitation at a single frequency, a time domain visualisation offers more physical insight in many simple cases. Time domain measurements on a variety of simple antennas, all using a large metallic ground plane, are described. Impulse response measurements include input reflection and input current, travelling wave current, and electric field at near and far points in the ground plane. Construction of balanced loop and capacitive probes, for current and electric field measurements respectively, is discussed, and a calibration technique is described which uses a horizontal conductor over the ground plane to make an approximation to an ideal TEM line. Approximate equivalent circuits for the probes are discussed. A specimen result (Figure 1) for an inverted vee antenna shows a reflection from the vertex at 0.5nS which is not insignificant compared to the end reflection.

A gating technique is used in an empirical design for a travelling wave vee antenna designed to give a broadband input match. The conductor is realised as a thin strip of variable profile, which is adjusted at the input end to reduce the first part of the reflection impulse response almost to zero. Gating the current probe response at various points along the structure allows the rate of attenuation of the current by radiation to be assessed without interference from the end reflection. These data provide a criterion for adjusting the radiating arm length to ensure true travelling wave behaviour, permitting an excellent broadband match to be obtained.

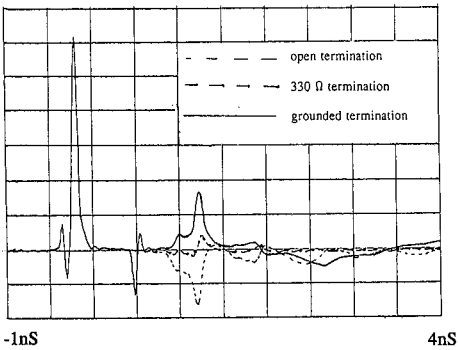

Figure 1. Input reflection impulse response (50 ohms source) of an inverted vee (half rhombic) antenna, of total length 20cm, vertex angle 45°, diameter 2mm.

URSI A **Session 76** **Salon St-Charles**

Antennas and EM Field Metrology
Co-chairs: J. Norgard, USA and M. Kanda, USA

13:10 76.1 Error Reduction of Measured Equation of Invariance, **K.K. MEI**, Y.W. LIU, K.N. YUNG, *City University of Hong Kong, Kowloon, Hong Kong*

13:30 76.2 Improving the Transient Performance of a TEM Horn Antenna Using Resistive Loading, **J.F. AURAND**, *Sandia National Laboratories, Albuquerque, NM, USA*

13:50 76.3 Near-Field Characterization of a Reflector Surface at 240 GHz, **M.T. CHEN**[1], C.E. TONG[2], S. PAINE[2], R. BLUNDELL[2], [1]*Academia Sinica, Taipei, Taiwan, China;* [2]*Harvard-Smithsonian Center for Astrophysics, Cambridge, MA, USA*

14:10 76.4 Fast Anechoic Chamber Diagnostic Testing via Modulated Scattering Arrays and the MUSIC Imaging Code, **B. COWN**[1], E. BEAUMONT[2], Ph. GARREAU[2], P. DUMON[3], J.M. LOPEZ[4], J. ESTRADA[4], [1]*SATIMO, Inc., Acworth, GA, USA;* [2]*SATIMO (SARL), Les Ulis and* [3]*CNES, Centre Spatial de Toulouse, France;* [4]*GTRI, Georgia Tech, Atlanta, GA, USA*

14:30 76.5 Spherical Back Transform for Microwave Holography, **G.G. CHENG**, *TRW Space and Electronics Group, Redondo Beach, CA, USA*

14:50 76.6 Metrics for Data Analysis and Error Control in EM Methods, **V. CABLE**, *Lockheed Martin Skunk Works, Palmdale, CA, USA*

15:10 76.7 Near-Field to Far-Field Transformation on Arbitrary Measurement Geometry Utilizing an Equivalent Electric Current, A. TAAGHOL, **T.K. SARKAR**, *Syracuse University, Syracuse, NY, USA*

15:30 76.8 Method of Time Domain Antenna Measurements and it's Application to Antenna Field Test, **D. PONOMAREV**, V. PROSHIN, K. NIKASHOV, *MERA Ltd., Nizhny Novgorod, Russia*

15:50 76.9 Finite Elements Calculation of Beam Patterns of Curvilinear Generants Horn Radiators, **A.V. GLUSHKOV**, I.I. SHUMLJANSKY, T. BUYADGI, I. SHPINAREVA, *OHMI, Odessa, Ukraine*

16:10 76.10 Synthesis of Electromagnetic Horns with Optimal Mismatch Factor, **A.V. GLUSHKOV**, Yu.A. KRUGLYAK, *OHMI, Odessa, Ukraine*

16:30 76.11 Synthesis of Electromagnetic Horns Featuring Optimal Conversion Coefficient into High-Order Waves, **S.V. AMBROSOV**, S. DAN'KOV, V.A. EFIMOV, V.A. CHERNETSKY, *OHMI, Odessa, Ukraine*

16:50 76.12 Solution of Internal Problem for Antenna Synthesis, **I.I. SHUMLJANSKY**, A.V. GLUSHKOV, *OHMI, Odessa, Ukraine*

A76.1

Error Reduction of Measured Equation of Invariance

K. K. Mei*, Y. W. Liu, and K. N. Yung
Department of Electronic Engineering
City University of Hong Kong

ABSTRACT

In the Measured Equation of Invariance (MEI) method, most of the effort is focused on finding the MEI coefficients (K. K. Mei, R. Pous, Z. Q. Chen, Y. W. Liu, and M. Prouty , IEEE Trans. on Antennas and Propagation, Vol. 42, No. 3, pp. 202-214, March 1994), because their accuracies directly affect the solutions. If we could find more accurate MEI coefficients at low frequencies, we may use the technique of the MEI coefficient interpolation and extrapolation (Y. W. Liu, K. K. Mei, K. M. Luk, and K. N. Yung, IEEE Antennas and Propagat. Intl. Symposium, pp. 946 - 949, Baltimore, Maryland, July 21 - 26, 1996), to obtain more accurate MEI coefficients at high frequencies. Since the time consumed in finding the MEI coefficients at the low frequencies is only hundredths or thousandths of the time of finding the MEI coefficients by using direct integrations, it is more advantageous to obtain the MEI coefficients by using interpolation and extrapolation technique. So, reducing the error of the MEI coefficients at the low frequencies becomes important. This paper proposes to minimize the error of total surface currents between the MEI and MoM by adjusting the original MEI coefficients that are obtained by direct integration process. Combined with the interpolation and extrapolation technique (Y. W. Liu, K. N. Yung, and K. K. Mei, "Interpolation, extrapolation and application of the measured equation of invariance to scattering by very large cylinders," Submitted to IEEE Trans. on Antennas and Propagation.), the solutions of many field problems shall reach a new region of high speed and high accuracy.

Improving the Transient Performance of a TEM Horn Antenna Using Resistive Loading

Dr. John F. Aurand
Sandia National Laboratories
High-Power Electromagnetics Dept. 9323
P.O. Box 5800, MS-1153
Albuquerque, NM 87185-1153

We recently modified a TEM (transverse electromagnetic) horn antenna with uniquely-placed resistive loading in order to improve the transient pulse response. The antenna consists of a conventional TEM horn configuration (two flat, 91-cm long triangularly-shaped conducting plates with a constant separation angle), and a solid dielectric lens placed in between the aperture end of the plates. The teflon™ lens collimates the internal wave for faster time-domain response. We have used this lens TEM horn for 1½ years, but there is an undesirable negative precursor feature in the receiving impulse response which we wanted to eliminate.

Because the lens does not extend past the two plates, it only interacts with the internal wave bound to the interior (facing) surfaces of the plates. Consequently, the external wave (defined by the surface currents on the exterior sides of the metal plates) experiences less propagation delay along the antenna structure than the internal wave. In addition, this external wave is of opposite polarity compared to the internal wave, due to the direction of the TEM-mode fields at the exterior/outer surfaces of the plates compared to the fields in between the plates. As a result, there is a leading negative precursor feature in the receiving impulse response due to the external wave arriving slightly earlier in time and with opposite polarity.

Modifying the antenna involved empirically determining the effect of carbon-loaded lossy-foam absorber when placed on the exterior surface of the two antenna plates. We found that the best configuration was a pair of long, narrow strips of absorber, located just inside the side edges of the triangular plates. This strongly attenuates the external wave fields, effectively eliminating the undesired negative precursor feature of the impulse response. For the same reason, it also increases the gain or sensitivity of the antenna because it eliminates the external-field reduction of the primary impulse response when superimposed on the internal wave fields at the antenna feedpoint.

This paper describes our antenna design, the experiments done in optimizing the antenna performance, and measurements of the resulting improvement. As a result of this modification, this type of antenna offers very good transient operation, with clean waveform behavior for ultra-wideband time-domain antenna work.

This work was supported by the U.S. Dept. of Energy under Contract DE-AC04-94AL85000. Sandia is a multiprogram lab operated by Sandia Corp., a Lockheed Martin Co., for the U.S. DOE.

A76.3

Near-field characterization of a reflector surface at 240 GHz

M. T. Chen[1*], C. E. Tong[2], S. Paine[2], and R. Blundell[2]

[1]Institute of Astronomy and Astrophysics
Academia Sinica, Taipei, Taiwan 115

[2]Harvard-Smithsonian Center for Astrophysics,
60 Garden St., Cambridge, MA 02138

ABSTACT: **We present the investigations to characterize a reflector surface from near-field measurements. In the techniques a bench-top, near-field range is set up to measure the beam pattern radiated from a corrugated feed horn through a reflected mirror at 240 GHz. Both the amplitude and phase of the E-field are measured on a scan plane. A near-field-to-near-field numerical transformation is implemented to model the beam propagation of the corrugated horn. Based on a vector Kirchhoff integral, the computing code can forward propagate a known radiating field to the scan plane through the mirror, or to backward propagate the measured field to the mirror, and then to the horn aperture. For our purpose the scanned field is backward transformed to the mirror surface. Our main concern is to understand the correlation between the transformed field pattern and the reflector surface irregularity, and consequently to reconstruct the reflector surface from further calculation. In this report we present the analysis of reflector surface from the measurements with beam reflected through a paraboloidal mirror, and through the same mirror but with known artifacts on its surface. The results are compared with the simulation to forward propagate an ideal field at the horn aperture to the mirror surface.**

The applicability of this near-field transformation to a large reflector is also studied. We present the simulations of forward transformation from an ideal aperture field to the 6-meter, primary reflector of the Sub-Millimeter Array (SMA) currently under construction by the Smithsonian Astrophysical Observatory.

Fast Anechoic Chamber Diagnostic Testing via Modulated Scattering Arrays and the MUSIC Imaging Code

B. Cown*, E. Beaumont, Ph. Garreau**, P. Dumon***, J. M. Lopez, and J. Estrada******

SATIMO, Inc., Suite E-116, 1318 Chandler Court, Acworth, GA, 30102 USA
***SATIMO (SARL), "Le Pin", rue de la Terre de Feu, Z. A. de Courtabouef, 91952, Les Ulis, France**
****CNES, Centre Spatial de Toulouse, 18 Avenue Edouard Belin, 31055 Toulouse, France**
*****GTRI, Antenna Technology Development Division, Georgia Tech, Atlanta, GA 30332 USA**

The technical feasibility of performing diagnostic testing of large ancechoic chambers by using 1) linear arrays of elements that utilize the Advanced Modulated Scattering Technique (A-MST) and 2) the MUSIC imaging algorithm has been demonstrated based on the outcome of experiments conducted at the compact range/anechoic chamber facility at the Centre Nationale de Recherches Spatiales (CNES) in Toulouse, France (B. J. Cown, Ph. Garreau, E. Beaumont, *et. al.*, " Advanced MST Automated Electromagnetic Field Probe for Anechoic Chamber Testing", Interim Technical Report, Phase I of AF96-222, Contract F04611-95-C-0060, Dec., 1996). In particular, the wideband (1.5 GHz-6.0 GHz) linear array of 64 dual-polarized modulated scattering probes, shown in Figure 1, was installed on the 7-axis positioner located in the quiet zone of the CNES compact range reflector, and the complex electric field existing at the location of each of the 64 probes along the 5.7-foot length of the array was measured in less than 10 milliseconds. In one series of measurements, the array was mounted horizontally and rotated in azimuth over ± 90.0 degrees to obtain a quick look at the chamber. A plot of the image obtained at 2.0 GHz by processing the measured data via the MUSIC imaging code is shown in Figure 2, for the case where the compact range feed is actively illuminating the reflector and a passive scatterer (an unexcited horn antenna) is located at approximately +38.5 degrees azimuth relative to the longitudinal axis of the quiet zone. The lobe at 0 degrees is due to the reflector mainbeam; the passive scatterer response is seen at approximately +38.5 degrees. The double-lobed response seen around + 54 degrees is due partly to scattering from a passive RF cable that was vertically draped from the aperture of the compact range transmitting room to the floor. A second set of measurements was performed to obtain 2-dimensional images of the chamber, and the results will be presented and discussed at the meeting.

1. A-MST Linear Array

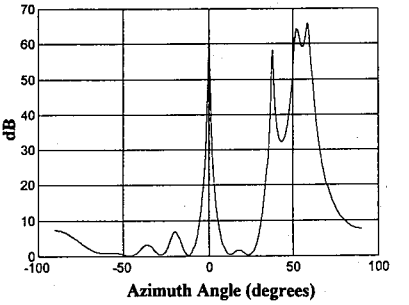

2. MUSIC image at 2.0 GHz

A76.5

Spherical Back Transform for Microwave Holography

Guan G. Cheng
TRW Space and Electronics Group
One Space Park, 66/1217
Redondo Beach, CA 90278

Microwave antenna holography is to some extent an inverse source problem. The goal of the spherical microwave holography is to determine the field on a spherical surface interior to a spherical measurement surface. Holographic techniques are widely utilized as a non-destructive method for the diagnosis of antennas, and more importantly, in my opinion, they provide a synthesis tool which is very useful for antenna design.

The computation of electromagnetic field on a spherical surface from that on a smaller, inner spherical surface with known field distribution is a classical boundary-value problem, and its numerical solution is straightforward. Conversely, field evaluation on an inner sphere based on a known distribution on a larger, outer sphere is rather cumbersome and computationally intensive because in this case an integral equation is involved. The inversion of a large matrix is required in the event that one chooses to rely on spherical modal expansions for field evaluation. Unlike planar microwave holography, which is numerically efficient due to the nature of the Fourier transform operation, the spherical back transform based on the spherical modal expansions normally takes hours of CPU time for a computer run.

We present here a novel spherical wave back transform for microwave antenna holography. This back transform is essentially an integration operation which calculates the field on an inner sphere from that on an outer sphere, with substantially the same CPU speed encountered when going from inner to outer spheres. Similar to the planar case, our work further shows that a pair of spherical nearfield-to-farfield and farfield-to-spherical nearfield transforms are indeed the inverse operations of one another, with identically the same degree of computational complexity.

Numerical results of various antenna holography simulations are described. Antenna designs utilizing holographic synthesis techniques are also shown.

Metrics for Data Analysis and Error Control in EM Methods

Vaughn Cable
Lockheed Martin Skunk Works
Palmdale, California 93599-2550

The Electromagnetic (EM) community does not have a generally accepted measure for comparing various antenna or scattering data. Although, the "sector average" approach is sometimes used, a quick scan of the EM literature reveals little use of any methods of error analysis, error bars, or use of a standard figure of merit.

Making comparisons between various data is the inevitable consequence of analysis and design. In the EM community, we make comparisons between measurements, between measurements and prediction, between different predictions, but we often only give a qualitative report. As a result, one backscatter pattern may be better or worse in one person's eyes, but not in another's. Reasonable people can disagree. The manner and format in which most EM data is prepared and compared varies, but the underlying issue is always the same. Namely, "What is the best way to report the result in order to enable the best possible decision?"

An array of quantifying statistical methods are available to engineers. They are the mainstay of detection and estimation theory, and TQM (Total Quality Management) for that matter. They play a part in target recognition and angle of arrival measurement. These methods include measures of central tendency (mean, variance, median, mode) and tests between these measures (t-test, F-test), tests to see if the data is derived from same or similar distributions (chi-square, K-S), correlation tests (linear correlation, Fisher's transform), and tests for associations between data (contingency analysis, entropy), to mention a few.

The "sameness" or "closeness" between EM data can be quantified and this paper will examine a series of statistical alternatives, including parametric and non-parametric measures which appear to be appropriate. Specific examples comparing RCS data using these methods will be presented.

A76.7

Near-Field to Far-Field Transformation on Arbitrary Measurement Geometry Utilizing an Equivalent Electric Current

A. Taaghol and T. K. Sarkar
Department of Electrical Engineering and Computer Science
121 Link Hall
Syracuse University
Syracuse, New York 13244-1240
Tel: 315-443-3775; Fax: 315-443-4441
Email: tksarkar@mailbox.syr.edu

Abstract: A general methodology for near-field to far-field transformation is presented utilizing measured data on an arbitrary measurement geometry. Conventionally near field vector data is measured on a planar, polar or spherical surface and then a near field to far-field transformation is carried out utilizing the classical model expansion method. In this paper, we utilize the surface equivalence principle and the method of moments to illustrate how near-field to far field transformation can be carried out utilizing measured data on an arbitrary shaped measurement surface. The basic philosophy is to encapsulate a surface close to the source by an equivalent electric current source. Given the equivalent electric current in free space one can find the near fields on any surface. Conversely, given the measured fields on an arbitrary surface one can obtain the equivalent surface unknown electric current via the method of moments. Once the equivalent electric current is known, the far fields can be obtained in a straight forward fashion. The advantages of this new technique are that the measurements need not be made at a conventional surface. Also there is no restriction on the rate of sampling of the measured field points. The measurement truncation error can be significantly reduced in this methodology as opposed to a planar near-field to far-field transformation. One can also do an error diagnosis on the actual antenna as the equivalent currents may illustrate how the structure is radiating.

The difficulty with this approach is that the moment matrix is ill-conditioned as the electric fields contain 2 derivatives. Also the size of the resulting field equations are large as the two components do not decouple as in some of the situations associated with the equivalent magnetic current. Numerical results will be presented to illustrate the efficacy of this methodology.

Method of Time Domain Antenna Measurements and it's Application to Antenna Field Test.

Dmitry Ponomarev E.E. Ph.D. Director, Scientific-Research company MERA, Nizhny Novgorod, Russia.
Vladimir Proshin Engineer, Scientific-Research company MERA, Nizhny Novgorod, Russia.
Konstantin Nikashov Researcher, Scientific-Research company MERA, Nizhny Novgorod, Russia.

Equipment of antenna field test based on Time-Domain method designed at MERA Ltd. allows serviceman to control whole antenna parameters and to locate failed elements in antenna arrays.

The basic idea of time-domain measurements is that antenna under test is radiated by a short electromagnetic pulse from different directions. The nature of electromagnetic pulse is that it is spatially concentrated. This allows one to separate antenna response excited by pulse from responses excited by its' reflections with a help of time window. This is equivalent to existence of unechoic area around antenna under test. The size of this unechoic area depends on such factors as length of antenna impulse response, distance between antenna under test and pulse radiating antenna, distance between both antennas and reflecting surface, etc. Test equipment records a set of antenna impulse responses and then calculates different antenna parameters (including directivity pattern, phase pattern, gain, etc.). Signal processing includes blanking of reflections with a help of time windows of different shapes, calculation of each impulse response spectrum, calculation and smoothing of antenna parameters such as gain, directivity, antenna pattern, phase pattern, etc.

Another feature of time-domain measurements is that each complex antenna usually has it's "characteristic" pulse responses corresponding to some directions. This "characteristic" responses looks like a set of easily locatable responses of individual antenna elements. This makes it possible to locate failed antenna elements by comparing reference "characteristic" response with a real one. In some specific cases this feature allows even to tune antenna array during field test.

Large practical experience of MERA engineers with many time-domain measurement system installations proved high efficiency of this method.

A76.9

FINITE ELEMENTS CALCULATION OF BEAM PATTERNS OF CURVILINEAR GENERANTS HORN RADIATORS

Glushkov A.V.[#*], Shumljansky I.I.&, Buyadgi T.[*], Shpinareva I.[#]

[#]Applied Math.Dept., OHMI, a/c 108, Odessa-9, SU-270009, Ukraine,
[*]Radiophys.&Electr.Center, a/c 108, Odessa-9, SU-270009, Ukraine
&Radiometeorology Dept., Odessa Hydrometeorological Institute,
a/c 108, Odessa-9, SU-270009, Ukraine

The problem of finding the beam patterns for horn radiators with curvilinear generants attracts a great interest. Some methods were used to calculate the beam patterns for simple form generants horns (on the basis of potentials of the corresponding fields & methods similar to those formulated for acoustic horns, etc.). In this paper we develop the general approach to calculation of the beam patterns for arbitrary form generants horns, which is based on the finite-differences and finite elements method. As an example, we solve the general equation for wave propagation in the horns with the exponential generants: $G \sim \exp[g\, z]$, g - constant, and compare with known solution. A more general task of finding the electric field potential for a substantially irregular horn with generants: $G \sim \exp[g(z)\, z]$ and $G = G(z)$ is considered and solved. There is the possibility to perform the series of calculations to find a horn, whose beam patterns agree with the required one within a given accuracy limit.

1. A.V.Glushkov, S.V.Malinovskaya, S.V.Ambrosov, Sci.Techn.Proc. N3, Odessa (1996).

SYNTHESIS OF ELECTROMAGNETIC HORNS WITH OPTIMAL MISMATCH FACTOR

Glushkov A.V.[#*],Kruglyak Yu.A.[@]

[#]Applied Math.Dept.,OHMI,a/c 108,Odessa-9,SU-270009,Ukraine,
[@]Molecular Electr.Dept.,State Univ.,a/c 108,Odessa-9,SU-270009,
[*]Radiophys.&Electr.Center,a/c 108,Odessa-9,SU-270009

Investigation of the main characteristics of antennas, horn radiators and improvement of them by means the use of the different factors, which affects the horn characteristics, for instance,of the form of the horn generants, the development of accurate theory for simplest types of the horn-type antennas (HA)and more complicated ones is of a great importance. The horn radiators offer such advantages as an unsophisticated construction,flat gain over the frequency range and reliability in service, which makes them widely applicable as wave guide adapters, antennas proper, exciters for reflector and lens-type antennas and elements of phased arrays. The problem of the electromagnetic horns treating and construction with optimal choice of main characteristics is under consideration in this paper. The aim is to find the optimal form for antenna curved generants, in particular,with minimum mismatching factor for a given horn lengths. It's considered a complex numeral approach to the solution of systems of firstorder differential equations for normalized amplitude of the field cross component expansion in the horn [1]. The approach is based on the complex use of the cross-section, finite-elements, Fourier transform and Optimal Governing theory methods. There is provided and controled the minimum mismatching factor. We consider synthesizing the shape of comparatively long horns with small variations of the input and output cross-section for designing the shape of comparatively short horns whose inlet and outlet cross-sections differ greatly.

1. A.V.Glushkov,S.V.Ambrosov, Sci.Techn.Proc.N3,Odessa (1995).

A76.11

SYNTHESIS OF ELECTROMAGNETIC HORNS FEATURING OPTIMAL CONVERSION COEFFICIENT INTO HIGH-ORDER WAVES

Ambrosov S.V.[@],Dan'kov S.[#*],V.A.Efimov[#], Chernetsky V.A.[#]

[#]Applied Math.Dept.,OHMI, a/c 108,Odessa-9,SU-270009,Ukraine,
[*]Radiophys.&Electr.Center,a/c 108,Odessa-9,SU-270009,Ukraine, [@]Institute of Technology, a/c 108,Odessa-9,SU-270009,Ukraine

The horn radiators were considered and their electrical characteristics were studied: radiators of stepped configuration (on the bases of electromagnetic principles with the use of different design methods, in particular, theory of stepped and tapered waveguide adaptors, the circuit theory). The results derived by means of the electrodynamic method (crosssection method) agree with the corresponding results, obtained within the circuit theory method for stepped horns. The problems of the matching the horn are considered with the feeding waveguide by selecting appropriate forms for the horn generants. The influence of the horn generant form variation upon the horn beam pattern has been studied. An effective approach is proposed for synthesis of a horn featuring an optimal conversion ratio of fundamental wave into higher-type waves. The optimal governing theory [1] method allows the calculation of the horn antenna configuration with minimal loss of electromagnetic energy under availibility the excitation of higher-type waves. The tests, carried out, have shown the expediency and efficiency of the curved horn application, when reducing the number of higher type waves (and, therefore, the power absorbed by them) and varing the shape of the beam pattern is necessary.

1. A.V.Glushkov,S.V.Malinovskaya,S.V.Ambrosov, Sci.Techn.Proc. N1,Odessa (1996).

SOLUTION OF INTERNAL PROBLEM FOR ANTENNA SYNTHESIS

Shumljansky I.I.&, Glushkov A.V.[#*]

[#]Applied Math.Dept.,OHMI, a/c 108,Odessa-9,SU-270009,Ukraine,
[*]Radiophys.&Electr.Center,a/c 108,Odessa-9,SU-270009,Ukraine, &
Radiometeorology Dept.,Odessa Hydrometeorological Institute, a/c 108, Odessa-9, SU-270009,Ukraine

It's considered an internal problem for antenna synthesis. The main task is to find the horn configuration providing the horn pattern with a given acuracy. We consider the horn with arbitrary (geometry) generants from some class of the curves. Using the method, similar to Sveshnokov-Ilijnsky, we find the reflection of the horn on the regular waveguide with a plane metallic flat-flange at the end.The length of the flat-flange is equal to length of the horn generant. The transverse cross-sections are the same.Further we find an electric field component E on the basis of the torsional boundary surfaces method [1]. The advantage of this procedure is the convergent approximation. In the limit, we get the waveguide field with the finite flat-flange. The following step is an inverse field transformation, which results in the initial horn field. By means of it, we construct the pattern diagram and compare with a given one. If the correspondence is absent, then the procedure is continued. Another horn is considered in order to obtain the admittable coincidence of the horns patterns. To simplify the synthesis procedure (the choice of the necessary horn form to provide the needed accuracy of the horn patterns), we are preparing a special atlas. It contains the corresponding horn patterns for different curvelinear generants. If the suitable horn pattern is absent, it is possible to choose the most closed horn pattern, which corresponds to the required one. Then it is necessary to fulfill additionally more specific calculations.

[1] Shumljansky I.I. Horn Radiators of Complex Configuration.- World Scientific Publ.,Singapore,1991.

URSI B **Session 1** **Salon Marquette**

Discrete Methods
Co-chairs: A.F. Peterson, USA and N. Simons, Canada

08:10	1.1	Characterization of Surface Mount Package Effects with the TLM Method, **G. TARDIOLI**, M. RIGHI, L. CASCIO, W.J.R. HOEFER, *University of Victoria, BC, Canada*
08:30	1.2	Accurate Determination of Loss of Symmetrical Reciprocal 2-Port Devices Using the Finite Element Method, **G.P. RIBLET**, *Microwave Development Laboratories, Inc., Needham, MA, USA*
08:50	1.3	Practical Vector Finite Elements, J.S. SAVAGE, **A.F. PETERSON**, *Georgia Institute of Technology, Atlanta, GA, USA*
09:10	1.4	On Accuracy of Field Representation by Edge-Elements of Various Shapes, **A. BOAG**, *Israel Aircraft Industries, Ben-Gurion Airport, Israel*
09:30	1.5	Construction of the Basis Functions for Nedelec's Finite Element Spaces for Triangular and Tetrahedral Meshes, **J.Y. WU**, R. LEE, *Ohio State University, Columbus, OH, USA*
09:50	1.6	The Spectral Lanczos Decomposition Method for Solving 3-D Low-Frequency Electromagnetic Diffusion by the Finite-Element Method, **M. ZUNOUBI**, J.-M. JIN, W.C. CHEW, *University of Illinois at Urbana-Champaign, Urbana, IL, USA*
10:10		Coffee Break
10:30	1.7	An Argument for the Use of Tetrahedral and Triangular Edge Elements for Modeling Electrically Large Geometries, J.Y. WU, **R. LEE**, *Ohio State University, Columbus, OH, USA*
10:50	1.8	Optimal Finite Difference Sub-Gridding Techniques Applied to the Helmholtz Equation, **J. NEHRBASS**, R. LEE, *Ohio State University, Columbus, OH, USA*
11:10	1.9	Frequency Extrapolation Analysis in Conjunction with Finite Element-Boundary Integral System, **Y.E. ERDEMLI**[1], J.L. VOLAKIS[1], J. GONG[1], C.J. REDDY[2], [1]*University of Michigan, Ann Arbor, MI and* [2]*Hampton University, Hampton, VA, USA*

B1.1

Characterization of Surface Mount Package Effects with the TLM Method

Giampaolo Tardioli, Mario Righi, Lucia Cascio, and Wolfgang J. R. Hoefer
NSERC/MPR Teltech Research Chair in RF Engineering.
Department of Electrical and Computer Engineering, University of Victoria,
Victoria, B.C. V8W 3P6, CANADA, e-mail: whoefer@ece.uvic.ca

The increase in clock rate and integration density in modern IC technology leads the designer to deal with problems for which traditional lumped circuit design methodology fails to accurately account for the complex interactions between different parts of the circuit. Problems such as dispersion, crosstalk and package effects require a full electromagnetic approach in order to predict their impact on the final configuration. A typical problem is the characterization of a MMIC once it is mounted in a package. The presence of leads, bond wires and grounding pins affects the MMIC behavior. These effects must be included in the early design stages. In order to avoid costly design cycles, an electromagnetic approach becomes attractive to predict accurately the performances of a packaged circuit.

In this paper we present the full wave time-domain analysis of a surface mount plastic package containing a simplified MMIC (a thru connection and a microstrip spiral inductor). Problems such as poor grounding terminations and crosstalk with neighboring lines are also considered as they can occur at relatively low frequencies. The significance of a full wave characterization of the component is shown. Results are validated with data available in the literature showing a good agreement.

Finally, we propose an approach to isolate the package effects. The whole structure is segmented and the package is characterized by its scattering parameters. In this way the package needs only to be modeled once for a given configuration. The package effects are extracted and combined with the MMIC parameters to predict the performance of the packaged circuit at a fraction of the computational costs. In addition, the MMIC circuit can be optimized by including the package effects from the design stages, thus significantly reducing costly cut-and-try cycles.

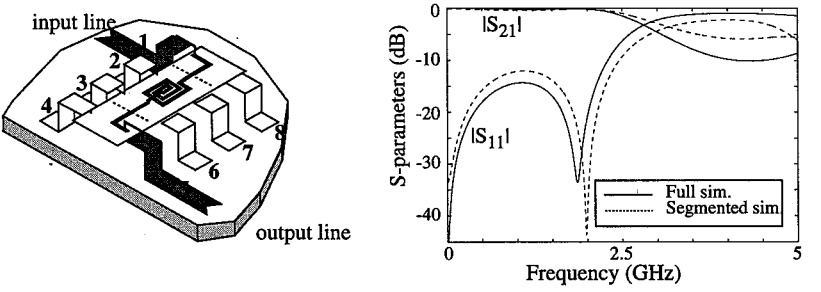

Segmentation sections in the plastic package and comparison with the full wave results

Accurate Determination of Loss of Symmetrical Reciprocal 2-Port Devices Using the Finite Element Method

G. P. Riblet, Microwave Development Laboratories Inc. Needham , MA 02194

A new method for analysing the performance of lossy symmetrical reciprocal microwave 2-port devices by the finite element method will be described. It is based on determining the even and odd mode reflection coefficients Γ_e and Γ_o. In the case of a lossy 2-port these magnitudes will be less than one. It represents an extension of a method which has been described recently (Itoh,T. , Pelosi,G. , and Silvester,P. (editors), Finite Element Software for Microwave Engineering , John Wiley & Sons, N.Y. , 1996, chapter 6) for determining Γ_e and Γ_o for lossless devices using the finite element method. The boundary value problem is solved with a constant unit amplitude field at the input and with an open (short) circuit at the symmetry plane. A layer of very thin elements is included close to any conducting surfaces but the surfaces themselves are assumed to be perfect conductors. The thickness of these thin elements can be the skin depth. The boundary value problem is then solved for the interior fields in both cases. From these solutions the stored energy and dissipated power P_D for both the even and odd mode terminations can be evaluated. These two quantities determine Γ uniquely. Only those thin elements close to conducting surfaces are used to evaluate the resistive losses. The method has been applied to determining the loss of waveguide bandstop filters. A comparison between theory and experiment will be given. An important class of microwave devices that this method can be applied to is that of microwave filters. Loss is an important parameter for filters which are almost always symmetrical.

B1.3

Practical Vector Finite Elements

J. Scott Savage and Andrew F. Peterson
School of Electrical and Computer Engineering
Georgia Institute of Technology
Atlanta, GA 30332

The finite element method using vector basis functions has far reaching applications. Most commonly, low–order vector basis functions, often called edge–elements, are used with little regard to the efficiency of the method. Unfortunately, any practical 3–D finite element application using edge–elements requires more unknowns than the average computational scientist is comfortable handling. Fortunately, many refinements and extensions to standard edge–elements are possible which move 3–D vector finite element analysis several steps toward practicality. This presentation will outline many such improvements.

The most significant improvement in the efficiency of vector finite elements is the use of higher–order basis functions. As the order of the basis functions increases, so too does the rate of convergence. Unfortunately, the number of unknowns per mesh element increases dramatically with higher–order elements. However, the increased rate of convergence allows the use of fewer total elements. In fact, the improvement in convergence rates supersedes the increase in unknowns per element, so that fewer total unknowns can be used without sacrificing accuracy. Perhaps the biggest advantage in using higher–order elements, though, involves mesh generation. The coarse meshes made practical by higher–order elements are much easier to generate than the dense meshes required using low–order elements. Indeed, the computational savings of higher–order elements have been verified.

One drawback to using coarse meshes is geometry modeling error. With fewer cells per unit length, curved boundaries are modeled less accurately. This error can overwhelm the benefits of using higher–order elements. However, using curved cells alleviates this conundrum, as will be demonstrated.

Another situation that affects the efficiency of finite elements is field singularities near corners and edges. Standard vector finite elements model only finite fields, so convergence rates are reduced in such applications. To restore the convergence rates, singular vector elements can be used in place of the original vector basis functions near singular points. Results will be presented which demonstrate the effect of field singularities and the advantages of singular elements.

Finally, open–region applications are often troublesome in a finite element formulation. This is especially true when using vector finite elements. The difficulty lies in the discontinuous nature of vector basis functions. This presentation will discuss a proposed implementation whereby complementary sets of vector basis functions are used to resolve the problems of basis function discontinuity.

On Accuracy of Field Representation by Edge-Elements of Various Shapes

Amir Boag
Israel Aircraft Industries, Department 4464
Ben-Gurion Airport 70100, Israel

The Finite Element Method (FEM) is often preferred over other techniques for solving electromagnetic problems involving inhomogeneous materials and complex geometries. However, accuracy and computational efficiency of the method are strongly affected by the type of elements employed in the analysis. Vector finite elements are widely used in electromagnetics thanks to two main advantages as compared to their scalar counterparts: freedom from spurious solutions and intrinsic handling of boundary conditions at material interfaces. Furthermore, the elements differ by shape and the order of polynomial approximation involved. While the effects of element order have been studied, apparently, the issue of element shape attracted less attention. The choice of element shape often appears to be based on "non-electromagnetic" considerations such as meshing. Tetrahedral elements are preferred by many researchers in the field, since tetrahedral meshing of arbitrary 3D geometries is easily performed by commercially available mesh generators. The use of pentahedral elements was advocated for layered geometries such as microstrip antennas. Tetrahedral and pentahedral edge-elements are also a natural choice if one desires to couple the FEM with the method of moments (boundary element method) using the popular Rao-Wilton-Glisson triangular expansion functions.

It is the purpose of this paper to study the accuracy of representation of electromagnetic fields in source-free regions by edge-based elements of various shapes. While the accuracy of the FEM equations can be tested using arbitrary source-free fields, in this study, we employ solely fields due to elemental dipoles. Since, arbitrary fields can be synthesized by superimposing dipole fields, we surmise that using fields of a large number of dipoles of various orientations we can satisfactorily characterize the accuracy of our FE formulation. To verify that the element shape (and not the formalism) is the one that affects the accuracy, we examine two ways of deriving the equations. First, we employ the conventional FEM, whereby the equations are obtained via the weighted residual Galerkin procedure. In addition, we obtained equations for the same geometry using the Measured Equation of Invariance (MEI) formalism. Since we use the same set of dipole fields for testing the accuracy and as metrons in MEI procedure, the residual error for MEI equations is slightly lower than that for conventional FEM ones. However, we show that both ways produce the same asymptotic accuracy. The hexahedral elements have same accuracy as a second order finite difference stencil. On the other hand, pentahedra and tetrahedra appear to be less accurate. Indeed, our numerical experiments involving a number of canonical scattering problems have clearly demonstrated the advantages of using hexahedral elements instead of tetra- and pentahedra.

B1.5

CONSTRUCTION OF THE BASIS FUNCTIONS FOR NEDELEC'S FINITE ELEMENT SPACES FOR TRIANGULAR AND TETRAHEDRAL MESHES

J. Y. Wu* and R. Lee

ElectroScience Laboratory
Department of Electrical Engineering
The Ohio State University
1320 Kinnear Rd.
Columbus, Ohio 43212-1191

A new and systematic approach is presented for constructing the basis functions for the triangular and tetrahedral finite element spaces proposed in Nedelec's 1980 paper (*Numer. Meth.*, vol. 35, pp.315–341, 1980). In that paper, finite element spaces of arbitrary order, that are both unisolvent and conforming in the $\mathcal{H}(curl)$ Hilbert space are presented. These spaces are now more commonly known as the tangentially continuous vector finite element (TVFEM) spaces; the famous edge element (Whitney 1-form) space happens to be the same as the lowest order Nedelec space (J. S. Savage and A. F. Peterson, *IEEE Trans. Microwave Theory Tech.*, vol. 44, pp. 874-879, June 1996), and the $\mathcal{H}_1(curl)$ space is the same as the next order Nedelec space.

The importance of Nedelec's 1980 publication has long been recognized and manifested in the fact that it has been cited in numerous papers. However, since it is not explicitly shown in the paper how to find the basis functions for the proposed spaces, its practical use has been limited. Many researchers have tried very hard to find these basis functions, and so far only those of the $\mathcal{H}_1(curl)$ space have been correctly found.

In this paper, we present a simple and systematic way of constructing the basis functions for Nedelec's spaces for triangular and tetrahedral meshes. The method makes use of Nedelec's theory directly, so it guarantees that the basis functions found are the same as proposed by Nedelec. Furthermore, the spaces so built are naturally hierarchical, which makes the method very suitable for adaptive FEM.

Numerical results for several electromagnetic scattering problems are shown for the hierarchical scheme that make use of both $\mathcal{H}_0(curl)$ and $\mathcal{H}_1(curl)$ finite elements.

The Spectral Lanczos Decomposition Method for Solving 3-D Low-Frequency Electromagnetic Diffusion by the Finite-Element Method

Mohammad Zunoubi*, Jian-Ming Jin, and Weng C. Chew
Center for Computational Electromagnetics
Department of Electrical and Computer Engineering
The University of Illinois at Urbana-Champaign
Urbana, IL 61801-2991

A common problem encountered in the numerical analysis of the electromagnetic fields is to solve Maxwell's equations in a low frequency regime when the fields are excited by a harmonic source and the effects of the displacement currents are neglected. Traditional methods suggest obtaining the solutions at each single frequency when a wide band of frequencies is considered. However, these techniques have proven to be quite time consuming and inefficient for multi-frequency simulations of the fields. Therefore, it is desirable to employ a technique which can treat the problem of solving for the electromagnetic fields in a general three-dimensional form at many frequencies with a negligible amount of extra computer time and memory.

Recently, a spectral decomposition method has been introduced by Druskin and Knizhnerman (1995 *Radio Science*, volume 29, pp. 937-953) for the solution of the low-frequency Maxwell's equations using the finite-difference method for the EM simulations in frequency and time domain. The technique is referred to as the Spectral Lanczos Decomposition Method (SLDM) and it is based on the approximations in a global Krylov subspace to the product of a matrix function and a vector.

In the present work, the finite-element method is used to discretize Maxwell's equations in a low frequency regime. The resulting equation is formed into a matrix equation whose homogeneous part has the form of a generalized eigenvalue problem. Consequently, SLDM is employed to solve the matrix equation. It is shown that SLDM yields accurate results in a minimal computation time. The electromagnetic fields are obtained for multiple frequencies with the same source term by performing the SLDM iteration only at one frequency while recomputing the matrix functional at other frequencies. It is further shown that the multi-frequency analysis of the fields takes a negligible amount of extra CPU time.

B1.7

AN ARGUMENT FOR THE USE OF TETRAHEDRAL AND TRIANGULAR EDGE ELEMENTS FOR MODELING ELECTRICALLY LARGE GEOMETRIES

J. Y. Wu and R. Lee*

ElectroScience Laboratory
Department of Electrical Engineering
The Ohio State University
1320 Kinnear Rd.
Columbus, Ohio 43212-1191

In the electromagnetics finite element community, most people use triangle or quadrilateral elements in 2D and tetrahedral or hexahedral elements in 3D. The triangular and tetrahedral elements have the advantage of being able to model very complex geometries. The usual criticism toward them is that they yield much more unknowns than the quadrilateral and hexahedral elements, when the same mesh size is considered.

A comparison can also be done between edge-based and node-based elements. The edge-based elements have advantages at modeling multiple material interfaces and perfectly conducting corners and edges; however node-based elements produce a higher order of polynomial approximation than edge-based elements for the same number of unknowns. Thus, one can argue that the node-based elements are more accurate. In this paper, we show that the exact opposite case occurs when we consider the numerical dispersion error of the tetrahedral and triangular edge elements. The numerical dispersion error is important because it is usually the dominant error in simulations involving electrically large geometries.

It is well known that the phase error is dependent on the direction the wave propagates through the element. For nodal elements and non-tetrahedral (non-triangular) edge elements, the phase error is all of the same sign no matter what the angle of incidence of the wave propagating through the elements; however, for the tetrahedral (triangle) edge element, the sign of the phase error changes depending on the direction of the wave propagating through the grid. Thus, for an unstructured grid containing tetrahedral edge elements, the error can be significantly reduced through phase cancellation. For example, for a grid spacing of $\lambda/10$ (λ being the wavelength), the maximum phase error for a sample structured mesh is 2.96° per λ when tetrahedral edge elements are used and 13.5° per λ when tetrahedral nodal elements are used. Because of the structured grid, the amount of phase cancellation is minimized. In truly unstructured grids, the reduction in phase error is even more significant. In this paper, we will show the details of the above analysis and provide some results for 3D unstructured meshes.

Optimal Finite Difference Sub-Gridding Techniques Applied to the Helmholtz Equation

J. Nehrbass and R. Lee
ElectroScience Laboratory
Department of Electrical Engineering
The Ohio State University
1320 Kinnear Rd.
Columbus, Ohio 43212-1191
nehrbass@osc.edu

Abstract --- When implementing finite difference schemes, uniform grids often simplify the simulation task and are therefore desirable. A grid is formed by selecting a spatial resolution which is typically a small fraction of the propagating wavelength. Within this grid there may be isolated locations where the spatial resolution may be insufficient. When energy propagates through dense materials the wavelength is reduced, thus finer spatial resolutions may be required. Physical geometries which contain smooth surfaces where the radius of curvature is small compared to the spatial resolution may require finer spatial resolutions. Objects that are small compared to the size of a single cell are poorly approximated and the placement of boundary locations are limited by their proximity to nearby cells. These and other factors may require one to reduce the spatial resolution until the smallest requirement is satisfied. The problem with globally using a fine resolution, is that this implies larger memory requirements and longer computation times. It would be preferable if a coarse resolution could be used over the majority of the computational domain, while fine resolutions are used in locally sensitive regions. The traditional way to accomplish this was to use meshes with different spatial resolutions and interpolate information where needed. If a field value was required in a location that was not sampled, an average value of the surrounding fields would be used. Unfortunately this technique causes large artificial reflections, and thus severely contaminates the solution. The reason that these interpolating schemes fail is that there are no physical justifications for the interpolating schemes used. In this presentation, a systematic method is presented which shows how to optimally choose the weights required in an interpolation scheme. Results are presented for 2D problems and for specific stencils. The ideas can then be applied to any dimension and any desired stencil in a straight-forward manner. The sub-gridding methods are numerically verified for accuracy through a study of the curved scattering geometries and dense penetrable materials.

B1.9

Frequency Extrapolation Analysis in Conjunction with Finite Element-Boundary Integral System

Yunus E. Erdemli*, John L. Volakis, J. Gong and C. J. Reddy+
Radiation Laboratory
Department of Electrical Engineering and Computer Science
University of Michigan, Ann Arbor, Michigan 48109-2122
yunusee@engin.umich.edu, volakis@eecs.umich.edu
+ Department of Electrical Engineering
Hampton University, Hampton, VA 23668

Being a frequency domain analysis, the finite element-boundary integral (FE-BI) method may not be appealing for broadband frequency computations as the case for antenna performance evaluations. For a highly frequency-dependent antenna parameter, it is necessary to execute the analysis at very fine frequency increments to obtain an accurate frequency response. This computationally intensive procedure can be avoided by using a technique referred to as the Asymptotic Waveform Evaluation (AWE). The AWE is a frequency extrapolation approach which provides a reduced-order model of a linear system. Using this technique, a Taylor series expansion of the matrix system is generated around a specific frequency. Subsequently, the Pade expansion is obtained by using the power series moments, yielding a rational function representation of two polynomials in the frequency variable. This representation provides an extension of the region of convergence of the power series, and as a result the accuracy of the analysis is increased to a larger frequency band.

Both scattering and radiation problems will be considered using this frequency extrapolation analysis. The frequency response of microstrip patch antennas will be examined with respect to input impedance characteristics with particular focus on the treatment of the intricate frequency dependence of the boundary integral subsystems. A convergence study will be also carried out to demonstrate the validity and capability of the technique.

URSI B **Session 5** **Galerie 4**

Array Antennas
Co-chairs: C. Christodoulou, USA and R.C. Hansen, USA

08:10	5.1	Analysis of Nonlinearly Loaded Antenna Array Including Mutual Coupling Effect, K.-C. LEE, **T.-H. CHU**, *National Taiwan University, Taipei, Taiwan, China*
08:30	5.2	Numerical Analysis of the Mutual Coupling in Finite Arrays of Rectangular Waveguides, **M. LEONCINI**[1], R. NESTI[1], E. PAOLETTI[1], G. RUGGERINI[2], [1]*University of Florence and* [2]*Space Engineering, Rome, Italy*
08:50	5.3	74GHz Waveguide-Fed Parallel Plate Slot Array Antenna, **J. HIROKAWA**, M. ANDO, *Tokyo Institute of Technology, Tokyo, Japan*
09:10	5.4	Infinite Periodic Array Analysis Using the Finite Difference Time Domain Method, **G.M. TURNER**, C.G. CHRISTODOULOU, *University of Central Florida, Orlando, FL, USA*
09:30	5.5	Application of the Hybrid FEM-MOM Formulation to the Analysis of a Ridge-Guide Phased Array, **T.P. FONTANA**, E.W. LUCAS, *Northrop Grumman Corporation, Baltimore, MD, USA*
09:50	5.6	A 12 Beam Cylindrical Array Antenna for AMPS Applications, **G. MARTEK**, T. ELSON, *Metawave Communications Corporation, Redmond, WA, USA*
10:10		Coffee Break
10:30	5.7	Performance Analysis of a Class of Cylindrical Conformal Array Antennas, **D. CHATTERJEE**, R.G. PLUMB, *University of Kansas, Lawrence, KS, USA*
10:50	5.8	Analysis of Phase Center Movement in Array Antennas, **J.U.I. SYED**, *PAF Academy, Risalpur, Pakistan*
11:10	5.9	Beam Synthesis from an Active Transmit Phased Array, **D.A. KSIENSKI**, *The Aerospace Corporation, El Segundo, CA, USA*
11:30	5.10	A Direct Matrix Approach to the Adaptive Space-Time Nulling Problem with Multiple Look Directions Utilizing the Conjugant Gradient Method, **S. PARK**, T.K. SARKAR, *Syracuse University, Syracuse, NY, USA*

B5.1

Analysis of Nonlinearly Loaded Antenna Array Including Mutual Coupling Effect

Kun-Chou Lee and Tah-Hsiung Chu*
Department of Electrical Engineering,
National Taiwan University, Taipei, Taiwan
Fax: 886-02-3638247, E-mail: thc@ew.ee.ntu.edu.tw

Scattering from single nonlinearly loaded antenna element has been widely studied for many years. The basic approaches to analyze its scattering response include the time domain approach and spectral domain approach. However it is inefficient and difficult to directly apply these techniques to a large antenna array due to the load nonlinearity and the array mutual coupling effects.

The response of a nonlinearly loaded antenna array is a total contribution from scattering part and radiating part respectively. The scattering part basically considers the antenna array scattering effect by the incident wave. They can be analyzed by the method of moments. The radiating part, however, includes the effect of nonlinear load to the antenna array. Therefore, the problem of a nonlinearly loaded antenna array becomes equivalent to a multiport nonlinear circuit problem, since all the equivalent exciting sources at each antenna terminal are coherent.

In this study, the method of nonlinear currents is used to solve the steady state response of a nonlinearly loaded antenna array, and the antenna array mutual coupling effect is calculated based on a power series expansion technique. The method of nonlinear currents is basically one approach in Volterra series analysis for microwave circuit, and is easier to be applied than the transfer function approach to analyze a large nonlinearly loaded antenna array. In this method, the current source components are calculated from the voltage components of lower order mixing frequency. Voltage components of the same order mixing frequency are then determined from these currents, and the current components of the next higher order mixing frequency can be found successively. It should be emphasized that the related equivalent circuit is linear in this approach, although each current source is a nonlinear function of the various order of mixing frequency of voltage components. With the use of power series technique for analyzing the antenna array mutual coupling effect, the matrix inversion operation in our calculation of nonlinearly loaded antenna array can be replaces by matrix multiplication operation. It is then much more numerically efficient that that of directly using Gaussian elimination technique for matrix inversion. In addition this operation can give insight into the antenna array mutual coupling mechanism at each intermodulation frequency component. Two numerical examples will be presented to illustrate the analysis given in this study.

NUMERICAL ANALYSIS OF THE MUTUAL COUPLING IN FINITE ARRAYS OF RECTANGULAR WAVEGUIDES

M. Leoncini*, R. Nesti and E. Paoletti
Electronic Engineering Department, University of Florence
Via C. Lombroso 6/17, 50134, Florence, Italy

G. Ruggerini
Space Engineering, Via dei Berio 91, 00155, Rome, Italy

Radiating elements like rectangular waveguides or apertures are commonly used in feed arrays for reflector antennas. However, one of the main problem in designing these illuminators is the accurate prediction of the mutual coupling between the elements which can alter the radiation pattern characteristics as well as the reflection coefficient of the feeder. Recently, a Green's function approach based on a modal expansion of the aperture field was proposed to quantify these coupling effects (T.S. Bird, IEEE Trans. AP, n. 2, 166-172, 1990), (G. Ruggerini, Proc. of ICAP 93, 772-775, 1993). This method, which allows to characterize the response for a large variety of actual configurations, needs the presence of a ground plane.

In the last few years, numerical methods like FDTD have been largely applied for the analysis of electromagnetic problems due to their straightforward implementation and versatility in dealing with complex and inhomogeneous structures.

The main advantages of FDTD are that no matrix inversion is required, it is not necessary to know the Green's function and the resulting code can be easily implemented on parallel architecture computers.

In this work, the FDTD method was used to analyze the EM coupling between arrays of a few rectangular open waveguides. The principal radiating planes of these elements were taken parallel to each other. Analysis was carried out by exciting propagation inside the waveguides and numerically determining the scattering parameters of the N-port system consisting of the N radiating elements. This was done both in presence and in absence of the ground plane. Results for the ground plane case have been compared with those obtained by using the above mentioned Green's function approach.

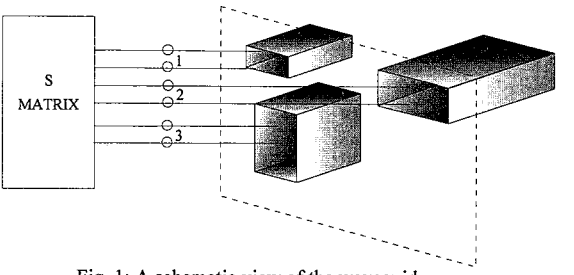

Fig. 1: A schematic view of the waveguide array.

B5.3

74GHz Waveguide-Fed Parallel Plate Slot Array Antenna

Jiro Hirokawa* and Makoto Ando
Dept. of Electrical & Electronic Eng.
Tokyo Institute of Technology, Japan

We have designed and fabricated a waveguide-fed parallel plate slot array antenna in use at 74GHz. This antenna is a planar antenna in which radiating slots are arrayed on one side of a square parallel plate waveguide and coupling slots occupy to be fed by a rectangular waveguide on the other side (J.Hirokawa et al., IEEE Trans. on Antennas & Propagat., 40-2, 218-223, 1992). We have already obtained an efficiency of 60% in a model antenna (size: 450mm square) at 12GHz band. The antenna is an attractive candidate of high-gain and mass-produceable planar arrays for millimeter-wave applications such as wireless LAN and automotive collision avoidance radar since the structure is very simple.

All the slots are paired in order to suppress undesired reflections and to assure the purity of the TEM plane traveling-wave mode in the parallel plate waveguide. The radiating slots are densely arrayed in the direction transverse to the TEM mode propagation. The slots are designed by using a rectangular waveguide with narrow walls satisfying the periodic boundary condition in order to simulate the coupling.

A model antenna has been designed and fabricated in use at 74GHz. The size is 85mm square. In the design at such a high frequency, the thickness (0.15mm) of a slotted plate must be included to estimate the slot coupling accurately since it cannot be neglected in comparison with the wavelength (4.05mm in free space). Furthermore, an aperture is placed at the input port and replaced with a coaxial-line adapter used in the 12GHz-band model. A waveguide matching section should be connected with a V-band (50GHz - 75GHz) standard waveguide for measurements. The section has been designed to suppress reflection below −16dB. In the presentation, we show experimental results of the 74GHz-band model antenna.

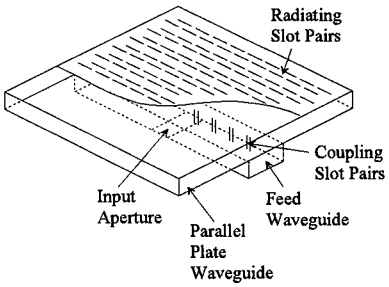

Waveguide-Fed Parallel Plate Slot Array Antenna

We are thankful to Dr. Hiroshi Kondoh and Ken Takei of the Central Research Laboratory of Hitachi Ltd. in Japan for supporting this work.

Infinite Periodic Array Analysis Using the Finite Difference Time Domain Method

Gregory M. Turner* and Christos G. Christodoulou
Department of Electrical and Computer Engineering
University of Central Florida
Orlando, Florida 32816

Advances in FDTD modeling concepts combined with advances in computer technology have expanded the scope, accuracy, and speed of FDTD modeling to the point where it is the preferred method for many problems involving complex three dimensional structures. Unique benefits of FDTD include its ability to model conducting or dielectric media of arbitrary shape and homogeneity and its ability to generate broadband data in a single run. The FDTD technique has been used extensively for the solution of two and three dimensional scattering problems and has more recently been applied with considerable success to the study of radiation and impedance characteristics of electrically small antennas.

For phased array antenna radiating element design, accurate numerical modeling techniques are particularly important due to the cost and effort associated with breadboard and development model fabrication and test. Performance of the individual radiating elements of an array can be significantly effected by the array environment due to mutual coupling between the elements. The performance of the majority of the inner elements of a large array can be accurately approximated by the uniform performance of the elements of an infinite array. The infinite array is particularly amenable to numerical modeling since the computational domain can be limited to a single unit cell. The FDTD is readily adaptable to the infinite periodic array case by applying appropriate periodic boundary conditions normal to the periodic axes.

Several examples of array active reflection coefficient calculations will be presented including waveguide and microstrip patch arrays.

B5.5

Application of the Hybrid FEM-MOM Formulation to the Analysis of a Ridge-Guide Phased Array

Thomas P. Fontana* and Eric W. Lucas
Northrop Grumman Corporation, Electronic Sensors and Systems Division
P.O. Box 746, Baltimore, Maryland 21203

In this presentation, we will discuss the analysis of a ridge-guide radiator in a scanned periodic array by using a combination of the method of moments (MOM) technique along with the vector finite-element method (FEM). An attempt was made to increase computational efficiency by using the analysis technique best suited to each region of the problem. Because suitable analytic modes for the ridge guide are not available, a finite element discretization was used for the ridge radiator. Our geometry also has an iris at the aperture as part of the matching structure, which is included in the FEM mesh. One side of the ridge-guide is fed by a semi-infinite ridge radiator port. The entire finite element portion consists of only few layers of meshing and contributes a relatively small sparse matrix to the system. It is coupled by means of aperture modes to a stratified MOM region above the radiator that describes the radome.

We use a two-dimensional vector finite element code to numerically generate multiple modes for the ridge waveguide input port. This code uses an E_t-H_t analysis in calculating the eigenmodes in which both the transverse electric as well as transverse magnetic fields are unknowns. (Fontana and Lucas IEEE AP/S Digest, Vol. 3, Seattle, WA, 1764-1767, 1994) . The technique has the property that it generates no spurious modes and is applicable to non-reciprocal propagating structures. To account for scattering by discontinuities near the aperture, we typically include between ten and twenty modes. The use of higher order modes also enables us to shrink the finite element region between port and aperture, thereby reducing computation time. We also use numerically generated modes for the basis that couples the finite element region to the MOM region.

Some numerical results are reported to show the overall efficiency of the technique. For this problem the port and aperture modes depend on frequency but not scan angle, reducing the computational cost of calculating modes. A ridge-guide radiator is a viable alternative to loading a rectangular waveguide. It is relatively easy to adjust the ridge-guide impedance by adjusting the slot width and ridge thickness. It also offers superior bandwidth. Fundamental engineering parameters such as reflection coefficient as a function of scan angle are shown.

A 12 Beam Cylindrical Array Antenna for AMPS Applications

by Gary Martek* and Todd Elson
Metawave Communications Corp., 8700 148th Ave NE, Redmond, WA 98052

One of the current trends in cellular technology is the use of sector antennas or multiple narrow beam antennas rather than omni-directional antennas. As property becomes more difficult to acquire for cellular communication purposes, the antennas atop the tower must be enhanced. Naturally, gain and front to back ratio are desired to be maximized with side lobes suppressed. Currently, panel antennas (dipole arrays with flat ground planes) are often implemented, with each panel scanning to provide, in many cases, multiple beams at equally spaced positions in the azimuth direction.

This paper details the design and test of a cylindrical 12 beam array antenna for use in AMPS applications. One immediate advantage of this design over panel antennas is the elimination of scan loss, as the shape of the array naturally generates equally spaced beams in the azimuth direction. The cylindrical design also makes for a smaller overall structure, i.e. a stealthier antenna. The current antenna generates 12 beams spaced by 30 degrees in the azimuth plane, each with a 30 degree beam width.

Two types of numerical routines were used in the design of the antenna: Numerical Electromagnetics Code (NEC) and Finite Difference Time Domain (FDTD). NEC, utilizing the method of moments, is more suited to this problem because of the straightforward Green's function and narrow bandwidth, but FDTD gives a "second opinion" as well as providing a basis for future work in the area of printed antenna elements.

The initial numerical model of the cylindrical array only depicts a conducting cylinder and dipoles set at a quarter wavelength away in the radial direction. A second, more detailed model includes a portion of the feed system, which is exposed and in close proximity to the elements. Slight differences in far field radiation patterns exist between the simplified model and the more detailed one.

Future work involves modification of the cylindrical array such that its beams are directed downward rather than towards the horizon. Use of parasitic elements is a subject of interest, as well as polarization states besides vertical. Some numerical simulations related to these subjects will be discussed.

B5.7

PERFORMANCE ANALYSIS OF A CLASS OF CYLINDRICAL CONFORMAL ARRAY ANTENNAS

D. Chatterjee* and R. G. Plumb

Radar Systems and Remote Sensing Laboratory
Department of Electrical Engineering and Computer Science
University of Kansas, Lawrence, KS 66045-2969

The use of arrays in wireless communications enhances the diversity performance of base-station antennas and the channel capacity [J. Liberti and T. Rappoport, *IEEE Trans. Veh. Technol.*, pp. 680-690, Aug. 1994], [A. F. Naguib *et. al.*, pp. 691-698, *ibid.*]. The results [Fig. 3, Naguib, *op. cit.*] also indicate that narrow-beam antennas increase the channel capacity at low bit-error rates (BER). The multipath effects associated with various link models are also reduced for arrays with low sidelobes [W. C. Jakes, *Microwave Mobile Communication Systems*, Plenum Press, NY, 1992]. Additionally it is important for improved diversity applications that the signals in various ports be uncorrelated. This requires modeling of the mutual coupling between the various radiating elements in the array. It was found [Jakes, *op. cit.*] that half-wavelength spacing provides the optimum diversity. However all antennas have a specified bandwidth and it turns out that the diversity can degrade over the whole bandwidth. Furthermore knowledge of mutual coupling and pattern control can help analyze the adaptivity performances [I. J. Gupta and A. Ksienski, *IEEE Trans. Antennas Propagat.*, pp. 548-553, July 1982]. Among the many choices of array antenna designs, the cylindrical conformal array appears to be very attractive. Rigorous analysis [J. C. Herper *et. al.*, *IEEE Trans. Antennas Propagat.*, pp. 259-272, March 1985] and experiment [J. C. Herper *et. al.*, *ibid.*, pp. 273-278] of such arrays have been reported earlier. Preliminary studies on the application of the Digital Beam Forming (DBF) technique [H. Steyskal, *Microwave Journal*, February 1996] to such arrays have been reported [D. Chatterjee and R. G. Plumb, *IEEE AP-S and USNC/ URSI Symp. Digest*, vol. 1, pp. 714-717, July 1996]. In this presentation, further results will be reported. The design technique has been extended to include the finite size of the array in the axial direction. A comparitive analysis of both rectangular and triangular grid structures will be presented from the channel capacity performance point of view. Emphasis will be placed on understanding the role of the interelement spacing on the respective pattern data for the two structures.

ANALYSIS OF PHASE CENTER MOVEMENT IN ARRAY ANTENNAS

Junaid Ul Islam Syed

College of Aeronautical Engineering,

PAF Academy Risalpur, Pakistan

The position of the phase center of an array becomes important when it is used as a feed in a reflector antenna or it is required to be focused at some finite distance. The shape and the direction of the maximum radiation of an array can be controlled by adjusting its amplitude and phase weighting co-efficient. The problem considered here is neither of beam scanning and nor of beam shaping, as the main objective is to move the phase center of the array antenna by adjusting its excitation coefficients to change the focusing distance. The focused antennas may be required for antenna measurement, energy concentration at some finite point or zooming.

In the case of cophasal excitation, the array is focused at infinity and the far-field phase taper is zero, which implies that the phase center lies over the radiating aperture. The focus distance reduces when the array is bent mechanically or electrically, this produces a taper in far-field phase and as a result the phase center moves away from the radiating aperture and shifts towards the caustics produced at some finite distance.

A numerical method will be presented to determine the location of the phase center of an array antenna. The best-fit phase center is determined numerically using the weighted least-squares criterion. For a given size of an array aperture, there is a limit to the movement of the phase center by phasing the elements. Beyond a certain value of phase taper across the array aperture, the maximum radiated energy does not remain along its boresight and the phenomenon of beam bifurcation in the plane of the linear array occurs. It can be deduced from the results that the shift in the apparent phase center of an array over a given angular region and phase taper will decrease with the increase in amplitude tapering at the array aperture.

B5.9

Beam Synthesis from an Active Transmit Phased Array

David A. Ksienski
Communication Systems Subdivision
The Aerospace Corporation
El Segundo, CA 90245-4691

Transmit phased arrays are capable of generating a variety of beam shapes through control of the field over the aperture. However, determining how to drive the elements of the array is a numerically intensive task. A novel algorithm to synthesize arbitrary beam shapes from a transmit phased array will be introduced. The algorithm incorporates an efficient underdetermined matrix formulation for rapid convergence. Beam shaping is accomplished with phase-only control of the elements.

The example to be considered is a geosynchronous active transmit phased array with 256 elements in a rectangular grid with 2.4-wavelength element spacing. Since each element contains a separate amplifier operating at a fixed back-off from saturation, only phase control is available to steer and shape the beam. The resultant numerical problem is a non-linear optimization in 256 variables.

The algorithm used for this optimization computes the gain at over 1000 far field locations, and then selects the 5 locations that have the minimum gain and are within the footprint of the desired beam. The gradient with respect to the phase settings of the 256 elements is then computed at these 5 locations. Thus, a non-linear function of 256 variables is reduced to an iterative solution of a 5×256 matrix. The matrix problem is solved using a singular value decomposition and backsubstitution to yield a "minimum-energy" solution vector. This formulation results in a rapid numerical determination of the phase settings needed for beam synthesis, about 30 minutes on a 120-MHz Macintosh.

Several spot beam synthesis results will be presented, including an Earth coverage beam. The bit depth of the element phase values will be shown to have a pronounced effect on the Earth coverage beam, and the effect of various element patterns will also be presented.

A Direct Matrix Approach to the Adaptive Space-Time Nulling Problem with Multiple Look Directions Utilizing the Conjugant Gradient Method

Sheeyun Park and Tapan K. Sarkar
Department of Electrical Engineering and Computer Science
121 Link Hall
Syracuse University
Syracuse, NY 13244

Abstract: In adaptive nulling problems, signal cancellation can occur if the direction of arrival (DOA) of the signal of interest (SOI) is unknown and the desired look direction is slightly off the actual DOA. In this case, the signal is considered a jammer and nulled by the adaptive algorithms. Target returns from within a finite extent indicate the presence of a target. This paper investigates the addition of multiple look directions to an adaptive Space-Time nulling problem in radar. In a complex environment, many sources of clutter and interference may degrade the performance of an adaptive system. A direct data domain approach has been taken to mitigate the problems arising due to a highly nonstationary environment. Without the need to estimate covariance matrices, this approach bypasses effects of nonhomogeneities in the secondary data. Also multipaths and other sources of coherent interference can be nulled out.

For a given look direction and Doppler, the expected phase delay is known. We can now subtract the delayed signal from its adjacent antenna element with the appropriate delay. This difference should just contain undesired interference. The noise power can be minimized while maintaining multiple look direction constraints. The solution of the resulting matrix equation can be obtained with a method of conjugant gradients. For a nonsingular matrix, this corresponds to the least squares solution due to the choice of minimized functional. In the singular case, the solution corresponds to the minimum norm solution.

With a single look direction, unless the array was steered to the exact direction of the incoming signal, the algorithm would null out the SOI. In the case of radar, where the DOA of target is unknown, it is desirable for target from within a certain angular extent to indicate a detection. Multiple look directions were added to solve this problem. Even in the presence of noise and clutter, targets can be detected. Also since this approach doesn't estimate covariance matrices, inhomogeneities in surrounding range cells or Doppler bins do not affect performance.

URSI B **Session 6** **Salon St-Laurent**

Reflector and Feed Antennas
Co-chairs: W.A. Imbriale, USA and S. Rengarajan, USA

08:10	6.1	Design of a New Dichroic Plate and Feed for a BWG Antenna, **W.A. IMBRIALE**, *California Institute of Technology, Pasadena, CA, USA*
08:30	6.2	Analysis of Circular Corrugated Horns Radiating in Presence of Conducting Structures, R. COCCIOLI[1], R. NESTI[1], **E. PAOLETTI**[1], G. PELOSI[1], R. RAVANELLI[2], [1]*University of Florence and* [2]*Alenia Spazio, Rome, Italy*
08:50	6.3	A Novel and Efficient Corrugated Feeder for Reflector Antennas, **R. GONZALO**, J. TENIENTE, C. DEL RIO, *Public University of Navarra, Pamplona, Spain*
09:10	6.4	An Efficient Gaussian Beam Technique for Reflector Antenna Analysis/Synthesis, **H.T. CHOU**, P.H. PATHAK, R.J. BURKHOLDER, L.C. POTTER, *Ohio State University, Columbus, OH, USA*
09:30	6.5	Gimbaled Parabolic Reflector for Limited Scan Application, **T.-K. WU**, *Antenna Product Center, Redondo Beach, CA, USA*
09:50	6.6	Large, Tiled Antennas Conforming to the Ruze Gain Loss, **J.A. GRZESIK**, *TRW Space and Defense, Redondo Beach, CA, USA*
10:10		Coffee Break
10:30	6.7	Dual Shaped Subreflector Synthesis Based on Laguerre-Gaussian Beam Modes, **H.D. FOLTZ**, M.C. NUNN, *University of Texas - Pan American, Edinburg, TX, USA*
10:50	6.8	Graphical Processing Techniques for Reflector Antenna Analysis, **M. VALLILOSSERA**, J.M. RIUS, A. CARDAMA, J. PLAZA, *Universitat Politècnica de Catalunya (UPC), Barcelona, Spain*
11:10	6.9	On Contoured Beam Reflector Antennas, **A.P. POPOV**, S.C. KANG, *Electronics and Telecommunications Research Institute, Taejon, Korea*

B6.1

Design of a New Dichroic Plate and Feed for a BWG Antenna

William A. Imbriale
Jet Propulsion Laboratory
California Institute of Technology
Pasadena, CA 91109

A BWG feed system is composed of one or more feed horns with a series of flat and curved mirrors arranged so that power can be propagated from the horn through the mirrors with minimum losses. Horns and equipment can be located in a large stable enclosure at an accessible location. The current NASA large ground station BWG antennas use conventional corrugated horns for feeds and thick dichroic plates with rectangular holes to separate multiple frequency bands. The dichroic plates are designed so that the lower frequencies are reflected and the upper frequencies are passed.

A new all metal dichroic plate was designed that is transparent at the lower frequencies and reflective at the upper frequencies. The basic concept of the new design is to use slots in a moderately thick metallic plate for the transmit band and to use chokes in the slots to reflect the upper frequency bands. Thus the dichroic plate is transparent at the lower frequency band and reflective at the upper frequency bands without using a dielectric. Two designs are under consideration for Deep Space Network (DSN) applications; 1) reflect Ka-band transmit and receive frequencies and pass X-band receive frequencies and 2) reflect Ka-band frequencies and X-band transmit frequencies, and pass X-band receive frequencies. Examples of both designs are given that have insertion losses as low as 0.04 dB at the narrow pass band as well as the ability to handle up to 20 KW of power.

Also, a new feed horn design is shown that produces a very gaussian type radiation pattern with very low sidelobes. This type of feed is ideally suited for illuminating BWG systems.

ANALYSIS OF CIRCULAR CORRUGATED HORNS RADIATING IN PRESENCE OF CONDUCTING STRUCTURES

R. Coccioli, R. Nesti, E. Paoletti*, G. Pelosi
Electronic Engineering Department, University of Florence
Via C. Lombroso 6/17, I-50134 Florence, Italy

R.Ravanelli
Alenia Spazio, Via Saccomuro 24, I-00131 Rome, Italy

Corrugated horns are often used as feeds in modern high performance reflector antenna systems because of their good features of low cross-polarization level and good impedance matching. For this reason they have been extensively studied and accurate and efficient design tools have been realized for their design. However, most of the available tools are suitable only for feeders radiating in free space. In this case, circular horns are usually analyzed by using the hybrid Mode Matching-Combined Field Integral Equation Method (MM-CFIE) (V.Hombach, E.Kuhn, *IEEE Trans. Antennas Propagat.*, vol. 37, no. 9, pp. 1093-1101, 1989). This analysis technique has also been employed in the framework of an optimization algorithm to realize a design software tool (R. Coccioli, G. Pelosi, R. Ravanelli, in *Software for Electrical Engineering Analysis and Design*, P.P. Silvester Ed., Computational Mechanics Publications: Southampton, 1996. pp. 265-273) which has proven very accurate and has been exploited for the design of state-of the-art feeders (R. Coccioli, G. Pelosi, R. Ravanelli, *La Recherche Aerospatiale*, 1997).

In this communication, the hybrid MM-CFIE technique is extended to the case of circular horns radiating in the presence of conducting structures large with respect to wavelength, as is the case in many practical instances. In particular, two main changes must be introduced in the method presented by R. Coccioli, G. Pelosi, R. Ravanelli (ibid.).

The first is relative to the MM technique used to treat the interior of the horn and consists in introducing all the general TE_{mn} and TM_{mn} modes in the modal expansion of the field inside the feeder. As a matter of fact, the presence of surrounding structures destroys the axial symmetry of the problem and consequently the simplified analysis used for the two-dimensional problem of isolated circular horns is not suitable anymore. This in turn affects also the set of basis functions used to expand the equivalent currents on the exterior surface of the feeder, that must present the same azimuthal variation as the modes used for the MM procedure.

The second main change concern the Green's function which appears into the CFIE exploited for the solution of the exterior problem. Assuming the structures surrounding the circular horn large with respect to the wavelength and placed sufficiently far from it, the Green's function of the exterior problem can be efficiently evaluated by means of the Uniform Theory of Diffraction (UTD).

B6.3

"A NOVEL AND EFFICIENT CORRUGATED FEEDER FOR REFLECTOR ANTENNAS"

Ramón Gonzalo, Jorge Teniente and Carlos del Río
Microwave and Millimeter Group. Public University of Navarra
Campus Arrosadía s/n. E-31006 Pamplona, Spain
Phone: 948 169023 Fax.: 948 169169 e.m.:ramon@upna.es

High-performance microwave satellite communications, radar and remote-sensing systems often use a reflector antenna as a final component of the transmitter and receiver front ends. The horn antenna is a crucial component because it must match the microwave signal from the source to the reflector antenna with the minimum losses and the maximum efficiency.

In this paper we present an original corrugated horn antenna profile to feed very efficiently reflector antennas. Starting from a monomode circular waveguide, we excite a far field radiation pattern with very low crosspolarization, high symmetry, low sidelobes and very high efficiency (bigger than 80% with a global aperture of 54 degrees) (see figure 1) in a wide frequency band.

The presented corrugated feeder has a gaussian profile (Gonzalo, R., Del Río, C., Teniente, J. and Sorolla, M. "Optimal horn antenna design to excite high purity gaussian beam using overmoded waveguides", Digest Int. Conf. On Infrared and Millimeter Waves, Berlin, Germany, July 1996.) with an impedance matching adapter at the throat from $\lambda/2$ corrugation depth (equivalent to smooth monomode waveguide) to $\lambda/4$. The corrugation period is $\lambda/3$. Because of this corrugated profile, the component has a very broad bandwidth.

The component has been successfully simulated using the mode matching and scattering matrix techniques.

As a result, a novel, very simple and efficient horn antenna profile is presented. It can be very useful in a quite many different applications that use reflector antennas.

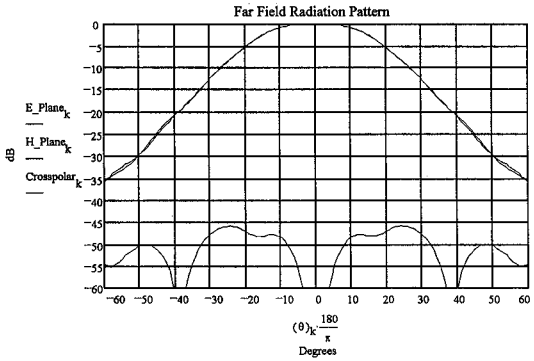

Figure 1: Far field radiation pattern obtained with a feeder (150 mm) and working at 8 GHz.

An Efficient Gaussian Beam Technique for Reflector Antenna Analysis/Synthesis

H.T. Chou*, P.H. Pathak, R.J. Burkholder and L.C. Potter
The Ohio State University ElectroScience Laboratory
1320 Kinnear Road, Columbus, Ohio 43212, USA

This paper presents a relatively efficient Gaussian beam (GB) based method for the synthesis of a planar array consisting of identical antenna elements which feeds a parabolic reflector, to produce a prescribed contoured beam, as is often required in communication satellite antenna applications. It has been demonstrated (H.T. Chou, P.H. Pathak, G. Zogbi & R.J. Burkholder, 1996 IEEE AP-S Intl. Symp. and URSI Radio Science Meeting, Baltimore, Md., Vol. 2, AP-S Symp. Digest, pp. 886-889) that the GB method provides a rapid analysis of electrically large reflector antennas since it requires no time-consuming conventional physical optics (PO) numerical integration over the electrically large reflector surface as is commonly employed in reflector radiation pattern analysis. The advantage of this GB approach stems from the fact that the feed illumination is expanded in a discrete set of a relatively few rotationally symmetric GB's whose fields adequately simulate the radiation field of the feed (in amplitude, phase and polarization). Each GB launched from the feed undergoes reflection from the interior reflector surface as well as diffraction from the reflector edge. Since the expressions for reflected and diffracted fields for each incident GB are obtained in closed form, this GB analysis of the radiation fields of a parabolic reflector are evaluated in a matter of a few seconds on a typical workstation; this is in contrast to several hours that are required in the conventional numerical PO integration on such a workstation. The efficient GB method is coupled here with an optimization algorithm based on the method of successive projections (S. Hay and G.T. Poulton, Radio Science, Vol. 31, No. 6, pp. 1671-1679, 1996) to arrive at the feed array distribution which produces the desired contoured beam. Since the iterative optimization algorithm requires one to repeatedly compute the reflector radiation fields a large number of times, the GB method can substantially speed up the overall synthesis computations. Depending on the overall size of the feed array in relation to the distance from the reflector, a set of GB's are launched radially out from the center of the whole array, or from the centers of the few subapertures into which the feed array is divided, using the rules developed in the earlier presentation mentioned above. It is assumed that the form of the field distribution over each antenna element in the feed array is known; this in turn allows one to know the radiated field pattern of each antenna element in the array. The complex weights for the array excitation are of course unknown and they need to be found. Hence, the actual radiation field of the array is known to within the array weights. First, the GB expansion can be found for the field radiated by a typical antenna element initially with a weight of unity, and the field radiated by the entire feed array can then be expressed as a superposition of GB fields which will automatically contain the unknown array weights as coefficients to be determined via the optimization routine. The optimization method based on successive projections tends to provide a solution for the array weights that yield a coutoured beam pattern whose field levels lie within some prescribed bounds.

B6.5

Gimbaled Parabolic Reflector for Limited Scan Application

Te-Kao Wu

TRW
Antenna Systems Department
Antenna Product Center
Electronic Systems and Technology Division
One Space Park, 66/1218
Redondo Beach, CA 90278
U.S.A.
Phone no. 310-814-5995
Fax no. 310-814-9082

Present and future GEO satellite communication systems require low mass, small volume, and low cost spaceborne antennas. In addition, the satellite antenna should provide fast scanning and shaped beams within ±9°, Earth field of view (FOV). Phased array and multiple beam antenna (MBA), such as reflector or lens antenna with multiple feeds and a beam forming network (BFN) are viable candidates for this application. But the development and fabrication costs of these electronically steered antennas are too high as compared to the mechanically gimbaled reflector antennas. In this paper, a hybrid approach is described using gimbaled parabolic dish to steer *mechanically* (over the ±9° FOV) a shaped beam *electronically* formed with a septet feed system.

There are two common ways to steer the antenna beams mechanically. First, one can gimbal the whole antenna system (including the reflectors and the feed system with or without a subreflector). Or one can further reduce the antenna system's weight and cost by gimbaling only the parabolic reflector. This is similar to the scanning beam reflector antenna with a fixed parabolic dish and a moving feed. In addition, as the reflector is gimbaled by θ°, the beam will be steered almost 2θ°. But the steered beam will suffer gain loss and pattern distortion. However, these performance degradations can be compensated by using a septet feed with both phase and amplitude adjustments.

Specifically, in this paper the steerable shaped beam capability of a gimbaled parabolic dish in an offset cassegrain antenna configuration will be evaluated. Three different offset cassegrain reflector antenna configurations will be considered and the trade in terms of weight, cost, and performance will be discussed in the presentation.

LARGE, TILED ANTENNAS CONFORMING TO THE RUZE GAIN LOSS

J. A. Grzesik
TRW Space & Defense
One Space Park
Redondo Beach, CA 90278

Space mission requirements for reflector antennas with ever higher gain are presently eliciting designs on a truly heroic scale. The concomitant weight penalties are being countered by having the reflecting paraboloid approximated with a fine mesh attached to a ribbed, graphite frame. It is clear that, even with the greatest of care, one can never achieve in this fashion a truly perfect conic and that, morever, asymmetric thermal loading during any realistic cycle of mission insolation will superimpose yet another level of distortion. It becomes then of considerable interest to have in hand some computational tool for assessing the extent of gain degradation to be expected in consequence of these various sources of surface distortion.

One global yardstick of such degradation is the celebrated Ruze formula relating gain loss to a root-mean-square [RMS] measure of surface distortion. The essential notions underlying Ruze's work are that: (i) surface distortion amounts to a local phase corruption; (ii) such phase corruption submits to a Gaussian statistical distribution at each point of the radiating mesh; and (iii) the implied statistical parameters, and, in particular, the crucial RMS value, are uniform across the antenna surface [J. Ruze, "The Effect of Aperture Errors on the Antenna Radiation Pattern," Nuovo Cimento Supplement, Vol. 9, pp. 364-380, 1952; "Antenna Tolerance Theory -- A Review," Proceedings of the IEEE, Vol. 54, No. 4, pp. 633-640, 1966]. Despite its seemingly radical assumptions, Ruze's formula has proved to be a quite reliable gauge of gain loss and, besides, has endeared itself to the antenna community by virtue of its extreme simplicity. Ruze's work further indicates an essentially diffuse broadening of the antenna pattern away from the degraded main beam.

We report here on finite-element codes evolved so as to tackle in an ab initio fashion with the patterns produced by mesh reflectors approximated as a collection of contiguous, triangular tiles. Internal mechanisms based on repeated edge bisection are provided for triangle refinement within the plane of each contributing antenna tile, with far-field patterns gotten simply as a vector superposition from the resulting myriad of mesh facets. Such tile refinement, across cascading powers of four, is pushed to a point of empirical pattern convergence, frequently attained at refinement levels no higher than three [i.e., sixty-four-fold tile fragmentation]. The radiating surface current within each facet is approximated by a standard physical optics form, with far-field phase estimates enforced as regards both facet-to-far field and facet-to-feed separations. While the former phase approximation is ipso facto guaranteed, the latter usually requires some preliminary level of tile refinement. In any event, with the current phase thus approximated, the radiation integral over each facet can be attained in a closed form only slightly more complicated than the usual {sin(x)/x}{sin(y)/y} diffraction form appropriate to the rectangle.

We have applied our code to realistic designs with results in perfect harmony with Ruze-type pattern degradation assessments. Moreover, by inducing auxiliary, code-generated surface tilings wherein all triangle vertices ridigly adhere to some parent paraboloid, we have been able to attain a quite compelling degree of encroachment upon smooth-surface patterns across wide ranges of beam angle. Our tiling/phase approximation stratagems emerge then as a sort of ad hoc, Riemann-style radiation quadrature estimate.

B6.7

DUAL SHAPED SUBREFLECTOR SYNTHESIS BASED ON LAGUERRE-GAUSSIAN BEAM MODES

H.D.Foltz and M.C.Nunn
Engineering Department, Univ. of Texas - Pan American, Edinburg, TX 78539

Beam guide systems are often analyzed using Gaussian beam techniques. In this paper we will present preliminary results of a method for designing dual shaped surfaces based on multimode Gaussian beams, rather than geometric optics. The technique should be useful for designing mode convertors and shaping beam profiles, subject to the usual Gaussian beam mode limitations. The reflectors are assumed to be shallow, with the deviations from conic sections representable by a simple phase shift at the surface, with no change in amplitude. The reflector synthesis problem is then reduced to finding the required phase shift profile for each surface.

The input beam and the desired output beam are given, while the beam profile in the interior region between the two reflectors is unknown. Rather than being represented directly by Laguerre-Gaussian modes, this interior beam h is represented by new sets of modes C_m and D_m:

$$h = \sum A_m C_m \quad and \quad h = \sum B_m D_m$$

where A_m and B_m are constants to be determined. C_m and D_m are given by

$$C_m = \sum G_{mp} L_p \quad and \quad D_m = \sum H_{mp} L_p$$

where G_{mp} and H_{mp} are constants and the L_p are axially symmetric Laguerre-Gaussian modes (the method could be extended to asymmetric cases). A set of sample points is chosen on each surface. The G_{mp} are chosen so that the C_m mode is one at the m-th sample point and zero at all others, on the first surface. Thus at the m-th sample point on this surface, only one mode P_m is nonzero, and the magnitude of A_m is given by the known amplitude of the input field at that point. The H_{mp} are chosen and the magnitude of B_m found according to a similar rule for the second surface. Thus only the phases of A_m and B_m remain to be found. Since both expressions for h represent the same beam, ideally it must be true that:

$$\sum A_m G_{mp} = \sum B_m H_{mp}$$

for each p. The phases of A_m and B_m which give the closest approximation to a solution of the above set of equations are found, which in turn gives the required deviation at each sample point on the surface. The rest of the surface is found by interpolation. A more detailed description of the method and comparisons with numerical simulations will be given in the presentation.

GRAPHICAL PROCESSING TECHNIQUES FOR REFLECTOR ANTENNA ANALYSIS

Mercè Vall-llossera, Juan M. Rius, A. Cardama, J. Plaza
Dpt. TSC, Universitat Politècnica de Catalunya (UPC)
Campus Nord, edifici D-3, Jordi Girona,1-3
08034 BARCELONA- Spain

The algorithms developed for analyzing electrically large conformed reflector antennas are generally based in high-frequency approximations. The main difficulty for reflector antennas analysis is to obtain the geometrical information, such as unit normal on the reflector surface. For that reason, classical techniques are based in geometrical symmetries and therefore each one is only suitable for a reduced group of structures. There are only a few algorithms for analyzing and designing conformed reflector antennas with arbitrary geometry using high frequency approximations.

We have developed a new approach for analyzing reflectors with arbitrary geometries. This algorithm takes advantage of the new concept introduced by GRaphical Electromagnetic COmputing technique developed in GRECO code for RCS prediction (J.M. Rius, Annals of Telecom., vol.50, No.5-6) in order to obtain the geometrical information of conformed reflector surface.

The most outstanding characteristics of the algorithm developed are:

- Physical Optics is used for surface reflection analysis.
- The contribution of edge diffraction is considered through the Method of the Equivalent Currents (MEC) using the Incremental Length Diffraction Coefficients (ILDCs) of Ando.
- The blockage effect is also considered through the approximation of null field on shadow areas, taking into account both fixed and mobile shadows.
- Graphical processing technique is used in order to get the geometrical information: Unit normals on the reflector surface, Edge detection for obtaining border diffraction, Detection of fixed and mobile shadows for accounting the blockage of the feeder and the struts.
- The radiation pattern of arbitrary antennas is obtained in lesser time than classical algorithms thanks to fast geometrical analysis by the graphical processing technique.

B6.9

On contoured beam reflector antennas

A. P. Popov, Sung C. Kang
Payload section, Electronics and Telecommunications Research Institute
161 Kajong-dong Yusong-gu Taejon 305-350, Korea

Abstract.

Contoured/shaped beam antennas are of interest in many applications such as surveillance radars base stations for mobile communications and satellite broadcasting.. In order to meet the coverage requirements and cross-polarization level, two-reflector antennas with shaped beam were introduced in recent time and successful design with both reflectors shaped were presented . However these design methods actually provide specified phase-amplitude radiation pattern, in spite of the fact that it is not clearly pointed out in the most of presentations. As for the most of practical important applications it is necessary to provide the specified power pattern regardless the properties of phase radiation pattern, it is possible to synthesize a reflector antenna that meets definite coverage requirements by shaping the one reflector only. The non-linear problem of synthesis of reflector antennas with specified power pattern has been well studied under geometric optics assumption. First geometrical optics design of single reflector antenna producing specified power pattern for radar application was introduced in 1948 (A.Dunbar, Proc.IRE, vol.36,no.10, pp.1289-1296,1948) and in (V.A.Kaloshin, A.P.Popov, Radioeng.&Electron., v.27, no.6, pp.1110-1119, 1982) was introduced geometrical optics design for shaped/contoured beam two-reflector antennas with specified shape of the main reflector by shaping the subreflector only. Recently, (H.Zhou, AP-S, 1995, pp.1194-1196) the attempt of purely numerical design of the two-reflector by shaping the subreflector and taking in account the diffraction effects was presented. However the presented design procedure is time consuming (work station is needed) and no results about the limitations of the procedure are available.

In the present paper an efficient method of synthesis for shaped/contoured beam dual-reflectors by shaping the subreflector only and taking in account the diffraction effects is presented. The method is based on solution for nonlinear problem of synthesis of power pattern by optimization of the phase distribution in the radiating aperture with specified amplitude distribution. Efficient iterative procedure suitable for PC based synthesis of the two-reflector offset-fed antenna with specified amplitude radiation pattern and a parabolic main reflector is described. This design is expected to be the more cost effective in comparison when the both reflectors are shaped, besides, as the main reflector could be a paraboloid, it is raised the possibility to reuse the main reflector aperture in multiband, multipurpose antenna systems. Another advantage is that, it is possible to compensate the errors of fabrication of the main reflector if the real shape of the reflector is measured.

URSI B **Session 15** **Salon Marquette**

Efficient Methods for Solution and Design
Co-chairs: F. Canning, USA and S. Avery, USA

13:10	15.1	Fast Multipole Method for Large Penetrable Scatterers, **J.M. SONG**, X.Q. SHENG, C.-C. LU, W.C. CHEW, J.-M. JIN, *University of Illinois, Urbana, IL, USA*
13:30	15.2	Solution of Electromagnetic Scattering Problems by Domain Decomposition, M. KUZUOGLU[1], **R. MITTRA**[2], [1]*Middle East Technical University, Ankara, Turkey;* [2]*Pennsylvania State University, University Park, PA, USA*
13:50	15.3	Fast Sparse Decomposition of Standard Moment Method Matrices, **F.X. CANNING**, *Rockwell Science Center, Thousand Oaks, CA, USA*
14:10	15.4	Fast Sparse Solution of Standard Moment Method Matrices, **F.X. CANNING**, *Rockwell Science Center, Thousand Oaks, CA, USA*
14:30	15.5	A Systematic Root-Finding Strategy for the Subspace Iteration Method with General Complex Sparse Matrices, **J. ARROYO**, J. ZAPATA, *Universidad Politécnica de Madrid, Spain*
14:50	15.6	High-Performance Computational Electromagnetic Modeling Using Low-Cost Parallel Computers, **D.S. KATZ**, *California Institute of Technology, Pasadena, CA, USA*
15:10		Coffee Break
15:30	15.7	Broadband Antenna Analysis and Scattering from Planar Structures Using a Fast Integral Method, S.S. BINDIGANAVALE[1], T. ÖZDEMIR[1], **J.L. VOLAKIS**[1], J. BERRIE[2], [1]*University of Michigan, Ann Arbor, MI and* [2]*Mission Research Group, Dayton, OH, USA*
15:50	15.8	Multilevel Fast-Multipole Algorithm for Solving Microstrip Structures, J.S. ZHAO, **W.C. CHEW**, C.C. LU, E. MICHIELSSEN, J.M. SONG, *University of Illinois at Urbana-Champaign, Urbana, IL, USA*
16:10	15.9	A Fast Method for Computing Current Distributions on Printed Circuit Boards Using the Method of Moments, V. JEVREMOVIC, **E.F. KUESTER**, *University of Colorado at Boulder, CO, USA*
16:30	15.10	The Progressive Numerical Method (PNM) for Electromagnetic Scattering of Three Dimensional Large Structures, Q. YE[1], **L. SHAFAI**[1], S. KASHYAP[2], [1]*University of Manitoba, Winnipeg, MB and* [2]*Defence Research Establishment, Ottawa, ON, Canada*
16:50	15.11	Reduced Expansion and Field Testing (REFT) for Matrix Thinning, B.Z. STEINBERG, **R. KASTNER**, *Tel-Aviv University, Tel-Aviv, Israel*

B15.1

Fast Multipole Method for Large Penetrable Scatterers

J.M. SONG*, X.Q. SHENG, C.-C. LU, W.C. CHEW, AND J.-M. JIN
CENTER FOR COMPUTATIONAL ELECTROMAGNETICS
DEPARTMENT OF ELECTRICAL AND COMPUTER ENGINEERING
UNIVERSITY OF ILLINOIS
URBANA, IL 61801

Fast multipole method (FMM) and multilevel fast multipole algorithm (MLFMA) have been applied for solving integral equations of electromagnetic (EM) scattering from a perfect electric conductor (PEC) iteratively. The FMM reduces the complexity of a matrix-vector multiply from $O(N^2)$ to $O(N^{1.5})$, where N is the number of unknowns. The MLFMA further reduces the complexity to $O(N\log N)$. It requires $O(N\log N)$ memory, and hence, can solve a large problem on a small computer.

Scattering of an electromagnetic wave by a PEC can be controlled or modified by coating the body with a lossy material sheet (partially penetrable scatterer). If the coating materials or totally penetrable scatterer are homogeneous media, surface integral equations can be solved for electromagnetic scattering. Both equivalent electric current and magnetic current should be considered as unknowns. The method of moments (MoM) is used to develop a matrix equation from the integral equation. The resultant matrix equation is solved iteratively by the conjugate gradient (CG) method. The FMM is used to speed up matrix-vector multiplies in the CG. The FMM formulations for operators related to magnetic currents are derived. The MLFMA reduces the complexity to $O(N\log N)$ for both the CPU time per iteration and memory requirements.

If the penetrable scatterers are inhomogeneous or have multi-layer coating, the hybrid finite-element boundary-integral (FE-BI) method is a powerful technique. It divides the problem into interior and exterior regions, and employs the finite-element method (FEM) to deal with the interior problem. The exterior problem is formulated using the boundary-integral method which, when coupled with the interior fields, provides an efficient solution to the original problem. But the capability of the technique is limited mainly by the full matrix generated by the discretization of the boundary-integral using the MoM. In this work, the FMM and MLFMA are used to speed up the matrix-vector multiply related to boundary integrals at a reduced complexity.

Solution of Electromagnetic Scattering Problems by Domain Decomposition

Mustafa Kuzuoglu
Department of Electrical Engineering
Middle East Technical University
06531, Ankara TURKEY

Raj Mittra
Pennsylvania State University
319 Electrical Engineering East
University Park, PA 16802-2705 USA

In this work, we present an overlapping domain decomposition method for the solution of electromagnetic scattering problems. In this approach, a coarse grid is implemented over the computational domain, and the weak form of the governing partial differential equation is discretized by the finite element method. Then, an arbitrary number of subdomains are chosen (composed of a union of coarse mesh elements) where the solution is expected to exhibit large gradients. Next, a finer mesh is generated over these subdomains, which may be allowed to overlap. Let Ω_i, $i = 1,2,\ldots n$ denote the i-th subdomain with n_i nodes, contained in the computational domain Ω, and let A_i be the finite element matrix associated with the subdomain Ω_i. The matrices A_i, $i = 1,2,\ldots n$ are used in the preconditioner part of the algorithm and, hence, accurate solutions of the subdomain linear systems $A_i \bar{x}_i = \bar{b}_i$ (where $\bar{x}_i, \bar{b}_i \in C^{n_i}$) are not required. There are basically two classes of preconditioners, the additive and the multiplicative. These operators are relatively inexpensive to evaluate and they lead to well-conditioned linear systems. Without preconditioning, the composite grid (the union of the coarse grid and the fine grids generated in the subdomains) will lead to an ill-conditioned system of equations, due to the difference in mesh sizes in the two grids. In the domain decomposition approach, the resultant preconditioner is obtained by summing up the preconditioners that have been previously constructed for the subdomain problems. The convergence rate of the iterative solution is independent of the mesh size and the coefficients of the differential equation. This approach can easily be parallelized, such that each subdomain problem is solved by a different processor. Thiis enables us to handle scattering or radiation problems involving a large number of unknowns that would otherwise be unmanageable.

B15.3

Fast Sparse Decomposition of Standard Moment Method Matrices

Francis X. Canning
Rockwell Science Center
1049 Caiman DOS
Thousand Oaks, CA 91360

Methods for efficiently calculating a sparse form of existing moment method matrices are developed. This method requires no knowledge of the geometry of the scattering surfaces. However, it does require that the unknowns are numbered appropriately. For example, for a three dimensional problem involving as ship, one would sort the unknowns according to their distance from the bow.

Previous work on the Impedance Matrix Localization (IML) method showed that using expansion functions which radiate narrow beams in the far field, a sparse matrix results. This work implied that blocks of the standard moment method matrix which do not cross its diagonal have a small number of singular values significantly different from zero. The singular value decomposition allows each block to be expressed using expansion functions chosen for that block; this allows near field interactions and gives more flexibility in choosing block sizes than in previous IML work. An m by m block of a moment matrix is written as:

$$\sum_{k=1}^{s} s_k \; \mathbf{v}_k \; \mathbf{u}_k^h \quad ; \; \mathbf{v}_k , \mathbf{u}_k \text{ vectors of length m}$$

This can always be done when s=m. However, we find that this is still an excellent approximation when s << m. Standard methods (e. g. CSVDC of Linpack) take roughly 5 m^3 operations. We show how this can be reduced by roughly the factor (s/m) using Lanczos bidiagonalization with complete reorthogonalization by Housedorf transformations. In a related paper we show how the resulting decomposed form allows a fast direct matrix inversion.

Fast Sparse Solution of Standard Moment Method Matrices

Francis X. Canning
Rockwell Science Center
1049 Caiman DOS
Thousand Oaks, CA 91360

Methods for efficiently calculating a sparse form of existing moment method matrices are developed in a related paper ("Fast Sparse Decomposition of Standard ..."). This paper uses that decomposition to solve the associated matrix equation. That is, a representation for the inverse of the moment method matrix is found. For N by N matrices where $O[N^3]$ operations were previously required, now only $O[N^2]$ are required for two-dimensional problems and about $O[N^{2.5}]$ are required for three-dimensional problems.

The moment method matrix is considered as four blocks of size N/2 by N/2. The off diagonal blocks have a low rank. If we have a solver for the diagonal blocks, then the off diagonal blocks may be included using the Sherman Morrison Woodbury formula. A solver may be constructed for the diagonal blocks by considering each of them to be four blocks of size N/4 by N/4. Proceeding recursively, a solver results. This is surprisingly easy to program in C, which allows recursion. The resulting method is very fast; unfortunately it has stability problems with respect to round off error as our numerical results show.

A stable method results from considering the moment method matrix as a banded part plus a collection of rectangular blocks. Using a banded matrix solver and the Sherman Morrison Woodbury formula to include the blocks gives a stable solver. The speed improvement over standard methods is modest, since all blocks are now related. Direct application of the matrix structure to standard inversion methods is used next. It is proven to be both stable and efficient. Numerical results confirm this substantial speed improvement over standard methods.

B15.5

A SYSTEMATIC ROOT-FINDING STRATEGY FOR THE SUBSPACE ITERATION METHOD WITH GENERAL COMPLEX SPARSE MATRICES

Javier Arroyo* and Juan Zapata
Departamento de Electromagnetismo y Teoría de Circuitos
E.T.S.I. Telecomunicación. U.P.M.
Ciudad Universitaria S/N
28040 Madrid Spain
Tel 34-1-5495700 Ext 315 Fax 34-1-3367348
email: jarroyo@gauss.etc.upm.es

For the class of waveguides that can be analyzed using a symmetrical or Hermitian positive definite formulation, the number of (real) eigenvalues within a given real interval can be computed using numerically efficient techniques based on well-known mathematical theorems. Besides, only the positive real axis needs be swept, which can be done in a straightforward way. However many structures require the use of formulations which yield generalized eigensystems of general complex sparse matrices being arbitrary the location of the eigenvalues in the complex plane in this case. A systematic root-finding strategy must be devised in order to prevent the potential loss of eigenvalues and to preclude or reduce the duplication of those which are found.

The subspace iteration method is one of the methods that may be applied for finding the eigenvalues and eigenvectors of these generalized eigensystems. The use of this method is specially convenient since it takes advantage of the sparsity of the matrices and allows the simultaneous obtention of a set of several eigenvalues, improving thus the efficiency. Since the convergence of the eigenvalues in the subspace iteration method depends on its distance from the center of the iterations, the complex plane must be swept using overlapping circles of variable radius in general.

The key parameter that controls the performance of the subspace iteration method is the dimension of the subspace that is (inversely) iterated. This dimension has a strong influence on the convergence rate and may affect the accuracy of the found eigenvalues. The choice is intimately related to the number of eigenvalues that actually exist within the circle that is being analyzed. Thus the ability to compute this number becomes essential for the success of the overall process.
It will be shown how to carry out this computation in a numerically efficient way, avoiding the difficulties that are encountered when other methods are used.

High-Performance Computational Electromagnetic Modeling Using Low-Cost Parallel Computers

Daniel S. Katz

Jet Propulsion Laboratory
California Institute of Technology
4800 Oak Grove Drive, MS 168-522
Pasadena, CA 91109
d.katz@ieee.org

This paper discusses the use of low-cost parallel computers, specifically the Beowulf system which was built at Caltech, to solve problems in computational electromagnetics. The focus of this paper is on application of the Finite-Difference Time-Domain (FDTD) method. Some discussion of applying the Finite-Element (FE) method to this type of machine is also be provided.

The Beowulf systems is composed of 16 200 MHz Pentium Pro-based personal computers connected with a fast 16-way crossbar switch. The hardware parts used to build the system are all commodity components, costing less that $60,000 for the entire system, and all the software used (compilers, operating system, etc...) is freeware. The highest sustained application speed measured on this system is 1.2 GFlops.

As the FDTD method can be parallelized through a simple domain decomposition, the initial set-up is quite simple. However, data communication is required from one processor, with a given computational domain A, to all the processors whose computational domains share a boundary with A at each time step. The data that must be communicated is equivalent to the field components at the shared boundary with A.

The FE method is more complicated, as the distribution of the initial mesh cannot simply be based on a partitioning of physical space. Once this problem has been solved, and the mesh or matrix is distributed, the solution of the matrix can be performed using standard parallel numerical libraries.

- Performance, including comparison with other parallel and sequential computers;
- An estimate of scaling to larger systems, since the Beowulf system is only 16 processors at this time; and
- User experiences with this class machine (non-commercial, not vendor-supported);

are included among the results discussed in this paper.

B15.7

Broadband Antenna Analysis and Scattering from Planar Structures using a Fast Integral Method

Sunil S. Bindiganavale, Tayfun Özdemir and John L. Volakis
Radiation Lab, EECS Dept.
University of Michigan
Ann Arbor, MI 48109-2122
bssunil@umich.edu, tayfun@umich.edu, volakis@umich.edu

J. Berrie
Mission Research Corp.
3975 Research Blvd.
Dayton OH 45340
jberrie@mrcday.com

The Finite Element - Boundary Integral (FE-BI) method has been very popular for scattering and radiation computations from composite structures. It is an "exact" method, since it employs the exact boundary integral equation. However, it leads to a partly full and partly sparse system and is thus computationally intensive. For special cases, where the termination boundary is convolutional, the FFT can be used to reduce the memory and CPU requirements to $N \log N$. In general, the CPU requirements will be of $O(N_b^2)$ where N_b denotes the unknowns on the boundary. Fast integral equation algorithms provide for a reduction of the computational complexity from $O(N_b^2)$ down to $O(N_b^\alpha)$ where alpha has a value less than 1.5. Two such algorithms have been recently proposed, and both have been applied to large scale scattering computations, namely, the fast multipole (FMM) and the adaptive integral equation (AIM) method. The FMM has an operation count of $O(N_b^{1.5})$ or $O(N_b^{1.33})$ depending on the specific version and level of nesting employed while the AIM has been demonstrated to reduce memory down to $O(N_b^{1.5})$ and complexity down to $O(N_b^{1.5} \log N_b)$ for surface problems.

In this paper, we apply a version of the Adaptive Integral Method (AIM), specialized to planar geometries, to reduce the storage and computational requirement of the boundary integral when the size of the aperture is large. By virtue of its $0(N^{1.5})$ memory requirement, the application of the AIM results in substantial savings in memory in the boundary integral portion of the code, independent of the shape of the BI contour. This technique while very accurate (see Figure 1) results in considerable savings in memory. We will discuss the efficiency of the method and present applications of the technique to scattering from planar structures with very fine geometrical details. Also hybridizations of AIM with the finite element method will be presented.

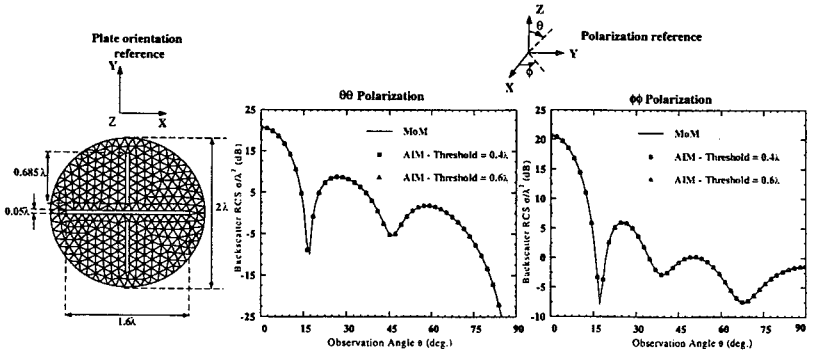

Figure 1: Monostatic RCS for a circular plate of diameter 2λ with 3 narrow slots computed with standard MoM & AIM

MULTILEVEL FAST-MULTIPOLE ALGORITHM FOR SOLVING MICROSTRIP STRUCTURES

J. S. Zhao, W. C. Chew, C. C. Lu, E. Michielssen, and J. M. Song
Center for Computational Electromagnetics
Department of Electrical and Computer Engineering
University of Illinois
Urbana, IL 61801

Abstract

In this paper, an accurate and efficient technique is presented for solving Maxwell's equations pertinent to the microstrip structure applications, which consists of the full-wave analysis method and the multilevel fast multipole algorithm (MLFMA). In this approach, a new form of electric field spatial-domain Green's function is introduced. When the method of moments is used to discretize the integral equation, the differential operators appearing in the Green's function are moved first from the singular Green's function to the differentiable basis and testing functions. Then, the remaining parts of the Green's function are less singular. The electric field dyadic Green's function includes the Sommerfeld-type integrals. The highly oscillatory and slowly converging behavior of the integrands makes numerical evaluation difficult. To accelerate the calculation of these Green's functions, the Fourier inversion contour is deformed to the vertical branch cut which is also the steepest descent path when the thickness of the substrate is small. For any fixed distance from the source point to the field point, only five Gaussian integration points are needed for a small errors. Subdomain triangular patch basis function is used to model the equivalent electric currents on the patch, so the patch may be of any arbitrary shape. To solve the matrix equation, conjugate gradient (CG) methods are preferred over direct methods. The major computational cost in CG lies in the matrix-vector multiplication. Multilevel fast multipole algorithm (MLFMA) is designed to speed up the matrix-vector multiplication. After deforming the the Fourier inversion contour to the vertical branch cut, MLFMA is applied to solve the microstrip structure. MLFMA reduces the computational complexity to $O(N \log N)$ from $O(N^3)$ for the Gaussian elimination method and $O(N^2)$ for the CG method. The memory requirement for MLFMA is $O(N \log N)$. Therefore this approach can solve a large problem on a small computer.

B15.9

A FAST METHOD FOR COMPUTING CURRENT DISTRIBUTIONS ON PRINTED CIRCUIT BOARDS USING THE METHOD OF MOMENTS

Vladan Jevremovic and Edward F. Kuester*
Electromagnetics Laboratory
Department of Electrical and Computer Engineering
Campus Box 425
University of Colorado at Boulder
Boulder, CO 80309
USA

The scope of this paper is to demonstrate an alternative method of the accurate prediction of current distribution on printed circuit boards (PCBs) or microwave integrated circuits (MICs) using a quasi-static Green's function approximation. A standard method to determine current distribution on PCB structure is to evaluate the impedance matrix of the structure using the Method of Moments (MoM) and a full-wave Green's function. A full wave Green's function is frequency dependent in a nontrivial way, and consequently the impedance matrix can be accurately determined only at a single frequency at a time. Oftentimes, current distribution of a fundamental clock frequency as well as its higher order harmonics on a PCB is needed. Moreover, the modeling of pulse propagation on PCBs requires solutions at a large number of frequency points, and MIC modeling must also often cover a wide frequency band. Since impedance matrix elements do not scale in a simple fashion with frequency, they must be recomputed for each new frequency separately. Impedance matrix computation and matrix inversion are thus very consuming of CPU time, and therefore the standard full-wave method becomes less efficient as the number of frequency points increases.

One way to speed up the computation of the impedance matrix is to use a static Green's function approximation to determine matrix elements. This will be a good approximation of the full-wave Green's function as long as the PCB is electrically small; when this is not the case, a correction needs to be made to the matrix elements. Each impedance matrix element for a given pair of MoM cells consists of four subterms (direct magnetic, magnetic image, direct electric, electric image). We propose a correction to the quasi-static impedance matrix element to be obtained by multiplying each of the four aforementioned matrix impedance element subterms with a unique phase shift, proportional to frequency. Each phase shift is otherwise only a function of the cell geometries, the substrate thickness and the relative positions of the two cells. The linear frequency dependence of each phase shift makes simple scaling with frequency possible. Therefore, each matrix element subterm needs to be calculated only once, at a fundamental frequency, using the quasi-static Green's function approximation. The impedance elements at other frequencies are then computed by multiplying the impedance element terms with the appropriate scaled phase shifts. This procedure thus speeds up the computation significantly.

As an example, a simple PCB circuit board will be presented, and comparison between the matrix elements and current distributions using the full-wave Green's function and those obtained using the approximation method described above will be shown.

The Progressive Numerical Method (PNM) for Electromagnetic Scattering of Three Dimensional Large Structures

Qiubo Ye*, L. Shafai* and S. Kashyap**

*Department of Electrical and Computer Engineering
University of Manitoba, Winnipeg, Manitoba, Canada, R3T 5V6

**Defence Research Establishment Ottawa
Ottawa, Ontario, Canada, K1A 0Z4

Recently the performances of the PNM on the electromagnetic scattering from two dimensional electrically large objects were investigated by the authors. It was shown that both TM-case and TE-case behave well for large objects. However, the TE-case was less accurate for small scatterers. Based on this study, the research is extended to three dimensional problems.

In this paper the application of the PNM is based on the conventional method of moment (MoM) with triangular surface patches. The implementation of PNM is to decompose the large object into a number of sub-regions. Then every sub-region is considered as a distinct object and is calculated for the current density by MoM. After the current distribution on the first sub-region is obtained the second one is calculated and the current on the first one is taken into account as an excitation. This procedure is continued over every sub-region, always using the latest updated currents as the excitations. An overlapping region may be used to improve the accuracy.

Numerical results will be presented to illustrate the ability of the PNM to handle large structures. These results will be shown graphically, including those of scattering on several three dimensional objects, and compared with the results of the full matrix MoM in which the entire objects are treated simultaneously. The accuracy and the efficiency of the PNM will be discussed. The saving of the computer memory and the execution time will also be provided.

B15.11

REDUCED EXPANSION AND FIELD TESTING (REFT) FOR MATRIX THINNING

B. Z. Steinberg and R. Kastner*

Faculty of Engineering, Tel-Aviv University, Tel-Aviv 69978, Israel

The RFT (Reduced Field Testing) method has been presented resecntly both in a heuristic form (R. Kastner and G. Nocham, "Matrix thinning with Reduced Field Testing (RFT)", *Microwave Optical Tech. Letters*, vol. 9, No. 6, pp. 329–333, 1995), and a systematic form (R. Kastner, G. Nocham and B. Z. Steinberg, "Multi–region systematic Reduced Field Testing (RFT) for matrix thinning", IEEE/AP-S International Symposium, Baltimore, MD, July 21–26, 1996). In its systemtic version, the method can be desribed either as a sequence of row operations over foursomes of rows of the MoM matrix $\mathbf{A}$, or as a multiplication of the system $\mathbf{A} \cdot \mathbf{J} = \mathbf{E}^{inc}$ by a sparse, unitary matrix $\mathbf{B}$. The resultant system, i.e., $\mathbf{B} \cdot \mathbf{A} \cdot \mathbf{J} = \mathbf{B} \cdot \mathbf{E}^{inc}$, is sparse because these operations generate rapidly varying testing functions which tend to average out the effect of slowly varying portions of the fields, such as exist in the far field region of any basis function ϕ. In this work, the idea is pursued further to incorporate "reduced expansion". The rationale of reduced expansion is dual to reduced testing: For a given testing point, one may consider only a limited number of expansion functions in the far field. To facilitate this reduction, we can use either column operations in addition to the aforementioned row operations, or transform the matrix using a block diagonal, unitary matrix $\mathbf{B}$ in the following way: $\mathbf{B} \cdot \mathbf{A} \cdot \mathbf{B}^T \cdot \mathbf{V} = \mathbf{B} \cdot \mathbf{E}^{inc}$, where the unknown current distribution is $\mathbf{J} = \mathbf{B}^T \cdot \mathbf{V}$. The sparse matrix $\mathbf{B}$ is composed of the following blocks along the diagonal:

$$\mathbf{b} = \begin{pmatrix} 1 & -1 & 1 & -1 \\ 1 & 1 & -1 & -1 \\ 1 & -1 & -1 & 1 \\ 1 & 1 & 1 & 1 \end{pmatrix} \quad \text{such that} \quad \mathbf{B} = \begin{pmatrix} \mathbf{b} & 0 & 0 & \cdots & 0 \\ 0 & \mathbf{b} & 0 & \cdots & 0 \\ 0 & 0 & \ddots & 0 & \vdots \\ \vdots & \vdots & 0 & \ddots & 0 \\ 0 & \cdots & \cdots & 0 & \mathbf{b} \end{pmatrix}$$

Using this transformation, the matrix $\mathbf{B} \cdot \mathbf{A} \cdot \mathbf{B}^T$ can have $10\% - 15\%$ more zero entries than the one obtained by reduced testing only. In the examples shown, the degree of thinning usually exceeds 75% with litle loss of accuracy in far field calculations.

URSI B

Session 25

Salon Peribonca

Chiral Media

Co-chairs: D.L. Jaggard, USA and K.A. Zaki, USA

13:10	25.1	Planar Chirowaveguides with Discontinuities, **X. WU**, D.L. JAGGARD, *University of Pennsylvania, Philadelphia, PA, USA*
13:30	25.2	Green Dyadic in Time Domain for Chiral Medium with Constant Material Parameters, **A.J. VIITANEN**, *Helsinki University of Technology, Espoo, Finland*
13:50	25.3	A Full-Wave Spectral Domain Analysis Method for Open Chirostrip Multilayered Structures, F. LUMINI[1], **J.C. DA S. LACAVA**[2], [1]*EMBRAER S.A. and* [2]*CTA-ITA, São Paulo, Brazil*
14:10	25.4	A Linear-Operator Formalism for the Analysis of Inhomogeneous Pseudochiral Planar Waveguides, **A.L. TOPA**, C.R. PAIVA, A.M. BARBOSA, *Technical University of Lisbon, Portugal*
14:30	25.5	Second Harmonic Emission from an Axially Excited Dielectric TFHBM Slab, V.C. VENUGOPAL, **A. LAKHTAKIA**, *Pennsylvania State University, University Park, PA, USA*
14:50	25.6	Exact Image Theory for Horizontal Sources above a Slightly Chiral Half Space, **L.H. RUOTANEN**, I.V. LINDELL, *Helsinki University of Technology, Espoo, Finland*
15:10		Coffee Break
15:30	25.7	Treatment of Chiral Property by Condensed Node Spatial Network for Vector Potential, **N. YOSHIDA**, *Hokkaido University, Sapporo, Japan*
15:50	25.8	Artificial Non-Reciprocal Magnetoelectric Composites, **S.A. TRETYAKOV**, S.V. ZAGRIADSKI, A.A. SOCHAVA, T.G. KHARINA, D.Ya. KHALIULLIN, *St. Petersburg State Technical University, St. Petersburg, Russia*
16:10	25.9	Electromagnetic Scattering and Diffraction Problems by Chiral and Biisotropic Bodies of Complicated Shape, F.G. BOGDANOV, **D.D. KARKASHADZE**, R.S. ZARIDZE, R.G. JOBAVA, *Tbilisi State University, Tbilisi, Georgia*
16:30	25.10	Excitation of the Electromagnetic Waves by a Current Placed on Chiral Layer Surface, **S.L. PROSVIRNIN**, A.E. SHEPILKO, *Ukrainian National Academy of Sciences, Kharkov, Ukraine*

B25.1

Planar Chirowaveguides with Discontinuities

Xinzhang Wu*, and Dwight L. Jaggard
Complex Media Laboratory
Moore School of Electrical Engineering
University of Pennsylvania
Philadelphia, PA 19104-6390

We propose, develop and implement an exact method to analyze the effect of discontinuities in open planar chirowaveguides. The method combines the building block approach of multimode network theory with a rigorous mode-matching procedure. Both the scattering of discrete spectra surface wave modes and the continuous spectra radiation and evanescent modes are discussed. The introduction of equivalent transmission line networks brings new physical insight into the overall behaviour of the discontinuities. The symmetry properties of the structure are also investigated.

Based on our analysis, numerical results of mode conversion by planar chirowaveguide sandwiched between two non-chirowaveguides (Fig.1) have shown that when the chirality parameter is small, mode conversion is weak; when the chirality parameter is moderate, mode conversion is strong; but when the chirality parameter is large, mode conversion becomes weak again due to strong radiation and reflection. Therefore, if we want to use chirowaveguide as a mode conversion device, the chirality parameter should be chosen to be an optimum moderate value.

We also examine guided wave propagation through double step discontinuity and air gap (Fig.2). We find both the mode conversion effect and radiation effect occur. Especially for the air gap, we find a considerable difference between R_0 mode incidence and L_0 mode incidence. When the distance of the air gap increases, the reflection of R_0 mode dominates for R_0 mode incidence; while the forward radiation dominates for L_0 mode incidence.

Finally, we study propagation properties of periodic structure with finite-length (Fig.3). We find the first Bragg reflection peaks of R_0-R_0, L_0-L_0, R_0-L_0 and L_0-R_0 coupling. The positions of these peaks are confirmed by simple physical reasoning and support the numerical results. In addition, the limits of the radiation is evaluated and agrees well with calculations.

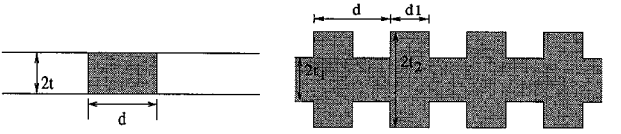

Fig.1

Fig.3

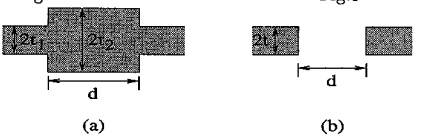

Fig.2

GREEN DYADIC IN TIME DOMAIN FOR CHIRAL MEDIUM WITH CONSTANT MATERIAL PARAMETERS

Ari J. Viitanen

Electromagnetics Laboratory
Department of Electrical and Communications Engineering
Helsinki University of Technology
Otakaari 5 A, FIN-02150 Espoo, Finland

The chiral medium is assumed to be lossless, reciprocal and isotropic. The time harmonic Green dyadic for a lossless isotropic chiral medium was presented in explicite form for a few years ago. The Green dyadic in time domain can be obtained by calculating the inverse Fourier transformation of the Green dyadic in frequency domain. To obtain the Green dyadic in time domain, one must know the frequency dependence of the material parameters. Also to obtain a real Green dyadic in time domain the chirality parameter must be an odd function and permittivity and permeability parameters even functions in frequency domain. This is a consequence of the general properties of the Fourier transformation. In this study the material parameters are assumed to have constant values at certain frequency band. Assuming constant material parameters it means that the chirality parameter is an odd constant, its sign is opposite at negative frequency range compared to the corresponding value at positive frequency range. The permittivity and permeability parameters are assumed to be constant at frequency range. As a result the Green dyadic is obtained which consists of two parts related to two separate fields which are propagating with different velocities. In frequency domain these two fields are known as right-hand and left-hand circularly polarized fields. Examples of the Green dyadic are calculated in cases when the material parameters are constant in narrow and wide frequency band. When the chirality parameter vanishes the Green dyadic reduces to the expression of the Green dyadic for isotropic medium.

B25.3

A FULL-WAVE SPECTRAL DOMAIN ANALYSIS METHOD FOR OPEN CHIROSTRIP MULTILAYERED STRUCTURES

Feliciano Lumini[+] **and J.C. da S. Lacava** [*]

[+] Division of Systems Engineering, EMBRAER S.A., 12227-901, S.J. Campos, SP, Brazil.

[*] Electronic Engineering Department, CTA-ITA, 12228-900, S.J. Campos, SP, Brazil.

INTRODUCTION. Printed circuit antennas in multilayered structures have been extensively analyzed in the last decade. Power gain and bandwidth are two important parameters that can be improved by using these structures. Recently, a new type of microstrip radiator, named chirostrip antenna, using a chiral material instead of a conventional dielectric substrate has been introduced. Due to the recent advances in the polymer science and in the manufacture of artificial dielectrics, open chirostrip structures have gained considerable attention in the microwave and millimeter-wave frequency ranges. Since a rigorous analysis method is required for integrated printed circuit applications, the purpose of this work is to present a full-wave spectral-domain analysis method for open chirostrip multilayered structures.

THEORY. An open chirostrip multilayered structure can be formed by adding M parallel chiral layers (with thickness $h_p = (d_p - d_{p-1})$) on a metallic ($\sigma_c=\infty$) xy plane. Perfect conducting chirostrip elements of area S_p, arbitrary shape and infinitesimal thickness are printed on $z = d_p$ interfaces ($1 \le p \le M$). Each chirostrip element supports surface current densities $\mathbf{J}_p$ and the p-th layer has relative dielectric constant ε_{rp}, magnetic permeability μ_o (non-magnetic material) and chiral admittance ξ_p. After the M-th chiral layer we have the free space region (ε_o, μ_o). The theory used in this work considers the chirostrip structure as a boundary problem where the current densities $\mathbf{J}_p$ are the virtual sources of the electromagnetic fields. The wave equations in the chiral layers and in the free space regions are solved in the Fourier domain. Then, the boundary conditions for the electromagnetic fields are applied on the interfaces $z = 0$ and $z = d_p$, resulting in a set of 4M+2 equations with 4M+2 unknowns. Solving this set of equations, the spectral electromagnetic fields in any point of region $z \ge 0$ can be determined. Finally, the electromagnetic fields in the space domain are obtained through the application of the inverse Fourier transform.

APPLICATIONS. Although the method may be used in the analysis of open chirowaveguides and chirostrip antennas, this paper discusses only aspects related to the fields excited by printed dipoles. The far electromagnetic fields radiated by the multilayered structure can be calculated using an asymptotic expression obtained by the application of the stationary phase method. Effects of chirality on radiation pattern, directivity function, cross-polarization level, axial ratio and radiation resistance are presented. On the other hand, near fields can also be analyzed through this method. Expressions for numerical evaluation of electromagnetic field components are obtained through the transformations $k_x = \beta\cos(\alpha)$, $k_y = \beta\sin(\alpha)$, $x = \rho\cos(\theta)$ and $y = \rho\sin(\theta)$. This procedure allows the calculation of these components in all points of the region $z \ge 0$. Effects of chirality on electromagnetic field components, including induced asymmetry, are also discussed. Finally, the behavior of electromagnetic field components on $z = d_p$ and $z = 0$ interfaces were also investigated. Two interesting things related to the magnetic field component H_z (normal to the interfaces) can be observed: H_z is not continuous on $z = d_p$ interfaces and is different from zero on $z = 0$ (perfectly conducting surface). Clearly, the standard boundary conditions for the magnetic field are not completely satisfied when chiral media are present.

A Linear-Operator Formalism for the Analysis of Inhomogeneous Pseudochiral Planar Waveguides

António L. Topa, Carlos R. Paiva, and Afonso M. Barbosa
Departamento de Engenharia Electrotécnica e de Computadores and Instituto de Telecommunicações, Technical University of Lisbon, Portugal

In this paper a linear-operator formalism for the analysis of inhomogeneous pseudochiral planar waveguides is presented. For these waveguides, using the theory of linear operators and through a suitable definition of a two-vector transverse mode function, the problem of guided electromagnetic wave propagation is reduced to an eigenvalue equation related to a 2×2 matrix differential operator. This mathematical framework is similar to the one developed by the authors for inhomogeneous chiral planar waveguides (*A. L. Topa, C. R. Paiva, and A. M. Barbosa, IEEE Trans. Microwave Theory Tech. 42, 629-634, 1994*).

Based on Maxwell's curl equations for source free regions together with the set of constitutive relations for pseudochiral media (N. Engheta and M. M. I. Saadoun, Proc. PIERS'91, 339, 1991) in the EH representation, the problem of electromagnetic wave propagation is reduced - after a suitable choice of the state vector Φ - to the following eigenvalue problem of rank two:

$$\overline{\mathscr{L}}\cdot\Phi=\beta^2\,\overline{\mathscr{W}}\cdot\Phi \qquad (1)$$

where $\overline{\mathscr{L}}$ is a linear differential operator and $\overline{\mathscr{W}}$ is the weight operator; β is the effective refractive index given by $\beta=k/k_0$, where k is the longitudinal wavenumber.

Using the concept of adjoint waveguide, bi-orthogonality relations are derived for the hybrid modes. In order to have a complete field representation in open pseudochiral waveguides, these relations are of utmost importance when choosing an appropriate set of mutually orthogonal radiation modes. As an example of application a general analysis of the radiation modes of a grounded pseudochiral slab is also presented. Finally, one should also note that this linear-operator formalism is applicable to multilayered planar waveguides with inhomogeneous layers. For homogeneous layers the general formalism is reduced to an algebraic 2×2 coupling matrix eigenvalue problem (*C. R. Paiva and A. M. Barbosa, Electromag. 11, 209-221, 1991*).

B25.5

SECOND HARMONIC EMISSION FROM AN AXIALLY EXCITED DIELECTRIC TFHBM SLAB

Vijayakumar C Venugopal and *Akhlesh Lakhtakia*
CATMAS – Computational and Theoretical Materials Sciences Group
Department of Engineering Science and Mechanics
The Pennsylvania State University, University Park, PA 16802–1401, USA.

Abstract

The electromagnetic properties of a thin film helicoidal bianisotropic medium (TFHBM) are totally delineated by a reference crystallographic symmetery as well as a helicoidal rotation matrix. The response of a dielectric TFHBM slab to an axially exciting plane wave is investigated here, assuming that second harmonic (SH) generation is possible inside the slab. The time–harmonic Maxwell postulates are used to formulate two 4×4 matrix differential equations. Analytical solution of these matrix differential equations is accomplished using an eigenvalue approach. The response of the TFHBM slab to axial planewave excitation is then set up as a boundary value problem.

The dependence of the linear and the SH responses on various structural—including geometric as well as constitutive—parameters is graphically illustrated for a TFHBM slab with Tetragonal $\bar{4}2m$ reference crystallographic symmetery. The geometric parameters include the helicoidal pitch as well as the so–called angle of rise above the transverse plane, and the slab thickness. Both positive uniaxial and negative uniaxial reference symmetries are considered. The response of the slab to both left and right circularly polarized incident plane waves is studied.

Zones of attenuative propagation inside the TFHBM are found, and a zonal classification scheme for the linear and the SH responses of the TFHBM slab is proposed. The intensities of the reflected/transmitted linear as well as the emitted SH plane waves are highly influenced by the handedness of the incident plane wave relative to the handedness of TFHBM. The possible existence of an optimal set of structural parameters of the chosen TFHBM slab to maximize the total intensity of the emitted SH plane waves is examined. Optical rotatory characteristics of the reflected/transmitted linear and the emitted SH plane waves are presented. Nanostructural implications for fabricating TFHBMs are discussed.

Exact image theory for horizontal sources above a slightly chiral half space

Leila H. Ruotanen and Ismo V. Lindell
Electromagnetics Laboratory
Helsinki University of Technology
Otakaari 5 A, FIN-02150 Espoo, Finland

The exact image method was originally introduced to improve various approximate image methods for the planar air-ground interface. Recently, the theory was simplified by introducing the Heaviside operational calculus as the tool for finding the images (I.V. Lindell, *J Electrom Waves Appl*, 11, 119-132, 1997). The theory has also been extended as a first-order theory to the interface between air and chiral ground, with the restriction that the chirality parameter be small (I.V. Lindell, *J. Electro. Waves Appl.*, 10, 1583-1594, 1996). Since large values for the chirality parameter are not easy to fabricate, the theory covers quite well problems appearing in practice. However, the theory was restricted to vertical dipole sources for simplicity.

The idea to find the image of a vertical dipole source was based on the wavefield decomposition, also called Bohren decomposition or self-dual decomposition, of the fields. To extend the theory to horizontal sources, no knowledge of the wavefield decomposition is needed. The elaborate dyadic analysis used previously is avoided too. The theory is extended to horizontal sources by applying the equivalent source concept. The horizontal source is first replaced by the equivalent vertical source and its known vertical image is finally replaced by an equivalent horizontal image. Thus, all that is needed for the construction of the image of a horizontal source is the expression for the image of a vertical source and the equivalence theorem. The assumption of slight chirality is still valid. However, when the image problem of vertical electric and magnetic dipoles has been solved for unrestricted chirality parameter values, the present method can be applied again to finding the image of horizontal dipoles.

B25.7

TREATMENT OF CHIRAL PROPERTY BY CONDENSED NODE SPATIAL NETWORK FOR VECTOR POTENTIAL

Norinobu Yoshida
Department of Electronics and Information Engineering
Hokkaido University, Sapporo 060 Japan

I have already proposed the treatment of dispersive and gyro-anisotropic properties in the Spatial Network Method of the condensed node for the vector potential [N.Yoshida; "Treatment of Gyro-anisotropic Properties in Spatial Network for Vector Potential," 1996 URSI Digest of Radio Science Meeting, pp.210]. The formulation of the chiral property is difficult in the expanded node time-dependent expression because of both the coupling properties between the electric and magnetic fields and the characteristic equation given by the steady state condition. But in the condensed node expression for the vector potential, the property is formulated easily by mutual equivalent conductances as follows.

The chiral property is given as follows;

$$\mathbf{D} = [\varepsilon]\,\mathbf{E} - j\,[\kappa]\,\mathbf{H} \qquad (1a), \qquad \mathbf{B} = [\mu]\,\mathbf{H} + j\,[\kappa]\,\mathbf{E} \qquad (1b)$$

On the other hand, for the dielectric medium with the conductive loss, the following relation is given;

$$\mathbf{D} = \varepsilon\,\mathbf{E} - j\frac{\sigma}{\omega}\mathbf{E} \;\rightleftarrows\; \varepsilon\,\mathbf{E} + \sigma\int \mathbf{E}\,dt \Rightarrow \varepsilon_0(1+\chi_e)\,\mathbf{E} + \sigma\,\Sigma\,\mathbf{E}\Delta t \qquad (2)$$

Equ. (1a) is rewritten as follows for the vector potential expression by using the relation between electric vector potential $\mathbf{S}$ and magnetic field $\mathbf{H}$; $\mathbf{H} = \partial\mathbf{S}/\partial t$. The equivalent circuit, for example, for scalar ε and κ is shown in Fig. 1.

$$\mathbf{D} = -[\varepsilon]\frac{\partial \mathbf{A}}{\partial t} + \frac{[\kappa]}{\Delta t}\,\mathbf{S} \;\Rightarrow\; \varepsilon_0(1+[\chi_e])\,\mathbf{E} + \frac{[\kappa]}{\Delta t}\,\Sigma\,\mathbf{H}\Delta t \qquad (3)$$

Each right hand side in equs. (2) and (3) corresponds to the finite difference forms in the numerical computation, respectively. From the analogy to that in equ. (2), the $[k]/\Delta t$ is considered as the equivalent mutual conductance between the magnetic vector potential and the electric vector potential nodes. The similar formulation can be obtained for equ.(1b). The result for an example problem is shown in Fig. 2.

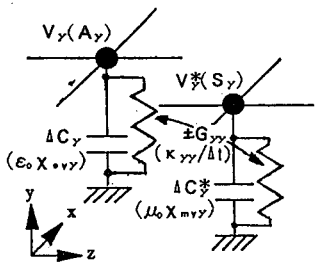

Fig.1 Equivalent Circuit of Chirality for y-Components in the Condensed Node.

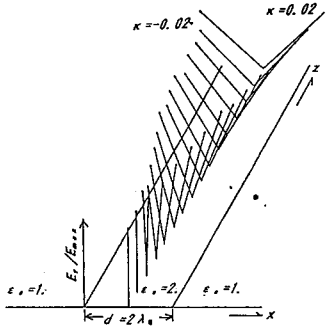

Fig.2 Rotation of Polarized Plane of Ey Vector in Chiral Media Slab.

Artificial non-reciprocal magnetoelectric composites

S.A. Tretyakov*, S.V. Zagriadski, A.A. Sochava, T.G. Kharina, D.Ya. Khaliullin

St. Petersburg State Technical University, Radiophysics Department
195251, St. Petersburg, Russia

Recently, E. Kamentskii put forward an idea of using magnetostatic wave (MSW) resonators to manufacture artificial bi-anisotropic materials (E. Kamenetskii, Microw. and Optical Technol. Lett., 11, 103-107, 1996).

Based on the Onsager-Casimir principle, we show that the suggested material is a non-reciprocal bi-anisotropic medium, similar to natural magnetoelectric crystals in its electromagnetic properties. Thus, the use of this technology possibly opens a possibility to create artificial non-reciprocal media for microwave applications (as using metal spirals it is possible to manufacture artificial chiral materials). The constitutive relations modelling the novel composites can be written as

$$\overline{D} = \overline{\overline{\varepsilon}} \cdot \overline{E} + \overline{\overline{\alpha}} \cdot \overline{H} \qquad \overline{B} = \overline{\overline{\mu}} \cdot \overline{H} + \overline{\overline{\alpha}}^{T} \cdot \overline{E}$$

where T denotes the transposed dyadics. The parameters are (frequency-dependent) dyadics. Note that both the coupling terms come with the same sign, in contrast to the case of reciprocal composites. Considered material is non-chiral (as is obvious from its geometrical structure).

We start from the question of practical realizability of the concept. For that purpose we estimate the magnetoelectric coefficient of a single MSW inclusion, assuming realistic sizes and ferrite film parameters. It appears that although the coupling efficiency is considerably weaker compared to reciprocal composites with metal inclusions (such as artificial chiral media), the effect is realizable.

Next, we consider plane waves in the uniaxial modification of the MSW composite (when the material parameters in the constitutive relations are uniaxial dyadics). This case can be realized with two orthogonal sets of MSW inclusions. Eigenwaves are seen to be linearly polarized. Looking at the properties of waves travelling in the opposite directions we find that their wave impedances are identical, but the propagation factors are different. This resembles reciprocal uniaxial omega composites (S.A. Tretyakov and A.A. Sochava, Electron. Lett., 29, 1048-1049, 1993) where the situation is the opposite: the impedances are "non-symmetric", but the propagation factors are the same.

These properties lead to interesting (non-reciprocal) features seen in reflection and transmission through plane layers of uniaxial composites. In particular, two important effects take place. The transmission coefficient is different for the opposite propagation directions (and different polarizations). Wave polarization changes as the wave crosses an MSW-layer. Both the effects are controlled by the external magnetic bias field.

B25.9

Electromagnetic Scattering and Diffraction Problems by Chiral and Biisotropic Bodies of Complicated Shape

F.G.Bogdanov, D.D.Karkashadze, R.S.Zaridze, R.G.Jobava

Laboratory of Applied Electrodynamics, Tbilisi State University
3, Chavchavadze Ave., 380028 Tbilisi, Georgia
Tel: +995-32 290821, Fax: +995-32 290845, e-mail: lae@resonan.ge

The problems of scattering and diffraction of electromagnetic waves by the bodies made of complex materials, such as chiral, biisotropic etc., are the subject of interest of numerous researchers due to characteristic properties of such materials producing the ample scope for potential applications. In this paper a uniform approach, efficient for solving of chiral and biisotropic problems for the bodies of complicated shape and for up to the rather high wavenumbers is developed. The given approach is based on the Method of Auxiliary Sources (R.Zaridze-Popovidi, Z.Tsverikmazashvili. Journal of Applied Mathematics and Mathematical Physics, No.7, Moscow, 1977, R. Zaridze, D. Karkashadze, etc., Radiotechnics and Electronics, Vol. 22, No.2, Moscow, 1978., D.Karkashadze, R.Zaridze. Latsis Symposium, Zurich, 163-180, 1995) and on generalization of one original method of solving of wave equation (H.Bateman. The Mathematical Analysis of Electrical and Optical Wave-Motion on the Basis of Maxwell's equations. Dover Publications Ing., 1955). This approach is suitable for any operator $\Im$ of wave equation and any kind of incident wave $\vec{U}_0(\vec{r})$.

The developed approach is based on the representation of the scattered field $\vec{U}(\vec{r})$ in each medium as the series of fundamental solutions of wave equation $\Im\,\vec{U}(\vec{r}) = 0$: $\vec{U}(\vec{r}) = \sum a_n \vec{F}_n(\vec{r}, \vec{r}'_n)$. The kind of basis functions is determined by the kind of wave operator $\Im$: so, in chiral and biisotropic media these functions are found as fundamental solutions of set of equations $\vec{\nabla} \times \vec{F}_n^{\pm} \mp k_{\pm}\vec{F}_n^{\pm} = 0$, $\vec{\nabla} \cdot \vec{F}_n^{\pm} = 0$ for different wavenumbers $k_{\pm}$. The coefficients a_n of series are interpreted physically as amplitudes of auxiliary sources and are found from boundary conditions by using of collocation method. The location of the auxiliary sources is connected with the sites of the main singularities of scattered field and is determined by the geometry of the problem, electrodynamic properties of media and excitation type.

On the basis of the created approach the two- and three-dimensional scattering and diffraction problems for the bodies of complicated shape and various electrodynamic properties at different excitation types are investigated and analyzed. The electrodynamic characteristics of far and near fields are computed, and the distinctive properties of different cases are detected and discussed The comparison of the obtained results with published data is conducted, and the efficiency of the developed approach is shown. The program complex for modeling and visualization of electromagnetic processes in the media with inhomogeneities of complicated shape and complex electromagnetic properties is designed and described.

Excitation of the electromagnetic waves by a current placed on chiral layer surface

S. L. Prosvirnin **A. E. Shepilko**

Institute of Radioastronomy of the Ukrainian National Academy of Sciences, Kharkov, Ukraine

SUMMARY In the presented study the problem of excitation of the electromagnetic waves by a 1-D current placed on a plane surface of the isotropic chiral layer is considered.

The solution is expressed in terms of the spectral Fourier-amplitudes of a radiated field in above-layer, in-layer, and below-layer regions and is represented by a continuous plane electromagnetic waves spectrum.

Using the Poisson's sum-formula the solution was extended on the case of a system of the periodically arranged currents placed on the chiral layer surface. In this case the electromagnetic field is represented by a discrete space-harmonics spectrum. Thus the spectral closed-form representation of the 2-D "periodical" Green's function was obtained.

The amplitude, phase, and polarization characteristics of the radiated field was analysed numerically. It was found out that in the case of synphase periodical excitation by system of longitudinal currents the zeroth harmonic of the radiated field is linearly polarized, so that in above-layer region the radiated field vector $\boldsymbol{E}$ is parallel to the currents direction, but in below-layer region it is rotated from it on a positive angle, magnitude of which depends on both a chirality parameter value and a relative layer thickness value.

The higher-order propagating harmonics have in general an elliptical polarization in both above-layer and below-layer regions. Polarization plane of the different harmonics may be rotated in different directions, but last ones prove to be opposite in above-layer and below-layer regions resp. for each harmonic propagated.

The results obtained in the presented work may be useful for the antennas theory and for analysis of more complicated problems, such as the problems of electromagnetic wave diffraction on perfectly conducting screens and periodical structures in chiral media.

URSI B | Session 27 | Salon Harricana

Classical Problems in Electromagnetics
Co-chairs: S. Babu, India and A. Lakhtakia, USA

13:10	27.1	Alternative Spectral Expansions for Sources in the Presence of a Dielectric Half Space, **B.A. BAERTLEIN**, *Ohio State University, Columbus, OH, USA*
13:30	27.2	Accuracy of King's Approximate Formulas for the Electromagnetic Fields Due to Electric Dipoles in the Presence of a Conducting Half-Space, **R. CHAITANYA BABU**, *University of Manitoba, Winnipeg, MB, Canada*
13:50	27.3	The Fikioris Approach for Source-Region Fields in an Uniaxial Dielectric-Magnetic Medium, **A. LAKHTAKIA**[1], W.S. WEIGLHOFER[2], [1]*Pennsylvania State University, University Park, PA, USA;* [2]*University of Glasgow, UK*
14:10	27.4	An Idea for Electromagnetic FeedForward/FeedBackward Media: I. Plane Wave Propagation in the Axial Direction, **C.A. MOSES**, N. ENGHETA, *University of Pennyslvania, Philadelphia, PA, USA*
14:30	27.5	General Formulas of Electromagnetic Fields Generated by a Horizontal Dipole in Arbitrarily Multilayered Dielectric Media, **K. LI**, *The University of Electro-communications, Tokyo, Japan*
14:50	27.6	On the Reciprocity Theorems for the Wave Scattering by Localized Discontinuities in Layered Dielectric Media, **A. ANDRENKO**, *Tokyo Institute of Technology, Tokyo, Japan*
15:10		Coffee Break
15:30	27.7	Double Excitation of Surface Plasmons at Uniaxial-Metal-Isotropic Films, R.A. DEPINE, **M.L. GIGLI**, *Universidad de Buenos Aires, Argentina*
15:50	27.8	New Translational Addition Theorems for Prolate Spheroidal Wave Functions, **T. DO-NHAT**, *Nhatrang, Vietnam*
16:10	27.9	Exact Solution for Electromagnetic Field Transformation in Medium with Time-Splashing Conductivity, **I.Yu. VORGUL**, *Kharkov State University, Kharkov, Ukraine*
16:30	27.10	On the Rigorous Theory of the Open Concentric Resonators, **E.D. VINOGRADOVA**, *Institute of Radiophysics and Electronics, NAS, Kharkov, Ukraine*
16:50	27.11	Equivalence between Physical Optics and Aperture Integration for Antenna and Scattering Problems, **S. MACI**[1], R. TIBERIO[2], P.Ya. UFIMTSEV[3], [1]*University of Florence and* [2]*University of Siena, Italy;* [3]*University of California at Los Angeles, CA, USA*

B27.1

Alternative Spectral Expansions for Sources In the Presence of a Dielectric Half Space

Brian A. Baertlein, ElectroScience Laboratory, Ohio State University
1320 Kinnear Road, Columbus, OH 43212

New spectral expansions are derived for sources over and in a homogeneous dielectric half space. The classical approach to problems of this kind, first used by Sommerfeld, involves a spectral expansion in the coordinates transverse to the interface and a closed-form (transmission-line like) formulation in the coordinate normal to the interface. Such a formulation is equivalent to treating space as a waveguide of unbounded homogeneous cross section with the "axial" direction normal to the interface. In the present work we treat the dielectric half space as an inhomogeneous waveguide of unbounded cross section by taking the direction of propagation transverse to the interface. This formulation is useful in treating scattering and radiation by planar structures oriented normal to the interface. To date, such problems have been treated either numerically or through approximations involving the impedance boundary condition.

Transforms associated with the new representations are defined and their properties are described. These transforms have the property of converting ordinary differential equations defined on regions with piecewise-constant media to algebraic equations. The presence of loss in the half space leads to operators which are not formally self-adjoint, and this fact significantly complicates the theoretical work. The problem is approached by using prior results for spectral expansions of non-self-adjoint operators on a bounded domain. By taking appropriate limits we obtain the expansion for the unbounded case. The relation of this work to results presented previously (L. B. Felsen and N. Marcuvitz, *Radiation and Scattering of Waves*, 1973) is discussed. To illustrate the use of the new representations we derive two and three-dimensional Green's functions for a variety of sources.

Accuracy of King's Approximate Formulas for the Electromagnetic Fields Due to Electric Dipoles in the Presence of a Conducting Half-Space

R. Chaitanya Babu

Department of Electrical and Computer Engineering
University of Manitoba,
Winnipeg, Manitoba R3T 5V6, Canada

Recently, in a series of papers, R. W. P. King and coworkers have reported simple approximate formulas for the electromagnetic fields due to electric dipoles radiating in the presence of a conducting half-space (Ref: R. W. P. King et al "Lateral Electromagnetic Waves", New York, Springer-Verlag, 1992). These formulas are derived subject to the approximation that, for $|k_1|^2 \gg |k_2|^2$ or $|k_1| > 3k_2$, significant contributions to the Sommerfeld-type integrals occur when the integration variable is of the order of k_2 (k_1 and k_2 are the wavenumbers in the lossy half-space and air respectively).

The purpose of this work is to investigate the accuracy of the formulas due to King et al for the fields of vertical and horizontal electric dipoles kept near a conducting half-space. This is conducted by making comparisons of the field strengths obtained from the approximate formulas with those from the direct numerical evaluation of the Sommerfeld-type integrals over a wide range of parameters. It will be shown that the above approximation is valid only for observation distances which are, typically, more than three times the skin depth in the conducting medium. However, in cases where the surface wave field is insignificant compared to the sum of direct and image fields, the formulas of King et al are seen to be accurate. Comparisons of the fields from the numerical evaluation of the integrals, King's formulas, and the quasi-static expressions will be presented.

B27.3

THE FIKIORIS APPROACH FOR SOURCE-REGION FIELDS IN AN UNIAXIAL DIELECTRIC-MAGNETIC MEDIUM

Akhlesh Lakhtakia

Department of Engineering Science and Mechanics

Pennsylvania State University, University Park, PA 16802-1401, USA

Werner S Weiglhofer

Department of Mathematics

University of Glasgow, Glasgow G12 8QW, Scotland, UK

Abstract

The time-harmonic electromagnetic field in an uniaxial dielectric-magnetic medium with constitutive relations

$$\mathbf{D}(\mathbf{r}) = \varepsilon_0 \underline{\underline{\varepsilon}}_r \bullet \mathbf{E}(\mathbf{r}) = \varepsilon_0 \left[\varepsilon_t \left(\underline{\underline{I}} - \mathbf{cc}\right) + \varepsilon_c \, \mathbf{cc}\right] \bullet \mathbf{E}(\mathbf{r}) \tag{1a}$$

$$\mathbf{B}(\mathbf{r}) = \mu_0 \underline{\underline{\mu}}_r \bullet \mathbf{H}(\mathbf{r}) = \mu_0 \left[\mu_t \left(\underline{\underline{I}} - \mathbf{cc}\right) + \mu_c \, \mathbf{cc}\right] \bullet \mathbf{H}(\mathbf{r}), \tag{1b}$$

is considered. Specifically, using the approach of Fikioris, expressions to estimate the electromagnetic field in a source region are obtained. Both the long-wavelength and the Rayleigh estimates are delineated; whereas the former are dependent on the shape as well as the size of an exclusion region, the latter depend only on the shape of the exclusion region. The derived results are specialized for an electrically small source region of arbitrary convex shape, and detailed calculations are presented for spherical exclusion regions to elucidate the role of anisotropy. Aciculate and cubical exclusion regions are also considered. Extension is made to all homogeneous media that are affinely equivalent to the uniaxial dielectric-magnetic medium (1a,b). The obtained results may be applied for scattering by an electrically small object as well as for the homogenization of particulate composites.

An Idea for Electromagnetic FeedForward/FeedBackward Media I. Plane Wave Propagation in the Axial Direction

C. A. Moses* and N. Engheta
Moore School of Electrical Engineering
University of Pennsylvania, Philadelphia, PA 19104

In recent years studies of the electromagnetic theory of complex media have gained considerable interest, particularly in regard to synthetically constructing such media by means of artificial materials. Here we present some of our theoretical work in analyzing the electromagnetic properties of a class of complex media that we name *FeedForward/FeedBackward* (FF/FB) media. The concept of FF/FB media was inspired by the research of *Saadoun and Engheta* [(1994), "Theoretical study of electromagnetic properties of non-local Ω media," in *Progress in Electromagnetic Research (PIER)* Monograph Series Vol. 9 on Bianisotropic and Bi-Isotropic Media and Applications, A. Pirou (Ed.), Chp. 15, pp. 351–397. EMW Publishing.] on a variation of artificial chiral media. Like chiral and Ω media, to our knowledge there are no *naturally occuring* FF/FB media for the *microwave* frequency band; for this reason we introduce an idea for artificial FF/FB media.

An artificial FF/FB medium can be conceptually proposed as follows: first, as in conventional artificial material, we would randomly distribute many electrically small conducting objects throughout some host dielectric; for example, in Figure (a) the pyramids represent generic inclusions with some fixed orientation. Then, as shown in Figure (b), we would conceptually link every inclusion to one other inclusion some fixed distance away. This link can be effected by means of a *tiny transmission line* (similar to the one proposed by Saadoun and Engheta). The connection between a tiny transmission line and an end-inclusion can be made by physically splitting the end-inclusion into two separate parts and connecting each of the two wires of the tiny transmission line to a different part. In this way, each end-inclusion acts like a small antenna and is influenced not only by the electromagnetic fields interacting directly with that inclusion, but also by the electromagnetic fields interacting with the opposite end-inclusion. The name *FeedForward/FeedBackward (FF/FB)* is meant to convey the notion that the medium samples the field at every *macroscopic* point and carries the effect of that sample forward and backward (in space) to induce polarization and/or magnetization at some displaced point, analogous to the feedback concept of lumped (or distributed) circuits.

In this theoretical study, we consider a special case of artificial FF/FB media in which the paired inclusions are short dipoles oriented perpendicularly to each other and to the connecting tiny transmission line (*Crossed-Dipole FF/FB* media). This medium is theoretically investigated by accounting for the effects of the inclusions through nonlocal constitutive relations (taking into account Lorentz theory) and then by solving the macroscopic Maxwell equations in the k domain. We present the dispersion equation for this medium and discuss the physical properties of its roots and their corresponding polarization eigenstates. Physical remarks and justifications of the findings are also discussed.

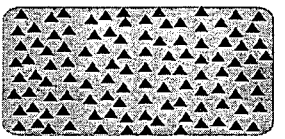

(a) Conventional artificial material

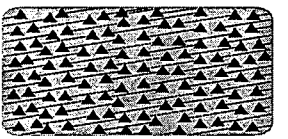

(b) An idea for artificial FF/FB media

B27.5

General Formulas of Electromagenetic Fields Generated by a Horizontal Dipole in Arbitrarily Multilayered Dielectric Media

Keren Li
The University of Electro-communications
1-5-1 Chofugaoka, Chofu-shi, Tokyo 182, Japan
Tel/Fax : +81-424-81-5713, E-mail: keren@light.ee.uec.ac.jp

Finding electromagnetic fields in a multilayered dielectric structure is a very tedious work for any specified number of layers. Fortunately, we discovered that by re-expressing the fields in two potentials introduced by Harrington (Harrington, "Time-harmonic electromagnetic fields," McGraw-Hill, New York, 1961), which are corresponding to two electromagnetic modes, transverse magnetic and transverse electric modes to the normal direction of the layer plane, the potentials and then the fields can be found in closed-form. This paper presents the general formulas of the potentials generated by a horizontal dipole in arbitrarily multilayered dielectric media.

Figure 1 shows a multilayered structure which consists of L isotropic dielectric layers with electric parameters ε_i (i = 1, 2, ..., L) and perfectly conducting ground conductors. The source point and the observation point are placed in jth and ith layer and denoted by (x_0, y_0) and (x, y), respectively. The source is a horizontal dipole. Coordinate systems are built in each local layer for convenience of analysis.

Denoting the two scalar potentials as ϕ^e and ϕ^h corresponding to TM-to-y and TE-to-y modes, and using their Fourier transform

$$\tilde{\phi}(\alpha, \beta) = \int_{-\infty}^{\infty} \phi(x, y)\, e^{j(\alpha x + \beta y)}\, dx$$

we obtain general closed-form formulas for the potentials as following.

$$\tilde{\phi}_{ij}^{m}(\bar{y}, \bar{y}_0) = \frac{j\tilde{s}_m}{\Delta_m} \begin{cases} \Delta_m^{i+}(\bar{h}_i - \bar{y})\, \Delta_m^{j-}(\bar{y}_0) \\ \quad i > j \text{ or } i = j,\ y \geq y_0 \\ \Delta_m^{i-}(\bar{y})\, \Delta_m^{j+}(\bar{h}_j - \bar{y}_0) \\ \quad i < j \text{ or } i = j,\ y \leq y_0 \end{cases}$$

where, $m = e, h$

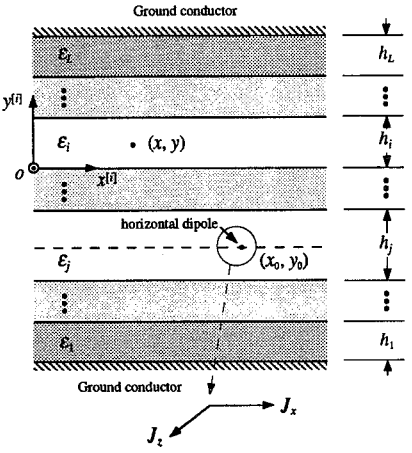

Fig. 1 Multilayered structure with a horizontal dipole

$$-\gamma_i^2 = k_i^2 - \alpha^2 - \beta^2,\ Y_i = j\gamma_i/\omega\mu_i$$

$$\tilde{s}_e = \frac{1}{\alpha^2 + \beta^2}\left(-\alpha \tilde{J}_x + \beta \tilde{J}_z\right)$$

$$\tilde{s}_h = \frac{1}{\alpha^2 + \beta^2}\left(\beta \tilde{J}_x + \alpha \tilde{J}_z\right)$$

$$\bar{h}_i = \gamma_i h_i,\ \ i = 1, 2, \cdots, L,\ \bar{y} = \gamma_i y,\ \ \bar{y}_0 = \gamma_i y_0$$

$$\Delta_m = \Delta_m\left(\bar{h}_1, \bar{h}_2, \cdots, \bar{h}_L\right)$$

$$\Delta_m^{i+}(\bar{y}) = \Delta_m\left(0, 0, \cdots, \bar{y}, \overline{h_{i+1}}, \cdots, \bar{h}_L\right)$$

$$\Delta_m^{i-}(\bar{y}) = \Delta_m\left(\bar{h}_1, \bar{h}_2, \cdots, \overline{h_{i-1}}, \bar{y}, 0, \cdots, 0\right)$$

$$\Delta(z_1, z_2, \cdots, z_L) = \prod_{k=1}^{L}\frac{1}{Y_k} \cdot \prod_{k=1}^{L-1}\left(Y_k \frac{\partial}{\partial z_k} + Y_{k+1}\frac{\partial}{\partial z_{k+1}}\right) \cdot \prod_{k=1}^{L} \sinh z_k$$

These formulas hold for any number of layers and are generated from a simple function.

On The Reciprocity Theorems For The Wave Scattering By Localized Discontinuities In Layered Dielectric Media

Andrey Andrenko
Dept. of Electrical and Electronic Engineering
Tokyo Institute of Technology
2-12-1 O-okayama, Meguro-ku, Tokyo 152, Japan

The well-known optical theorems and reciprocity relations give the general aspects of the electromagnetic scattering problems and, at the same time, play the role of independent tests of the correctness of numerical solutions. In particular, the need to obtain such an independent check becomes very important when a solution to the canonical problem is not available as in the case of wave scattering by arbitrary shaped obstacles or screens imbedded in a layered medium. The derivation of the optical theorems for the wave scattering from obstacles in layered media has been reported in (P.G. Petropoulos and G.A. Kriegsmann, IEEE Trans. Antennas Propagat., vol. 39, .8, 1119-1124, 1991) and since an optical theorem provides a necessary, but not sufficient condition that must validate a numerical calculation, the accurate analysis should be completed with the reciprocity theorem (A.S. Andrenko, A.I. Nosich, and V.P. Shestopalov, Sov. Phys. Dokl., 35, .4, 366-368, 1990).

The purpose of this paper is to present the general derivation of two-dimensional reciprocity theorems for the problems of wave scattering by localized irregularities in layered media such as grounded dielectric slab and multilayered dielectric guide. The scattering of both slab's guided modes and plane wave or cylindrical wave incident from surrounding free half-space has been studied. The analysis is based on the application of Green's formula to the pair of functions describing the total fields in the cases of wave incidence in two different directions. Considering the scattering of guided modes, we obtain the simple formula connecting the amplitudes of transmitted modes but not reflected ones and field of radiation. In particular, for any inhomogeneity having a symmetry plane the transmission coefficient of the incident wave is invariant under the sign of angle of this plane with respect to the plane of slab's cross section, although the remaining energy distributes between the radiation field and all other slab's modes in a different way.

In the analysis of cylindrical wave scattering from an arbitrary inhomogeneity imbedded in a grounded dielectric guide, we arrive at the statement of the reciprocity theorem which enables one to obtain the correspondence between the amplitude of coupled guided mode due to the scattering of space wave and the directivity of outgoing radiation field produced by the incident slab's guided mode. As the example useful for the modeling of open guide's excitation, we can estimate the optimal cylindrical-to-guided wave coupling efficiency of the finite periodic grating couplers, i.e. the direction of incident wave providing the maximum amplitude of the excited guided mode, without the solving of above-mentioned diffraction problem but using the results of alternative problem of guided mode scattering and conversion by the same inhomogeneity. In both cases, the reciprocity theorem serves as the independent check for the confidence in the numerical data.

B27.7

Double excitation of surface plasmons at uniaxial-metal-isotropic films

Ricardo A. Depine and Miriam L. Gigli, Grupo de Electromagnetismo Aplicado, Departamento de Fisica, Facultad de Ciencias Exactas y Naturales, Universidad de Buenos Aires, Ciudad Universitaria, Pabellón I, (1428) Buenos Aires, Argentina

We perform a theoretical study about the interaction between light and surface plasmons at metallic films that separate a negative uniaxial crystal from an isotropic medium. Depending on the angle of incidence, an incident wave (from the crystal side) can excite two different surface modes in these structures: one at each interface. We show that tuning film parameters, the angles of incidence for which these different excitations occur can be near enough as to have almost simultaneous excitation.

To do so, first we study the homogeneous scattering problem (R. Petit, ed., *Electromagnetic theory of gratings*, Heidelberg: Springer, 1980) for the film. Solutions to this problem exist if the determinant of the inverse of the 2x2 reflection matrix R is zero. This condition holds only for certain values of the tangential components of the wavevectors $\alpha_0 = \alpha_0^p$ (poles of the reflection matrix). In this work we have found constitutive parameters for which there are two values of the propagation constant α_0^p; one of them is associated to a single uniaxial-metal interface (α_{01}^p) and the other is related to a single metal-dielectric interface (α_{02}^p). The first mode exists only for certain orientations of the optic axis $\hat{c}$, and the real part of its propagation constant is located in a region where only ordinary waves can propagate (R. A. Depine and M. L. Gigli, Optics Letters v. 20, 2243-2245, 1995). We show that the relative position of these poles in the complex plane depend on the refractive index of the substrate and that this value can be tuned as to have $\mathrm{Re}(\alpha_{01}^p) \approx \mathrm{Re}(\alpha_{02}^p)$. Thus, each surface mode can be excited by an incident *ordinary* wave, with a (real) propagation constant $\alpha_0 \approx \mathrm{Re}(\alpha_{0j}^p)$. This excitation is accompanied by an increase of the power absorbed by the film. The excitation of surface modes can be optimized for values of the propagation constant that verify the condition: $R_{11} = 0$, for which the ordinary reflected amplitud is zero. For critical parameters (for example, for a critical value of the film width ℓ) the later condition can be verified for real values of α_0, and so, there will be no reflected energy if an ordinary wave is incident with that propagation constant. This phenomenon is illustrated in Figure 1, where we plot the reflected energy as a function of α_0/k_0 ($k_0 = 2\pi / \lambda_0$ is the wave number in vacuum), for several film widths. For each curve, two narrow peaks can be observed due to the excitation of surface modes. For example, if $\ell / \lambda_0 = 0.11$, almost all the power is absorbed at $\alpha_0/k_0 = 1.42$ and $\alpha_0/k_0 = 1.44$.

The variation of the components of the fields along the direction normal to the interfaces have also been studied. We found that the electromagnetic field is enhanced on the two surfaces at angles of incidence near the resonances.

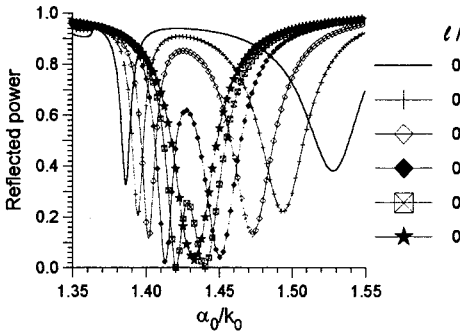

Figure 1. Reflected power vs. α_0/k_0, for different film widths ℓ. The ordinary wave is incident from sodium nitrate ($n_o = 1.584$, $n_e = 1.336$) onto a metallic film (gold, $n_m = 0.15 + 4.65\,i$ at $l_0 = 800$ nm). The refractive index of the isotropic substrate is $n_i = 1.3638$. The angle between the optic axis $\hat{c}$ and the normal to the interface is 14°, and the projection of $\hat{c}$ onto the interface forms an angle of 45° with the plane of incidence.

New Translational Addition Theorems for Prolate Spheroidal Wave Functions

Dr. Tam Do-Nhat[1], 7 Ngo Si Lien Nhatrang, Vietnam.

Summary

The conventional addition theorems applied to incoming and outgoing spheroidal waves, developed by Dalmas, Deleuil, Sinha and MacPhie [Quart. Appl. Math., 44, 1987, 737-749] possess a property of having convergence spheres which, in some cases, may meet the spheroid's surface. This limits the application of many interesting electromagnetic problems in Physics and Engineering such as the scattering of an array of thin prolate spheroids closely spaced. In the new approach the prolate scalar wave functions are first transformed into the complete set of a spectrum of cylindrical wave functions of correct types. These spectral densities are evaluated in closed forms by considering either the far field condition or the near field condition [T. Do-Nhat and R. H. MacPhie, Quart. Appl. Math., 55, 1996, 677-685] of the prolate scalar wave functions. The next step is to use the well known translational addition theorems for these cylindrical wave functions to represent the spheroidal wave in another coordinate system. In the final step, by using the orthogonality properties of the angle spheroidal functions related to the new coordinate system, the cylindrical wave functions are transformed back to the spheroidal wave functions of the new system. By utilizing the procedures outlined above, the new translational addition theorems are derived. In particular, for thin spheroids these theorems exhibit a rapidly convergent series for fields of *any type* on the translated spheroid's surface.

[1] Mailing Address: 1210-812 King Street W., Kitchener, Ontario, Canada, N2G 1E9; email: tdonhat@golden.net

B27.9

Exact solution for electromagnetic field transformation in medium with time-splashing conductivity

I.Yu.Vorgul
Applied Electrodynamics Dept., Kharkov State University,
4 Svoboda Sq., Kharkov, 310077 Ukraine

Time-varying electrodynamic properties, in particular media conductivity, take place as a result of atmospheric fluctuations, environmental changes or can be specially created, for example, in some types of semiconductors. In this work one considers the case of time-splashing conductivity as, for example, atmospheric or capacitor discharges. Mathematically the conductivity time-dependence law is considered as difference of reducing exponents.

In previous works on field transformation in transient media, except abrupt conductivity time-changes, the problems usually were solved numerically or approximately. Exact solutions could have some advantages allowing to carry out a qualitative analysis of physical processes here and more detail quantitative analisis as well.

One has managed to obtaine the exact solution for electromagnetic field in the medium with the time-splashing conductivity when initial field (the field before the medium change) is a plane harmonic wave. Mathematically the problem was formulated as Rikkatti differential equation. The obtained solution has not a very complicated integral form.It can be calculated without principal difficulties for different parameters of the conductivity time-splashing and initial field frequencies. A theoretical analysis of this formula also is carried out. It can, particulary, point the time moments of maximal and minimal values of electrical component of the field for arbitrary values of the initial field frequency and the medium change parameters and consider the dependence of this extremal points number on these parameters.

ON THE RIGOROUS THEORY OF THE OPEN CONCENTRIC RESONATORS

E.D.Vinogradova
Institute of Radiophysics and Electronics,
12 Ac.Proskura st., Kharkov 310085, Ukraine

Introduction

The asymptotic methods are usually used to analyse the features of the open resonators (OR). It's well known that these methods not provide the accurate investigation of the electromagnetic field (EMF) polarization features and EMF distribution in the focal region of OR. The goal of this paper is to develop the rigorous approarch to analysis of a type of concentric OR composed from spherical and plane mirrors (Fig.1) and to evaluate the limits of the applicability of the asymptotic methods for diffraction and quasi-optic frequency ranges.

Problem definition

The wave diffraction problem is considered associated with a magnetic horizontal dipole exitation of the spherical mirror in the presence of an infinite plane. Due to coupling between the E- and H- types of waves the analysed problem is reduced to two coupled infinite matrix equation sets of the second kind by using the triple series approach and regularization method.

Numerical results

Based on the obtained solution a number of OR characteristics have been analyzed numerically from diffraction range to quasi-optics ($0.5 \le a/\lambda \le 50$). There are the radiation resistance, stored energy, Q - factor, EMF distribution in focal region. As example, in Fig.2 the frequency dependence Q is plotted (here Q is ratio of the stored energy to energy loss), for a case of dipole location on the plane mirror surface (b=0). Resonant spikes correspond to Q - factor of OR.

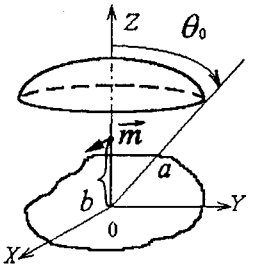

Fig. 1

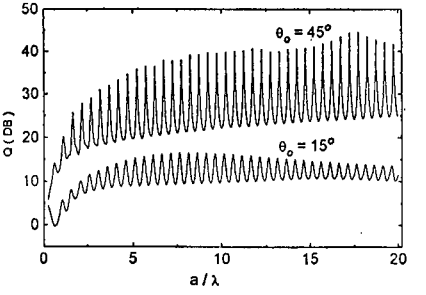

Fig. 2

The barrell-type OR can be studied by the similar way. The using of the addition theorems for the spherical wave functions makes it possible to investigate the confocal OR in the frames of presented approach.

B27.11

EQUIVALENCE BETWEEN PHYSICAL OPTICS AND APERTURE INTEGRATION FOR ANTENNA AND SCATTERING PROBLEMS

S. Maci[1], *R. Tiberio*[2], *P. Ya. Ufimtsev*[3]

[1] *Dep. of Elec. Eng., Univ. of Florence, Via S.Marta 3, Florence, Italy*
[2] *College of Eng., Univ. of Siena, Via Roma 77, 53100, Siena, Italy*
[3] *Electrical Eng. Dept., Univ. of California at Los Angeles, CA 90095-1594, USA*

In describing electromagnetic radiation and scattering in the high-frequency regime, two basic techniques are often used for their simplicity; i.e. the Kirchhoff-Kottler aperture integration (AI) and the physical optics (PO). Despite of their simplicity, these techniques are found accurate for most practical applications, also for moderate size of the radiating object. Although AI and PO approximations are very simple and well established techniques, the relationship between them has not yet been fully exploited in the literature. A rigorous relationship was established by Altintas *et al.* [*Radio-Sci,* No 6, 1994] for the scattering from a perfectly conducting half-plane, and by Oodo and Ando [*AP-S Symp.*, Baltimore, 1996] for metallic corners; also the same authors have performed a numerical investigation for reflector antennas.

Recently, the authors [*IEEE Trans. Antennas Propagat.* No. 1, 1997] have demonstrated the AI-PO equivalence for the radiation by an open-ended waveguide of arbitrary cross-section. In this paper, the above equivalence is extended to a class of radiation and scattering problems, provided that the PO currents are defined by using the modal field of the infinite canonical structure, whose surface partially superimposes with that of the actual radiating structure. Perfectly conducting corners and parabolic reflectors, open-ended waveguides, screens and other structures of practical interest undergo this equivalence. When the radius of curvature of the local perfectly conducting reflector is large in terms of a wavelength, the above definition of the PO currents tends to recover the ordinary definition in terms of the incident magnetic field.

The physical interpretation of this equivalence involving the classical theory of the black bodies is discussed, and its importance in the framework of incremental diffraction theories is investigated.

URSI B | Session 30 | Salon Marquette

Numerical Methods for Microstrip Antennas
Co-chairs: J. D'Angelo, USA and P. Bhartia, Canada

08:10	30.1	Comparison of Integral Equation and Finite Element Methods for the Analysis of Infinite Microstrip Antenna Arrays, J. D'ANGELO[1], **J. HERD**[2], K. OMMODT[3], [1]*Skyblue Systems, Troy, NY,* [2]*Rome Laboratory, Hanscom AFB, MA and* [3]*Texas Instruments, Dallas, TX, USA*
08:30	30.2	FDTD Analysis of Stacked Annular Patch Microstrip Antennas, **J. GOMEZ TAGLE**, C.G. CHRISTODOULOU, *University of Central Florida, Orlando, FL, USA*
08:50	30.3	Analysis of Staked Microstrip Patches Using Closed from Green's Functions, **A. BADAWI**, A.R. SEBAK, *University of Manitoba, Winnipeg, MB, Canada*
09:10	30.4	Radiation Efficiency of Ferrite Based Linear Microstrip Antenna Array Inside Plasma Medium, **S.S. PATTNAIK**, *University of Utah, Salt Lake City, UT, USA*
09:30	30.5	Dual Frequency Circularly-Polarized Electromagnetically-Fed Microstrip Antennas, A. HOORFAR[1], **A. PERROTTA**[2], [1]*Villanova University, Villanova, PA and* [2]*Motorola Inc., Plantation, FL, USA*
09:50	30.6	Effects of Mutual Coupling and Finite Dielectric Extent on Complex Resonant Frequency of Unbounded Regular and Irregular Microstrip Patch, **X. JIANG**, K. WU, *POLY-GRAMES Research Center, Montréal, QC, Canada*
10:10		Coffee Break
10:30	30.7	The Meander Loop Microstrip Antenna, **M.A. SAED**, *State University of New York at New Paltz, NY, USA*
10:50	30.8	Analysis of the Resonant Modes of Stacked Circular Microstrip Patches in Multilayered Anisotropic Media, V. LOSADA, R.R. BOIX, **M. HORNO**, *Universidad de Sevilla, Spain*
11:10	30.9	Analysis of Infinite Arrays of Probe-Fed Patches, **M. DAVIDOVITZ**[1], A. SOLOVEY[2], [1]*Rome Laboratory and* [2]*System Resources Corporation, Hanscom AFB, MA, USA*
11:30	30.10	Optimum Design of a Cross-Shaped Dual-Polarized Microstrip Patch Antenna, **A. TAVAKOLI**, B. MOHAMMADI, R. MOINI, *Amirkabir University of Technology (Tehran Polytechnic), Tehran, Iran*

B30.1

Comparison of Integral Equation and Finite Element Methods for the Analysis of Infinite Microstrip Antenna Arrays

John D'Angelo, Skyblue Systems, Troy, NY
Jeffrey Herd, Rome Laboratory, Hanscom AFB, MA
Kevin Ommodt, Texas Instruments, Dallas, TX

This paper will discuss the modeling of infinite microstrip antenna arrays with an integral equation method and with a finite element based method. A comparison of the two approaches on the same antenna geometry will be performed to distinguish the capabilities and limitations of each. Included in the comparison will be the man-time geometric modeling effort, the computational timing, and the accuracy against measurements.

The infinite array element used for comparison consists of two stacked patches. The lower patch is fed by four vertical coaxial probes to achieve balanced circular polarization, and the upper patch is capacitively coupled to the lower patch. This type of geometry gives a wider scanning bandwidth than a conventional patch antenna array.

The integral equation analysis uses the infinite array spectral dyadic Green's function for periodic electric current sources embedded in a multilayer grounded dielectric slab. The unknown current distribution on the patches is expanded in a set of basis functions, and a Galerkin method of moments is applied. The four feeding probes are modeled as idealized vertical electric current sources. The resultant patch currents are then used to calculate the 4x4 S-matrix of the feeds.

The finite element method consists of a high-order edge element formulation solving for the magnetic vector potential and the electric scalar potential. Coupled to the finite element method for the antenna feed are waveguide mode harmonics. These harmonics are used to excite the probe feed and to calculate the S-parameters. For the exterior region, the finite elements are coupled to a Floquet harmonic expansion. The Floquet modes model the periodic structure of the antenna and directly calculate the main and grating lobe modes.

A 9x9 array of the analyzed element geometry has been fabricated. The embedded radiation pattern of the central element has been measured as a function of frequency, with all surrounding elements terminated in matched loads. The measured results will be compared with the calculated results of the two analysis methods described above.

Measured data is from work supported by Air Force Rome Laboratory, Space and Missile Systems Center, and Materiel Command under contract F30602-95-C-0055.

FDTD ANALYSIS OF STACKED ANNULAR PATCH MICROSTRIP ANTENNAS

J. Gomez Tagle* and C. G. Christodoulou
Electrical and Computer Engineering Department
University of Central Florida
Orlando, FL. 32816

Abstract

The input impedance of stacked microstrip ring antennas is obtained using the three dimensional Finite Difference Time Domain Method. These antennas have been shown to be useful for mobile communications applications (J.C. Batchelor and R. J. Langley, "Microstrip Ring Antennas Operating at Higher Order Modes for Mobile Communications", *IEE Proc. H.*, vol. 142, no. 2, pp. 151-155, 1995).

Different feeding methods are analyzed, like the microstrip-line feed, the coaxial probe feed and a proximity coupling feed.

A staircase approximation is done for both the annular patches and the coaxial probe. A Gaussian pulse excitation is used to obtain the time samples of voltage and current and to predict the frequency response of the antennas. Mur's first order absorbing boundary conditions are utilized to truncate the solution region.

The return loss and input impedance are plotted for the various feeding techniques. The fields distributions are are displayed for several time steps. The results are compared with both experimental data and data obtained through other numerical techniques.

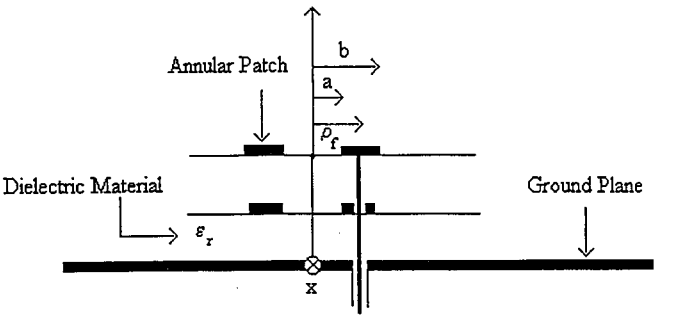

Fig. 1. Geometry of a stacked annular microstrip antenna

B30.3

Analysis of Staked Microstrip Patches Using Closed From Green's Functions

Ashraf Badawi and Abdel Razik Sebak
Department of Electrical and Computer Engineering
University of Manitoba
Winnipeg, Manitoba, Canada R3T 5V6

In analysing planar microstrip structures the method of moments (MoM) can be applied in spectral or spatial domain. The latter has the advantage that the integrands of the MoM matrix elements needs to be evaluated only over a finite range for the subsectional basis and testing functions. On the other hand it conventionally requires the evaluation of Sommerfeld type integrals, which is a computationally intensive operation and very time consuming.

A method that was recently developed (Y. L. Chow *et al.*, IEEE Trans. MTT-39, 588-592, 1991) drives asymptotic closed form expressions for the Green's function which decreases the time required to fill the MoM matrix by almost two orders of magnitude. The method was used for single layer patches and for a single layer with a superstrate. This technique is attractive because of its relative accuracy and capability to handle several layers of dielectric.

In this paper the derivation is extended to handle the multiple layers case. The quasi-static images and the surface wave poles are extracted from the integrand of the Sommerfeld inetgral. Their contribution is handled through the residue theorem. Next the remaining integrand is approximated via a set of complex exponentials through the generalized pencil of functions (GPOF) method. Once the Green's functions are calculated, the MoM solution proceeds normally using roof-top basis functions for the current cells and pulse type basis functions for the charge cells.

A number of cases are simulated to test the validity of the numerical code and compared well with published results (I. Park *et al.*, IEEE Trans. MTT-29, 394-400, 1995). The details of the derivation and numerical results for the different cases tested will be presented.

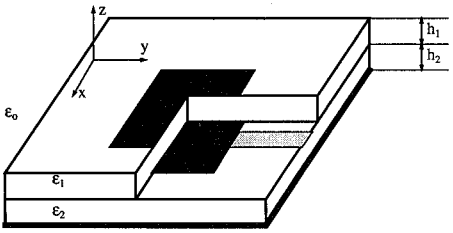

Fig. 1. Staked patch antenna configuration showing two dielectric layers and two conducting patches above an infinite ground plane

RADIATION EFFICIENCY OF FERRITE BASED LINEAR MICROSTRIP ANTENNA ARRAY INSIDE PLASMA MEDIUM

SHYAM S. PATTNAIK
ELECTRICAL ENGINEERING DEPARTMENT, UNIVERSITY OF UTAH,
3280 MEB, SALT LAKE CITY, UTAH-84112, U.S.A,
E-Mail: pattnaik@ee.utah.edu Fax: (801) 581-5281

ABSTRACT: Ferrite based microstrip antennas have emerged as a potential radiators due to their many attractive features.In the recent time,the ferrite based microstrip antenna arrays are having paramount significance due to growing demands on LEO sattellite communications.However,the satellite or space vehicle boarded antennas encounter plasma medium of different electron densities in their voyage.As has been reported,the antenna parameters such as resonant frequency,radiation efficiency,radiation patterns etc are altered by the presence of plasma medium.The effect is more severe when the plasma frequency is nearer to operating frequency of the antenna thus leading to the phenomenon of black-out.The radiation efficiency of all radiators including dielectric based microstrip antennas drops down in the region where plasma frequency is less than the operating frequency i.e plasma frequency to operating frequency ratio is less than one.In this paper an attempt is being made to study the radiation efficiency of a linear microstrip antenna array on ferrite substrarte inside plasma medium.Numerical simulations are carried out to see the radiation efficiency of this ferrite based linear array at different plasma frequencies a space vehicle suppose to encounter.Also theoretical expressions are derived for the radiated power of this linear array both in electromanetic mode and plasma mode.The variation of radiation conductance with different plasma to source frequency ratios are numerically calculated for both the modes i.e electromagnetic mode and plasma mode. Experimental measurements are carried out at three different plasma frequencies to validate the numerical results. The experimental results are in good agreement with numerical findings.

As has been shown in the figure,the radiation efficiency of ferrite based linear microstrip antenna array shows multi-resonance peaks even when the plasma to source frequency ratio(Fp/Fr) is less than one.This is in contrary to the results achieved so far for different radiators inside plasma medium.This result in conjuction with the suggested method of tuning and pattern control of ferrite based antenna (Pozar et al) can be gainfully exploited to achieve high efficiency and directive radiation pattern inside plasma medium.

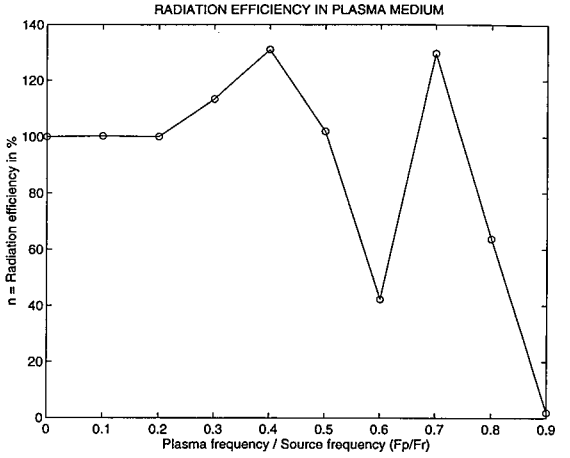

B30.5

DUAL FREQUENCY CIRCULARLY-POLARIZED ELECTROMAGNETICALLY-FED MICROSTRIP ANTENNAS

Ahmad Hoorfar
Dept. of Elec. & Comp. Eng.
Villanova University
Villanova, PA 19085

Alessandro Perrotta*
iDEN Subscriber Division
Motorola Inc.
Plantation, FL 33334

Many of the present and future satellite and wireless communication systems require low-profile, light weight and low cost circularly-polarized (CP) antennas. In addition some applications require dual frequency operation. Examples include GPS, regional mobile-sat arrays, large feed arrays for offset reflectors and other common transmit & receive antennas. Another important requirement for most of these applications is a low intermodulation distortion which demands minimum metal to metal contacts in feeding the radiating elements. In this presentation we discuss the design feasibility of multilayer stacked microstrip patch antennas to meet the aforementioned requirements.

We have developed several concepts for design of dual-band circular-polarized microstrip antennas. These concepts all use a three-layer structure in which two rectangular or circular patches resonant at two desired bands are located on top of the first and third dielectric layers, while the microstrip line feed is sandwiched between the two on top of the second layer. In one concept nearly square patches are electromagnetically fed either along their diagonal or off-diagonal by a single microstrip line. Alternatively, square patches with center slots and an off-diagonal feed can be used to generate CP. To achieve good match and low axial ratio at the two desired frequencies, the two radiating patches are first designed separately using a cavity model. A moment-method based simulation code is then used to model the entire three-layer structure. Relative locations of the patches are varied and/or small tuning tabs at the two sides of the square patches are added until good return loss and low axial ratio at the two desired frequencies are achieved. Preliminary simulation results, based on these concepts, for an antenna resonating at the two GPS frequencies of L1 and L2 show return losses of better than - 20 dB and broadside axial ratio of less than 2 dB. We are also presently studying an alternative configuration in which the microstrip line electromagnetically feeds the two sides of each patch via a cross-feed in order to provide the required 90° phase shift for a wider CP bandwidth. Again, the relative locations of the patches are optimized or tuning tabs are added for low axial ratios at both frequencies. Detailed simulation results on these designs as well as a parametric study of the effects of feed position on return loss and axial ratio at the two bands will be given in the presentation. In addition, measured data on some selected designs will be presented.

EFFECTS OF MUTUAL COUPLING AND FINITE DIELECTRIC EXTENT ON COMPLEX RESONANT FREQUENCY OF UNBOUNDED REGULAR AND IRREGULAR MICROSTRIP PATCH

*Xiaohong JIANG and Ke WU**

POLY-GRAMES Research Center
Dépt. de Génie Electrique et de Génie Informatique
École Polytechnique de Montréal
C.P. 6079, Succ. Centre-Ville, Montréal, Québec
Canada, H3C 3A7

* On leave from the above institution and currently with
Telecommunication Research Center
Department of Electronic Engineering, City University of Hong Kong
Tat Chee Avenue, Kowloon, Hong Kong

ABSTRACT

A field-theoretical model is presented for characterizing radiative electrical performance of a class of microstrip patches and patch arrays. The proposed model is based on the method of lines, allowing the consideration of regular and irregular patch geometries (see Fig. 1a and Fig. 1b) formed on dielectric substrate having a finite extent. Effects of mutual coupling of multiple patches and finite dielectric extent on complex resonant frequency are taken into account for these resonant structures in the model. An absorbing boundary condition with the Pade approximation is implemented in the proposed algorithm to simulate any potential radiation and leakage waves. Examples are shown for electrical characteristics of their complex resonant frequencies including a microstrip patch and two coupled patch resonators printed on finite dielectric substrates. The proposed model has been validated through comparison with the results available to date.

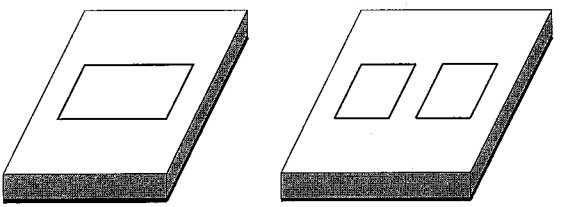

(a) (b)

Fig. 1 (a) Single microstrip patch on a finite dielectric substrate
(b) Two coupled patches on a finite dielectric substrate.

B30.7

THE MEANDER LOOP MICROSTRIP ANTENNA

Mohammad A. Saed
Department of Electrical Engineering
State University of New York at New Paltz
New Paltz, New York 12561

Microstrip antennas are low cost, low profile, light weight, and can be easily integrated. Such characteristics made them popular in many applications such as mobile communications, satellite communications, radar applications, and even quasi-optical power combining and amplification techniques. The most common microstrip antenna shapes are the rectangular, circular, and ring patches. These shapes have been extensively treated in the literature. For applications that use low microwave frequencies, the size of these conventional patches becomes large. This can be prohibitive if large arrays are to be used or if miniaturization is very important. In this paper, a novel microstrip antenna shape is proposed. It provides a significant size reduction over conventional patch shapes. The proposed shape is a "Meander Loop". It occupies an area less than half of that occupied by the ring, rectangular, or circular patch shapes operating at the same frequency. This is an important advantage since miniaturization is highly desirable, specially at the lower frequencies allocated for mobile communications.

The antenna can be fed using a microstrip line on the same side of the substrate, either gap-coupled or directly. It can also be fed using probe feeding, aperture coupling, or electromagnetic coupling. Like other microstrip patch shapes, it radiates linearly polarized waves. Circular polarization can be achieved by using a square loop with a small shape perturbation.

The proposed antenna with the various feeding mechanisms is analyzed using the Finite-Difference Time-Domain Method. The method is well known. It is based on discretizing the differential form of Ampere's law and Faraday's low using a second order finite difference approximation of the time and space derivatives. As a result, the whole structure is replaced with a mesh. Furthermore, the electric field components are displaced by a half step in time and space from the magnetic field components to enable computer implementation in a leap-frog time-stepping scheme. Results for radiation patterns, input impedance, and return loss for directly coupled, probe-fed, electromagnetically coupled, and aperture coupled meander loop antennas will be presented at the conference.

Analysis of the resonant modes of stacked circular microstrip patches in multilayered anisotropic media

Vicente Losada, Rafael R. Boix, Manuel Horno
Microwave Group, Dpt. of Electronics and Electromagnetism
Avda. Reina Mercedes s/n, 41012 Sevilla, Spain
E-mail losada@cica.es. Tph: #345 455 2891, Fax: #345 423 9434

Although microstrip patch antennas are widely used because of their low profile, light weight, low price, conformability, mass productivity, etc., these antennas suffer from narrow bandwidth. It is well known that the bandwidth of a microstrip patch antenna can be enlarged by stacking a parasitic patch above the antenna [A. N. Tulintseff. S. M. Ali, J. A. Kong, *IEEE-AP*, 39, 381–390, 1991]. This configuration of stacked microstrip patches can also be used in the design of dual–frequency operation antennas when the upper patch is fed through a clearance hole in the lower patch [S. Long, M. D. Walton, *IEEE-AP*, 27, 270–273, 1979]. In general, the operating frequency band of an antenna consisting of two stacked microstrip patches is mainly determined by the resonant frequencies of the structure.

In this work, the authors focus on the analysis of the resonant modes of two stacked microstrip patches. In particular, the authors carry out a rigorous full-wave analysis in the Hankel trasform domain of the stacked microstrip patches [K. Araki, H. Ueda, T. Masayuki, IEEE-AP, 34, 1390-1394, 1986] in order to obtain the resonant frequencies, the quality factors and the radiation patterns of the first resonant modes of the patches. Thanks to the use of a suitable dyadic Green's function in the Hankel transform domain, the analysis is carried out in the case in which the two circular microstrip patches are embedded in a multilayered media consisting of materials which may show dielectric and/or magnetic anisotropy.

In order to check the validity of the numerical results obtained by the authors, these numerical results have been compared with measurements carried out for the resonant frequencies of the first ten resonant modes of stacked circular microstrip patches fabricated on isotropic substrates ($\epsilon_r \simeq 2.5$). In all cases, the agreement has been found to be within 2 %. As shown in [K. Araki, H. Ueda, T. Masayuki, IEEE-AP, 34, 1390-1394, 1986], the resonant frequencies of stacked circular microstrip patches can be tuned by introducing an air gap between the lower patch and the substrate of the upper patch, and by adjusting the air gap width. The results obtained in this work indicate that the aforementioned resonant frequencies can be also tuned by using magnetized ferrite substrates, and by adjusting the magnitude of the bias magnetic field [D. M. Pozar, *IEEE-AP*, 40, 1084-1092, 1992].

B30.9

Analysis of Infinite Arrays of Probe-Fed Patches

Marat Davidovitz*,
Rome Laboratory,Hanscom AFB, MA 01731
Alex Solovey, System Resources Corporation

Accurate determination of scanning characteristics of probe-fed microstrip patch arrays requires careful modeling of the region containing the feed. In particular, account must be taken of the finite probe radius and care exercised to ensure continuity of current at the probe-patch junction. The proposed approach to the problem is briefly outlined as follows:

- An integral equation for the patch-probe currents and the fields in the aperture of the coaxial feed-cable is formulated using the dyadic Green function for the unit-cell of the periodic structure.
- The unknown patch and probe currents are approximated with entire-domain basis functions satisfying the appropriate continuity requirements. The basis can be constructed for arbitrarily-shaped patch geometries, including multi-probe and stacked configurations. Where feasible, perturbation techniques are employed to modify existing entire-domain bases to incorporate probe-to-patch current continuity.

Use of the entire-domain basis results in a relatively low-order ($\simeq$ 30-50) system of equations and the associated solution time is negligible. Various mathematical and computer algorithms are applied to reduce the effort associated with the moment-method matrix calculation.

Favorable comparisons with measured data has been obtained to date, and selected results will be presented.

Optimum Design of a Cross-Shaped Dual-Polarized Microstrip Patch Antenna

Ahad Tavakoli, Badiozaman Mohammadi, and Rouzbeh Moini
Amirkabir University of Technology (Tehran Polytechnic)
424 Hafez Ave., Tehran, Iran
Tel: +98-21-6406591; email: tavakoli@cic.aku.ac.ir

Dual-polarized antennas with two linear orthogonal polarizations are widely used in communication systems and radars. Due to their simplicity in use and fabrication, dual-polarized microstrip patches are getting more attention in various applications. Low isolation and high cross-polarization are among the major disadvantages of using rectangular dual-polarized patch antennas. Earlier, dual linear polarization with low cross polarization and high isolation was reported for a cross shaped microstrip patch antenna (A. Tavakoli, *etal,* 1995 IEEE AP-S symposium, pp. 994-997). Antenna characteristics such as resonant frequency, input impedance, scattering parameters, and radiation patterns are calculated applying the segmentation method, the multiport network theory, and employing Green's functions derived from cavity models (K. C. Gupta, *etal,* Computer Aided Design of Microwave Circuits, Artech House, 1981). Significant improvement of the cross polarization and the isolation between the input ports compared to the conventional dual-polarized rectangular microstrip patches was reported. In this paper, making a couple of improvements in the model, an optimization procedure is used in designing the optimum antenna. By adding an impedance between the input ports, the coupling between them is taken into account. As a result, a considerable improvement in calculation of the isolation that is confirmed by measurements is achieved. The iterative calculation routine is also modified so that no assumption about the field distribution around the periphery is made in advance.

Only a limited number of papers on the optimization of microstrip antennas are reported that mostly focus on the input impedance of the antenna (M. A. Saed, Microwave Journal, Jan. 1993, pp. 123-124). Here, using the simplex optimization method to find the global minimum, input impedances, antenna efficiency, isolation between the ports, and radiation cross polarizations are all considered in the optimization process. Therefore, based on the desired specifications, the computer code generates the dimensions of the antenna. By applying the optimization routine, a 22.5 dB improvement in isolation, 5 dB in cross polarization, and 5 dB in maximum directivity compared to the previously reported results is achieved that is confirmed by measurements.

URSI B **Session 39** **Salon Bersimis**

Monopoles, Dipoles and Resonators
Co-chairs: A.D. Olver, UK and T. Milligan, USA

08:10	39.1	Currents Induced in Human Body by Incident 50-60 HZ or 10-30 KHZ Electric Field When the Arms are Raised, **R.W.P. KING**, *Harvard University, Cambridge, MA, USA*
08:30	39.2	Numerical and Experimental Study of Dielectric Resonator Antennas, A. SANGIOVANNI, **J.-Y. DAUVIGNAC**, C. PICHOT, *Université de Nice-Sophia Antipolis/CNRS, Valbonne, France*
08:50	39.3	Dielectric Resonator Antennas Operation at Two Polarizations, **G. SÉGUIN**[1], Y.M.M. ANTAR[2], N. SULTAN[1], Z. FAN[1], [1]*Canadian Space Agency, Saint-Hubert, QC and* [2]*Royal Military College of Canada, Kingston, ON, Canada*
09:10	39.4	Dielectric Rod Waveguide with Unequally Spaced Radial Variations, **H. KUBO**, Y. MAHARA, *Yamaguchi University, Yamaguchi, Japan*
09:30	39.5	Analysis of a Cavity-Backed Monopole, **J.-F. KIANG**, *National Chung-Hsing University, Taichung, Taiwan, China*
09:50	39.6	Top Loaded Monopoles with Parallel Strip Elements, **H.D. FOLTZ**[1], J.S. McLEAN[2], L. FRANCAVILLA[2], G. CROOK[2], [1]*University of Texas - Pan American, Edinburg, TX and* [2]*University of Wisconsin, Madison, WI, USA*
10:10		Coffee Break
10:30	39.7	The Center-Fed Dipole with a Finite Gap, **R.C. BOOTON, Jr.**, *Boulder, CO, USA*
10:50	39.8	Analysis of Monopole Antennas with a Coaxial Feed Line by the Method of Lines, **R. PREGLA**, *Fern Universität, Hagen, Germany*
11:10	39.9	Radiating Circumferential Slots on a Coaxial Cable, **J.-F. KIANG**, *National Chung-Hsing University, Taichung, Taiwan, China*
11:30	39.10	Radiation Properties of a Tapered Coaxial Radiator, **J.-F. KIANG**, *National Chung-Hsing University, Taichung, Taiwan, China*

B39.1

CURRENTS INDUCED IN HUMAN BODY BY INCIDENT 50–60 HZ or 10–30 KHZ ELECTRIC FIELD WHEN THE ARMS ARE RAISED

Ronold W. P. King
Gordon McKay Laboratory, Harvard University, Cambridge, MA 02138-2901

A current $I(z)$ is induced in a man standing on the ground near a power line or VLF antenna where the incident field is $E_z^{\rm inc}$. When his arms touch his sides this is given by (13) in King and Sandler (*Radio Sci.* **31**, 1153, 1996). With the arms raised to an angle Θ as shown in the figure, the current $I_1(z)$ in the body and legs is increased, $I_2(z)$ in the neck and head is decreased, and $I_3(x)$ and $I_4(x)$ are generated in the arms. Graphs will be shown. The formulas are

$$I_1(z) = \frac{j2\pi k h^2 E_z^{\rm inc}}{\zeta_0 \Psi_h}\left\{1 - \frac{z^2}{h^2} - \frac{Z_L}{Z_0+Z_L}\left(\frac{h-z+2Cl}{h+2Cl}\right) + C\left(\frac{4h_1 l}{h^2} - \frac{2l^2}{h^2}\cos\Theta\right)\right.$$
$$\left.\times\left[1 - \frac{Z_L}{Z_0+Z_L}\left(\frac{h-z+2Cl}{h+2Cl}\right)\right]\right\};\quad 0 \le z \le h_1,$$

$$I_2(z) = \frac{j2\pi k h^2 E_z^{\rm inc}}{\zeta_0 \Psi_h}\left\{1 - \frac{z^2}{h^2} - \frac{Z_L}{Z_0+Z_L}\left(\frac{h-z}{h+2Cl}\right) + C\left(\frac{4h_1 l}{h^2} - \frac{2l^2}{h^2}\cos\Theta\right)\right.$$
$$\left.\times\left[k^2 h h_1\left(1-\frac{z}{h}\right) - \frac{Z_L}{Z_0+Z_L}\left(\frac{h-z}{h+2Cl}\right)\right]\right\};\quad h_1 \le z \le h_1+h_2 = h,$$

$$-I_3(-x) = I_4(x) = \frac{j2\pi k h^2 E_z^{\rm inc}}{\zeta_0 \Psi_l}\left\{\left(1-\frac{x}{l}\right)\left[\frac{2h_1 l}{h^2} - \frac{Z_L}{Z_0+Z_L}\left(\frac{l}{h+2Cl}\right)\right]\right.$$
$$- \left(1-\frac{x^2}{l^2}\right)\frac{l^2}{h^2}\cos\Theta - C\left(1-\frac{x}{l}\right)\left(\frac{l}{h+2Cl}\right)\left(\frac{Z_L}{Z_0+Z_L}\right)$$
$$\left.\times\left(\frac{4h_1 l}{h^2} - \frac{2l^2}{h^2}\cos\Theta\right)\right\};\quad 0 \le x \le l.$$

Here, $\zeta_0 = 120\pi\ \Omega$, $h_1+h_2 = h$, $l_1 = l_2 = l$, $\Psi_h = 2\ln(2h/a_h) - 3$; $\Psi_l = 2\ln(2l/a_l) - 3$, a_h is the mean radius of the body, a_l of the arms, $C = \Psi_h/\Psi_l$, $Z_L = -j/\omega C_0$ is the impedance between the soles of the feet and their image in the earth, and $Z_0 = -j\zeta_0\Psi_h/2\pi k(h+2Cl)$ is the impedance of the body where $I_1(z)$ is maximum.

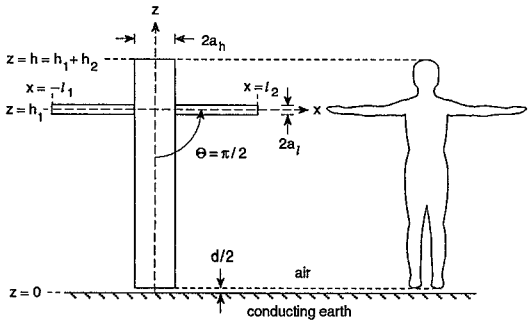

NUMERICAL AND EXPERIMENTAL STUDY OF DIELECTRIC RESONATOR ANTENNAS

A. Sangiovanni, J-Y. Dauvignac and Ch. Pichot
Laboratoire d'Electronique, Antennes et Télécommunications,
Université de Nice-Sophia Antipolis/CNRS, 06560 Valbonne, France

In recent years, different works have been carried out on dielectric resonator antennas (DRA) due to some advantages over microstrip patch antennas in the microwave and millimeter wave region. These different studies were mainly dealing with bandwidth enhancement techniques and for this, various dielectric antenna configurations have been proposed e.g. two stacked cylindrical or annular ring elements (A. A. Kishk, B. Ahn, and D. Kajfez, Electron. Lett., 25, 1232-1233, 1989).

Here, we present a study based on numerical simulations and experimentations to investigate new antenna configurations for bandwidth improvement. In the numerical simulation, we use a surface Finite Element method (P. Brachat, P. Ratajczak, C. Dedeban, and T. Bousquet, JINA'96, 425-438, 1996) which enables us to compute the different resonant frequencies as well as the field distribution associated to each mode in the DRA and the near-field mapping. Moreover, we are able to model arbitrary geometry with various excitations such as coaxial probe feed, microstrip feedline, slot or waveguide coupling.

In order to validate the numerical method, first results for simple structures were obtained. Field distributions of the $TE_{01\delta}$ and $HEM_{11\delta}$ modes for a cylindrical DRA operating at resonant frequencies are computed. These preliminary numerical results have been compared with experiments and with some published data (D. Kajfez and P. Guillon, *Dielectric Resonators*, Artech House, 1986). A very good agreement has been observed.

A study of new configurations of DRA offering interesting features as a wider bandwidth and other characteristics (compactness, geometry, ...) are reported as well near-field mappings. One aim for developing such antennas is to use them as a transmitter/sensor in a microwave imaging system.

B39.3

DIELECTRIC RESONATOR ANTENNAS OPERATION AT TWO POLARIZATIONS

G. Seguin*, Y.M.M. Antar**, N. Sultan*, Z. Fan**

*Space Systems, Canadian Space Agency
Saint-Hubert, Québec, Canada

**Department of Electrical and Computer Engineering
Royal Military College of Canada
Kingston, Ontario, Canada

Recently, dielectric resonator antennas (DRA) have been suggested and investigated for use as efficient and wideband radiators especially in microwave and millimeter wavebands. These types of antennas offer several advantages as they exhibit wide impedance bandwidth, small size in view of the high dielectric constant used, higher radiation efficiency and no excitation of surface waves.

In this paper, we report on an experimental and theoretical study to investigate the feasibility of using rectangular DRA's to realize a dual-polarized antenna. Theoretical analysis based on the modal expansion method and the spectral domain approach is developed. The accuracy of the theory is verified by comparison with both numerical results obtained using TLM approach and experiments. Expressions for natural resonant frequencies, factors and radiation patterns are obtained. Several dual-polarized DRAs operating at L and C bands with various feed schemes using slot coupling are fabricated and measured. These feed schemes, for example, include using offset slots fed by two microstrip lines on the same substrate and two microstrip lines located on different surfaces of multilayer substrate to excite the DR via two crossed centered slots. For these various configurations, input port isolation and cross-polarization are examined. Measured results for return loss, isolation and radiation patterns for copolarized and cross-polarized fields show that by suitable designs isolator between ports and cross polarization levels better than -20 dB can be achieved. This study demonstrates the feasibility of using this new type of antenna for dual polarization operation.

Dielectric Rod Waveguide with Unequally Spaced Radial Variations

Hiroshi Kubo and Yukihiro Mahara
Dept. of Electrical and Electronics Eng., Yamaguchi University
Tokiwadai, Ube-shi 755, Japan

Introduction Recently the interests in mobile satellite communications and indoor millimeter-wave wireless networks have been growing rapidly. The radiation pattern directional in the elevation direction and omni-directional in the azimuth direction is demanded of the antennas in some of these systems. In the present article, the dielectric rod waveguide with the radial variations of the surface shape is presented.

Antenna form and radial variations

Figure 1 shows the dielectric rod waveguide whose surface varies at unequal intervals. The radius of a variation section is given by

$$\rho = f(z) \begin{cases} f(z) = a + h & \text{for } z_i - w \le z \le z_i \\ f(z) = a - h & \text{for } z_i \le z \le z_i + w \end{cases}$$
$$i = 0, 1, 2, \cdot, \cdot \ ,$$

where a denotes the average radius of the waveguide and z_i denote the center of the sections. In the waveguide the fundamental mode is propagating. The wave energy is radiated in the air at the sections. Owing to the axial symmetry, the radiation pattern is omni-directional in the azimuth direction. The pattern in the elevation direction depends on z_i, which determine the phase of the radiated waves and their wave path differences in the air. z_i are chosen so that the error of the pattern may be minimized. For obtaining z_i we use two approaches: 1) making the groups consisting of the same number of variations, the relative locations in the group are chosen; all possible configurations of groups locations are examined; 2) the generic algorithm known as a optimum search technique is applied to this problem.

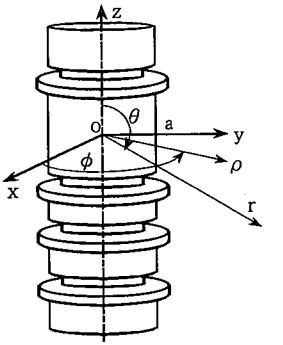

Fig. 1 Dielectric rod waveguide.

Radiation pattern

We have designed the waveguide with the pattern directional in the range between θ=30[deg.] and 60. The solid line of Fig.2 shows the pattern designed by using the first approach. The experimental pattern from one variation is plotted by the broken line. The results by generic algorithm and the experimental patterns will be shown in presentation.

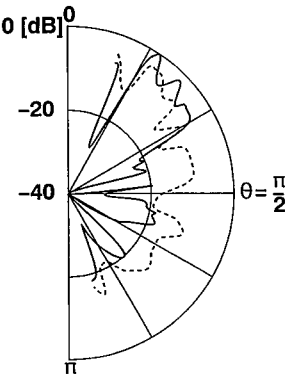

Fig. 2 Radiation patterns.

B39.5

Analysis of a Cavity-Backed Monopole

Jean-Fu Kiang
Department of Electrical Engineering
National Chung-Hsing University
Taichung, Taiwan

Cavity-backed slot radiators are widely used in airplanes because of their small size, light weight, conformability, and power handling capacity. They do not have the surface waves induction problem that occurs to microstrip patch antennas. The bandwidth of a patch antenna can also be significantly increased by enclosing it within a cavity. A horizontal stripline current probe extending from the sidewall of a cavity is used to drive a slot backed by this cavity, and a wide bandwidth is also observed.

In this work, we analyze a cavity-backed monopole antenna to see if it has the wide bandwidth characteristics of the cavity-backed stripline probe. A Galerkin's method is developed to calculate the input impedance and radiation patterns of a cavity-backed monopole. A stationary formula is also derived to obtain results for comparison. The effects of cavity dimension, strip size, strip depth, and cavity filling permittivity on the radiation characteristics are studied.

It is observed that inserting a dielectric layer to the bottom of the cavity significantly increases the frequency range in which the impedance variation is little. This will simplify the design of matching network in the feeding circuits. It is also found that this antenna is suitable for mobile communication because the radiation pattern in the E plane is almost omnidirectional, and is insensitive to the strip size, strip location, and cavity filling permittivity.

TOP LOADED MONOPOLES WITH PARALLEL STRIP ELEMENTS

H.D.Foltz[1], J.S.McLean[2], L.Francavilla[2], and G.Crook[2]
[1]Engineering Department, U. of Texas - Pan American, Edinburg, TX 78539
[2]Dept. of Elec. and Comp. Engin., U. of Wisconsin, Madison, WI 53706

Folded, top-disk loaded monopoles can be designed to give broadband antenna performance with a small electrical size. Typically, the vertical element consists of two or more parallel cylindrical conductors. The currents in these conductors can be decomposed into antenna (radiating) and transmission line (nonradiating) modes. Through proper tuning the susceptance of the transmission line mode can be used to compensate for that of the antenna mode, resulting in a broad double tuned response. The top disk lowers the resonant frequency of the antenna mode, thus permitting a smaller antenna. However, lumped tuning elements, with their associated losses, must be added to align the resonance and adjust the susceptance slope of the transmission line mode. To allow the addition of these tuning elements, the top loading disk must often be segmented.

In this paper we consider replacing the vertical element with a pair of parallel strips separated by a dielectric material (see figure below). The dielectric allows the transmission line mode to resonate with a short physical length; furthermore, by adjusting the separation between the strips the susceptance slope can be controlled with relatively little effect on the resonant frequency of the antenna mode. If the parallel strips are allowed to have unequal widths the impedance level of the overall antenna can be scaled to permit convenient matching to the feedline. The result is an antenna structure which is self-resonant, double-tuned, and electrically small without the use of lumped element loading or matching networks. In addition, the top disk need not be segmented, thus simplifying analysis and construction.

Approximate analytical techniques useful for designing these antennas will be presented, along with the results of numerical simulations and measurements.

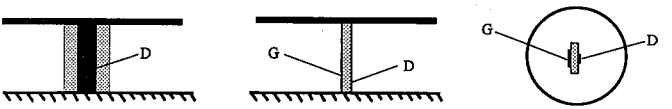

G - Grounded Strip Element D - Driven Strip Element

B39.7

The Center-Fed Dipole with a Finite Gap

Richard C. Booton, Jr.
2983 Foothills Ranch Road
Boulder, Colorado

Many studies have been performed of the center-fed dipole. Almost all of these studies, however, have assumed the limiting case of the infinitesimal gap. Analytic results have long shown that the susceptance of such a dipole is infinite, a result of the infinite capacitance across the antenna terminals. Nevertheless, numerical results are still being produced showing finite susceptance. More careful numerical solutions using the moment method show a susceptance that increases logarithmically without limit with the number of basis functions, consistent with the analytical results..

This paper considers the dipole with a finite (noninfinitesimal) gap. A few studies of the finite-gap dipole have been reported but these are based upon questionable assumptions such as sinusoidal current. An integral equation that determines the current can derived. For simplicity, narrow lossless dipole arms are assumed. Because the E-field for a lossless dipole arm is zero, the expression for the magnetic vector potential can easily be derived as the solution of a differential equation, which leads in turn to an expression for the electric scalar potential. Relating this potential to the source voltage leads to the integral equation

$$\int_0^{0.5L} G(z,z')\, I(z')\, dz' = -\frac{j2\pi V_G}{\eta_0} \sin(k_0|z-0.5g|) + C\cos(k_0|z-0.5g|)$$

To solve this equation, some assumption must be made concerning the source region of the dipole, in the form of the variation of either the E-field or the current in the gap. In this paper, the current is assumed to be constant (independent of position) in the gap. A equivalent source model is one that places concentrated charges on the antenna terminals. A straightforward application of the moment method yields the admittance as the ratio of current into the antenna terminals to the voltage across the terminals. Triangular basis functions with point matching are used. For a small number of basis functions, the susceptance agrees with the infinitesimal-gap result and then converges to a finite result rather than diverging as the number of basis functions is increased. Use of Richardson extrapolation decreases the number of basis functions required to obtain an accurate solution.

Analysis of Monopole Antennas with a Coaxial Feed Line by the Method of Lines

Reinhold Pregla
Allgemeine und Theoretische Elektrotechnik
FernUniversität, D-58084 Hagen, Germany

Vertical monopole antennas over a grounded plane are easy to construct and widely used for measurements. There are several applications for these structures, even if the monopole is submerged partially or entirely in soil or water. In this contribution different types of monopole antennas fed by a coaxial line (see Fig. 1) will be analyzed by the method of lines (MoL) – a special finite difference method, highly suitable and flexible for the analysis of electromagnetic field problems, as shown in numerous papers.

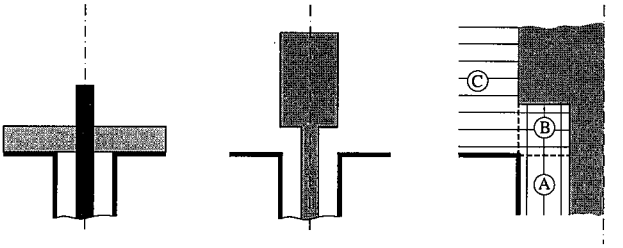

Fig. 1: a) Monopole antenna partially buried in a grounded dielectric substrate b) Thick monopole with a coaxial feed line c) Discretization scheme

For analysis of the above mentioned structures the field in the coaxial line is discretized in radial direction (see Fig. 1c). Accordingly, the discretization lines on which the field is described analytically coincidence with the propagation direction. In the region above the ground metallization the discretization is carried out in vertical direction, using Bessel functions for the analytical solution in radial direction. In the transition region the two line systems cross each other perpendicularly. At the boundary of this region the potential is suitably matched. An impedance transfer technique (R. Pregla, *AEÜ*, Oct. 96, pp. 293–300) is employed to obtain the input impedance. The impedance of the outer region is transferred by the radial line into the input impedance of coaxial line. Finally, a source wave is introduced in the coaxial line allowing to calculate the field in the whole structure.

Results of the study of input impedances and field distributions for various monopole antennas, e.g. thick monopoles or monopoles partially buried in a grounded dielectric substrate, will also be presented.

B39.9

Radiating Circumferential Slots on a Coaxial Cable

Jean-Fu Kiang
Department of Electrical Engineering
National Chung-Hsing University
Taichung, Taiwan

Slot antennas have been used on vehicle surfaces due to their conformability and power handling capacity. The structures with slots that were studied recently are cylindrical waveguide surface, cylindrical cavity, sectoral waveguide, and so on. Also, an annular aperture can be formed by attaching a ground plane to the opening of a coaxial cable, and serves as a slot antenna or a sensor. Segments of coaxial cables can be connected to form a coaxial collinear antenna.

In this work, we study the radiation properties of slots on a coaxial cable which can be used to distribute signals in a wireless local area network. The coaxial cable is used to transmit signals over a much longer distance than antennas. Slots are then opened on the coaxial cable around an end user cluster to radiate signals to them without interfering with other electronic equipments at a distance.

The dominant TEM mode propagating in the cable induces higher order modes around the slots, and is itself partly reflected. Hence, we will first study the reflection and radiation characteristics of a circumferential slot on the outer conductor of a coaxial cable by using both the Galerkin's and the mode-matching methods. The reflections induced by different slots along the cable may accumulate and reduce the transmission efficiency. Then, a Monte Carlo simulation will be used to analyze the accumulated effects of multiple slots on the reflected power.

Radiation Properties of a Tapered Coaxial Radiator

Jean-Fu Kiang
Department of Electrical Engineering
National Chung-Hsing University
Taichung, Taiwan

Coaxial cables have been widely used to feed power to patch or cavity-backed antennas. The coaxial cable openings can also serve directly as radiators. A coaxial-fed monopole antenna can be implemented by extending the center conductor as the radiator. When the coaxial outer conductor is flush with a ground plane, the junction reflects most of the power due to discontinuity and significantly reduces its radiation efficiency. The structure near the junction can be modified to make the transition smooth, thus reducing the reflection and increasing its efficiency.

Tapered lines have been used in the transmission line design for impedance matching. The idea also applies to the dielectric waveguides and other microwave components. For example, a horn antenna can be perceived as a tapered version of the feeding waveguide.

In this work, we extend the tapering technique to the coaxial cable near the junction with the ground plane to study its effects on the radiation properties. The tapered section of the coaxial antenna are constructed by expanding the outer conductor gradually toward the aperture flush mounted to the ground plane. It can be approximated by concatenated sections of coaxial cables with incremental change of outer conductor radius. A mode-matching technique is developed to calculate the input impedance and radiation patterns of this antenna.

It is observed that the tapered coaxial antennas have a broader bandwidth in the sense of input impedance. The radiation pattern is mostly affected by the coaxial aperture in direct contact with the half space, and is insensitive to tapering. The antenna designers may focus on meeting the input impedance requirements by changing the tapered sections once the aperture size is chosen.

URSI B **Session 47** Salon Marquette

Finite Difference Time Domain
Co-chairs: C. Trueman, Canada and J. LoVetri, Canada

13:10 47.1 Improvements in the Simulation of Absorbing Boundaries for the Finite-Difference Time-Domain Method, N. CALVÉ, **A.E. ROS**, *Laboratoire d'Electronique et Systèmes de Télécommunications, Brest, France*

13:30 47.2 FDTD Analysis and Measurements of Shielded Cellphone Antenna, B. YILDIRIM, **E.-B. EL-SHARAWY**, *Arizona State University, Tempe, AZ, USA*

13:50 47.3 Using Time-Domain Complex-Envelope Representations of Band-Pass Limited Signals in the Finite-Difference Solution of the Wave Equation, **P.M. GOGGANS**, J.D. PURSEL, *University of Mississippi, University, MS, USA*

14:10 47.4 Analysis of a Time Domain FEM with Edge Elements of Different Form, G. MANARA[1], **A. MONORCHIO**[1], G. PELOSI[2], [1]*University of Pisa and* [2]*University of Florence, Italy*

14:30 47.5 Derivation and Verification of a Dispersion Optimized Fourth Order FD-TD Method, **G. HAUSSMANN**, M. PIKET-MAY, *University of Colorado at Boulder, CO, USA*

14:50 47.6 Source Modeling in the Finite-Difference Time-Domain Method, **M.A. SAED**, *State University of New York at New Paltz, NY, USA*

15:10 Coffee Break

15:30 47.7 A Comparative Study of the FDTD and the FVTD Schemes, **R. SIUSHANSIAN**[1], J. LO VETRI[1], N.R.S. SIMONS[2], [1]*University of Western Ontario, London and* [2]*Communications Research Centre, Ottawa, ON, Canada*

15:50 47.8 An FDTD Method with Nonuniform Cylindrical Grids for Inhomogeneous Conductive Media, **J. HE**, Q.H. LIU, *New Mexico State University, Las Cruces, NM, USA*

16:10 47.9 Limitations of Precise Simulations of Handheld Mobile Phones with FDTD, O. VOLEŠ, K. POKOVIĆ, **M. BURKHARDT**, N. KUSTER, *Swiss Federal Institute of Technology (ETH), Zürich, Switzerland*

16:30 47.10 Design of Composite Grating Assisted Mode Couplers for Ultrafast Pulses, **T. LIANG**, R.W. ZIOLKOWSKI, *University of Arizona, Tucson, AZ, USA*

B47.1

Improvements in the Simulation of Absorbing Boundaries for the Finite-Difference Time-Domain Method

N.Calvé, A.E.ROS*
Laboratoire d'Electronique et Sytèmes de Télécommunications
6,Av.Le Gorgeu - BP 809 - Brest Cédex - France
E-mail : Alain.Ros@lest-gw.univ-brest.fr

On account of the very fast increasing of power of microcomputers in terms of CPU time and memory size, numerical methods using a discretization of space in order to simulate the propagation of the electromagnetic field regained interest during the 80's .

Many results have already been published for resonant cavities, microstrip lines, fin lines, discontinuities in homogeneous or inhomogeneous media

Nevertheless, difficulties introduced by open media due to the necessary limitation of the spatial extension of the simulated domain are not conveniently solved at this time . In order to simulate the radiation and the propagation of the electromagnetic field in open space of a microwave device, it is necessary to introduce or simulate "absorbing boundaries" .

Two different types of boundaries have been proposed : purely numerical (or "mathematical") solutions consisting in the cancelling of the reflected field on these boundaries; others, more "physical", absorb the components of the incident field reaching the boundaries under some pre-defined angles . In each cases, the chosen boundaries conditions generally introduce parasitic solutions ("spurious modes") that damage the accuracy of the calculated characteristics .

In this paper, we intend to compare the solutions proposed by authors (1,2,3) in terms of efficiency, dispersion, spurious modes,...These solutions will be tested in the two formulations of the FD-TD method : expanded nodes (Yee's scheme) and condensed nodes .

The conclusions of these comparisons will give us the ability to suggest some improvements in the simulation of absorbing boundaries such as the use of non-centered finite-differences formulas for the Mur's absorbing boundaries (4) . The comparison of the expanded nodes and condensed nodes formulations will be extensively developed in the case of the Berenger's absorbing boundaries (3) .

FDTD Analysis and Measurements of Shielded Cellphone Antenna

Bahadir Yildirim and El-Badawy El-Sharawy
Department of Electrical Engineering
Telecommunication Research Center
Arizona State University, Tempe Arizona, USA

Analysis and Measurements of a cellular phone antenna that has the following features

1-Minimum radiation toward the human user to reduce potential health hazards that may be associated with exposure to EM signals.

2-To achieve the above goal without adversely altering the electrical performance of the antenna and the range of the cellular phone. In fact, the new antenna is expected to have more range than conventional cellular phone antenna.

3-To keep the size of the antenna as small as possible to follow the trend in today user's electronics.

4-To address technical features of antenna configuration including bandwidth, input impedance and gain.

5-To achieve the polarization diversity required for maximum range and reception

The above goals have are achieved using a dual resonance antenna with back shielding in the near field while maintaining a near omni-directional characteristics in the far field. An internal as well as external version of the antenna will be described. FDTD analysis is used to predict the antenna performance and is in good agreement with the measurements.

B47.3

Using Time-Domain Complex-Envelope Representations of Band-Pass Limited Signals in the Finite-Difference Solution of the Wave Equation

Paul M. Goggans* and Jeffrey D. Pursel
Department of Electrical Engineering
University of Mississippi
University, MS, 38677, USA

The usual finite-difference time-domain (FDTD) solution of the electromagnetic wave equation uses time and spatial sampling according to the low-pass limited (LPL) sampling theorem. For time sampling this means that the time step must be set in accordance with maximum frequency in the source signal. However, for scattering problems the source signal is usually band-pass limited (BPL) rather than low-pass limited. The band-pass limited sampling theorem states that, using the proper techniques, the signal can be sampled in accordance with the bandwidth of the signal source rather than its maximum frequency. This suggests that the FDTD method can be modified so that the required time step for BPL signals is significantly increased compared to the conventional FDTD.

One way of modifying the FDTD method is to use the complex envelope representation of BPL signals (Simon S. Haykin, Communication Systems, 2nd ed., John Wiley & Sons Inc., 1983). The complex envelope representation of a real BPL signal yields a complex LPL signal with a maximum frequency equal to one half the bandwidth of the original signal. For a real BPL signal a(t), the complex envelope representation $\tilde{a}(t)$ is related to a(t) by the following expression:

$$a(t) = \mathrm{Re}\left[\tilde{a}(t)\exp(j2\pi f_o)\right] \tag{1}$$

where f_o is the center frequency of a(t). The one-dimensional electric-field wave equation in a source free homogeneous region is

$$\frac{\partial^2}{\partial t^2}E_z(x,t) = c^2\frac{\partial^2}{\partial x^2}E_z(x,t) \tag{2}$$

for an z directed electric field which is constrained to propagate in the $\pm$ x direction. The phase velocity in Eqn. (2) is c. Eqn. (2) can be rewritten in terms of the complex envelope representation of the electric field yielding the BPL wave equation

$$\frac{\partial^2}{\partial t^2}\tilde{E}_z(x,t) + j4\pi f_o\frac{\partial}{\partial t}\tilde{E}_z(x,t) - (2\pi f_o)^2\tilde{E}_z(x,t) = c^2\frac{\partial^2}{\partial x^2}\tilde{E}_z(x,t). \tag{3}$$

In this paper we discuss the finite difference solution of the BPL wave equation. Included in the presentation is an algorithm for the solution of Eqn. (3).

Analysis of a Time Domain FEM with Edge Elements of Different Form

G. Manara, A. Monorchio *
Department of Information Engineering, University of Pisa
Via Diotisalvi 2, I56126 Pisa, Italy

G. Pelosi
Department of Electronic Engineering, University of Florence
Via C. Lombroso 6/17, I50134 Florence, Italy

The Finite Element Method (FEM) has been widely used in frequency domain for solving both two- and three-dimensional problems. In time domain, the simplicity and popularity of another numerical technique, the Finite Difference Time Domain (FDTD) method, has actually limited its application. However, in its simple original form, FDTD does not allow to easily model complex structures with curved or irregular interfaces. In this context, a time domain FEM may constitute a powerful tool for analyzing time domain problems with complex geometries and material constitution.

A specific Time Domain FEM (FETD) formulation is devised here, which employs interpolating functions of different order in space. The technique has presently been implemented for analyzing two-dimensional problems. It resorts to triangular edge elements; indeed, due to their geometrical properties, triangular elements are suitable to match very complex geometries, providing a significant improvement in space-domain interpolation with respect to FDTD. Vector edge elements of different forms (Whitney 1-form and Whitney 2-form) have been used in the implementation for comparatively testing the convergence and accuracy of the corresponding numerical procedures. A marching on in time scheme is introduced for a direct solution of the problem in time domain. The possibility of introducing quadratic interpolating functions in time is also being considered.

Numerical tests have been performed with reference to a set of closed problems in two-dimensions and will be shown at the conference. The main purpose is to compare the efficiency and effectiveness of the different formulations.

B47.5

Derivation and Verification of a Dispersion Optimized Fourth Order FD-TD Method

G. Haussmann* and M. Piket-May
Department of Electrical and Computing Engineering
University of Colorado at Boulder
Boulder CO 80309-0425

In this study we examine a Finite-Difference Time-Domain (FD-TD) method which is fourth order in space and second order in time. This method is optimized to minimize numerical dispersion error in all propagation directions. Multiple fourth order terms are utilized to produce more flexibility in the optimization method (in the form of a higher dimensional search space).

The resultant method has lower global dispersion error than either the standard second order or fourth order methods. Numerous variants, based upon the principle of using multiple higher order terms, produce a similar gain in optimization over the normal fourth order method.

While the original work and analysis of this method was performed for two dimensional FD-TD simulations, subsequent study has been done extending the method to full three dimensional simulations. The need for dispersion and stability analysis of numerous higher order methods dictated the derivation of more generalized equations, utilizing a generic difference operator, which could be used to quickly analyze numerous higher order methods by simple substitution. These generalized equations facilitated rapid examination of several closely related variants upon the original fourth order method.

The presentation will examine the generalized dispersion and stability equations, and demonstrate certain requirements not revealed in the two dimensional analysis. Simulation results will be shown for long distance, free space propagation, where the numerical dispersion error normally produces the most dramatic effect. The results include validation tests as well as a comparison involving the variants of this fourth order method.

SOURCE MODELING IN THE FINITE-DIFFERENCE TIME-DOMAIN METHOD

Mohammad A. Saed
Electrical Engineering Department
State University of New York at New Paltz
New Paltz, New York 12561

The Finite-Difference Time-Domain method (FDTD) is well known and very widely used in various applications such as scattering, microwave circuits, bioelectromagnetic simulations, antennas, subpicosecond photonic devices, and high speed electronic circuits. Among other factors, the accuracy of all these simulations is strongly dependent on accurate modeling of the excitation sources. Usually, in FDTD implementations, the source-free Maxwell's equations are discretized in a leap-frog time-stepping scheme. Then, hard sources are added to the computational domain by forcing some field components at some locations to equal the desired excitation pulse or sinusoid. Pulse sources must be placed far enough from the first discontinuity so that they expire and then removed before seeing the first reflection. This is computationally inefficient since it necessitates a large computational domain. Furthermore, such sources may be impossible to remove before the arrival of the first reflection in many applications such as high speed electronic circuits. Sinusoidal sources cannot be removed and must be turned on for the entire simulation time. This causes spurious reflections since the field components representing the sources are not updated using Maxwell's equations, but instead are forced to equal the desired sinusoidal function all the time.

In this paper, we present source models that solve the above problems associated with commonly used source models. Our FDTD implements the discretized Maxwell's equations for regions with sources. The sources do not need to be removed and all the field components at those locations are updated according to Maxwell's equations. The sources do not cause spurious reflections and can be placed close to the discontinuities saving valuable computation time. The details of the implementation, numerical results, and source models for probe and aperture coupling will be presented at the conference.

B47.7

A Comparative Study of the FDTD and the FVTD Schemes

R. Siushansian*, J. LoVetri
Department of Electrical Engineering
The University of Western Ontario
London, Ontario, Canada N6A 5B9
(email: riaz@gauss.engga.uwo.ca)

N. R. S. Simons
Directorate of Antennas & Integrated Electronics
Communications Research Centre
P.O. Box 11490, Station H
Ottawa, Ontario, Canada, K2H 8S2

This work involves a comparative investigation of the Finite Difference Time Domain (FDTD) method (K. S. Yee, IEEE Trans. Antenna & Propagation, v. AP-14, pp.302-307, May 1966) and Shankar's application of the Finite Volume Time Domain (FVTD) technique (V. Shankar, *et al*, Computer Physics Communication, v. 68, pp. 175-196, 1991). The FDTD method has become popular due to its ease of formulation and implementation, as well as its relatively low overhead (*i.e.* very little extra memory is required to define the problem) as compared to analogous methods. However, Yee's FDTD algorithm has many disadvantages due to its reliance on rectangular (and often uniform grids). For example, a rectangular grid representation of curved surfaces (stair stepping) leads to an ambiguity in the location of material boundaries. This has motivated many researchers to investigate extensions to the Yee's FDTD scheme or to utilize algorithms (such as the FVTD technique) that are capable of using a body-fitted coordinate representation of geometrically complex objects. This results in a better representation of the curved surfaces and allows for locally condensed meshes for finer discretization of small geometrical features.

There are however, several inherent problems associated with Shankar's finite volume technique. The first problem is the added overhead of the algorithm that increases both memory requirements and computation time. The second is the artificial viscosity term associated with the Lax-Wendroff scheme that renders the FVTD method dissipative (whereas the FDTD method is a conservative technique). The purpose of this work is to compare the FDTD and FVTD methods for several cases with analytic or well-established numerical solutions. Useful benchmark problems include various waveguide geometries such as finned and elliptical waveguides. Computational issues such as memory requirements and computation time will also be discussed.

AN FDTD METHOD WITH NONUNIFORM CYLINDRICAL GRIDS FOR INHOMOGENEOUS CONDUCTIVE MEDIA

J. He* and Q. H. Liu
Klipsch School of Electrical and Computer Engineering
New Mexico State University
Las Cruces, NM 88003

Many applications require time-domain solutions of Maxwell's equations in inhomogeneous, conductive media involving cylindrical interfaces. The conventional finite-difference time-domain (FDTD) method discretizes the continuous space with a uniform Cartesian grid which may result in a large staircasing error. Alternatively, a cylindrical grid can be used to remove this staircasing error and improve the accuracy. However, many problems consist of both electrically small and large structures. If a straightforward uniform grid is used, many unnecessary cells will be wasted in the regions with large structures in order to accommodate the accurate geometrical representation in regions with small structures. Although nonuniform grid has been used for Cartesian coordinates (e.g., Sheen, *Numerical Modeling of Microstrip Circuits and Antennas*, Ph.D. Dissertation, Massachusetts Institute of Technology, 1991), apparently there is no report on the use of nonuniform cylindrical grid.

In this work, an explicit second-order FDTD method with a nonuniform cylindrical grid is developed for time-domain Maxwell's equations. A refined lattice is used near sharp edges and within fine geometrical details, while a larger lattice is used outside these regions. This provides an efficient use of limited computer memory and computation time. We also extend the Liao's absorbing boundary condition and Berenger's perfectly matched layers to the nonuniform cylindrical grid. Numerical results will be shown to demonstrate the effectiveness of the nonuniform grid and the absorbing boundary conditions. Various applications in waveguides and subsurface sensing will be illustrated.

B47.9

Limitations of Precise Simulations of Handheld Mobile Phones with FDTD

O. Volež, K. Pokovič, M. Burkhardt* and N. Kuster
Swiss Federal Institute of Technology (ETH)
8092 Zurich, Switzerland
Phone:+41-1 632 2151, Fax:+41-1 632 1057, e.mail: burkhardt@ifh.ee.ethz.ch

Introduction

Several authors have recently proposed the use of FDTD techniques to perform the dosimetric evaluation of handheld mobile phones prior to equipment authorization or use, as required by the Federal Communication Commission of the United States (FCC 96-326, Report on Guidelines for Evaluationg the Environmental Effects of Radiofrequency Radiation). Other authors have expressed strong reservations with regard to such an approach since the modeling of the test object is *per se* critical.

Objectives

The objective of this study was to assess the possible sources of uncertainties of FDTD simulations of geometrically and electrically well-defined transmitters in the very close proximity of lossy scatterers.

Methods

A generic phone was developed which consists of a metal box on which different types of antennas can be mounted. For this study a monopole antenna as well as a helix antenna were used. The device was constructed in such a way that it enabled experimental determination of the feeding point impedances.

Two lossy scatters were used: 1) a simple flat phantom filled with brain simulating liquid; 2) the left-hand-usage side of the generic twin phantom (N. Kuster et al., invited paper in IEICE, submitted). The latter was developed on the basis of an anatomical study to represent the maximum absorption among at least 90% of the users. Since the CAD data set was available, a precise numerical as well as experimental phantom could be generated.

For the experimental evaluation new near field probes were developed for highly precise measurements in the very close near field. The H-field probe has a spatial resolution which is better than $<0.1\,\mathrm{cm}^3$ and a deviation from spherical isotropy of only $< \pm 0.2\,\mathrm{dB}$. The E-field probe has about the same spatial resolution with a deviation from spherical isotropy of $< \pm 0.4\,\mathrm{dB}$. Another probe was used for the evaluation in the brain simulating liquid (spatial resolution: $<0.1\,\mathrm{cm}^3$, deviation from isotropy: $< \pm 0.4\,\mathrm{dB}$). The basis of the evaluation was the dosimetric near field scanner described in (T. Schmid et al., IEEE MTT-44, pp. 105-113, 1996).

The far field radiation pattern was measured in a tapered anechonic chamber with automated instrumentation and control. The dimensions of the anechoic chamber are 4.9x4.9x16.5 m with a 1 m quiet zone 2.3 m above the floor level.

The simulations were performed with two different numerical codes: 1) The commercial package MAFIA which is based on the Finite Integration Technique (FIT) and 2) an in-house FDTD code.

The near and far fields of the devices were first carefully analyzed and compared in free space. In the next step the induced E- and H-field distributions in the tissue simulating liquid were compared for different distances. The last comparison was performed with the twin phantom using the standard position as defined by CENELEC (CENELEC 3rd draft, 1996).

In addition, experimental and numerical evaluations of a commercial DCS phone were compared and discussed.

Conclusion

FDTD is of limited use to conduct dosimetric evaluations of mobile phones, since relatively large safety margins of several dB are required due to the uncertainties in modeling the physical phone. On the other hand, numerical techniques complement efficient CAD tools to design and optimize antennas for mobile communications, since tight margins of absolute values are of minor relevance for design applications.

DESIGN OF COMPOSITE GRATING ASSISTED MODE COUPLERS FOR ULTRAFAST PULSES

Tao Liang* and Richard W. Ziolkowski
Department of Electrical and Computer Engineering
University of Arizona, Tucson, AZ 85721

As the techniques for generating ultrafast laser pulses advance and the potential for their applications increases, there is a corresponding need to understand the interaction between such ultrawide-bandwidth optical pulses and advanced materials and devices. In this paper we will develop an efficient time domain numerical modeling tool that can be used to simulate mode conversion of optical pulsed modes by grating structures in planar dielectric waveguides. The purpose of modeling such grating structures with ultrafast pulse interactions stems from the recognition that optical communication systems are being driven to shorter pulse regimes to increase the available information bandwidths. Devices will then need to be designed for these ultrafast pulses to meet traditional needs.

A number of methods have been proposed to analyze grating structures for single frequency excitation. Most of them treat the gratings as periodic structures of infinite extent. However, the ultrafast pulse environment will require aperiodic finite grating structures that can be effective over a few optical cycles, hence, over a large frequency bandwidth. It is thus desirable to have an efficient way to model the behavior of grating structures interacting with ultrafast optical pulses. The finite-difference time-domain method (FDTD) is a very good choice for this purpose. It has become a very popular method in the microwave regime and has been used recently to model ultrafast optical pulse propagation in linear and nonlinear media, and to model the interactions with linear and nonlinear interfaces and gratings. It provides an extremely flexible simulation environment that can model arbitrary geometries and material distributions, including dispersion and nonlinearities.

We have developed an efficient real-time mode extraction technique for use with our FDTD simulator. This augmented FDTD simulator has enabled us to carry out a thorough investigation of grating-assisted mode convertors for pulsed modes in dielectric waveguides. The results for various aperiodic grating structures that could be used to mode convert ultrafast optical pulses will be presented. It will be shown that a composite aperiodic grating structure can be designed that results in a nearly thirty percent increase in the converted mode energy for an ultrafast six-cycle optical pulsed mode over that achieved with a standard uniform grating designed for a single operating frequency.

URSI B

Session 63

Salon Jolliet

New Materials

Co-chairs: R. Ziolkowski, USA and S.M. El-Ghazaly, USA

15:30 63.1 The Analysis and Design of Passive Maxwellian Electromagnetic Absorbers, **R.W. ZIOLKOWSKI**[1], F. AUZANNEAU[2], [1]*University of Arizona, Tucson, AZ, USA;* [2]*Commissariat à l'Énergie Atomique, Le Barp, France*

15:50 63.2 The Analysis and Design of Maxwellian Smart Skins, R.W. ZIOLKOWSKI[1], **F. AUZANNEAU**[2], [1]*University of Arizona, Tucson, AZ, USA;* [2]*Commissariat à l'Énergie Atomique, Le Barp, France*

16:10 63.3 Electromagnetic Field of a Horizontal Dipole below the Surface of a Spherical Earth, **D. MARGETIS**, *Harvard University, Cambridge, MA, USA*

16:30 63.4 One-Dimensional Photonic Band Gap Reflectors, **H. CONTOPANAGOS**[1], N. ALEXOPOULOS[2], E. YABLONOVITCH[1], [1]*University of California, Los Angeles and* [2]*University of California, Irvine, CA, USA*

16:50 63.5 Bruggeman Formalism for Composite Media with Aligned Short Fibers, **A. LAKHTAKIA**[1], B. MICHEL[2], W.S. WEIGLHOFER[3], [1]*Pennsylvania State University, University Park, PA, USA;* [2]*Max-Planck-Gesellschaft, Jena, Germany;* [3]*University of Glasgow, UK*

B63.1

The Analysis and Design of Passive Maxwellian Electromagnetic Absorbers

Richard W. Ziolkowski *

Department of Electrical and Computer Engineering, University of Arizona, 1230 E. Speedway, Tucson, AZ 85721-0104, Tel: (520) 621-6173, Fax: (520) 621-8076, E-mail: ziolkowski@ece.arizona.edu

and

Fabrice Auzanneau

Commissariat à l'Énergie Atomique, Centre d'Études Scientifiques et Techniques d'Aquitaine, Boite Postale n°2 , 33114 Le Barp, France

A Maxwellian material interpretation of a perfect absorber using polarization and magnetization fields has been developed [R. W. Ziolkowski, to appear in *IEEE Trans. Antennas and Propagat.*, 1997]. The resulting time-derivative Lorentz material medium has been shown to lead to absorption characteristics in the 90 dB range for large angles of incidence. Moreover, a suggestion as to its realizability through an artificial material construction has been made which deals with the introduction of a lattice of small loaded antenna elements that are embedded in some host medium.

In this paper we analyze the types of passive microstructure circuit elements which could be used to achieve an electromagnetic absorbing material. This basic problem reduces to analyzing the complete response in the far-field to a loaded antenna structure which reradiates after it has been excited by an incident wave. The basic antennas to be discussed will include the electric (linear) and magnetic (loop) dipoles that are much smaller than a wavelength in size. They are loaded with simple combinations of passive LRC components. The equivalent polarization and magnetization fields of these artificial molecules and their defining differential equations will be presented. This analysis leads to a representation of the electric and magnetic properties of the resulting artifically realized material.

Several material models can be recovered with these artificial molecules. They include the standard Debye and Lorentz materials. Moreover, novel materials including the time-derivative Debye, the time-derivative Lorentz, and the two time-derivative Lorentz models can be obtained. These material models will be described and contrasted for their use as electromagnetic absorbers. Various interesting parameter regimes of these material models will be indicated and assessed using FDTD calculations. As was done with the time-derivative Lorentz material, the generalized polarization and magnetization field equations can be coupled with Maxwell's equations in a natural way and solved numerically with the FDTD approach. Several test cases in both one and two dimensions will be shown to quantify the behavior of these electromagnetic absorbers.

The Analysis and Design of Maxwellian Smart Skins

Richard W. Ziolkowski

Department of Electrical and Computer Engineering, University of Arizona, 1230 E. Speedway, Tucson, AZ 85721-0104, Tel: (520) 621-6173, Fax: (520) 621-8076, E-mail: ziolkowski@ece.arizona.edu

and

*Fabrice Auzanneau**

Commissariat à l'Énergie Atomique, Centre d'Études Scientifiques et Techniques d'Aquitaine, Boite Postale n°2 , 33114 Le Barp, France

Various types of artificial materials constructed from a lattice of small loaded antenna elements that are embedded in some host medium have been considered. These artificial molecules consist of electrically small electric (linear) and magnetic (loop) dipoles loaded with simple, passive LRC circuits. The equivalent polarization and magnetization fields of these artificial molecules and their defining differential equations have been obtained. Several material models can be recovered with these artificial molecules. They include the standard Debye and Lorentz materials but also novel choices including the time-derivative Debye, the time-derivative Lorentz, and the two time-derivative Lorentz models. Various interesting parameter regimes of these passive material models have been studied for their use as electromagnetic absorbers.

In this paper we analyze the modifications to these material models which result from the introduction of active circuit elements, such as diodes and transitors, into the circuits which load the elemental antennas. The artificial molecules then become active rather than passive. The actual usefulness of the resulting active materials as a "smart skin" will be assessed using FDTD calculations. By a "smart skin" we mean a surface that could actively respond to variations in the incident field. As was done with the passive artificial material models, the generalized polarization and magnetization field equations have been coupled with Maxwell's equations in a natural way and solved numerically with the FDTD approach. Several test cases in both one and two dimensions will be shown to quantify the behavior of these "smart skins" and to assess their potential usefulness.

B63.3

ELECTROMAGNETIC FIELD OF A HORIZONTAL DIPOLE BELOW THE SURFACE OF A SPHERICAL EARTH

Dionisios Margetis
Gordon McKay Laboratory, Harvard University, Cambridge, MA 02138-2901

The electromagnetic field at the boundary between air and earth of a horizontal electric dipole located just below the surface of a homogeneous and isotropic spherical earth is examined analytically when the earth is optically dense, has a radius which is large compared to the wavelength in air, and is surrounded by a homogeneous atmosphere. The geometry of the problem is depicted in Figure 1. It consists of an x-directed horizontal electric dipole located inside a homogeneous, isotropic and non-magnetic sphere (region 1, $r < a$) at a distance b from the origin. The sphere is centered at the origin and is surrounded by air (region 2, $r > a$).

The starting point for the analysis is the derivation, directly from Maxwell's equations without the use of the Debye potentials, of the exact solution for the field in the form of series representations of the Mie type involving spherical Bessel functions and Legendre polynomials. These series are subsequently converted into a set of series of integrals via the application of the Poisson summation formula. Each term in the new representation is evaluated approximately by asymptotic methods.

The analysis emphasizes the physics of the problem, revealing a non-trivial creeping-wave structure of waves propagating along the surface through the air while accompanied by an infinite number of rays bouncing inside the earth. When the earth is lossy, the proposed analytical treatment provides a good alternative to tedious numerical computations based on the formal series expansions.

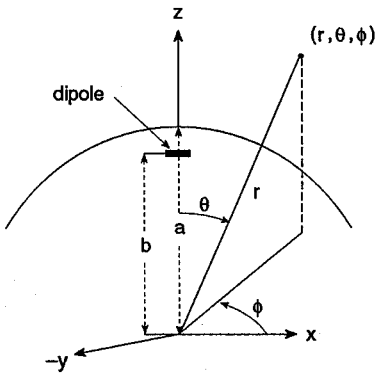

Fig. 1. Spherical coordinates and horizontal dipole inside a spherical earth.

One-dimensional Photonic Band Gap Reflectors

H. Contopanagos* [a], N. Alexopoulos[b] and E. Yablonovitch[a]

[a]Department of Electrical Engineering
University of California, Los Angeles
405 Hilgard Avenue
Los Angeles, CA 90095

[b]Department of Electrical and Computer Engineering
University of California, Irvine
Irvine, CA 92697

Abstract

High-Reflectivity systems are both theoretically very interesting and practically very important for a variety of engineering applications in communication systems, high-Q cavities and Lasers, among others. We address the issue of designing a system, composed of a very good conducting material, of higher reflectivity than the intrinsic reflectivity of the material itself. We study a finite one-dimensional periodic array of plane conductors of finite thickness, equivalent to a one-dimensional Photonic Band Gap architecture of finite size in the periodicity axis. We arrive at an exact analytical formula for the reflection coefficient, which is in fact valid for arbitrary electrical properties of the layers. The formula is derived using a matrix representation for the amplitudes of the transmitted and reflected waves within the structure, and explicit evaluation of the resulting scattering matrix by expansion on the Pauli spin matrices and usage of the corresponding SU(2) group algebra. The final formula is exact, and needs a minimal amount of programming (essentially focused on computing polynomials of complex variables of degree equal to the number of layers) to compute the reflectivity. By a Taylor expansion of the exact formula as a series in the dimensionless variable $1/\Delta \equiv (\sigma/2\omega\epsilon_0)^{-1/2}$ we derive an analytical approximation, arbitrarily accurate, that needs no numerical implementation (except for graphical purposes), and involves no large cancellations. Applying this formula to the case of very good conductors at microwave frequencies, and in particular to Copper, we fully explore the 3-dimensional parameter space of the structure. This space consists of the number of layers, their thickness and their spacing. For specific regions of the parameter space, the reflectivity of the structure is significantly enhanced relative to the intrinsic reflectivity of the material. We finally discuss design characteristics and error tolerances for practical systems at a variety of operating frequencies.

B63.5

BRUGGEMAN FORMALISM FOR COMPOSITE MEDIA WITH ALIGNED SHORT FIBERS

Akhlesh Lakhtakia

Department of Engineering Science and Mechanics

Pennsylvania State University, University Park, PA 16802–1401, USA

Bernhard Michel

Max–Planck–Gesellschaft, AG "Staub in Sternentstehungsgebieten"

Schillergäßchen 2–3, D–07745 Jena, Germany

Werner S. Weiglhofer

Department of Mathematics

University of Glasgow, Glasgow G12 8QW, Scotland, UK

Abstract

Aligned short–fiber composite media consist of electrically small aciculate inclusions dispersed randomly in a host medium, all inclusions aligned parallel to each other. The identical orientation imparts the composite medium the ability to discriminate between illuminating plane waves of different polarization states. These polarization–discriminating properties are of particular importance for low–weight high–strength radomes, aircraft structures and striplines, as well as for high shielding effectiveness in the electromagnetic compatibility industry. Uniaxial composite media also have considerable appeal for the production of functional gradient materials.

The Bruggeman formalism is rigorously implemented here on two models for homogenizing an aligned short–fiber composite medium. The inclusion medium is supposed to be dispersed in the homogenized composite medium (HCM) as cylindrical particles in both models. However, the host medium is dispersed as cylindrical particles in the first model and as spherical particles in the second. Although the two models yield different estimates of the anisotropic dielectric properties of the HCM, the Wiener bounds are satisfied in both instances. Both models also exhibit percolation. Benchmarking against careful experiments appears necessary to evaluate the adequacy of either model. The described models may eventually find use for on–line inspection and control of manufacturing processes for aligned short–fiber composite media.

URSI B Special Session **Session 68** **Salon St-Maurice**

Model Order Reduction for Rapid EM Field Simulation
Co-chairs: A.C. Cangellaris, USA and J.-F. Lee, USA

13:10 68.1 **Invited:** Illustrative Examples of Reduced Order Representation for Efficient Electromagnetic Computation, **R. MITTRA**, *Pennsylvania State University, University Park, PA, USA*

13:30 68.2 **Invited:** Model-Order Reduction in Computational Electromagnetics Using Model-Based Parameter Estimation, **E.K. MILLER**, *Santa Fe, NM, USA*

13:50 68.3 **Invited:** Application of Total Least Squares in Parametric Modelling of Responses of Electromagnetic Systems, **T.K. SARKAR**, *Syracuse University, Syracuse, NY, USA*

14:10 68.4 **Invited:** A Brief Survey of Krylov-Subspace Based Model-Order Reduction, **I. ELFADEL**, J. PHILLIPS, M. SILVEIRA, J. WHITE, *Massachusetts Institute of Technology, Cambridge, MA, USA*

14:30 68.5 **Invited:** A Lanczos Model-Order Reduction Technique for Time-Domain Electromagnetic Simulations, **P.M. VAN DEN BERG**, R.F. REMIS, *Delft University of Technology, Delft, The Netherlands*

14:50 68.6 **Invited:** Application of the Padé via Lanczos Process to Rapid Broadband Simulation of Distributed Electromagnetic Systems, **A.C. CANGELLARIS**, L. ZHAO, *University of Arizona, Tucson, AZ, USA*

15:10 Coffee Break

15:30 68.7 **Invited:** A Rational Lanczos Method-Reduce Modeling of Electromagnetic Field Computation, **X. ZHANG**, D.K. SUN, J.-F. LEE, *Worcester Polytechnic Institute, Worcester, MA, USA*

15:50 68.8 **Invited:** Model-Reduction Techniques for EM and Mixed EM/Circuit Simulation, **M. NAKHLA**, R. ACHAR, M.A. KOLBEHDARI, *Carleton University, Ottawa, ON, Canada*

16:10 68.9 Fast Transient Analysis via Electromagnetic Reduced-Order Models, E. BRACKEN, **Z.J. CENDES**, *Ansoft Corporation, Pittsburgh, PA, USA*

16:30 68.10 Adaptive Stopping Criteria for the Padé via Lanczos Algorithm Applied to Electromagnetic Problems, **R.D. SLONE**, Z. BAI, W.T. SMITH, *University of Kentucky, Lexington, KY, USA*

B68.1

Illustrative Examples of Reduced Order Representation for Efficient Electromagnetic Computation

Raj Mittra
EE Department & Applied Research Laboratory
Pennsylvania State University, University Park, PA

In this paper we present two examples that illustrate the use of the reduced order representation for the solution of large-body scattering problems with applications in RCS computation, and the construction of closed form Green's functions for MMIC analysis. Despite the advent of high speed computers, and innovative approaches to reducing the operation counts in the solution techniques, the solution of large-body scattering problems using the conventional numerically-rigorous techniques remains an elusive goal at frequencies even moderately above the resonance range. Thus one must typically resort to asymptotic methods, e.g., the ray techniques to tackle these problems. This situation presents us with the following dilemma: Should we accept the limitations of the asymptotic techniques in terms of accuracy and flexibility relative to the numerical techniques, or use the more reliable and accurate numerical schemes instead, but resignedly settle for the solution of a smaller-size problem that is manageable within the limits of the available CPU memory and time? In this paper we present a technique based on the reduced order representation of the induced current distribution in the smooth regions of large scatterers in terms of a small number of complex exponentials. This representation is subsequently extrapolated to previously-unreachable higher frequencies in a systematic manner, from the results derived by using conventional numerical techniques, e.g., MoM, FEM or FDTD, at two or more lower frequencies, for which the problem size is still manageable in terms of memory size and CPU time. The extrapolation algorithm is based on a selective scaling of the individual traveling wave components of the current distribution on the surface of the scatterer, whose scaling properties with frequency depend upon the nature of the traveling wave.

In the second example, we consider the problem of expressing, in closed form, the Green's function for MMIC problems involving microstrip circuits etched on a multi-layered substrate. We again seek to represent the integrand of the Sommerfeld integral in terms of a set of complex exponentials – relatively few in number. Such a representation not only enables us to evaluate the integral in a closed form, but to subsequently express the elements of the MoM matrix also in closed forms. The time saving resulting from the use of the closed form Green's function and MoM matrix element representation can be substantial, and renders this technique suitable for incorporation into a CAD tool for MMIC analysis.

MODEL-ORDER REDUCTION IN COMPUTATIONAL ELECTROMAGNETICS USING MODEL-BASED PARAMETER ESTIMATION

Edmund K. Miller
3225 Calle Celestial
Santa Fe, NM 87501-9613
emiller@esa.lanl.gov

Although computer speed and memory continue to grow at their times-ten trend every five years or so, the resource requirements of solving electromagnetic boundary-value problems remain daunting for a wide variety of applications. Consequently, much attention has been devoted in recent years to the strategy of reducing, for example, the number of unknowns needed to model a problem, the computer-operation count required in developing a solution, and the number of samples needed to represent that solution for subsequent use. Broadly speaking, these kinds of strategies can all be described as belonging to the topic of model-order reduction.

One particular approach to model-order reduction is model-based parameter estimation (MBPE), a name borrowed from the signal-processing community. MBPE uses an analytical description (the model, preferably physics-based) whose unknown coefficients (the parameters) are quantified by fitting the model to samples of a process or data to be approximates [E. K. Miller and G. J. Burke (1991), "Using Model-Based Parameter Estimation to Increase the Physical Interpretability and Numerical Efficiency of Computational Electromagnetics," Computer Physics Communications, 68, 43-75]. Applications of MBPE to computational electromagnetics (CEM) can be found in all of the areas above, though not necessarily always referred to by that name. Specific uses of MBPE in CEM include reducing the operation count required for computing an integral-equation impedance matrix, estimating the frequency dependence of the impedance and admittance matrix coefficients, simplifying computation of radiation patterns, and estimating the accuracy of a numerical solution. This presentation will include a brief background discussion of MBPE and its implementation, and illustrate its use for for several CEM applications.

B68.3

Application of Total Least Squares in Parametric Modelling of Responses of Electromagnetic Systems

Tapan K. Sarkar
Department of Electrical Engineering and Computer Science
121 Link Hall
Syracuse University
Syracuse, New York 13244-1240

Abstract: Conventionally one utilizes least squares when it is necessary to approximate some data Y in the system AX = Y where A is the System matrix and X is the unknown to be solved for. Generally, it is assumed that these are more equations than unknowns and Y is contaminated by noise. However, least squares tacitly assume that the system matrix A contains no errors and that all the errors are in Y. However, in the parametric modelling of EM responses, this assumption is no longer valid. The system matrix A is also contaminated by noise, either computational or otherwise. In that case, the application of least squares would not provide accurate solutions. One has to take recourse to the Total Least Squares. Total least squares take care of noise in both the system matrix A and in the data Y. Hence the application of Total Least Squares provide significantly stable results and the statistical variations are considerably smaller. The application of this principle has been incorporated in the Matrix Pencil Method and in the Cauchy Technique. The Matrix Pencil Method is a technique to approximate a function by a sum of complex exponentials. This technique is highly suitable for extrapolating free transient responses from conducting objects. In this procedure early time domain date (i.e. after the incident pulse has crossed the object) can be utilized to extrapolate late time responses utilizing the SEM concept. The utilization of Total Least Squares provides a stable solution.

The Cauchy Method is another method for approximating a function by a ratio of two polynomials given the values of the function and/or a few of its derivatives at some points not necessarily equally spaced. Cauchy's method developed in 1821 predates most parametric methods and the various other techniques like Pade and so on are really special cases of this method. This method is useful for interpolating/extrapolating frequency domain responses of electromagnetic systems which may contain sharp resonances. Again utilization of total least squares provide a stable solution procedure. Performance of both of these techniques in the presence of noise will be illustrated.

A Brief Survey of Krylov-subspace Based Model-Order Reduction

Ibrahim Elfadel, Joel Phillips, Miguel Silveira, and Jacob White
Department of Electrical Engineering and Computer Science
Massachusetts Institute of Technology
Cambridge, MA 02139

There are now a variety of robust methods for automatically generating reduced-order models from frequency-domain analysis of linear electromagnetic systems with a few inputs and outputs, with electronic interconnect being the most common example. These various model-reduction methods begin differently, depending primarily on whether the system is represented by tabulated data, finite-element or finite-difference spatial discretization, or discretized integral formulations such as the method-of-moments. However, these robust methods all share the same final stage, where a Lanczos or Arnoldi method is used to generate suitably orthogonalized Krylov subspaces. In this talk, we will survey these recently developed methods and describe the problem of insuring that the reduced-order model is both stable and passive. We will show that for quasistatic problems, these issues are nearly entirely resolved. We will also show that for full-wave analysis, propagation delays play an important roles, there are still significant challenges.

B68.9

FAST TRANSIENT ANALYSIS VIA ELECTROMAGNETIC REDUCED-ORDER MODELS

Eric Bracken and Zoltan Cendes
Ansoft Corporation
Four Station Square, Suite 660
Pittsburgh, PA 15219

We present a efficient alternative to time-stepping methods for computing transient electromagnetic signals. First, we use fast-sweep methods such as AWE (X. Yuan and Z. Cendes, "A Fast Method for Computing the Spectral Response of Microwave Devices over a Broad Bandwidth", AP-S/URSI International Symposium, Ann Arbor, MI, June 1993, p. 196) or ALPS (D. Sun, "ALPS: An Adaptive Lanczos-Pade Approximation for the Spectral Solution of Mixed-Potential Integral Equations", AP-S/URSI International Symposium, Baltimore, MD, July 1996, p. 30) to determine the frequency response of an electromagnetic system over a broad bandwidth. This information is then used to compute a reduced-order model of the transfer function of the system. From this reduced-order model an equivalent circuit is derived. This equivalent circuit is subsequently used in circuit analysis to determine the transient response of the system using circuit simulators such as SPICE or SPECTRE.

This procedure is to be compared to classical time-stepping methods in the space domain such as the FDTD algorithm. In that approach, the geometry of the structure is represented by thousands of grid points and the electromagnetic field at each point is computed at thousands of time steps directly from Maxwell's equations.

The new approach has several advantages over the time-stepping with fields approach: First, the electromagnetic field is computed only once. Since the electromagnetic behavior of a linear system is completely characterized by a few dozen parameters, these can be derived from a single field solution. Second, the electromagnetic analysis may be performed by using either differential or integral equation based methods. In this paper, we employ both finite element analysis and boundary element analysis to perform the frequency domain electromagnetic field computation. Third, the time-domain solution is computed in the circuit domain. This means that the transient simulation is very fast and memory efficient since it is based on reduced-order models involving only a few dozen parameters. Fourth, the resulting electromagnetics model is readily combined with external sources and loads. Since both the electromagnetic fields and the external sources and loads are represented by circuit elements, they are simulated simultaneously in the circuit simulator. And fifth, it is very easy to use these reduced-order models in what-if design variations. Since the electromagnetics is performed only once, it is possible to pass these detailed electromagnetics models on to design groups working at the system level.

The new transient/fast sweep procedure has been implemented in the Ansoft product the High-Frequency Structure Simulator HFSS. The full paper will illustrate the theory with solutions from antenna design obtained by using this new feature in Ansoft HFSS.

Adaptive Stopping Criteria for the Padé Via Lanczos Algorithm Applied to Electromagnetic Problems

Rodney Daryl Slone[1*], Zhaojun Bai[2], William T. Smith[1]

[1] Dept. of Electrical Engineering
453 Anderson Hall
University of Kentucky
Lexington, KY 40506-0046 USA

[2] Dept. of Mathematics
751 Patterson Office Tower
University of Kentucky
Lexington, KY 40506 USA

The Padé Via Lanczos (PVL) algorithm was developed in the CAD area for efficient time or frequency domain analysis of electrical interconnects [Feldman and Freund, 1995]. The PVL technique can be used to obtain the dominant poles and residues of an electromagnetic system model. It is straightforward to find the transient response or the frequency domain response of the model using these poles and residues. Typically, to determine the response using the standard PVL technique, one had to run the algorithm for a user-specified number of poles, rerun the algorithm to generate a higher order approximation, and compare both sets of data to heuristically determine if the reduced model had captured the characteristics of the original system. In this talk, a new computationally inexpensive error bound for the PVL procedure is presented. This error bound resulted from a new matrix based derivation of the PVL technique. Using this error bound as a stopping criterion, it is possible for the first time to adaptively implement the PVL algorithm. This PVL with error bound (PVL-WEB) technique takes a user-defined error tolerance and iterates the Lanczos process until the error in the reduced model is less than the user-requested tolerance.

The applications of the PVL-WEB technique to electromagnetic problems will be illustrated by modeling planar conducting circuits using the Partial Element Equivalent Circuit (PEEC) full wave solution method. PEEC analysis can generate large systems of equations but the PVL-WEB algorithm provides an efficient solution without the previously required heuristic determination of convergence.

Results of applying the PEEC method to analyze a patch-type antenna structure will be presented. The PVL-WEB algorithm will be used to develop a reduced-order model of the radiator. Characteristics such as input impedance and current distribution will be computed and will be compared to results generated using other modeling techniques.

URSI B Special Session **Session 71** **Salon Peribonca**

Image Construction from Real Data
Co-chairs: R.V. McGahan, USA and R.E. Kleinman, USA

13:10 71.1 **Invited:** Target Recognition from Limited-Angle Backscatter Data, R.A. MARR[1], **D.A. POMMET**[2], U.H.W. LAMMERS[1], R.V. McGAHAN[1], M.A. FIDDY[2], [1]*University of Massachusetts-Lowell and* [2]*Rome Laboratory, Hanscom AFB, MA, USA*

13:30 71.2 **Invited:** Imaging of Unknown Targets from Measured Scattering Data, **D.A. POMMET**[1], S. BHAGAVATULA[1], J.B. MORRIS[2], R.V. McGAHAN[2], M.A. FIDDY[1], [1]*University of Massachusetts-Lowell and* [2]*Rome Laboratory, Hanscom AFB, MA, USA*

13:50 71.3 **Invited:** The Reconstruction of Hybrid Media from Real Electromagnetic Scattering Data, P. MAPONI[1], **F. ZIRILLI**[2], [1]*Università di Camerino and* [2]*Università di Roma "La Sapienza", Rome, Italy*

14:10 71.4 **Invited:** Image Reconstruction from the 1997 Ipswich Data Using Conjugate Gradient Algorithm Enhanced with Edge-Preserving Regularization, **P. LOBEL**, Ch. PICHOT, L. BLANC-FÉRAUD, M. BARLAUD, *Université de Nice-Sophia Antipolis/CNRS, Valbonnne, France*

14:30 71.5 **Invited:** Modified Gradient Methods Applied to the Ipswich Real Data, **B. DUCHÊNE**, D. LESSELIER, *Laboratoire des Signaux et Systèmes (CNRS-Supélec), Gif-sur-Yvette, France*

14:50 71.6 **Invited:** The Application of Backpropagation Algorithms to the Ipswich Data, **G.F. CROSTA**, *Università Degli Studi di Milano, Italy*

15:10 Coffee Break

15:30 71.7 **Invited:** Image Reconstruction from Ipswich Data-III, **P.M. VAN DEN BERG**[1], B.J. KOOIJ[1], R.E. KLEINMAN[2], [1]*Delft University of Technology, Delft, The Netherlands;* [2]*University of Delaware, Newark, DE, USA*

B71.1

Target Recognition From Limited-Angle Backscatter Data

R.A. Marr*, D. A. Pommet, U. H. W. Lammers*, R. V. McGahan* and M. A. Fiddy

Department of Electrical Engineering, University of Massachusetts-Lowell, Lowell, MA 01854
*Rome Laboratory, Hanscom AFB, MA 01731

Inverse scattering methods typically require scattered field measurements to be taken at all scattering angles for all illumination directions. This is rarely feasible in practice and one usually has only limited data to work with. Under ideal circumstances, the scattered field data are placed on arcs in k-space which are then processed to recover information about the target. This processing is particularly straightforward for weakly scattering targets. We demonstrate how targets can be recognized when only limited backscatter data are available for a small range of illumination angles. In this paper we assume that the first Born approximation is valid, which is reasonable when the backscatter data are dominated by a limited number of independent specular scatterers. These limited data can be used, along with prior estimates of possible target shapes, to determine which target is present. This step is based on the extrapolation of the measured scattered field data in k-space. The method used to do this, the PDFT algorithm, requires that a set of equations of the form:

$$f(k) = \sum_{n=-N}^{N} a_n p(k-n), \; k = -N,\ldots,N \qquad (1)$$

is solved where f(k) are the data and the values p(m) (m = -N, ..., N) are taken from the discrete Fourier transform of the prior knowledge, P(r), of the target shape. The estimate of the object is given by

$$PDFT(r) = P(r) \sum_{n=-N}^{N} a_n e^{inr} \qquad (2)$$

The quality of the reconstruction depends on the number of data points and quality of the prior estimate of the target. There is a trade-off between the number of data values and the amount of target information incorporated into P(r). Using this approach one can determine how *few* data points are required, for a given prior, to reliably identify a target from a set of likely candidates. We illustrate the technique with both real and simulated data.

Imaging of unknown targets from measured scattering data

D. A. Pommet, S. Bhagavatula, J. B. Morris*, R. V. McGahan*, and M. A. Fiddy

Department of Electrical Engineering, University of Massachusetts-Lowell, Lowell, MA 01854
* Rome Laboratory, Hanscom AFB, MA 01731

Using data provided, we employ several inverse scattering methods to recover and estimate an image of the permittivity distribution responsible for the scattering. The Born approximation as well as a rigorous Fourier-based technique, known as differential cepstral filtering, will be applied to the data.

The differential cepstral filtering technique remains computationally simple but is not limited by a weakly scattering condition. The technique is based on recognizing that scattering data captured from single view illumination is related to the product of the target's permittivity and the (unknown) internal field. In the cepstral domain, spectral information about the sum of these functions are available. By filtering backpropagated images in the differential cepstral domain, one can remove the contribution from the unknown field to recover the target distribution.

B71.3

The reconstruction of hybrid media from real electromagnetic scattering data

Pierluigi Maponi
Dipartimento di Matematica e Fisica
Università di Camerino
62032 Camerino (MC), Italy

Francesco Zirilli
Dipartimento di Matematica "G. Castelnuovo"
Università di Roma "La Sapienza"
00185 Roma, Italy

We consider the propagation of electromagnetic waves in an inhomogeneous medium. The inhomogeneity is assumed to be cylindrically symmetric and the polarization of the incident time harmonic electromagnetic field is either parallel or orthogonal to the symmetry axis. Under these assumptions the scattering problem can be reduced to an inverse problem for the two dimensional Helmholtz equation where the unknown is a complex refraction index $n(\underline{x}) = n_1(\underline{x}) + i\ n_2(\underline{x})$. The medium is hybrid in the sense that both $n_1(\underline{x})$ and $n_2(\underline{x})$ are non zero.
In the Born approximation the refraction index appears as the unknown of a Fredholm integral equation of the first kind or more precisely a system of two Fredholm equations for the two unkonwn $n_1(\underline{x}), n_2(\underline{x})$. The solution of this system of equaions is ill posed. A special algorithm is suggested to solve this system that attempts to reach high resolution avoiding ill conditioning. This is done using an iterative method that makes use of several grids to discretize the integral equations and in a heuristic strategy to choose the location of the unknown to be solved along the iteration.
This algorithm is tested on the IPSWICH data provided by Rome Laboratory Hascom, MA, (USA).
The results obtained will be shown and are very satisfactory.

Image Reconstruction from the 1997 Ipswich Data using Conjugate Gradient Algorithm enhanced with Edge-Preserving Regularization

P. Lobel[1*], Ch. Pichot[1], L. Blanc-Féraud[2] and M. Barlaud[2]

[1] Laboratoire d'Electronique, Antennes et Télécommunications,
[2] Laboratoire Informatique, Signaux et Systèmes de Sophia Antipolis,
Université de Nice-Sophia Antipolis/CNRS,
250 rue Albert Einstein, 06560 Valbonne, France

The reconstruction of the complex permittivity contrast profile for 2D-TM objects using scattered far-field data is considered. In order to solve this nonlinear and ill-posed inverse scattering problem, an iterative algorithm based on a conjugate gradient method with edge-preserved regularization is used (P. Lobel, Ch. Pichot, L. Blanc-Féraud, and M. Barlaud, 1996 Digest IEEE AP-S, Baltimore, 1, 644-647). The problem is formulated by means of the minimization of a two-term cost functional. The first term matches the measured scattered data with computed ones of the forward problem. The forward problem is solved by means of an EFIE and the moment method. A second term is added for regularizing the solution in order to enhance the reconstruction i.e the convergence and stability versus signal to noise ratio.

With the regularization procedure, the object to be reconstructed is modeled as a set of homogeneous areas separated by borderlike discontinuities. It involves the use of a non-quadratic regularizing function which could be seen as a potential function φ of a Markov Random Field. During the minimization process, this φ function allows a smoothing in the homogeneous areas of the object while edges are preserved. Various convex and non-convex φ functions exist in the literature having different behaviors for edge detection and enhancement. The complete iterative algorithm can be described as an alternate minimization involving, in one hand, the minimization of the edge mapping and, on the other hand, the minimization of the contrast using a Polak-Ribière conjugate gradient algorithm.

B71.5

Modified gradient methods applied to the Ipswich real data.

B. Duchêne and D. Lesselier
Division Ondes – Laboratoire des Signaux et Systèmes (CNRS-Supélec)
ESE – Plateau de Moulon, 91192 Gif-sur-Yvette Cedex, France

Binary-based modified gradient solution methods are applied to the new set of experimental Ipswich Data. As is now well-known, nonlinearized modified gradient methods attempt to solve both the observation equation and the coupling equation, this being done simultaneously for all excitations. (The first equation relates the scattered field data to the sources induced inside the target which are proportional to the unknown contrast function; the second equation links these sources to themselves.) Extensions of such methods that are capable to iteratively build up "binary" structures whose contrast with respect to the ambient medium electric or acoustic parameter takes only two values (say, 1 when a given pixel is inside the object, and 0 when it is outside) have been shown effective as is demonstrated in L. Souriau *et al., "A modified gradient approach to inverse scattering for binary objects in stratified media," Inverse Problems, 12, 463-481, 1996.*

Modified gradient methods and their binary extensions apply to many wavefield inversion problems, from both nearfield and farfield, full-view or aspect-limited data, in the space-diversity mode and/or the frequency-diversity mode, and they suitably handle high-contrast targets or perfectly conductive ones —though a domain integral formulation of the wavefield is to be chosen in the analysis. However so far the binary extensions dealt with a purely real or purely imaginary-valued contrast function, i.e., with lossless dielectric targets or perfectly conductive ones. Here, in addition, the case of possibly lossy dielectric objects is attacked using two contrast functions, one associated with the real part and the other with the imaginary part of the contrast, each being allowed to take two values only but in an independent fashion (in practice, it means that three directions of updating are built up at each iteration, one for the complex-valued field, and one for each contrast function).

Key theoretical and numerical aspects of the binary-specialized methods and results of inversions carried out on both known and mystery targets, will be discussed in the presentation, and comparisons with diffraction tomographic schemes tailored for the cylindrical measurement scheme will be made.

THE APPLICATION OF BACKPROPAGATION ALGORITHMS TO THE IPSWICH DATA

GIOVANNI F CROSTA
UNIVERSITÀ DEGLI STUDI DI MILANO
Dipartimento di Scienze dell' Ambiente e del Territorio
via Emanueli, 15 – I 20126 MILANO (IT); e_mail: crosta@imiucca.csi.unimi.it

ABSTRACT

The IPSWICH data provide a unique opportunity for the validation of the approximate backpropagation (ABP) methods [see e.g., G F CROSTA, 1994, *The Backpropagation Method in Inverse Acoustics*, in M CHENEY, P KUCHMENT, E T QUINTO, Editors, *Tomography, Impedance Imaging and Integral Geometry*, **LAM 30**, pp 35 – 68, AMS: Providence, RI], which were originally developed to identify the shape of a sound soft, axially symmetric obstacle and have so far provided satisfactory numerical results on a class of simulated data in the resonance region. Said methods rely on the properties of complete families of solutions to exterior problems for the HELMHOLTZ equation e.g., the outgoing wave functions $\{v_\lambda \mid \lambda \in \Lambda(L)\}$, where λ is a multi–index and L the approximation order. The unknown is the (admissible) shape parameter vector, $\vec{\psi}$; the objective function to be minimized (by e.g., conjugate directions) is the boundary defect, B, of order L

$$B^{(L)}[\vec{\psi}] := \| \sum_{\lambda \in \Lambda(L)} \tilde{c}_{\lambda}^{(L)} v_\lambda + u \|^2_{L^2(\Gamma)},$$

where u is the incident plane wave. The approximate scattered wave, $v^{(L)}$, on the unknown obstacle boundary, Γ, depends on a few expansion coefficients, $\tilde{c}_{\lambda}^{(L)}$. The latter come from suitably transforming (propagating backwards) the known far field coefficients, $\tilde{f}_\lambda$. In fact, the two ABP methods available to date, $\mathbf{W}^{(L)}$ and $\mathbf{M}^{(L)}$, differ by the operator, which maps $\tilde{f}_\lambda$ to $\tilde{c}_{\lambda}^{(L)}$. In order to deal with the IPSWICH data, some procedures of the ABP algorithms have to be modified. The basis functions for two dimensional problems have to be used and the derivatives of the ABP operator have to be obtained and coded. The parameters in the phase offset of the scattered field are additional unknowns in the boundary defect. All suitable subsets of the IPSWICH data are being processed. The outcome will be discussed and justified in any case.

B71.7

Image Reconstruction from Ipswich Data–III

P. M. van den Berg and B.J. Kooij

Laboratory of Electromagnetic Research, Faculty of Electrical Engineering, Centre for Technical Geoscience, Delft University of Technology, P.O. Box 5031, 2600 GA Delft, The Netherlands

R.E. Kleinman

Center for the Mathematical of Waves, Department of Mathematical Sciences, University of Delaware, Newark, Delaware 19716, USA

In this paper we describe the results obtained by using variants of the modified gradient algorithm developed earlier (e.g. R.E. Kleinman and P.M. van den Berg, *J. Comp. and Appl. Math.*, **42**, 17–35, 1992) together with some of the Ipswich datasets to reconstruct the shape, location, and/or index of refraction of unknown two-dimensional scatterers.

This method was used previously in connection with two Ipswich datasets (IPS001 and IPS002) corresponding to TM polarization (electric field polarized along the cylinder axis of the cylindrical 2-D scatterer) or VV in the Ipswich designation for two perfectly conducting objects, the circular cylinder and the strip. The experimental data were renormalized by multiplying the circular cylinder data by an unknown complex constant and this constant is determined by minimizing the L^2 norm of the difference with the exact data as computed using the representation in cylindrical wave functions. This constant, which is essentially a phase correction, was then used as a multiplier of the measured data for all other cases. Good reconstructions were obtained and these results were reported three years ago. Two years ago, a third dataset (IPS003) for a penetrable object (a square polystyrene cylinder) became available, but good reconstruction was not possible because the data were measured in a different setup and calibrated differently.

Since last year, the new Ipswich datasets are all given in the same form and a perfectly conducting cylinder set (IPS006) was also given which enables a consistent renormalization, but it only applies to the TM case. We were able to reconstruct images successfully from the datasets IPS005 (a dielectric dihedral) and IPS007 (a dielectric tube with a smaller inner tube). The reconstructed image from the last dataset, IPS008 (the two tubes filled with a sand/salt mixture), was not really satisfactory; in this case we either need more datapoints or we have to reconstruct assuming that the permittivity is complex-valued rather than real-valued.

The dataset IPS004, the aluminium dihedral, corresponds to TE polarization (electric field polarized transversal to the cylinder axis) or HH in the Ipswich designation. But the problem was that no experimental data with respect to TE scattering from a circular cylinder has been supplied, so that no proper calibration of the data can be carried out.

In the present paper, we hope to report reconstructions from new datasets using the modified gradient method. In case also datasets (including a dataset of a circular cylinder for calibration purposes) are available for the TE (HH) case, reconstructions from these datasets will be reported as well.

URSI B

Session 74

Salon Chaudière

Scattering by Periodic Structures
Co-chairs: E.W. Lucas, USA and M. Lecours, Canada

13:10	74.1	Ray Analysis of Scattering by a Periodic Array of Strips on a Material Half Space for Nearby Source and Observer Locations in ITS Applications, H.T. CHOU, F. BIRBIR, **P.H. PATHAK**, B. BAERTLEIN, *Ohio State University, Columbus, OH, USA*
13:30	74.2	EM Scattering from Periodic Gratings of Lossy Conductors, **H.A. KALHOR**, *State University of New York, New Paltz, NY, USA*
13:50	74.3	Entire Domain Modal-Based MOM Analysis for Infinite Periodic Array Radiation and Scattering Problems, **E.W. LUCAS**, T.P. FONTANA, R.G. SCHMIER, *Northrop Grumman Corporation, Baltimore, MD, USA*
14:10	74.4	Millimeter-Wave Radar Phenomenology of Power-Lines, **K. SARABANDI**, M.S. PARK, F.T. ULABY, *University of Michigan, Ann Arbor, MI, USA*
14:30	74.5	TM-Mode Scattering from Multiple Notches in a Dielectric-Covered Ground Plane, K.H. PARK[1], H.J. EOM[1], **W.J. CHUN**[2], [1]*Korea Advanced Institute of Science and Technology, Taejon and* [2]*Korea Telecom, Seoul, Korea*
14:50	74.6	TE Blazing of Finite Periodic Strip Grating on a Grounded Dielectric Slab, **J.I. LEE**, Y.-K. CHO, *Kyungpook National University, Taegu, Korea*
15:10		Coffee Break
15:30	74.7	Scattering Characteristics of Bigratings, **R.B. HWANG**[1], S.T. PENG[2], [1]*National Center for High-Performance Computing and* [2]*National Chiao Tung University, Hsinchu, Taiwan, China*
15:50	74.8	Backscattering by Periodical Surfaces with Dielectric Filling, **J.-F. KIANG**, *National Chung-Hsing University, Taichung, Taiwan, China*

B74.1

Ray Analysis of Scattering by a Periodic Array of Strips on a Material Half Space for Nearby Source and Observer Locations in ITS Applications

H.T Chou, F. Birbir, P.H. Pathak* and B. Baertlein
The Ohio State University ElectroScience Laboratory
1320 Kinnear Road, Columbus, Ohio 43212, USA

A radar based method for automatic guidance of vehicles as part of the intelligent transportation system (ITS) requires one to analyze and design an appropriate periodic linear array of scatterers located along the surface of a highway that is locally illuminated by a nose mounted automobile radar. The periodic array must be designed to produce a sufficiently strong reflected wave back to the radar to provide guidance information for the steering mechanism. Such a configuration may be modeled initially in two dimensions by a periodic array of perfectly conducting strips located on a material half space (simulating concrete); the illumination for this array is a nearby directive source simulating a radar antenna on an automobile. In this paper, a relatively efficient analysis of this configuration is developed based on a generalization of ray methods for periodic structures. Here, the transmitting antenna is fairly directive, and the excitation of the array by this antenna is therefore sufficiently localized to the region of the array illuminated by the directive antenna beam. Consequently, the excitation of the array is very different from a periodic excitation. Clearly, the scattered fields due to non-periodic excitation cannot be directly expanded in a set of discrete Floquet modes, but instead requires a continuous spectral integration over each term of the Floquet mode series thereby making such analysis cumbersome. Thus, an asymptotic approximation of the spectral integral obtained earlier in (Felsen & Ribas, IEEE Trans. AP-S, vol. 44, No. 3, pp375-382, 1996) is utilized to obtain only a Floquet mode series that contains a generalized ray interpretation for describing the scattering in both the specular and non-specular directions. Such a ray picture for describing the phenomenology of scattering from periodic structures excited by a non-periodic illumination proves to be very useful in the design of periodic arrays for the present application to ITS. It is also shown in this paper how the relevant ray parameters can be obtained rather efficiently from the standard numerical solution of the corresponding related but more conventional problem of the plane wave scattering from the same periodic array configuration; however, since the plane wave excitation is periodic, the numerical solution based here on an integral equation formulation for either the unknown electric current on the strips or the unknown equivalent magnetic currents in the apertures (or gaps) between the metal strips is obtained by solving for these unknowns only within the unit cell of the periodic structure. Also, it is seen that the coefficients of the Floquet mode expansion for plane wave excitation can be computed relatively efficiently for all incident plane wave directions necessary in the evaluation of the ray parameters. Numerical results illustrating the utility of this ray analysis to ITS application will be presented. Also, the effect of a thin coating of a high dielectric constant material that can be viewed as a superstrate on the periodic array of strips over the half space will be discussed; this superstrate serves to model a thin coating of rain water over the concrete highway.

EM SCATTERING FROM PERIODIC GRATINGS OF LOSSY CONDUCTORS

Hassan A. Kalhor
Department of Electrical Engineering
State University of New York
New Paltz, N.Y. 12561-2499

Metallic gratings of different groove shapes have many applications in optics, electromagnetics, and microwaves because of their strong frequency dependent behavior. Many ingenious numerical analysis techniques have been developed for the analysis of such structures. Most of the analytical methods assume that the metal is a perfect conductor and placed in air. In practice, all the scatterers are made of finitely conducting materials, and many times, they are located in a lossy medium as well. The effect of finite conductivity in gratings with triangular groove shape has been previously calculated by using a surface impedance model (Kalhor and Neureuther, J. Opt. Soc. Am., Nov. 1973). Gratings of resistive strips have also been analyzed for their potential in reducing their scattering in reflector antennas (Hall, IEEE Trans. Antennas Propogat. Sept. 1985).

In this presentation, the scattering from imperfect conducting gratings is solved by a combined wave expansion and finite difference method which gives the field within the material as well as the scattered fields. Conductor losses and their impact on the scattered fields can, therefore, be determined accurately. The scattered fields above and below the structure are expanded in terms of outgoing travelling wave modes. In the groove region, the wave equation is discretized in a finite difference form. The fields in the three regions are coupled together through the application of the required boundary conditions at the two interfaces. The solution of the system yields the reflected and the transmitted wave coefficients as well as the fields in the groove region. Conductor losses are calculated from the calculated fields in the grating material and compared with the difference between the incident and all the scatettered power to establish the accuracy and the adequacy of the proposed technique.

B74.3

Entire Domain Modal - Based MOM Analysis for Infinite Periodic Array Radiation and Scattering Problems

*Eric W. Lucas, Thomas P. Fontana and Robert G. Schmier
Northrop Grumman Corporation, Electronic Sensors and Systems Division
P.O. Box 746, Baltimore, Maryland 21203

In this presentation we will discuss an application of the method of moments (MOM) technique for the efficient radiation and/or scattering analysis of some infinite periodic array structures. The simplifying assumption of infinite periodicity is known to be very practical for the electromagnetic performance predictions of large planar arrays, and is commonly invoked for the industrial designs of many phased array antennas, frequency selective surfaces, stratified polarizers and other such periodic rf devices. The assumption is simplifying because it permits the analysis to focus on a single periodic 'unit-cell' of the array provided that a suitable representation of the periodic Green's function is used. This is readily accomplished through a Floquet vector-mode expansion of the periodic dyadic Green's function. Since this is a plane-wave oriented vector mode expansion, it is quite simple to take into account the effects of isotropic stratified dielectric layers directly into this Green's function, as is well known. This is vital since stratified dielectric layers play an important role in shaping the rf performance of these devices.

In this particular formulation, we use a reation-oriented approach combined with the concepts of the equivalence principle. The approach thus handles combinations of PEC (electric-type) scatterers along with multiple aperture (magnetic-type) scatterers. The efficiency of the approach lies in the selection of entire-domain vector-mode basis functions, which can often be integrated in closed-form in the moment procedure. This also allows for the use of very small numbers of basis functions, usually on the order of 10 or so per scatterer to accurately describe the unknown currents. Of course this does limit the geometric generality of the pec patches and apertures which can be appropriately modeled by such bases. The canonical cross-sectional shapes of circular waveguides, rectangular waveguides, coaxial waveguides, and parallel-plate waveguides are used here. This limited set fortunately provides for the analysis of many practical and high-performance phased-arrays and frequency-selective surfaces. Some representative examples will be reported.

Millimeter-Wave Radar Phenomenology of Power-Lines

Kamal Sarabandi, Moon Soo Park, Fawwaz T. Ulaby
Radiation Laboratory
Department of Electrical Engineering and Computer Science
The University of Michigan, Ann Arbor, MI 48109-2122
Tel :(313) 936-1575, Fax:(313) 747-2106
email: saraband@eecs.umich.edu

High voltage power lines and power line towers create hazardous condition for low flying aircrafts and helicopters. Army aviation and other services have an urgent need for an automated system to alarm pilots of the existence, direction, and distance of nearby cables. Many collision warning techniques have been suggested in the past. An electro-optical laser radar is currently pursued as a solution for this problem. Major limitations of laser systems include: 1) limited range, 2) significant atmospheric attenuation under inclement weather conditions, and 3) limited ability to automate the wire detection warning for pilots. As a result of these limitations, the laser systems has not preceded beyond the technology demonstration phase. In this paper the feasibility of power line detection using millimeter-wave radars is investigated. The fact that a high voltage power-line is made up of strands of wires in a helical arrangement can be exploited with regard to backscattering detection of the power-lines. At high frequencies the helical geometry of power-lines becomes an important factor influencing the scattering behavior of electromagnetic waves which can be taken advantage of in detecting power lines at off-specular directions. Power line samples of different diameters were acquired and their polarimetric backscatter responses over a wide range of incidence angles were measured at X-, Ka-, and W-band. The effect of the helicity and the periodicity of the surface in backscatter at millimeter wave frequencies manifest themselves in strong Bragg scattering at vertical and cross polarization. A polarimetric detection algorithm for detecting power-lines in a strong clutter background is developed and tested.

B74.5

TM-Mode Scattering from Multiple Notches in a Dielectric-Covered Ground Plane

Kyung H. Park and Hyo J. Eom
Department of Electrical Engineering
Korea Advanced Institute of Science and Technology
373-1, Kusong Dong, Yusung Gu, Taejon, Korea
Phone 82-42-869-3436, Fax 82-42-869-3410

Wan J. Chun*
Satellite Communication Research Office
Korea Telecom, Seoul, Korea
Phone 82-2-458-6116, Fax 82-2-458-6430

The problem of TE-mode scattering from a finite number of notches in a dielectric-covered ground plane has been extensively studied and well understood for leaky wave antenna applications (K. Uchida, IEEE Trans. Microwave Theory Tech. vol. MTT-35, no. 5, pp. 481-486, May, 1987). TM-mode scattering from a single notch in a dielectric-covered ground plane has been also considered in (R.D. Nevels and C.M. Butler, Journal of Applied Physics, vol. 52, no. 5, pp. 3145-3147, May, 1981). In this paper, we analyze TM-mode scattering from a finite number of rectangular notches which are periodically engraved in a dielectric-covered ground plane. We formulate the problem of TM-scattering from multiple notches using the Fourier transform and the mode-matching technique, thus obtaining a rapidly-converging series solution. Simultaneous equations for the modal coefficients are obtained by enforcing the boundary conditions on the notch apertures. Using the Fourier transform, the mode orthogonality, and the residue calculus, it is possible to evaluate the transmission and reflection of the surface wave very efficiently from computational view point. Numerical computations are performed to investigate the behaviors of transmission, reflection and radiation. The angular pattern of the far-zone scattered field above the ground plane is examined as the number of notches increases and the size of notch varies. The behavior of the total radiation power versus the number of notches is discussed. Our theoretical analysis is useful for the leaky wave antenna design using multiple notches in a dielectric-covered ground plane.

TE Blazing of finite periodic strip grating on a grounded dielectric slab

Jong Ig Lee* and Young Ki Cho

Department of Electronics, Kyungpook National University, Taegu, 702-701, Korea

Phone : 82-53-950-5536, Fax : 82-53-950-5505,

E-mail : ykcho@ee.kyungpook.ac.kr

So far Off-Bragg blazing phenomena have been observed in reflection gratings such as rectangular groove grating as well as sinusoidal and triangular grating but only for TM polarization(magnetic field parallel to the grating axis). Recently experimental result that periodic strip grating on a grounded dielectric slab behaves like a rectangular groove grating was reported. And so it would be interesting to investigate blazing phenomena in the periodic strip grating on a grounded dielectric slab.

For this purpose, we consider the electromagnetic scattering problem of a Gaussian beam wave by finite periodic strip grating on a grounded dielectric slab, which is more practical than the infinite geometry case. The desired integral equation for the unknown current induced on the conducting strip is derived and solved numerically by use of the method of moments(pulse basis expansion and point matching scheme). From knowledge of the strip currents, scattering patterns are computed. In particular, we are to concentrate our attention on investigating blazing characteristics of the geometry under analysis for the appropriately chosen geometrical parameters which have been determined from the preliminary study on the infinite geometry case from the viewpoint of both the leaky wave radiation problem and the reflection grating problem.

The results are summarized as :

First, there are Bragg blazing phenomena of two types ; one which is observed for the case that the lowest TE_1 mode is cutoff in the parallel plate waveguide region under the strip and so the leaky wave guiding structure cannot be formed between two adjacent periodic cells, the other for the case that the lowest TE_1 mode is propagating in the parallel plate waveguide region under the strip and so the leaky wave guiding structure can be formed(that is, resonance type).

Second, TE Off-Bragg blazing phenomenon also is observed in the present geometry unlike the rectangular groove grating. It is worthy of noting that this Off-Bragg blazing is observed only for the case that leaky wave guiding structure is formed in the present geometry.

And some difference between blazing phenomena in the present geometry and the finite periodic slot geometry in a parallel plate waveguide filled with a homogeneous dielectric(J. I. Lee and Y. K. Cho, *Proc. 1996 International Symposium on Antennas and Propagation, Chiba, Japan*, vol. 1, pp. 29-32, Sept. 1996) is discussed. The validity of the numerical results are assured by a check of the power conservation relation.

B74.7

Scattering Characteristics of Bigratings

R.B. Hwang*
National Center for
High-Performance Computing

S.T. Peng
Dept. of Comm. Engineering
National Chiao Tung University

We present here a thorough investigation of the plane-wave scattering by a class of bigratings, each of which consists of a uniform dielectric layer sandwiched between two separated gratings that may have different periods and may be oriented with a crossing angle between them. Inherently, this is a three-dimensional boundary value problem, regardless of the incidence condition. An exact formulation based on the method of mode matching is carried out, taking into account the effect of polarization couplings. Wood's anomalies and Bragg phenomenon in the presence of a bigrating are carefully examined and the results are interpreted in terms of the interaction between the two constituent gratings. As an example, Fig. 1 shows the effect of the crossing angle on the transmitted intensity diffracted by a bigrating. There exist regions of rapid variation, which can be explained as Wood's anomalies. To substantiate such an explanation, the normalized transverse propagation constants along the grating structure are plotted against the crossing angle in solid curves in Fig. 2, for various harmonics. The effective indices of the surface waves supported by the limiting case of a uniform dielectric waveguide (in the absence of the gratings) are included as the dashed lines. An intersection of a solid curve with a dashed curve determine the condition of phase matching and hence strong coupling between the diffracted wave and a guided wave; consequently, this determines the region of rapid variation of the diffraction efficiency. The two sets of curves in Figs, 1 and 2 illustrates such a relationship on physical basis. For application, it is found that a bigrating may be designed to perform two functions: beam splitting and polarization purification, as will be explained in detail.

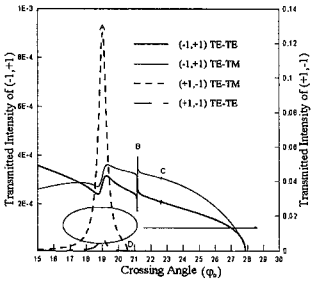

Fig.1 Effect of the crossing angle on the diffraction efficiencies.

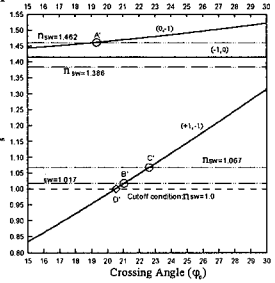

Fig.2 Normalized transverse propagation constant versus incident angle

Backscattering by Periodical Surfaces with Dielectric Filling

Jean-Fu Kiang
Department of Electrical Engineering
National Chung-Hsing University
Taichung, Taiwan

Periodical structures have been widely studied for applications such as filters and leaky wave antennas, wave transmission and reflection, scattering, diffraction by a Fourier grating, scattering from conductive surfaces with a sinusoidal height profile, reflection and transmission by conductive or dielectric gratings embedded in a dielectric slab, and so on.

When a plane wave is incident upon a periodical surface, higher order (Floquet) modes other than the specularly reflected mode are scattered in directions determined by the periodical boundary conditions. The higer order modes carry away part of the incident power, hence reduce the specularly reflected power. It is observed that the profile depth of the surface affects the ratio between the specularly reflected power and the power carried by the first order Floquet modes. This property can be used to reduce the radar cross section of moving objects of which the grooves need be filled by dielectric materials to have an aerodynamically smooth surface. Thus, the effects of the dielectric cover on the backscattering cross section need to be considered.

In this work, we develop a mode-matching method by which periodical surfaces of arbitrary profiles filled with layered dielectric can be analyzed. Several types of periodical surfaces are studied on their backscattering to a normally incident plane waves. The effects of frequency, surface profile shape, period-to-depth ratio, and cover permittivity are analyzed.

The use of dielectric cover reduces the frequency at which surface waves start to be guided, hence reduces the reflected power at certain low frequencies in the $0 \leq P/\lambda_o \leq 1$ band at which total reflection occurs when without cover. The sawtooth profile with $h = 0.25\lambda_o$ reflects very little power at $P/\lambda_o \geq 2$ with or without cover. The sawtooth, concave and convex elliptical profiles with $h = 0.125\lambda_o$ reflect a much higher power when $P/\lambda_o \geq 1$. For the sinusoidal, concave and convex elliptical profiles, the addition of cover tends to reduce the backscattering power. The results obtained can be applied to reduce radar cross section of moving objects.

URSI B | Session 75 | Salon Matapedia

Hybrid Methods
Co-chairs: M.P. Deshpande, USA and W.J.R. Hoefer, Canada

13:10 75.1 Analysis of Matched Waveguide Bends by a Combination of Numerical Methods, **W. PASCHER**, *Fern Universität, Hagen, Germany*

13:30 75.2 New TLM Algorithm for the Study of Axially Symmetric Structures (AS-TLM), S. LE MAGUER, **M.M. NEY**, *Ecole Nationale Supérieure des Télécommunications de Bretagne, Brest, France*

13:50 75.3 A Hybrid Method Combining Integral Equations and a Modal Technique for Air Intake Modelling, **P. SOUDAIS**, A. BARKA, *ONERA, Chatillon, France*

14:10 75.4 A Hybrid FEM-MOM Formulation for Stratified Problems Using Triangular Prism Elements, **E.W. LUCAS**[1], T.P. FONTANA[1], R.G. SCHMIER[1], J.-F. LEE[2], [1]*Northrop Grumman Corporation, Baltimore, MD and* [2]*Worcester Polytechnic Institute, Worcester, MA, USA*

14:30 75.5 Hybrid MoM/SBR Method to Compute Scattering from a Slot Array in a Complex Geometry, **A.D. GREENWOOD**, J.-M. JIN, *University of Illinois at Urbana-Champaign, Urbana, IL, USA*

14:50 75.6 Practical Analysis of Microwave Filters by FDTD and Model S-Parameter Extraction, **P.C.K. YAU**, C. WU, K.-L. WU, J. LITVA, *McMaster University, Hamilton, ON, USA*

15:10 Coffee Break

15:30 75.7 Application of AWE for Frequency Domain Electromagnetics, **C.J. REDDY**[1], M.D. DESHPANDE[2], C.R. COCKRELL[3], F.B. BECK[3], [1]*Hampton University,* [2]*ViGYAN Inc. and* [3]*NASA Langley Research Center, Hampton, VA, USA*

15:50 75.8 Exact Subdomain FEM and MOM Method for Large Inlet Scattering, T. VOLPERT, **A. BARKA**, *Office National d'Études et de Recherches Aérospatiales (ONERA), Châtillon, France*

16:10 75.9 On the Use of Decoupled Meshes in the Analysis of Printed Antennas, **L.C. KEMPEL**, *Mission Research Corporation, Valparaiso, FL, USA*

16:30 75.10 Two-Dimensional Radiation Transport Across Fibrous Media, **J.A. GRZESIK**, *TRW Space and Defense, Redondo Beach, CA, USA*

B75.1

Analysis of Matched Waveguide Bends by a Combination of Numerical Methods

Wilfrid Pascher
Allgemeine und Theoretische Elektrotechnik
FernUniversität, D-58084 Hagen, Germany

The designs of compact rectangular waveguide circuits include inevitably both bends and matching elements, e.g. steps or diaphragms in a confined space. Because of the occurring interactions the curvature of the bends as well as the edges of the matching elements have to be considered accurately.

In this paper a combination of the Method of Lines (MoL) and the Generalized Multipole Technique (GMT) for the analysis of matched waveguide bends is presented. The GMT is employed for round elements (Ch. Hafner, *The Generalized Multipole Technique for Computational Electromagnetics*, Artech House, 1990) whereas the angular parts are investigated by the MoL (W. Pascher, R. Pregla, *IEEE T-MTT 43*, 2649-2653, Dec. 1995). This ensures a good modeling since each circuit element is analyzed by the best-suited method. More complicated structures can be investigated by the hybrid approach than by any of the two methods alone. Both methods use different series expansions and are compatible concerning the field matching at the interfaces between the individual solution domains.

The MoL is particularly appropriate for the analysis of matching elements since the electromagnetic field is very accurate even near metallic and dielectric edges. In case of rectangular waveguide structures in the E- or H-plane the wave equation is discretized and numerically solved in one transverse direction only. The solution in the other transverse direction and in longitudinal direction is obtained analytically.

On the other hand the GMT is favorable for modeling of round objects, e.g. cylinders of arbitrary cross-sections. The wave equation is solved analytically by the GMT in the corresponding domain using a superposition of several line multipoles. The outlines of the bends need not be concentric circles and can even deviate from circular shape. In this way tapers and bends with varying radii can be analyzed and optimized easily. — A generalized point matching technique is employed which uses a higher number of matching points than unknowns and thus yields an overdetermined system of equations. This means increases the precision of the results considerably.

Using this hybrid approach a full-band matched 90° E-plane bend and a taper in a rectangular X-band waveguide are investigated. Frequency response and field distributions are presented. — The approach proposed in this paper can be easily extended to bends in other waveguides, e.g. optical slab waveguides.

NEW TLM ALGORITHM FOR THE STUDY OF AXIALLY SYMMETRIC STRUCTURES (AS-TLM)

S. Le Maguer and M.M. Ney
Laboratory of Electronics and Communication Systems (LEST) UMR CNRS no. 6616,
Ecole Nationale Supérieure des Télécommunications de Bretagne (Telecom Bretagne),
BP 832, 29280 Brest Cedex, France

Abstract - The TLM method is a well-known numerical time domain technique which has been widely used for solving electromagnetic field problems. Axially symmetric structures are frequently encountered in microwave engeneering. For this purpose, a first memory-saving TLM algorithm was developped in the particular case of uniform guiding structures (S. Le Maguer and M. M. Ney , PIERS Proc.,334, 1996). Based on the classical Symmetrical Condensed Node (SCN), this approach leads to a one-dimensional mesh array using 18 complex voltages. Low memory requirement and simple algorithm make this method a very versatile tool. Extension of this model to general axially symmetric structures (two-dimensional mesh array) is not memory competitive compared to other time domain methods as BOR-FDTD (A. Taflove, Computational Electr., 1995). In this paper, we propose a new TLM node for this kind of geometries: The Axial Symmetry Symmetrical Condensed Node (AS-SCN). This node is directly deduced from Maxwell equations expressed in the case of body of revolution with the approach proposed by Jin and Vahldieck (IEEE MTT. .42, 2554-2561, 1994). It leads to a new diffusion matrix using 14 real voltages including losses. The new node is validated on a large scale of structures. Example is given in Table I. Further discussion is made on the center of cylindrical coordinates system. Finally, Hybrid (11 voltages) and Super-Condensed (8 voltages) versions of the algorithm are proposed using Maxwell integral equations and the general TLM formulation introduced by Peña and Ney (ACES 96 Conf. Proc., 262-269, 1996). These last features make this method very attractive and competitive as compared to other time-domain schemes.

Modes	Azimutal index	AS-SCN (Ghz)	Theoretical (Ghz)	Error (%)
TE11	1	17.43	17.39	0.25
TM01	0	18.97	18.89	0.4
TE21	2	21.02	20.92	0.5
TM11	1	23.73	23.66	0.3
TE01	0	23.73	23.66	0.3

Table I. First resonance frequencies in a cylindrical metalic resonator of radius of 1 cm and 1-cm-length (20x10 cells and 8000 steps).

B75.3

A Hybrid Method Combining Integral Equations and a Modal Technique for Air Intake Modelling

Paul SOUDAIS*, André Barka
ONERA B.P. 72 92322 Chatillon Cedex FRANCE

In many scattering or electromagnetic compatibility problems, the model can be separated in several domains. In each domain, the most suitable numerical method may be different. The Method of Moment is very efficient to compute the scattering in an unbounded medium. The Finite Element Method is well suited for bounded and possibly inhomogeneous domains. Dividing the domain into subdomains is also a way to compute higher frequencies.

In the air intake scattering problem, we separate the domain into subdomains by introducing fictitious surfaces. The solution is performed independently in each subdomain. The continuity condition on fictitious surfaces is written with an expansion on the guided modes of the section in order to reduce the number of unknowns of the condensed problem.

A general 3D MoM code has been modified in order to perform these subdomain solutions with modal excitations. Validations have been carried out that show no significant discrepancies between the entire domain solution and the solution obtained by assembling the subdomains solutions.

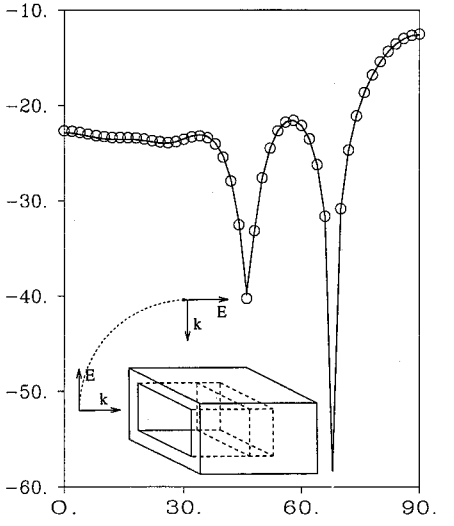

Comparison of entire domain and subdomain computation of the monostatic radar cross section of a rectangular wave guide (5 travelling modes).

Entire domain computation ———
Subdomain computation o

A Hybrid FEM-MOM Formulation for Stratified Problems using Triangular Prism Elements

*Eric W. Lucas, Thomas P. Fontana and Robert G. Schmier
Northrop Grumman Corporation, Electronic Sensors and Systems Division
P.O. Box 746, Baltimore, Maryland 21203

Jin-Fa Lee
ECE Department, Worcester Polytechnic Institute
Worcester, MA 01609

In this presentation, we will discuss a hybrid formulation which makes use of a combination of the method of moments (MOM) technique along with the vector finite-element method (FEM). This particular formulation will concentrate on periodic array geometries as well as closed EM problems which can be geometrically described by stratified construction. Many phased-array radiators as well as other waveguide and microstrip geometries fall into this category. The use of right triangular prisms as the finite-element of choice is sensible for such planar geometries for obvious reasons. On the other hand, many FEM practitioners recognize that difficulties may arise when using the more commonly accepted tetrahedral elements to model thin dielectric layers or other thin structures which have large transverse dimensions relative to their thickness. The prism elements can also experience some difficulty if the layers get too thin, but still seen to offer some advantage over the tetrahedral elements in many cases.

The MOM side of the formulation uses a reaction-oriented approach with diverse vector-mode expansions for the appropriate dyadic Greens functions. Stratified dielectric layers are easily incorporated into these vector-mode expansions as is well known. Both entire-domain vector-mode bases as well as triangular sub-domain bases are used. We have formulated the MOM procedure for infinite periodic arrays as well as several closed waveguide geometries. Both electric (PEC) as well as magnetic (aperture) scatterers may be simultaneously handled.

The MOM and FEM representations are coupled using a methodology we call the hybrid surface reaction method (HSRM) which is derived from Jeng's variational electromagnetic (VEM) methodology. These surface reactions are formed at the FEM-MOM interfaces and are incorporated into the overall functional to preserve the variational nature of the coupled formulation. Some numerical examples will be reported to demonstrate the technique.

B75.5

Hybrid MoM/SBR Method to Compute Scattering from a Slot Array in a Complex Geometry

Andrew D. Greenwood*
Rome Laboratory and
University of Illinois
Urbana, IL 61801

Jian-Ming Jin
ECE Department
University of Illinois
Urbana, IL 61801

Recently, a method of moments (MoM) procedure has been introduced to compute the scattering from a cylindrically conformal slotted-waveguide array antenna (see G. Fan and J.M. Jin, 1996 IEEE Antennas and Propagation Society International Symposium Digest, volume 2, pp. 1394-1397). Because the MoM cannot efficiently model a complex, 3-D geometry, this method does not account for the geometry surrounding the slot array. High frequency methods, such as the shooting and bouncing ray (SBR) method, can account for the geometry, but cannot accurately model the slots due to their small sizes. To overcome these problems, the MoM computation is hybridized with the SBR method to compute the electromagnetic scattering from a large, 3-D target which includes a slotted-waveguide array antenna.

To compute the scattering using the hybrid method, the apertures of each slot are first covered with perfect electric conductor (PEC), and equivalent magnetic currents are introduced according to the field equivalence principle. Then, an integral equation is derived by enforcing the continuity of the tangential magnetic fields across each slot aperture. The incident magnetic fields on each slot aperture, which are found using the SBR method, form the excitation of the system. The integral equation is solved using the MoM, giving numerical values for the equivalent currents on the slot apertures. Using the reciprocity theorem and the SBR method, the radiation of the equivalent currents is found in the presence of the large, 3-D body. This radiation is added to the scattered field from the large, 3-D body with the slot apertures covered by PEC, which is found using the SBR method.

The computations of the two methods are decoupled in one of two ways. The first expands the incident field on the slot apertures in terms of basis functions and uses the MoM to find the equivalent current response to each basis function. Alternatively, the second ignores the interactions between individual slots in the array. The procedure assumes a single isolated slot, finds the current response to a field of unit magnitude on this slot, and assumes that this current is present on each slot. This approximation is accurate only when the frequency is not equal to the working frequency of the slot array.

The hybrid method is validated by comparing it with previously published work. Numerical results show that at some incidence angles and frequencies, the scattering from a slot array may dominate the scattering from the entire target. Thus, it is important to include the slot array in a scattering model. The hybrid method allows the scattering from a large, 3-D target with a slotted-waveguide array antenna to be accurately and efficiently computed.

Practical Analysis of Microwave Filters by FDTD and Model S-parameter Extraction

Patrick C.K. Yau, Chen Wu, Ke-Li Wu and John Litva
Wireless Technology Group
Communications Research Laboratory
McMaster University
1280 Main Street West
Hamilton, ON L8S 4K1

Abstract

A combination of finite-difference time-domain method and model S-parameter extraction, for extracting S-parameters of complicated waveguide structures, is presented. With the application of model S-parameter extraction, a special index indicates the accuracy of the resulting S-parameters. By considering this index, the simulation process can be terminated as certain accuracy of S-parameters is reached. It is useful when the FDTD algorithm is implemented into software. Various waveguide structures are verified by applying this method. The following examples also show that the dispersive absorbing boundaries are proved to be more efficient than using the standard Mur's absorbing boundaries for these applications.

B75.7

Application of AWE for Frequency Domain Electromagnetics

C. J. Reddy*
Dept. of Electrical Engg.
Hampton University
Hampton VA 23668

M.D.Deshpande
ViGYAN Inc.
Research Drive
Hampton VA 23681

C.R.Cockrell and F.B.Beck
Mail Stop 490
NASA Langley Research Ctr.
Hampton VA 23681

ABSTRACT

Frequency domain numerical techniques such as Method of Moments (MoM), Finite Element Method(FEM) and hybrid FEM/MoM have become popular over the last few years due to their flexibility to handle arbitrarily shaped objects and complex materials. One of the disadvantages of frequency domain techniques is the computational cost involved in obtaining solutions over a frequency range as the computations have to be repeated for each frequency over a frequency range. To over come this problem, a technique called Asymptotic Waveform Evaluation(AWE) is used for finite element analysis of microwave circuits(*Yuan and Cendes, URSI Meeting, 196, 1993).* In this paper, application of AWE for electromagnetic scattering and radiation problems(*Cockrell and Beck, NASA TM 110292,1996*) is presented. MoM in conjunction with AWE technique is applied to obtain radar cross section of an arbitrarily shaped three dimensional PEC objects over a frequency band (*Reddy and Deshpande, NASA CR 4758, 1996*). AWE technique is also applied along with FEM/MoM to calculate the input characteristics of cavity-backed-aperture antennas over a frequency range. In figure 1, normalized input impedance of a cavity-backed square microstrip patch antenna is presented. Comparison of numerical data obtained from AWE calculations agree well with the values computed at each frequency over the frequency range. More numerical examples will be presented at the conference.

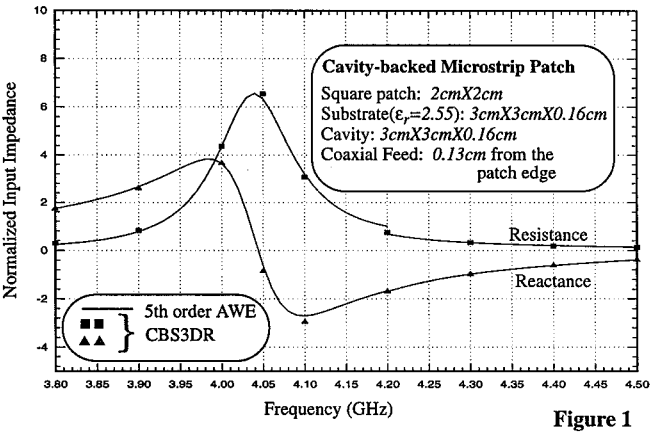

Figure 1

EXACT SUBDOMAIN FEM AND MOM METHOD FOR LARGE INLET SCATTERING

A. Barka,T.Volpert
Office National d'Études et de Recherches Aérospatiales
ONERA, BP 72, 92322 Châtillon Cedex, France

The electromagnetic scattering from the interior of complex jet engine inlet contributes significantly to the overall radar cross section (RCS) of a modern jet aircraft. The scattering mechanisms in jet or missile inlets are complex and difficult to accurately simulate. The difficulty being the geometrical complexity (engine face , strutural obstacles , materials) and the large size of the problem. Traditionally, asymptotic techniques are employed, such as the geometrical optics ray method, hybrid combination of asymptotic high frequency and modal methods (P.H Pathak,R.J Burkholder, IEEE Trans. APS-37 pges 635-647, 1989). However , the high frequency techniques break down for complex targets. Recent investigations have been done for the accurate simulation of the engine face using a three-dimensional finite element analysis combined with modal or ray methods (D.C Ross,J.L Volakis, H.Hannastassiu , Finite Element-Modal Analysis of Jet Engine Inlet, IEEE Trans. Vol 43 , $n°3$, March 1995).

In this paper we discuss an original multi domain and multi method approach for large and complex inlets (several millions of unknowns) totally based on exact formulations of the Maxwell equations. The global target is splitted in N subdomains separated by interfaces . In each domain, the generalized Scattering matrix is computed with differents methods such as the three-dimensional Finite Element Method or the Electric Field Integral Equation in relation with a generalized modal base representation of the fields on the interfaces. Then, the different objects are connected by cascading the different matrices. We will discuss the different avantages of this approach like the space and time unlocalization of the different subdomains computations, parallelism, accuracy in each volume, computation time, CAO and object-oriented conception of this application. A significant computation in terms of size and complexity will be presented.

B75.9

On the Use of Decoupled Meshes in the Analysis of Printed Antennas

Leo C. Kempel*
Mission Research Corporation
Valparaiso, FL 32580

Traditionally, conformal printed antennas have been modeled using the finite element method using coupled meshes. For example, a finite element-boundary integral (FE-BI) formulation utilizes an integral equation to terminate the finite element mesh. In a coupled scheme, the basis functions associated with the boundary integral are identical to and collocated with the surface evaluation of the volume basis functions associated with the finite element method. This approach leads to the fewest number of unknowns at the expense of mesh rigidity, e.g. the surface features may constrain the volume discretization.

An alternative approach is the use of decoupled meshes. In this scheme, the basis functions associated with the boundary integral are not related to the basis functions used in the volume finite element method. Rather, field continuity is explicitly enforced via coupling equations. In addition, the various boundary conditions such as those associated with perfect electric conductors are also explicitly enforced. Figure 1 illustrates such a decoupled mesh.

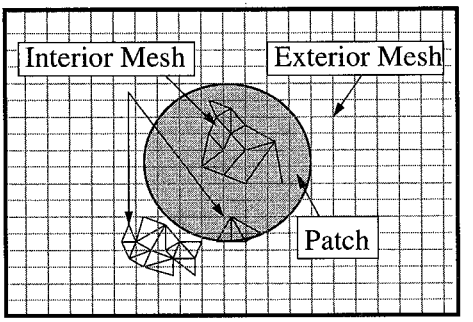

Figure 1. Decoupled mesh representation of a printed antenna. The interior finite element mesh uses triangles while the exterior finite element mesh utilizes rectangular patches.

During the presentation, the advantages and disadvantages of this decoupled mesh scheme will be discussed in regards to conformal antenna modeling. In particular, the following will be discussed:

1. Memory and compute cycle demands.
2. Matrix conditioning.
3. Radiating element flexibility.
4. Implications for other finite element applications.

TWO-DIMENSIONAL RADIATION TRANSPORT ACROSS FIBROUS MEDIA

J. A. Grzesik
TRW Space & Defense
One Space Park
Redondo Beach, CA 90278

The emerging prominence of reinforced fiber composite materials for lightweight airframe/spacecraft construction defines an arena of radiation heat transport/shielding wherein the underlying electromagnetic [EM] propagation is confined to well-defined cones around fiber axes. Although practical analysis techniques seeking to evaluate/modify macroscopic shielding properties are naturally anchored around the primitive EM attribute of a scattering amplitude at the micron wavelengths characteristic of the infrared regime, they nevertheless quickly revert to a photonic viewpoint which submits instead to a Boltzmann equation expressing quantum conservation across flight directions and any available mechanisms of energy transfer and emission/absorption.

The physical picture of photon movement along cone generators around fiber axes has the evident consequence of rendering the Boltzmann transport equation effectively two-dimensional, with flight azimuth around fiber axes serving as the key independent parameter. A very close analogue is produced thereby of the standard model involving transport symmetry around some preferred direction [S. Chandrasekhar, Radiative Transfer, Dover Publications, New York, 1960; K. M. Case & P. F. Zweifel, Linear Transport Theory, Addison-Wesley Publishing Co., Reading, Mass., 1967], with photon flight azimuth around fiber axes replacing the more usual polar angle with respect to the symmetry direction. The analogue ceases however to be strict as regards the angular measure, with the usual sine weighting being relinquished in favor of a uniform, unit value.

An EM/transport interface in the physical context thus motivated can be traced from [S.-C. Lee, "Dependent Scattering of an Obliquely Incident Plane Wave by a Collection of Parallel Cylinders," J. of Applied Physics, Vol. 68, No. 10, 1990, pp. 4952-4957] and [S.-C. Lee & J. A. Grzesik, "Scattering Characteristics of Fibrous Media Containing Closely Spaced Parallel Fibers," J. of Thermophysics & Heat Transfer, Vol. 9, No. 3, 1995, pp. 403-409]. Here, however, we wish to report on codes evolved in the specifically two-dimensional, fibrous transport context, and on their validation by comparison with an analytic, Wiener-Hopf [WH] solution of the corresponding half-space albedo problem. Our WH albedo solution is modeled on canonical techniques [G. Placzek & W. Seidel, "Milne's Problem in Transport Theory," Physical Review, Vol. 72, No. 7, 1947, pp. 550-555], but it is of course modified as necessary to account for the simplified angular measure. The codes themselves exploit both coupled differential solvers and eigenvalue/eigenvector decomposition packages assisted by subroutines drawn from the IMSLIB library. Albedo agreement attained on the basis of these disparate approaches imparts confidence in code use vis-à-vis realistic fiber scattering amplitudes.

We present also some of our preliminary attempts to transpose to the two-dimensional, azimuthal scattering/transport context the singular eigenfunction decomposition apparatus elaborated by K. M. Case in his cited text.

URSI B **Session 85** Salon Bersimis

Microstrip Lines and Circuits
Co-chairs: A.W. Glisson, USA and L. Shafai, Canada

08:10	85.1	Computation of Resistance and Internal Inductance of Rectangular and Trapezoidal Cross Section Conductors, J. GUO, **A.W. GLISSON**, D. KAJFEZ, *University of Mississippi, University, MS, USA*
08:30	85.2	Efficient Characterization of Microstrip Structures Using Higher Order Boundary Operators, **O.M. RAMAHI**, *Digital Equipment Corporation, Maynard, MA, USA*
08:50	85.3	Analysis of Stripline-Fed, Slot-Coupled Patch Antennas with Vias for Parallel-Plate Mode Suppression, **A. BHATTACHARYYA**, O. FORDHAM, Y. LIU, *Hughes Space and Communications, Los Angeles, CA, USA*
09:10	85.4	Modal Analysis of Coupled Cylindrical Microstrip Transmission Lines, **C.-H. LEE**[1], Y.-W. WANG[1], C.-I.G. HSU[2], [1]*National Changhua University of Education and* [2]*Da-Yeh Institute of Technology, Changhua, Taiwan, China*
09:30	85.5	Quasi-TEM Analysis of Microstrip Lines with Inhomogeneous Substrates, **J.-F. KIANG**, *National Chung-Hsing University, Taichung, Taiwan, China*
09:50	85.6	Optimization Design of Impedance Transforming Branch-Line Hybrids with Single-Fold Symmetry, **C.-L. LI**, C.-Y. LI, *Tamkang University, Taipei, Taiwan, China*
10:10		Coffee Break
10:30	85.7	Analysis of Shielded Transmission Lines on Anisotropic Substrates, **V.V. KHOROSHUN**, I.E. PEDCHENKO, N.A. SYVOZALIZOV, *Kharkov State University, Kharkov, Ukraine*

B85.1

Computation of Resistance and Internal Inductance of Rectangular and Trapezoidal Cross Section Conductors

Jing Guo, Allen W. Glisson*, and Darko Kajfez
Department of Electrical Engineering
University of Mississippi, University, MS 38677

At very low frequencies the effective resistance of a conductor trace is dependent almost exclusively on the material properties and cross sectional area of the conductor. At higher frequencies, the shape of the cross section of a conductor affects the surrounding field distributions and influences the effective resistance and internal inductance of the conductor. Over-etching of a circuit trace, for example, may result in a conductor with a trapezoidal cross section. This effect needs to be taken into account in the computation of the effective resistance and internal inductance of the trace. Once the effective values are determined, they can be incorporated into simpler models as lumped elements or as distributed resistance and inductance per unit length.

This paper will present the computation results of resistance and internal inductance per unit length for conductors of rectangular and trapezoidal cross sections over a relatively wide frequency range. To determine these quantities we consider the problem of an infinite bar excited by a transverse magnetic (TM_z) plane wave as shown in the adjacent figure, where w and τ are the width and thickness of the conductor respectively, and α is an angle chosen to change the shape of the trapezoidal. The bar with its conductivity σ is situated in free space. A pair of surface integral equations (SIE) are formed by applying the equivalence principle to obtain two separate equivalent situations. For the exterior region equivalence, the bar is replaced by an electric surface current J_z^+ that radiates in free space. In the interior region equivalence, the bar is replaced by an electric surface current J_z^- that radiates in a homogeneous space with the conductivity of the bar. Continuity of the electric and magnetic fields at the surface of the bar leads to a pair of coupled integral equations that can be solved by the method of moments for J_z^+ and J_z^-. The electric and magnetic fields just inside the bar surface can be computed from knowledge of J_z^-. The ac resistance and internal inductance can be determined in terms of the power flow into the conductor and the total current induced in the bar.

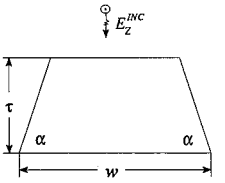

Conductor cross section

The computed results of resistance and internal inductance of rectangular and trapezoidal cross sections versus frequency will be presented and compared with other available data.

Efficient Characterization of Microstrip Structures Using Higher Order Boundary Operators

Omar M. Ramahi
Digital Equipment Corporation
PKO3-1/R11, 129 Parker St.
Maynard, MA 01754, U.S.A.
ramahi@poboxa.enet.dec.com

The Finite Difference Time Domain (FDTD) method is a powerful and efficient technique for obtaining wide band characteristics of printed circuits. For the class of problems involving dispersive structures, the choice of the Absorbing Boundary Condition (ABC) can have a significant impact on the efficiency and accuracy of the analysis. Earlier work found that Higdon ABC can be very effective. However, in these implementations, the effectiveness of the ABC was found to be highly dependent on good prediction of the effective permittivity of the medium over the frequency band of interest. This unfortunately puts a sever limitation on the general applicability of those ABCs. Also, while higher order ABCs, of the Higdon type, give higher accuracy, their previous applications gave highly unstable solution.

In this work, we design a set of boundary operators that take advantage of the field behavior in the guiding structure. We employ a 4th order Higdon ABC on the far end of the structure (transverse to the signal trace,) such that this ABC favors the absorption of traveling waves. On the remaining four walls, we apply a 4th order Higdon ABC that favors the absorption of evanescent waves. This combination of Higdon's 4th order ABCs results in a very accurate solution while keeping the computational domain appreciably smaller than what was needed in previous work. However, the most significant advantage of this ABC construction is its stability. Typical ABCs give a reflection coefficient of unity or slightly close to unity along the boundaries parallel to the trace. Consequently, any perturbation in the computationally intensive FDTD method can tip the reflection coefficient above unity, and thus the potential for instability increases. By adjusting only the ABC on the upper terminal boundary, the reflection factor can be made less than unity, thus resulting in a very stable solution . This construction was found to be highly effective and highly independent of the line shape and parameters, and more importantly, it does not call for accurate estimate of the effective permittivity.

B85.3

ANALYSIS OF STRIPLINE-FED, SLOT-COUPLED PATCH ANTENNAS WITH VIAS FOR PARALLEL-PLATE MODE SUPPRESSION

Arun Bhattacharyya*, Owen Fordham and Yaozhong Liu
Hughes Space and Communications
S12/V348, Box 92919
Los Angeles, CA 90009

The slot-coupled patch is an attractive radiating element for phased arrays since it is simple to fabricate, and the feed circuit does not disturb the radiated pattern. There has been an increasingly large interest to integrate patch antennas with MMIC devices such as phase shifters and solid state power amplifiers (SSPAs) for phased array applications. For efficient use of space and to allow direct interface with a heat sink, the MMICs are typically placed underneath the ground plane of the patches. The SSPA's input often must be isolated from the feed circuit with another ground plane, to avoid potential feed-back/oscillation problems. However, introduction of this second ground plane allows parallel plate modes to exist in the feed circuit layers, which have a 'stripline' configuration. The lowest order parallel plate mode has zero cutoff frequency, and unlike a surface wave mode (microstrip configuration), the intensity of excitation does not depend strongly on the dielectric medium. When a significant amount of power is launched into the parallel plate modes, there is a corresponding reduction in the radiated power, hence the radiation efficiency of the patch antenna is reduced. Also, the parallel-plate mode can cause mutual coupling problems between elements of the array, which may alter the amplitude and phase distributions from their intended values.

In a stripline-fed, slot-coupled patch antenna, the parallel plate modes are excited at the slot discontinuity in the upper ground plane. To achieve a reasonable input impedance for the antenna, the coupling slots are usually between one-quarter and one-half wavelength, and strongly excite the parallel plate mode. A practical way to supress the parallel plate modes, without significantly affecting the stripline mode, is to introduce via holes around the slot. However, the input impedance of the patch antenna changes significantly due to scattering of the parallel plate mode from the vias. To achieve first-pass design success, the effect of the via holes must be included in the analysis.

In this paper, we introduce a model to analyze stripline-fed, slot-coupled patch antennas with vias around the slots. We also present a comparison of simulated and measured results to verify the model's accuracy. The via holes are modeled as cylindrical scatterers with ground planes at both ends. Our model allows two dielectric layers with different permittivities to be specified for the 'stripline' feed. A higher permitivitty layer between the strip and the slot concentrates more current in the upper ground plane, where it will be interupted by the slot. This design flexibility is often required to obtain a reasonable input impedance for the antenna. Also, the thickness ratio between the upper and lower layers may be reduced for the same purpose. This asymmetric stripline feed sustains microstrip-like fields, but still requires via holes to suppress the parallel plate mode.

Our formulation applies the method of moments (MoM) with Galerkin's procedure in the spectral domain. The entire problem is divided into two coupling problems: (a) coupling between the slot and the stripline feed in the presence of vias, and (b) coupling between the slot and the patch. To make the analysis accurate and very general, several mutually orthogonal modal fields are considered on the slot aperture. Lorentz's reciprocity theorem is then invoked to construct a generalized equivalent circuit for the coupling between the slot modes and the feed line. The equivalent circuit consists of a generalized transformer and two generalized shunt admittances (admittance matrices). One admittance matrix represents radiation from the slot on the feed side of the ground plane and includes the effect of scattering from the vias. The other admittance matrix represents radiation on the patch side of the ground plane and includes the scattering from the patch metallization. A general matrix formulation is presented to handle the scattering problems in both sides, and the input impedance seen by the feed line is deduced from the equivalent circuit.

Modal Analysis of Coupled Cylindrical Microstrip Transmission Lines

Ching-Her Lee* and Yen-Wen Wang
Department of Industrial Education
National Changhua University of Education
Changhua, 500, Taiwan

Chung-I G. Hsu
Department of Electrical Engineering
Da-Yeh Institute of Technology
Changhua, 500, Taiwan

Cylindrical microstrip transmission line is the canonical structure of many integrated microstrip devices on curved surfaces. It finds many applications in microwave and communication circuits with cylindrically shaped substrates. In this paper, a spectral domain, full-wave approach is used to accurately analyze the modal characteristics of the coupled microstrip transmission lines with cylindrical multidielectric-layered background structure. The system governing equation expresses the electric field as a product of the strip currents and an electric dyadic Green's function which is appropriate to the cylindrical-layered background structure. To obtain numerical solutions, a Galerkin's method of moments is implemented. The trigonometric functions incorporated appropriate edge factors are chosen for transverse and longitudinal current expansion and testing.

Some sample structures are computed in this work. The dimension parameters used are as follows: the substrate thickness h, the thickness of superstrate t, and the microstrip line width (for both) w are all about 3 mm; the ratio of the radius of the conducting cylinder to that of the substrate, a/b, varies from 0.8 to 0.95. The dielectric constants used for substrate is 9.6, and that for superstrate is 2.32 or 5.0. It is seen that the solution using the electric dyadic Green's function approach relies on the substrate surface electric field and current, so when considering the closely coupled microstrip lines, the transverse electric field is no longer negligible. In this case, the field strength of the odd mode between the two lines becomes strong enough to compensate for the weak transverse current, and full-wave (including transverse and longitudinal wave components) computation should be implemented (A. Nakatani and N. G. Alexopoulos, IEEE MTT-35, 1392-1398, 1987). In our work, both current components are considered, and three expansion functions are used for numerical computation.

In this paper, we will present the effective dielectric constants and the current distributions of the fundamental and higher-order modes. From the obtained results, we see that the effective dielectric constants of the even and odd modes diverge increasingly from that of single strip line as the spacing decreased. The effective dielectric constant of the odd mode increases relatively speed than that of the even mode as the dielectric constant of the superstrate increased.

B85.5

Quasi-TEM Analysis of Microstrip Lines with Inhomogeneous Substrates

Jean-Fu Kiang
Department of Electrical Engineering
National Chung-Hsing University
Taichung, Taiwan

Microstrip lines embedded in multilayered media have been widely studied. Conventionally, each dielectric layer is assumed homogeneous when the spectral domain methods or mode-matching techniques are used. However, some practical substrate materials contain inhomogeneities. For example, glass fibers are implanted within an epoxy circuit board to enhance its mechanical strength. A notch can be cut in the substrate amidst two microstrips to reduce their coupling. The dielectric constant underneath the microstrip can also be increased locally to focus the power guided by the strip. In such cases, conventional spectral domain methods or mode-matching techniques do not apply, and the spatial domain approaches may render too many unknowns to model the equivalent surface charge especially when the dielectric constant is a continuous function of coordinates.

In this work, a mode matching approach combined with Galerkin's method is proposed to calculate the capacitance matrix of microstrip lines embedded in an inhomogeneous stratified medium. Eigenmodes in each layer is first solved numerically, and the potential in each layer can be expressed in terms of these eigenmodes. Coupling between two sets of eigenmodes in contiguous layers are described by defining reflection matrices. A Green's function is thus obtained in terms of these eigenmode sets to relate the potential to a line charge. Integral equation is then constructed relating the charge distribution and the imposed voltage on the microstrip surface. Galerkin's method is next applied to solve the charge distribution and hence the capacitance matrix. Several inhomogeneous profiles are studied to understand the effects of inhomogeneities on the capacitance and relevant parameters like effective dielectric constant and phase velocity.

OPTIMIZATION DESIGN OF IMPEDANCE TRANSFORMING BRANCH-LINE HYBRIDS WITH SINGLE-FOLD SYMMETRY

Ching-Lieh Li* and Chin-Yi Li
Department of Electrical Engineering
Tamkang University
Tamsui, Taipei Hsien, Taiwan 25137
China

The branch-line coupler is one of the fundamental microwave components, and is most suitable for planar structure. In this paper, we conduct the investigation on an arbitrary two-section hybrid with single-fold symmetry.

The single-section branch-line hybrid has a narrow bandwidth, which is usually improved by adding additional sections. For some application, it may be sufficient to employ a conventional two-section hybrid with two-fold symmetry which has ideal performance at the center of the desired frequency band. However, wider bandwidth can be achieved by either relaxing the two-fold symmetry to single-fold symmetry or allowing the hybrid to operate non-ideally at the center frequency f_o.

First, for a hybrid with single-fold symmetry and ideal performance at f_o the impedance transformation between the input ports and output ports is also made possible (R.K.Gupta, S.E. Anderson, and W.J. Getsinger, IEEE Trans. on MTT,1303-1307, 1987). In this case, the bandwidth for the 20dB return loss and isolation up to 30% can be achieved. However, more careful examination shows that the allowance of impedance transformation may reduce the isolation bandwidth dramatically. Secondly, if a hybrid with two-fold symmetry is allowed to operate non-ideally at all frequencies of the desired band, it can achieved better bandwidth, for example, more than 37% for both return loss and isolation were reported (M. Muraguchi, T. Yukitake, and Y. Naito, IEEE Trans. on MTT, 674-679, 1983).

In this paper, we conduct the investigation on an arbitrary two-section hybrid with single-fold symmetry. As the power division ratio and the impedance transformation ratio are specified and the hybrid is required to operate ideally at the center frequency f_o of the desired frequency band in our study such that the design equations for three impedances out of five branches are derived, while the other two branch impedances are adjusted to improve the bandwidths. By allowing simultaneous optimization for return loss and isolation bandwidth, the isolation reduction due to impedance transformation can be largely improved. It is also found that for those hybrids that have coupling values other than 3dB (i.e. non equal power division between output ports) the bandwidths may be largely increased. For example, more than 37% and 40% for return loss and isolation bandwidth, respectively, can be achieved at 2:1 power division ratio. Various numerical results for the bandwidths of return loss, isolation and output power imbalance under various specifications will also be shown.

B85.7

ANALYSIS OF SHIELDED TRANSMISSION LINES ON ANISOTROPIC SUBSTRATES

V.V.Khoroshun, I.E.Pedchenko, N.A.Syvozalizov

Kharkov State University, Department of Radiophysics,
Svobody Sq., 4, Kharkov 310077, Ukraine

ABSTRACT. Characteristics of shielded transmission lines for microwave and millimeter-wave integrated circuits have been investigated in the past by means of many methods. However, in spite of numerons attemps a rigorous theory is not fairly well established.

This communication presents a rigorous analysis applied to shielded transmission lines on anisotropic substrates. The analysis is based on the method of the Riemann-Hilbert problem in order to obtain determinantial equations for the propagation constants and electromagnetic field components (V.P.Shestopalov, The method of the Riemann-Hilbert problem ..., Kharkov, Univ.Press, 1971,in Russian). The constructed procedure of an analytical regularization equivalently reduces the initial boundary value problem to the set of linear algebraic equations of the second kind. The obtained numerical results have shown that developed method allows to construct efficient numerical algorithms. Certain approximations are introduced to allow the solution in the form of simple approximate formula. The characteristics of propagation of the dominant mode in microstrip line with anisotropic substrate are studied. The dispersion characteristics for microstrip line are computed over a wide freguency band including resonanse region.

In the method of the Riemann-Hilbert problem the condition zero metallization thickness is used, therefore modified reexpanding method for calculation of characteristics of transmission lines with nonzero thickness is suggested (V.V.Khoroshun Electromagnetic theory of diffraction gratings, Intern. Simp. "Physics and Eng. MM and SubMM Waves", vol.1, Kharkov, 1994). Comparison of numerical results obtained by both methods is presented.

URSI B | Session 92 | Salon Matapedia

Propagation, Scattering and Radiation in Complex Media
Co-chairs: V.I. Tatarskii, USA and R. Olsen, Canada

08:10	92.1	New Formulation of Rough-Surface Scattering Theory in Terms of Phase Factors and Related Approximate Solutions, **V.I. TATARSKII**, *University of Colorado, Boulder, CO, USA*
08:30	92.2	Universal Behavior of Scattering Amplitudes for Scattering from a Plane in Average Rough Surface for Small Grazing Angles, **V.I. TATARSKII**[1], M. CHARNOTSKII[2], [1]*University of Colorado and* [2]*Science and Technology Corporation, Boulder, CO, USA*
08:50	92.3	Multiple Scattering Theory with Size Corrections of Inclusions for Particulate Composites, **A.J. STOYANOV**[1], H. ÜBERALL[2], B.F. HOWELL[1], E.C. FISCHER[1], [1]*NSWC, West Bethesda, MD and* [2]*Catholic University of America, Washington, DC, USA*
09:10	92.4	Decomposition of Electromagnetic Sources for a Class of Anisotropic Media, **I.V. LINDELL**[1], F. OLYSLAGER[2], [1]*Helsinki University of Technology, Espoo, Finland;* [2]*University of Ghent, Belgium*
09:30	92.5	Scattering of the Electromagnetic Waves on the Rough Cone and Paraboloid, **V.G. SPITSYN**, *Tomsk State University, Tomsk, Russia*
09:50	92.6	The Averaged Boundary Conditions for Some Grids in Anisotropic and Moving Media, **A.V. TYUKHTIN**, *St. Petersburg University, St. Petersburg, Russia*
10:10		Coffee Break
10:30	92.7	The Excitation and Propagation of Surface Waves in an Absorbing Layer, R.T. LING, J.D. SCHOLLER, **P.Y. UFIMTSEV**, *Northrop Grumman Corporation, Pico Rivera, CA, USA*
10:50	92.8	The Vector Problem of EM Wave Propagation in an Impedance Waveguide with a Large-Scale 3D Wall Irregularity, **O.V. SOLOVIEV**, *University of St. Petersburg, Russia*
11:10	92.9	Mode Structure Formation Length in an Inhomogeneous Media, **N.I. PETROV**, *All-Russian Electrotechnical Institute, Istra, Russia*

B92.1

New Formulation of Rough-Surface Scattering Theory in Terms of Phase Factors and Related Approximate Solutions

Valerian I. Tatarskii
University of Colorado/CIRES and NOAA/ERL/ETL
325 Broadway, Boulder, CO 80303-3328, USA

This paper presents the formulation of rough-surface scattering theory in which the phase shift factors $\exp[i\alpha\zeta(\mathbf{r})]$ replace the elevation $\zeta(\mathbf{r})$. The integral equations for secondary sources (surface currents) are obtained for the Dirichlet and for the Neuman problems that contain in their kernels only this phase function. The representations of the scattering amplitude that contain only the source functions and the phase factor $\exp[i\alpha\zeta(\mathbf{r})]$ are obtained for both problems. It follows from this formulation of the scattering problem that the scattering amplitudes and scattering cross-sections are some functionals depending not on elevations $\zeta(\cdot)$, but on the phase factors $\exp[i\alpha\zeta(\cdot)]$ only. Elevations cannot enter to the solution in any other form. This formulation of the scattering problem corresponds to the partial summation of the conventional perturbation theory in powers of elevations. In contrast to the conventional formulation, the formulation based on the phase function deals only with the bounded functions

$$|\exp[i\alpha\zeta(\mathbf{r})]| \leq 1$$

even for the case $|\alpha\zeta(\mathbf{r})| \gg 1$.

This representation of the scattering theory seems to be more adequate both from the physical and mathematical points of view. The Neuman series for the solutions of derived integral equations are a series in powers of these phase factors, not in powers of the elevations. In the case of small Rayleigh parameter ($\alpha\zeta \to 0$) the Neuman series turns out to be the standard Born expansion, describing Bragg scattering. Using the Neuman series and Fredholm formulae we obtain several uniform (with respect to $\alpha\zeta$) approximate solutions that contain, as limiting cases, Bragg scattering, Kirchhoff approximation, small-slope approximation, and the tilt-invariant approximation. These new approximations are more useful for numerical calculations because they contain the random function $\zeta(\mathbf{r})$ only in the exponents and therefore provide simple formulae after averaging.

Universal behavior of scattering amplitudes for scattering from a plane in average rough surface for small grazing angles

Valerian I. Tatarskii† and Mikhail Charnotskii‡
†University of Colorado/CIRES and NOAA/ERL/ETL
325 Broadway, Boulder, CO 80303-3328, USA
‡Science and Technology Corporation

The problem of rough surface scattering at low grazing angles has attracted significant interest at least since the mid - 1950s. Approaches vary from the use of exact solutions for specifically constructed surface models to development of sophisticated analytical techniques, and extensive use of numerical methods. The present paper is different in that we use the most general properties of the scattered fields for the investigation of the low grazing-angle behavior of the scattering amplitudes. Our analysis is limited to the scalar scattered fields under the simplest Dirichlet and Neuman boundary conditions, without involvement of any analytical or numerical approximations. We consider such an approach to be advantageous because it provides precise results.

It is shown that for scattering from a plane in average rough surface, the scattering cross section of the range of small grazing angles of the scattered wave demonstrates a universal behavior. If the angle of incidence is fixed (in general it should not be small), the diffusive component of the scattering cross section for the Dirichlet problem is proportional to θ^2 where θ is the (small) angle of elevation, and for the Neuman problem it does not depend on θ. For the backscattering case these dependencies correspondingly became θ^4 and θ^0. The result is obtained from the structure of the equations that determine the scattering problem rather than use of approximation.

B92.3

MULTIPLE SCATTERING THEORY WITH SIZE CORRECTIONS OF INCLUSIONS FOR PARTICULATE COMPOSITES

A. J. Stoyanov*, H. Überall+, B. F. Howell and E. C. Fischer

Carderock Division NSWC
9500 MacArthur Boulevard
West Bethesda, MD 20817-5700, USA

+Department of Physics, The Catholic University of America
Washington, DC 20064, USA

Multiple scattering effects in the complex permittivity, as exhibited to a passing electromagnetic wave, of particulate composites (treated as an effective medium) are described by the theory of Tsang and Kong. We have previously used this theory (as reported at URSI and PIERS conferences) in order to obtain effective complex permittivites (including the absorptivity) of particulate composites composed of randomly distributed spherical inclusions with complex internal permittivity (consisting of graphite with relatively high conductivity imbedded in a matrix of complex permittivity (consisting of epoxy with low or negligible conductivity), plotted as a function of frequency in the GHz or multi-GHz region. Thre sizes of the imbedded microspheres considered there correspond to a radius of about 100μm, and their volume concentrations ranged from 5% to 25%.

The Tsang-Kong theory (in its most easily accessible form), being essentially a long-wavelength theory, has its applications restricted to particle sizes much smaller than a wavelength. If the particle size becomes comparable to the wavelength, numerical calculations showed the occurrence of instabilities and divergences in the effective permittivity. We are able to correct for these spurious effects by introducing corrections into the Tsang-Kong theory that extended its applicability to larger particles sizes, approaching the electromagnetic wavelength. We were able to introduce these corrections without having to resort to a full-fledged extension of the (complicated) theory, by patterning the corrections after those of a previous theory by Lewin that had provided a partial solution for the effective material parameteres, but in which larger-size corrections for the particulate inclusions had been taken into account. It was found possible to intoduce the same type of size corrections into the Tsang-Kong theory, and we shall present results for effective permittivities and absorptivities, plotted vs. particle radius up into the mm-region, as compared with the (unstable) predictions where no size corrections had been taken into account.

DECOMPOSITION OF ELECTROMAGNETIC SOURCES FOR A CLASS OF ANISOTROPIC MEDIA

Ismo V. Lindell*, Frank Olyslager**
*Electromagnetics Laboratory, Helsinki University of Technology
Otakaari 5A, Espoo FIN-02150 FINLAND
** Department of Information Technology, University of Ghent
Sint-Pietersnieuwstraat 41, Ghent B-9000 BELGIUM

A class of anisotropic media considered in the present paper is defined by a relation between its permittivity and permeability parameter dyadics as $\overline{\overline{\mu}} = \tau\overline{\overline{\epsilon}}^{T} + \mathbf{ab}$ with τ a scalar and $\mathbf{a}, \mathbf{b}$ two vectors. $()^T$ is the dyadic transpose operation. This condition allows the medium to be nonreciprocal. It can be shown that an electromagnetic field in such a medium can be decomposed outside the sources in TE and TM parts with respect to the respective vectors $\mathbf{a}$ and $\mathbf{b}$, i.e., in partial fields satisfying either $\mathbf{a} \cdot \mathbf{E} = 0$ or $\mathbf{b} \cdot \mathbf{H} = 0$. Actually, the above condition defines the most general anisotropic medium for which the TE/TM decomposition can be made for electromagnetic fields. A generalization to bi-anisotropic media has also been done and will be presented elsewhere.

To see how the decomposed fields arise from a given electromagnetic source, the corresponding decomposition principle is formulated for the electromagnetic sources. Thus, any source can be split in two individual problems with either TE_a or TM_b fields being generated. It is also shown that electromagnetic fields in each of the split problems can be solved by replacing the medium of the problem by a simpler equivalent medium possessing an analytic Green dyadic expression. This makes it possible, without knowing an analytic Green dyadic for the original problem, to find the field from a point source in terms of its decomposed sources and their Green dyadics.

B92.5

SCATTERING OF THE ELECTROMAGNETIC WAVES ON THE ROUGH CONE AND PARABOLOID

V.G. Spitsyn, Tomsk State University, Russia

In this paper we consider scattering of the electromagnetic waves on the rough bodies of revolurtion: cone and paraboloid. It is assumed that the falling wave is plane, and the measurement of whole rerflection body of revolution surpass by far length of the wave. Roughes are statistic independent and they are distributed uniform on the surface of the body of the turn.

Three types of diagrams over-radiation elements of rough surface: isotropic, Lambert and quasi-mirror are analysed. The diagram of over-radiation of rough surface of quasi-mirror type is asymmetrical. The main part of energy scattering signal is concentrated in the vicinity of the direction of mirror reflection wave from surface (V.G. Spitsyn, Journ. of Communicat. Technol. and Electronics. 6, 730-734, 1996). The analitic expressions for scattering indicatrix were received for three types of diagrams over-radiaion elements of rough surface.

The scattering of the electromagnetic waves on inside surface rough bodies of revolution: cone and paraboloid the second and the fourth orders are considered. In this case the field of scattering wave is formed in the result of multiple over-reflection wave from rough surface. For solution of the task is taken the method of statistic modeling of the process of multiple scattering electromagnetic waves on chaoticly disposing roughes.

In the result of the calculations the dependence of angular spectrum of signal, scattering on cone and paraboloids of revolution the second and the fourth orders, from type of the diagram of over-radiation rough surface was investigated. It was determinated that with increase the order equation, describing the surface, the focusing of energy scattering signal to the axis of body of the turn takes place.

THE AVERAGED BOUNDARY CONDITIONS FOR SOME GRIDS IN ANISOTROPIC AND MOVING MEDIA

Andrey V. Tyukhtin
Institute of Radiophysics, St.Petersburg University
1, Ul'yanovskaya, Petrodvorets, St.Petersburg 198904, Russia
E-mail:tyukhtin@onti.niif.spb.su

The method of the averaged boundary conditions (ABC) has been developed in detail for grids positioned in vacuum (M.I.Kontorovich et al., Electrodynamics of grid structures, Moskow, 1987, in Russian). Also, it is effective for grids in some non-trivial media (A.V.Tyukhtin. Sov. J. Commun. Technol. Electron., 14, 118-123, 1989). In given report some new results in this area are presented. Special attention is given to systems of parallel thin strips with arbitrarily oriented cross sections.

Anisotropic medium

An infinite periodic system of parallel perfect conductors is supposed to be situated into an electrically-anisotropic stationary nonabsorbing homogeneous medium. The incident electromagnetic field is harmonic. It is assumed that $r \ll a \ll \min(\lambda, \Lambda)$, where r is a characteristic cross size of conductors, a is a period of the system, λ is a characteristic length of wave, Λ is a characteristic distance the incident field is varied in the grid plane. Under these conditions the ABC have been obtained. Both general case of an arbitrary tensor of permittivity and some special cases (one-axis hyrotropic medium etc.) have been analysed. The ABC has been shown to contain two "effective" radii of conductor. One of them depends on some elements of the permittivity tensor, and another is identical to the radius in the case of vacuum. The values of radii for circular cylinders and for thin strips have been obtained. As example of ABC application the scattering of plane waves on a grid situated in an one-axis crystal has been considered.

Moving medium

The periodic systems of conductors in a moving medium have been considered, also. The medium is supposed to be isotropic, homogeneous and nondispersive. Generally speaking, its velocity is relativistic and has an arbitrary direction. It is only supposed that the field of each conductor is governed by an elliptic equation. This condition gives some limitation on the value of the medium motion velocity. The ABC for systems of circular wires and thin strips have been obtained. It has been shown that in relativistic case the effective radius of conductor depends on the motion velocity and electromagnetic properties of medium. The interaction of plane waves with the grid has been considered.

B92.7

The Excitation and Propagation of Surface Waves in an Absorbing Layer

R.T. Ling, J.D. Scholler, P.Y. Ufimtsev *

Northrop Grumman Corporation
8900 E. Washington Blvd.
Pico Rivera, CA 90660-3783

Abstract

A theory is developed to study TM-type surface waves propagating along a thin absorbing layer on an infinite perfectly conducting plate. It is assumed that the layer is homogeneous and isotropic. The loss mechanism includes both electric and magnetic losses as both permittivity and permeability of the layer are complex. A new phenomenon, which indicates the existence of an *upper cutoff frequency* for surface waves, has been discovered. This phenomenon does not exist in the case of isotropic lossless layers. It was known probably only for magneto-static surface waves on lossless ferrite substrates. Differences in principle are found between surface waves on an absorbing isotropic layer and magneto-static surface waves. One of them concerns the phase velocity near the upper cutoff frequency. This quantity for surface waves on absorbing isotropic layers is higher than the light speed, while the phase velocity of magneto-static waves tends to zero. All basic characteristics of surface waves on an absorbing layer are analyzed. They include the attenuation factors due to electric and magnetic loss mechanism, spatial orientations of phase and amplitude fronts inside a layer, phase and energy velocities, resonance behavior, and launching efficiency. The latter is calculated for surface waves excited by aperture-limited plane waves. A new value for the product of the energy velocity and phase velocity is found. The difference is emphasized between these characteristics and those for surface waves propagating along lossless isotropic layers. In particular, it is shown that in the case of lossless layers, the energy velocity is one half of the phase velocity.

The vector problem of EM wave propagation in an impedance waveguide with a large-scale 3D wall irregularity

Oleg V. Soloviev
Radiophysics Department, University of St.Petersburg
198904 St.Petersburg, Russia. Fax: +7 (812) 428-72-40, E-mail: soloviev@ovs.usr.pu.ru

Up to now the most of 3D problems pertaining to the theory of electromagnetic wave propagation in the presence of localized irregularities in a various model waveguides are considered in scalar approximation. The scalar problem is formulated for the only one component of the Hertz's vector which corresponds to a given source. That statement of a scalar problem ignores the vector effects (e.g. field depolarization). We strive to fill up this gap.

The problem to be considered is the radiation of the point source in the waveguide of the height h, bounded by the surfaces S_e and S_i, characterized by impedance functions $\delta_e = const$ and $\delta_i = \delta(r,\varphi)$. We assume later that $\delta(r,\varphi)=\delta_{io}$ if $(r,\varphi)\in S_{io}$; $\delta(r,\varphi)=\delta_{ip}$ if $(r,\varphi)\in S_{ip}$ and $\delta(r,\varphi)=\delta_{i\gamma}(r,\varphi)$ if $(r,\varphi)\in S_{i\gamma}$, where S_{ip} the area of inhomogeneity of arbitrary shape and size, S_{io} - unperturbed part of the surface S_i, $S_{i\gamma}$ - intermediate curved ring between S_{ip} and S_{io}, where the impedance function changes its value from δ_{io} to δ_{ip}. The unknown EM field components obey Maxwell's equations inside the guide and Leontovitch's impedance boundary conditions. Using them we derive the expressions for normal derivatives on $S_{i\gamma}$, for example to E_z: $\dfrac{\partial E_z}{\partial z} = ik\delta E_z - Z_0 H_\varphi \dfrac{\partial \delta}{\partial r} - \dfrac{\partial \ln\delta}{r\,\partial\varphi} E_\varphi$. This formulae above is substantially different from the commonly used (V.A.Fok, Electromagnetic diffraction and propagation problems. Pergamon, N.Y., 1965) boundary conditions on an irregular surface which contains only first item in the right hand sides and do not allow to step out from restrictions of scalar approximation. Our assessments exhibit significance of the terms with derivatives of impedance in comparison with $ik\delta E_z$. Using the vector form of the Green's theorem we transform the differential equations into the integral equations which relates the field components inside the guide and the boundary values of the unknown functions and their normal derivatives on $S=S_e\cup S_i$. In order to reduce the integration from the infinite surface S to the inhomogeneous area $S_{ip}\cup S_{i\gamma}$ we employ dyadic Green's function. The two parts of this function are $W^{(e)}$ and $W^{(m)}$ - dimensionless vertical components of electric and magnetic Hertz's vectors corresponding to the case of regular guide of the same height h with homogeneous impedance walls (δ_e, δ_{io}) excited by vertical electrical and magnetic dipole, respectively. Thus, the problem is reduced to the system of four coupled surface integral equations for E_Z, H_Z, E_φ, H_φ field components. Taking into account narrowness of the $S_{i\gamma}$ we succeed to convert the surface integral over it into the linear integral along the contour γ - the boundary of $S_{i\gamma}$. As an example we write out here only one equation of the system:

$$E_z(r',\varphi',z') = E_z^0 + \frac{ik}{2\pi}\iint_{S_{ip}} (\delta_{ip}-\delta_{io}) W^{(e)}(\bar{R}',\bar{R}) E_z(\bar{R})\, dS -$$

$$\frac{1}{2\pi}\left\{ Z_0(\delta_{ip}-\delta_{io})\int_\gamma W^{(e)}(\bar{R}',l) H_\varphi(l) \frac{A(l)\,dl}{\sqrt{1+A^2(l)}} + \ln\frac{\delta_{ip}}{\delta_{io}} \int_\gamma W^{(e)}(\bar{R}',l) E_\varphi(l) \frac{dl}{\sqrt{1+A^2(l)}} \right\}$$

where E_z^0 is the field of the source in uniform waveguide, $A = r/r'_\varphi$, $r = r(\varphi)$ - equation which specifies the contour γ. As it may be seen from the derived formulae the first two terms in the right hand side are similar to those in the scalar problem. Therefore the surface integral over S_{ip} can be asymptotically ($kr' >> 1$) reduced (O.V.Soloviev, Izv.VUZ. Radiofiz., 33(9), 1078-1087, 1990) to the contour integral along γ. So the depolarization effect may be evaluated with the aid of the successive approximations using known scalar solution as a starting point.

B92.9

Mode structure formation length in an inhomogeneous media

N.I.Petrov
All-Russian Electrotechnical Institute,
19-39, Lenina str, Istra,
Moscow region, Russia
Phone: (096) 3153258; Fax: (095) 5603134; E-mail: alex@rdiees.msk.ru

Both the ray and mode representations are used for investigation of propagation of radiation in inhomogeneous media. Choice of the convenient representation (the full set of basic functions) is determined by the conditions of excitation. So, at the distances from the source which do not exceed the mode structure formation length it is convenient to use the ray approach, and at long distances from the source - expansion in terms of modes of medium. However the boundaries of the applicability of ray description is the open question.

In this paper the boundaries of the applicability of ray description and formation of mode structure in an inhomogeneous graded-index medium are determined. It is shown, that the length of mode structure formation and the average number of excited modes are determined by the axis displacement or the slope of the incident beam at initial plane of the medium.

Exact analitical expressions for the trajectory and width of nonparaxial wave packets propagating in graded-index medium are obtained using the coherent states formalism for the solution of the Helmholtz wave equation. It is shown, that the nonaxial wave beam diverges at the propagation in graded-index medium and the trajectory of wave beam relaxes on the axis of the medium. The width of the beam increases only up to value determining by the axis displacement or incidence angle of the beam at initial plane. The length of mode structure formation decreases at the increasing of axis displacement or incidence angle of the beam, wavelength of radiation and gradient parameter of the medium. Note, that the mode structure formation length is more sensitive to the change of gradient parameter of medium. Therefore for the image transmission in optical fibres it is necessary to use the fibres with small value of gradient parameter. In typical graded-index optical fibres with the radius 50 μm and gradient parameter $5 \cdot 10^{-3}$ μm^{-1} the mode structure is formed on the distance ~ 30 cm.

URSI B **Session 98** **Galerie 4**

Antennas

Co-chairs: P. Strickland, Canada and S.A. Long, USA

13:10 98.1 A Dual-Polarized, Dual-Band Array for Spaceborne SAR, **P.C. STRICKLAND**[1], L. SHAFAI[2], G. SEGUIN[3], [1]*CAL Corporation, Ottawa, ON,* [2]*University of Manitoba, Winnipeg, MB and* [3]*Canadian Space Agency, Montréal, QC, Canada*

13:30 98.2 A Compact Circular Polarized Antenna with Integrated Feed for UMTS Satellite Portable Terminal, M. CLENET[1], A. SHARAIHA[2], C. TERRET[2], **J. SAILLARD**[1], [1]*EP CNRS 63, IRESTE, Nantes and* [2]*Université de Rennes I, Rennes, France*

13:50 98.3 Enhancement of Wide-Flare Pyramidal Horn E- and H-Plane Performance Using Metal Baffles, **M.A. KOERNER**, R.L. ROGERS, *University of Texas at Austin, TX, USA*

14:10 98.4 On the Design of Conformal Array Antenna, **G.G. CHENG**, C. KCHAO, F.C. CHANG, *TRW Space and Electronics Group, Redondo Beach, CA, USA*

14:30 98.5 Theoretical Study of Two-Dimensional, Highly Directive Current Distributions, **G. FIKIORIS**[1], D. MARGETIS[2], J.M. MYERS[2], T.T. WU[2], [1]*Rome Laboratory, Hanscom AFB and* [2]*Harvard University, Cambridge, MA, USA*

14:50 98.6 Design and Modelling Considerations for a Zoned Bootlace Antenna, **P.J. WOOD**, *CAL Corporation, Ottawa, ON, Canada*

15:10 Coffee Break

15:30 98.7 Fractal-Element Antenna (FEA) Applications in Hand-Held Wireless/PCS Systems, **N. COHEN**[1], R. FERRA[2], [1]*Fractal Antenna Systems, Inc., Belmont, MA and* [2]*US Army/CECOM, USA*

15:50 98.8 A Novel Thin Planer Antenna for One-Side Radiation Wireless Phone Terminal, **K. TAKEI**, H. OKABE, *Hitachi Ltd., Tokyo, Japan*

16:10 98.9 Transmission Line Model for CPW Antennas Using ANN Modeling Approach, **K.C. GUPTA**, P. WATSON, *University of Colorado at Boulder, CO, USA*

B98.1

A Dual-Polarized, Dual-Band Array For Spaceborne SAR

Peter C. Strickland*, CAL Corporation
Lot Shafai, University of Manitoba
Guy Seguin, Canadian Space Agency

Abstract

The next generation of civilian, satellite based synthetic aperture radar is likely to be multispectral with polarization synthesis, cross polarization and multi-mode capabilities. In order to minimize the overall size of the antenna subsystem, techniques are being developed which allow the aperture to be shared between multiple frequency bands and multiple polarization channels. In this work, a multi-layered windowed microstrip implementation is being used in order to provide simultaneous L-band and C-band operation with simultaneous vertical and horizontal polarization in each band.

The multilayer patch implementation results in a thin, lightweight and rigid structure while allowing broad bandwidths to be achieved at both L and C bands. With a radiating panel thickness of only 0.44", a bandwidth of 160 MHz has been achieved at C-band and 70 MHz has been achieved at L-band with a mass of only 400 grams per square metre. The lower resonator layers are printed on a thermally stable substrate, with slot coupling being used at C-band in order to avoid the need for large numbers of plated-through holes. The upper resonators are passive, requiring no interconnection to the driven elements below. In order to minimize feed losses, and increase overall system reliability, the array may be either fed in a semi-active manner with T/R modules devoted to sub-arrays, or by a hybrid scheme whereby low loss square-ax is used to distribute power to the sub-arrays. The azimuth sub-arrays have been implemented using compact broadband microstrip feeds, printed on a thin substrate layer behind the feed slots.

The figure below illustrates one panel of the proof-of-concept array which is currently under construction. Eight of these panels will be configured to give a 32 by 32 element array at C-band and an 8 by 8 element array at L-band. At C-band this provides nearly the same aperture height as CAL Corporation's Radarsat SAR antenna panels, and consequently will allow similar shaped sector beams to be produced. A 32 way unequal split power divider has been developed for this purpose.

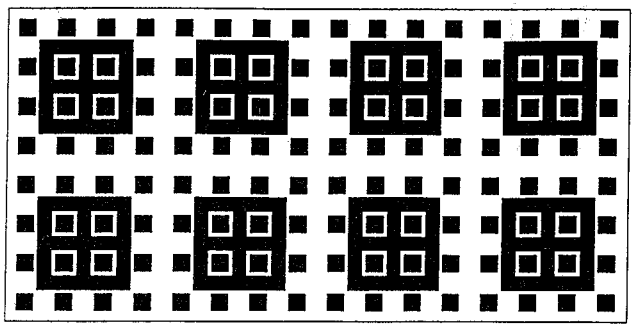

A Compact Circular Polarized Antenna with Integrated Feed for UMTS Satellite Portable Terminal

M. CLENET*, A. SHARAIHA**, C. TERRET**, J. SAILLARD*
* Laboratoire SEI, EP CNRS 63, IRESTE, La Chantrerie, 44087 NANTES, FRANCE
** Laboratoire Structures Rayonnantes, U.R.A au CNRS $n°$ 834, Université de Rennes 1
Av. du Général Leclerc, 35042 RENNES CEDEX, FRANCE

Introduction

In this paper, we present the structure of a circular polarized antenna with integrated feeding network. This antenna can be mounted on a portable terminal for satellite communications according to the UMTS (Universal Mobile Telecommunication System) standard (1.98-2.01 GHz for the reception and 2.17-2.2 GHz for the emission). The main characteristic of this antenna is to have an integrated feed which do not increase the size. The characteristics of the antenna were measured over an infinite ground plane and mounted on a portable terminal.

The ***microstrip antenna*** consists of two substrate layers (fig. 1). The lower layer is made of a high permittivity material (ε_r = 10.8) to reduce the dimensions. The upper layer is printed on a 2.55 permittivity material. Both printed radiating elements are square shape. The lower patch is fed on the diagonal by two orthogonal ports in phase quadrature in order to obtain the required circular polarization.

Thus, we obtain a 15% bandwidth for a Standing Wave Ratio (SWR) less than two around F_o=2.092 GHz, and the coupling between the two feeds is less than -20 dB.

The ***feeding system*** is introduced between the two layers. The lower patch is used as the ground plane of the feed. The feeding system is a 90° hybrid coupler designed in a semi-lumped technology, as shown in fig. 2, in order to obtain a size reduction of the structure (A.C. Tarot, C. Terret, MOTL, vol.12, june 96, pp77-79). Thus, the optimized circuit is contained on a 20 mm^2 square surface. It is printed on a dielectric substrate of permittivity 2.92 and 125 µm thickness.

The experimental results show that the SWR of this circuit is less than 1.5 in the useful bandwidth, the magnitude error between the two feeds is less than 0.5 dB and the maximum phase error is 2 degrees.

The characteristics of the ***antenna with its integrated feed*** was also measured. The bandwidth obtained is 18.5%. The axial ratio equals 1.4 dB in a 60° beamwidth in the two main planes when the antenna is over an infinite ground plane. This value is a little greater when the antenna is mounted on a portable terminal. The measured gain is about 3.5 in the transmitting band and 5 dB in the recieving band.

Conclusion

A compact microstrip antenna with integrated feeding system has been realized. It produces a circular polarized wave with low axial ratio. A good matching is obtained on a bandwidth of 18.5%. The antenna is a good candidate for satellite communications according to the UMTS standard.

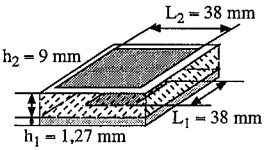

fig. 1 : The microstrip antenna

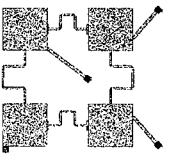

fig. 2 : The feeding system

Acknowledgment: This work is supported by the CNET (contract number 94 1B 005).

B98.3

ENHANCEMENT OF WIDE-FLARE PYRAMIDAL HORN E- AND H-PLANE PERFORMANCE USING METAL BAFFLES

Matthew A. Koerner *, Robert L. Rogers
Applied Research Laboratories
The University of Texas at Austin
Austin, TX 78713-8029

Work underway to develop small, economical, high-gain antennas for microwave and millimeter wave systems led to a simple scheme for enhancing the performance of wide-flare pyramidal horn antennas. The scheme consists of loading horns with small, planar, metal baffles. These baffles alter aperture fields much like a lens, resulting in greatly enhanced gain, beam-patterns, and aperture efficiency. Calculations and measurements for metal baffle loading schemes which enhance the E-plane parameters of wide-flare pyramidal horns have been presented by Koerner and Rogers (M. A. Koerner and R. L. Rogers, USNC/URSI National Radio Science Meeting, 9-13 Jan. 1996). These results were then expanded through further analysis and development (M. A. Koerner, Master's Thesis, The University of Texas at Austin, August 1996). Recently, a new loading scheme has been discovered which enhances H-plane parameters of wide-flare horns as well as E-plane parameters.

Two dimensional calculations discussed previously lead to E-plane metal baffles which reduce phase curvature across antenna apertures much like a lens. The E-plane baffles proved effective in an experimental wide-flare X-band horn where they increased the antenna's gain by 3dB over a 1.4 GHz frequency band with a bandwidth of 12.4% (M. A. Koerner, Master's Thesis). Unfortunately, the E-plane baffles alone do little to enhance the H-plane parameters of the antenna.

Due to the success of the E-plane two-dimensional calculations and the need for H-plane improvements, a two-dimensional H-plane model was employed to study simple metal baffles in this plane. Introductory studies have produced H-plane baffles which enhance antenna gain by 2dB over wide frequency ranges in the experimental horn used in the E-plane measurements. Calculations show that the H-plane baffles introduce higher order modes to the aperture fields and reduce phase curvature resulting in enhanced antenna performance.

Simultaneous studies of E- and H-plane baffles can not be accomplished using two-dimensional calculations, but preliminary measurements of an E-plane/H-plane combination baffle have produced excellent experimental results. One combination found increases the gain of the experimental wide-flare X-band horn by 4dB over a frequency band of 1 GHz. The aperture efficiency in this frequency band is above 50% and peaks to 65%.

On The Design Of Conformal Array Antenna

Guan G. Cheng*, Chamroeun Kchao, and F.C. Chang

TRW Space and Electronics Group
One Space Park, 66/1217
Redondo Beach, CA 90278

A direct, closed-form solution for the design of a conformal array antenna via pattern synthesis is presented. This design procedure enables a desired far-field pattern to be theoretically realized by an array antenna with weighted elements laying on a spherical surface. A new pattern synthesis technique which determines the amplitude and phase distribution for these array elements has been developed. Both far-field amplitude and phase patterns are required for the synthesis, which basically back transforms the desired far field directly onto a spherical cap in the near-field region with arbitrary radius. This back transform is merely a double-integration operation, and is indeed the inverse transform of the spherical near-field to far-field transformation, with identically same degree of computational complexity.

Three design issues which pose direct impacts to the hardware implementations, are under investigation. They are phase pattern of the desired far-field, the curvature of spherical surface of interest, and the discrete version of surface field distribution. First, the determination of phase pattern has arisen since the desired far field is normally an amplitude (power) pattern, and the back transform requires both amplitude and phase field data. Algorithm which generates different, reasonable phase patterns for far-field is analyzed and it results in interesting near-field distributions. Second, the difference in spherical curvature gives rise to different near-field distributions and is also related the size of the cap. Proper selection of the curvature minimizes the size. Third, the discrete near-field distribution due to array hardware implementation affects the far field performance. All these three issues are considered to be design parameters in the array design process.

Antenna designs and their hardware realization for various desired far field patterns are described, along with the impacts on the antenna performance for the selections of input far field phase pattern, the spherical curvature, and the discrete near-field distribution.

B98.5

THEORETICAL STUDY OF TWO-DIMENSIONAL, HIGHLY DIRECTIVE CURRENT DISTRIBUTIONS

George Fikioris*
Rome Laboratory
Electromagnetics and Reliability Directorate
Hanscom AFB, MA, 01731, and

Dionisios Margetis, John M. Myers, Tai Tsun Wu
Gordon McKay Laboratory
Harvard University
Cambridge, MA, 02138

In this paper, we propose a general scheme for investigating two-dimensional, highly directive current distributions, and illustrate its application to a particular geometry: For the two-dimensional case of surface currents invariant along an axis, we maximize the directivity in the far field while constraining $C = N/T$. N is the integral of the square of the current density, and T is the total radiated power. For current-carrying regions made of highly conducting materials, N is proportional to the ohmic losses. The method of Lagrange multipliers leads to a Fredholm integral equation of the second kind for the unknown current density, in which C enters as a parameter implicitly.

We expect our integral equation to be a valuable tool for obtaining insight into the nature of highly directive antennas. We apply it to the case of the infinitely long cylindrical shell of electrical radius ka. Here, ohmic losses are obtained by multiplying $\frac{N}{ka}$ by a quantity independent of a; thus, $\frac{ka}{C}$ measures the efficiency. In this simplest case, the solution of the integral equation can be obtained in closed form. However, the optimum current and the resulting optimum directivity D depend on C and ka in a complicated way.

A certain value C_0 of C yields the reference case, in which currents of uniform amplitude produce the maximum directivity D_0 by constructive interference. Combining analytical and numerical techniques, we investigate the function $D(\frac{C}{ka})$ for $\frac{C}{ka} \geq \frac{C_0}{ka}$ and $ka \gg 1$. Qualitatively, the curve first increases rather rapidly, then eventually increases extremely slowly. The behavior in the latter region, which is to be expected, is quantified analytically. We show that the slope in the first region increases with increasing ka. Generalizations of this last result must hold for more complex geometries; this encourages further research into electrically large, moderately superdirective antennas.

DESIGN AND MODELLING CONSIDERATIONS FOR A ZONED BOOTLACE ANTENNA

Peter J. Wood, CAL Corporation

The double membrane concept has been developed by CAL Corp. to provide a method of realizing large spacecraft antennas which have (simultaneously) a very low mass, minimal stowed volume, and low cost (see Raab et al, CASI 9th Conference on Astronautics, 1996, pp. 90-98). DDM lens antenna technology is well suited to many spacecraft communications and radar applications. In this paper, the DDM (deployable double membrane) is made to function as a zoned bootlace artificial lens. The radiating elements on each of the two lens outer surfaces are configured as a special form of microstrip patch radiator, and are interconnected by flexible two-wire transmission lines.

Three major electrical design issues may be cited for a membrane lens:

a) The radiating elements must be matched to an incident wave, and to one another via the bootlace lines. Matching conditions are quite different for membrane-supported arrays, as compared to individual patches operated in a free-space environment.

b) The radiating elements and their interconnecting lines should be configured so as to maximize bandwidth.

c) The design needs to be tolerant of the membrane surface distortions which occur in a typical in-orbit environment.

This paper will discuss the special techniques which have been developed for the electromagnetic modelling of artificial lens structures. The model is based around the University of Syracuse Wire-Plate Method of Moments code. Special extensions to this code have been developed by CAL. The two lens surfaces, together with their interconnecting lines, are treated as a single electromagnetic unit. 'Immersed element pattern' and 'active match' design rationales will be compared.

The electromagnetic model has been used to determine the optimal configuration for a DDM patch. It has been established that the DDM lens can offer an electrical performance which is fully comparable to that of a conventional offset reflector realization, in pencil beam, shaped beam, or reconfigurable shaped beam applications. In-orbit distortions have a virtually negligible effect for a 10m. L-band design, and it appears to be possible to extend the concept to much higher frequencies.

B98.7

FRACTAL-ELEMENT ANTENNA (FEA) APPLICATIONS IN HAND-HELD WIRELESS/PCS SYSTEMS

Nathan Cohen, Fractal Antenna Systems, Inc.,
and Robert Ferra,US Army/CECOM

We describe several options for miniature fractal antennae for wireless transceivers operating at 800-950 MHz or 1.9-2.4 GHz. All the antennae have substantially flat form factors with typical size reductions of 2-4 compared to Euclidean conterparts such as: monopoles; dipoles; loops; and patches. Complexity in the fractal patterns produces fractal loading, yielding reduced resonant frequencies, and size compression. There is a clustering of higher resonances which produce broadbandedness/multiband operation.

No discrete loading components are utilized. The antennae are etched onto flexible, thin substrates. They can be embedded or mounted covertly, when the load characteristics of adjacent material is taken into account.

At their lowest resonances, each FEA typically produces power patterns, field strengths, and feed impedances compatible with appropriate requirements. Bandwidths are typically 4-10% for 2:1 VSWR to 50 ohms.

A Novel Thin Planer Antenna for One-Side Radiation Wireless Phone Terminal

Ken Takei* and Hiroshi Okabe
Communication Systems Research Dept. Central Research Lab. Hitachi Ltd., Japan

We have developed a novel thin planer antenna. Our antenna is a board consists of three metal layers. (as shown in figure 1.) The first layer is a conducting plate with a radiating slot, whose length is about a half operation wavelength. An inner strip conductor is formed on the second layer and serves as feeding line to the radiating slot. The third layer is a finite ground plane. Four sides of the first and third layers are electrically connected to plated side. One end of the strip conductor is connected to the center conductor of a coaxial line through a hole on the grounding layer. RF power is input through the coaxial line to feed this antenna structure. The radiation source of our antenna is a finite magnetic line current along the slot. This antenna can create an one-side radiation pattern because the source current locates on the center of the finite ground plane.

We measured the radiation pattern of a small wireless phone terminal with our antenna. The antenna is mounted on the back surface of a shield case which contains an RF circuit board. The antenna and the terminal measure 30x40x0.8 mm and 180 cc, respectively. Figure 2 shows experimental radiation patterns measured indoors in two cases. The terminal is located far from human body in one case. In the other case the terminal is held near a human head by hand. These pattern are not so far different, since our antenna effectively reduce the radiation power toward the user. To demonstrate the antenna directivity in actual use outdoor environment, we measured radiation power from 1.9Ghz PHS (Personal Handy-phone System) base station by using this terminal. The terminal was held in front of a user's face by his hand. He changed the position in order to vary the angle, i.e. 0, 90, 180, 270 degrees, between the main beam direction of antenna and the site direction of the base station. As shown in figure 3, the change of measured intensities of the electric field with the beam angle verifies the antenna directivity measured indoors.

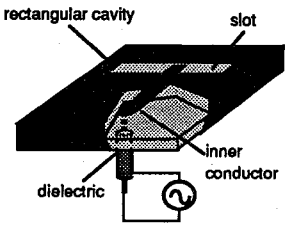

Fig. 1 Antenna Structure.

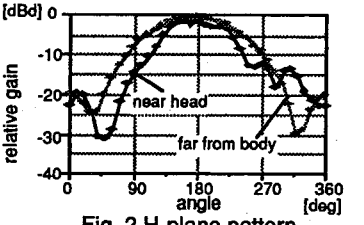

Fig. 2 H-plane pattern.

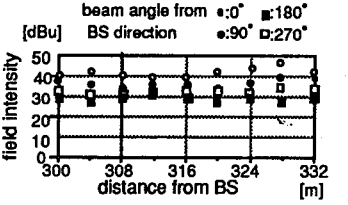

Fig. 3 Measured Field Intensity.

B98.9

Transmission Line Model for CPW Antennas Using ANN Modeling Approach

K.C. Gupta and Paul Watson
University of Colorado at Boulder
Center for Advanced Manufacturing and Packaging of
Microwave, Optical and Digital Electronics (CAMPmode)
Department of Electrical and Computer Engineering
Boulder (Colorado) 80309-0425

Radiating elements using open-ended CPW resonators (Fig. 1) provide an alternative for printed slot antennas. Motivation for exploring these antenna structures arises from the ease of connecting CPW resonators to CPW lines which are conveniently fed by coaxial connectors. Further investigation of these radiating structures requires development of simple network models (like transmission line model for microstrip patches) which may be used for designing these antennas. This presentation will discuss development of a transmission line model for CPW antennas based on Artificial Neural Network (ANN) models for CPW line, CPW open-end, and a CPW T-junction. These ANN models could be used in a microwave network simulator (like HP's MDS) for design of CPW antennas.

The concept of developing ANN models for microwave/mm-wave components using a fullwave electromagnetic simulator for training these models has been presented earlier (Watson and Gupta, IEEE Trans. Microwave Theory Tech., vol. 44, pp. 2495-2503). For the current work, this methodology has been used for developing efficient and accurate models for CPW lines on Duroid substrates, CPW open-ends (including radiation conductance modeling), and CPW T-junctions used for connecting CPW resonators to CPW lines. HP's Momentum was used for training these ANN models. These component model are used in HP's MDS to develop a Transmission Line Model for CPW patches. Antenna performance derived from this Transmission Line Model is compared with the full-wave analysis results to verify the validity of the antenna model developed. Detailed results will be presented at the meeting.

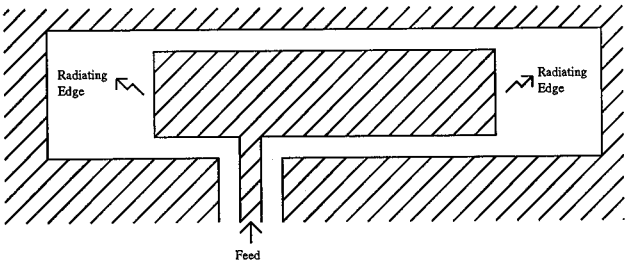

Fig. 1 A CPW antenna fed by a CPW line.

URSI B | Session 102 | Salon Bersimis

Guided and Leaky Wave Structures
Co-chairs: T. Tamir, USA and M. Ando, Japan

13:10 102.1 Higher Order Modes of Coupled Stripline Structures, **D. INFANTE**, D.P. NYQUIST, *Michigan State University, East Lansing, MI, USA*

13:30 102.2 Analysis of Cylindrical Microstrip Lines Embedded in a Two-Layer Substrate inside a Ground Cylinder, **C.-I.G. HSU**[1], S.-U. HWU[2], C.-H. LEE[3], [1]*Da-Yeh Institute of Technology, Chang-Hua, Taiwan, China;* [2]*Lockheed Martin Engineering and Sciences Company, Houston, TX, USA;* [3]*National Chang-Hua University of Education, Chang-Hua, Taiwan, China*

13:50 102.3 Using Equivalent Impedance Approach to Analyze Quasiperiodic Corrugated Waveguides, **A.E. SEREBRYANNIKOV**, *Radio Astronomy Institute, Kharkov, Ukraine*

14:10 102.4 Pole-Migration with Scan-Angle of Planar Leaky-Wave Antennas, **E. SCHMIDHAMMER**, J. DETLEFSEN, *Technische Universität München, Germany*

14:30 102.5 Leaky-Wave Formulation of Wave Scattering and Guiding by Periodic Structures, K.C. HO, **T. TAMIR**, S. ZHANG, *Polytechnic University, Brooklyn, NY, USA*

B102.1

HIGHER ORDER MODES OF COUPLED STRIPLINE STRUCTURES

D. Infante* and D. P Nyquist
Department of Electrical Engineering
Michigan State University
East Lansing, MI 48824

Stripline structures have found increasing use in areas such as integrated circuit devices and the electromagnetic characterization of materials. In spite of the fact that the symmetric structure of stripline devices lends itself well to analysis, little has been documented regarding higher order modes (including leaky modes) which may exist on these structures. In particular little is known about the interaction of coupled strips which are operated at frequencies which excite modes beyond the fundamental mode. Knowledge of the propagation mode spectrum, including possible leaky modes which arise on a coupled stripline structure, would be useful in reducing or preventing crosstalk and other interference effects in circuits which utilize these structures.

In order to determine the propagation mode spectrum, a Hertzian potential Green's function is established for a generalized impressed current source suspended in free space between two infinitely wide conducting plates. This Green's function is then specialized to the coupled strip structure by enforcing boundary conditions for tangential fields at the (not necessarily co-planar) conducting strip surfaces. This results in a pair of coupled electric field integral equations for currents on the strips. Guided mode solutions are determined by Fourier transforming on the axial variable and examining the resulting EFIEs:

$$\hat{t}\cdot(k_o+\tilde{\nabla}\tilde{\nabla}\cdot)\left[\lim_{y\to h_1}\int_{x_1-\frac{w_1}{2}}^{x_1-\frac{w_1}{2}}\tilde{\vec{g}}_\zeta(x,y|x',h_1)\cdot k_{1p}(x')dx'+\int_{x_2-\frac{w_2}{2}}^{x_2+\frac{w_2}{2}}\tilde{\vec{g}}_\zeta(x,h_1|x',h_2)\cdot k_{2p}(x')dx'\right]=0 \qquad (1)$$

$$\hat{t}\cdot(k_o+\tilde{\nabla}\tilde{\nabla}\cdot)\left[\int_{x_1-\frac{w_1}{2}}^{x_1-\frac{w_1}{2}}\tilde{\vec{g}}_\zeta(x,h_2|x',h_1)\cdot k_{1p}(x')dx'+\lim_{y\to h_2}\int_{x_2-\frac{w_2}{2}}^{x_2+\frac{w_2}{2}}\tilde{\vec{g}}_\zeta(x,y|x',h_2)\cdot k_{2p}(x')dx'\right]=0 \qquad (2)$$

Here $\tilde{\nabla}$ is the transform-domain differential operator, $\tilde{\vec{g}}$ is the transform-domain Green's function, and $k_{\alpha p}$ are the transform-domain currents existing on the conducting-strip cross-sections which extend from $x_\alpha - w_\alpha/2$ to $x_\alpha + w_\alpha/2$ at distances h_α from the center of the structure ($\alpha = 1,2$). Equations (1) and (2) have non-trivial solutions only for discrete values of ζ which are the propagation constants for the guided wave modes. The coupled EFIEs are converted to matrix form via Galerkin's method, employing Cheybechev basis functions. The resulting matrix equation has non-trivial solutions only for discrete $\zeta = \zeta_p$, which are determined numerically.

This paper will discuss a full-wave integral equation formulation for coupled strip currents and propagation constants. Results will include current distributions associated with various modes, and propagation-mode dispersion characteristics, indicating cutoff frequencies of higher order modes, and the existance of leaky-wave modes.

Analysis of Cylindrical Microstrip Lines Embedded in a Two-layer Substrate inside a Ground Cylinder

Chung-I G. Hsu[1*], Shian-Uei Hwu[2], Ching-Her Lee[3]
[1]Dept. of Elect. Eng., Da-Yeh Inst. of Tech., Chang-Hua, Taiwan 51505
[2]Lockheed Martin Eng. and Sciences Company, Houston, TX 77058, USA
[3]Dept. of Industrial Edu., National Chang-Hua Univ. of Edu., Taiwan 50058

The objective of this article is to study the dispersion characteristics of a cylindrical microstrip line mounted inside a grounded conducting cylinder, as shown in Fig. 1, where each dielectric layer is characterized by (ε_i,μ_i),i=1,2,3 and layers 2 and 3 are the substrates. The conducting strip lies on a cylindrical surface of arbitrary radius (i.e., not necessarily on interfaces between adjacent dielectric layers). A rigorous full wave analysis is applied to formulate an electric field integral equation, which is subsequently solved numerically using the method of moments. A spectral dyadic Green's function that relates the electric fields to the surface currents on the strip is derived. Entire domain basis functions that incorporate the edge conditions are employed to approximate the longitudinal and the transverse surface currents on the strip in the numerical computation. The numerical results presented in this article include the effective dielectric constants and the characteristic impedances of the propagation modes. The effects of the locations of the strip on the dispersion characteristics are examined. Since investigations for the present structure have not been reported elsewhere, the computed frequency-dependent results can only be compared with data available in the literature for some special cases. The computer code developed in this research can be used as a computer aided tool in the pre-fabrication stage in the circuit design process.

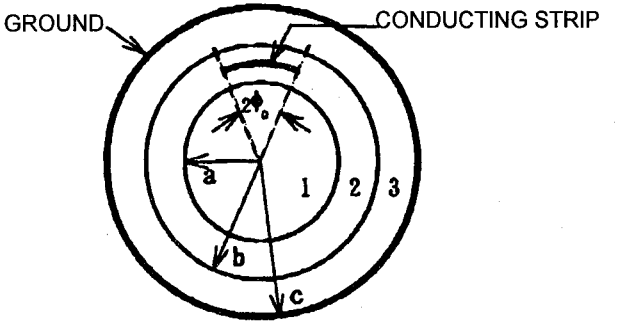

Fig.1 The cross-sectional view of a cylindrical microstrip line mounted inside a ground cylinder.

B102.3

Using Equivalent Impedance Approach to Analyze Quasiperiodic Corrugated Waveguides

A.E.Serebryannikov
Radio Astronomy Institute, Kharkov, Ukraine

The method of equivalent boundary conditions (MEBC), based on the equivalent surface impedance (ESI) approach, is an efficient tool to analyze periodically-corrugated waveguiding structures. In the present paper the MEBC is developed for the quasiperiodic coaxial corrugated waveguide. We use both formulae for the ESI and for the imaginary part of natural frequencies, that were obtained by Illinsky and Slepyan for imperfectly conducting plane structure (A.S.Illinsky and G.Ya.Slepyan, Oscillations and Waves in Lossy Electrodynamic Systems, Moscow, 1983), as the entry point. At the first stage, using the fundamental-harmonic approximation of the characteristic equation of the azimuthally-periodic waveguide, and comparing one with the general formula for the surface impedance, we obtain the formula allowing to estimate the imaginary part of the ESI for TE-modes of the considered frequency-selective surface. Formula for the real part of the ESI ($Re\,\mathbf{Z}^{e}_{(1)}$) remains without change. In such a way we take into account both cylindricity of the combed structure and the υ-dependence of ESI (υ is the aperture opening of each cell).

At the second stage we solve the eigenvalue problem for the quasiperiodic corrugated waveguide. We consider the case of the most practical interest when one of the cells is loaded so, that the periodicity of the structure is disrupted. In this case it is necessary to consider the diffractive losses and the ohmic ones simultaneously. Assuming smallness of the structure period in comparison with the wavelength, and using the averaging method with respect to the azimuthal variable φ, we obtain the ESI for the outer conductor of equivalent coaxial waveguide as $\mathbf{Z}^{e} = [(1-\upsilon)\mathbf{Z}^{e}_{(1)} + \upsilon\,\mathbf{Z}^{e}_{(2)}]/2\pi$. (Here $\mathbf{Z}^{e}_{(2)}$ is the equivalent impedance of the loaded cell). Since the diffractive losses are taken into account by using $\mathbf{Z}^{e}_{(2)}$, both the real and imaginary parts of natural frequencies can be calculated equating the ESI obtained above ($\mathbf{Z}^{e}$) and the input impedance of the space between the inner and outer conductors.

The modification of the MEBC, proposed in this paper, gives an efficient apparatus for analysis of the both azimuthally-periodic and quasiperiodic combed structures with losses. The possibilities of the practical use of the developed approach have been studied on the basis of comparison with the numerical data obtained by using more strict models. The recent results show that it can be used to analyze the quasiperiodic structure when its natural frequency is located closely to natural frequency of the key periodic structure. The method has been applied to investigate the geometric parameters effect on the complex natural frequencies of the loaded magnetron-like cavity with the complex load and to compare the loading effect appearing for different modes. As a result, recommendations for choosing the working mode have been given.

POLE-MIGRATION WITH SCAN-ANGLE OF PLANAR LEAKY-WAVE ANTENNAS

E. Schmidhammer*, J. Detlefsen
Lehrstuhl für Hochfrequenztechnik
Technische Universität München, 80290 München, Germany

Leaky-wave antennas, consisting of multiple dielectric layers above a ground-plane, become more and more interesting due to their flatness. One important point of these type of antennas is the ability to radiate in any direction under a specific scan-angle. This can be achieved by properly dimensioned layers (D. R. Jackson et al., IEEE Trans. AP, Vol. 33, No. 9, pp. 976-987, Sept. 1985). Dependend of the permittivities of the different layers, leaky-waves are strongly excited which are responsible for sharp peaks in the farfield pattern. Up to now, only the frequency dependence of the dominant leaky waves was studied in detail (D. R. Jackson et al., IEEE Trans. AP, Vol. 36, No. 7, pp. 905-910, July 1988). If the scan-angle is near 90° and additionally the lowest layer is filled with air, more and more leaky-wave modes are excited and show their influence in the farfield.

In this presentation we want to explain the physical behaviour of these poles in the steepest-descent plane. By determining the pole locations and calculating the attenuation and propagation constants a dependence between scan-angle and higher-order leaky-wave modes can be given for either TE and TM polarization. Furthermore we want to show the influence of the permittivities of the different layers, whether a higher-order mode can be launched or not. If we generalize the problem to a two-layered structure, the lower layer is always responsible for the excitation of leaky-waves, while the upper layer counts for the strongness e.g. amplitude of the mode.

As a result of these investigations some fundamental properties of the structure can be concluded. If the lower layer is air-filled, all leaky-waves will end in the branch point at k_0 when the scan-angle reaches 90°. After (S. Barone et al., Microwave Res. Inst., Polytechnic Inst. Brooklyn, R-698-58, PIB-626, Dec. 1958) always an infinite number of leaky-wave poles exist. Therefore more and more are captured by the steepest-descent path and hence directly contribute to the farfield. By increasing the permittivity of the lower layer up to a specific value, the number of peaks in the radiation pattern can be adjusted. In this way it is possible to achieve a single-mode radiation, even if the scan-angle is near 90°. Now higher-order modes are either suppressed, because they are no more captured by the steepest-descent path or have become surface-waves, which do not contribute to the farfield.

B102.5

LEAKY-WAVE FORMULATION OF WAVE SCATTERING AND GUIDING BY PERIODIC STRUCTURES

*K.C. Ho, T. Tamir and S. Zhang**

Department of Electrical Engineering, Polytechnic University
Six Metrotech Center, Brooklyn, NY 11201

Numerous electromagnetic studies of multilayered periodic configurations have recently been motivated by planar optoelectronic components that function as lasers, couplers, switches, filters, etc. by scattering or guiding light beams. The analysis and design of such devices has been carried out mostly by using coupled-wave techniques or by applying numerical methods to exact field solutions. However, these approaches may become unwieldy when the number of layers and/or periods is large. We have therefore developed an alternative modal approach that more effectively expresses the fields in multilayered periodic configurations. By using leaky-wave concepts, this approach brings novel insights into the operation of such devices and serves as a systematic tool for deriving design criteria.

Fields in planar periodic structures are usually viewed as waves that progress along the longitudinal (horizontal) z direction of the layers. These waves are then represented mostly as coupled but generally non-orthogonal modes, or as local normal modes that vary over the length of a periodic interval. By contrast, our approach uses a space-harmonic (Floquet) analysis that basically combines the two other representations into a rigorous and global formulation. An important advantage of this approach is that it can view the fields as propagating also along the perpendicular (vertical) x direction of the layers, in which case transverse-resonance techniques can be applied to describe field solutions in terms of equivalent transmission-line networks along x. Due to periodicity, each layer must then be represented by a set of separate transmission lines which are associated with space harmonics. Those transmission-line sets couple at the layer boundaries by means of well defined interface transformers. However, the transmission-line sets for periodic layers can be treated by matrix expressions that follow the same formal rules obeyed by scalar relations used in homogeneous (nonperiodic) layers. As a result, generalized transverse networks describing periodic configurations can be handled by a straightforward extension of conventional transmission-line-network techniques.

When considering configurations of practical application, we then find that the field supported by the periodic region is well characterized by only one or two discrete leaky waves, rather than by a more complicated field representation that includes continuous spectra. As a result, wave scattering or guiding by multilayered gratings can be treated by relatively simpler models that describe the operation of practical devices in terms of radiation-leakage effects. Cross-sectional discontinuities in such devices can also be evaluated by the leakage-wave approach, which thus provides a systematic and effective technique having phenomenologically useful interpretations. Our results will be illustrated by examples whose analysis by means of other techniques has already been reported in the literature.

---

* S. Zhang was on leave from the Hangzhou Institute of Electronics Engineering, Hangzhou, P.R. China.

URSI B **Session 103** Salon Bersimis

Characterization of Transient Antennas
Co-chairs: K. Virga, USA and E. Heyman, Israel

15:30 103.1 On the Near Field Properties and Radiation Efficiency of Short Pulse Antennas, A. SHLIVINSKI, **E. HEYMAN**, R. KASTNER, *Tel-Aviv University, Tel-Aviv, Israel*

15:50 103.2 Experimental Characterization of the Effect of Aperture Design on the Time-Domain Response of Impulse-Radiating Antennas with Application to Arrays, **C.J. BUCHENAUER**, J.S. TYO, J.S.H. SCHOENBERG, *USAF Phillips Laboratory/WSQW, Kirtland AFB, NM, USA*

16:10 103.3 Transient Characteristics of Antennas for Wireless Communications Systems, **K.L. VIRGA**[1], Y. RAHMAT-SAMII[2], [1]*University of Arizona, Tucson and* [2]*University of California, Los Angeles, CA, USA*

16:30 103.4 Study of the Pulse Antenna with Resistance and Capacitance Loading, **J.-H. WANG**, *Northern Jiaotong University, Beijing, China*

16:50 103.5 Short Video Pulse Radiation by a Slot Metal-Dielectric Antenna, **N.N. KOLCHIGIN**, S.N. PIVNENKO, *Kharkov State University, Kharkov, Ukraine*

B103.1

On the Near Field Properties and Radiation Efficiency of Short Pulse Antennas

Amir Shlivinski, Ehud Heyman and Raphael Kastner

Faculty of Engineering, Tel-Aviv University, Israel
Fax: +972-3-6423508, e-mail: heyman@eng.tau.ac.il

With the increasing interest in the radiation and detection of ultra wideband (UWB) short pulses, there is a need for the design and analysis of appropriate antennas. One approach would be to utilize the traditional frequency domain (FD) antenna analysis on a frequency-by-frequency basis. However, because of the broad frequency band of the short-pulsed fields, direct treatment of the antennas in the time domain (TD) is more efficient and physically transparent than the inversion of FD solutions. The dividends of a self-sustained TD description call for a development of a comprehensive methodology and phenomenological analysis for TD antennas.

In a recent paper [A. Shlivinski, E. Heyman and R. Kastner, Antenna characterization in the time domain, IEEE Trans. Antennas Propagat., 1996, submitted], we have developed a unified TD system theory for antenna characterization, emphasizing the source-to-far-field transition as well as the receiving properties of the antenna. These results provided a complete TD transmit-receiver (Friis-type) equation. The analytical framework there has been structured upon the TD plane wave spectrum, defined via the slant stack transform of the antenna current distribution.

In the present work we explore the near field properties of the antenna directly in the time-domain. We start by extending the well known multiple (or spherical wave) expansion of the field to the TD. Using this new representation we then define the pulsed (i.e., time-dependent) reactive field and power and the pulsed reactive energy. By considering time-dependent energy balance we then clarify the transition of the pulsed reactive energy, that dominates essentially in the near zone, to the pulsed radiation power. Finally, we introduce a quality (Q) factor to quantify the radiation efficiency of the pulsed antenna.

Experimental Characterization of the Effect of Aperture Design on the Time-Domain Response of Impulse-Radiating Antennas with Application to Arrays

*C. J. Buchenauer, J. S. Tyo, and J. S. H. Schoenberg,
USAF Phillips Laboratory / WSQW, Kirtland AFB, NM 87117

Impulse-radiating antennas (IRA's) are a class of ultra-wideband nondispersive focused-aperture antennas that offer unique advantages for time-domain applications. These antennas employ focusing optics to transform the inhomogeneous spherical wavefront of the TEM mode of a conically-symmetric transmission-line feed structure into a plane wave. IRA's have been studied extensively as transmitting antennas and as E-field replicating sensors. (C. E. Baum, Sensor and Simulation Note #321, Nov. 89, Phillips Laboratory, Albuquerque, NM) When driven by a step-function signal, these antennas radiate an approximately impulsive field on boresight. Used as receiving antennas, they can generate signals that closely replicate the incident E-field for a finite time. (C. J. Buchenauer and J. R. Marek, in *Ultra-Wideband Short Pulse Electromagnetics 2*, L. Carin and L. B. Felsen Editors, pp. 197-208, Plenum Press, 1995) The early-time performance of an IRA is determined by the field distribution of the TEM mode across the focused aperture. The late-time response may be determined from the asymptotic current distribution on the antenna. The prompt response can be tailored by a suitable choice of focused aperture. For example, when operating as a field replicating sensor, the prompt response of a lens IRA can be made to overshoot or undershoot the asymptotic late-time response. (C. J. Buchenauer, J. S. Tyo, and J. S. H. Schoenberg, to appear in *Ultra-Wideband Short-Pulse Electromagnetics 3*, Plenum Press, in publication) The intermediate-time response (the transition between early- and late-time responses) has not been treated theoretically. In this investigation, we measure the transmission and receiving response of IRA's with differently constructed apertures over extended time scales.

To achieve optimal early-time performance from an impulse radiating antenna, we develop a concept of aperture efficiency that predicts lower-impedance planar TEM horns to produce the highest prompt radiated fields for a given input power and aperture area. Thus, for highest prompt efficiency, a low-impedance lens IRA is preferable to a high-impedance reflector IRA. The considerable weight of a lens for a large aperture system may be greatly reduced or eliminated by constructing an array of many smaller elements. The total weight of N smaller lenses scales inversely with the square root of N for fixed horn geometry and fixed total aperture area. If the time dispersion within a single horn element becomes smaller than the risetime of the signal, the lenses may be eliminated altogether without loss of performance.

Antenna arrays are seen to offer several advantages: array elements with high aperture efficiencies may be used while minimizing the weight of optical elements; limited electronic beam steering may be achieved through source timing; and lower voltage sources may be used to drive the individual elements. Measurements are planned to investigate the mutual-interaction effects on the performance of TEM horns in dense arrays.

B103.3

Transient Characteristics of Antennas for Wireless Communications Systems

Kathleen L. Virga*
Department of Electrical & Computer Engineering, University of Arizona
Tucson, AZ 85721

Yahya Rahmat-Samii
Department of Electrical Engineering
University of California, Los Angeles
Los Angeles, CA 90095

In recent years there has been quite a bit of research directed at the characterization of the frequency behavior of antennas for wireless communications systems. As new applications, such as those involving digital and/or broadband communications, evolve it will become increasingly important to understand transient antenna performance in the communications system environment. This paper investigates the short-pulse time-domain characteristics of several types of antennas commonly used in wireless communications applications. The types of antennas to be investigated range from circular helices to Planar Inverted F Antennas (PIFAs) to spiral antenna configurations.

Algorithms based upon the Finite-Difference Time-Domain (FDTD) and Method of Moments (MoM) approaches are used to analyze the antenna performance with short-pulse excitation. FDTD and MoM each have specific advantages and disadvantages, thus both approaches allow for the analysis of diverse types of antennas. The FDTD method predicts radiator performance under short-pulse excitation in a single simulation. The use of a three-dimensional Cartesian FDTD grid results in a stairstep approximation for geometries with curved or flared boundaries and thus limits the complexity of the antenna structures that can accurately be modeled with this method. The surface patch MoM model incorporates a variable mesh structure that allows detailed features to be modeled with a locally dense mesh. Curved and flared boundaries can easily be modeled by a linear approximation of the boundary. The time-domain response of the MoM simulation is computed by using an inverse Fourier transform of frequency domain data taken at many points over a large frequency band.

This paper quantifies the transient behavior of antennas used in wireless communications systems. It includes a comparison of the transient response computed using both FDTD and MoM. The output parameters of interest include the source current at the antenna feed and the far-field radiation characteristics given short-pulse excitation. These parameters can be used to identify the effects, such as undesirable antenna resonances, due to EMI from unshielded circuits within a wireless package or between basestation and remote terminal units. This insight can be used to identify preferred antenna configurations, set the criteria for the front-end filtering performance, or define package shielding requirements in the wireless system.

Study of the Pulse Antenna with Resistance and Capacitance Loading

Jun-Hong Wang
Institute of the Light Wave Technology,
Northern Jiaotong University, Beijing, P.R.China

As we know that pulse antenna is an important part of the nonsinusoidal wave exploring system, higher radiation efficiency of the pulse antenna and less ringing of the radiation waveform will lead higher sensibility of the system. Unfortunately, the radiation efficiency and the waveform ringing are always contradiction, for we usually load the pulse antenna with resistance to get less ringing pulse waveforms, thereby the radiation efficiency reduces. But if the pulse antenna is loaded with capacitance or simultaneously loaded with resistance and capacitance, maybe a higher efficient pulse antenna with good radiation waveforms can be obtained, the work of this paper is in this respect.

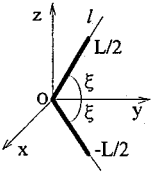

Fig.1 antenna structure

The structure of the antenna is shown in fig.1, it is loaded with distributed capacitance and resistance, and is excited by gaussian pulse. When analyzing, the time dependent distributing voltage along the antenna surface, caused by the distributed capacitance, is considered into the time domain equation derived from the boundary condition, by solving this equation in time domain directly, the radiating characteristic of the pulse antenna loaded with the capacitance can be obtained. Fig.2 gives the radiating waveforms of the straight wire dipole with capacitance loading only, the results without any loading are also given. By comparison, we found that the capacitance loading antenna can restrain the ringing of the radiating waveforms. Fig.3 gives the radiating waveforms of the V-dipole antenna with capacitance loading only, also the results without any loading are given. Besides the similar conclusion as obtained from the straight wire antenna, one can see that a higher peak pulse can also be obtained by the V-dipole antenna. Fig.4 gives the radiating waveforms of the V-dipole antenna loaded with resistance and capacitance simultaneously, we can see from it that the radiation waveforms are better, but the antenna efficiency decreases little.

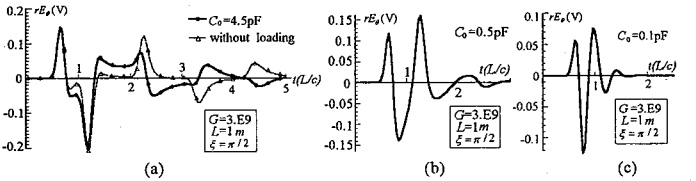

Fig. 2 Computation results of the straight wire dipole antenna with capacitance loading only

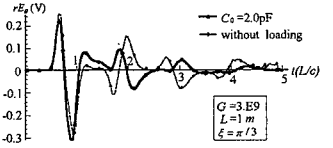

Fig.3 Computation results of the V-dipole antenna with capacitance loading only

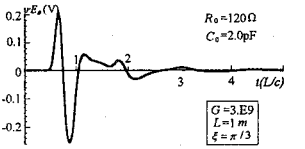

Fig.4 Computation results of the V-dipole antenna with resistance and capacitance loading

B103.5

SHORT VIDEO PULSE RADIATION BY A SLOT METAL-DIELECTRIC ANTENNA

N. N. Kolchigin[*], *and S. N. Pivnenko*

Chair of Theoretical Radiophysics, Kharkov State University,
Svobody Sq. 4, Kharkov 310077, Ukraine

This report presents the results of experiments involving a linearly tapered slot metal-dielectric antenna (LTSA) excited by short video pulses of duration less than 1ns. The aim of experiments was to investigate how the pulse shape depends upon the type of a load and parameters of a transmission line employed, and to determine optimal pulse excitation and propagation conditions.

In the experiments, the excitation was provided by a short pulse generator connected to a slot input of the antenna via a coaxial line. We used a pulse generator based on an avalanche transistor. The generated pulses ($\tau \sim 1ns$) were additionally sharpened with the help of two step-recovery diodes. The pulses obtained had a front and drop duration of about 250 ps. An orthogonal transition from a coaxial line to a slot line was utilized for the excitation of the latter. The matching of the coax-to-slot transition for short pulses with frequency spectrum ranging from 0.2 GHz to 2 GHz was provided by choosing appropriately the slot width and substrate thickness. The ratio of peak magnitudes of pulses launched to and reflected from the transition was 20 to 1, and the difference between their shapes was almost negligible. The coincidence of the reflected pulses in shape and amplitude was achieved by the replacement of the antenna with an appropriate load depending upon the tapering angle of the antenna. Thus we were in a position to determine the load which was equivalent to the LTSA in the radiation regime.

Time characteristics of the reflected pulse have been measured for the following cases: (1) – the slot line is opened at the end, (2) – the slot line is short-circuited by a shunt of various width, and (3) – the slot line is loaded by a resistive load. It has been experimentally shown that the pulse reflection from the LTSA can be essentially reduced with the help of a smooth diminution of substrate thickness nearby antenna aperture. Space-time characteristics of the radiated pulse have been obtained in the E- and H-planes at various distances from the antenna. From the analysis of these characteristics it follows that there exists an opportunity to provide minimum distortion of the radiated pulse and achieve maximum concentration of energy ($\sim 60\%$) in a section of space of angular width 90^o along an axis of principal radiation by properly selecting the antenna parameters. This substantiates our initial guess about applicability of the LTSA for radiating short pulses.

URSI B **Session 112** Salon Marquette

Method of Moments
Co-chairs: D. Wilton, USA and R. Graglia, Italy

08:10 112.1 Space Domain Method of Moments Solution for a Thin Strip on a Finite Dielectric Slab, **I. TEKIN**, E.H. NEWMAN, *Ohio State University, Columbus, OH, USA*

08:30 112.2 Capacitance of Finite Width Metalized Surface on a Truncated Dielectric Substrate above an Infinite Ground Plane, T.-L. LIN, **D.L. SENGUPTA**, C.-J. LIN, *University of Detroit Mercy, Detroit, MI, USA*

08:50 112.3 Scattering of Waves by a Homogeneous Dielectric Sphere Using the Method of Moments with Solenoidal Basis Functions, S. ANTENOR, **L. MENDES**, *Universidade Estadual de Campinas, Brazil*

09:10 112.4 Particular Applications of an Advanced Spectral Domain Approach, **T. VAUPEL**, V. HANSEN, *Bergische Universität/Gesamthochschule Wuppertal, Germany*

09:30 112.5 Computation of Potentials for Higher-Order Bases on Curvilinear Elements, **R.D. GRAGLIA**[1], D.R. WILTON[2], [1]*Politecnico di Torino, Italy;* [2]*University of Houston, TX, USA*

09:50 112.6 Higher-Order Modeling of Surface Integral Equations, **W.J. BROWN**, D.R. WILTON, *University of Houston, TX, USA*

10:10 112.7 The Multiple Sweep Method of Moments (MSMM) Analysis of Wideband Antennas, **D. ÇOLAK**, E.H. NEWMAN, *Ohio State University, Columbus, OH, USA*

10:30 112.8 RCS and Antenna Modeling Using Hybrid Meshes Incorporated into CARLOS-3D, J.M. PUTNAM[1], **J.D. KOTULSKI**[2], [1]*McDonnell Douglas Corporation, St. Louis, MO and* [2]*Sandia National Laboratories, Albuquerque, NM, USA*

10:50 112.9 A Study of Wire-to-Surface Junctions: Numerical Modelisation and Input Impedance Measurements, **H. JEULAND**, B. UGUEN, G. CHASSAY, *LCST, Rennes, France*

11:10 112.10 Heating of a Material Sample in an Electromagnetic Cavity, **J. ZHANG**, K.M. CHEN, *Michigan State University, East Lansing, MI, USA*

11:30 112.11 Closed-Form Green's Functions for Cylindrically Stratified Media, Ç. TOKGÖZ, **G. DURAL**, *Middle East Technical University, Ankara, Turkey*

11:50 112.12 To Calculation of the Two-Dimensional Integrals with Weak Singularity in the Scattering Theory, **Z.T. NAZARCHUK**, O.I. OVSYANNIKOV, *Karpenko Physico-Mechanical Institute, NAS, Lviv, Ukraine*

B112.1

Space Domain Method of Moments Solution for a Thin Strip on a Finite Dielectric Slab

I. Tekin* and E.H. Newman
The Ohio State University ElectroScience Laboratory
1320 Kinnear Road, Columbus, Ohio 43212

This paper presents a space domain method of moments (MM) solution to the problem of a strip dipole printed on a dielectric slab of finite length and width. The goal is to permit standard space domain MM codes (such as the authors *Electromagnetic Surface Patch Code*) which can treat dielectric volumes and metallic strips, to be able to treat metallic strips on the surface of a dielectric volume, i.e., a printed circuit antenna. The conventional method for analyzing printed circuit antennas is via a spectral domain MM solution in which the Green's function for the dielectric slab is expressed in terms of Sommerfeld integrals. The limitation of the spectral domain formulation is that it is directly applicable only to infinite slabs, and it would be extremely difficult to combine it with a space domain MM code.

In order to analyze a thin strip on the surface of a dielectric slab we have developed a special junction expansion function which is placed directly under the strip in the dielectric slab. The purpose of this junction expansion function is to model the extremely large electric fields which exist in the dielectric in the vicinity of the strip/dielectric interface, and which can not be modeled by standard dielectric expansion functions. The shape of the junction mode is obtained from the 2D problem of a strip in free space. Numerical results will be shown for a strip dipole on the surface of a finite sized dielectric slab.

Capacitance of Finite Width Metalized Surface on a Truncated Dielectric Substrate above an Infinite Ground Plane

by
Tsung-Lung Lin, Dipak L. Sengupta and Chun-Ju Lin

Department of Electrical Engineering
University of Detroit Mercy
Detroit, MI 48219 U.S.A.

ABSTRACT

Capacitance values of finite-width metalized surface on a truncated dielectric substrate above an infinite ground plane have been obtained by numerical means. Typical geometry considered consist of a metalized square section of dimension 2a×2a on a dielectric substrate of dimension 2L×2L and of the thickness h placed above an infinite ground plane, as shown in Fig. 1. For a given potential of the plate, integral equations have been developed for the charge (free and/or bound) densities at the dielectric-air and dielectric-conductor boundaries. Method of moments has been applied to solve the above equations to determine the unknown charge densities. The capacitance of the plate is then obtained from the knowledge of the free charge on the plate and its potential. Details of the numerical calculation will be discussed in the full paper.

For a given thickness of the substrate capacitances have been calculated for various values of a and L. Parametric studies of the capacitance indicate that for a given dimension of the metalized surface the substrate may be considered to be of infinite extent for $2L/2a \geq 3.6$; this limiting value does not depend appreciably on the thickness and dielectric constant of the substrate. This observation is of some theoretical as well practical interest.

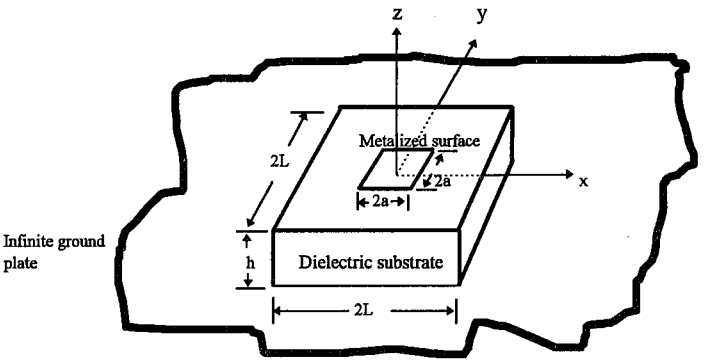

Fig . 1 Geometry of finite-width metalized surface on a truncated dielectric substrate above an infinite ground plane.

B112.3

SCATTERING OF WAVES BY A HOMOGENEOUS DIELECTRIC SPHERE USING THE METHOD OF MOMENTS WITH SOLENOIDAL BASIS FUNCTIONS

Sérgio Antenor
and
Leonardo Mendes*

The use of the Method of Moments with volume basis functions to analyze the scattering of EM waves has always suffered from convergence problems. It has been shown that the source of the numerical problems in the volume approach is the spurious charges generated by the basis functions in the interior of the object. In this work one uses a 3D solenoidal volume basis function with the Method of Moments to solve the problem of scattering of waves by dielectric objects. The function, besides eliminating the spurious charges, is based on a tetrahedra that permits a better fitting of the object to be discretized. The approach is applied to the scattering of a plane wave by a dielectric sphere. Bellow one shows some of the results obtained.

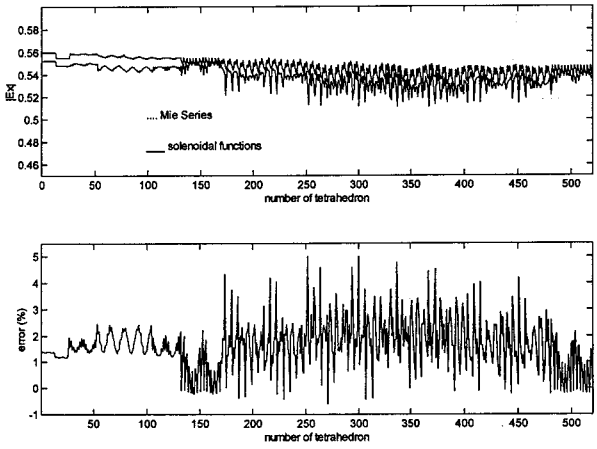

Figure1 - Fields inside a lossless homogeneous dielectric sphere; $\varepsilon_r = 4.0, \kappa_0 = 0.408$

Particular Applications of an Advanced Spectral Domain Approach

Thomas Vaupel* and Volkert Hansen,
Lehrstuhl für Theoretische Elektrotechnik,
Bergische Universität/Gesamthochschule Wuppertal, D-42097 Wuppertal — Germany

At present a large number of commercial software tools based on integral equation formulations are available. These software packets are well suited for standard problems like microstrip circuits in common multilayer environments. Nevertheless they often fail if they are applied to particular applications. Therefore the development of additional software tools with enhanced abilities is required.

Integral equation based software tools, which solve for the current distribution with the Method of Moments, can be divided into space domain and spectral domain approaches. Most commercial software packets are based on space domain techniques which have provided a good computational efficiency in recent time. The advantage of spectral domain approaches lies in the analytically available Green's function guaranteeing numerical convergence for all kinds of layer arrangements even in the case of strongly different layer thicknesses. Accordingly we have developped an enhanced spectral domain field solver. In order to achieve a high computational efficiency we use various numerical and analytical acceleration strategies like special treatment of surface wave poles, a generalized asymptotic Green's function subtraction technique, a special database approach and redundance reduction algorithms [T. Vaupel, V. Hansen, Efficient Spectral Domain Analysis of Planar Circuits Using Higher Order Expansion Functions Combined With Fast System Matrix Computation Methods IEEE AFRICON '96 Symp. Digest, Stellenbosch, South Africa] as well as adapted Clenshaw Curtis integration schemes. For an improved modeling flexibility we use several kinds of expansion functions on nonuniform meshes as well as different excitation mechanisms with improved source modelings.

With this spectral domain field solver we can investigate many special structures and field problems. As applications we will present two very different examples, the first is a ringslot antenna with a coplanar feeding line and additional printed bridges in the slot circumference for embedding into a mixer structure in the submm-region (f=650 GHz), using the magnetic field integral equation. Furthermore the computation of coplanar structures with finite ground is possible, also the consideration of 3-D elements like airbridges. The computation of coupled line sections embedded in a very thin quartz layer will be presented as a further application. Fig.1 shows a computed coupler structure and the layer arrangement consisting of the quartz layer with thickness $2.6\mu m$ mounted on a silicon substrate with thickness $0.5mm$ and reflector. Due to the very thin quartz layer the reaction integrals converge very slowly despite the utilized asymptotic Green's function subtraction technique. Nevertheless we get stable results with an appropriate extended integration range. Such structures play an important role in the development of amplifiers used for fast digital data transmission on optical fiber links. Further examples and details of analytical and numerical schemes will be given in the oral presentation.

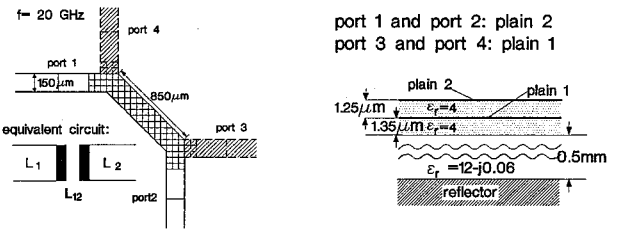

Fig. 1: Line sections embedded in a very thin dielectric layer

B112.5

Computation of Potentials for Higher-Order Bases on Curvilinear Elements.

Roberto D. Graglia, Politecnico di Torino, Torino, Italy*
Donald R. Wilton, University of Houston, Houston, TX, USA

Fully interpolatory higher-order divergence-conforming vector basis functions on surface patches of triangular and quadrilateral shape were recently defined in [1]. These basis functions become very effective in the numerical solution of the electric or the magnetic field integral equation provided one is able to compute with a good accuracy the moment integrals. The kernel of the moment integrals is the free space Green's function $\exp(-jkR)/R$, and these integrals are quite difficult to compute when the integration patch contains or is close to the observation point.

A feature of the bases derived in [1], is that they contain a factor $1/\mathcal{J}$, where $\mathcal{J}$ is the Jacobian of the curved patch, which cancels with a similar factor in the differential surface area, allowing evaluation of the moment integrals in parent coordinates (ξ_1, ξ_2). Furthermore, in parent coordinates, the bases are a product of a polynomial P of degree p times a low order vector function, a feature which facilitates determining a Taylor's series expansion of each basis function near the observation point for arbitrarily high polynomial order p.

We present two integration schemes, both based on integration in the plane tangent to the surface of the patch at the observation point, or its projection onto the patch surface. The first scheme considers the case of observation points located on the patch surface. The second is used to deal with observation points not lying on the integration surface. In the first case we define a new quadrature function $q_m(n, \alpha)$ used to analytically integrate in one direction $[Q\, R^m \exp(-jkR)]$, for $m \geq -1$, where Q is a monomial of n-th degree (for a plane patch it suffices to consider $m = -1$); the moment integrals are then reduced to one-dimensional integrals along the patch contour. The functions $q_m(n, \alpha)$ satisfy recursive formulas which permit their evaluation from knowledge of $q_{-1}(0, \alpha)$.

The second integration scheme is based on a systematic (recursive) procedure able to express the integrand as the divergence of a finite vector sum, so that surface integration is easily reduced to an integration along the patch contour. In the presentation we point out and discuss some difficulties encountered in considering curved patches.

[1] R. D. Graglia, D. R. Wilton, and A. F. Peterson, "Higher-order interpolatory vector bases for computational electromagnetics," *IEEE Trans. Antennas Propagat.*, vol. 45, no. 3, 1997.

Higher Order Modeling of Surface Integral Equations

William J. Brown* and Donald R. Wilton
Department of Electrical and Computer Engineering
University of Houston
Houston, TX USA 77204-4793

In this study, higher order modeling of both geometry and equivalent surface currents is employed in the problem of electromagnetic scattering by arbitrarily shaped objects. Higher order modeling is desirable because of the potential savings in computation time for a given level of accuracy. The electric field integral equation is formulated in the frequency domain using the vector and scalar potential descriptions. A formulation using higher order bases on curvilinear elements is introduced. The bases are constructed as products of zero-order basis functions (the usual triangular patch basis functions) and a complete polynomial of order p. The basis functions are of Nédélec type and are divergence-conforming (only normal continuity across element boundaries is enforced). They are also complete in their divergence to the same order as the basis functions themselves. The Lagrange polynomials are employed to give the bases interpolating properties. Results are presented for the first-order case, for which it is found that fewer unknowns are generally needed to obtain a given level of accuracy compared to the zero-order case.

Higher order bases generally perform poorly near edges; hence, basis functions which incorporate charge singularities are derived and tested. These basis functions provide a more accurate description of the current in the neighborhood of sharp edges than basis functions that do not account for charge singularities. The new singular basis functions are still divergence-conforming and their divergence has the correct behavior near an edge. They can also be used on planar as well as curvilinear surfaces. Results are presented comparing the performance of singular and nonsingular bases for the case of scattering by a square plate and a sphere with a circular aperture. The nonsingular basis functions exhibit a nonphysical dip near the edges which does not appear with the singular basis functions. Solutions obtained using singular bases also agree better with the quasi-exact solution than solutions using nonsingular bases with little increase in computation time.

B112.7

The Multiple Sweep Method of Moments (MSMM) Analysis of Wideband Antennas

D. Çolak* and E.H. Newman
The Ohio State University ElectroScience Laboratory
1320 Kinnear Road, Columbus, Ohio 43212

This paper presents the Multiple Sweep Method of Moments (MSMM) analysis of electrically large wideband antennas. The MSMM is an $\mathcal{O}(N^2)$ recursive method for solving the large matrix equations which arise in the method of moments (MM) analysis of electrically large bodies. In the MSMM a large body of size L is split into P smaller sections of size $D_p = L/P$, and with $N_p = N/P$ unknowns per section. The currents on the P sections are found in a recursive manner until they hopefully converge to the value which would have been obtained by a direct solution of the MM matrix equation. In the MSMM the first sweep across the body corresponds to the dominant or first order reflection and diffraction mechanisms, while subsequent sweeps correspond to higher order mechanisms. The result is a method which typically converges to engineering accuracy in a few sweeps, and actually converges faster as the electrical size of the body increases.

In the design of electrically large wideband antennas one generally wants a structure which permits the current to flow from the generator onto the antenna surfaces with as little reflection as is possible. As compared to the standard MM which employs a direct solution of the matrix equation, the MSMM has two features which make it useful in the *design* of electrically large wideband antennas. First the MSMM is an $\mathcal{O}(N^2)$ method ($\mathcal{O}(N^{3/2})$ if combined with the Fast Multipole Method), as compared to $\mathcal{O}(N^3)$ for the standard MM. More importantly, although the MSMM is a frequency domain method, it has a time domain interpretation which allows it to locate and assess the strengths of points of current reflection on the antenna. When a point of reflection has been found, one can change the local geometry and recompute the current in only $\mathcal{O}(N^2/P)$ CPU time. Results will be shown for the 3D problems of a long dipole antenna with a reactive load in the center of each arm and a TEM horn antenna with a bend.

RCS and Antenna Modeling Using Hybrid Meshes Incorporated into CARLOS-3D

J.M. Putnam
McDonnell Douglas Corporation
PO Box 516
MC 064-2263
St. Louis, MO 63166-0516

J.D. Kotulski *
Sandia National Laboratories
Radiation and Electromagnetic Analysis Department
MS 1166
PO Box 5800
Albuquerque, NM 87185-1166

During the last decade, the method of moments(MOM) has become a robust technique for solving electromagnetic problems for arbitrary three-dimensional geometries. There are several reasons why the MOM technique has become so widely used. First, modeling fully three-dimensional geometries has been facilitated by the development of robust basis functions, such as the roof-top functions introduced by Rao-Wilton-Glisson (RWG) for triangular meshes. Secondly, complex boundary conditions can be readily incorporated into the formulation. These boundary conditions, for example, can include conducting, dielectric, resistive, magnetically conducting, and the impedance boundary condition. Finally, the advent of modern fast parallel and vector computer architectures has permitted the solutions of larger and more complex problems.

CARLOS-3D is a three-dimensional scattering code based on the Galerkin method of moments formulation that models arbitrary geometries composed of multiple conducting and homogeneous dielectric regions. The code is cast in operator notation which allows the use of different representations for the basis functions to be incorporated in a straightforward manner. The code was originally structured to run on either a workstation or Intel Paragon. By incorporating the parallel message passing protocol MPI (Message Passing Interface) it can now be run on a workstation, workstation cluster, or a massively parallel machine that supports MPI.

In this presentation, we will investigate the use of hybrid meshes for modeling RCS and antenna problems in three dimensions. We will consider two classes of hybrid basis functions. These include combinations of quadrilateral and triangular meshes for arbitrary 3D geometries, and combinations of axisymmetric body-of-revolution (BOR) basis functions and triangular facets. In particular, we will focus on the problem of enforcing current continuity between two surfaces which are represented by different types of surface discretizations and unknown basis function representations. We will illustrate the use of an operator-based code architecture for the implementation of these formulations, and how it facilitates the incorporation of the various types of boundary conditions in the code. Both serial and parallel code implementation issues for the formulations will be discussed.

Results will be presented for both scattering and antenna problems. The emphasis will be on accuracy, and robustness of the techniques. Comparisons of accuracy between triangularly meshed and quadrilateral meshed geometries will be shown. The use of hybrid meshes for modeling BORs with attached appendages will also be presented.

B112.9

A study of Wire-to-Surface Junctions : Numerical Modelisation and Input Impedance Measurements.

H. JEULAND, B. UGUEN, G. CHASSAY
LCST, 20 avenue des buttes de Coesmes, 35043 Rennes cedex, France
Phone: +33-2 99 28 65 07, Fax: +33-2 99 38 62 48
e-mail: herve.jeuland@insa-rennes.fr

The accurate prediction of antenna features mounted on complex structures is a critical task owing to the geometry of the surrounding structure (corner on satellite structure, edge on aircraft...). Our purpose deals with the incorporation of a numerical model to treat arbitrary systems of body with connected wire(s) into a general-purpose computer code. The problem is solved for the whole perfectly conducting structure (wire+body) by the Method of Moment [1]. Our choice to check the code ability consists in comparing computed results to experimental data. The input impedance of the antenna is the pertinent parameter. Its behavior follows the variations of surface current densities more closely than far-field characteristics.

Starting from the theoretical analysis of solutions which are presented in previous papers, our study underlines the principal steps of an accurate modelisation as for example the main principles for the junction basis function (current dependency in the junction region...) and the analytical treatment of integrals having singular kernel. The solution [2] adopted in our numerical procedure has been chosen for its ability (i) to describe arbitrary shaped configurations of wire-to-surface junctions and (ii) to approach the current variations in the vicinity of the attachment point. It is based on Rao's surface patch modeling technique. Vector and scalar potential calculations require the evaluation of integrals whose kernel becomes singular as the source point gets closer to the observation point or to the junction vertex. Various analytical solutions are compared and a rigorous treatment is performed for accurate modelisations.

Input impedance are measured using a computer-controlled network analyser. Our measurement technique includes a new additional step in the usual calibration process in order to exactly define a measurement plane. Comparisons between plots of computed and measured data versus frequency are made for canonical configurations of junctions on smooth surface or near geometrical discontinuities. These configurations include wire mounted at the center, the corner or on the edge of a plate, near trihedral or dihedral corner or directly attached on a cube vertex. The agreement between measured and numerical results illustrates the versatility of the integrated model.

[1] RAO S.M., "Electromagnetic scattering and radiation of arbitrarily shaped surfaces by triangular patch modeling", Ph. D. Thesis, Univ. of Mississipi, 1980.
[2] HWU S.U., WILTON D.R., "Electromagnetic scattering and radiation by arbitrary configurations of conducting bodies and wires", Naval Ocean Systems Center, Technical doc. 1325, August 1988.

Heating of a Material Sample in an Electromagnetic Cavity

Jianping Zhang * and K.M. Chen
Department of Electrical Engineering
Michigan State University
East Lansing, MI 48824
Tel: (517) 355-6502, Fax: (517) 353-1980

In the study of the interaction of microwave radiation with non-ionic materials, a material sample is placed in a cylindrical EM cavity which is excited with a fundamental cavity mode. We aim to quantify the electric field inside the material sample induced by the cavity mode, and then determine the temperature rising behavior inside material molecules.

The first task is to find appropriate dyadic Green' s function for the cavity. Due to the presence of a material sample inside the cavity, the divergence of the electric field does not vanish, the induced electric field inside the material sample has an irrotational component. Thus, it can not be expanded into simple cavity modes which are purely solenoidal. We have derived an electric dyadic Green' s function in terms of vector wave functions, $\vec{M}, \vec{N}$ and $\vec{L}$ functions. We also derived an electric dyadic Green' s function based on the magnetic field using a magnetic dyadic Green' s function. After appropriate dyadic Green' s functions are obtained, the electric field integral equations (EFIEs) for the induced electric field inside the material sample are derived. These EFIEs are then numerically solved by discretizing the sample into a large number of volume elements.

After the induced electric field inside the material sample is accurately quantified, the dissipated power density inside the material sample is calculated. This dissipated power density acts as the heating source to raise the temperature of the material sample. The behavior of temperature rising as a function of time is determined by solving a heat diffusion equation.

The temperature rise inside the material sample and the EM field of the cavity with the presence of a material sample will be probed experimentally and compared with theoretically predicted values.

B112.11

CLOSED-FORM GREEN'S FUNCTIONS FOR CYLINDRICALLY STRATIFIED MEDIA

Çağatay Tokgöz and Gülbin Dural*
Middle East Technical University
Department of Electrical and Electronics Engineering
06531 Ankara Turkey

The closed-form Green's functions of the electric and magnetic fields in the spatial domain are presented for the sources of electric and magnetic dipoles embedded in a general, cylindrically stratified medium. In an arbitrary observation point, the spectral domain expressions for electric and magnetic fields of coupled TE and TM modes are obtained through the electric and magnetic fields of the source layer by using a recursive algorithm. Then closed-form Green's functions are obtained with a two level approximation of spectral domain representations. The approximation procedure can be outlined as follows:

1. First, spectral domain Green's function is approximated in terms of complex exponentials, $\sum_i a_i e^{-k_\rho b_i}$, for large values of k_ρ, using the Generalized Pencil of Functions (GPOF) Method, then it is represented with Hankel functions with the use of asymptotic properties of Hankel functions. Closed-form expression for large k_ρ values is obtained using the following identity:

$$\frac{e^{-jk|\vec{r}-\vec{r}'|}}{|\vec{r}-\vec{r}'|} = \frac{-j}{2}\int_{-\infty}^{\infty} dk_z e^{-jk_z(z-z')} H_o^{(2)}(k_\rho|\bar{\rho}-\bar{\rho}'|)$$

2. The spectral domain Green's function approximated for large k_ρ values is subtracted from the original Green's function: the remaining function will decay rapidly outside a small range and can be approximated by complex exponentials of k_z, $\sum_i c_i e^{-k_z d_i}$, making analytical evaluation of the spatial domain Green's functions possible.

The computational efficiency in the calculation of spatial domain Green's functions is increased with the use of closed-form approximations.

To Calculation of the Two-Dimensional Integrals with Weak Singularity in the Scattering Theory

Nazarchuk Z.T., Ovsyannikov O.I.
Karpenko Physico-Mechanical Institute of the National Academy of Sciences of Ukraine,
5 Naukova St. Lviv, 290601 Ukraine, tel.: (380 322) 637038, e-mail: nazarch@ah.ipm.lviv.ua

The aim of this report is to present a method of calculation of the two-dimensional integrals with weak singularity. We suppose this approach can be applied to obtain numerical scheme of solutions of three-dimensional scattering problems.

Let us consider an integral in the following form

$$E(T)=\int_S \frac{f^*(t)\exp[i\chi r(T,t)]}{r(T,t)}dS,\ T\in S, \qquad (1)$$

where $f^*(t)$ is density; t, T are points on the surface S, dS is the element of surface at the point t, χ is wave number of the medium; $r(t,T)=|t-T|$.

Let us assume the forms of the surface S are a rectangle or a circle. To evaluate the integral (1) we propose to present surface S by parameters ξ,ψ=[-1;1]. We present the density f by two-dimensional Lagrange interpolation polynomial at the nodes which are zeros of Chebyshev polynomials of the first kind

$$f(\xi,\psi)\approx\frac{\pi^2}{n_1 n_2}\sum_{l=1}^{n_1}\sum_{k=1}^{n_2}S_l^{n_1}(\xi)S_k^{n_2}(\psi)f(\xi_l,\psi_k);\ \xi,\psi=[-1;1],$$

$$S_k^n(\tau)=\frac{1}{\pi}\left(\frac{\cos((n-1)\varphi_k)\cos(n\arccos(\tau))}{\tau-\cos(\varphi_k)}\right),\ \varphi_k=\frac{(2k-1)}{2n}\pi.$$

Now it is easy to obtain numerical analog of the integral (1) and to calculate this integral. In the case when we have integral equations and density f is unknown it is allow us to obtain finite linear algebraic equations.

B119.1

Object-Oriented Programming(OOP) and Data Base(OODB) for Radar Target Identification: Part I: Development of OO Data Base

Asoke K. Bhattacharyya
E-Mail: BHATTACH@LINCOLNU.EDU
Computer Science and Technology
Lincoln University
Jefferson City, MO 65109

***Abstract*:** All target identification and classification schemes use some kind of a radar signature data base. The most widely used type is the conventional relational data base. Recently, Object Oriented Programming(OOP)[J.P. Cohoon and J.W. davidson-'C++ Program Design', Irwin, 1997] and Object Oriented Data Bases (OODB)[A. Stevens-'C++ database Development',MIS Press, New York, N.Y.,1994] are being increasingly used in many applications such as, payroll processing, personnel Dbs et cetera. To the best of the knowledge of the author OOP and OODB have not been used in radar target identification studies. In these two presentations, the author describes the development of an OODB for radar signatures and the use o the DB for target identification. Unlike traditional conventional DBs, A 'persistent object' is used in OOP and OODB. An object is a declared instance of data type including standard C++ data types as well objects of classes. An object is said to be persistent when it has an ability to succeed its creator and to subsequently exist in a space other than the space in which it was created. Some of the advantages of an OO development are (1) Encapsulation (2) Inheritance and (3) Polymorphism.The basic ten steps of OODB design are:(1) Identifying the basis for the data base requirements (2) Defining the DB's functional and performance requirements (3) Idenfying the data terms (4) Separating the data members from the persistent classes (5) Building a data member dictionary (6) Gathering data members into persistent classes (7) Identifying the key data members of each class (8) Identifying the relationships between classes (9) Identifying the class methods, (10) Adding the inheritence and number functions to make the classes persistent. and finally (11) Repeatedly refining the ten steps above leading to an acceptable solution. The basic software 'Persistent Almost Relational Object Oriented DB Development'(called PARODY version 2) has been used and a application software RTI.EXE has been prepared for radar target identification to work with the hierarchy of PARODY2. The details of the different key features, such as, classes, constructor, destructor, changing, creating and deleting of the persistent objects will be described. Fig. 1 shows a rough sketch of what the target persistent object consists of. Details of the target DB development on a PC will be presented.

Object-Oriented Programming (OOP) and Data Base(OODB) For Radar Target Identification Part II: Radar Target Idenfication

Asoke K. Bhattacharyya
E-Mail: BHATTACH@LINCOLNU.EDU
Computer Science and Technology
Lincoln University
Jefferson City, MO 65109

Abstract: The second part of the presentation deals with the application of the OODB developed earlier to radar target identification and classification . The data base consists of the information about many targets particularly the complex resonant frequencies under various parametrs including environmental conditions, such as, soil parameters and the trial depth of the object. The input to the DB is a set of resonant frequencies for the test target obtained by processing the received signal in presence of a noise using a signal processing technique, such as matrix pencil method. The data base finds the closest match and decides on the most probable object. If it finds no correlation with the a priori known signatures, the target is considered to be unknown to the signature library in the DB. The 'abstraction' in the OODB provides some additional security since the object hides information. Results for typical case studies and the limitations of the DB will be presented. A comparison of the performances of the commonly used relational and the proposed OODB will be discussed. Further scope of work following the two presentations will also be described.

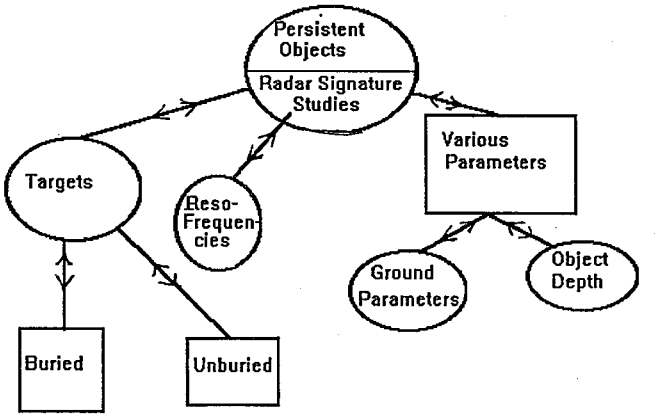

Fig. 1: Persistent Object Oriented Data Base

B119.3

Utilization of CAD Files Representing Realistic Aircraft Models for Electromagnetic Computations - Geometrical and Computational Issues

Professor Vladimir I. Oliker
Emory University, Atlanta, Georgia 30322
& Matis, Inc., Atlanta, Georgia 30329
e-mail: matis@netcom.com

Building a high-quality realistic aircraft model suitable for high-accuracy electromagnetic computations can be a very expensive task. On the other hand, the significant progress achieved in recent years in computational electromagnetics has led to development of algorithms capable of solving scattering problems over complete aircraft represented by realistic models not limited to unions of cones, cylinders, plates, etc. Clearly, the demand for high-quality realistic aircraft models will grow together with the demand for more accurate electromagnetic computations.

With rapid development of CAD/CAM and scanning technologies the issue of re-usability of available electronic aircraft models for electromagnetic computations has become of substantial practical significance. However, it is well known that CAD files developed for particular purposes (manufacturing, for example) may be completely useless if one attempts to use them for purposes not intended by the designer. Thus, the idea of utilizing existing models for multiple applications introduces the need to carry out a pre-processing step consisting of diagnostic evaluation of such models with subsequent modifications and/or repairs required to produce models suitable for performing required computations.

Here is a partial list of some typical irregularities that we observed in faceted CAD models: overlapping parts, branching facets, disconnected parts, missing facets, degenerate facets, incorrect facet orientation, inconsistencies in triangulation, bad aspect ratio in polygons, etc. Of course, models come in many different electronic formats and "translation" from one format to another may introduce new defficiencies.

The purpose of this talk is to describe our experience in dealing with the above described issues. We will also discuss software packages with capabilities to solve some of the tasks required in pre-processing CAD files representing aircraft models.

Electromagnetic Visualization Using Virtual Reality Tools

J. Nehrbass
ElectroScience Laboratory
Department of Electrical Engineering
The Ohio State University
1320 Kinnear Rd.
Columbus, Ohio 43212-1191
nehrbass@osc.edu

Abstract --- When calculating the electromagnetic fields scattered from three dimensional objects, very large data sets may be generated. It is often difficult to visualize this information without advanced visualization tools. When data from time varying simulations are examined, visualization problems are intensified by the addition of another dimension. As a result, information is often compromised by observing only selected cross-sectional snapshots of three dimensional time varying sets of data. In this talk, the capability of a few visualization tools are presented. Results from various electromagnetic research projects are presented by exploiting the technology of select visualization tools. These tools allow the user to change the desired observation viewpoint while the data is being observed as a function of time. Illustrative examples from the software packages FAST, AVS, and MATLAB are included among these examples. Additionally, the ImmersaDesk, a virtual reality tool, is introduced as a powerful electromagnetic visualization tool. The ImmersaDesk is a semi-immersive, stereoscopic projection based system which uses stereo glasses, head tracking, and hand tracking virtual reality input devices. By programming these input devices to respond to the users motions rather then the traditional keyboard input device, the user is more free to concentrate on observing the desired characteristics of the chosen model. Thus, this tool allows real time visualization of three dimensional penetrable objects in a modern dynamic environment. In an attempt to motivate and encourage the style of future presentations, only a LCD projection converter, a laptop computer, and a overheard projector are used in this presentation.

URSI B — Session 121 — Salon Bersimis

Analysis of Guided Wave Structures
Co-chairs: T. Tamir, USA and E. Kuester, USA

08:10	121.1	A Variational Calculation of Coplanar Waveguide Short-Circuit Parameters in the Quasistatic Regime, **E.F. KUESTER**, *University of Colorado at Boulder, CO, USA*
08:30	121.2	Computation of [C], [L], [G] and [R] Matrices of Multiconductor Lines with Polygonal Cross Sections, J. BERNAL, F. MEDINA, **M. HORNO**, *Universidad de Sevilla, Spain*
08:50	121.3	Quick and Accurate Analysis of CPW Structures Using Complex Images, J. BERNAL, F. MEDINA, **M. HORNO**, *Universidad de Sevilla, Spain*
09:10	121.4	A New Perturbation Approach for Computing the Line Parameters of Strip Transmission Lines with Nonzero Metallization Thickness, **E.F. KUESTER**, *University of Colorado at Boulder, CO, USA*
09:30	121.5	Pseudo-TEM Modes, **E.F. KUESTER**, *University of Colorado at Boulder, CO, USA*
09:50	121.6	Fast Transient Simulation of Eddy Current Problems Using Reduced-Order Models, S. JAN, **Z.J. CENDES**, *Ansoft Corporation, Pittsburgh, PA, USA*
10:10		Coffee Break
10:30	121.7	Analysis of a Microstrip Transmission Line Incorporating Ground Plane Perforations, A.W. MATHIS, **A.F. PETERSON**, *Georgia Institute of Technology, Atlanta, GA, USA*
10:50	121.8	Analog Hardware Description Language for Modeling Microstrip Circuits and Discontinuities, **H. GHALI**, *Ain Shams University, Cairo, Egypt*
11:10	121.9	Numerical Analysis of Traveling Waves in Slotted Waveguide of Arbitrary Cross Sections, **C.-Y. CHU**, S.-K. JENG, *National Taiwan University, Taipei, Taiwan, China*

B121.1

A VARIATIONAL CALCULATION OF COPLANAR WAVEGUIDE SHORT-CIRCUIT PARAMETERS IN THE QUASISTATIC REGIME

Edward F. Kuester
Electromagnetics Laboratory
Department of Electrical and Computer Engineering
Campus Box 425
University of Colorado at Boulder
Boulder, CO 80309
USA

Compared to more popular microwave transmission lines such as microstrip, coplanar waveguide (CPW) has found slower popular acceptance by microwave circuit designers in spite of the substantial practicaal advantages which it offers. Perhaps one of the most important reasons for this is the relative lack of accurate and efficient models for discontinuities in CPW, which at present can be obtained only through substantial numerical effort, and are inconvenient for computer-aided design (CAD) methods.

In this paper, we present a new approach to the simple but accurate calculation of the equivalent inductance of a CPW short circuit. Excess capacitance or excess inductance for a microstrip junction has often been determined by directly solving for and integrating "excess" (in comparison to what would be present on an infinitely extended uniform transmission line) charge or current densities on the strip conductor in order to avoid the numerical error associated with the subtraction of two nearly equal quantities. Here we will use a *variational* version of this formulation. The static inductance problem is formulated as an integral equation for the normal component of the magnetic field in the CPW slots as follows. A scalar magnetic potential is calculated from the unknown density in the slot using an appropriate Green's function. The potential, followed along a path encircling the central strip conductor of the CPW, increases by an amount I, the total current on that strip, when we return to the starting point of the path: this gives the desired integral equation for the slot field. The normal component of magnetic field at the slot is now expressed as the sum of a uniform CPW's field (assumed known) and a local (excess) portion concentrated near the short circuit. The excess inductance is now calculated from a variational expression obtained from the resulting modified integral equation.

This formulation allows trial distributions of modest complexity to give values of the excess inductance L of the CPW short circuit which have quite good accuracy. The results for the simplest trial functions are in closed form, and in no event is numerical effort greater than the evaluation of a finite, definite integral by numerical means required. The requisite computational requirements are in any case far less than those of traditional full field modeling. Results of this analysis are thus easily calculated on readily available general-purpose mathematical software, and are arrived at so fast as to be virtually instantaneous (an important consideration for CAD applications). A comparison of these results with others available in the literature will be made, showing good agreement with those of more time-consuming numerical approaches.

Computation of [C], [L], [G] and [R] matrices of multiconductor lines with polygonal cross sections

J. Bernal, F. Medina, M. Horno
Microwaves Group, Dpt. of Electronics and Electromagnetism
Avda. Reina Mercedes s/n, 41012 Sevilla, Spain
E-mail: medina@cica.es. Tel.: +34 5 455 2891, Fax: +34 5 423 9434

The computation of the per unit length characteristic matrices ([C], [L], [G] and [R]) of a multiconductor transmission system is a classical problem that has been attacked by using a variety of analytical and numerical methods. Purely numerical methods such as FD (H.E. Green, IEEE–MTT, vol. 13, pp. 676–692, Sept. 1965) or FE (Z. Pantic and R. Mittra, MOTL, vol. 9, pp. 244–249, Aug. 1995) are very general and suitable for complicated geometries. However they are too time consuming to be used in iterative optimization schemes (even if we take into account that subtle refinements have been introduced in those techniques to speed up computations). A satisfactory compromise between generality, accuracy and computational speed seems to be provided by methods based on the resolution of the integral equation for the free surface charge distribution on the conductors (F. Olyslager et al., IEEE–MTT, vol. 39, pp. 901–909, June 1991; K.S. Oh et al., IEEE–MTT, vol. 42, pp. 1443–1453, Aug. 1994; G. Plaza et al., IEEE–MTT, vol. 43, pp. 1623–1626, July 1995) or a coupled integral equation for the free surface charge and the polarization charge at the dielectric boundaries (C. Wei et al., IEEE–MTT, vol. 32, pp. 439–450, April 1984; J. Venkataraman et al., IEEE–MTT, vol. 33, pp. 952–959, Oct. 1985). The technique proposed in this communication corresponds to the former type.

In the present work we propose a method that combines the advantages of different formulations in order to built up a quick quasi–static computer solver for polygonal–shaped conductors embedded in a multilayered dielectric medium. The method is based on solving the space domain integral equation for the free charge distribution on the conducting slabs. The appropriate space domain Green's function (the kernel) is conveniently obtained from the spectral one by means of system identification techniques, by using the complex images concept (Y.L. Chow et al., IEEE–MTT, vol. 39, pp. 1120–1125, July 1991). Entire domain basis functions are then used in a Galerkin scheme with the aim of keeping small the size of the final Galerkin matrix. In addition, the computation of the elements of this matrix is carried out in a very efficient way by using suitable numerical quadratures and closed form integration. Putting together all these elements leads to an efficient and accurate computer code which is suitable for quick computations on a PC platform. The numerical efficiency of the method will be discussed in the presentation. The Wheeler's rule is finally used to compute [R] from [L] (G. Plaza et al., IEEE–MTT, vol. 43, pp. 1623–1626, July 1995).

B121.3

Quick and accurate analysis of CPW structures using complex images

J. Bernal, F. Medina, M. Horno
Microwaves Group, Dpt. of Electronics and Electromagnetism
Avda. Reina Mercedes s/n, 41012 Sevilla, Spain
E-mail: medina@cica.es. Tel.: +34 5 455 2891, Fax: +34 5 423 9434

The quasi-TEM model is often used to analyze single or multiconductor strip-like transmission lines due to its simplicity and accuracy at the lower end of the microwave frequency spectrum. In fact, very accurate tools, suitable for CAD purposes, have been developed even for relatively complicated geometries, including multiple strips in multilatered medium (G.E. Howard et al., IEEE-MTT, vol. 40, pp. 628-636, April 1992; E. Drake et al., IEEE-MTT, vol. 41, pp. 260-267, Feb. 1993; D. Homentcovschi et al., IEEE-MTT, vol. 43, pp. 363-372, Feb. 1995). This analysis could be also extended to coplanar waveguide structures (CPW) (in fact, the range of validity of a quasi-TEM analysis is usually larger for CPW geometries than for microstrip ones), but CPW's have received considerably less attention (E. Drake et al., IEEE-MTT, vol. 42, pp. 2328-2335, Dec. 1994; K.K.M. Cheng et al., IEEE-MTT, vol. 42, pp. 1958-1965, Oct. 1994).

The purpose of this contribution is to provide a quasi-analytical static solution for laterally open multiconductor CPW structures printed on layered media. Although the numerical effort is still larger than the one involved in conformal mapping approaches, the method is more general and accurate – we do not approximate the slot region with a magnetic wall –, and also quick enough from a practical point of view. Essentially we propose to adapt previously reported ideas (G.E. Howard et al., IEEE-MTT, vol. 40, pp. 628-636, April1992; E. Drake et al., IEEE-MTT, vol. 42, pp. 2328-2335, Dec. 1994) to our case problem. Thus, we partially adapt the elegant technique reported by Howard et al. for strip geometries to the CPW geometry. Although the physical meaning of the "complex images" introduced in that work is not straightforward, the mathematical procedure can still be used to transform the original spectral domain integral equation for the slot electric field into a space domain equation. Due to some distinct features of the CPW problem, some theoretical difficulties have to be removed before going on with this technique, as it will be discussed in the presentation of this communication. In addition we do not use the multipipe model proposed by Howard et al.. Instead we use the conventional Galerkin method. However, most of the, in principle, lenghty numerical integrations are carried out in closed form. Since the basis functions are the natural ones for our problem, the final result is a small size system of linear equations whose coefficients are evaluated in quasi closed form, giving place to a very efficient and accurate computer code.

A NEW PERTURBATION APPROACH FOR COMPUTING THE LINE PARAMETERS OF STRIP TRANSMISSION LINES WITH NONZERO METALLIZATION THICKNESS

Edward F. Kuester
Electromagnetics Laboratory
Department of Electrical and Computer Engineering
Campus Box 425
University of Colorado at Boulder
Boulder, CO 80309
USA

The line parameters of planar microwave transmission lines such as microstrip, coplanar waveguide (CPW), etc., are often calculated with the simplifying assumption that the strip conductors are perfect conductors of zero thickness. For thin conductors, the error committed by making this assumption is often small, especially for structures such as microstrip when the capacitance per unit length is dominated by a parallel plate term that is relatively large. On the other hand, for structures like CPW whose line capacitance is predominantly due to a slot effect, the thickness of the metallization can have a pronounced effect. Cohn [1960] and Garb *et al.* [1968] have made some general attempts to provide thickness corrections for strip and slot geometries, but none of these works provides a *local* correction for the thickness.

In this paper, we introduce a new perturbation method for the approximate calculation of the effect of nonzero conductor thickness on the capacitance and inductance per unit length of planar perfectly conducting transmission lines. This method provides a way to correct for thickness that depends only on behavior local to the edge itself. We start from a classic perturbation formula of Poincaré [1890] for the perturbation of the capacitance of a conducting body due to a slight indentation of the conductor surface. If applied to the present case, where the unperturbed conductor has zero thickness, the capacitance correction computed in this way is divergent, due to the inverse square root singularity of the charge density at the conductor edge. To get around this problem, we use the "stopping-point trick" first developed by Lewin [1984] for computing conductor loss of thin metallizations. That is, the perturbation integral is stopped short of the edge by an amount that depends only on the local features of the edge itself, and not on the characteristics of the rest of the conductor.

As a result, we obtain a closed-form expression for the corrected capacitance per unit length of a CPW, and therefore its characteristic impedance in the quasi-TEM range. Computed results will be presented which demonstrate excellent agreement with those obtained by more numerically intensive means, even in the case of relatively substantial ratios of metallization thickness to strip and slot widths.

B121.5

PSEUDO-TEM MODES

Edward F. Kuester
Electromagnetics Laboratory
Department of Electrical and Computer Engineering
Campus Box 425
University of Colorado at Boulder
Boulder, CO 80309
USA

The behavior of many types of lossless transmission line is described by the telegrapher's equations, wherein a shunt capacitance per unit length and a series inductance per unit length serve to determine the propagation constant and characteristic impedance of the structure. If the cross section of a waveguide is occupied only by two (or more) perfectly conducting boundaries, and otherwise by a homogeneous (μ and ϵ constant) material, then the waveguide supports a mode which is said to be TEM: the fields are transverse to the direction of propagation. Other structures containing two or more conductors that are inhomogeneously filled (microstrip, coplanar waveguide, etc.) support so-called quasi-TEM modes in the limit when the cross-sectional dimensions are small compared to a wavelength. In this case, the longitudinal fields are small in the sense that there are still unambiguously defined capacitance and inductance per unit length, as well as voltage and current so that the telegrapher's equations still apply.

For most types of waveguide, however, neither the TEM nor quasi-TEM description adequately accounts for the behavior of the dominant modes. Nevertheless, there are certain kinds of waveguide which appear to share at least some of the properties of quasi-TEM modes. In such cases, critical portions of the guide cross section are small compared to a wavelength, and the dominant mode is either: (1) a quasi-TM mode, for which current is well defined but voltage is not; or (2) a quasi-TE mode, for which voltage is well defined but current is not. Examples of the former are Goubau lines, suspended striplines and the higher-order modes of coplanar stripline; the latter include finlines, slotlines and the higher-oreder modes of coplanar waveguide. In this work, we use the term "pseudo-TEM modes" to characterize this type of mode.

We will describe such modes using an extension of the classical transmission line theory. The waveguide cross section is divided into two parts: a quasi-static part where the voltage or current is defined, and a "package" part comprising the rest of the cross section. Each of these contributes a portion of the series inductance and shunt capacitance per unit length, but the package portions are in general both spatially and temporally dispersive (that is, they depend on frequency and the yet unknown propagation constant). The fields of the two regions are matched to each other by a sort of transverse resonance procedure, from which there results a transcendental equation which must be solved to obtain the propagation constant. The characteristic impedance (either power-current or power-voltage definition) can then be found from these line parameters alone using the variational energy identity for Maxwell's equations.

A wide variety of pseudo-TEM modes may thus be modeled by "mixing and matching" various combinations of packages and quasistatic parts. This in turn leads to quick methods for calculating the behavior of these modes and to greater understanding of the physics behind their operation. As an illustration, a finline will be examined using this technique.

FAST TRANSIENT SIMULATION OF EDDY CURRENT PROBLEMS USING REDUCED-ORDER MODELS

Seaway Jan and Zoltan J. Cendes
Ansoft Corporation
Four Station Square, Suite 660
Pittsburgh, PA 15219

In this paper, a procedure is developed to simulate the time domain response of transmission lines including skin effect. This procedure combines the modeling accuracy of the finite element method and the efficiency of transient simulation with reduced-order models. The finite element method (FEM) is employed to model eddy currents in arbitrary geometries. For transient simulation, Asymptotic Waveform Evaluation (AWE) provides a general, efficient and accurate way to determine the transient responses of large linear circuits in terms of the dominant poles and residues. Once the poles and residues are obtained, transient simulation is performed by using recursive convolution.

The major task of this paper is to generate reduced pole/residue macromodels that incorporate skin effect. The two main components of this task are the generation of lumped circuit parameters that account for electromagnetic effects such as skin effect and crosstalk, and the generation of a stable frequency-dependent lossy transmission line model. The generation of frequency dependent system parameters is accelerated by using the Pade Via Lanczos (PVL) procedure. PVL is a more stable method for obtaining poles than AWE as long as problem in question can be formulated as eigenvalue problem. A reliable generalized macromodel, which is expressed in terms of the dominant poles and residues generated by AWE, is then derived for lossy transmission lines based on the two dimensional circuit parameters obtained from the FEM/PVL procedure.

In the generation of the frequency dependent lossy transmission line model, frequency dependent modal analysis coupled with Complex Frequency Hopping (CFH) is applied to obtain the pole distribution of the multiple transmission lines. Transmission line delays, attenuation and dispersion are fully captured in the pole distribution graph. A mathematically sound method of residue computation is then devised to provide stable residues. Stable poles and residues together provide accurate macromodels for lossy transmission lines. These enhancements make it possible to analyze practical interconnect problems accurately and efficiently.

The theory presented here has been implemented in the computer program Maxwell Spicelink. Examples from industry simulated using the method discussed in this paper will be presented. It is shown that skin effect indeed plays a significant role in predicting transient behavior of transmission lines at high frequencies.

B121.9

Numerical Analysis of Traveling Waves in Slotted Waveguide of Arbitrary Cross Sections

Chin-Yi Chu* and Shyh-Kang Jeng
Department of Electrical Engineering
National Taiwan University
Taipei, Taiwan

Traveling waves in slotted waveguide have been the bases of some leaky wave antennas. However, the related researches before were focused on waveguides of regular shape. In this research, we developed a numerical scheme to analyze the traveling wave in a slotted waveguide of arbitrary cross sections. This numerical analysis method is based on a set of magnetic field integral equations(MFIE) that is solved by the method of moment. To derive the MFIEs, an equivalent magnetic current is introduced on both sides of the slot aperture, and the original problem is split into two regions: a half free space region and a cavity region. This surface magnetic current excites fields in these two regions. Boundary conditions are then applied on the aperture and on the waveguide walls as following to obtain a set of MFIEs: The tangential magnetic fields in the two regions must be continues on the slot aperture, and the tangential magnetic field in the cavity region must equal to the surface electrical current on the waveguide walls. The derived MFIEs can be reduced to a matrix equation by the method of moment. This matrix equation consists of a matrix whose element expressions involve the propagation constant. Since this matrix equation must be with non-trivial solutions, the determinant of the matrix must be zero. The propagation constant thus can be determined from this restriction. The Newton-Raphson iteration technique has been used to solve this nonlinear equation to find the propagation constant. Multiple solutions can be found that represent different waveguide modes. In the presentation we will show and discuss the computed results for some slotted waveguides.

URSI B

Session 123

Salon Richelieu

Inverse Problems
Co-chairs: J.-W. Ra, Korea and C.J. Reddy, USA

08:10 123.1 Numerical Solution of the Inverse Source Problem for a Circular Dielectric Cylinder under Oblique Incidence, **M. LE BLANC**, G.Y. DELISLE, *Université Laval, QC, Canada*

08:30 123.2 Neural Network Approach to Inverse Scattering for Binary Object Identification in Stratified Media, **M.N. RYCHAGOV**[1,2], B. DUCHÊNE[1], [1]*CNRS-SUPELEC, Gif-sur-Yvette, France;* [2]*Moscow Institute of Electronic Engineering, Moscow, Russia*

08:50 123.3 Scattering Mechanism Characterization Using Matching Pursuits with a Weighted Exponential Dictionary, **N.S. SUBOTIC**, J.W. BURNS, D. PANDELIS, *Environmental Research Institute of Michigan, Ann Arbor, MI, USA*

09:10 123.4 A New Method Applied to Inverse Scattering Problem of Layered Media, **M. NAKHKASH**, Y. HUANG, M.T.C. FANG, *University of Liverpool, UK*

09:30 123.5 Applications of the Wigner Distributions in Resonance-Based Target Identification, **G. TURHAN-SAYAN**, *Middle East Technical University, Ankara, Turkey*

B123.1

Numerical Solution of the Inverse Source Problem for a Circular Dielectric Cylinder under Oblique Incidence

Mario Le Blanc, Gilles Y. Delisle
Department of Electrical and Computer Engineering
Laval University, Quebec City (QC), Canada G1K 7P4

When a lossy dielectric cylinder of known properties is illuminated by a plane, linearly polarized wave of known frequency, a certain distribution of internal and external electromagnetic fields is obtained. The incident wave is characterized by 4 unknonws: the amplitude E_0, and the incidence, azimuth and polarization angles (θ, ϕ, ξ). If the unknowns can be determined, the internal fields can be calculated, leading to the evaluation of the Specific Absorption Rate (SAR) in a straightforward manner. The use of a network of 24 small E-field probes (8 each for E_r, E_ϕ and E_z), radially mounted near the surface of the cylinder, has been proposed as a means of obtaining data for solving the inverse source problem (Le Blanc and Delisle, Proc. Canadian Conf. Electrical and Computer Engineering, Sept. 1994, pp. 572-575). The purpose of this communication is to present numerical examples showing that the solution can be found with good accuracy in a number of cases.

The first step towards the solution is to consider only ratios of measured (or calculated) field magnitudes. Thus, the amplitude E_0 is eliminated, effectively reducing the solution space to 3 dimensions. After the angles have been determined, E_0 is easily recovered. Error functions are defined by summing the absolute values of the differences between the expected and measured field ratios (robust function) or the squares of those differences (quadratic function). In the absence of measurement errors, the point in the solution space that corresponds to the actual source parameters yields a zero value of the error function. In practice, the minimum of the error function over the solution space is sought.

Simulations were performed using a cylinder made of a low-loss dielectric shell, of inner and outer radii 14.6 and 15.24 cm, respectively, filled with saline water, as described by Misra and Chen (IEEE Trans. Microwave Theory Tech., 33, 6, 447-452, 1985). The signal frequency was 9.27 GHz. The spacing between the measurement points was 2.5 mm. The measurement results were simulated by perturbating the exact field values with uniformly distributed random coefficients corresponding to maximum errors of +/- 2 dB. The minima of the error functions were found using the algorithm AMOEBA (Press et al, Numerical Recipes. Cambridge U. Press, 1986, pp. 289-293). Using the quadratic error function, 64 typical points in the (θ, ϕ, ξ) space were considered. With the nearest probe located 2.5 mm away from the cylinder surface, the solution was within a 10 degree radius of the actual point of the space in 55 of the 64 cases. With the probes moved 20 mm outwards, 46 solutions were within the same radius. Further results, as well as discussions of more realistic error models will be presented.

NEURAL NETWORK APPROACH TO INVERSE SCATTERING FOR BINARY OBJECT IDENTIFICATION IN STRATIFIED MEDIA

Michael N. Rychagov [1,2] and Bernard Duchêne [1]

[1] *Laboratoire des Signaux et Systémes, CNRS-SUPELEC, Plateau de Moulon, F-91192 Gif-sur-Yvette Cedex, France*
FAX: +33-1-69.85.17.58; E-mail: duchene@supelec.fr

[2] *Moscow Institute of Electronic Engineering, MIET, Moscow 103489 Zelenograd, Russia*
FAX: +7-095-530.22.33; E-mail: mr@org833.zgrad.ru

Multilayer neural network, trained via the backpropagation rule, is used for solving a special class of inverse scattering problems, the electromagnetic or acoustic characterization of objects (defects or structures) embedded in stratified media. A $2-D$ frequency-diverse, aspect-limited data configuration (L. Souriau, B. Duchêne, D. Lesselier and R. E. Kleinman *Inverse Problems*, **12**, 463-481, 1996) is considered. It is assumed that the test object is homogeneous with known parameters so that the identification problem using neural network approach consists of reconstructing the shape and location of the object. A labeled dataset, each pattern of which being constituted of a pair of input signals and target results, is obtained during the numerical modelling of the direct scattering problem for simple lossless inhomogeneities. As input signals, the amplitudes and phases of the scattered field calculated with accounting for the multiple scattering inside the medium under investigation are used. The target results represent a limited set of parameters which describe the characteristics of the inhomogeneities: i.e., the geometrical components of the translation and the rotation angle in the particular case of an elliptical object. The questions of the determination of the optimal design parameters for the neural network as well as the optimal measurement parameters (frequencies, number of receivers etc.) are also analysed.

B123.3

SCATTERING MECHANISM CHARACTERIZATION USING MATCHING PURSUITS WITH A WEIGHTED EXPONENTIAL DICTIONARY

Nikola S. Subotic*, Joseph W. Burns and Dimitrios Pandelis
Environmental Research Institute of Michigan
P.O. Box 134001 Ann Arbor, MI 48113-4001
subotic@erim.org, burns@erim.org, pandelis@erim.org

The ability to classify and characterize target scattering mechanisms in radar data is useful for radar cross section diagnosis and automatic target recognition applications. One method of classification is to identify the scattering mechanism's frequency dependence. The approach is motivated by the observation that asymptotic solutions for the high frequency scattering from targets, such as the Geometric Theory of Diffraction (GTD), describe the scattering from canonical local geometries by simple models with distinct frequency dependencies. Model-based optimization algorithms, such as the technique described by Potter, et al. [. Potter, D.-M. Chiang, R. Carriere, and M. Gerry, "A GTD-Based Parametric Model for Radar Scattering," *IEEE Trans. Ant. Propagat.*, Vol. 43, No. 10, pp. 1058-1967, 1995] have been developed to estimate scattering mechanism dependence from frequency diverse data. Existing algorithms, however, are computationally intensive and are generally formulated to decompose the radar signal with only a single class of function, which limits the range scattering mechanisms that can be identified.

To overcome these limitations we investigated the use of recently-developed adaptive methods for scattering mechanism identification. Adaptive techniques decompose radar signals using a very general "dictionary" of functions which can represent disparate scattering mechanisms and are chosen to closely model anticipated characteristics of the signal. The goal of adaptive decomposition is to obtain fast and stable signal representations that are sparse and offer separation of disparate phenomena. The specific adaptive decomposition technique considered was the Matching Pursuit algorithm of Mallet and Zheng [S. Mallat and Z. Zhang, "Matching Pursuit with Time Frequency Dictionaries," *IEEE Trans. Sign. Proc.*, Vol. 41, 1993, pp 3397-3415]. To estimate scattering mechanism frequency dependence, the Matching Pursuit technique was used with a GTD-based dictionary similar to that described in Potter, et al. [1995]. The algorithm was implemented with an extension of the Atomizer software of Chen and Donoho [S. Chen and D. Donoho, *Basis Pursuit*, Technical Report, Department of Statistics, Stanford University, 1995, http://playfair.stanford.edu/reports/chen_s].

In the presentation, we will describe the formulation and implementation of the algorithm. We will show the mechanism classification performance obtained when the algorithm was applied to numerically-simulated and experimentally-measured data, and algorithm performance determined from Monte Carlo simulations will be compared to Carmer-Rao bounds. We will show that the technique provides fast and accurate estimates of scattering mechanism frequency dependence when the radar data have adequate fractional bandwidth and signal-to-noise ratio.

A New Method Applied to Inverse Scattering Problem of Layered Media

M. Nakhkash*, Y. Huang and M. T. C. Fang
University of Liverpool, Liverpool, L69 3BX, UK

The 1-Dimensional Electromagnetic Inverse Scattering (1-D EIS) problem is to reconstruct the electrical parameters (e.g. permittivity and conductivity) of a layered medium illuminated by a plane wave from scattering data, which may be obtained from the fourier transform of the impulse response of the medium (e.g. reflection coefficient). The EIS methods fall into two categories :

1. Inverse mapping methods, which are based on integral-inverse algorithms or differential-inverse algorithms, such as layer stripping algorithms.
2. The best fitting methods or the iterative procedures which are usually formulated by the source-type integral equation and relate the constitutive parameters of the medium to the scattering field.

We propose a novel 1-D EIS method which belongs to the best fitting methods. Instead of using the source-type integral equation, the method is formulated by a closed-form equation which represents the reflection coefficient as an explicit function of parameters of a half-space multi-layer medium. The permittivity, conductivity and thickness of the medium are reconstructed by successive minimisation of Mean Square Error (MSE), which is obtained from the difference between the measured values and the values calculated from the closed-form equation for reflection coefficient at discrete frequencies. In another word, the 1-D EIS problem is turned into parameter optimisation of a cost-function which here is MSE function.

The main advantage of using the closed-form equation is that the reflection coefficient is not only function of permittivity and conductivity of the layers but also function of the thickness of the layers. In this way, there is no need for discretization of the medium to thin layers. Consequently, the number of unknown parameters is reduced significantly and so the new method is much more efficient comparing with previous methods from the computation time point of view.. Another remarkable advantage is that for the case of simultaneously reconstructing permittivity and conductivity profiles, the reflection coefficient for normal incident is sufficient for the proposed EIS method. But in previous 1-D EIS methods the reflection coefficients in two angles of incidence or both TE and TM reflection coefficients are required.

Computer simulations have demonstrated the accuracy and efficiency of this new method.

B123.5

Applications of the Wigner Distributions In Resonance-Based Target Identification

Gönül Turhan-Sayan

Department of Electrical and Electronics Engineering
Middle East Technical University, 06531 Ankara, Turkey

It is well known that a target's pole pattern uniquely identifies that target in an aspect and polarization independent manner. However, the resonance-based target identification techniques usually make indirect use of target's natural resonance frequencies (i.e., poles) due to practical difficulties of pole extraction. The indirect approach is based on synthesizing an input signal whose Laplace domain zeros are the same as the target poles over the application bandwidth. This design objective can be, at least approximately, met by minimizing the natural resonance related target response energy with respect to input signal design parameters. When this energy minimization procedure is performed in time domain, a considerable amount of error may occur due to taking the inverse Fourier transformation of a band-limited data. In general, such error increases as the signal bandwidth decreases and the lower frequency limit of the available data increases.

This paper introduces an alternative approach to input signal shaping where the target response is essentially formed in the frequency domain. The natural resonance related part of the response energy is then computed by means of the Wigner Distributions (WD's) and/or its smoothed versions in the joint time-frequency domain to be minimized afterwords. As the WD of a signal satisfies the so called marginal properties, it can be interpreted as a distribution of the signal energy over time and frequency. Therefore, the WD of a signal provides much more information about the natural resonances of a target as compared to that provided by the Fourier transform pair. Both the advantages and the disadvantages of using WD's in a resonance-based target identification problem will be discussed in this paper in detail. Effects of the signal bandwidth and the band's lower frequency level on the target identification performance will also be demonstrated for various canonical targets.

URSI B | Session 124 | Salon Richelieu

Non-Conventional Computational Methods
Co-chairs: E.H. Newman, USA and O.B. Kesler, USA

10:30 124.1 An Implicit Solution to Integral Equation Time-Domain Scattering Problems, **S.M. RAO**[1], T.K. SARKAR[2], [1]*Auburn University, Auburn, AL and* [2]*Syracuse University, Syracuse, NY, USA*

10:50 124.2 The Path Integral Time-Domain Method: A New Numerical Method for Electromagnetic Scattering, **R. NEVELS**, J. MILLER, R. MILLER, *Texas A&M University, College Station, TX, USA*

11:10 124.3 The Method of Lines for the Analysis of Traveling-Wave Antennas, **L. VIETZORRECK**, R. PREGLA, *Fern Universität, Hagen, Germany*

11:30 124.4 Wave Interaction with Heterogeneous Dielectric Objects Using Lattice Gas Automata, **D. CULE**[1], M. ZHANG[1], N. SIMONS[2], G. BRIDGES[1], M. CUHACI[2], [1]*University of Manitoba, Winnipeg, MB and* [2]*Communications Research Centre, Ottawa, ON, Canada*

11:50 124.5 Multi-Bit Lattice Gas Automaton for Computational Electromagnetics, **G. BRIDGES**[1], N. SIMONS[2], [1]*University of Manitoba, Winnipeg, MB and* [2]*Communications Research Centre, Ottawa, ON, Canada*

B124.1

An Implicit Solution to Integral Equation Time-Domain Scattering Problems

S. M. Rao*, Department of EE, Auburn University, Auburn, AL 36849.

T. K. Sarkar, Department of ECE, Syracuse University, Syracuse, NY 13244.

In this work, we present an implicit solution method to solve the integral and integro-differential equations directly in the time-domain. Starting from Maxwell's equations and using potential theory, for conducting, as well as dielectric bodies, it is possible to derive integral equations. Usually for these problems, the unknown quantity is the induced surface current. The time-domain integral equations (TDIE) are more appealing to electromagnetic scattering problems than the differential equation solution methods such as FDTD and TLM, because the solution space is confined to the object and the radiation condition is enforced in an exact sense.

It may be noted that the solution to the TDIE problems have been carried out, at least, for the last thirty years. These equations are solved numerically using the marching-on-in-time technique in conjunction with the method of moments. In the numerical solution scheme, the TDIE is approximated as a matrix equation. However, the matrix equation is solved numerically in an iterative fashion by selecting the time step less than the smallest discretization in space divided the wave velocity. This particular numerical scheme is known as *explicit solution method* and for this technique the computer storage requirements are minimal. If applied intelligently, one can entirely eliminate the storage of the system matrix which is a definite advantage for scattering problems. Unfortunately, this scheme is plagued by late-time instabilities which may be reduced in some cases using special averaging procedures.

In this paper, we present a different numerical solution method to solve the TDIE problem. In this case, we still apply the method of moments to reduce the operator equation into a matrix equation. In the next step, we solve the matrix equation by developing the *implicit solution scheme.* It has been noted that the implicit solution method did not exhibit any late-time instabilities. Obviously, this is a great advantage. Further, the method is more accurate since no averaging procedures are needed to arrest the oscillations. The method is also more efficient since one can use a larger time-step. This is because the time-step is no longer controlled by the discretization in space. However, this procedure requires the storage/inversion of a sparse moment matrix. We present several numerical results illustrating the capabilities of the present method.

The Path Integral Time-Domain Method: A New Numerical Method For Electromagnetic Scattering

Robert Nevels*, Jeffrey Miller and Richard Miller
Department of Electrical Engineering
Texas A&M University
College Station, TX 77843-3128

The path integral was proposed by P.A.M. Dirac and later developed by Nobel Laureate Richard Feynman as an alternative to the Schrodinger and Heisenberg treatments of quantum mechanics. It can be described as a universal Green's function, expressed as a nested sequence of integrals, for a parabolic type equation.

The lack of mathematical generality or flexibility of previous attempts to apply the path integral to electromagnetic scattering is in part due to the starting point, which has been the frequency domain form of Helmholtz equation. Helmholtz equation is an elliptic equation which, because path integrals are known to exist only for parabolic equations, must be converted to parabolic form. This has been accomplished by operator splitting techniques, with the parabolic approximation method and by pseudo time domain transformation (R. D. Nevels, C. Huang, Z. Wu, *IEE Proc., Part H,* 488-492, 1993). These methods prevent effective scattering analysis because in the first case only one-way propagation is allowed, in the second the medium parameters are restricted to gradual change in the direction of propagation, and the latter case is applicable only to scalar scattering.

Here we will present a new path integral method for electromagnetic field scattering in the time domain. This formulation will be shown to give a remarkably simple expression in which, at each time step, each field component is found by a Fourier and an inverse Fourier transformation of each of the previous time fields. This path integral time-domain method is completely general, applicable, for example, to the case of scattering from a three dimensional general shaped body that can contain inhomogeneous, anisotropic and nonlinear material. Because Fourier transformation can be accomplished numerically with a fast Fourier transform (FFT) algorithm, the calculation of each field component at N points in a three-dimensional numerical lattice requires on the order of $3\times N ln N$ operations. The path integral is a complete expression and as such the boundary conditions are not explicitly enforced, but rather are inherent in its expression. Other attractive features of this path integral numerical method are that in its simplest form it is 3rd order accurate and because the FFT is a unitary operation, it is unconditionally stable.

B124.3

The Method of Lines for the Analysis of Traveling-Wave Antennas

Larissa Vietzorreck and Reinhold Pregla
Allgemeine und Theoretische Elektrotechnik
FernUniversität, D-58084 Hagen, Germany

Traveling-wave antennas are of increasing interest for numerous millimeter-wave applications. They are inexpensive in production and easy to implement on arbitrary surfaces. Their radiation pattern featuring a narrow main lobe and a high side lobe attenuation makes them very suitable for traffic control and anticollision radars.
These antennas can be regarded as a microstrip line with evenly spaced stubs. The size of the stubs can vary both in length and width (see Fig. 1a). The analysis of such an antenna with a common numerical method, e.g. MoM or FDTD, where the whole surface has to be discretized, is very difficult. The small deviations in size require such a fine discretization, that even for small structures with only a few stubs the capacities in computer memory are exceeded.

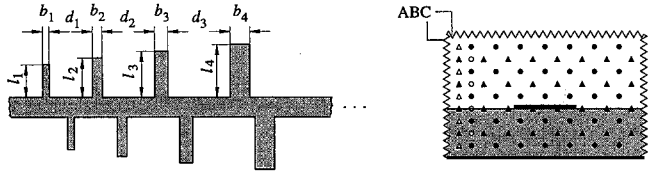

Fig. 1: a) Top view of a traveling-wave antenna b) Cross-section with discretization scheme

Recently, the Method of Lines (MoL) has been further developed for analysis of cascaded discontinuities (L. Vietzorreck and R. Pregla, *IEEE T-MTT 44*, 2580-2586, Dec. 1996). Using this new concept, the structure is divided into longitudinal sections. Each section has to be homogeneous in propagation direction, but can have an inhomogeneous cross-section including metallizations. The cross-section is discretized, the solution in propagation direction being analytical. Matching the tangential field components at all interfaces results in a generalized scattering matrix. For a given input the field distribution in the whole structure is calculated easily.

An extension of the MoL is proposed in this paper for the analysis of traveling-wave antennas. Absorbing boundary conditions (ABC) are implemented at the top and the side walls of the cross-section to model the free space (see Fig. 1b). Furthermore, a new discretization scheme is introduced, allowing the ends of the stub metallizations to be positioned between the discretization points. This reduces the number of discretization points in the cross-section. Because of the analytical solution in propagation direction the stub width and spacing b_i, d_i do not influence the required memory, so that the characteristic parameters are computed with a reasonable numerical effort, using the proposed algorithm.

Wave Interaction with Heterogeneous Dielectric Objects Using Lattice Gas Automata

D. Cule*, M. Zhang, N. Simons†, G. Bridges and M. Cuhaci†

Department of Electrical and Computer Engineering
University of Manitoba
Winnipeg, Canada R3T 2N2

†Directorate of Antennas and Integrated Electronics
Communications Research Centre
3701 Carling Avenue, P.O. Box 11490, Station H
Ottawa, Canada K2H 8S2

Lattice Gas Automata (LGA) are an alternative to the traditional differential equation based numerical methods now widely used in computational electromagnetics. LGA are a special class of cellular array processors and are comprised of a large regular lattice of cells. The cells are very simple, with only a few bits being used to represent all possible states, and are all updated in synchronism according to the same deterministic rule. We have previously demonstrated that very simple LGA constructed with only 4 bits per cell and operating on a rectangular lattice are capable of simulating two-dimensional electromagnetic field problems [N. Simons, N. Adnani, G. Bridges, M. Cuhaci, Intl. J. Num. Modelling, 8, 301, 1995]. The simplicity of the LGA algorithm makes them ideally suited to implementation in a parallel processing architecture. In contrast to the traditional differential equation based approach in electromagnetics, LGA use only a few bits of memory per cell, and simple binary logic to manipulate information. This also results in unconditionally stable behaviour.

We have recently developed new lattice gas automata based algorithms for modelling wave propagation in inhomogeneous dielectric media with a large range of dielectric constants. In this paper we report on these algorithms and discuss their application to the analysis of scattering off heterogeneous dielectric cylinders. Comparisons with standard numerical methods, such as the Symmetric-Condensed Transmission Line Matrix and Finite-Difference Time-Domain methods as well as analytical solutions will be given. Due to its fine lattice structure and the minimal memory required for each cell, the lattice gas approach has the ability to model fine geometrical details. This enables the scattering structure to be defined with a high precision within the spatial grid, an advantage when modelling complex problems such as wave interaction with biological media.

B124.5

Multi-Bit Lattice Gas Automaton for Computational Electromagnetics

Greg Bridges* and Neil Simons

Electrical and Computer Engineering
University of Manitoba
Winnipeg, Canada R3T 2N2

Directorate of Antennas and Integrated Electronics
Communications Research Centre
3701 Carling Avenue, Ottawa, Canada K2H 8S2

In this paper we present a new computational technique based on the lattice gas automata approach. Lattice gas automata are an alternative to the traditional differential equation based numerical methods now widely used in computational electromagnetics. A lattice gas automaton (LGA) is an extremely large regular lattice of interconnected cells. The cells are very simple, usually only a few bits being used to define all possible states. All cells are updated in synchronism according to the same deterministic rule which is local spatially and temporally. LGAs have received the most attention in the modelling of fluid dynamics, where the individual bits of the lattice cells mimic interacting particles. In the small perturbation limit a fluid will behave according to the linear wave equation, and thus by making an analogy between fluid and field parameters we have utilized this simple particle interaction paradigm as a tool for computational electromagnetics. We have previously shown how LGA algorithms are capable of simulating a variety of electromagnetic propagation and scattering problems [N. Simons, N. Adnani, G. Bridges, M. Cuhaci, Intl. J. Num. Modelling, 8, 301, 1995]. One of the main motivations for exploring LGA numerical techniques is that they are inherently simple parallel systems. Cells require only a few bits of memory and simple logical operations for their evaluation. This makes LGA ideally suited to computation using fine-grained parallel architectures, unlike their difference equation counterparts which require floating point processors. Futher, first generation special purpose computing architectures, referred to as cellular automata machines, already exist [N. Margolus, in Pattern Formation and Lattice Gas Automata, Am. Math Soc. Fields Inst. Ser., 1995]. We have used these to implement the algorithms presented in this paper.

The LGA algorithms we have previously demonstrated for two-dimensional field problems utilize only 4 bits per cell on a rectangular lattice (one bit per direction). This means that binary variables are passed between adjacent cells and a simple 2^4=16 state transition table is required to update a cell, making it extremely efficient for implementation in a parallel computing architecture. However, one of the drawbacks of this binary variable approach is that statistical averaging over a group of cells is necessary to obtain macroscopic field quantities over a reasonable dynamic range. Thus, a larger mesh is required than when using a real-number variables as in the differential equation methods. From experiments with various field problems increased mesh densities are on the order of 10-30 per dimension for the LGA technique. Further, even though the LGA technique does not exhibit the numerical dispersion errors inherent with difference equation approximations, it does exhibit dissipative effects (similar to viscosity in a fluid). To reduce these two problems we have developed a multi-bit variable LGA model (4 bit variables per lattice direction for example). Even though the number of bits is increased it is still amenable to implementation on special purpose hardware. Our model is similar to a quantized transmission line matrix algorithm where variables are allowed only 16 states. To handle truncation and round-off during cell updating we use a technique that conserves fields exactly and energy statistically so that proper linear wave behaviour on the lattice is maintained. The LGA algorithm and comparisons with differential equation based techniques will be given in the presentation.

URSI B | Session 127 | Salon Marquette

Mesh Truncation Approaches
Co-chairs: B. Stupfel, France and S.M. Rao, USA

13:10 127.1 Mesh Truncation by Non-Planar Perfectly Matched Absorbers in the Finite Element Time Domain Method, M. KUZUOGLU[1], **R. MITTRA**[2], [1]*Middle East Technical University, Ankara, Turkey;* [2]*Pennsylvania State University, University Park, PA, USA*

13:30 127.2 Perfectly Matched Layer (PML) Absorbers Studies for Truncating Finite Element Meshes, Y.Y. BOTROS, J. GONG, **J.L. VOLAKIS**, *University of Michigan, Ann Arbor, MI, USA*

13:50 127.3 Improved Numerical Implementation of Conformal Absorbing Boundary Conditions in an Edge Based Finite Element Formulation, **B. STUPFEL**, *Commissariat à l'Énergie Atomique, Le Barp, France*

14:10 127.4 A Perfectly Matched Layer Method for Node-Based Finite Elements, J. TANG, **K.D. PAULSEN**, S.A. HAIDER, *Dartmouth College, Hanover, NH, USA*

14:30 127.5 Application of the Transparent Absorbing Boundary (TAB) in Finite Methods, **J. PENG**, C.A. BALANIS, *Arizona State University, Tempe, AZ, USA*

14:50 127.6 Profiling the Perfectly Matched Layer to Improve Large Angle Performance, **S.C. WINTON**, C.M. RAPPAPORT, *Northeastern University, Boston, MA, USA*

15:10 Coffee Break

15:30 127.7 Analysis of Scattering and Radiation Problems by Means of a Finite Element Iterative Method, **L.E. GARCIA-CASTILLO**[1], T.K. SARKAR[2], M. SALAZAR-PALMA[1], T. ROY[2], A. DJORJEVIC[3], [1]*Polytechnic University of Madrid, Spain;* [2]*Syracuse University, Syracuse, NY, USA;* [3]*University of Belgrade, Yugoslavia*

15:50 127.8 Electromagnetic Solution for Three-Dimensional, Arbitrarily-Shaped Inhomogeneous Bodies Using FIT/MEI, **J.H. HENDERSON**, S.M. RAO, *Auburn University, Auburn, AL, USA*

16:10 127.9 The Integral Equation MEI for Three-Dimensional Scatterers, **J.M. RIUS**, E. ÚBEDA, J. PARRÓN, A. CARDAMA, *Universitat Politècnica de Catalunya, Barcelona, Spain*

16:30 127.10 Concurrent Implementation of the Complementary Operators Method, **O.M. RAMAHI**, *Digital Equipment Corporation, Maynard, MA, USA*

B127.1

Mesh Truncation by Non-planar Perfectly Matched Absorbers in the Finite Element Time Domain Method

Mustafa Kuzuoglu
Department of Electrical Engineering
Middle East Technical University
06531, Ankara TURKEY

Raj Mittra
Pennsylvania State University
319 Electrical Engineering East
University Park, PA 16802-2705 USA

Perfectly matched absorbers have been extensively used in the Finite Difference Time Domain (FDTD) and Finite Element (FE) formulations for mesh truncation. In this work, we propose a formulation that employs perfectly matched anisotropic absorbers in the Finite Element Time Domain (FETD) technique, that has some advantages over the other two methods for certain type of problems.

In a perfectly matched absorber, the differential equation satisfied by the $\vec{E}$ field is given by

$$\nabla \times \left([\Lambda]^{-1} \nabla \times \vec{E} \right) - \omega^2 \varepsilon_0 \mu_0 [\Lambda] \vec{E} = 0$$

where $[\Lambda]$ is a tensor whose entries are chosen to enforce the decay of the wave within the absorber in the direction normal to the boundary. The tensor $[\Lambda]$ can be expressed as the product $[\Lambda] = T^t [\tilde{\Lambda}] T$, where T is a rotation matrix and $[\tilde{\Lambda}]$ is a diagonal matrix. Defining new variables $\vec{P}_1 = [\Lambda]^{-1} \nabla \times \vec{E}$ and $\vec{P}_2 = [\Lambda] \vec{E}$, the original equation is reduced to the following coupled system of equations

$$[\Lambda] \vec{P}_1 = \nabla \times \vec{E}, \qquad \vec{P}_2 = [\Lambda] \vec{E} \quad \text{and} \quad \nabla \times \vec{P}_1 - \omega^2 \varepsilon_0 \mu_0 \vec{P}_2 = 0$$

The equations in time domain can be obtained by employing the inverse Fourier transform. The first two equations contain first order derivatives with respect to time, whereas the second time derivative of $\vec{P}_2$ appears in the last equation. After generating the weak forms of the partial differential equations, the finite element method is utilized to obtain the space-time discrete equations. In order to determine $\vec{P}_{1,n}$, $\vec{P}_{2,n}$ and $\vec{E}_n$ (where n denotes the time step), $\vec{P}_{1,n-1}$, $\vec{P}_{2,n-1}$, $\vec{P}_{2,n-2}$ and $\vec{E}_{n-1}$ (i.e., 12 quantities) must be known. In this respect, the storage requirements of this approach are the same as those in Berenger's split-field formulation, for FDTD applications, which also utilizes the same number of unknowns. The main advantage of the PML/FETD combination is that, the absorber can be chosen to be conformal to the scatterer (or radiator) and, hence, the white space of the computational domain can be minimized considerably for many problems of interest.

Perfectly Matched Layer (PML) Absorbers Studies for Truncating Finite Element Meshes

Youssry Y. Botros, Jian Gong and John L. Volakis
Radiation Laboratory
Department of Electrical Engineering
and Computer Science,
The University of Michigan
Ann Arbor, MI 48109-2212

Abstract

Perfectly Matched Layer (PML) absorbers have superior performance over other truncation schemes such as Absorbing Boundary Conditions (ABCs) or isotropic material absorbers. In this paper, we present improvements in the PML performance for truncating finite element meshes. Previous examinations undertook parametric studies of the PML parameters and presented optimal values of certain constants to improve the overall PML performance. In our paper, we will look at all parameters affecting the PML performance including the absorber location, thickness, material constants and discretization. We will carefully study the effect of these parameters on the resulting system condition, convergence rate and system size. First, the effect of the PML absorber constants on the absorption is considered. Using the optimal values of these parameters, the system condition will be examined and improved if necessary. Simple preconditioning schemes can improve the system convergence without much computational effort. Three different iterative solvers and their performance are considered. Namely, the Biconjugate Gradient (BCG), the Quasi Minimal Residual (QMR) and the Generalized Minimal Residual (GMRES) are tested for solving the FEM system with the PML implemented and optimized. The convergence rate, storage requirements and number of operations will be discussed for each of these solvers. Several examples for microwave structure simulations with multiport circuits will be considered as applications.

B127.3

IMPROVED NUMERICAL IMPLEMENTATION OF CONFORMAL ABSORBING BOUNDARY CONDITIONS IN AN EDGE BASED FINITE ELEMENT FORMULATION

Bruno Stupfel

CESTA, Commissariat à l'Énergie Atomique, B.P. 2, 33114 Le Barp, France.

The finite element method (FEM) is well-suited for solving scattering problems involving inhomogeneous, arbitrarily-shaped objects. For open region problems, the FEM used in conjunction with a local, hence approximate, radiation condition called the absorbing boundary condition (ABC) leads to a sparse FE matrix. However, the feasibility of an FE solution of the scattering problem by electrically large objects requires the minimization of the size of the computational domain comprised between the surface of the scatterer S_0 and the terminating boundary S upon which the ABC is prescribed. One possibility is to choose S to be "conformal" to S_0, and to prescribe on S high-order boundary conditions which can be either analytical ABCs [B. Stupfel, IEEE Trans. Ant. Prop. 42, 773-780, 1994] or numerical ABCs (NABCs) [B. Stupfel, R. Mittra, IEEE Trans. Ant. Prop. 44, 1015-1022, 1996]. Accurate calculations of the Radar Cross Section have been presented in [B. Stupfel, PIERS96 Proceedings, 113, Innsbruck, 1996] when second- or third-order ABCs or NABCs are prescribed on the surface of a parallelepiped whose distance from S_0 is small (typically $\lambda/10$ - $\lambda/15$). However, the numerical implementation of these ABCs when edge based elements are employed necessitates a regular meshing of S which constitutes a severe drawback for industrial applications. In addition, a special treatment is required for the edges of the parallelepiped which leads to a non symmetric FE matrix and, consequently, to a computationally expensive solution of the final linear system.

In this paper we present, for an edge based FEM, an enhanced numerical implementation of the second-order ABC which does not require a regular meshing of S. Also, it is shown that the use of a smooth conformal terminating boundary allows the symmetrization of the FE matrix and, consequently, reduces the computational costs. As such, this ABC can be employed in conjunction with the corresponding second-order transmission condition in the domain decomposition method proposed in [B. Stupfel, IEEE Trans. Ant. Prop. 44, 1375-1385, 1996]. Numerical results are presented, together with those obtained when implementing the higher-order NABC with a double layer distribution of the points M_js, as defined in the previously mentioned paper by Stupfel and Mittra.

A Perfectly Matched Layer Method for Node-Based Finite Elements

J. Tang, K.D. Paulsen and S.A. Haider
Thayer School of Engineering, Dartmouth College, Hanover, NH, USA
phone: 603-646-2695; fax: 603-646-3856; email: keith.paulsen@dartmouth.edu

There has been considerable interest in the development and implementation of the perfectly matched layer (PML) concept first introduced by Beringer as an effective mesh truncation scheme for differential equation solvers in computational electromagnetics. The majority of attention to date has been devoted to FDTD considerations, although there has been a significant increase in the development and use of the PML in finite element calculations as well. In this regard, edge-element formulations have served as the primary focus and have dominated the advances which have been reported in the literature.

We have been developing the analogs for PML implementation on node-based finite element discretizations. In this presentation, we demonstrate that the PML concept can be efficiently and effectively incorporated into existing node-based finite element codes. Specifically, we show that this can be readily accomplished in either scalar/vector potential or direct field formulations on simple linear tetrahedral elements. An interesting feature of our numerical approach is the fact that both the anisotropic media and stretched coordinate viewpoints of mesh truncation in this context lead to the same discrete systems of equations and hence are numerically identical. Further, implementation of the PML on node-based finite elements can be readily generalized to non-cartesian mesh terminations which not only preserves the flexibility of the finite element method in terms of accommodating complex geometries but also relieves the imposition of any constraints on the already difficult task of 3D mesh generation when the PML is employed. Results from several sample benchmark problems will be highlighted to demonstrate the validity and overall performance of the PML within the node-based finite element computational framework.

B127.5

Application of the Transparent Absorbing Boundary (TAB) in Finite Methods *

Jian Peng and Constantine A. Balanis
Department of Electrical Engineering
Telecommunications Research Center
Arizona State University
Tempe, AZ 85287-7206

A new approach to truncate computational domains without reflection is proposed for finite methods, such as finite difference and finite element. Instead of solving Maxwell's equations in an open space, an auxiliary field system defined in a closed domain is introduced. By establishing the equivalence between the physical and auxiliary systems, one can solve for the auxiliary fields in the closed domain and then find the actual fields from them.

The auxiliary system is designed such that its field magnitudes decrease outwardly and become zero at the exterior boundary of the computational domain. Thus, field absorption in the auxiliary system provides the additional homogeneous boundary condition needed for domain truncation. Meanwhile, the wave impedance and phase velocity in the auxiliary system are kept identical to those of the physical system so that no artificial reflections will be introduced in the auxiliary system. That is, the transformation of solution domain seems *transparent.*

Like the well-known Perfectly Matched Layer (PML), the TAB is independent of frequency, incident angle and material properties. The unique feature of this method is that the TAB does not need the absorption region of the PML. Field attenuation takes place in the domain of interest, and the actual fields can be found from the attenuated auxiliary ones through an inverse transformation. Thus, the computational efficiency can be improved.

The TAB approach is applied to truncate computational domain for finite methods, such as the finite-difference method. The challenge in the numerical solution is that the loss responsible for domain truncation is no longer conductive. The numerical approximation to the partial differential equations must reflect these new lossy terms. Formulation and numerical results are discussed, respectively, for the finite methods.

*This work was sponsored by NASA Langley Research Center Grant NAG1-1082 and the Advanced Helicopter Electromagnetics (AHE) Industrial Associates Program.

PROFILING THE PERFECTLY MATCHED LAYER TO IMPROVE LARGE ANGLE PERFORMANCE

Scott C. Winton and Carey M. Rappaport
Center for Electromagnetics Research
Northeastern University
Boston, MA 02115

Absorbing Boundary Conditions (ABCs) are used in Finite Difference Time Domain (FDTD) scattering problems in order to prevent reflections off the lattice edges. The introduction of the Perfectly Matched Layer (PML), (Berenger, *J. Comp. Phys.*, Oct. 94), revolutionized ABCs. In continuous time and space, the PML completely absorbs waves, independent of frequency and angle of incidence and can attenuate these waves at an arbitrary rate. Despite the obvious utility of the PML, its numerical implementation is problematic. The amount of attenuation experienced by waves incident on a PML drops off sharply as the angle of incidence, θ increases. Despite considerable effort in interpreting, adapting and improving it, little success has been achieved in modifying the PML in such as way as to achieve consistent performance over a wide range of angles, until now. Presented are the constitutive values of conductivity σ that will allow the PML to achieve a total reflection of -100 dB(.0001%) through angles beyond 60°. Also presented is the background and methodology required to determine these values.

In order to understand the problems in discretizing the PML, consider that it has been established that the decay rate of the PML in continuous time and space is $\alpha = \sigma\eta\cos\theta$. When discretized, the total two way loss for the an N-layer PML is $L = \mathrm{Exp}(-2\sum_{n=0}^{N-1}\sigma_i\eta\cos\theta\Delta)$, assuming perfectly conducting termination. The value of σ at a spatial point within the PML is σ_i, Δ is the spatial increment and i is the spatial index. Because the decay rate per PML layer, defined by $S_i = \sigma_i\eta\Delta$ is a source of discretization error, the values of S_i must be chosen carefully (Rappaport, *IEEE Trans. Magn.*, May 96) and clearly any S_i may not be arbitrarily large. The minimization of computational overhead requires that N be as small as possible. However, since L is inversely proportional to $\cos\theta$, if N and the values of σ_i are too small, L may become unacceptably large. Berenger found that varying the conductivity parabolically $\sigma_i = \sigma_f(i/N)^2$, where σ_f is a constant, optimized absorption. Still, Berenger's published results indicate that reflections from the discretized PML increase rapidly as θ increases.

To find a set of σ_i that will allow the PML to achieve consistent results over a wide range of angles requires one assumption and two observations. Consider an 8 layer PML, this allows for profiling of 16 half-layers, since at every spatial point, there is a σ_i associated with both $\overline{E}$ and $\overline{H}$ fields.

Based on Berenger's results, it is assumed that there exists a profile of the form $\sigma_j = \sigma_f(j/16)^p$, $j = 1,2..16$ $(i = [j/2])$ where σ_f and p must be found to optimize performance. The first observation is that reflections off the PML at small angles are dominated by discretization error. Finding the best set of σ_j's for small angles is simply balancing the discretization error against L. An increase in σ_f will increase the discretization error and decrease L. The value of p effects the change in one value of σ_j to the next. If this "contrast" is large, reflections from adjacent spatial points are increased. The *overall* effect of changes in p are difficult to predict. The second observation is that reflections from the PML at large angles are dominated by L. It will be shown that discretization error goes down with an increase in θ. The key then, is to have σ_f large enough to provide a suitable attenuation at large angles and to adjust p to minimize both the discretization error and L at low angles.

One-dimensional FDTD simulations (Winton, Rappaport, *97 ACES Syp. Dig.*, to be published) are used for an automated search for σ_f and p. The gaussian pulse width and FDTD parameters are those used by Berenger to facilitate comparison. Reflections were analyzed for angles from normal to 60°. When an appropriate set of parameters was found, several angles were tested with the 1-D simulations and verified with 2-D simulations.

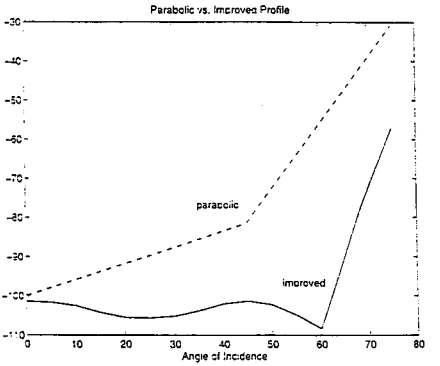

The results above clearly indicate that significant improvement over the parabolic profile has been achieved for angles between 0° and 75°. In some cases this improvement is as much as 40 dB.

B127.7

ANALYSIS OF SCATTERING AND RADIATION PROBLEMS BY MEANS OF A FINITE ELEMENT ITERATIVE METHOD

L.E. Garcia-Castillo*, T.K. Sarkar**, M. Salazar-Palma*, T. Roy**, A. Djorjevic***
*Polytechnic University of Madrid, **Syracuse University, ***University of Belgrade
Email: luise@gmr.ssr.upm.es Tel. 34-1-3367358, Fax. 34-1-3367362

Finite Element Method (FEM) has demonstrated to be a very flexible and powerful tool to analyze a wide variety of electromagnetic problems. Complex geometries can be easily analyzed due to the independence of the FEM code on the particular shape of the problem domain. Anisotropies, inhomogeneities, and so on, are also easily handled by the FEM. However, when dealing with open region problems an artificial boundary must be used to truncate the mesh in order to keep the number of unknowns finite. A boundary condition must be written over the artificial boundary that should be able to simulate the electromagnetic field behaviour on the external region; it should also produce a mesh with a low number of unknowns. Two main kinds of boundary conditions can be used. First type is derived from the boundary integral equations and provide an exact boundary condition for mesh termination. These are the so called hybrid FEM/BEM methods. However, the use of Green's function leads to dense matrices, which are expensive to solve and store. On the other hand, local boundary conditions, also known as "Absorbing Boundary Conditions" (ABC), come from the discretization of the differential operator in which the sparsity of the matrices is retained but are not exact and the boundary must be placed at some distance from the sources in order to obtain an accurate solution. Also, there are undesirable effects at reentrant corners. Other approaches have become popular in the recent years as the "Measured Equation of Invariance" (MEI) and the "Perfectly Matched Layer" (PML).

In [L. E. García-Castillo et. al., 1996 USNC/URSI Radio Science Meeting (pp. 54), Baltimore, Maryland, USA, Julio 1996] a different technique, namely an iterative procedure, was proposed for the truncation of the FEM mesh in 3D scattering and radiation problems and preliminary results were presented. In the mentioned approach, the boundary condition at the external boundary, S, appears as a Dirichlet condition for the nodes on S at each iteration step. The values to be imposed as the Dirichlet boundary conditions are computed from equivalent currents (tangential components of the FEM electric and magnetic fields obtained in the previous iteration) on an auxiliary surface S', using the Green's function and the Equivalence principle. Therefore, sparse matrices are obtained. Also, the use of the Green's function allows to terminate the mesh close to the original sources of the problem (the scatterer or the radiation sources), providing thus a mesh with less number of unknowns than a conventional ABC approach.

Double curl formulations with the electric or magnetic field as the vectorial variational unknown have been employed in the implementation of the iterative procedure. Tethraedral edge elements are used for field discretization, providing a consistent approximation of the electromagnetic field avoiding the problem of spurious modes. An under relaxation factor may be introduced in the iterative process for the nodes on S when needed. The proposed approach has been applied to different structures. Differences between electric field and magnetic field formulations have been observed for the same structure due to the differences in the excitation and imposition of boundary conditions processes between the two formulations. The communication will present the obtained results compared with the analytic solution (when available) and with those obtained with other methods in order to show the features of the method.

Electromagnetic Solution for Three-Dimensional, Arbitrarily-Shaped Inhomogeneous Bodies Using FIT/MEI

John H. Henderson* and S. M. Rao
Department of Electrical Engineering
200 Broun Hall
Auburn University, AL 36849-5201

A numerical method for solving open-region EM scattering problems involving arbitrarily-shaped, inhomogeneous objects that results in a system matrix that is small as well as sparse is desired. This has been achieved by applying the Measured Equation of Invariance (MEI) mesh-truncation technique to the Finite Integral Technique (FIT).

FIT uses tetrahedral discretization of the object and the surrounding space, explicit edge- based basis functions for the electric field, and face- based functions for the magnetic flux density. The integral form of Maxwell's equations are applied to paths surrounding faces and edges, resulting in a sparse system matrix relating the electric field at each edge to the edges forming the tetrahedra that share that edge. The constitutive parameters may be different for each tetrahedron, allowing the modelling of inhomogeneous objects.

The MEI method is based on the premise that sparse-matrix methods, such as Finite Element (FE), Finite Difference (FD) and Finite Integral, are simply sets of linear equations that relate each unknown to some number of neighboring unknowns with coefficients determined by the method. When the mesh is truncated, FE, FD and FIT do not result in valid coefficients. MEI uses a set of linearly independent current distributions on the body and applies the free space Green's function to measure the weights at the boundary. The resulting weights are geometry-, but not excitation-dependent. Since MEI makes no assumption about the geometry, the mesh may be truncated as close as two tetrahedra layers to the body, unlike other mesh-truncation methods such as absorbing boundary conditions. The method also maintains sparsity of the matrix, unlike integral equation methods.

Basic conducting and dielectric bodies are analyzed with this method, and compared against results obtained by the Method of Moments and analytical solutions.

B127.9

THE INTEGRAL EQUATION MEI FOR THREE-DIMENSIONAL SCATTERERS

Juan M. Rius*, Eduard Úbeda, Josep Parrón, Angel Cardama
Dpt. Teoria del Senyal i Comunicacions, Universitat Politècnica de Catalunya,
Campus Nord UPC, Edifici D-3, Jordi Girona, 1-3,
08034 - BARCELONA, Spain

Boundary element methods (BEMs) are widely used for the numerical analysis of electromagnetic radiation and scattering. However, their application to three-dimensional (3-D) scatterers is limited to electrically small or resonant size objects due to the fact that the computational requirements increase rapidly with the electrical size.

Recently, several techniques have been proposed to reduce the computational cost of BEMs. These new techniques are commonly based on iterative solution of the system of equations, where the matrix-vector products are optimized either exploiting the physical or mathematical properties of the matrix or using sets of basis and testing functions that radiate narrow beams and thus produce almost-sparse impedance matrices. Most of this techniques share a common limitation: the application to 3-D arbitrary boundaries is difficult due to the use of analytically derived transformations that depend on the topology of the boundary.

A new approach, called the integral equation MEI (IE-MEI), is an approximate sparse matrix boundary element method in which the matrix coefficients are numerically derived (J.M. Rius, Elect. Lett., vol. 32, no. 1, pp. 23-23). This allows easy application to 3-D arbitrary surfaces.

The figure below shows the bistatic RCS of an sphere of diameter equal to one wavelength discretized in 512 triangles. Basis functions are Rao, Wilton and Glisson triangle pairs, with 768 unknowns. The sparsity of the matrices is 4.5% and the memory usage is less than 2 MB. The IE-MEI computation is compared with the MoM solution and the exact spherical Bessel functions series, showing excellent agreement.

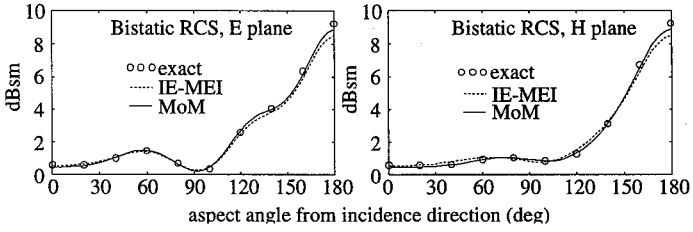

Concurrent Implementation of the Complementary Operators Method

Omar M. Ramahi
Digital Equipment Corporation
PKO3-1/R11, 129 Parker St.
Maynard, MA 01754, U.S.A.
ramahi@poboxa.enet.dec.com

The Complementary Operators Method (COM) was introduced as a mesh truncation technique for open region Finite Difference Time Domain (FDTD) simulations [Ramahi, *IEEE Trans. Antennas Propagat.* 43:697-704, 1995]. The basic premise of COM is the cancellation of the first order reflections that arise from the terminal boundaries which truncate the computational domain. This cancellation is made possible by averaging two independent solutions of the problem. The two solutions are obtained by imposing boundary operators that are complementary to each other in the sense that the errors generated by the two operators are equal in magnitude but 180° out of phase.

Although COM requires two independent FDTD simulations, which result in doubling the operation count, it was still found to be highly effective and more efficient than other available mesh truncation techniques. Ideally, however, one would like to perform the averaging of the two complementary solutions at the boundary and in a single simulation. If this was possible, then not only will the operation count remains unchanged, but also first order reflections will be canceled, leading to the elimination of all subsequent secondary reflections. This effectively creates an exact local boundary operation. Is such complementary operation possible?

In this presentation, we show that the concept of COM can be applied to the fields at locations close to the boundary. By performing the averaging concurrently, i.e., for each time step, a filtering effect is created which insures that the fields away from the boundaries are not contaminated with any artificial reflections. This operation produces a local boundary condition that is highly accurate and efficient. The "exactness" of this boundary operation will be discussed within the analytical, discretized and numerical contexts. In addition, representative examples will be discussed showing the performance of this new boundary operation in comparison to other mesh truncation techniques.

URSI B **Session 129** **Salon Duluth**

Microstrip Antennas
Co-chairs: H. Nakano, Japan and D. Jackson, USA

13:10 129.1 Analysis and Optimization of a "Yagi-Like" Printed Stacked Dipole Array for High Gain Applications, **A. HOORFAR**[1], R.J. TETI[2], [1]*Villanova University, Villanova, PA and* [2]*Lockheed Martin Government Electronic Systems, Moorestown, NJ, USA*

13:30 129.2 An Adaptive Multibeam Microstrip Antenna Array for PCS, **X. YU**, Z. LI, C. WU, J. LITVA, *McMaster University, Hamilton, ON, Canada*

13:50 129.3 Efficient Design of Printed Circuit Antenna Systems Based on Macromodeling Concepts, **K.F. SABET**[1], K. SARABANDI[2], L.P.B. KATEHI[1], [1]*EMAG Technologies, Inc. and* [2]*University of Michigan, Ann Arbor, MI, USA*

14:10 129.4 Performance Characteristics of Large Arrays in Microstrip and Inverted Microstrip Configurations, R. CHAITANYA BABU[1], **L. SHAFAI**[1], D.J. ROSCOE[2], A. ITTIPIBOON[2], [1]*University of Manitoba, Winnipeg, MB and* [2]*Communications Research Centre, Ottawa, ON, Canada*

14:30 129.5 New Dual-Band Single-Fed Printed Antennas, **H.F. HAMMAD**[1], A.P. FREUNDORFER[1], Y.M.M. ANTAR[2], [1]*Queen's University and* [2]*Royal Military College of Canada, Kingston, ON, Canada*

14:50 129.6 High Gain Microstrip Phased Array Antenna for MMWave Applications, **R. TELIKEPALLI**, E. BOCH, *Lockheed Martin Canada, Kanata, ON, Canada*

15:10 Coffee Break

15:30 129.7 Horizontally Polarized Microstrip Patch Array Operating at 18.86-19.26 GHz, **C. WU**, L. ZHAONIAN, M. NGUYEN, J. LITVA, *McMaster University, Hamilton, ON, Canada*

15:50 129.8 Linear Imaging Arrays for Millimeter-Wave Applications, **A.J. PARFITT**, *University of Adelaide, Australia*

16:10 129.9 An Aperture-Coupled Microstrip Array for PCS Shaped-Beam Basestation Antennas, **H. KIM**[1], K. KIM[1], S. HONG[2], W. YEO[1], [1]*Hanyang University and* [2]*Korea Mobile Telecom, Seoul, Korea*

B129.1

ANALYSIS AND OPTIMIZATION OF A "YAGI-LIKE" PRINTED STACKED DIPOLE ARRAY FOR HIGH GAIN APPLICATIONS

Ahmad Hoorfar*
Department of Electrical and Computer Engineering
Villanova University, Villanova, PA 19085

Richard J. Teti
Lockheed Martin, Government Electronic Systems, Moorestown, NJ 08057

The Yagi-Uda array of wire dipoles are widely used in communications and radar for high-gain applications. A typical three element Yagi array with optimized dimensions can achieve a gain as high as about 10 dBi. Although the Yagi-array has a relatively simple structure made of thin-wire elements, its overall length could become very large for high gain and/or low-frequency applications mainly due to the large number of directors and the required spacing between the elements. In addition, a mast must be used to structurally support the array elements in air.

In this paper we propose two alternative high-gain structures that alleviate the above disadvantages of a conventional Yagi array. Structure I, shown in the figure, is a multi-layer printed-circuit version of the Yagi array in air; it consists of a reflector, a driver and a finite number of embedded director strip elements. Structure II is a microstrip version of the array in the figure and has a ground-plane in place of the reflector element.

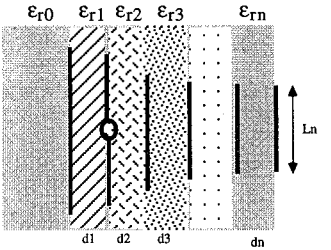

A printed Yagi Array in a multi-layer dielectric medium

These structures give a few more degrees of freedom (i.e., the dielectric constants of the layers) when optimizing their design. They can also be made conformal to curved surfaces. Due to the presence of the ground-plane, the structure II is expected to provide a higher directivity than the structure I, at the expense of a smaller bandwidth. We have used a spatial-domain moment method solution to develop a numerical model for optimum design of these "Yagi-like" arrays. For a given resonance frequency and a given number of dielectric layers, the optimization is performed with respect to the lengths of the radiating elements as well as the dielectric constants and thickness of the layers. It is found that it is possible to obtain high gain from these structures without a need for a high permittivity layer as is the case when only a single microstrip element is used and the dielectric layers are chosen according to a resonance condition (Jackson and Alexopoulos, IEEE Trans. Antennas Propagat., pp. 976-987, Sept.1985). For the case of a three layer medium with $\varepsilon_{r1}= \varepsilon_{r2}= \varepsilon_{r3} =2$, gains of approximately 9 and 11 dBi are obtained for structures I and II, respectively. In this example the total thickness is about 0.6 wavelength in the dielectric. Other examples involving 4 and 5 layer structures will be discussed in the presentation.

An adaptive multibeam microstrip antenna array for PCS

X. Yu, Z. Li, C. Wu and J. Litva
Wireless Technology Group
Communications Research Laboratory
McMaster University
Hamilton, ON, Canada, L8S 4K1
E-mail: yu@aerostar.crl.mcmaster.ca

The spatial filtering properties of adaptive antenna arrays in wireless communications makes it possible to confine the radio energy associated with a given user to a small addressed volume. Here, we summarize the work we have done to exploit the capability of a multibeam antenna array. A multibeam antenna system is built aiming for use in Personal Communication System (PCS). Such an antenna system has the advantage of low cost and robustness while maintaining fairly impressive performance compared to an omnidirectional and sectorized base station antennas. It has multiple beams that can be switched on and off. By selecting the appropriate beams for each user (both receive and transmit), the antenna system can increase CIR (or SINR) as well as reduce the fading rate. By scanning the changing of both incoming signals and interferences, this system adaptively assign appropriate beams to keep track of the movement of the mobile users.

It consists mainly of 4-element microstrip antenna array, beamforming network, repeaters and 10-db directional couplers, microwave switches, RF amplifier and detector, control and scanning circuits and amplifiers. The four microstrip antennas are mounted on one side of the box which houses the rest part of the system. The main beam width of each beam covers 22.5°. 90° angle range is covered with the 4 beams.

one of the major challenges is to maintain equal coverage in angular range for each beam covering 90°,which is 22.5° for this case, low sidelobe levels, and identical radiation pattern of each beams with regard to characteristics such as mainbeam width, mainbeam gain, sidelobe levels, etc .

Another thing which is worth mentioning here is scanning speed and switching rate. As the scanning and switching beam process is how the antenna system modifying the beam direction to allow the mobile to keep the link with the fixed base station while moving, one would intuitively think that the faster the scanning speed and the higher the switching rate, the better the system would performance. But this is not the case. Our computer simulation as well as the real measurement, all show there is a limit upon which the performance actually deteriorate when the scanning speed and switching rate go over a certain level. The actual values of that level is dependent heavily on the environment in which the system operates. one of the main reasons for this is that the noise introduced by switching beams actually increase with the rate of switching. The other reason is that signals strength from the mobile (and to mobile as well) fluctuates. The use of our antenna system greatly reduce the fading rate, and signal levels fluctuate less rapidly. Too fast scanning speed would result in too frequent switching of beams which is the result of the scanning catching up with the fluctuation of the signal, which is not desirable because it gives false switching as well as increase noise introduced by switching. We are not going into details here but this is a important finding we got when building this antenna system.

The antenna array we built covers 90° angle range, but it can readily be incorporated into situations where more than 90° coverage is needed. For example, for a 360° full coverage, one can use 4 of this kind of antenna array arranged properly. As a next stage research, a 8-element multibeam microstrip antenna array will be built with extensive capabilities of digital signal processing (DSP) and power control.

B129.3

EFFICIENT DESIGN OF PRINTED CIRCUIT ATNENNA SYSTEMS BASED ON MACROMODELING CONCEPTS

Kazem F. Sabet†, Kamal Sarabandi‡, and Linda P.B. Katehi‡

† EMAG Technologies, Inc., 2901 Hubbard Rd., Suite E-116, Ann Arbor, MI 48106
‡ Department of Electrical Engineering and Computer Science, The University of Michigan, Ann Arbor, MI 48109-2122

Abstract. The accuracy in the design of printed circuit antenna systems highly depends on the accurate modeling of the electromagnetic couplings not only among the radiating elements alone but also among these elements and various components of the antenna feed circuit. Such couplings affect both near-field and far-field characteristics of the antenna system. In complex printed antenna arrays, the full-wave modeling of these effects oftentimes amounts to sophisticated large-scale numerical problems. The scope of the computational effort needed for the solution of such problems is hardly amenable to a fast iterative design or optimization process. When quasi-static or other approximate CAD models prove inadequate, the antenna designer has no choice other than resorting to a tedious design-through-analysis approach based on the repetitive numerical simulation of the system.

This paper addresses the current pressing need for a fast and efficient design methodology for printed circuit antenna systems, which preserves the accuracy and rigor of full-wave electromagnetic modeling. To this end, some basic concepts of the macromodeling theory are borrowed from CAD-based electronic circuit design. Invoking general principles of dimensional analysis, almost real-time macromodels are developed for various radiating antenna elements and feed circuit components. These macromodels, which are computationally very simple and efficient, are constructed from full-wave simulation data, and therefore provide the same level of accuracy as a direct numerical simulation. Although appearing very tempting, the macromodels have a limited range of validity especially as the relevant parameter space becomes large. But this is also the case in most design situations, where a variety of physical and manufacturing constraints often limit the scope and range of various design parameters. The full-wave macromodels of the radiating elements and circuit components are interconnected in a multiport microwave network context. The interconnection takes into account the coupling among the various segments of the overall structure. Both near-field and far-field response of the antenna system can be simulated in this manner.

In this paper, we apply the macromodeling approach to the design of a printed microstrip patch antenna array. A typical corporate feed circuit is considered for the excitation of the array. The coupled patches and various microstrip discontinuities such as bends and T junctions are mocromodeled using full-wave numerical data. Some of the underlying design parameters include the permittivity and thickness of the substrate and various geometrical aspect ratios concerning the radiating patches or microstrip feed lines. The result of the macromodel-based design is validated by direct full-wave numerical simulation of the overall geometry using a wavelet-based sparse moment method (MoM) code, which is described in a separate paper submitted to this symposium.

Performance Characteristics of Large Arrays in Microstrip and Inverted Microstrip Configurations

R. Chaitanya Babu, L. Shafai, D. J. Roscoe*, and A. Ittipiboon*

Department of Electrical and Computer Engineering
University of Manitoba,
Winnipeg, Manitoba R3T 5V6, Canada

* Communications Research Centre
3701, Carling Avenue
Ottawa, Ontario K2H 8S2, Canada

Microstrip antenna arrays have been used extensively in a broad spectrum of applications including satellite communication and radar systems. In the design of large complicated microstrip arrays, the use of microstrip line feeding the array of patch elements leads to constructional simplicity. However, ohmic and dielectric losses and parasitic radiation associated with the feed network adversely affect the array characteristics, particularly at Ku/Ka band frequencies. Some investigations have been reported in the literature on the use of low loss dielectric image line and insular image guide as feed structures for microstrip arrays. The main disadvantage of such configurations is the complexity involved in the design of power division networks for two dimensional arrays. On the other hand, a variant of microstrip line, i.e. inverted microstrip line has the advantages of lower conductor loss and compatibility with printed technology. For example, calculations have indicated that, for a line impedance of 50 Ohms, the conductor and dielectric losses in an inverted microstrip line are typically less than those in a microstrip by 1.4 dB/m at 15 GHz and 2.6 dB/m at 35 GHz.

The purpose of this work is to investigate and compare the performance characteristics of parallel series fed and corporate fed microstrip arrays of rectangular/square patches in conventional and inverted microstrip configurations. This study is intended to validate the achievable advantages of the inverted microstrip architecture.

B129.5

NEW DUAL-BAND SINGLE-FED PRINTED ANTENNAS

H.F.Hammad*, A.P.Freundrofer
Electrical and Computer Engineering
Queen's University , Kingston , Ont.

Y.M.M. Antar
Electrical and Computer Engineering
Royal Military College of Canada
Kingston, Ont., Canada

Considerable research has been carried out on methods for achieveing dual frequency operation as well as frequency agility for printed antennas. Techniques using multilayer patches, shorting posts, varactor diodes, multiple slots in rectangular patches, and inclined slot feeds have been used. Recently other techniques that combine spur-line band-stop filters (D. Sanchez-Hernandez and I.D. Robertson, IEEE. AP., Vol. 43, No. 2, pp.201-205, 1995) or aperture-coupled resonators (F.Croq and D.M. Pozar, IEEE. Trans. AP, Vol. 40, pp. 1367-1374, 1992) have been reported. The trend is toward practical attractive features such as reduction in size and ease of integration for possible MMIC applications.

In this paper dual frequency operation using the concept of spur-line band stop filters is examined and applied to two configurations of printed antennas that are suitable for MMIC applications. An aperture coupled patch is designed using modal analysis for the patch, combined with a spur-line filter, that can be optimized to control the frequency of operation. The filter sections are situated near the non-radiating edges of the patch and several designs have been considered and successfully simulated. In the second configuration, a CPW (coplanar waveguide) - fed slot loop antenna, with the spur-line filter also, inside the loop is considered. CPW offers several advantages over conventional microstrip lines, and the antenna structure has the advantage of easier integration with solid state devices for MMIC's applications. Several configurations were designed and simulated around 35 GHz. Both antenna configurations are being fabricated and tested. Results should provide useful insight into the operation and design of these type of antennas.

HIGH GAIN MICROSTRIP PHASED ARRAY ANTENNA FOR MMWAVE APPLICATIONS

Radha Telikepalli* and Erik Boch
Lockheed Martin Canada
3001 Solandt street
Kanata, Canada

Development of microstrip phased array antennas poses a challenging problem at millimeter wave frequencies. This is due to several factors that include feed losses, issues of bandwidth, cost testability. Bandwidth enhancement techniques that are applicable at lower frequencies may not be applicable at these frequencies. Advantages of this approach are the low profile, economical solution with a proper choice of materials, and the feasibility of interface with other appropriate electronics.

The objective of this work is to develop a 28 GHz phased array antenna with a high gain of 30 dB by means of a pencil beam. To minimize the feed losses, a series feed has been chosen. Measures were taken to limit dispersion in the frequency range of interest. The array was linearly polarized with a bandwidth of 3% and a cross polarization level of more than 30 dB.

The present paper gives the design of the antenna from sub array level, feed network and designed patterns. The paper also presents technical difficulties encountered in development.

B129.7

Horizontally Polarized Microstrip Patch Array Operating at 18.86-19.26 GHz

C. Wu, L. Zhaonian, M. Nguyen, J. Litva

Communications Research Laboratory, McMaster University

1280 Main Street West, Hamilton, Ontario, Canada L8S 4K1

1 Abstract

Cochannel interference in a cellular system may be decreased by replacing a single omni-directional antenna at the base station by several directional antennas, each radiating within a specified sector. By using directional antennas, a given cell will interfere only with a fraction of the co-channel cells. In our case, the cell is partitioned into four 90° sections.

A waveguide-fed linear series array of corner-fed square patches with horizontal polarization is proposed to realize a broad-band antenna with high efficiency and low cross polarization. A waveguide to microstrip line transition was also built to interface a waveguide with the antenna's microstrip feed network. High efficiency is achieved by having proper impedance matching throughout the array. The beam pattern of the antenna in H-plane has a 90° beamwidth at broadside direction. The antenna elements are mounted on a low dielectric constant RT Duroid subtrate ($\epsilon_r = 2.33$) in order to increase the bandwidth and the radiation efficiency.

The paper consists of three sections. In the first section, the theoretical design of the antenna element with the aid of FDTD (Finite Difference Time Domain) method was discussed. In addition, coupling effect between the elements was studied to determine the spacing between the elements in the array. Array pattern was then synthesized in the next section to provide the necessary weight of each element in the array. From the weighting factor, the feed network was calculated as a tapered linear series' array. The next section contains results of the analysis and experiments.

Linear Imaging Arrays for Millimeter-Wave Applications

Andrew J. Parfitt

Department of Electrical and Electronic Engineering
The University of Adelaide
South Australia 5005

Abstract

A number of imaging applications may be usefully supplemented by millimeter-wave technology to take advantage of the propagation characteristics at millimeter wavelengths. For commercial applications, a low cost technology is desirable, and passive millimeter-wave imaging may provide a compact, low-cost and low-power system. For some collision avoidance and proximity sensing systems a linear array providing azimuthal resolution of a few degrees may be suitable for reliable detection provided that sufficient sensitivity can be achieved.

In this paper an antenna array, beamforming network and receiver on a single substrate is described. A 37GHz prototype and 5GHz scaled test circuit are described. Consideration is given in the design to the following factors:

- architectural considerations and housings.
- low-cost fabrication on hard or soft substrates and associated resolution and surface condition issues.
- antenna design for 20% bandwidth on relatively thick, high permittivity substrates.
- planar constrained lens beamforming for multi-receiver systems.
- millimeter-wave losses, transmission line and integrated amplifier considerations.
- detection and direct-conversion receiver circuits for testing and operation.
- potential for active enhancement in radar-like systems.
- simple post-detection processing systems.

This paper focuses on the design of the antenna array and a Rotman Lens beamforming network to provide ten beams for testing purposes. Some preliminary results will be presented that indicate the feasibility and limitations of such systems.

B129.9

An aperture-coupled microstrip array for PCS shaped-beam basestation antennas

Hyeongdong Kim, Kwangjo Kim, Woonsik Yeo* and Seongcheol Hong**
*Hanyang University, Dept. of Radio Science and Eng., Seoul, Korea
**Korea Mobile Telecom, Digital Cellular Div., Seoul, Korea

This paper presents a design and fabrication of a shaped-beam antenna which will be used for CDMA PCS (personal communication service) basestation; 1.725 Ghz for receiving and 1.815 Ghz for transmitting, respectively. In the mobile cellular communication, a basestation antenna is required to radiate electromagnetic energy uniformly inside the service cell than having a high directive gain in the special direction. The basestaion antenna is also required to radiate at as low a level as possible toward the adjacent cell. In this work, a shaped beam antena having the above-mentioned characteristics is developed using 7 element aperture-coupled microstrip arrays. The required beam shape can be obtained by an antenna array of elements that are fed with unequal amplitudes and phases which are synthesized by a antenna synthesis method. A modified Woodward Lawson method has been used. Mutual coupling between array elements has been taken into account in the designs. To provide the synthesized unequal amplitudes and phases for each array elements, the feed network has been designed by employing unsymmetrical Wilkinson power divider and delayed transmission lines.

In the presentation, we will present the detailed design procedures and the measured beam pattern of the developed shaped beam antenna. The preliminary measurements show that the interfering sidelobe level is below -20 dB and the pattern is of the cosecant squared beam without null (refer to Fig. 1).

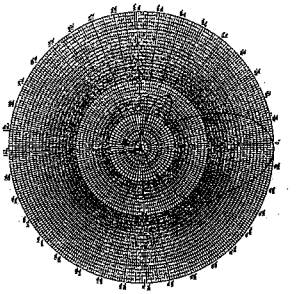

(Fig. 1) Measured vertical (E-plane) beam pattern of the developed shaped-beam antenna (f=1.815 Ghz).

URSI B | Session 139 | Salon Richelieu

Transient Propagation and Scattering in Dispersive Media
Co-chairs: V.N. Bringi, USA and S. Saoudy, Canada

13:10	139.1	Operational Options for Forward and Inverse Born-Type Scattering Using Pulsed Beam Pre- and Post-Processing Strategies, **T. MELAMED**[1], E. HEYMAN[2], L.B. FELSEN[1], [1]*Boston University, Boston, MA, USA;* [2]*Tel-Aviv University, Tel-Aviv, Israel*
13:30	139.2	The Scattering of Long and of Short Radar Pulses from Wires and from Chaff, Y. GUO[1], H. ÜBERALL[2], **Y.J. STOYANOV**[3], A.J. STOYANOV[3], [1]*Johns Hopkins Applied Physics Laboratory, Laurel, MD,* [2]*Catholic University of America, Washington, DC and* [3]*NSWC, West Bethesda, MD, USA*
13:50	139.3	Bistatic Time-Domain Imaging of Radar Targets for Limited-View Reconstruction, **Y. DAI**, E.J. ROTHWELL, K.M. CHEN, D.P. NYQUIST, Y. HUANG, *Michigan State University, East Lansing, MI, USA*
14:10	139.4	A TD-UTD for Transient Radiation by Pulsed Antennas Placed Directly on a Smooth Convex Surface, **H.T. CHOU**[1], P.H. PATHAK[1], P. ROUSSEAU[2], [1]*Ohio State University, Columbus, OH and* [2]*Aerospace Corporation, El Segundo, CA, USA*
14:30	139.5	Wavepacket Propagation in an Inhomogeneous Plasma, **G. SAMELSOHN**, R. MAZAR, *Ben-Gurion University of the Negev, Beer-Sheva, Israel*
14:50	139.6	Transmission and Reflection of Normally Incident, Electromagnetic, Finite-Cycle Sine Waves on a Lorentz Half Space, **E.L. MOKOLE**, S.N. SAMADDAR, *Naval Research Laboratory, Washington, DC, USA*
15:10		Coffee Break
15:30	139.7	Analysis of the Depletion of the Spectral Components of the Modified Power Spectrum Pulse, A.M. SHAARAWI[1], M. ABDEL-RAHMAN[2], **I.M. BESIERIS**[2], [1]*Cairo University, Giza, Egypt;* [2]*Virginia Polytechnic Institute and State University, Blacksburg, VA, USA*
15:50	139.8	A Comprehensive Analysis of Propagation of Localized Wave Pulses in Collisionless Plasma Media, M. ABDEL-RAHMAN[1], **I.M. BESIERIS**[1], A.M. SHAARAWI[2], [1]*Virginia Polytechnic Institute and State University, Blacksburg, VA, USA;* [2]*Cairo University, Giza, Egypt*
16:10	139.9	Transient Polarisation and Charge of Condencor with Unsettled Dielectric Parameters, **A.L. GUTMAN**, *Voronezh State Forestry Engineering Academy, Voronezh, Russia*
16:30	139.10	Short Pulses Dispersion and Attenuation in the Dielectric Media with Unsettled Parameters, **A.L. GUTMAN**, *Voronezh State Forestry Engineering Academy, Voronezh, Russia*
16:50	139.11	Numerical Description of the Wave Packet Propagation in Time Dispersive Media Via Nonstationary Parabolic Wave Equation, **V. KOPEIKIN**, *IZMIRAN, Moscow, Russia*

B139.1

Operational Options for Forward and Inverse Born-Type Scattering Using Pulsed Beam Pre- and Post-Processing Strategies

T. Melamed[1], E. Heyman[2], L.B. Felsen[1]

[1]Dept. of Aerospace and Mechanical Engineering, and the Dept. of Electrical and Computer Engineering, Boston University. Fax: (617)-353-5866.

[2]Dept. of Electrical Engineering – Physical Electronics, Tel-Aviv University, Israel. Fax: +972-3-6423508, e-mail: heyman@tau.eng.ac.il.

Recent activities in forward and inverse scattering of electromagnetic waves by complex environments have emphasized the importance of short-pulsed time domain (TD) interrogation because of the high spatial-temporal localization achieved thereby, which is enhanced further if the incident signal is a pulsed beam (PB) wavepacket. When coupled to pre- and post-processing in the (space-time) - (wavenumber-frequency) phase space, which takes advantage of the concept of slant-stacked (SS) tomography, the forward and inverse localized interrogation strategy is pushed to its ultimate potential [T. Melamed, E. Heyman and L.B. Felsen, PIERS 1997;to be submitted to IEEE Trans. Antennas Propagat.]. The versatility of this procedure with respect to weak (Born-type) scattering is explored here further, with emphasis on the resolution achieved when exercising various options. The algorithm is based on TD-PB interrogation (pre-processing), which can direct the incident wavepacket to any region in the scattering environment and place the observer at an arbitrary location. Due to the degree of localization in the pre- and post-processing, the entire 3D scattering process reduces approximately to a pseudo-1D process along the beam axes. Moreover, it is found that the incident-scattered PB configuration arranges itself along Fermat ray paths which modal the space-time scattering phenomenology as reflection from a pseudo-1D stratified scattering cell oriented along the bisector between the incident and scattered beam. Taking advantage of this approximated pseudo-one-dimensionalization along the beam axes, the forward and inverse scattering algorithms can be reduced explicitly to closed forms. The present contribution examines the advantages and drawbacks, especially as regards resolution, associated with various options in the direct and inverse procedures: obliquity in the Fermat pseudo-reflection process, beam width (processing window), etc., either individually or in some hybrid combination.

THE SCATTERING OF LONG AND OF SHORT RADAR PULSES FROM WIRES AND FROM CHAFF

Yanping Guo+, H. Überall++, Y. J. Stoyanov*, and A. J. Stoyanov

Carderock Division, NSWC
9500 MacArthur Boulevard
West Bethesda, MD 20817-5700, USA

+ Johns Hopkins Applied Physics Laboratory
Laurel, MD 20723, USA

++Department of Physics, The Catholic University of America
Washington, DC 20064, USA

We present the results of a calculation of the transient response to incident radar pulses of perfectly conducting wires, and its extension to chaff clouds consisting of multiple, randomly distributed and oriented wires (modeled by several thousands of wires of equal length). While some of our short-pulse results were presented earlier at some conferences (AMEREM at Polytechnical University and at Albuquerque), we here discuss in addition the effects encountered in the scattering of long pulses from chaff clouds.

For the case of single wires, wide-band pulses lead to a well-defined series of multiple returns that are a superposition of decaying sinusoids representing the response of each resonating mode; they can be interpreted as the radiation of pulses of traveling waves (Y. Guo and H. Überall, J. Electromag. Waves Applic. 8, 355, 1994) that reradiate from the wire ends as the traveling waves get reflected at the wire ends. Narrow-band pulses, however, exhibit the individual mode resonances which in turn can be interpreted as the in-phase superposition of traveling-wave components that form standing waves between the wire ends.

For the case of a chaff cloud, wide-band pulses lead to a superposition of multiple pulse returns from all wires in the cloud that in the time domain combine to a quasi-continuum of an extent that depends on the size of the cloud. Fourier analysis of this continuous echo, however, clearly reveals the existence of the individual wire resonances in frequency space. Narrow-band pulses, on the other hand, lead to a superposition of specular reflections from the individual wires in the time domain (again a quasi-continuum), followed this time by the superposed ringing (decaying sinusoids) of the individual wires if the incident carrier frequency coincides with their resonant frequency.

B139.3

Bistatic Time-Domain Imaging of Radar Targets for Limited-View Reconstruction

Y. Dai*, E.J. Rothwell, K.M. Chen, D.P. Nyquist and Y. Huang
Department of Electrical Engineering
Michigan State University
East Lansing, MI 48824

The development of viable short-pulse radar systems has renewed interest in target imaging performed directly in the time-domain with temporally measured signals. The short-pulse response of a target provides significant information about the positions and strengths of scattering centers. If observations are made over a wide range of aspect angles, sufficient information is gained to obtain an image of the target. A time-domain imaging technique has been developed based on a space-time magnetic field integral equation, using a sine modulated exponential pulse, and employing the inverse Radon transform. Images of various aircraft models were created from measured target responses over a wide band of frequencies and over the entire range of aspect angles.

In this paper, we will extend the approach to the more practical case of the limited-view problem. Image reconstruction from limited-view data has been extensively studied by many researchers in the area of computed tomography. Among those methods, the method of projection onto convex sets (POCS) in particular has shown great flexibility in dealing with known geometric constraints and with noise. The basic principle of POCS is that each piece of a priori knowledge must be represented by a convex set onto which the current image estimate can be projected. It has been shown that if the intersection of these convex sets is nonempty then the sequence of cyclic projections will converge weakly to a point in this intersection. We will extend this method to radar imaging, combining it with linear prediction. Since the scattered field of a target can be written as a superposition of distinct specular reflections arising from scattering centers on the target, the trace of the scattering centers can be predicted using linear prediction with the change of the observation angle. Thus the missing data may be predicted before reconstructing the image by POCS.

Examples will be generated using scatted field data measured in the Michigan State University scattering laboratory. The time-domain responses of several aircraft targets will be synthesized from ultra-wideband measurements (2-18 GHz) using the inverse Fourier transform. Measurements will be made within a plane for varying azimuthal aspect angle, producing images corresponding to the thickness of the target.

A TD-UTD for Transient Radiation by Pulsed Antennas Placed Directly On a Smooth Convex Surface

H.T. Chou*, P.H. Pathak and P. Rousseau†
The Ohio State University ElectroScience Laboratory
1320 Kinnear Road, Columbus, Ohio 43212, USA
† Aerospace Corp., El Segundo, Calif., USA

Recently, a time domain (TD) version of the uniform geometrical theory of diffraction (UTD), or TD-UTD, has been developed for analytically describing the transient electromagnetic scattering by a perfectly conducting arbitrary curved wedge, and arbitrary smooth convex surface, respectively when each of these is excited by an arbitrary time impulsive astigmatic wavefront (P.R. Rousseau, Ph.D. dissertation, Dept. of Electrical Engineering, The Ohio State Univ., Columbus, Ohio, USA, 1995). These TD-UTD solutions have been constructed from the corresponding frequency domain UTD solutions by an application of the analytic time transform (ATT). The advantage of the ATT is that it avoids some of the serious difficulties that result in the use of conventional Laplace/Fourier inversion techniques. Furthermore, the ATT allows one to essentially obtain a closed form (as opposed to numerical) convolution when the TD-UTD response to a realistic finite energy pulse excitation is to be obtained from the TD-UTD response to a time impulsive excitation; this is a significant advantage which maintains the efficiency of the TD-UTD ray analysis. In addition, TD-UTD employs the same ray paths as in the UTD, and like the UTD it remains uniformly valid across the geometrical optics shadow boundary transition regions. In this paper, the TD-UTD is extended to analyze another important situation, namely that of analytically predicting the transient radiation by elemental pulsed antennas located directly on a perfectly conducting arbitrary convex surface. While the previous TD-UTD scattering solutions were restricted to source and observer both sufficiently far from the wedge or smooth convex surface, the present TD-UTD radiation solution allows for the pulsed source to lie directly, and hence conformally, on the convex surface while the observer is located sufficiently far from the convex surface. This new TD-UTD solution is also obtained from the corresponding frequency domain UTD solution via the use of ATT when the elemental (point) antennas are excited as a step function in time. The major difficulty in the development of the TD-UTD analysis here is due to the presence of the radiation type Fock integrals in the frequency domain UTD fields which are to be inverted into the TD via ATT. However, this latter step in the analysis can be performed in a manner somewhat analogous to that developed earlier for the TD-UTD solution for scattering by a smooth convex object. It is noted that the UTD Fock function for scattering are different from those of the UTD radiation Fock functions which provide a uniform ray solution for this radiation problem of interest in the present paper. Some numerical results illustrating the utility of this TD-UTD solution will be presented. The TD-UTD analysis of more general conformal antennas on a convex body can be obtained via an appropriate superposition of the response to the elemental antennas.

B139.5

WAVEPACKET PROPAGATION IN AN INHOMOGENEOUS PLASMA

Gregory Samelsohn and Reuven Mazar

Department of Electrical and Computer Engineering,
Ben-Gurion University of the Negev, Israel

In this work we consider the propagation of transient waves in an inhomogeneous plasma. We start with the so-called plasma wave equation,

$$\nabla^2 G - c^{-2}\partial_t^2 G - k_p^2(\mathbf{R})G(\mathbf{R},t|\mathbf{R}_0,t_0) = -\delta(\mathbf{R}-\mathbf{R}_0)\delta(t-t_0)\,, \qquad (1)$$

which describes approximately the propagation of a transverse electromagnetic wave in a cold plasma with fluctuating electronic concentration, when electron collisions and static magnetic fields are negligible. To solve Eq. (1) we apply the method of proper time, originally proposed by Fock for the integration of quantum mechanical equations (V. Fock, Sow. Phys. **12**, 404-425, 1937). The method is based on the introduction of an additional pseudotime variable τ and a transfer to a higher-dimensional space, in which the propagation process is governed by the generalized parabolic equation

$$2ik\partial_\tau g + \nabla^2 g - k^2\varepsilon(\mathbf{R})g(\mathbf{R},\tau|\mathbf{R}_0,\tau_0) = 0\,, \quad \tau > \tau_0 \qquad (2)$$

which coincides formally with the nonstationary Schrodinger equation in quantum mechanics. Defining initial condition $g(\mathbf{R},\tau_0|\mathbf{R}_0,\tau_0) = \delta(\mathbf{R}-\mathbf{R}_0)$ and assuming an infinitesimally small absorption, it can be shown that the propagators of Eqs. (1) and (2) are connected by the following integral transform

$$G(\mathbf{R},t|\mathbf{R}_0,t_0) = \frac{i}{2k}\int_{\tau_0}^{\infty} d\tau h(t,\tau|t_0,\tau_0)g(\mathbf{R},\tau|\mathbf{R}_0,\tau_0)\,, \qquad (3)$$

where the kernel $h(t,\tau|t_0,\tau_0)$ describes the wave propagation in an one-dimensional *homogeneous* medium. Therefore the initial formulation is divided to the two independent problems. In the first one we consider the time evolution of the wavefield in a homogeneous medium, and exact results can be obtained for pulses having arbitrary shapes, including the Gaussian pulse with linear frequency modulation which is important in applications. The second problem is related to the propagation of a time-harmonic wave through an inhonogeneous medium. Since our formulation deals with the *parabolic* problem instead of the elliptic one, the solution of Eq. (2) can be presented in a form of the Feynman path integral, which provides an efficient technique for the analysis of wave propagation in random media (G. Samelsohn and R. Mazar, Phys. Rev. E **54**, 5697-5706, 1996). Using this formulation we investigate asymptotic behavior of the wavefield in a weakly inhomogeneous dispersive medium. As an example of the approach we consider the mean intensity of a pulse wave propagating in a plasma with fluctuating electronic concentration.

TRANSMISSION AND REFLECTION OF NORMALLY INCIDENT, ELECTROMAGNETIC, FINITE-CYCLE SINE WAVES ON A LORENTZ HALF SPACE

E. L. Mokole
S. N. Samaddar
Radar Division (Code 5340)
Naval Research Laboratory
Washington, DC 20375-5336

One dimensional propagation of a normally incident, electromagnetic, finite-cycle sine wave on an isotropic, spatially homogeneous, dispersive half space is investigated analytically and numerically. The medium is characterized by a single-resonance Lorentz model of the refractive index. Past formulations at optical frequencies by Sommerfeld, Brillouin, and Oughstun and Sherman are generalized. These formulations ignore the field outside the medium by specifying the field at the medium's boundary and analyze the transmitted field under the assumption that the transmission coefficient is unity. The generalizations are: (1) a formulation that is applicable to propagation at any frequency for which the Lorentz model of a dispersive medium is appropriate; (2) accommodating a source external to the medium; (3) accounting for reflection from the medium; and (4) inclusion of a frequency-dependent transmission coefficient in the transmitted field. Moreover, inclusion of the reflection coefficient provides a diagnostic capability for learning about the dispersive medium. Also, early-time and high-frequency representations of the reflected field are obtained, and the high-frequency approximation is shown to subsume a previous approximation of Colby by including attenuation from absorption as well as additional terms.

The inversion integral for the time-domain reflected field is presented in terms of pole contributions and branch-cut integrals which are computed numerically; whereas the uniform asymptotic methodology of Oughstun and Sherman is applied to the transmitted field. An example shows that contributions from the reflection and transmission coefficients should not always be ignored, even at optical propagation frequencies. Specifically, for Brillouin's choice of the medium's physical parameters, the reflected field has a peak value which is 21% of the incident field's amplitude and which corresponds to a 21% decrease in the main signal (pole contributions) of the transmitted field when the transmission coefficient is unity. In addition, contributions to the transmitted field from the distant saddle points (Sommerfeld precursor) are shown to be negligibly affected by including the transmission coefficient that differs from unity.

B139.7

ANALYSIS OF THE DEPLETION OF THE SPECTRAL COMPONENTS OF THE MODIFIED POWER SPECTRUM PULSE

Amr M. Shaarawi
Department of Engineering Physics and Mathematics
Faculty of Engineering, Cairo University
Giza 12211, Egypt

and

Mohamed Abdel-Rahman and Ioannis M. Besieris*
The Bradley Department of Electrical Engineering
Virginia Polytechnic Institute and State University
Blacksburg, VA 24061

The purpose of this analysis is to explain the mechanism of depletion of the spectral content of the modified power spectrum (MPS) pulse as it propagates away from its source plane. The generation and propagation of the MPS pulse has been thoroughly investigated by Ziolkowski who derived it as a weighted superposition of infinite energy focus wave modes (FWM). This synthesis yields a closed form, finite energy solution to the scalar wave equation in free space. In recent studies, a different approach of deriving finite energy localized wave (LW) pulses generated by flat dynamic apertures has been used. This approach uses a time-limited FWM wave field to excite a flat aperture characterized by a time-dependent radius. A localized wave generated from a "finite time" FWM aperture exhibits a slow decay as it travels away from its source plane and has finite energy content.

The decay in the amplitude of the centroid of the finite time FWM is attributed to the oscillations introduced into the ω windows centered around the various χ spatial spectral components. As the pulse travels to farther distances, the oscillations progressively remove the ω windows centered around the small χ values. This spectral depletion is different from that exhibited by quasi-monochromatic signals for which the oscillations are introduced over the entire χ spectrum. Since the MPS pulse is a finite energy superposition of FWMs, one expects that it should exhibit a spectral structure analogous to that of the finite time FWM. The most prominent features of such a structure are the spectral $\omega - \chi$ coupling and the form of the ω windows. The shape, width and χ - dependence of the ω windows strongly affect the spectral depletion of the propagating LW pulse and determine its decay behavior. In this work, the spectral structure of the MPS pulse is investigated in an attempt to determine its $\omega - \chi$ coupling and show how the associated ω windows affect the decay of the centroid of the propagating MPS wavefield.

A COMPREHENSIVE ANALYSIS OF PROPAGATION OF LOCALIZED WAVE PULSES IN COLLISSIONLESS PLASMA MEDIA

Mohamed Abdel-Rahman and Ioannis M. Besieris*
The Bradley Department of Electrical Engineering
Virginia Polytechnic Institute and State University
Blacksburg, VA 24061

and

Amr M. Shaarawi
Department of Engineering Physics and Mathematics
Faculty of Engineering, Cairo University
Giza 12211, Egypt

In this work, it is demonstrated that localized wave (LW) pulses propagating in dispersive media modeled by the Klein-Gordon equation display unusual decay patterns. This is especially true when a source spectral parameter k_s is tuned to the plasma frequency k_p of the medium. Under this provision, the radiated LW pulses exhibit decay rates slower than those characterizing analogous LW pulses traveling in free space. This slow decay rate is attributed to the extraordinary depletion of the spectral components of the LW pulses as the latter travel away from their source plane. Unlike quasi-monochromatic signals, the depletion of the spectral components of the carrier-free, ultra-wideband LW pulses is controlled by a coupling between the spatial and temporal spectral components. For the LW pulses studied in this work such a coupling includes the k_s parameter. The existence of this spectral parameter effectively places the ω windows scanning the spatial spectrum at higher values. As a consequence, the depletion of the spectral components is reduced. In turn, this results in a reduction of the decay rate of the centroid of the Klein-Gordon LW wavefield.

B139.9

TRANSIENT POLARISATION AND CHARGE OF CONDENCOR WITH UNSETTLED DIELECTRIC PARAMETERS

A.L.Gutman
Voronezh State Forestry Engineering Academy
Physics Department
RUSSIA 394613 Timiryazeva St, 8
fax: 7—0732—560—435
E—mail: olc@vlti.voronezh.su
mail to: RUSSIA 394000 Mira St, 3. apt 102

In the previous author's researches (A. Gutman. Reports of the Russian Academy of Sciences, v. 351, №2, November, 1996; A. Gutman. 25th General Assembly U.R.S.I., Lille, France, "Abstracts", p. 122, 1996) the transient polarization, dielectric coefficient and conductance were obtained for a dielectric with elastically tied charges at zero initial conditions. In this work we, first of all, obtain the generalized correlation between nonstaniory field and the polarization at general form for initial conditions. Secondly, we study the charge of the condencor with dielectric at the single step and rectangular pulse voltage. The obtained generalized correlation enables us to receive the integral equation for the field in the condencor. For the Laplace transformation of the field the equation is reduced to an algebraic one. Its solution has an exact inverse Laplace transformation. The resulting establishment is described by the sum of the four terms. The first term is the established field in the condencor, the three others describe the type of the establishment process. The correlations between these terms determine the dynamics of the correlation between the voltage in the condencor and on the inner resistance of the voltage source. There are two kinds of the establishment process:
1) all three terms are real ones and are three exponents with negative power, and
2) one term is a real function of time (exponential attenuation), and two others are complex conjugate ones (attenuation with oscillations).
These kinds are conditioned with the correlation between the time constant of the condencor without dielectric and microscopic parameters of dielectric. The numerical calculations highlight these dependences. In addition to this, we study the modification of the pulse form and duration in the condencor. The possibilities of the pulse form and duration optimization are considered.

B139.10

SHORT PULSES DISPERSION AND ATTENUATION IN THE DIELECTRIC MEDIA WITH UNSETTLED PARAMETERS

A.L. Gutman
Voronezh State Forestry Engineering Academy
Physics Department
RUSSIA 394613 Timiryazeva St., 8
fax: 7-0732-560-435
E-mail: olc@vlti.voronezh.su
mail to: RUSSIA 394000 Mira St., 3. apt. 102

This paper contains the continuation of previous author's researches (A. Gutman. Amerem-96, UWB, SP-3, Albuquerque, New Mexico, May 27-31, 1996, Abstracts, p. 264. A. Gutman. 25th General Assembly U.R.S.I., Lille - France, 1996, Abstracts, p. 122). In this work we obtain the generalized wave equation for the pulse propagation at general form of initial conditions in the dielectric media with unsettled parameters. The Laplace transformation method reduces this partial differential equation into the ordinary one. The Green function and solution of the equation for the Laplace transformation field is obtained. But a precise general inverse Laplace transformation of the solution is not obtained. Therefore, the approximate general methods for the inverse Laplace transformation are discussed; and where it is possible to obtain the inverse Laplace transformation, the particular examples are considered. These results are used to precise the formerly obtained estimations of the pulse dispersion and attenuation. It is found out that the pulse dispersion depends essentually on the establishment process phase, in which the action of the pulse back front begins. We study the impact of the pulse form and pulse dispersion upon the attenuation. The results obtained in the other paper (A. Gutman. Transient Polarization and the Charge of Condencor With Unsettled Dielectric Parametrers. Montreal, Canada, 1997) is also used here. On the basis of these results the comparison between pulse absorption in the lumped capacitance with dielectric and at the propagation in the dielectric media becomes possible. Together with dispersion and attenuation estimation precising, we find out the presence of partial energy return from a media to the pulse.

B139.11

Numerical description of the wave packet propagation in time dispersive media via nonstationary parabolic wave equation.

V. Kopeikin, IZMIRAN, Troitsk, Moscow region, 142092, Russia.

In time dispersive media, distortion of the wave packets take place. In case of one-dimensional propagation this effect manifests itself as longitudinal spread of the wave form. In 2D and 3D media this effect may be accompanied by the transversal shift of the packet. We will refer to this phenomenon as dispersive refraction.

Both these effects have the same nature because they are governed by a nonlinear relationship between frequency and the wave number in the dispersion equation. However, whereas the former one has been studied and widely used for the radar pulse compression, the latter one (transversal distortion of the wave packet in 2D and 3D media) is not investigated so far. For its description, the nonstationary parabolic wave equation can be applied.

In this paper, some results of numerical calculations of 2D wave packets via parabolic wave equation are presented. As a primary model wave equation taking into account dispersive properties of the propagation medium we use Klein-Gordon equation. A two-dimensional parabolic equation in Cartesian coordinates can be obtained by substitution into the primary equation a modulated plane wave Ansatz and neglecting the second derivatives with respect to time and longitudinal spatial coopdinate. In order to solve it numerically, we use finite-difference approximation.

We have calculated the propagation of 2D wave packets with transversal frequency modulation in homogeneous nondispersive and dispersive media. Numerical results show that all packets in a homogeneous nondispersive medium are propagating rectilinearly, being slightly diffused due to difraction. In dispersive media, both longitudinal spread and transversal shift of the wave packet take place.

URSI B **Session 141** **Salon Chaudière**

Scattering by 2 and 3D Dielectric Objects
Co-chairs: D.E. Wolfe, USA and P.L.E. Uslenghi, USA

13:10	141.1	Exact Solutions for Scattering from Vertical Half Planes above and in a Dielectric Half Space, **B.A. BAERTLEIN**, *Ohio State University, Columbus, OH, USA*
13:30	141.2	Electromagnetic Wave Scattering by Cracks - E Polarization Case, R. SATO, **H. SHIRAI**, *Chuo University, Tokyo, Japan*
13:50	141.3	Electromagnetic Plane Wave Scattering from a Perfectly Conducting Cube, **R.H. MacPHIE**[1], K.-L. WU[2], [1]*University of Waterloo and* [2]*COM DEV Ltd., Cambridge, ON, Canada*
14:10	141.4	Analysis of Scattering from a Cavity-Backed Aperture in a PEC Wedge Using a Multifilament Current Model, **P.-R. RENAUD**[1], J.-J. LAURIN[1], G. PELOSI[2], [1]*École Polytechnique de Montréal, QC, Canada;* [2]*University of Florence, Italy*
14:30	141.5	Scattering by a Cylinder and a Sphere Coated with a Layer of Isorefractive Material, **S. ROY**, P.L.E. USLENGHI, *University of Illinois at Chicago, IL, USA*
14:50	141.6	Inhomogeneous Plane Wave Scattering by a Polygonal Cylinder Embedded in a Lossy Medium, F. BERTONCINI[1], **G. MANARA**[1], P. NEPA[1], R.G. KOUYOUMJIAN[2], [1]*University of Pisa, Italy;* [2]*Ohio State University, Columbus, OH, USA*
15:10		Coffee Break
15:30	141.7	Oblique Incidence Scattering from Eccentric Cylinders, H.A. YOUSIF[1], **A.Z. ELSHERBENI**[2], [1]*University of Pittsburgh, Bradford, PA and* [2]*University of Mississippi, University, MS, USA*
15:50	141.8	EM Scattering by Two-Dimensional, Cavity-Backed Aperture in a Ground Plane, **G.K. GOTHARD**, S.M. RAO, *Auburn University, Auburn, AL, USA*
16:10	141.9	Electromagnetic Analysis of Cavity Structures with Aperture Opening Using the Method of Auxiliary Sources, **R. ZARIDZE**[1], D. KARKASHADZE[1], R. JOBAVA[1], D. ECONOMOU[2], N. UZUNOGLU[2], [1]*Tbilisi State University, Tbilisi, Georgia;* [2]*National Technical University of Athens, Greece*
16:30	141.10	Dual-Surface Electric-Field Integral Equation for Bodies of Revolution in Electromagnetic Scattering, **J.L. SCHMITZ**, *Rome Laboratory/ERCS, Hanscom AFB, MA, USA*
16:50	141.11	Extension of the Sheet Approximation to Electromagnetic Scattering by Thin Layers in the Earth, **I.G. IARMAKHOV**, S.B. POPOV, *Institute of Radioengineering and Electronics RAS, Moscow, Russia*

B141.1

Exact Solutions for Scattering From Vertical Half Planes Above and In a Dielectric Half Space

Brian A. Baertlein, ElectroScience Laboratory, Ohio State University
1320 Kinnear Road, Columbus, OH 43212

In this talk we derive exact solutions for diffraction by a vertical conducting half plane located above or in a lossy half space (see figure). The solution procedure is analogous to that used for diffraction by a half plane in free space, which is briefly reviewed. For the half-space problem novel spectral representations, described in a separate presentation, permit us to take a transform in the vertical coordinate. Next, we develop a generalized Wiener-Hopf (WH) method that is based on a modified Hilbert transform. The conventional Hilbert transform, which is implicitly based on the Fourier transform, has the property that it separates its image domain into disjoint sets. The modified Hilbert transform defined here has the same property, but it employs the spectral representation appropriate for the problem at hand. A significant problem encountered in applying the generalized WH method is development of a criterion that separates contributions from the half plane and from the aperture. (For the conventional WH method the criterion is analyticity in the upper and lower complex planes.) An analogous criterion is described and used to obtain exact integral expressions for the fields. Asymptotic evaluation of the integrals yields edge diffraction coefficients in which the effects of the half space are readily identified. It is shown that the solution satisfies the edge condition, and the cases of free space and a perfectly conducting half space are obtained as the appropriate limits. Numerical calculations of the diffracted components are presented for both the exact expression and a method of moments solution.

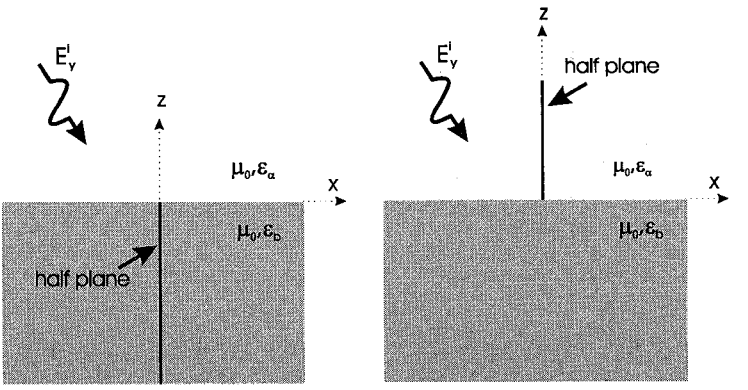

ELECTROMAGNETIC WAVE SCATTERING BY CRACKS
– E Polarization Case –

Ryoichi SATO and Hiroshi SHIRAI

Department of Electrical and Electronic Engineering
Faculty of Science and Engineering, Chuo University
1-13-27 Kasuga, Bunkyo-ku, Tokyo 112 Japan.

Identification and detection of defects on a material surface is one of the important tasks for industrial products. Even for a small crack, its existence may be fatal. In order to develop fast and reliable non-destructive test procedure using waves, one may need to understand behavior of wave scattering mechanism by cracks.

In this paper, electromagnetic plane wave scattering by cracks has been analyzed by utilizing the Kobayashi and Nomura's method, which is based on the characteristics of Weber-Schafheitlin's discontinuous integrals for Bessel functions. As the simplest model of cracks, the scattering by a narrow trough and thick slit has been studied here. In the previous investigation, we have already reported for H polarization case. In this paper, formulation for E polarization case will be derived.

For both geometries, the scattered field is first formulated rigorously as a boundary value problem. The scattering field for the half space is expressed as an integral of eigen functions. By choosing appropriate weighting functions, this integral can be identified as a canonical form of Weber-Schafheitlin's discontinuous integrals, so that the boundary condition on the perfectly conducting ground plane can be satisfied automatically. The field inside the trough and the slit can be expanded in terms of the corresponding parallel plate waveguide modes with unknown excitation coefficients. Continuity conditions for the tangential fields at the aperture is then used to determine these coefficients.

Using the results of the above formulations, the simple formulas have been derived for the case when the aperture is electrically narrow. Validity of this approximation has been confirmed by comparing with the rigorous solution. Comparison with other low frequency solutions, and differences between H and E polarizations will also be discussed.

B141.3

ELECTROMAGNETIC PLANE WAVE SCATTERING FROM A PERFECTLY CONDUCTING CUBE

Robert H. MacPhie*
Elect. & Comp. Eng. Dept.
University of Waterloo
Waterloo, ON N2L 3G1
Canada

Ke-Li Wu
COM DEV Ltd.
155 Sheldon Drive
Cambridge, ON N1R 7H5
Canada

The classical problem of plane wave scattering from a perfectly conducting sphere was solved almost a century ago by Mie (Ann. Physik, 25, p.377, 1908) in terms of the vector fields of multipoles. Since these fields are given in spherical coordinates and are orthogonal over the surface of a sphere, a simple closed form solution for the amplitudes of the scattered multipole fields can be obtained by field matching on the surface of the sphere.

Another very simple scattering object is the perfectly conducting cube. In this paper it is assumed that the field scattered from the cube can also be expressed in terms of the fields of multipoles located at its center. In order to field match over the six planar sides of the cube the multipole fields are transformed into cartesian coordinates by means of a plane wave series expansion of their potential functions from which we deduce the vector multipole fields. This is the spherical analog of the transformation of Bessel-Fourier potential functions in circular cylindrical coordinates into a plane wave series which has recently been reported by the authors (IEEE Trans. MTT-43, pp.2041-2045, Sept. 1995).

With the scattered multipole fields expressed in cartesian coordinates it is relatively straightforward to perform the field matching on the six surfaces of the cube. Using Galerkin's method we deduce a matrix equation for the multipole field amplitudes. Numerical results will be presented and the generalization to other scatterers with planar surfaces, e.g., rectangular cylinders of finite length, will be discussed.

Analysis of Scattering from a Cavity-Backed Aperture in a PEC Wedge Using a Multifilament Current Model

Pierre-Richard RENAUD* and Jean-Jacques LAURIN
Department of Electrical and Computer Engineering
École Polytechnique of Montreal
P.O. Box 6079, Station Centre-Ville, Montreal (QC), Canada H3C 3A7

Giuseppe PELOSI
Department of Electrical Engineering
University of Florence
Via C. Lombroso 6/17, I-50134 Florence, Italy

The presence of a small aperture (gap or crack) in the surface of a target can provide a significant contribution to its scattering pattern. Furthermore, if the target is a shielded enclosure, its shielding properties can be severely damaged. It is then necessary to develop methods for predicting these effects.

A typical problem of this nature is the analysis of the 2-D scattering from a cavity-backed aperture in a perfectly conducting (PEC) wedge. Numerical solutions based on moment methods, finite element techniques and the uniform geometrical theory of diffraction (UTD) are already reported in the literature (e.g. M. Calamia, R. Coccioli, G. Pelosi and G. Manara, COMPEL, 13 A, 229-235, 1994). Our objective is to introduce the multifilament current method (MFCM) to this kind of study and investigate its abilities.

The MFCM is a semi-analytical technique inspired from the MoM and point-matching procedures. It has been formulated by Leviatan *et al.* (Y. Leviatan and A. Boag, IEEE Trans. Antennas Propagat., 35, 1119-1127, 1987) for the scattering problem of a homogeneous dielectric cylinder, and applied successfully to the shielding analysis of a complex cylindrical structure involving high-loss layers (P.-R. Renaud and J.-J. Laurin, CCECE Proc., 2, 901-904, 1995). The basic concept of the MFCM is to express the induced fields within a designated region in terms of free space radiating monopoles, namely fictitious filamentary current sources located outside the physical boundaries of the region.

In this communication, a hybrid approach that combines the MFCM and Green's function formulation, respectively for the inner and outer regions of the cavity, will be presented. By means of equivalent magnetic currents at the surface of the aperture separating the two regions, the original problem is replaced by two simpler ones. The coupling of the two solutions is obtained by the application of suitable continuity conditions across the aperture. Numerical results will complete the presentation.

B141.5

SCATTERING BY A CYLINDER AND A SPHERE COATED WITH A LAYER OF ISOREFRACTIVE MATERIAL

Soma Roy * and Piergiorgio L. E. Uslenghi
Department of Electrical Engineering and Computer Science (M/C 154)
University of Illinois at Chicago
851 South Morgan Street, Chicago, Illinois 60607-7053, USA

The scattering of a plane electromagnetic wave by a perfectly conducting body covered by a layer of isorefractive material is considered. The conducting body is selected to be either a circular cylinder or a sphere, so that the effect of curvature on the scattering process may be examined in both two- and three-dimensional cases. The coating layer has uniform thickness, and, therefore, its outer surface is either coaxial (in the case of a cylinder) or concentric (in the case of a sphere) to the surface of the conductor. The analysis is conducted in the frequency domain.

The material of the coating layer is isorefractive to the infinite medium which surrounds the scattering structure. This means that the two media have the same refractive index, but different intrinsic impedances; that is, the product of electric permittivity and magnetic permeability is the same for both media, but the ratio of these two parameters assumes different values in the two media. Isorefractive materials could be constructed, for example, by imbedding minute spherical particles of diamagnetic material in a dielectric matrix with a low dielectric constant.

Isorefractive materials exhibit some interesting properties. For example, when a plane wave is incident on a planar interface separating two isorefractive half-spaces, the transmitted wave proceeds in the same direction of the incident wave, while both reflection and transmission coefficients are independent of direction of incidence and polarization of the primary wave. The purpose of this analysis is to study whether the use of isorefractive coatings introduces some peculiar properties in the field scattered by a coated curved surface. Both the exact solutions and their high-frequency asymptotic approximations are examined.

INHOMOGENEOUS PLANE WAVE SCATTERING BY A POLYGONAL CYLINDER EMBEDDED IN A LOSSY MEDIUM

F. Bertoncini, G. Manara*, P. Nepa
Dept. of Information Engineering, University of Pisa
Via Diotisalvi 2, I-56126 Pisa, Italy

R. G. Kouyoumjian
Dept. of Electrical Engineering, The Ohio State University
2015 Neil Avenue, Columbus, OH 43210, USA

A uniform high-frequency solution has been recently presented for the diffraction of an inhomogeneous plane wave by a perfectly conducting wedge (R.G. Kouyoumjian et al., *Radio Science*, vol. 31, no. 6, pp. 1387-1397, Nov.-Dec. 1996). This solution, derived in the format of the Uniform Geometrical Theory of Diffraction (UTD), is valid when the medium surrounding the wedge is lossy. It is applied here to analyze the scattering from a metallic, polygonal cylinder embedded in a lossy medium. This problem is relevant to remote sensing applications, since a plane wave incident on an interface between air and a lossy medium excites an ihnomogeneous plane wave in the lossy medium. When the latter interacts with buried metallic objects, the resulting scattered field can be used to detect the presence of these objects. In the present case we note that interactions between the edges of the polygonal cylinder may play an important role in the scattering mechanism. Consequenly, the main part of the paper is concerned with the derivation of uniform expressions to account for the field contributions associated with doubly and triply diffracted rays.

Specific uniform asymptotic expressions for double diffraction are derived which contain the UTD transition function with complex argument. Special attention is given to the description of the discontinuity compensation mechanisms, which take place at the shadow boundaries of the incident, reflected and diffracted fields. The displacement of these boundaries from their conventional locations and the extent of the corresponding transition regions are given, and the effect of loss is discussed.

Numerical results will be shown to demonstrate the effectiveness and accuracy of the UTD solution. The accuracy is checked by comparing the numerical results obtained from the UTD solution with those obtained from a moment method solution.

B141.7

Oblique Incidence Scattering from Eccentric Cylinders

Hashim A. Yousif
Natural Sciences Division
University of Pittsburgh
Bradford, Pa 16701
yousif@vms.cis.pitt.edu

Atef Z. Elsherbeni*
Electrical Engineering Dept.
University of Mississippi
University, MS 38677
atef @ olemiss .edu

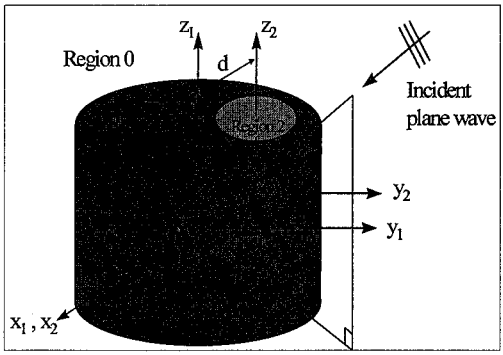

The solution of the scattering of electromagnetic waves from a single and coaxial cylinders are available, however to our knowledge, no solution exists for the more general case of the eccentric cylinders at oblique incidence as shown in the figure. This paper provides a semi-analytical solution for the scattering from infinitely long eccentric cylinders. The cylinders are made of homogeneous isotropic dielectric material with circular cross sections. The method of solution starts by expressing the incident, scattered and internal fields in cylindrical harmonic functions with eight sets of unknown coefficients. The application of the appropriate boundary conditions along with the additional theorem of Bessel functions are utilized to derive eight coupled equations for the unknown scattering and internal coefficients. These exact equations are then solved numerically by truncating the infinite sets of coefficients into finite sets. The near and far electric and magnetic fields are found from these coefficients. The numerical procedure is verified by comparing our results for several special cases (such as a single cylinder, coaxial cylinders, and eccentric cylinders at normal incidence) against results based on the corresponding exact solutions or other available solutions for normal incidence. Excellent agreement is obtained in all test cases. Numerical calculations with emphasis on the radar scattering cross section for the eccentric cylinders are then obtained as functions of the eccentricity parameter and the tilt angle of the incident plane wave. The numerical results based on the investigated examples show that the eccentricity parameter enhances the back scattering cross section. Thus it is easier to separate eccentric cylinders from coaxial cylinders based on the back scattering cross-section.

EM Scattering by Two-Dimensional, Cavity-Backed Aperture in a Ground Plane

G. K. Gothard* and S. M. Rao
Department of Electrical Engineering
200 Broun Hall
Auburn University, AL 36849-5201

In this work, we analyze the electromagnetic scattering by a cavity-backed, two dimensional slot in a ground plane by either a transverse electric (TE) plane wave or a transverse magnetic (TM) plane wave. The analysis is based on the generalized network formulation developed by Harrington and Mautz. In the numerical solution scheme, the arbitrary slot is modeled by planar triangular cylinders. In order to model the inhomogeneous materials of the slot, a separate ϵ and μ may be independently assigned. Further, the cavity is analyzed using the finite integral technique (FIT) which generates a sparse system matrix and free of spurious solutions.

The basic steps involved in the numerical scheme may be enumerated as follows:

- Using equivalence principle, the problem at hand may be separated into three sub-problems, *viz.* a) radiation problem, b) short-circuit problem, and c) the cavity problem.
- The radiation problem may be easily solved using the radiation integrals.
- The short-circuit problem is trivial using image theory.
- Lastly, the cavity problem is solved using the FIT technique.

In the FIT technique, the integral form of Maxwell's equations are applied to a discrete conformal grid. Next, the unknown electric and magnetic fields are approximated by a set of specially designed basis functions with unknown coefficients. These basis functions let us satisfy all the required continuity conditions on the electric and magnetic fields at every material boundary. Since all the electromagnetic conditions are properly satisfied in the present technique, the solution obtained is the only solution according the to the uniqueness theorem.

Finally, we present several numerical results illustrating the capabilities of the present method.

B141.9

ELECTROMAGNETIC ANALYSIS OF CAVITY STRUCTURES WITH APERTURE OPENING USING THE METHOD OF AUXILIARY SOURCES

R.Zaridze*, D.Karkashadze*, R.Jobava*, D.Economou, N.Uzunoglu****

* Laboratory of Applied Electrodynamics, Tbilisi State University
3, Chavchavadze Ave., 380028 Tbilisi, Georgia
Tel: +995-32 290821, Fax: +995-32 290845, e-mail: lae@resonan.ge

** Department of Electrical and Computer Engineering
National Technical University of Athens
9, Iroon Polytechniou Street, Zografou 15773, Athens, Greece
Tel: ++ 301-7723556, Fax ++301-7723557, e-mail: nuzu@zeus.central.ntua.gr

Analysis of conductive wall resonator structures with aperture opening is required in many cases such as calculation of radar cross sections of vehicles or open resonators. The conductive walls could have finite conductivity and thickness. The coupling of the inner and outer space fields poses difficulties in applying standard numerical techniques such as Method of Moments, Finite Difference or Finite Element Techniques. In this article the Method of Auxiliary Sources (MAS) [1-3] in two variations is presented to solve structures of the types mentioned in the title.

The MAS is based on description of fields using some auxiliary sources placed in depth of boundaries on which the fields are requested to satisfy appropriate boundary conditions. The type of the sources is chosen according the fundamental solutions of wave equations in appropriate media. The complex amplitudes of the auxiliary sources are selected to satisfy the boundary conditions accurately.

In the first variation, all auxiliary sources are placed within the thick conductor walls. Then the boundary conditions for the short circuiting of tangential electric fields are requested at points inside and outside the resonator structure leading into a linear system of equations in terms of the unknown source amplitudes. Selecting sufficient number of sources and boundary matching points only on the conductor walls highly satisfactory results are obtained. This method is very easy to be programmed and highly complex structures could be analyzed.

The second alternative variation of the method is based on defining in the first place "inner" and "outer" volumes and placing sources associated with the opposite spaces. Then the boundary conditions for both metallic walls and coupling apertures should be satisfied. In this case the method is more suitable to thin conductors while significantly less numerical cost is needed compared to the first technique.

In order to test the method two and three dimensional structures have been analyzed and comparison with corresponding solutions based on Method of Moments shown to be in good agreement. The results of computational experiments for various structures are discussed from physical point of view.

References:

1. R.Zaridze-Popovidi, Z.Tsverikmazashvili. Journal of Applied Mathematics and Mathematical Physics, No.7, Moscow, 1977.
2. R.Zaridze, D.Karkashadze, etc., Radiotechnics and Electronics, Vol. 22, No.2, Moscow, 1978.
3. D.Karkashadze, R.Zaridze. Latsis Symposium, Zurich, 163-180, 1995.

DUAL-SURFACE ELECTRIC-FIELD INTEGRAL EQUATION FOR BODIES OF REVOLUTION IN ELECTROMAGNETIC SCATTERING

James L. Schmitz
Rome Laboratory/ERCS, Hanscom AFB, MA 02174

Numerical difficulties in computing the induced currents on perfectly conducting scatterers illuminated with plane electromagnetic waves increase rapidly with the electrical size of the scatterer. Integral equation solutions to these problems by the method of moments are effective and efficient for electrically small scatterers. However, as the electrical size increases beyond a few wavelengths, conventional solutions of both the magnetic-field integral equation (MFIE) and electric-field integral equation (EFIE) fail to produce a unique solution at frequencies equal to the resonant frequencies of the interior cavity. These spurious resonances severely corrupt the numerical solution of the MFIE and EFIE.

A unique solution can be found by linearly combining the equation, for example the combined-field integral equation (CFIE). Yaghjian, et al. discovered a robust technique using "dual-surface integral equations" that eliminates these spurious resonances from either the MFIE or EFIE alone. A second surface is placed interior to and within $\lambda/2$ of the surface of the scatterer on which the integral equation is applied. This second surface ensured uniqueness of the solution by providing an additional boundary condition, without changing the form of either the MFIE or EFIE.

The focus of this paper is the numerical implementation of the dual-surface electric-field integral equation (DEFIE) for a body of revolution (BOR). The uniqueness, stability, and simplicity of the dual-surface equations provide advantages not found in other methods used to eliminate spurious resonances. The DEFIE solution for plane wave scattering from a BOR will be formulated using two different moment method solutions. The first formulation of the DEFIE will parallel the BOR formulation used by Mitschang and Putnam. This moment method solution uses a Galerkin method with triangle basis functions. The second formulation follows the method of Wilton and Glisson and uses a staggered-pulse moment method. Numerical results are shown for perfectly conducting BORs using the DEFIE for the first time. The numerical accuracy and computational efficiency of the two different moment method approaches will be demonstrated quantitatively. The monostatic radar cross section results from the two solutions will be compared to measurements for conespheres and right circular cylinders of various electrical sizes. A comparison of the DEFIE and CFIE is performed for electrically large scatterers, critically evaluating the numerical predictions of both equations.

B141.11

EXTENSION OF THE SHEET APPROXIMATION TO ELECTROMAGNETIC SCATTERING BY THIN LAYERS IN THE EARTH

Dr. I.G.Iarmakhov*, Dr. S.B.Popov.
Inst. of Radioeng. & Electronics RAS, Mokhovaya Str.11, 103907, GSP-3, Moscow, Russia. Fax: (095) 203-84-14.

This work is concerned with an extension of the sheet approximation (R.F.Harrington and J.Mautz, T-AP No.4,531-534, 1975; T.B.A.Senior and J.Volakis, Radio Sci., No.7,1261-1272,1987) for an arbitrary system of thin dielectric layers (see fig.). This model is applicated in the geophisical problems such as the oil/gas reservoir exploration (I.G.Iarmakhov, Radiotech.& Electr.(in Russian),No.12,1789-1797,1995).

The results of the paper have been used to detect and evaluate oil /gas saturated layers immersed into the dissipative Earth as well as to control the petroleum reservoir engineering.

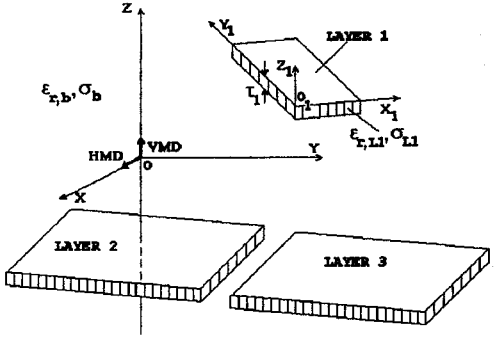

Geometry of the problem

In this work the system of integro-differential equations to determine for every thin dielectric layer both tangential and normal to the layer polarization currents is developed. This equations are transformed to the system of linear algebraical equations with block-Toepliz matrix by a grid approximation of the differential and integral operators. The received system is solved either by direct Gaussian method or by an iterative method. The computer code SCREEN was developed to evaluate of the electromagnetic interaction of several arbitrary displaced finite layers exited by magnetic dipole.

Solutions for three layered test problems representative of electromagnetic fields inside and outside of an ifinitely extended thin layer calculated by means of the SCREEN program show good agreement with the corresponding Sommerfeld solutions.

URSI B/F/K | Session 135 | Salon Gatineau

Volume and Surface Wave Propagation
Co-chairs: E.E. Altshuler, USA and J. Whitteker, Canada

13:10	135.1	An Interferometric Synthetic Aperture Radar Simulation for Urban Areas, **B. HOUSHMAND**, *California Institute of Technology, Pasadena, CA, USA*
13:30	135.2	Using Genetic Algorithms in Designing and Evaluating a Wide-Angle Bistatic Radar, **C.J. McCORMACK**, J.L. SCHMITZ, E.E. ALTSHULER, *Rome Laboratory, Hanscom AFB, MA, USA*
13:50	135.3	A Scanned-Frequency Ground-Coupling Radar, **P.M. GOGGANS**, W. YANG, C.E. SMITH, *University of Mississippi, University, MS, USA*
14:10	135.4	The Real-Time Seismic Warnings by Electromagnetic Phenomena in the Atmosphere, **E. ASARI**, *Hokkaido College of Arts and Sciences, Hokkaido, Japan*
14:30	135.5	On Laser Sounding of the Atmosphere with the Use of Nonlinear Spectroscopic Effects, **S.V. AMBROSOV**, S.A. BORIK, N.Yu. KOLTZOVA, O. GOLOSHCHAK, *OHMI, Odessa, Ukraine*
14:50	135.6	Nonlinean Optical Effects in the Inflammable Aerosol in Atmosphere, **A.V. GLUSHKOV**, Yu.A. KRUGLYAK, A.K. BALAN, *OHMI, Odessa, Ukraine*
15:10		Coffee Break
15:30	135.7	Theoretical Model of Forming the Discharge Centers of the Complicated Chemical Substances Gases by a Laser Radiation in Atmosphere, **S.V. MALINOVSKAYA**, V.N. POLISCHUK, O. GOLOSHCHAK, *OHMI, Odessa, Ukraine*
15:50	135.8	Intercepting and Identification of the Vehicle's Technological Characteristics by Radar and AAS Systems, **A.V. GLUSHKOV**[1,2], S.V. DAN'KOV[1], V.A. EFIMOV[1], [1]*OHMI and* [2]*Private Theoretical Center of Strategical Researches (TCSR), Odessa, Ukraine*
16:10	135.9	Modeling of Propagation Electromagnetic Waves in a Turbulent Flows of Plasma, **V.G. SPITSYN**, *Tomsk State University, Tomsk, Russia*

BFK135.1

An Interferometric Synthetic Aperture Radar Simulation for Urban Areas

B. Houshmand
Jet Propulsion Laboratory
California Institute of Technology
4800 Oak Grove Drive
Pasadena, CA 91109-8099

Interpretation of the Interferometric Synthetic Aperture Radar (IFSAR) measurements over urban areas are complicated due the complex interaction of the radar signal with the urban environment. The returned radar signal from an urban environment is, in general, a coherent sum of a direct returned signal plus signals which have gone under a number of reflections. The accuracy of height measurements from interferometric measuremnets is affected as a result of multiple scattering. Furthermore, shadowing and overlay effects introduce additional inaccuracies in the computed height profiles. In this talk the simulation results for IFSAR over urban areas are presented, and compared with measurements. The simulation is carried out in two steps. First the forwad scattering data is synthsized using a three dimensional scattering model based on Geometrical Optics (GO). The urban profile is represent by a facet based model, and a forward ray tracing algorithm is used to provide efficient computation of multiple paths for arbitrary geometrical arrangements. The second step is to invert the generated data for a high resolution image of the the urban scene. A convensional range-Azimuth algorithm is used to produce a complex (magnitude, phase) image of the scene. An estimate of the height profile is then computed from two complex images derived from two synthesized receivers displaced in the range direction by a baseline length. The relative phase difference between the complex images is used to locate the position of the dominant scattering center for each resolution cell on the scene. It is of interest to characterize the multiple scattering and shadowing effects in the derived height profile. Multiple scattering in the range direction, in general, displaces the scattering center position due to the increase in the effective path lenght of the contributing signal. In this presentation a number of geometrical configurations which produce single and multiple scattering, layover , and shadowing effects are considered. The derived height accuracy as a function of radar parameters, angle of incidence, and the height profile will be disccused. The simulated results will be compared with the IFSAR measurements over a selected number of urban areas.

Using Genetic Algorithms in Designing and Evaluating a Wide-Angle Bistatic Radar

Christopher J McCormack
James L Schmitz
Edward E Altshuler
Rome Laboratory
Hanscom AFB, MA 01731

We use a genetic algorithm to help select parameters for a wide-angle bistatic radar system. The basic scenario shown below involves a transmitter and receiver pair protecting an asset from an inbound threat. The strength of the received signal depends on a large number of factors, including the ranges from transmitter and receiver to the target, the target's orientation or aspect angle, θ, the bistatic angle, β, and antenna polarizations for the transmitter and receiver.

Genetic algorithms were chosen due to the large number of interacting parameters involved. The genetic algorithm approach allows us to start with a severely constrained system, then add additional parameters and complexity. This incremental design approach gives us tremendous insight to the system's robustness and performance. The genetic algorithm also provides a good basis for incorporating random parameters in the system design as well as allowing a competing algorithm to actively selecting threat parameters attempting to degrade the radar's performance.

A particular effect we examine is the depolarization of the radar signal by the target. Varying the polarizations of the transmit and receive antennas provides widely varying power levels for the scattered signal depending on the exact geometric relationship between the radar components and the threat. The depolarization caused by the target is also a function of the target's structure. This was one area where we employed competing genetic algorithms to find the best overall radar performance regardless of changes in the target.

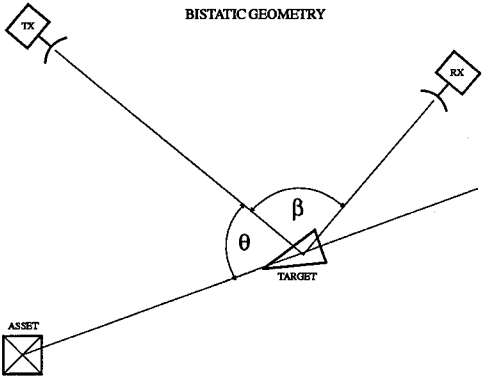

BFK135.3

A Scanned-Frequency Ground-Coupling Radar

Paul M. Goggans*, Wenhai Yang, and Charles E. Smith
Department of Electrical Engineering
University of Mississippi
University, MS, 38677, USA

Because of current efforts to clean up former artillery ranges, there exists a need to develop an electromagnetic system to locate and identify subsurface artillery shells. Here, we investigate scanned-frequency ground-coupling radar for this application.

The system we investigate uses a CW radar which slowly scans a band of frequencies in the vicinity of the fundamental resonant frequency of each type of unexploded shell in the former artillery range. Because the shells have enhanced coupling with the antenna at their resonant frequencies, this technique can be used to detect the shell by sensing the enhanced coupling at the resonant frequency. Shells are axisymmetric bodies with relatively high length to maximum diameter ratios. As a result, the fundamental resonance frequency of a shell can be determined approximately from the length of its generating curve. The resonant frequency is approximately the frequency at which the length of the generating curve is one-half of a wavelength. Because the fundamental resonance occurs at a frequency related to the dimension and shape of the shell this technique may allow for identification based on shell size.

Using the relatively low frequency band associated with the shells resonant frequencies helps mitigate the ground/air boundary reflection problem observed in radars in which the antenna is not touching the ground. If the antenna is less than approximately a wavelength from the boundary, the wave impedance at the boundary is not the characteristic impedance of air as it is for a plane wave, but rather is determined by the characteristics of the antenna (of course the actual near field region also has to do with the antenna size). Loop antennas have a larger proportion of magnetic field than electric field (relative to a plane wave) in the near field region so that the wave impedance in the near field region is less than the characteristic impedance of air. By placing the boundary in the near field region of a loop antenna, the impedance of the wave can be more nearly matched to the impedance of the ground, thus reducing the reflection of the incident wave.

The antenna and target geometry investigated here consist of a wire loop antenna operated below its resonant frequency in air and a thick wire target in air and in soil. We report the results of our initial numerical and experimental studies to establish the feasibility of our ground coupling radar concept.

This material is based upon work supported by the U. S. Army Research Office under contract number DAAH04-95-1-0403.

The Real-time Seismic Warnings by Electromagnetic Phenomena in The Atmosphere

Eikichi ASARI
Hokkaido College of Arts and Sciences
Bunkyoudai-Midori-Machi 582, Ebets, Hokkaido, 069 Japan
Tel. +81113861111. Fax. +81113875848

The purpose of this study is to propose immediate warning methods against earthquakes that use of electromagnetic observations in the atmosphere or underground points where the seismic electromagnetic radiation detecting. It will be useful for making decisions about how warn people against seismic disasters. On the earthquake zones, seismic predictions and warnings are very important for people's safeties and preventions against seismic disasters to the public in general. At present, we are knowing that electromagnetic phenomena are accompaniments of every geophysical phenomena. One of the electromagnetic phenomena is the extraordinary variations of earth-currents, and another one is the electromagnetic radation characteristic of seismisms.

An example of the first is a seismic prediction technique that called VAN-method was developed by three Greeks, namely, Varotsos, Alexopoulos and Nomicos. VAN-method provides the early warnnings of strong earthquakes and the forecasts of scales of the earthquakes including locations of the epicenters by watching to transitions of earth-currents in observation networks over the country.

The second seismic predictions' technique is the watching of burst out electromagnetic radiatings accompanied with destructions of the crust. Recent experiences proved the bursts inform us of the omens of earthquakes. We can predict the earthquake will be arriving on the spot from the epicenter at least several seconds before.

The seismic predictions are classified two categories on period, 'Forecasts' as long-range or long period, and 'Nowcasts' means short-range or short period predictions. Author took notice of usefulness of shortest period predictions and warnings which called as 'Real-time warnings'. When an epicenter occur in the crust, the earthquake propagated through the crust to the surface of the earth. The propagation needs several seconds or more, we feel weaker mechanical vibrations called P-Wave last few seconds first and then attacked strong swings called S-Wave. P and S-Wave propagated from their epicenter to around in the crust by 6-7km/sec of speed on P-Wave and 3-4km/sec of speed on S-Wave. The difference of speeds between P-Wave and S-Wave is very useful quantity for make real-time warnings of earthquakes. Moreover, if we catch burst out electromagnetic radiating on the spot from the epicenter immediately, we can get more useful time for our safeties and preventions than the difference of speeds between P-Wave and S-Wave, even only several seconds. The real-time warnings is a surest method of seismic predictions and warnings. However, at present time, we have no systems for the warnings, but detections of burst out electromagnetic radiating provide to us good immediate signs of earthquakes. Detecting techniques of the radiations were already developed.

Of earthquakes, the general public are wishing someone to inform believable seismic predictions for them because they heared 'cry wolf' too often for many years. Administrators of government should inform certain seismic predictions even if we can provide only scores seconds real-time warnings now. However, it may builds up national movements for preventions against natural disasters. The movements will be bring the advancements of all kinds of sciences and technologies on seismic predictions.

BFK135.5

ON LASER SOUNDING OF THE ATMOSPHERE WITH THE USE OF NONLINEAR SPECTROSCOPIC EFFECTS

Ambrosov S.V.[*],S.A.Borik[#],Koltzova N.Yu.[#],Goloshchak O.[#]

[#]Applied Math.Dept.,OHMI, a/c 108,Odessa-9,SU-270009,Ukraine, [*@]Institute of Technology, a/c 108,Odessa-9,SU-270009,Ukraine

At present a great interest attracts the possibility of the use of nonlinear and coherent interactions as a physical origin of new methods for laser and optoacoustic sounding of the atmosphere [1]. In process of the IR laser radiation resonance absorption it occurs the redestribution of molecules on the energy levels of internal freedom degrees. Creation of the excited nitrogen molecules in the atmosphere due the resonance excitation transmission from carbon dioxide molecules leads to the medium polarizability changing. As result it could be substantionally changed the IR- laser pulses propogation conditions. At present paper we consider the role of the resonance spectroscopic effects in the forming of the nonlinear behaviour of the gas atmosphere for propogation of the powerful pulsed laser radiation in it under different conditions and models of the atmosphere.As a basic model for the absorbed energy relaxation description it's used 3-mode kinetic processes model. It's numerically demonstrated the change in the time dependence of the resonance radiation absorption coefficient for carbon dioxide under different atmospheric conditions. We also consider effects of stimulated light scattering in atmospheric gases under realistic conditions. These are indicated the perspective possibilities of the air pollution on the base of examined effects.

1.Zuev V.E.,Zemlyanov A.A.,Kopytin Yu.D.Nonlinean athmosphere optics.- L., 1989.
2.Glushkov A.V., Preprint Inst.for Spectroscopy of Russian Acad.Sci., N2-AS, Moscow,1993;

BFK135.6

NONLINEAN OPTICAL EFFECTS IN THE INFLAMMABLE AEROSOL IN ATMOSPHERE

Glushkov A.V.[#*],Kruglyak Yu.A.[#],Balan A.K.[#]

[#]Applied Math.Dept.,OHMI, a/c 108,Odessa-9,SU-270009,Ukraine,
[*]Radiophys.&Electr.Center,a/c 108,Odessa-9,SU-270009,Ukraine

It has been considered the problem for the self-action of the intensive laser radiation in the inflammable aerosol, in particular,the oilproducts drops.The correct problem solution includes the combined solution of the quasi-optics nonlinean parabolical equation for the comlex field amplitude E and the aerothermochemistry equations set (thermoconductivity & mass, impulse, energy transfer equations).It has been fulfilled the modelling of a entire system of equations.It has been received the relative radius and flammable oilproduct drop surface temperature dependences for the different waves lengths and power density under action of the laser radiation. It has been noted the threshold character of the oil products ignition under achieving the threshold radiation intensity [2].

1.Zuev V.E.,Zemlyanov A.A.,Kopytin Yu.D. Nonlinean athmosphere optics.- L., 1989.
2.Glushkov A.V. et al, Nonlinean Optical effects in the inflammable aerosol.-Preprint OHMI,Odessa,1995.

BFK135.7

THEORETICAl MODEL OF FORMING THE DISCHARGE CENTERS OF THE COMPLICATED CHEMICAL SUBSTANCES GASES BY A LASER RADIATION IN ATMOSPHERE

Malinovskaya S.V.[#*],Polischuk V.N.[#],.Goloshchak O.[#]

[#]Applied Math.Dept.,OHMI, a/c 108,Odessa-9,SU-270009,Ukraine,
[*]Radiophys.&Electr.Center,a/c 108,Odessa-9,SU-270009,Ukraine

In last years the considerable interest attracts the problem of the appearance the plasma formations in an air medium under action of the powerful laser radiation, that is stimulated by the set of important applications, in particular, the distant analysis of the inert gases and aerosol substances, the athmosphere zonding for definition og the meteorological parameters etc [1]&A great number of papers has been devoted to the optical discharge of single- atom gases by laser radiation [1]. In our paper it is considered the problem of the first time laser discharge of the vapor oreol for chemical complex substances (the oilproducts vapor), mixture with air. The master equations system contains the quantum differences equation for an energy spectrum of free electrons, the equation for the concentration of the vapor particles in the main and first excited state, the energy conservation, motion, continuity and state equations. In the difference from the analogous single-atom equations system, in above indicated master system there is carried out the summation of the partial contributions of the interaction with every kind of atoms.There are presented the results of the numeral modelling.

1.Zuev V.E.,Zemlyanov A.A.,Kopytin Yu.D. Nonlinean athmosphere optics.- L., 1989.
2.Glushkov A.V. et al, Nonlinean Optical effects in the inflammable aerosol.- Preprint OHMI,Odessa,1995.

INTERCEPTING AND IDENTIFICATION OF THE VECHICLE'S TECHNOLOGICAL CHARACTERISTICS BY RADAR & AAS SYSTEMS

Glushkov A.V.[#*$], Dan'kov S.V.[#*],Efimov V.A[#]

[#]Applied Math.Dept.,OHMI, a/c 108,Odessa-9,SU-270009,Ukraine, [*]Radiophys.&Electr.Center,a/c 108,Odessa-9,SU-270009,Ukraine, [$]Private Theoretical Center of Strategical Reserches (TCSR)

The question of how to identify & inspect possible orbital target is one of the most complicated questions. Indeed, it is extremely difficult to determine the nature of space vechicle purely from ground observations. The vechicle could be held in orbit for long periods and its intentions would be hard to predict-much harder, f.e,than those of an aircraft which flies a certain course. One can hardly find out more about unidentified objects in orbit than can be obtained by analysing their orbital motion and checking on any changes that may take place in orbit. It's possible to identify the satellite's radio signals but, it is not possible to interpret the results of its instruments.Although space track system contribute information from satellites,tracking radars,Doppler devices etc.,a precise idea of the vechicle's shape,covering materials structure etc. can hardly be obtained in full degree. We develope a new technology providing information about vechicle's characteristics. It's based on the complex use of radar system& activation analysis system (AAS) [1]. In AAS, the identification of elements is fulfilled by means the measurement of intensity & emission energy of the radiactive or excited nuclei, which are a result of the nuclear reactions after exposing to radiation by neutrons (n) or (Y)-quants flow. We consider the AAS variants: n -AAS [feasible detection limit: 10(-4)-10(-6)%],Y-AAS [10(-7)%]) & instrumental AAS without damage of the intercepting unidentified object.In any case it may be possible to deduce something of its designed mission. It is related to more complex objects (IRBMs or ICBMs). Something might be also said of its internal workings especially from the amount &type of emitted radiation. If the satellite contained nuclear device,it might even be possible to check the amount of the contained fissile material.

1.Glushkov A.V. Sci.Techn.Proc.N13,TCSR,Odessa (1995);

BFK135.9

MODELING OF PROPAGATION ELECTROMAGNETIC WAVES IN A TURBULENT FLOWS OF PLASMA

V.G. Spitsyn, Tomsk State University, Russia

In this paper we consider multiple scattering of electromagnetic waves on the strong fluctuation dielectric penetration the flow of plasma. It is found the analytic expression for frequency spectrum scattering signal on the external surface of turbulent flow of plasma. The numerical model of multiple scattering waves in turbulent flows of plasma is proposed. We consider propagation wave through flow with unhomogeneous profiles velocity and concentration of turbulences. The results of calculations show, that with growth of angle sounding flow increase coherent component in spectrum and decrease uncoherent scattering component take place. It explains thereby, that probably of travelling beams through flow without interaction in case big angles of falling grows, but scattering beams - falls.

We consider sounding turbulent flow of plasma along its axis. Multiple scattering of waves on the inside surface of turbulent plasma bodies of the turn is modeled. Dependence of angle and frequency spectrums of scattering signal from form of scattering surface and width diagram of over - radiation turbulences is investigated. Growth of width of diagram of over-radiation turbulences quasi - mirror type is accompained by displacement of maximum uncoherent component of frequency spectrum on side greater meanings displacement of frequency scattering signal.

The results calculations of frequences spectrums electromagnetic waves multiple scattering on the inside surface of turbulent plasma bodies of revolution are compared with experimental observation spectrum, got at electromagnetic sounding turbulent flow of plasma (J.S. Draper , P.O. Jarvinen, T.D. Conley, AIAA J..9, 1568-1573, 1970). Similarity of form of experimental spectrum and curves, carried out in result of numerical modeling, permits to make up the conclusion, that this spectrum of reflection of signal appears in result of multiple scattering of electromagnetic waves on the inside surface of turbulent paraboloid of revolution.

URSI C **Session 122** **Salon Peribonca**

Communications and Signal Processing
Co-chairs: J. Morris, USA and T. Denidni, Canada

08:10	122.1	On Generation of Non-Stationary Random Processes, **S. PRIMAK**, *University of Western Ontario, London, ON, Canada*
08:30	122.2	NMR FID Parameter Estimation Using Gabor Transform, **J.M. MORRIS**, S. JOSHI, *University of Maryland Baltimore County, Baltimore, MD, USA*
08:50	122.3	Multi-Beam Phased Antenna Array for Cellular Mobile Communications, **T.A. DENIDNI**, *Université du Québec à Rimouski, QC, Canada*
09:10	122.4	A Non-Linear Weighted Least Squares Approach to Radar Array Processing, **J. ERIKSSON**, *Chalmers University of Technology, Göteborg, Sweden*
09:30	122.5	Performance Analysis of Optimal/Adaptive Arrays for Reduction of Signal Spatial Coherence, **G.V. SEREBRYAKOV**, *University of Nizhny Novgorod, Russia*
09:50	122.6	Digital Computer Simulation of a Concatenated Coding System for Reliable Satellite and Space Communications, **A.A. EL-AZM**, J. KASPARIAN, *Menoufia University, Menouf, Egypt*
10:10		Coffee Break
10:30	122.7	Irreducible Error Performance of MQAM in Indoor Multipath Environment, **P. SHI**, K. GONG, *Tsinghua University, Beijing, China*
10:50	122.8	Performance of a Decorrelating Receiver in High-Data Rate, High-Processing-Gain, Spread-Spectrum Systems, **P. KANAGARATNAM**, *University of Kansas, Lawrence, KS, USA*
11:10	122.9	The Cepstrum Processing of Electromagnetic Signals, **S.V. MALINOVSKAYA**, G. PREPELITSA, S.A. BORIK, V. POLISCHUK, *OHMI, Odessa, Ukraine*
11:30	122.10	The Analytical Signal for the Radio Pulse with Rectangular Envelope, **I.D. ZOLOTAREV**, *Omsk State Engineering University, Omsk, Russia*
11:50	122.11	8PSK Signaling over Non-Linear Satellite Channels, **R. CABALLERO**, *New Mexico State University, Las Cruces, NM, USA*

C122.1

ON GENERATION OF NON-STATIONARY RANDOM PROCESSES

Sergey Primak
Dept. of Electrical Engineering, The University of Western Ontario, London, Ontario, Canada, N6A 5B9, e-mail: primak@gauss.engga.uwo.ca

The generation of non-Gaussian random processes with a given Probability Density Function (PDF) and correlation function is of high interest during last two decades. The very general approach to solve this problem using Stochastic Differential Equations (SDE) was recently suggested (V. Kontorovich, and V. Lyandres, IEEE Trans. Sig. Proc., Vol. 43, # 10, 1995, pp. 2372-2385).

In this publication we extend the SDE approach to generate random processes with given non-stationary PDF $p_x(x, t)$. In contrast to the original approach, which requires the knowledge of the stationary solution we will use the Fokker-Planck equation to obtain the drift and the diffusion of the process with the desired non-stationary distribution.

Let the desired process be generated by the following non-linear system (Ito form)

$$\dot{x} = f(x, t) + g(x, t)\xi(t) \tag{1}$$

The corresponding Fokker-Planck equation is then

$$\frac{\partial}{\partial t}p(x, t) = -\frac{\partial}{\partial x}[K_1(x, t)p(x, t)] + \frac{1}{2}\frac{\partial^2}{\partial x^2}[K_2(x, t)p(x, t)] \tag{2}$$

where

$$K_1(x, t) = f(x, t),\ K_2(x, t) = g^2(x, t) \tag{3}$$

Equation (2) can be solve with respect to unknown function $K_1(x, t)$ as

$$f(x, t) = K_1(x, t) = \frac{1}{2}\frac{\frac{\partial}{\partial x}[K_2(x, t)p(x, t)]}{p(x, t)} - \frac{\int_{-\infty}^{x}\frac{\partial}{\partial t}p(x, t)dx}{p(x, t)} \tag{4}$$

The last equation allows us to model a non-stationary random process with given non-stationary PDF as the solution of the proper SDE. Applying well known disretization schemes to SDE one can obtain non-linear recursion to generate a non-stationary non-Gaussian random sequence with given PDF. A number of examples will be presented.

NMR FID Parameter Estimation using Gabor Transform

Joel M. Morris* and Sanjay Joshi
Computer Science and Electrical Engineering Department
University of Maryland Baltimore County
1000 Hilltop Circle, Baltimore, MD 21250, USA

Abstract

Nuclear magnetic resonance (NMR) spectroscopy is an important tool in understanding the chemical structures of molecules. An NMR signal is modeled as a free induction decay (FID) signal, i.e., a finite mixture of modulated, exponentially decaying sequences. The signal parameters give information about the chemical bonds. The methods to estimate these parameters can be classified as time-domain methods and frequency-domain methods (M. Joliot *et al.*, *Magn. Res. Med.*, 18, 358-370, 1991). In this paper, the discrete-time Gabor transform (DTGT) is used to estimate the parameters of the FID.

The FID signal $s(k)$ can be modeled as $s(k) = \sum_{m=1}^{M} b_m e^{-\pi d_m k} e^{j2\pi\nu_m k} e^{j\phi_m}$, where M is the number of components. For each of the components the parameters to be estimated are the amplitude b_m, the exponential decay constant d_m, the modulation frequency ν_m, and the phase ϕ_m.

In this work, we propose to use the discrete-time Gabor transform (DTGT) that represents a signal in the joint time-frequency domain (JTFD). Using a DTGT, a signal can be represented, using its DTGT coefficients c_{mn}, as $s(k) = \sum_{m=0}^{M-1} \sum_n c_{mn} g_{mn}(k)$, where $g_{mn}(k) = g(k - nN) \exp(j2\pi mk/M)$ and $M \geq N$. The sequence $g(k)$ is known as the synthesis sequence. The coefficients c_{mn} are computed using the analysis sequence $\gamma(k)$ as $c_{mn} = \sum_k s(k)\gamma^*_{mn}(k)$, where $\gamma_{mn}(k)$ is defined similar to $g_{mn}(k)$.

By choosing $g(k)$ similar in shape to the signal model, the coefficients can be localized to a small region in the joint time-frequency domain (JTFD), whereas the noise will be almost uniformly distributed across the JTFD. Here, $g(k)$ is chosen as the exponentially-decaying sequence $g(k) = \exp(-\pi dk)$, where $0 \leq k \leq Q - 1$, with Q the length of $g(k)$. The analysis sequence $\gamma(k)$, denoted the dual sequence, is computed using the biorthogonal-like sequence theory (J. M. Morris and Y. Lu, *IEEE Trans. SP*, 44(6), 1378-1391, 1996). For $M = Q$ and $N \leq Q$, the dual sequence $\gamma(k)$ can be written as $\gamma(k) = 1/g(k)$ for $0 \leq k \leq N - 1$.

We show how the parameters are estimated using the coefficients c_{mn}. The results are compared with the results via the standard methods in the time and frequency domains.

C122.3

Multi-beam Phased Antenna Array for Cellular Mobile Communications

Tayeb A. Denidni
Department of mathematics, computer science and engineering,
University of Quebec at Rimouski, Canada

Abstract

In the last few years, the wireless communications systems have become a significant worldwide market. We can find a large range of new products and services and this trend can only increase in the future. At the same time, the cellular radio networks constitutes probably the largest public interest. However, this area suffers from the fading problem caused by the cochannel interference. Due to this problem, this system may be lost its spectral efficiency. Consequently, the channel capacity will be reduced. To overcome this problem, we propose in this paper a new multi-beam phased antenna array which will be used at the mobile base station in the context of cellular mobile communications.

In order to adapt the antenna array pattern to its environment, the proposed system uses an electronically steerable antenna array beam control. This approach is based on the principal of combining the time and the space multiplexing. In others words, the time-space multiplexing method is a switching concept which considers time-division beam scanning of antenna array pattern. With this kind of system, the base station antenna array redirects, at each time-slot, its beam to a desired mobile. With this technique, the transmitter employs a TDMA radio link system for time multiplexing while an electronic scanning antenna array is used at the same time. The antenna system is consisted of number of fixed antennas elements with beam formation achieved by the phase adjustment at each element of the array. Based on mobile location information that is available at the base station, the antenna system is able to automatically phase compensate, at an element level, in order to form a beam in desired direction.

The aim of this system is to form in automatic manner a narrow beam in direction of desired signal. In the context of cellular mobile communications, the principal advantage: this system offers very considerable flexibility in its ability to shape and alter the radiation pattern electronically. Therefore a narrow antenna array pattern beam will significantly suppress interference from surrounding transmitters in the same frequency. Using this technique in cellular mobile radio area, we expect that it is possible to boost the capacity even more.

A mathematical description of this system and comparison with classical techniques will be presented. In order to examine the system performance, the numerical results will be reported. In conclusion, we expect with this approach that the performance would exceed the performance of conventional systems.

A Non-Linear Weighted Least Squares Approach to Radar Array Processing

JONNY ERIKSSON*
Department of Applied Electronics
Signal Processing
Chalmers University of Technology
412 96 GÖTEBORG, SWEDEN

Abstract

A signal model that is common in active pulsed Doppler radar is the sinusoidal source signal model. In this paper, the problem addressed is the simultaneous estimation of the amplitudes, phases, frequencies and directions of arrival of p source signals observed in spatially colored noise. Since the *maximum likelihood* method results in a computationally complex algorithm, the simpler *weighted least squares* technique is investigated instead. A detailed treatment of this method applied to the scenario described herein seems not to be available in the signal processing literature. The criterion can be concentrated with respect to the complex amplitudes, leaving a $2p$ dimensional criterion function which is minimized in order to obtain the estimates of the frequencies and the DOA:s. Consistent estimates are produced provided that the sources are separated in the two-dimensional parameter space defined by the direction of arrival and the frequency. This means that sources can be located at the same direction of arrival if the frequencies are distinct. The asymptotic distribution of the parameter estimation error is given and Monte Carlo simulations are carried out that support the theoretical results. The optimal weighting, which gives estimates that are efficient, is the inverse of the covariance matrix. However, simulations show that estimates that are close to being efficient can be obtained by using the inverse of the estimated array correlation as weighting.

*Telephone:+46 31 772 1787, fax: +46 31 772 1782, e-mail: eriksson@ae.chalmers.se

C122.5

Performance analysis of optimal/adaptive arrays for reduction of signal spatial coherence

Georgij V.Serebryakov

Research Institute of Applied Mathematics and Cybernetics, University of Nizhny Novgorod,10 Ul'janov st., Nizhny Novgorod, 603005, RUSSIA
fax: +7 8312 39 04 11, e-mail: gvs@focus.nnov.su

Optimum array processing is generally studied and used in the case of perfectly known wavefronts. In sonar and in presence of non-rigid arrays or in shallow water, the wavefronts may be randomly distorted.

A concern wnich arises, when considering the use of a very large aperture in order to achieve high array gain, is that the signal received at widely separated sensors may have reduced spatial coherence due to complexities in the propagation of the sound waves from the source to spatially separated receivers. Causes of distorsions are very diversified: they are of two types. The first type relates to mechanical deformation of the array. The second type is inherent to the propagating medium. Actually, the medium is neither isotropic, nor homogeneous, nor deterministic. Different causes of perturbation of the propagation are for instance the existence of multipaths, local heterogeneites and diffusion.

The sucess of optimal beamforming is limited by the ability to precisely predict the Green's function. In addition to deterministic effects, small-scale random inhomogeneities perturb the Green's function, causing decorrelation, or loss of coherence, across a large receiving array. Thus a central problem in large-array optimal beamforming is the signal and interference coherence which limits the detection performance.

The purpose of this paper is to examine the effect of reduced signal and interference coherence on the performance of an optimal processor, which maximizes the output signal-to-noise ratio (SNR) for coherent signal and interferences.

For simplicity, the single interference case is studied. The spatial coherence of the interference is assumed to fall off exponentially with separation of the elements.

Analytical expressions for the optimal weight vector, directional pattern and output SNR are derived in terms of the coherence coefficient of interference, interference power and parameters of the adaptive processor. It is shown that the performance of optimal/adaptive beamforming is substantially degraded for large arrays and typical coherence lengths.

The different models of interference coherence are studied. Finally, to illustrate the theory, several numerical results are given.

Digital Computer Simulation of a Concatenated Coding System for Reliable Satellite and Space Communications

***Dr. Atef Abou El-Azm and ** Eng. Jeff Kasparian**

* Faculty of Elecronic Eng., 32952-Menouf, Egypt, Fax:(048) 360 716

** e-mail: jeff@spri.levels.unisa.edu.au

This paper presents a design methodology of a concatenated coding system. The system is with rate 1/2 convolutional code and NASA standard RS (255, 223) code. The decoder for convolutional code is the Viterbi decoder and is designed with different values of quantization levels. An interleaver and deinterleaver between the two codes with depth eight is also included. The software signal processing worksystems SPW is used for analysis the presented system. Simulation results of bit error rate (BER) for both hard and soft decisions decoding, i.e. q=2 and 8 respectively, and for depth eight of interleaver are given in Fig.1. From these results we see that at the decoded bit error rate 4 x 10^{-4} with the interleaver depth 8 and the differential encoding/decoding is ON, the system achieves 2.2 dB. To get good results, the simulation needs to be at least 1000 bit errors counted, probably 3000. To achieve a decoder BER of 10^{-5} as shown in the NASA/ESA system (*J.L.Massey, Control and Information Sciences, Vol.182, Berlin-Springer-Verlag, 1992*) and presented by a square point in Fig.1, the required value of E_b/N_0 will be very close to 2.4 dB. The obtained results of our designing system show a good agreement with the NASA/ESA system This design mehodlogy offers the designer of such systems new options. He can set the interleaver depth to any value in the range (1-20). Also he can adjust the quantization level from 2 to 16. Differential encoding/decoding can set ON/OFF. In general, most of all parameters within those blocks used in the designed system can be changed and then analyse the data after the simulation is performed with the new specifications.

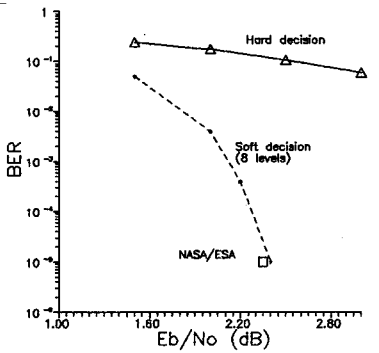

Fig.1 Error Performance of the concatenated system.

C122.7

Irreducible Error Performance of MQAM in Indoor Multipath Environment

Pengyu Shi & Ke Gong

Department of Electronic Engineering, Tsinghua University

Abstract:

The paper analyzes the irreducible errors introduced by time dispersion in a frequency-selective Rayleigh and Rician fading channel. The MQAM modulation is considered with coherent detection in a channel without noise. The symbol combinations which do or do not lead to errors in the two-path model are given. For the special case of two paths with small delay, a simple formulation is derived which shows that the BER is proportional to the square of the mean delay spread (normalized to the bit length) in two-path Rayleigh fading channel and it decreases monotonically with the increase of roll-off factor from 0 to 1, which match the previous results very well. In Rician fading channel, BER cannot be simply related to the mean delay spread but does have a specific relation to Rician parameter and variances as well as time delay of the two paths. Increase the number of levels of QAM, the multipath effects on MQAM system become worse in both Rayleigh and Rician fading cases. Two typical cases of Rician fading are investigated, and it is found for a maximum phase system the LOS path might lead to even worse BER in some cases. Based on the measured indoor propagation data, BER is predicted for MQAM. If the channel is characterized by two-path Rayleigh fading model, it is shown that up to 64-QAM with 1 MS/s symbol rate in an indoor environment could perform well (BER < 0.01) even without an equalizer. Since a dominate path (LOS or a strong reflecting path) often exists in indoor radio channel, Rician fading is more suited to real case. A method is proposed to calculated the parameters of two-path Rician fading model, which reveals that the system performance is largely improved due to the existing of dominate path and higher level QAM (M>64) may be adopted for indoor radio channel even without any equalizer.

Performance of a Decorrelating Receiver in High-Data Rate, High-Processing-Gain, Spread-Spectrum Systems

Pannirselvam Kanagaratnam*

Abstract

Spread-spectrum (SS) systems are used in mobile communications to combat the effects of fading and narrowband interference. The processing gain, which is defined as the ratio of the transmission bandwidth to the data bandwidth, dictates the performance of the system. The higher the processing gain, the higher the interference rejection capability, CDMA user capacity and other important system attributes.

Unfortunately, limited spectrum allocation will limit the processing gain of high-data-rate systems. Parallel spread-spectrum signaling schemes have been shown to increase the processing gain of SS systems. The processing gain is increased by multiplexing successive bits in a data stream and spreading it with shifted versions of the same PN code sequence. This reduces the data rate of each branch by a factor equal to the number of branches, thus increasing the processing gain. In the design of the receiver for this system, the interference from spread waveforms from the other parallel branches must be minimized. This can only be achieved if the receiver has a priori knowledge of all the spreading waveforms in the channel.

The decorrelating receiver is one such receiver that has been used in CDMA environments to minimize interference due to other users signals. Decorrelating receivers also have the advantage of not requiring power control. In this paper, we present the derivation of the bit error rate (BER) for a parallel spread spectrum-system using a decorrelating receiver. The analytical results of the performance of this system against single-tone jamming and fading using constant and exponential multipath delay profiles are also presented. The results show that system immunity against these hostile conditions increases with an increase in the number of parallel data streams.

C122.9

THE CEPSTRUM PROCESSING OF ELECTROMAGNETIC SIGNALS

Malinovskaya S.V.*,Prepelitsa G.#,Borik S.A.#,Polischuk V.#

*Radiophys.&Electr.Center,a/c 108,Odessa-9,SU-270009,Ukraine, #Applied Math.Dept.,OHMI, a/c 108,Odessa-9,SU-270009,Ukraine

The cepstrum method is widely used for processing in a whole numberof fields including radiolocation etc. Its application in processing for the nonlinear electro- & radiosygnals especially effective in the complicated situations with the superposition of signals.In paper it's considered an application of the cepstrum method in processing of the electromagnetic signals in the atmosphere duct. We consider the electromagnetic waves spreading in the ionosphere(its form is determined by the spectroscopical characteristics of the source and dispersion properties of the athmosphere duct),the long (as a result of the signal spreading from the source till magnetic-conjucted point & back) and short (excite in the region which is magnetic-conjucted to reception zone) piping athmospherics signals. The complicated situation is realized for ones which are affected to the multiple reflection from magnetically conjucted ionosphere regions. It results in a appearance of the echo-signals. The cepstrum method is used for analysis data,contained reflection or reverbation of the ground wave. The power cepstrum is used to define the return time moment for elementary wave, its reflections,relative amplitudes. Quite sophisticated study uncludes the spectral,pseudocorrelation and cepstrum analysis [1].

1. A.V.Glushkov,S.V.Ambrosov,S.V.Malinovskaya, "The Radiosygnals Cepstrum Processing",Kiev,(1995);

The Analytical Signal for the Radio Pulse with Rectangular Envelope

Ilya D. Zolotarev
Omsk State Engineering University
11, Mira avenue, 644050, Russia
Phone: +3812 63 04 39, Fax: +3812 65 26 98
E-mail: zol@omgu.omsk.su

The solution of the problem of unequivocal determination of Amplitude, Phase, Frequency (APF), which correspond to the physical adequate of this parameters, is one of the fundamental problems of modern Electronics. The researching of presentation of radio pulse with rectangular envelope by analytical signal (AS) were carried out by A.K.Smolinski [1]. In the present work for radio pulse with rectangular envelope some fallacious postulates, which were attributed to AS, are eliminated.

D.E. Vakman and L.A. Vainshtein, trying to give fundamental study of AS in their works, considered this model as universal and exclusively true. It is suggested to consider correct and objective in mathematical, physical and technical sense the results, which issue only from AS applications, and to consider other determinations of signal's parameters valid to use even whereas they coincide with AS [2]. Moreover, basing upon the works of A.K.Smolinski [1] even it is suggested energetic handling of fore-runner and trace out of the interval of pulse's existence (with the help of special schemes).

Careful researches showed, that AS doesn't result in contradictions concerning given fore-runner and trace. In a short form it can be shown the next way. As far as in these time domains $f(t) \equiv 0$, we will write AS in the form of $\hat{f}(t)=0+j\hat{f}(t)$. Hence, though envelope $A(t)=|\hat{f}(t)|$ can exist, phase $\Phi(t)=\arg \hat{f}(t)= \pm \pi/2$ and therefore $f(t)=A(t)\cos\Phi(t)\equiv 0$ out of interval of radio pulse's existence. And what about the oscillations on the top of radio pulse, got from AS, which decay rapidly while withdrawal from its edges, there we have a phenomenon, which is similar to Gibbs phenomenon in Spectrum Theory, that was noticed for the first time in [3]. In frequency domain it is connected with initial signal spectrum's truncation on the frequencies negative semiaxis as necessary and sufficient condition of signal to be analytical. It is necessary to consider AS as one of approximative methods of complex signal presentation for solution of APF problem in electronics.

It was shown, that AS gives real signal's mathematical model, for which approximation defect is inherent. For the APF problem's solution the unicity of accordance of the representing function to its original is suggested to use [4,5]. This also outspreads on the solution of differential equipment of the system in the space of images.

References

[1] A.K.Smolinski. Bull. de L'Acad. Polon. des Sciences. V. XIX, No 4, pp.473-484, 1971.
[2] D.E.Vakman, L.A.Vainshtein. The Successes of Physical Sciences, vol.23, pp.657-682, 1977.
[3] I.D.Zolotarev. Digest "Electronic and Magnetic measuring devices", Omsk, OmPI, pp. 119–124, 1984.
[4] I.D.Zolotarev. Nonstationary processes in resonance amplifiers of phase-pulse measuring systems. Novosibirsk, Nauka, Siberian Division of Academy of Sciences of USSR, 1969.
[5] I.D.Zolotarev. Abstracts of the XXV General Assembly URSI. Lille, France, p.148, 1996.

C122.11

8PSK SIGNALING OVER NON-LINEAR SATELLITE CHANNELS

by
Rubén Caballero

Center for Space Telemetry and Telecommunications Systems
Klipsch School of Electrical and Computer Engineering
New Mexico State University

ABSTRACT

A study of 8 Level Phase Shift Keying (8PSK) modulation with respect to bandwidth, power efficiency, spurious emissions, interference susceptibility and the non-constant envelope effect through a non-linear channel is presented.

An end-to-end system performance, including the InterSymbol Interference (ISI) and the Bit Error Rate (BER) as a function of the Bit Energy to Noise Ratio (Eb/No) on 8PSK modulation was conducted on Signal Processing Worksystem (SPW) software installed on a SUN Sparc Station 10 and Hewlett Packard Model 715/100 Unix Station. The simulations were based on the Non-Return to Zero (NRZ) modulation format. The end-to-end system evaluation was performed using ideal and non-ideal data with ideal system components and three baseband filter types: Butterworth 5th Order, Bessel 3rd Order and Square Root Raised Cosine (SRRC) (α = 1) to observe the effect of pulse shaping on bandwidth and Symbol Error Rate (SER).

The simulations show that in-band spurious emissions are more present and more evident for the Bessel Filter than the Butterworth Filter (BT=1). With respect to the sideband attenuation, it was found that the values of attenuation for the 3rd Order Bessel filter are comparable to the 5th Order Butterworth filter. For SRRC filters with $\alpha = 0.5$, the bandwidth is narrower than the Butterworth and Bessel filters but the attenuation is less at high frequencies. Nonetheless, the absence of spurious emissions is a net advantage. For SRRC $\alpha = 1$, the bandwidth is wider than the two previous SRRC filters and the absence of in-band spurious emissions was again noticed. Less side band attenuation was recorded for this roll-off factor compared with $\alpha = 0.25$ and $\alpha = 0.5$. For SER, it was found that the Butterworth and Bessel filters just barely meet the threshold of ISI loss <0.4 dB at SER = 10^{-3}. Also the SRRC filters do not meet this specification. From these results, it can be stipulated that the 5th Order Butterworth filter has a small advantage compared to the other filters. Overall, it was shown by using baseband filtering that the bandwidth utilization can be improved by a factor of 12 to 24 with BT=1 and 8PSK which can significantly increase the spectrum utilization. Also a study on the tradeoffs between non-constant envelope and bandwidth in a non-linear system (SSPA) is discussed.

URSI D/A Special Session **Session 40** **Salon Peribonca**

Packaging and Interconnects
Co-chairs: G. Pan, USA and C.M. Rappaport, USA

08:10	40.1	Simulation Strategies Employing Electromagnetic Modeling Methodologies to Ensure First-Pass Design Success of an 8-Bit 2 GHz Gallium Arsenide Analog-to-Digital Converter Multichip Module for a Digital Radar Receiver, **R.L. THOMPSON**, M.J. DEGERSTROM, W.L. WALTERS, B.K. GILBERT, *Mayo Foundation, Rochester, MN, USA*
08:30	40.2	Quantification of Interconnect Coupling Mechanisms in Multilayer Substrates with Perforated Ground Planes, Y.-S. TSUEI[1], **A.C. CANGELLARIS**[2], [1]*Tandem Computers Inc., Cupertino, CA and* [2]*University of Arizona, Tucson, AZ, USA*
08:50	40.3	Coupling Effects in Vies and Flip-Chip Interconnects, **H. GHOUZ**, E. ELSHARAWY, *Arizona State University, Tempe, AZ, USA*
09:10	40.4	Port Size Effect on Power/Ground Plane Input and Transfer Impedances, **G.T. LEI**, R.W. TECHENTIN, B.K. GILBERT, *Mayo Foundation, Rochester, MN, USA*
09:30	40.5	Distributed Circuit Parameter Extraction from Field Theory in Full Wave Analysis, J. TAN[1], **G. PAN**[2], [1]*Compact Software Inc., Paterson, NJ and* [2]*Arizona State University, Tempe, AZ, USA*
09:50	40.6	High Density Multiconductor Transmission Line Parameters: Modeled Versus Measured, S. JAGANNATHAM, R. RUSSELL, M. KESLER, **J. GRIFFITH**, *W.L. Gore and Associates, Inc., Phoenix, AZ, USA*
10.10		Coffee Break

DA40.1

Simulation Strategies Employing Electromagnetic Modeling Methodologies To Ensure First-Pass Design Success of an 8-Bit 2 GHz Gallium Arsenide Analog-to-Digital Converter Multichip Module for a Digital Radar Receiver

Rick L. Thompson, Michael J. Degerstrom,
Wayne L. Walters, and Barry K. Gilbert
Special Purpose Processor Development Group
Mayo Foundation, Rochester, MN 55905

The digital radar receiver multichip module presently being developed as an upgrade to the U.S. Navy E2-C Hawkeye Airborne Early Warning Aircraft's APS-145 radar system uses heterojunction bipolar transistor monolithic A/D converter integrated circuits to directly digitize a radar signal in the 400-450 MHz UHF frequency band, without the need for traditional analog downconversion. The performance required for the digital radar receiver (DRR) demanded a 65 dB spurious free dynamic range with seven bits of resolution, while sampling at a clock rate greater than 2 GHz. The aggressive performance requirements dictated that the multichip module (MCM) be designed to provide a noise free environment throughout the intended bandwidth of operation.

It was crucial to the success of the project to predict the electrical behavior of the A/D converter chips in their packaging environment in order to direct the physical design of the components before fabrication and assembly. A critical component of the electrical modeling is the detailed and accurate simulation of all the module parasitics. These parasitics were computed with Mayo's multilayer multiconductor transmission line (MMTL) electromagnetic simulation tool suite. The MMTL electromagnetic simulator was used to extract the capacitive and inductive reactance matrices for the geometrically complex structures that comprise the multichip module.

This paper will describe the intensive application of MMTL in the electrical analysis of these A/D converter MCMs. MMTL was used to predict the even and odd mode characteristic impedances of analog and digital signals on both the DRR MCM and its supporting test fixture. The analysis of noise coupling from digital signals to the A/D converter preamplifier through the analog power planes will be presented. Further studies included the investigation of the integrated circuit digital output buffers' tendency to oscillate, which was induced by multichip module parasistics. Finally, a simultaneous switching noise analysis will be presented to demonstrate the utility of MMTL as it is employed in the modeling of very large numbers of conductors.

QUANTIFICATION OF INTERCONNECT COUPLING MECHANISMS IN MULTILAYER SUBSTRATES WITH PERFORATED GROUND PLANES

Yuh-Sheng Tsuei
Tandem Computers Inc.
19333 Vallco Parkway, LOC 3-09
Cupertino, CA 95014-2599

*Andreas C. Cangellaris**
Department of Electrical and Computer Engineering
Center for Electronic Packaging Research
University of Arizona
Tucson, AZ 85721
Phone: 520/621-4521 FAX: 520/621-2999
email: cangellaris@ece.arizona.edu

The electromagnetic characterization of interconnects in multilayer substrates with perforated ground/power planes has been an issue of concern for several years. Several investigators have proposed and used a variety of methodologies to calculate interconnect characteristic impedance, propagation constant, as well as coupling coefficients for crosstalk analysis, and establish their dependence on perforation dimensions and perforation orientation with respect to the interconnect axis. However, very little attention has been given to other electromagnetic effects associated with the perforated characteristics of the power ground planes and their impact on signal integrity.

In this paper, a rigorous, full-wave electromagnetic field solver is used to model high-speed pulse propagation in interconnect structures with perforated reference planes. Contrary to previous modeling approaches, the true three-dimensional characteristics of the interconnect structure are modeled. Consequently, the simulation results provide for a thorough investigation of all electromagnetic effects associated with these waveguiding structures. In particular, attention is paid to a specific noise interaction mechanism that has not been investigated thoroughly in previous studies. This mechanism is associated with the surface waves excited at interconnect discontinuities and supported by the perforated planes. It is well-known that such perforated planes exhibit inductive surface impedance properties and thus can support transverse magnetic (TM) surface waves. These waves have field distributions similar to that of the quasi-TEM mode supported by the interconnects. Consequently, their presence can lead to an unexpected noise coupling mechanism which is quite different from the familiar inductive and capacitive coupling. Three-dimensional field visualization, as well as visualization of the current flow on the perforated planes is used to facilitate the discussion and interpretation of the aforementioned electromagnetic effects.

DA40.3

Coupling Effects in Vies and Flip-Chip Interconnects

By

Hussein Ghouz and Elbadawy Elsharawy, Senior Member IEEE

Arizona State University

Tempe, AZ85287-7206

Phone: (602) 965-8591, Fax: (602) 965-8591, email: elsharawy@envs10.eas.asu.edu

Flip chip technology is emerging as the lead technique in backing passive and active microwave and millimeter wave integrated circuits (MMIC). This technology permits the use of different integration levels and several combinations of substrate and superstrate materials (mother board and chip). In addition, low cost, high density and short interconnects are considered to be the main advantages of the flip chip technique. However, there are several problems associated with this technology. Interconnect discontinuities (bumps), losses and electromagnetic coupling are among the main problems associated with the flip chip technique. In this paper, the transition discontinuities of flip chip circuits are modeled and investigated using FD-TD method to predict the s-parameters of different packages. The coupling effects between two different discontinuities are investigated. The computed s-parameters of the package including coupling are compared to those obtained by ignoring the coupling effects. The limits at which the coupling effects become prominent are studied and presented. The paper also includes the evaluation of the coupling between multiple signal lines including a flip chip or a via transition to study the interference between these lines due to package discontinuity.

Port Size Effect on Power/Ground Plane Input and Transfer Impedances

G. T. Lei, R. W. Techentin, and B. K. Gilbert
Special Purpose Processor Development Group
Mayo Foundation, Rochester, MN 55905

Accurate modeling of Power/Ground plane noise is becoming increasingly important in the design of high speed digital and mixed signal modules. The effect of port size (corresponding to via hole size) on the input and transfer impedances of the structure can have a significant impact on the system noise characteristics. It has been demonstrated that ignoring the port size effects can introduce significant simulation errors, and a numerical method has been introduced to compensate. (Z.J. Fang, and Y. Liu, Proceedings of the 10th Annual Review of Progress in Applied Computational Electromagnetics, March 1994, pp. 38-45).

We present a new semi-analytical approach to evaluate the effects of port size on the input and transfer impedances based on the "full-wave" field model which we have employed to characterize power/ground plane structures of printed wiring boards (PWBs) and multichip modules (MCMs) (G.T. Lei, R.W. Techentin, P.R. Hayes, D.J. Schwab, and B.K. Gilbert, IEEE Transactions on Instrumentation and Measurement, Vol. 44, No. 2, April. 1995). The Z matrix elements are obtained from

$$Z_{ij} = \sum_{m=0}^{\infty}\sum_{n=0}^{\infty} \left(\frac{j\omega\mu d C_m^2 C_n^2}{P_x P_y\left(k_{xm}^2+k_{yn}^2-k^2\right)}\right) \cos\left(k_{yn}T_{yi}\right)\cos\left(k_{xm}T_{xi}\right)\cos\left(k_{yn}T_{yj}\right)\cos\left(k_{xm}T_{xj}\right)\times$$
$$\left[\frac{\sin\left(k_{yn}\frac{L_{yi}}{2}\right)}{k_{yn}\frac{L_{yi}}{2}}\right]\left[\frac{\sin\left(k_{xm}\frac{L_{xi}}{2}\right)}{k_{xm}\frac{L_{xi}}{2}}\right]\left[\frac{\sin\left(k_{yn}\frac{L_{yj}}{2}\right)}{k_{yn}\frac{L_{yj}}{2}}\right]\left[\frac{\sin\left(k_{xm}\frac{L_{xj}}{2}\right)}{k_{xm}\frac{L_{xj}}{2}}\right]$$

where m and n represent the m'th and n'th modes associated with the x and y dimensions; P represents the metal plane dimensions; T is the port center-point coordinates; L represents the port widths, which are much shorter than the wavelengths of interest; k represents the real wave number for the lossless case; $k = \omega\sqrt{\mu\epsilon}$, $k_{xm} = \frac{m\pi}{P_x}$ and $k_{yn} = \frac{n\pi}{P_y}$; d is the dielectric thickness; μ and ϵ are the dielectric permeability and permittivity; ϵ_r stands for the relative dielectric constant; Here, $C_m = 1$ if $m = 0$, and $C_m = \sqrt{2}$ if $m \neq 0$. Similarly, $C_n = 1$ if $n = 0$, and $C_n = \sqrt{2}$ if $n \neq 0$.

Simulations were performed for an MCM typical of a front-end of an all-digital receiver. Input and transfer impedances were calculated for a number of port sizes and locations over a wide frequency range. The impedance effects of differing port sizes were analyzed by computing the algebraic difference, as a function of frequency, between the impedances of zero-size and finite-size ports. It will be shown that the finite-size ports contribute a frequency independent negative inductance to the input impedance for any given port, but that the transfer impedance is essentially unaffected. The additional inductance is most pronounced for ports located at the corners of the module, and increases with port size.

This discovery enables us to easily modify any other numerical simulations of unloaded power/ground plane structures to compensate for the effects of finite-size vias by simply adding an appropriate inductor at the port location.

DA40.5

Distributed Circuit Parameter Extraction from Field Theory in Full Wave Analysis

Jilin Tan
Compact Software Inc.
Paterson, NJ 07432
George Pan
Arizona State University
Tempe, AZ 85287

In this paper we present a technique that extracts frequency dependent circuit parameters of multiconductor transmission lines with arbitrary cross-sections and embedded in an arbitrary dielectric environment. The technique is solely based upon the field superposition principle and power equivalence concept.

The Newly developed formulation is suitable to any full wave analysis in the spectral domain, where the eigenvalues and eigenvectors of the system have been obtained. In particular, the new method is appropriate for use in combination with the edge element formulation, which latter totally suppresses the spurious modes. At low frequencies these parameters are essentially the same as those from the quasi-static solutions. However, at high frequencies, it is found that the substrate loss can cause not only the conductance but also the resistance; while conduct loss can contribute not only to resistance, but also to conductance. Physical examples support the formulas.

The new method is mathematically simple and accurate, physically clear and unambiguous, and is easily converted into a computer aided engineering (CAE) tool.

High Density Multiconductor Transmission Line Parameters: modeled versus measured

Swamy Jagannatham, Rob Russell, Matt Kesler, Jim Griffith*

During the past few decades investigators [1,2] have developed powerful numerical tools for analyzing/predicting the electrical parameters of MTL. The method-of-moments (MOM) approach is often used because of its speed and ease of application from existing codes. For calculating inductance and capacitance, MOM methods generally assume perfect conductors with all the current flowing on the surface rather than being somehow distributed through the conductor cross section. Theoretical and measured parameter values combine to show that the perfect conduct assumption produces accurate results for many applications. However for high density applications where round-conductor spacing approximates the wire diameter, accuracy of the computed values is not established.

We have compared MOM predicted parameters to measured parameters for several high density MTLs. Cables fabricated by the Signal Transmission Group of W.L. Gore and Associates, code from previous investigators [1,2], and a multi-port network analyzer (HP4380S) from Hewlett-Packard were used in this investigation.

Preliminary results with two different cable cross-sections show that the modeled values of MTL inductance, and capacitance are within +/- 20% of the corresponding measured values. We conclude that the perfect conductor assumption is reasonable for calculating approximate inductance and capacitance values. Obtaining close tolerance (say +/- 10%) values for closely spaced round wires will likely require inclusion of internal inductance and proximity effects.

References:

[1] G.W. Pan, et.al., "The simulation of high-speed, high-density digital interconnects in single chip packages and multichip modules," IEEE Trans. Components, Hybrids, and Manufacturing Technol., vol. 15, pp. 465-477, Aug. 1992.

[2] A.R. Djordjevic, T.K. Sarkar, and R.F. Harrington, "Time-domain response of multiconductor transmission lines", Proceedings of IEEE, vol. PROC-75, pp.743-764, June 1987.

* presenter

URSI D/A Special Session **Session 56** **Salon Peribonca**

Microwave Integrated Circuits for Commercial Applications
Co-chairs: G. Hegazi, USA and A.M.K. Saad, Canada

13:10 56.1 Low Temperature Co-Fired Ceramics - An Enabling Technology for 3D Integrated Circuits for Wireless Applications, **A.E. FATHY**, M. LIBERATORE, D. CHIN, B. THALER, J. FIELDS, B. GELLER, *David Sarnoff Research Center, Princeton, NJ, USA*

13:30 56.2 Evanescent Mode - Ridge Waveguide Technology: An Effective Tool to Design Passive Microwave Components, **A.M.K. SAAD**, *Scientific Microwave Corporation, Mississauga, ON, Canada*

13:50 56.3 **Invited:** Millimeter-Wave P-HEMT Low-Noise and Power MMIC Amplifiers for the Commercial Market, **T. LEE**, L. PHELPS, J. SINGER, G. HEGAZI, S.W. CHEN, J. BASS, W. LI, J. REDUS, *MA-COM Inc., Clarksburg, MD, USA*

14:10 56.4 **Invited:** Point to Multi-Point Radio for Data Communications, **K. PANDE**, *Synoptel, Inc., Gaithersburg, MD, USA*

14:30 56.5 Electromagnetic Wave Effects on High Frequency Transistors, S.M. HAMMADI, **S.M. EL-GHAZALY**, *Arizona State University, Tempe, AZ, USA*

DA56.1

Low Temperature Co-Fired Ceramics - An Enabling Technology for 3D Integrated Circuits for Wireless Applications

Aly E. Fathy, Michael Liberatore, Daniel Chin, Barry Thaler,
John Fields, Bernard Geller
David Sarnoff Research Center
201 Washington Road, Princeton, New Jersey 08540

Low Temperature Co-fired Ceramic (LTCC) circuits provide a low cost means of realizing real 3D microwave integrated components. Several circuits that are difficult to fabricate in a single planar configuration can be easily implemented using this multi-layer technology. Various lumped passive and distributed rf components can be conveniently embedded using this multi-layer stacking approach.

Wireless communication products, for example, utilize mixed signal designs (containing both high-speed digital and analog circuits). These designs require a large number of discrete passive components that use a sizable percentage of the module/PWB area, greatly limiting the potential for miniaturization as well as adversely affecting the performance of these products. The embedding of these passive components in a 3D stack will result in integration of rf, microwave, and high speed digital functions. Even the antennas can be integrated thus achieving a high packaging density at low cost.

We will present our efforts in developing this enabling technology for microwave circuits, integrated antennas, and packaging applications. Circuit modeling, rf measurement results, new design considerations, and the leverage this technology provides will be emphasized.

EVANESCENT MODE - RIDGE WAVEGUIDE TECHNOLOGY

AN EFFECTIVE TOOL TO DESIGN PASSIVE MICROWAVE COMPONENTS

BY
DR. A. M. K. SAAD
SCIENTIFIC MICROWAVE CORPORATION
MISSISSAUGA, ONTARIO, CANADA

THIS PRESENTATION WILL HIGHLIGHT THE POTENTIAL OF THE EVANESCENT MODE - RIDGE WAVEGUIDE TECHNOLOGY IN THE DESIGN, DEVELOPMENT AND REALIZATION OF VARIOUS TYPES OF PASSIVE MICROWAVE COMPONENTS FOR MILITARY, SPACE AND COMMERCIAL APPLICATIONS.

TO DEMONSTRATE THE VERSATILITY OF THIS TECHNOLOGY VARIOUS RIDGE WAVEGUIDE STRUCTURES IMPLANTED IN AN EVANESCENT MODE WAVEGUIDE WERE USED IN THE DESIGN AND MANUFACTURING OF DEFFERENT CLASSES OF PASSIVE MICROWAVE COMPONENTS.

THE RIDGE WAVEGUIDE STRUCTURES WHICH WILL BE CONSIDERED IN THIS PRESENTATION ARE:
- SINGLE RIDGE;
- SINGLE RIDGE WITH TM COUPLING;
- DOUBLE ANTIPODAL RIDGE;
- DOUBLE ANTIPODAL RIDGE WITH GROOVE;

THESE STRUCTURES WERE USED IN THE DESIGN OF THE FOLLOWING CLASSES OF PASSIVE MICROWAVE COMPONENTS:
- LOWPASS HARMONIC FILTERS;
- BANDPASS HARMONIC FILTERS WITH SERRATED OR UNSERRATED RIDGE;
- 3-PORT CIRCULATORS;
- RIDGE SHAPED HYBRIDS AND COUPLERS.

IT WILL BE SHOWN THAT BY USING THIS TECHNOLOGY, PASSIVE MICROWAVE COMPONENTS WITH WIDE BANDWIDTH AND HIGH POWER HANDLING CAPABILITY WITH COAX OR WAVEGUIDE (STANDARD OR RIDGED) INTERFACES CAN BE ACHIEVED.

IT IS IMPORTANT TO MENTION THAT THE ABOVE MENTIONED TECHNOLOGY WAS DEVELOPED TO SOLVE REAL TECHNICAL PROBLEMS TO FACE THE CHALLENGES OF THE EVER GROWING DEMAND FOR WIDEBAND AND HIGH POWER PASSIVE MICROWAVE COMPONENTS.

DA56.3

Millimeter-wave P-HEMT Low-Noise and Power MMIC Amplifiers For The Commercial Market

Submitted by:
T. Lee, L. Phelps, J. Singer, G. Hegazi *,
S. W. Chen, J. Bass, W. Li, and J. Redus

MA-COM Inc.
IC Business Unit
Millimeter IC Products +
Clarksburg, MD 20871

Abstract

MA-COM's Millimeter IC Products (MICP) has developed a family of advanced P-HEMT based millimeter-wave MMIC amplifiers to address the commercial market which is currently driven by the point-to-point digital radio applications and near term automotive sensor systems. In the area of low-noise amplifiers, MICP has developed a family of 15-GHz, 18-GHz, 23-GHz, 26/28-GHz, and 38-GHz P-HEMT MMIC LNAs based on a 0.18-micron low-noise P-HEMT process. Typical chip performance achieved include 1.64-dB NF and 19-dB gain at 15 GHz, 2.20-dB and 20-dB gain at 23 GHz, to 4.5-dB with 18-dB gain at 38 GHz. Experimental wafers with 0.18-micron T-gate indicates that a 0.3- to 1-dB improvement in MMIC NF can be achieved, depending on the particular frequency band. MICP has also developed power amplifier MMICs to cover the same millimeter-wave radio bands using MICP's power P-HEMT process. The 18 to 23-GHz PA exhibits 20-dB gain and greater than 24.5 dBm P1dB, the 26-GHz PA exhibits 20-dB gain and greater than 23 dBm P1dB across the 24.2 to 26.5 GHz band and the 38-GHz PA exhibits 18-dB gain with greater than 22 dBm P1dB across the 37 to 40 GHz frequency band. Both families of LNAs and PAs will be translated to the base-lined LH5 and PH5 MMIC processes once they are released for production. In addition to the radio market, many of these MMICs will find applications in automotive electronics for collision avoidance/warning and autonomous-intelligent-cruise control systems where 18-GHz and 38-GHz parts can form the basis of a frequency multiplier chain to achieve 77-GHz signal generation.

* G. Hegazi is currently with Motorola.

+ Millimeter IC Products is a Division of Amp Incorporated.

Point to multi-point radio for data communications

Krishna Pande
Synoptel, Inc.
12200 Galesville Drive
Gaithersburg, MD 20878

ABSTRACT

Point to multi point radio market is witnessing ~30% growth for PCS cell site link and data communications. Speed and channel capacity of such radios are critical parameters for addressing large packet of data transmission. This presentation will address the architecture of radios and associated transceivers that can provide more than 8 channels and higher than 16Mbit/sec. speed. The design of components and subsystems based on P-HEMT MMIC technology will be reported for transmitter/ receiver amplifiers that can deliver more than 250 milliwatt output power and less than 5.5 dB noise figure. An unique power amplifier design that can deliver linearity without sacrificing efficiency will be highlighted.

DA56.5

Electromagnetic Wave Effects on High Frequency Transistors

Samir M. Hammadi, and Samir M. El-Ghazaly

Department of Electrical Engineering
Arizona State University
Tempe, AZ 85281-5706

Abstract

Conventionally, physical modeling and numerical simulation of semiconductor devices are developed totally independent from electromagnetic wave effects on electron dynamics. At very high frequencies, however, the carriers relaxation times become comparable to the period of the propagating waves inside the device, and the electron-wave coupling becomes significant and cannot be neglected. Moreover, for short gate-length devices high time-varying electromagnetic fields can be present and a strong electromagnetic coupling between device electrodes is also present and adds to parasitics effects in the device operation. Therefore, the conventional semiconductor modeling and simulation should be reviewed for very high frequency devices and more accurate models that takes into account the electromagnetic wave effects needs to be developed.

In this presentation an FDTD scheme that incorporates the full-wave solution of maxwell's equations into the simulation of a MESEFT transistor is discussed. Many results illustrating various aspects of device simulation will be presented. First an accurate hydrodynamic model for the semiconductor device is developed. Next a full-wave solution of Maxwell's equation is developed for the passive structure of the device. Finally the two models are coupled together using the relation between electric field and the conduction current.

To illustrate the electromagnetic wave effects on the MESFET operation, results are given for three different cases. In the first case results are computed from the simulation of the semiconductor model only. In the second case results from the full-wave electromagnetic model for the passive structure are given, and finally results from the coupled models is illustrated.

URSI E | Session 28 | Salon Chaudière

Electromagnetic Compatibility and Interference (EMC/EMI)
Co-chairs: A. Pinchuk, Canada and J.-J. Laurin, Canada

13:10	28.1	Numerical Modeling of Printed Circuit Boards for EMI/EMC Compliance, **A.H. MOHAMMADIAN**, W.F. HALL, V. SHANKAR, *Rockwell International Science Center, Thousand Oaks, CA, USA*
13:30	28.2	Transient Simulation of Noise Interactions in Printed Circuits, **T. LIANG**, A.C. CANGELLARIS, *University of Arizona, Tucson, AZ, USA*
13:50	28.3	Dyadic Green's Function Formulation Applied to the EMC/EMI Modeling in Planar Circuits, P. BERNARDI, **R. CICCHETTI**, A. FARAONE, *University of Rome "La Sapienza", Rome, Italy*
14:10	28.4	Cross Coupling between the Power and Signal Traces on Printed Circuit Boards, **Z. PANTIC-TANNER**[1], E. SALGADO[1], D. TANNER[2], F. GISIN[3], [1]*San Francisco State University, San Francisco,* [2]*Lockheed Martin, Sunnyvale and* [3]*Silicon Graphics, Mountain View, CA, USA*
14:30	28.5	Efficient Calculation of Line-to-Line Parasitics in MMIC Circuits, **J.M. DUNN**, D. GINES, H. MacMILLIAN, J. PEETERS-WEEM, *University of Colorado, Boulder, CO, USA*
14:50	28.6	A Multi-Wire Formalism for the FDTD Method, **J.-P. BERENGER**, *Centre d'Analyse de Défense, Arcueil, France*
15:10		Coffee Break
15:30	28.7	Coupling of High Frequency Waves to an Overhead Cable: Influence of the Insulating Jacket, F. LABARRE, **P. DEGAUQUE**, *Université des Sciences de Lille, Villeneuve d'Ascq, France*
15:50	28.8	Experimental Validation of Models for External Field Coupling to MTL Networks with Nonlinear Junctions, **T. LAPAHOS**[1], J. LOVETRI[1], J. SEREGELYI[2], [1]*University of Western Ontario, London and* [2]*Defence Research Establishment Ottawa, ON, Canada*
16:10	28.9	Optimizing System Peak Responses Caused by High Power Microwaves, **D.P. McLEMORE**, S. KOKOROWSKI, K.S.H. LEE, *Kaman Sciences Corporation, Albuquerque, NM, USA*

E28.1

Numerical Modeling of Printed Circuit Boards for EMI/EMC Compliance

A. H. Mohammadian[†,*], W. F. Hall, and V. Shankar
Rockwell International Science Center
1049 Camino Dos Rios
Thousand Oaks, California 91360
†*E-mail: ahm@hertz.risc.rockwell.com*

Printed circuit boards (PCB) (for both digital and analog circuits) must comply with regulatory directives which limit the amount of radiative emission from most electronic devices. It is of interest to the designers of these devices to estimate the amount of radiation from their devices in the design stage and before a prototype is built.

The radiation from PCBs are often the result of either electrically long conductors that behave like dipole antennas, or closed circuits that act like loop antennas. Therefore, to compute the radiation from these antennas one would need to compute either the current distribution on the PCB or the electromagnetic field around it. Generally, the accurate way to compute these quantities is to solve Maxwell's equations numerically. However, most PCBs are so complex that a full wave numerical solution is out of question at the present time. There are approximate methods based a quasi-TEM assumption for the traces (microstrips and striplines) that reduce this complexity and circumvent a full wave solution. These methods can only be applied to a limited class of digital PCBs that follow certain design rules. Even then the accuracy of radiation prediction has not yet been established.

Therefore, it seems to be almost inevitable to use a full wave numerical solution method to obtain some estimate of the radiation from a PCB or at least from regions on a PCB that are more likely to be responsible for excess radiation. Most analog or mixed PCBs used in power electronics such as power drives, rectifiers, etc., fall in this category.

In this research effort, we have tried to investigate the feasibility and usefulness of a full wave numerical simulation of critical traces and metalized areas on a PCB for PCB designers. We will present scopes and limitations of some popular numerical techniques including the method of moments (MoM), finite elements method (FEM), and finite-difference time-domain method (FD-TD) for the type of problems that we previously explained. In our numerical simulations, both commercial software tools and in-house research codes have been used. Also the simulations cover both simple PCBs such as a wide trace over a ground plane with a slot, and complex multilayer PCBs used in power electronics. The emphasis is to define and identify suitable numerical methods and software tools for these kinds of simulations.

TRANSIENT SIMULATION OF NOISE INTERACTIONS IN PRINTED CIRCUITS

Tao Liang* and Andreas C. Cangellaris
Electromagnetics Laboratory
Department of Electrical and Computer Engineering
University of Arizona, Tucson, AZ 85721

As digital circuit clock frequencies begin approaching the GHz regime, full-wave electromagnetic analysis becomes necessary for the accurate prediction of the various types of electromagnetic noise induced by the interconnect and package in performance-driven electronic systems. In addition, the aggressive integration of both digital and high-frequency, RF/microwave sensitive circuitry, further enhances the need for accurate electromagnetic compatibility analysis of the system. Accurate quantification of these noise effects is essential for proper system partitioning and layout, not only for preserving signal integrity, but also for avoiding electromagnetic interference problems that may prevent the component from meeting FCC electromagnetic compatibility regulations.

Of particular interest to this work is the prediction of electromagnetic noise coupling to interconnects on printed circuit boards. There are numerous studies in the literature that have shown that such coupling can be predicted with sufficient engineering accuracy using transmission line theory. However, most of the results are limited to plane wave radiation coupling. In this paper, the validity of this theory for other types of electromagnetic radiation noise, often occuring in printed circuit board environments, is examined.

In particular, the finite-difference time-domain (FD-TD) method is used to investigate radiation coupling to printed circuit board interconnects. Due to the complexity of the interactions in a practical circuit layout, we assumed the radiation to be arbitrary incident fields. More specifically, the emphasis of the simulation is placed on the noise generated by discontinuities in the layout in the vicinity of the victim interconnection. The calculated voltages are compared with those obtained from FD-TD simulations with the victim interconnects in place. The results from these comparisons are then used to establish the frequency range over which the transmission line model approach leads to results of acceptable engineering accuracy.

E28.3

Dyadic Green's Function Formulation Applied to the EMC/EMI Modeling in Planar Circuits

Paolo Bernardi, Renato Cicchetti, and Antonio Faraone*

University of Rome "La Sapienza", Department of Electronic Engineering,
Via Eudossiana 18, 00184 Rome, ITALY

A reliable prediction of microwave and millimeter wave planar integrated circuit and antenna behavior requires the inclusion of all physical phenomena that influence their performance. These phenomena are related with the excitation of volume and surface waves, which remarkably affect the circuit behavior when substrates with high dielectric permittivity are employed. Degradation of circuit performance may occur if the effects associated with these phenomena are not properly accounted for at design stage, frequently resulting in EMC/EMI intrasystem problems and longer design practices.

In this frame, full-wave methodologies are gaining wider interest as reliable prediction tools for MIC's and MMIC's design, given their versatility in handling complex structures within reasonable computation time (J. X. Zheng, *Int. J. MIMICAE,* 384-395, 1994). Methodologies based on integral equation formulations that employ the dyadic Green's function to express the electromagnetic field are well suited for the frequency-domain analysis of planar microstrip circuits and antennas (T. Itoh Ed., *Numerical Techniques for Microwave and Millimeter-Wave Passive Structures*, New York: John Wiley & Sons, 1989).

In this contribution, a SDA-based modeling approach, suitable for the full-wave analysis of wide classes of planar integrated structures, as well as to predict their EMC/EMI characteristics, is presented. Upon adopting the appropriate dyadic Green's function (P. Bernardi, R. Cicchetti, *IEEE MTT Trans.*, 8, 1474-1483, 1994) a significant number of typical EMC problems, ranging from discontinuity effect characterization to susceptibility analysis with respect to external electromagnetic sources operating in the near-field region, can be studied (P. Bernardi, R. Cicchetti, A. Faraone, *Annales des Telecom.*, 3-4, 1997). For example, in fig. 1 the current induced along a microstrip line excited by an external horizontal magnetic dipole source is shown. Upon deriving an equivalent network representation, the model allows the inclusion of more realistic exciting/loading configurations.

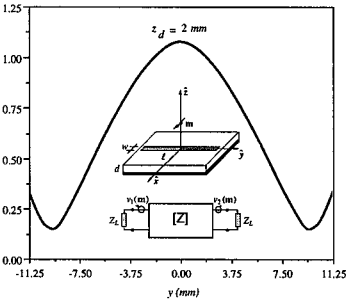

Fig. 1 *Current magnitude induced along a matched microstrip interconnect (d=1.57 mm, w=1.38 mm, ε_r=10) excited by a unitary magnetic dipole.*

The electrical behavior of circuital layouts of medium complexity can be predicted in realistic operation with a high degree of reliability, so that possible EMI problems can be individuated and reduced already during the design stage. Dyadic Green's function formulations can be also employed in hybrid models useful for fast analysis of transient electromagnetic phenomena. In particular, the transient emission from microstrip interconnects can be predicted by adopting a transmission-line model including dispersion for signal propagation, with a subsequent asymptotic evaluation of the radiation integral involving the Green's function (R. Cicchetti, A. Faraone, *IEEE EMC Trans.*, 3, 367-375, 1996).

Further extensions in the range of applicability of the methodology, for example with the inclusion of uniaxial anisotropy, are under way, and the relevant results will be presented at the Symposium.

CROSS COUPLING BETWEEN THE POWER AND SIGNAL TRACES ON PRINTED CIRCUIT BOARDS

Z. Pantic-Tanner, and E. Salgado*
San Francisco State University
San Francisco, CA 94132

D. Tanner
Lockheed Martin
Sunnyvale, CA 94088-35

F. Gisin
Silicon Graphics
Mountain View, CA 94039

Switching power supplies and other power switching circuits produce high frequency components in currents on power traces and power ground in printed circuit boards (PCBs). These currents are then electromagnetically coupled to low level signal traces and can cause significant interference. The goal of this paper is to evaluate the coupling mechanisms in order to develop ground rules for circuit board design that would minimize this interference.

For lower frequencies a quasi-static model will be used. The distributed parameters (inductance, capacitance, resistance and conductance) of the equivalent multi-conductor transmission line will be calculated using commercially available software packages Maxwell by Ansoft and EMC-Workbench by Incases. The coupling at the near and far ends of the line will be determined using the SPICE program. The effect of proximity and position of power switching circuits with respect to the signal traces will be examined. Also, the effect of the properties of the dielectric substrate will be evaluated. Practical solutions for noise reductions such as decoupling capacitors and ferrite beads will be consequently included in the SPICE model.

For higher frequencies a full wave model will be used. The S-parameters of the equivalent multi-conductor transmission line will be calculated using commercially available software packages Maxwell by Ansoft and EMC-Workbench by Incases. Frequency dependence of the dielectric material will be taken into account. The placement of the components on the board will be studied in order to optimize their relative position. Also, advantages of the divided ground plane versus single ground plane will be examined.

Single and multi-level boards will be considered. Firstly, the PCBs with widely spaced planes and low capacitance will be examined and the number and values of the decoupling capacitors determined. Secondly, the newly emerging circuits with small spacing between layers and corresponding high-capacitance low-inductance power planes will be evaluated.

E28.5

Efficient Calculation of Line-to-Line Parasitics in MMIC Circuits

John M. Dunn*, David Gines, Hugh MacMillian, and Jan Peeters-Weem
Department of Electrical and Computer Engineering
University of Colorado
Campus Box 425, Boulder, CO, 80309-0425

Parasitic coupling is defined to be unintended electromagnetic interactions between various portions of a circuit. This type of coupling is normally quite weak; however, it can have deleterious effects on the circuit's performance if sensitive portions are coupled. Although the coupling can be calculated by using a full wave field simulation tool, it is usually to slow to be useful to the engineer. In this talk, we will discuss an approximate technique for calculating the coupling between microstrip lines in a circuit, which overcomes this disadvantage.

The method is based on an approximate solution of the standard, electric field, integral equation (EFIE) for the problem. A typical geometry consists of N lines lying on a substrate. The conventional moment method would calculate the coupling between the lines using a moment method with an appropriate basis. Most commonly, "roof top" basis and testing functions would be used for the current. Essentially, our technique speeds up the solution of the coupling calculation by using transmission line basis functions, and throwing out non-essential elements of the resulting matrix equation.

The method will not be as accurate as a conventional moment method if the lines are close together. Therefore, the technique is not considered a design tool. Rather, it is to be regarded as a design verification tool, in which the engineer can quickly see if parasitics are a problem. If they are, further redesign is indicated.

We will present details of the basic algorithm, and give results of benchmark cases. The benchmark cases will be examined for both speed and accuracy of the algorithm.

A MULTI-WIRE FORMALISM FOR THE FDTD METHOD

J.-P. BERENGER

Centre d'Analyse de Défense
16 bis, Avenue Prieur de la Côte d'Or 94114 Arcueil, France
Berenger@cad.etca.fr

The thin wire formalism (R. Holland and L. Simpson - IEEE EMC, May 1981) permits wires whose radius are small as compared to the size of the cells to be set within a FDTD computational domain. Such a formalism allows problems involving thin wires or both thick structures and thin wires to be easily solved by means of the FDTD method. In past years, it has been extensively used in EMC applications. Nevertheless, the use of this formalism is limited by the fact that the separation between wires must be at least equal to one cell, in other words only one wire can be set through a given cell. For this reason, with the intention of extending its domain of application, we have generalized the initial formalism to a multi-wire formalism that allows bundles composed of parallel wires to be taken into account. With the multi-wire formalism, the separation between wires of the same bundle can be as small as needed.

The first part of the paper will present the principle and assumptions of the multi-wire formalism and the equations governing the currents on the multi-wires. Numerical comparisons with the integral equation method (TWTD method) will show that the interactions between the wires of a bundle are well taken into account with the generalized formalism, on the contrary to the initial formalism.

The second part will be devoted to the important problem of connecting multi-wires. The method allowing a multi-wire to be connected either to a wire or another multi-wire will be presented. This allows complex structures (i.e. circuits) composed of wires and multi-wires to be modeled and set within a FDTD computational domain. In order to validate the connections, a comparison with the integral equation method will be shown, for a loop composed of wires and multi-wires.

The conclusion will be that the thin wires formalism can be generalized to a multi-wire formalism that enables the FDTD computer codes to deal with bundles and arbitrarily close wires.

E28.7

COUPLING OF HIGH FREQUENCY WAVES TO AN OVERHEAD CABLE : INFLUENCE OF THE INSULATING JACKET

F. Labarre and P. Degauque
Université des Sciences de Lille, Electronics Dept, Batiment P3
F- 59655 Villeneuve d'Ascq Cedex, France

Many theoretical studies deal with the coupling of an incident plane wave to a bare wire parallel to the air-ground interface. The problem is usually solved by means of an integral equation relating the incident field to the current distribution or by assuming that the height of the wire is small enough so that a transmission line model can be applied. Furthermore, explicit solutions can be obtained at low frequency, the conduction current in the ground being much higher than the displacement current ($\sigma_g >> \omega\varepsilon_g$). This leads to the well-known quasi-TEM approximation.

The purpose of this contribution is to show that the transmission line approach can be extended to the high frequency range ($\omega\varepsilon_g >> \sigma_g$) and that the dielectric jacket covering the cable may play an important role on the induced current amplitude. We present a comparison between transmission line and antenna theory and, in order to get explicit expressions, which are easiest to compare, we restrict the problem to the coupling of a plane wave to an infinitely long wire.

In the antenna theory, the longitudinal electric field radiated by the wire is calculated on the surface of the jacket and, by introducing the concept of surface impedance, the induced currents are expressed in terms of the height of the wire and of of the characteristics of the ground and of the dielectric jacket covering the cable. In the transmission-line approach, the per unit length impedance Z and admittance Y are expressed in terms of the same variables as previously but they also depend on the propagation constant of the current induced on the wire. In other words, it means that Z and Y are no more intrinsic parameters of the overhead line but depend on the angle of incidence of the plane wave illuminating the structure. In the usual quasi TEM approximation, this is not important since the terms in which the angle of incidence appears are within the Sommerfeld integrals characterizing the radiation of the structure and which do not play a dominant role in the low frequency range. Furthermore, even by taking these integrals into account, it appears from the mathematical expressions, that the effect of the angle of incidence of the disturbing wave on the values of Z and Y are negligible if $\sigma_g >> \omega\varepsilon_g$. In our case, we will show the limits of such an approximation.

In order to illustrate the theoretical approach, results on the coupling of high frequency waves to an horizontal cable will be presented. In the case of a grazing angle of incidence, giving rise to important induced currents, it appears that the effect of the insulating jacket covering the cable remains negligible up to 100 MHz. However, above this frequency, the jacket tends to decrease considerably the amplitude of the induced current. In the time-domain,the peak amplitude of short rise time induced currents (on the order of few ns) and due, for example, to a NEMP, will thus be reduced by the influence of this jacket as it can be shown on few examples.

Experimental Validation of Models for External Field Coupling to MTL Networks with Nonlinear Junctions

Tibor Lapahos *Joe LoVetri*
Dept. of Electrical and Computer Eng.
The University of Western Ontario
London, Ontario, Canada N6A 5B9
Phone: (519) 679-2111 ext. 8342
Email: joe@gauss.engga.uwo.ca
tibor@gauss.engga.uwo.ca

Joe Seregelyi
Defence Research Establishment Ottawa
Electronic Countermeasure Section
3701 Carling Avenue
Ottawa, Ontario, Canada, K1A 0Z4
Phone: (613) 998-5576
Email: Joe.Seregelyi@dreo.dnd.ca

We presents a series of practical experiments aimed at validating the numerical modelling of external field coupling to multiconductor transmission line (MTL) networks with non-linear junctions. The measurements are performed in both the frequency and the time domain using a GTEM cell where the circuits subjected to analysis are printed circuit boards (PCB) containing MTLs above a ground plane and terminated with diodes and passive elements. The transmission lines are modelled by the quasi-TEM transmission line equations and they are solved using FDTD techniques (C.R. Paul, Analysis of Multiconductor Transmission Lines, John Wiley, 1994). The modelling equations are:

$$\partial_x v(x,t) + L\,\partial_t i(x,t) + R\,i(x,t) = V_F(t),\ \partial_x i(x,t) + C\,\partial_t v(x,t) + G\,v(x,t) = I_F(t)$$

where L, C, R, and G are the per unit length inductance, capacitance, resistance and conductance matrices respectively, $v(x,t)$ is the time domain voltage along the line, and $i(x,t)$ is the time domain current along the line, $V_F(t)$ and $I_F(t)$ model the external field coupling. The MTL per-unit-length parameters involved in the MTL equations are determined with the finite-element software package: MSC Aries, EMAS and XL. At the boundaries, the non-linear circuits are solved for by employing iterative procedures (Newton-Raphson) applied to the MNA problem formulation (D. Mardare, J. LoVetri, IEEE Trans. on EMC, **37**, pp. 252-259, 1995). One of the issues at this point is the fine-tuning of these procedures in order to increase the accuracy of the numerical solutions. Among the possibilities to increase simulation accuracy and computational speed are: the adaptation of time steps of the iterative procedures to the local characteristics of the signal, and the variation of the linear multistep formulas (LMS) that form the seed of these algorithms. The accuracy of the problem formulation may also be analysed through a comparison of the modelled and measured responses of non-linear components. In the numerical schemes the diodes are implemented by making use of models with different complexities. Special attention is given to the inclusion of junction capacitance in order to emulate realistic devices. The diode models implemented are similar to those in SPICE.

E28.9

Optimizing System Peak Responses Caused By High Power Microwaves

*Donald P. McLemore
Stan Kokorowski
K.S.H. Lee
Kaman Sciences Corporation
6400 Uptown Blvd. NE, Suite 300E
Albuquerque, NM 87110
505-889-7009

For linear systems, the impulse response transfer function defines the ratio of the response of the system to some excitation and is denoted by $\tilde{T}(\omega)$ in the frequency domain. For our purposes in this paper, we assume that the excitation is a plane-wave electromagnetic field and the response is a current or a voltage at a circuit node in the system.

The theoretical maximum response for any system, at fixed energy, occurs when the incident threat spectrum is some constant multiple of the complex conjugate of this transfer function. We denote the magnetic field portion of the conjugate threat spectrum, $\tilde{H}_{np}^{(inc)}(f)$, and

$$\tilde{H}_{np}^{(inc)}(f) = constant \times T_n(f)^*$$

Therefore the conjugate response at test point n is:

$$i_{np}(t) = \int_{-\infty}^{\infty} \tilde{T}_n(f)\tilde{H}_{np}^{(inc)}(f)e^{j2\pi ft}df = constant \int_{-\infty}^{\infty} \tilde{T}_n(f)\tilde{T}_n(f)^* e^{j2\pi ft}df$$

The value of the constant is obtained from the normalization requirement that all incident waveforms $(\vec{E}^{(inc)}, \vec{H}^{(inc)})$, including the conjugate threat, have the same energy density, F, or:

$$\int_{-\infty}^{\infty} \vec{E}^{(inc)}(t) \times \vec{H}^{(inc)}(t)dt = \frac{1}{\eta}\int_{-\infty}^{\infty} \left|\vec{H}^{(inc)}(f)\right|^2 df = F$$

A quantitative method to compare the ability of various HPM sources to produce maximum amplitude responses at a given test point in a system is proposed in this paper. We define a coupling efficiency, η_{nm}, which gives a scalar number between 0 and 1 relating the peak response created by source *m*, as compared to that produced by the conjugate response (source *p*) at test point *n*, or

$$\eta_{nm} \equiv \frac{\left[i_{nm}(t)\right]_{\max}}{\left[i_{np}(t)\right]_{\max}} \text{ at fixed energy density}$$

The maximum response created from any source *m* (at some fixed energy density), can be found knowing the transfer function, $\tilde{T}(\omega)$, and the frequency domain incident field of the source (i.e. $\vec{H}^{(inc)}$); the maximum response caused by the conjugate source *p* (at the same energy density) can be found as described above. Thus the coupling efficiency can be found for numerous sources by knowing this transfer function, $\tilde{T}(\omega)$ The coupling efficiency can also be calculated a number of combinations of measured transfer functions and candidate sources, at all the measured test points. One can then ask which candidate threat produces the highest efficiency, on average. The average efficiency, then, provides an quantitative, objective way to quantity and compare the effectiveness of the different candidate sources.

URSI E **Session 44** Salon Chaudière

Electromagnetic Noise
Co-chairs: C. Dubé, Canada and D. Hill, USA

08:10 44.1 Statistical Characterization of VLF Radio Noise and Improvement of VLF Signal Detection, **D.A. CHRISSAN**, *Stanford University, Stanford, CA, USA*

08:30 44.2 Using Signal to Noise Ratio to Describe Different Noise Sources, **J. NUUTINEN**[1], F. HAN[2], [1]*Nokia Telecom, Oulu and* [2]*Nokia Research Centre, Helsinki, Finland*

08:50 44.3 Noise in a Cavity with Active Microwave Devices, **V.B. YURCHENKO**[1,2], L.V. YURCHENKO[2], [1]*Bilkent University, Ankara, Turkey;* [2]*Institute of Radiophysics and Electronics, NAS, Kharkov, Ukraine*

09:10 44.4 Photodetector Quantum Noise Distribution, **M. STEFANOVIC**, Z. NIKOLIC, A. VIDOVIC, D. MILOVIC, *University of Nis, Yugoslavia*

09:30 44.5 Detection of Optical Signals in Colored Gaussian Noise, **M. STEFANOVIC**, D. MILOVIC, A. VIDOVIC, *University of Nis, Yugoslavia*

E44.1

STATISTICAL CHARACTERIZATION OF VLF RADIO NOISE AND IMPROVMENT OF VLF SIGNAL DETECTION

D. A. Chrissan (Space, Telecommunications and Radioscience Laboratory, Stanford University, Stanford, California 94305)

The Space, Telecommunications and Radioscience (STAR) laboratory at Stanford University has been conducting a global survey of extremely-low frequency (ELF) and very-low frequency (VLF) radio noise since February 1985. Eight measurement stations around the world have collected thousands of hours of ELF and VLF time-series data; these data have been used to test known statistical models and develop new ones in an effort to fully characterize naturally occurring ELF/VLF radio noise in a statistical sense.

The primary goal of the work presented here is optimization of signal detection for digital communication signals with a carrier frequency in the VLF range. This optimization generally refers to a minimization of bit error rate over all possible receiver structures given a specific received signal format and power, and it requires a complete description of the received additive noise in order for it to be determined. Noise in the VLF range, however, is impulsive (due to individual lightning strokes) and non-stationary (due to seasonal and diurnal variations and the passing of storms), making even first-order statistics such as amplitude probability distributions quite complicated to determine.

The data are analyzed in two ways: the inter-arrival times of impulses in the noise are characterized and modeled, and the joint probability distributions of the noise at successive points in time are determined. The results of these two methods are found to be related in that the marginal distribution at a given time depends on the history of previous impulses. The specific results to be presented can be summarized as follows: (1) Of all the statistical models to which the data are compared, the optimal choice given its remarkable accuracy and simplicity is that which specifies the noise as a stable random process. (The so called *stable* distribution varies from highly impulsive to Gaussian depending on one of its parameters, and thus can be accurate over a wide range of impulsive activity in the noise.) Typical parameters of the stable distribution as a function of time, location and bandwidth are presented. (2) The time spacings between impulses indicate that lightning events are clustered according to a Poisson clustering model. Several variations of this model are compared to the data; results indicate that impulses cluster on the order of one second. (3) The low-level component of VLF noise is found to be uncorrelated in time, but the high-level impulses are related due to clustering. Because of this clustering, the marginal distribution of the stable process at a given time can be determined from the history of impulses prior to that time. A fairly simple, accurate and complete statistical characterization is thus determined. (4) Finally, using this characterization, an optimal maximum-likelihood receiver is determined for digital data corrupted by VLF noise and real data are used to compare its performance to other receiver structures.

Using Signal to Noise Ratio to Describe Different Noise Sources

Jukka Nuutinen*
Nokia Telecom
Kaapelitie 4
SF-90650 Oulu
jukka.nuutinen@ntc.nokia.com
Phone: +358 (08) 5654389
Fax: +358 (08) 5655140

Fang Han
Nokia Research Centre
Hekkilantie 7
Helsinki 00210, Finland
fang.han@research.nokia.com
Phone: +358 (09) 43766246
Fax: +358 (09) 4376 6856

Keywords: System EMC analysis, Signal to noise ratio, cellular systems.

Abstract: This paper presents a novel approach to describe various noise sources. A very efficient way of describing the is to use signal to noise ratio (SNT) defined as

$$SNT = 20\log_{10}\left|\frac{U_{noise}}{U_{signal}}\right|, \qquad (1)$$

where U_{noise} is the unwanted noise signal generated by external or internal noise sources, and U_{signal} the wanted signal level. The aim of this paper is to give expressions for the U_{noise} in various situations, including the radio path interference. The cumulative effect of various interference sources can be analysed by superposition principle, giving an estimate of the system functionality. Thus this means, that SNT can be used as a general measure of EMC quality in various systems. Using SNT we can estimate the worst case situation in larger systems, giving complete amount of interference in the system concept.

The expressions for noise voltage in linear circuits and in non-linear circuits are derived using well known Maxwell's equations. The effect of frequency and amplitude to noise is also discussed in linear and non-linear circuits.

In cellular systems we are interested in the radio interface of the system. The trend nowadays seems to be towards higher frequencies and lower power levels. Paper will show, that from the EMC point of view, lower frequencies and lower power level will suit better in indoor applications. In outdoor applications, we can use high frequencies and high powers. The conclusion of this paper is that recent developments in GSM system suit well into indoor solutions.

E44.3

NOISE IN A CAVITY WITH ACTIVE MICROWAVE DEVICES

V. B. Yurchenko[1,2] and L. V. Yurchenko[2]

[1] Electrical and Electronics Engineering Dept, Bilkent University
Bilkent, Ankara 06533, Turkey

[2] Institute of Radiophysics and Electronics, NAS of Ukraine
12 Proskura St., Kharkov 310085, Ukraine
e-mail: yurchenko@ire.kharkov.ua

Electromagnetic noise arising due to dynamical chaos in a 2-D rectangular cavity with array of active devices located at the cavity wall is investigated. A layer of semiconductor of N-type current-voltage characteristics is considered as a model of the active array when the device spacing is small as compared to the typical wavelength.

Microwave self-excitation is computed at the voltage operating conditions, with the operating point fixed in the negative differential resistance region, and with GaAs parameters of semiconductor being assumed. Two-dimensional linear wave equation in z-component of the electric field satisfying the nonlinear boundary condition at the active wall $x = D$ is solved by applying finite cosine and sine transforms in spatial coordinates x and z, respectively, to reduce the original initial-boundary-value problem to the Cauchy problem for a set of nonlinear ordinary differential equations.

The electric field at the wall is computed as a function of time t. The power density spectrum of the field E_z at the middle point of the active wall is evaluated, Fig.1, and Poincare section (E_z, $\partial E_z/\partial t$) plotted, Fig.2. Appearance of the dynamical chaos accompanied with multi-frequency generation is demonstrated. The noise is shown to increase, and the power spectra become smooth, when the coupling constant of the field-to-array interaction increases. The wavelet analysis is used to study the properties of the noise.

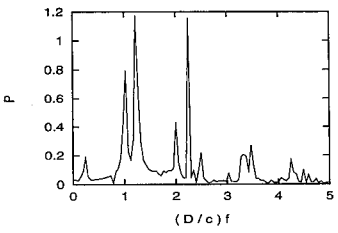

Fig. 1. Power Density Spectrum of $E_z(t)$

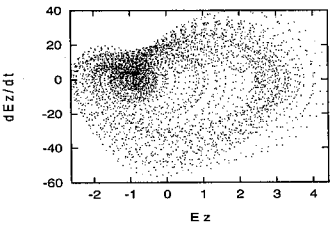

Fig. 2. Poincare Section ($E_z, \partial E_z/\partial t$)

Photodetector Quantum Noise Distribution

Mihajlo Stefanovic, Zorica Nikolic, Aleksandra Vidovic, Daniela Milovic

Faculty of Electronic Engineering, University of Nis, Beogradska 14, 18000 Nis, Yugoslavia
Phone: +381 18 45 466 655, Fax: +381 18 46 180, E-mail:dacha@europa.elfak.ni.ac.yu

Actual optical receivers use a photodetector which inevitably introduces quantum noise. When intensity of light that comes on photodetector is constant, photodetector quantum noise is Poisson distributed. Under the influence of various noises and interferences in optical cable, the light intensity changes and photodetector quantum noise distribution depends on probability density distribution of the incoming light intensity. Three different models of intensity changes are provided in this paper and the photodetector quantum noise distribution is evaluated for each model.

The conditional probability density function of photodetector quantum noise can be expressed as [1]:

$$p(n/\lambda) = \frac{\lambda^n}{n!} e^{-\lambda} \quad , \quad n \in \{0,1,2,3,\ldots\} \tag{1}$$

where λ denotes intensity proportional to the square amplitude of the signal coming to the photodetector's input:

$$\lambda = kA^2 \tag{2}$$

In the presence of various noises on line such as fiber modal noise, different reflexional noises, signal A is Gaussian distributed.

$$p(A) = \frac{1}{\sqrt{2\pi}\sigma} e^{-\frac{A^2}{2\sigma^2}} \quad , \quad A \in \{-\infty, +\infty\} \tag{3}$$

Meanwhile, in some systems, when more random optical rays encounter signal A may be considered as Rayleigh or Rician distributed [1],[2], .

$$p(A) = \frac{A}{\sigma^2} e^{-\frac{A^2}{2\sigma^2}}, \text{ Rayleigh distribution}$$
$$p(A) = \frac{A}{\sigma^2} e^{-\frac{A^2+A_0^2}{2\sigma^2}} I_0\left(\frac{AA_0}{\sigma^2}\right), \text{ Rician distribution} \tag{4}$$

The analysis presented in this paper accounts for each of three mantioned distribution. Some of obtained results are shown on figure.

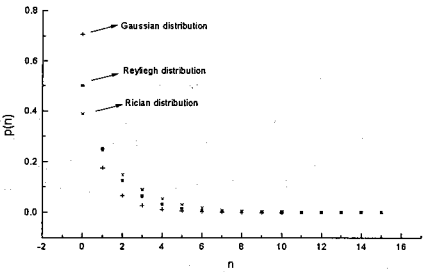

References:

[1] R. M. Gagliardi, S.Karp, *Optical Communications*, John Wiley & Sons, 1976.
[2] G. Jacobsen, *Noise in Digital Optical Transmission Systems*,Artech House, Boston, London 1994.
[3] D. S. Mitrinovic, "Uvod u specijalne funkcije", Gradjevinska knjiga, Beograd 1972.
[4] Antony D. Whalen, "Detection of signals in noise", Academic press, New York and London 1971.

E44.5

Detection of Optical Signals in Colored Gaussian Noise

Mihajlo Stefanovic, Daniela Milovic, Aleksandra Vidovic
Faculty of Electronic Engineering, University of Nis, Beogradska 14, 18000 Nis, Yugoslavia
Phone: +381 18 45 466 655, Fax: +381 18 46 180, E-mail: sanda@europa.elfak.ni.ac.yu

In this paper detection of Amplitude Shift Keying (*ASK*) optical signals in colored Gaussian noise is performed. The optical signal is amplitude modulated. The arriving signal in the optimal receiver, for hypotheses H_0 is:

$$r(t) = n(t) \qquad 0 \le t \le T \tag{1}$$

and for hypotheses H_1:

$$r(t) = A\cos\left(\omega_0 t + \theta\right) + n(t) \qquad 0 \le t \le T \tag{2}$$

n(t) is colored Gaussian noise with zero mean and autocorrelation function:

$$R_n(\tau) = \frac{1}{4} N_0 \omega_0 \exp\left(-\omega_0|\tau|\right) \tag{3}$$

Because of the laser phase noise, the carrier phase has Gaussian probability density function (Barry 1990):

$$p(\theta) = \frac{1}{\sqrt{2\pi}\sigma_\theta} \exp\left(-\frac{\theta^2}{2\sigma_\theta^2}\right) \qquad \theta \in [-\pi, \pi] \tag{4}$$

The cases of phase θ, being uniformly distributed and having Viterbi distribution, have been considered in literature. Here, the laser phase noise is produced by the finite width of the laser ray spectrum. This is the result of the laser spontaneous emission in the transmitter and the receiver of the optical system.
The likelihood ratio is determined:

$$\lambda(r) = \exp\left(-\frac{A^2}{4}\int_0^T\int_0^T R_n^{-1}(t-\tau)\cos\left[\omega_0(t-\tau)\right]dtd\tau\right)\left[I_0(Aq) + 2\sum_{n=1}^{\infty} I_n(Aq)\exp\left(-\frac{n^2\sigma_\theta^2}{2}\right)\cos n\theta_0\right] \tag{5}$$

wher is:

$$\begin{aligned} q\cos\theta_0 &= \int_0^T r(t) f_1(t)dt \\ q\sin\theta_0 &= \int_0^T r(t) f_2(t)dt \\ f_1(t) &= \int_0^T R_n^{-1}(t-\tau)\cos\omega_0\tau d\tau \\ f_2(t) &= \int_0^T R_n^{-1}(t-\tau)\sin\omega_0\tau d\tau \end{aligned} \tag{6}$$

The above equation specifies the optimal receiver construction procedure. For the received signal r(t), the receiver calculates random variables q and θ_0 and at last, the likelihood ratio $\lambda(r)$ which it compares with λ_0 and makes decision about which signal is sent by transmitter. Also, the error probabilities have been evaluated for the optimal receiver suggested in this work for detection of optical signals in colored Gaussian noise.

References

[1] M. S. Kao, J. Wn, *"Performance analysis of ASK optical receivers in the presence of optical channel noise"*, IEE Proceedings, Vol. 137. Pt. J. No. 5, October 1990.
[2] John R. Barry and Edward A. Lee, *"Performance of coherent optical receivers"*, Proceedings of the IEEE, Vol. 78, No. 8, August 1990.
[3] Harry L. Van Trees, *"Detection, estimation and modulation theory"*, John Wiley and Sons, Inc. New York-London-Sydney
[4] Anthony D. Whalen, *"Detection of signals in noise"*, Academic press, New York and London, 1971.
[5] D. S. Mitrinovic, *"Uvod u specijalne funkcije"*, Gradjevinska knjiga, Beograd, 1972.

URSI E Special Session **Session 45** **Salon Chaudière**

High Power Electromagnetics
Co-chairs: R.L. Gardner, USA and D. Kajfez, USA

10:30 45.1 Complexity and Its Consequences for Electromagnetic Vulnerability and Lethality, **R.L. GARDNER**, *Directorate for Space and Nuclear Deterrence, U.S. Air Force, Washington, DC, USA*

10:50 45.2 **Invited:** Dielectric Jackets as Lenses and Application Generalized Coaxes and Bends in Coaxial Cables, **C.E. BAUM**, *Phillips Laboratory WSQW, Kirtland AFB, NM, USA*

11:10 45.3 Azimuthal TEM Waveguides in Dielectric Media, **C.E. BAUM**, *Phillips Laboratory WSQW, Kirtland AFB, NM, USA*

11:30 45.4 Energy Loss and Velocity of Energy Propagation of Impulse-Like Waveforms Including Free Carrier and Polarization Relaxation Contributions, **I. KOHLBERG**[1], K. MIN[2], [1]*Kohlberg Associates, Inc., Alexandria, VA and* [2]*Wright Laboratory Armament Directorate, Eglin AFB, FL, USA*

11:50 45.5 Design of Chebyshev and Binomial Transformers for Wide Bandwidth High Power Microwave Radars, **A.W. BIGGS**, *University of Alabama in Huntsville, AL, USA*

E45.1

Complexity and Its Consequences for Electromagnetic Vulnerability and Lethality

R. L. Gardner
Directorate for Space and Nuclear Deterrence
Office of the Assistant Secretary of the Air Force (Acquisition)
1060 Air Force, Pentagon
Washington, DC 20330-1060

A large part of the business of the electromagnetic theorist and test engineer is to conclude if a class of individual systems is susceptible to a particular electromagnetic stimulus. The incident electromagnetic wave or current can generally be described easily, but systems of interest usually cannot. Systems or interest qualify as complex, and hence the total interaction cannot be exactly simulated experimentally or computationally. What can be done is to apply a number of physical rules, limits and the results of example problems to effectively bound the results of the interaction. Most simulations assume that the sample system they are testing is exactly the same as all *similar* systems of interest. Normally, there are design changes, aging, and other differences between real systems, even those with the same model designation. These variations and those of the source result in an engineering margin for the susceptibility or lethality conclusion.

Variations in the source are relatively easy to model, although all of the components of the incident waveform must be considered, not just the incident power density. Bounding the interaction of the source and system requires the topological decomposition of the system into a convenient set of component parts [Lee, *EMP Interaction*, Taylor and Francis, 1980]. This topological decomposition is like a management plan with which to consider the coupling of the electromagnetic wave with the stimulus. Its main advantages are that the technique is not overly dependent on the details of the geometry of the system and can accommodate excursions easily.

As we go deeper into the system, we depend on testing and other empirical evidence to help us consider each of the elements of the topological decomposition. There are small variations in the system topology which can change the conclusion about vulnerability [Gardner and Jones, System Design and Assesment Note 32, EMP Note Series, Kirtland AFB, NM]. Unless we are careful, these small variations will increase the errors in the system assessment to conclusions that are not useful. Such a system is chaotic. In this paper, we will outline the decomposition and show the consequences of small changes on the nodes and connections of some canonical system geometries.

Dielectric Jackets as Lenses and Application Generalized Coaxes and Bends in Coaxial Cables

Carl E. Baum
Phillips Laboratory WSQW
3550 Aberdeen Avenue SE
Kirtland AFB, New Mexico 87117-5776

In the design of lenses for transporting transverse electromagnetic (TEM) waves in desirable ways, there are techniques from differential geometry and the concepts of transit-time and differential-impedance matching (C.E. Baum and A. P. Stone, *Electromagnetic Symmetry,* Taylor & Francis, 1991). In its most general form such lenses are three-dimensional structures in which wavelengths are allowed to be small compared to characteristic dimensions in all three coordinate directions. In such cases, one can consider the full Maxwell equations for appropriate solutions. Under appropriate conditions, the propagation of electromagnetic waves as governed by the Maxwell equations can be reduced to propagation in less than three dimensions. A common case is that of a transmission line in which the two cross-section dimensions are typically assumed to be small compared to wavelength. If the transmission line is constructed of straight perfect conductors in a uniform isotropic medium the dominant mode of propagation is a TEM mode, and one can even go to frequencies high enough that the cross section is not electrically small if one is careful not to introduce higher order (E and H) modes.

The concept of a jacket as a two-dimensional space for TEM-wave propagation can lead to some practical dielectric lens designs. From a theoretical point of view, this is of interest as a two-dimensional wave concept, midway between a one-dimensional duct or transmission line, and a full three-dimensional lens. Constraining the permeability to be uniform and isotropic (e.g., μ_0) and the permittivity to be isotropic, this still leaves the spatial variation of the permittivity to consider. Examples of both uniform (generalized coax) and nonuniform (bend in coax) permittivity are considered. This paper considers the general properties of a jacket consisting of two closely spaced, but curved, conducting plates separated by a medium of uniform isotropic permeability and nonuniform isotropic permittivity for propagating dispersionless TEM waves. A simple form of this is a body of revolution with generalized axial propagation (generalized coax) which can be synthesized with a uniform permittivity. One can also use a nonuniform permittivity for a bend in a coaxial cable.

E45.3

Azimuthal TEM Waveguides in Dielectric Media

Carl E. Baum
Phillips Laboratory WSQW
3550 Aberdeen Avenue SE
Kirtland AFB, New Mexico 87117-5776

Dielectric lenses for bending the direction of propagation of transverse electromagnetic (TEM) waves have been investigated in recent papers. A common feature of these lenses, and those to be discussed here, is that they are portions of a dielectric body of revolution (BOR) with permittivity ε proportional to Ψ^{-2} where Ψ is the cylindrical radius from the axis of revolution (the z axis). This has led to several cases involving planar, circular cylindrical, circular conical and spherical boundaries. Special cases of these include E- and H-plane bends. One can also approach this problem from the point of view of a jacket in which the spacing of the two conductors perpendicular to the electric field is electrically small, and small compared to the dimensions in the direction of the magnetic field. Such a low-impedance structure is basically two-dimensional in terms of dimensions that can be large compared to wavelength and thereby admit propagation. This jacket technique gives an approximate solution for a bend in a coaxial cable.

The present paper continues the discussion of such dielectric bending lenses by exploring the general properties of the TEM waves with azimuthal (ϕ-directed) propagation. Recalling the properties of previous solutions, it was noted how the transverse behavior of the magnetic field was like a static magnetic field multiplied by a waveform function propagating in the ϕ direction. As we shall see, this is a characteristic of the general solution. An interesting canonical magnetostatic solution is that of a filamentary circular current loop. The closed magnetic field lines encircling the current can be used to define closed conducting surfaces which look like a circularly bent coaxzial cable. By superposition of such loops, any ϕ - independent static ϕ - directed current distribution and the associated magnetic field can be produced for defining "coaxial" bends with various cross-section shapes.

We now have a theory of TEM modes in a BOR section with ε proportional to Ψ^{-2}. This gives the desired dispersonless character of TEM modes for propagating pulses through bends in coaxial cables, thereby extending the bandwidth of such bends to higher frequencies, or equivalently preserving shorter rising times. This still leaves questions of how best to transition into and out of such a bend, and how to best manufacture such a bend while closely approximately the required conductors and permittivity.

ENERGY LOSS AND VELOCITY OF ENERGY PROPAGATION OF IMPULSE-LIKE WAVEFORMS INCLUDING FREE CARRIER AND POLARIZATION RELAXATION CONTRIBUTIONS

Ira Kohlberg*
Kohlberg Associates, Inc.
Alexandria, VA 22304

Kwang Min
Wright Laboratory Armament Directorate
EGLIN AFB, FL 32542-6810

Interpretation of GHz impulse-like wide-band signals in dispersive media such as sand and concrete using the common optical frequency dispersion formula for dielectrics appears to have limited applicability. This is due to the fact that optical resonances lie well above the dominant frequences for these waveforms. Recent experimental observations suggest that attenuation and pulse spreading are better understood using material models consisting of a combination of free carriers having relaxation time, τ_{rc}, and/or molecules having polarization relaxation relaxation time, τ_{rm}. For free carriers the current density, $\vec{J} = N_c\vec{v}$, where N_c is the concentration, $\vec{v}$ is the velocity determined from the equation $d\vec{v}/dt + \vec{v}/\tau_{rc} = q\vec{E}/m$, $\vec{E}$ is the electric field, q is the carrier charge, and m is the carrier mass. The molecular polarization response is composed of two parts: $\vec{P} = \vec{P}_1 + \vec{P}_2$, where $\vec{P}_1 = \varepsilon_0\chi_1\vec{E}$, and $\vec{P}_2$ is determined from the equation: $d\vec{P}_2/dt + \vec{P}_2/\tau_{rm} = \varepsilon_0\chi_2\vec{E}/\tau_{rm}$. The physical constants in these equations are experimentally determined from attenuation and reflection coefficient measurements in a manner that is consistent with causality requirements.

Using the aforementioned material models in conjunction with a corpuscular model for pulse propagation leads to a prediction of pulse width, τ_p, that minimizes attenuation. Critical parameters are the ratios τ_p/τ_{rc}, and τ_p/τ_{rm}. When $\tau_p/\tau_{rc} \ll 1$ the free carriers cannot respond, and the pulse passes with minimal energy loss and dispersion. The converse is true when $\tau_p/\tau_{rc} \gg 1$. On the other hand, saturation of polarization and accompanying reduction in energy loss favor larger τ_p/τ_{rm} for molecular polarization relaxation. An exact space-time expression is derived for the velocity of energy propagation, V_E, required in the corpuscular model; V_E is approximated using the principle of stationary phase.

E45.5

DESIGN OF CHEBYSHEV AND BINOMIAL TRANSFORMERS FOR WIDE BANDWIDTH HIGH POWER MICROWAVE RADARS

Albert W. Biggs
University of Alabama in Huntsville
109 South Emerson Avenue
Wenatchee Washington 98801 USA

This paper describes some methods for design of transformer structures capable of matching slow wave transmission lines with different characteristic impedances for specified bandwidths and of reduction of sidelobe levels of linear in-phase broadside antenna arrays. The design techniques were developed by Cohn [MTT-3, pp 16-21, Apr 1955] for fast wave lines. These were extended to slow wave lines. The slow wave structure is a series of different characterictic impedances spaced by equal electrical lengths of slow wave lines.

One method for designing transformer structures with maximally flat passband responses uses W. Hansen's [MIT Rad. Lab.] Binomial coefficient design. The logarithms of the characteristic impedance ratios of adjacent transmission line sections are made equal to the ratios of the Binomial coefficients. The use of Binomial transformers is applied to match slow wave line sections to fast wave lines of equal electrical lengths where the line impedances are determined by phase velocities instead of media dielectric constants. Phase velocities exceed that of light in metallic waveguides, and are less than that of light in waveguides loaded with diaphragms. These elements may be rectangular serrations in the form of very thin fins or thick rectangular. or square, teeth. The Binomial coefficients are easily found with Blaise Pascal's triangle.

The "equal ripple" response ripples in the band with Chebyshev polynomials instead of the maximally flat response of the Binomial transformers. The ratio of Binomial coefficients is replaced by a ratio of Chebyshev coefficients. Derivation of Chebyshev reflection coefficients is greatly simplified with an algorithn developed by Ross Graves, Stanford University, in an unpublished memo. The algorithm starts with the value $x_o = [\cos 180^o/(1+BW)]^{-1}$, where BW is the bandwidth of the section and cos $180^o/(1+BW)$ is the phase length between guide lengths. For BW=1.0, the Binomial and Chebyshev coefficients are equal, while for BW=2.0, phase length is 60^o. With BW=3.0, it is 45^o, et cetera.

URSI E Special Session **Session 72** **Salon Richelieu**

Spectrum Management Issues: A Perspective on Recent Technical, Economic and Policy Developments
Co-chairs: D. Cohen, USA and M. Fournier, Canada

13:10 72.1 **Invited:** A Changing International Spectrum Management Environment, **R.D. PARLOW**, *NTIA/U.S. Department of Commerce, Washington, DC, USA*

13:30 72.2 **Invited:** Moving from Apparatus Licensing to Spectrum Licensing: The Economic and Public Policy Rationale, **I. MUNRO**, *Industry Canada, Ottawa, ON, Canada*

13:50 72.3 **Invited:** Latest Developments in Public Spectrum Management in the USA, **W.A. LUTHER**, *Federal Communications Commission, Washington, DC, USA*

14:10 72.4 **Invited:** Measures of Spectrum Utilization, **R.H.M. HAFEZ**, G.K. CHAN, [1]*Carleton University and* [2]*Industry Canada, Ottawa, ON, Canada*

14:30 72.5 **Invited:** Spectrum Planning for Wireless Multimedia, **D.J. COHEN**, *University of Maryland, College Park, MD, USA*

14:50 72.6 **Invited:** Can Radio Astronomy Survive? The Impact of Technological Developments on Sensitive Services, **T.E. GERGELY**, *National Science Foundation, Arlington, VA, USA*

15:10 Coffee Break

15:30 72.7 **Invited:** Case Study of a Real Time Remotely Controlled Monitoring System, **P. VACCANI**, *Industry Canada, Ottawa, ON, Canada*

15:50 Panel Discussion

E72.1

A Changing Intenational Spectrum Management Environment

Richard D. Parlow
Associate Administrator for Spectrum Management
National Telecommunications & Information Administration
U.S. Department of Commerce
Washington, D.C.

Management of the radio spectrum has seen many changes during the past decade. Spectrum dependent radiocommunication services have benefited from the broad introduction of solid state devices, new digital modulation techniques and an unquenchable thirst for information transfer by public and governmental interests. With an expanding ability to communicate, business, industry and government started developing new and innovative radiocommunication services. The need and interest in the radio frequency spectrum began to grow and its real value in technological, and financial terms became evident.

With the end of the "Cold War", the global military industrial complex and the private sector recognized that technologies in many defense systems were transferable to civil telecommunications applications in a rapidly expanding global market place. The globalization of telecommunications infrastructures pioneered by intergovernmental organizations such as Intelsat was only the tip of iceberg--the competitive race to expand global, regional and domestic telecommunication insfrastructures started to explode.

What has evolved is a market place filled with new services and equipment--cordless telephones, baby monitors, national/regional/global cellular/PCS networks, local area networks, advanced GEO satellites, big/little LEOS, broadband LEO systems, satellite navigation systems, resource monitoring, meteorological systems, multi--point distribution systems, enhanced sound/TV broadcasting, enhanced public safety & transportation systems, national security infrastructures, etc.. In the environment, competition & a flexible regulatory environment are keys to success for the consumer, investors, the mobile communicator. But, the most important key is the availability of spectrum, flexible allocations, standards and the opportunity to sell products and services in the global market.

Within this context, this paper will discuss current activities within the International Telecommunications Union (ITU) concerning spectrum availability, standards setting, new radiocommunication services and application, and the 1997 World Radiocommunications Conference. It will also present information regarding efforts to increase the rights and obligations of private sector members of the ITU, and initiatives to improve the financial base of the ITU and delivery of services to all members.

Moving from Apparatus Licensing to Spectrum Licensing: The Economic and Public Policy Rationale

Ian Munro
Senior Economist
Radiocommunications and Broadcasting Regulatory Branch
Industry Canada

Industry Canada is working towards the goal of better incorporating economic principles into its spectrum management activities, as are many other spectrum management organizations throughout the world. One means by which this goal is being pursued, both in Canada and in a number of other countries, is the trend towards assigning licences for the use of specified frequencies over a specified geographic area, as opposed to the more traditional practice of assigning licences for individual radio apparatus.

The *Radiocommunication Act* was amended in 1996 to create the spectrum licence, defined as an authorization "in respect of the utilization of specified radio frequencies within a defined geographic area" and recent licensing processes have utilized this new approach.

There are many benefits to the use of spectrum licensing, including increased flexibility for spectrum users, reduced administrative burdens for both licensees and spectrum managers, and a high degree of compatibility with other Departmental policy initiatives such as licence fee reform and the introduction of spectrum auctioning.

Any break with traditional methods also, of course, will always present its own challenges. With regard to spectrum licensing these challenges include answering the questions of how spectrum licences should be defined for various services in terms of geographic area and band-width, what technical parameters may be required to make these definitions meaningful and practical, and how to ensure that the move to spectrum licensing in no way hinders Industry Canada's ability to implement various policies designed to achieve a wide range of economic and social goals.

E72.3

Latest Developments in Public Spectrum Management in the USA

William A. Luther
Chief, Radiocommunication Policy Branch
International Bureau
Federal Communications Commission
2000 M Street, NW.
Washington, D.C.

Within the USA, there have been resounding, permanent changes in radio spectrum management within the last several years. The use of lotteries to identify new, public sector radio license holders has ben replaced with auctions. As of this abstracts, about 23 billion dollars has been pledged so far in either "outcry" or simultaneous, multiround, computer-driven auctions for new spectrum authorizations in the personal communications services, the direct broadcast satellite service and the interactive video service. Auctions for additional services, e.g., local multipoint (video) distribution services, are pending.

Along with the introduction of auctions, a new philosophy of spectrum management is being applied in the USA. Tenets of the new philosophy include a more open, transparent process; a stated commitment to competition; and the opening of U.S. telecommunication markets to foreign entities on a reciprocal, "effective competitive opportunities" test. U.S. domestic telecommunication satellites have been declared available for international use, and vice-versa, under an FCC Domestic-International Satellite Consolidation Order (DISCO I). The FCC has developed a similar proceeding called DISCO II toward reciprocal opening of domestic telecommunication markets to foreign satellite operators under a similar "effective competitive opportunities" test. Outcome of DISCO II is predicated upon successful completion of World Trade Organization negotiations working toward a deadline of February 15, 1997.

These newly applied spectrum management techniques will be presented and explained at the symposium, including the foreseen results from DISCO II, updated from the trade agreements scheduled to finish in February. The newly adopted FCC spectrum management philosophy will be examined. The FCC agenda and goals as seen by its Chairman for 1997 and 1998 will be considered.

Measures of Spectrum Utilization

Gerald K. Chan
Director, Terrestrial Engineering
Spectrum Engineering Branch
Industry Canada

Roshdy H.M. Hafez*
Carleton University
Ottawa, Ontario

It is widely recognized that the radio spectrum operates in three dimensions: space, frequency and time, i.e. at a particular frequency and with a particular bandwidth, at a given location, and at a particular time. The term "spectrum utilization" usually refers to the amount of information (measured in bits) that is being carried by a spectrum unit, and is measured in Hz. sq. m. Sec. Therefore, an appropriate "theoretical" measure for spectrum utilization is the average bits/sec/sq.m./Hz. However, the maximum achievable rate of information per unit spectrum depends on many factors ranging from the physical propagation conditions such as path loss, fading, delay spread, etc. to the state of technology and system design including antenna pattern. In this paper, we attempt to summarize the known definitions of the spectrum utilization and discuss their applicability to existing radio services and their practical usefulness.

In general, the measures of spectrum utilization fall into two categories: (1) absolute measure and (2) relative measures. Absolute measures tend to be less practical because accurate analysis of the maximum utilization is theoretically complicated, and often the results of such analysis do not readily relate to known practical systems. Relatives measure, on the other hand, are more practical and useful in pointing out areas of deficiencies. It can also be used to compare how a particular system operates from year to year or from location to location.

In the paper, we discuss the tools developed to monitor and evaluate spectrum utilization including the amount of spectrum denied to other users. The information used to determine utilization varies from radio service to radio service and relevant databases are crucial instruments in providing accurate measures. Examples are the spatial and spectral distributions of radio stations, and channel occupancies which are measures of spectrum utilization in the time dimension, in given bands, as well as demographic distribution of users and applications. Finally, a methodology to measure spectrum utilization in the form of an index will also be presented.

E72.5

Spectrum Planning for Wireless Multimedia

David J. Cohen
Associate Director, Information and Telecommunications Studies
University of Maryland, University College
University Blvd. at Adelphi Road
College Park, MD. 20742

This paper reviews the new wireless multimedia technology from a spectrum management perspective. The wireless telecommunication infrastructure in the future will need to transfer multimedia information including voice, video, videoconferencing, data, images and text. The bit rates needed to transfer these information sources will vary from, kb/s to Mb/s and the information may be bursts or continuous. Spectrum management will need to help assure the radio spectrum accommodates the wide variety of information sources along with increasing volume of wireless traffic.

Spectrum planners, previously could plan with a reasonably assured knowledge of the required RF channel bandwidths. For example conventional broadcast analog video requires a channel bandwidth of 6 MHz. However with the move to digitization, compression, and new modulation methods required RF bandwidths for video sources varies over a wide range (kHz to MHz) depending upon the desired quality. Two important examples, which illustrate this variable video bandwidth, are presented. First, the Advanced Television "over the air standard" is reviewed and second, the new H.324 (ITU-T) Multimedia Communication Standard is discussed. H.324 is an analog voice bandwidth modem with the capability to transmit multimedia sources such as videoconferencing. Under development, Annex C of the H.324 standard pertains to wireless networks.

Several spectrum planning alternatives are presented which may be applicable for the current era of dynamic and uncertain changes in the wireless technology. Spectrum allocation planning is difficult given the uncertainty of the two factors "technology push" and "requirement pull". An important technology allocation issue is "licensed" vs "unlicensed" use. Devising frequency channeling plans is difficult because of the ever changing bandwidth requirements brought on by compression and RF modulation technology advancements.

Can Radio Astronomy Survive? The Impact of Technological Developments on Sensitive Services

Tomas E. Gergely
Division of Astronomical Sciences
National Science Foundation
4201 Wilson Boulevard
Arlington, VA 22230

Radio astronomers worldwide are taking advantage of technological developments to refine and upgrade existing telescopes, to build more sensitive new instruments and to expand the scpectral range they cover, particularly in the mm-wave region of the spectrum. Technological developments also fostered a huge number of new radio services during the last few years, and this trend is expected to continue. Coordinating the operation of these new services and technologies with radio astronomy facilities is often difficult.

Radio astronomy observations are particularly impacted by: a) the large increase in the number of satellite borne transmitters, regardless of where in the spectrum they transmit; b) the failure of satellite and other airborne transmitters to curb their out-of-band and spurious emissions and; c) The increasing use of the mm-wave spectral range (30 Gz and above) for commercial and other applications. Radio observatories have traditionally been located at the remote sites to avoid sources of man made interference. A remote location however does not help with satellite transmissions, which deny access to portions of the spectrum by astronomers at most, and sometimes all locations on the surface of the Earth, by design. As for the mm-wave region of the spectrum, there are hundreds of spectral lines above 30GHz. Many of these provide unique information about astronomical phenomena, and loss of access to them would have very serious consequences for astronomy.

E72.7

Case Study of a Real Time Remotely Controlled Monitoring System

Paul Vaccani
Manager Systems Engineering
Spectrum Engineering Branch
Industry Canada

The Canadian administration identified in 1992 a need for monitoring facilities accessed at district offices in the major population centres across Canada to assist in the resolution of radio interference problems and to gather data on the use of the radio spectrum. District offices are typically located in the downtown area of major urban centres making these sites poor locations for spectrum radio monitoring; hence the need for a capability of remoting the monitoring facilities to more suitable monitoring sites. To meet this challenge the Canadian administration has developed the **INTEGRATED SPECTRUM OBSERVATION CENTRE (ISOC)** system.

The ISOC is a versatile multi-user, multi-remote site system for monitoring the radio frequency spectrum from 10 kHz to 2700 MHz depending on instrument selected and antennas. The ISOC concept uses computer controlled monitoring equipment at remote sites to automatically gather monitoring data that can either be transmitted to the control site in real time, or stored at the remote site computer for transmission at a later time. The ISOC system has a star network configuration allowing a central site to control up to four monitoring sites and support simultaneously a number of users. The remote site monitoring equipment consists of a primary receiver capable of doing simultaneous level, modulation and frequency measurements, a secondary receiver, spectrum analyzer, modulation analyzer, tone decoder, a line of bearing or a netted direction finding capability, a RF switch and audio matrix, antenna system, and a multi-channel audio tape recorder. The system is designed to be modular to allow the deletion of a given instrument or the addition of a new one.

The ISOC design philosophy will be presented. The results from the field trial will be described along with the resulting enhancements. In addition the current operational capabilities and the national implementation will be described.

URSI F Special Session **Session 8** **Salon Gatineau**

Applications of Rough Surface and Volume Scattering Methods
Co-chairs: K. Sarabandi, USA and G. Edwards, Canada

08:10	8.1	**Invited:**An Application of the Contour Path Finite Difference Time Domain Method to Rough Surface Scattering, F.D. HASTINGS, S.L. BROSCHAT, **J.B. SCHNEIDER**, *Washington State University, Pullman, WA, USA*
08:30	8.2	**Invited:** Pulsed Beam Scattering from a Layer of Discrete Random Medium: A Three Dimensional Model, **O. KILIC**[1], R.H. LANG[2], [1]*COMSAT Laboratories, Clarksburg, MD and* [2]*George Washington University, Washington, DC, USA*
08:50	8.3	**Invited:** Modelling and Measurements of Scattering from Road Surfaces at Millimeter-Wave Frequencies, **K. SARABANDI**, E.S. LI, A. NASHASHIBI, B. LITKOUHI, *University of Michigan, Ann Arbor, MI, USA*
09:10	8.4	**Invited:** Applications of Estimation Theory to the Forward and Inverse Scattering Problem, **J.M. STILES**, *University of Kansas, Lawrence, KS, USA*
09:30	8.5	**Invited:** Microwave Scattering Experiments on Artificial Dielectric Surfaces at the EMSL, **G. NESTI**[1], P. COPPO[2], D. TARCHI[1], A.J. SIEBER[1], [1]*JRC, Space Applications Institute, Ispra and* [2]*Firenze, Italy*
09:50	8.6	**Invited:** Time-Frequency Correlations and Angular Memory Effects for Waves Scattered by Random Media, **A. ISHIMARU**, Y. KUGA, T.-K. CHAN, J.-H. YEA, *University of Washington, Seattle, WA, USA*
10:10		Coffee Break
10:30	8.7	**Invited:** Polarimetric Bistatic Measurement Facility for Point and Distributed Targets, B. HAUCK, R. DEROO, **F. ULABY**, *University of Michigan, Ann Arbor, MI, USA*
10:50	8.8	Ocean Radar Backscatter Statistics: From Mid Incidence to Near Grazing, **B.L. GOTWOLS**, R.D. CHAPMAN, D.R. THOMPSON, *Johns Hopkins University, Laurel, MD, USA*
11:10	8.9	Application of the Music Algorithm to a Multi-Frequency HF Ocean-Wave Radar, **C.C. TEAGUE**, *Stanford University, Stanford, CA, USA*
11:30	8.10	GeoSAR: A New Radar Terrain Mapping System for the New Millennium, **T. THOMPSON**[1], J. VAN ZYL[1], S. HENSLEY[1], G. DILDINE[2], J. SEIB[2], J. BURTON[3], R. YOHA[3], M. GARDNER[3], R. BARTMAN[1], K. WHEELER[1], [1]*California Institute of Technology, Pasadena,* [2]*Calgis, Incorporated, Fresno and* [3]*California Department of Conservation, Sacramento, CA, USA*
11:50	8.11	Signal Processing Methods for Sub-Surface Detection, **H. RAEMER**, E. MILLER, *Northeastern University, Boston, MA, USA*

F8.1

AN APPLICATION OF THE CONTOUR PATH FINITE DIFFERENCE TIME DOMAIN METHOD TO ROUGH SURFACE SCATTERING

Frank D. Hastings, Shira L. Broschat, and John B. Schneider *
School of Electrical Engineering and Computer Science
Washington State University
Pullman, WA 99164-2752

Over the past few years there has been considerable interest in developing numerical approaches for the study of electromagnetic scattering from rough surfaces [see, for example, Fung *et al.*, *IEEE Trans. Geosci. Remote Sensing*, 32, 986-994, 1994; Hastings *et al.*, *IEEE Trans. Antennas Propagat.*, 43, 1183-1191, 1995; and Sarabandi *et al.*, *IEEE Trans. Antennas Propagat.*, 34, 425-432, 1996]. These approaches can be used to benchmark approximate models and to study problems for which no accurate approximate models exist. Several investigators have used the Finite-Difference Time-Domain (FDTD) method in their approach. However, previously we have shown that for one-dimensional (1-D), perfectly conducting surfaces with horizontal polarization the staircase approximation of the continuously varying physical surface can lead to significant numerical artifacts. Although a finer grid can be used to obtain more accurate results, the increased computational cost may be prohibitive. Fortunately, staircasing errors can be virtually eliminated with the use of the contour path technique. In this technique the grid conforms locally to the rough interface; it is relatively simple to implement and computationally inexpensive.

In this paper, we consider the case of scattering from 1-D, randomly rough dielectric surfaces for horizontal polarization. We find again that staircasing errors are appreciable, particularly at low grazing angles in the backscattered direction. However, as for the case of perfectly conducting surfaces, use of the contour path technique gives more accurate results. We present results for a Gaussian roughness spectrum as well as for a modified power law spectrum. In addition to the contour path technique, we discuss other enhancements to the standard FDTD method—such as correcting for numerical grid dispersion in the specular direction—which were used to improve the accuracy of the results. For this study, Gaussian-tapered harmonic illumination was used since it can be implemented easily. However, because it is a time domain technique, the FDTD method holds the promise of providing results over a broad spectrum of frequencies by means of a single simulation.

Pulsed Beam Scattering from a Layer of Discrete Random Medium: A Three Dimensional Model

O. Kilic[(1)*], R. H. Lang[(2)]
[(1)] COMSAT Laboratories, 22300 COMSAT Drive, Clarksburg, MD 20871
(301) 428-4722 (Tel) (301) 426-3686 (FAX)
ozlem.kilic@comsat.com (e-mail)
[(2)] The George Washington University, Dept. of EECS, Washington, DC 20052

The problem of a pulsed aperture illuminating a layer of discrete random medium over a flat, homogenous background is considered. The layer consists of sparsely distributed dielectric scatterers that are randomly oriented in space. The behavior of the backscattered signal from the medium is examined in the time domain for the case of a short pulse incidence. The study is an extension of a previously developed two dimensional model (O. Kilic and R. H. Lang, Proc. IGARSS, pp.760-762, 1996) to the three dimensional representation. The radiated fields from the antenna are approximated by a three dimensional Gaussian beam, which enables the model to take into account the bounded nature of the illuminated fields and the variation of intensity as a function of propagation direction. Furthermore, with an appropriate choice of the beamwidth, the Gaussian beam representation can closely match the main lobe of a realistic antenna pattern.

A solution for the backscattered power is obtained for an arbitrary pulse by first decomposing the radiated signal into its time harmonic components. The scattered field from the medium is determined for each frequency component by applying the Distorted Born Approximation, which is a single scatter model. The interaction of the Gaussian beam with the random medium is accounted for in the calculations of the backscattered field by decomposing the incident beam into its plane wave components, and employing the well known time harmonic plane wave solutions. The dimensions of the particles inside the medium is assumed to be small enough so that the spread and decay of the incident field over a particle size can be neglected, and a local plane wave approximation can be used in the calculation of scattered fields from each particle.

The solution for the received power is dominated by three terms: direct, direct-reflected and reflected. Due to the different nature of the paths they follow, these components carry information on different aspects of the medium. The direct term is associated with the volume scattering from the layer and arrives first at the antenna. The second term observed at the antenna is the direct-reflected component, which results from a single interaction between the scatterer and the ground. The reflected term which involves a double bounce from the ground arrives last due to the relatively longer path it travels. The response of the medium to the incident signal is analyzed in terms of these different components.

F8.3

Modelling and Measurements of Scattering from Road Surfaces at Millimeter-wave Frequencies

K. Sarabandi, Eric S. Li, A. Nashashibi, and B. Litkouhi
Radiation Laboratory
Department of Electrical Engineering and Computer Science
The University of Michigan, Ann Arbor, MI 48109-2122
Tel :(313) 936-1575, Fax:(313) 747-2106
email: saraband@eecs.umich.edu

Abstract- Millimeter-wave radar-based sensors are being considered for a number of automotive applications including obstacle detection and collision warning, true-speed, and traction sensors. In this paper, interaction of electromagnetic waves with asphalt road surfaces, possibly covered with ice or water, at millimeter-wave frequencies is studied. First an experimental procedure for determining the effective dielectric constant of bituminous mixtures used in road surface constructions is developed. In this procedure the effective dielectric constant is derived using a simple inverse scattering algorithm to the measured radar cross sections of cylindrical specimen of a standard asphalt mixture. Then vector radiative transfer equation is used to formulate the scattering from a multi-layer medium representing an ice- or water-covered asphalt surface. The University of Michigan Polarimetric 94 GHz radar system was deployed for characterizing the polarimetric backscatter responses of asphalt surfaces under many physical conditions near grazing incidence angles ($70° - 88°$). The measured backscatter coefficients and parameters of co-polarized phase difference statistics of a dry asphalt surface with smooth interface at one incidence angle were used to derive the phase matrix of the asphalt medium. The experimentally determined phase matrix is substituted in the radiative transfer formulation to predict the scattering from asphalt surfaces under all conditions. Excellent agreement between the theoretical predictions and measured quantities is obtained.

Applications of Estimation Theory to the Forward and Inverse Scattering Problem

James M. Stiles
Radar Systems and Remote Sensing Laboratory
The University of Kansas, Lawrence Kansas
Tel: (913) 864-7744, Fax: (913) 864-7789
e-mail: jstiles@rsl.ukans.edu

Abstract

To provide an accurate representation of the scattering from a random medium, scattering models must explicitly comprehend each physical parameter of the medium that affects the scattering response. Unfortunately, many of these physical parameters are often not those of ultimate interest to the scientific investigator, and their addition to the scattering model greatly increases the difficulty of the inverse problem. These nuisance variables can be eliminated (either explicitly or implicitly) by setting them to a fixed (e.g., mean) value, thereby reducing the number of variables and thus moderating model complexity. This is perhaps even a requirement for performing inversion - that is to provide a problem which is well-posed.

However, by modeling as constants, or ignoring completely, the media parameters which affect scattering response (and are in fact variable and unknown), the accuracy of the scattering model is decreased. This degradation in model accuracy can lead to erroneous results from the inversion process, particularly when considering the non-linear relationships found in scattering.

An alternative to model inversion is to approach the task as an estimation problem, wherein *a priori* knowledge about a scattering medium, as well as knowledge of model accuracy, can be used to determine the most likely set of media parameters given a set of scattering observations. Although this solution is in many ways superior to the inversion problem, its complexity is equivalently affected by nuisance parameters. However, estimation theory also allows for the numeric evaluation of information (i.e., the ability of observed data to reduce the uncertainty of an unknown variable). By numerically quantifying information content, specific methodologies can be implemented to transform (linearly) the set of variables that describe a random medium into a new set of lower dimension (i.e., fewer variables), while maximizing the information content associated with this simplified model. In this way, model complexity is reduced in a manner that attempts to minimize the adverse impact on model accuracy.

F8.5

Microwave Scattering Experiments on Artificial Dielectric Surfaces at the EMSL

G. Nesti*, P. Coppo**, D. Tarchi* and A. J. Sieber*
*JRC, Space Applications Institute - Advanced Techniques,
21020 Ispra (Va) - Italy
**Via G.Mazzoni 17, 50134 Firenze - Italy

ABSTRACT

Within the frame of the thematic subgroup on scattering properties of non vegetated terrains of the European Microwave Signature Laboratory (EMSL), a number of scattering experiments on artificial surfaces with known statistical parameters and dielectric properties have been realised. Polarimetric measurements have been performed over samples of 2 m in diameter in the frequency range 2 to 18 GHz. Backscattering data have been acquired with variable incidence angle (10°-50°) while bistatic data have been taken at two incidence angles (20° and 40°) with the scattering angle variable in the range ±50°. Data have been collected also outside the principal scattering plane using the fixed antennas array of the EMSL. Azimuth target rotation has been used to obtain independent measurement samples and, as additional verification, in selected cases the scattering coefficient (σ^o) obtained from scatterometric measurements has been compared with the results obtained from high resolution SAR images of the same target.

The artificial material has been realised with a mixture of fine sand, water and ethanediol. Its dielectric constant has been estimated with two independent methods: 1) by means of a surface contact coaxial probe and 2) through the measurement of the perpendicular reflection coefficient of a thin layer of material backed by a metallic plate. The value of $\underline{\epsilon}_r$ ranges between $8.5 - j3.5$ at 2 GHz and $5.5 - j1.5$ at 18 GHz with a reasonable agreement between the two methods (typically 10% discrepancy).

The roughnesses of the surfaces has been determined by using moulds (isotropic in azimuth) with pre-defined statistical parameters. Three types of surfaces have been realised: 1. relatively smooth with Gaussian Autocorrelation Function (ACF), (height RMS: 4 mm, Autocorrelation Length (ACL): 60 mm), 2. medium rough with mixed ACF (height RMS: 9 mm, Gaussian ACL: 30 mm, Exponential ACL: 18 mm) and 3. very rough with Gaussian ACF (height RMS: 25 mm, ACL: 60 mm). Given the wide frequency range considered, these three samples allow the investigation of a significant set of scattering conditions.

The backscattering data have been calibrated by applying, in addition to a full polarimetric calibration on the antenna boresight, specific correction factors to take into account the effect of the antenna pattern and the variation of the local incidence angle. For the bistatic case, due to lack of suitable polarising targets, a simpler calibration procedure which assumes ideal antenna characteristics has been used. The maximum error of the experimental data (after averaging in azimuth) is estimated in ±1.0 dB for the copolar channels where the signal is typically well above the system sensitivity level. The signal of the cross-polar channels is more critically affected by system noise and antenna cross-polarisation purity.

Time-Frequency Correlations and Angular Memory Effects for Waves Scattered by Random Media

*Akira Ishimaru, Yasuo Kuga, Tsz-King Chan and Ji-Hae Yea
Department of Electrical Engineering
University of Washington
Box 352500
Seattle, Washington 98195-2500 USA
Telephone: 206-543-2169, Fax: 206-543-3842, E-mail: ishimaru@ee.washington.edu

Time-frequency correlations of scattered waves are generalized to include the relationships with the two-frequency mutual coherence function and the Wigner distribution. The correlations are expressed in average and difference times and average and difference frequencies. Parallel formulations for spatial correlations are given in terms of the average and difference positions and spatial frequencies. The relationships with the specific intensity and the flux in the radiative transfer theory are given. As an example, the Wolf effect, which is the shift of source spectrum due to the correlation effect, is shown for the turbulence case.

The angular correlations of the scattered waves and the memory effects are generalized to include the circular memory effect. Two cases are examined in detail. One is the forward scatter case when the reference transmitter and the receiver are in opposite sides of the scattering medium. In this case, the correlation is insensitive to the azimuthal angular changes. The other is the backscattering case when the reference receiver is close to the transmitter. In this case, the correlation is sensitive to the change of the azimuthal scattering angle. The use of this circular memory effect in object detection is discussed, and millimeter wave experiments with rough surfaces are shown to illustrate the method. Generalizations of the memory effects in three-dimensional space are also considered showing the general matching conditions for transverse wave vectors including two different frequencies.

F8.7

Polarimetric Bistatic Measurement Facility For Point and Distributed Targets

Bryan Hauck, Fawwaz Ulaby, and Roger DeRoo

Electrical Engineering and Computer Science
University of Michigan
Ann Arbor, Michigan 48109-2122
Phone: (313)764-0501
Fax: (313)647-2106

Abstract

Whereas extensive measurements have been made over the years to characterize the backscattering response of point and distributed targets at microwave and millimeter-wave frequencies, very few measurements have been reported in the literature for the general bistatic-scattering case in which the transmitter and receiver are not co-located. The purpose of this paper is to describe the operational characteristics of a polarimetric bistatic radar facility that was designed and constructed at the University of Michigan for the purpose of characterizing the three-dimensional bistatic scattering responses of certain types of distributed targets, such as rough dielectric surfaces and surfaces covered with short vegetation, as well as the scattering response of small point targets. One of the distinguishing features of the facility is its ability to measure the complete polarimetric scattering matrix of a target over a wide range of incidence and scattering direction. Even though the facility is capable of operation at 10, 35, and 94 GHz, for the sake of brevity this presentation will be limited to the 10-GHz system only.

To calibrate the radar system, the radar cross section (RCS) of a point target with a known RCS pattern was measured. The target chosen was a hemisphere on a ground plane. This target had the advantage of having a known scattering pattern. The results of these measurements indicated that the system accuracy is well within $\pm$ 1 dB. A random rough surface was then prepared for measurement. This surface was created by milling a computer generated rough surface with known statistics on forty-two $9'' \times 12'' \times 6''$ floral foam blocks. Results of the measurements are presented with comparisons to theoretical predictions for the surface.

OCEAN RADAR BACKSCATTER STATISTICS: FROM MID INCIDENCE TO NEAR GRAZING

B. L. Gotwols*, R. D. Chapman, and D. R. Thompson
Johns Hopkins University
Applied Physics Laboratory
Johns Hopkins Road
Laurel, MD 20723

This talk will focus on the transition that takes place in ocean backscatter statistics as the incidence angle varies from 20° to near grazing. Recently a model for the amplitude pdf of the microwave field backscattered from the ocean surface was proposed by the JHU/APL group, which fits the data at all amplitudes. The same model has also been used successfully to compute the phase. The cornerstone of the proposed model is based on the observation that the backscattered field is locally normally distributed. By this it is meant that for a given long wave slope (wavelength greater than the radar footprint) the complex field is normally distributed, but with a variance that depends on the underlying slope. The model successfully describes the statistics of the complex backscattered field based on sound physical principles, without the need for an ad hoc assumption of the underlying statistical distribution. Originally the model was meant to apply at intermediate incidence angles in the range 20° to ~60°.

Comparison of the JHU/APL model with approximately 1 Tbyte of data collected during the SAXON, COPE, and MISE experiments shows exceptionally good agreement at wavelengths ranging from 2 - 20 cm, and incidence angles from 20° to >60°. Somewhere around 70° the model starts to deviate from the measurements, but by a surprisingly small amount.

The measurements will be compared with both the JHU/APL mid incidence model, and the K distribution, which applies at near grazing incidence. Reasons for the transition in the character of the backscatter from mid incidence to near grazing will be discussed.

F8.9

APPLICATION OF THE MUSIC ALGORITHM TO A MULTI-FREQUENCY HF OCEAN-WAVE RADAR

Calvin C. Teague
STAR Laboratory, Stanford University, Stanford Calif. 94305

A new multi-frequency HF (4–30 MHz) ocean backscatter radar system, recently constructed jointly by the University of Michigan, the Environmental Research Institute of Michigan (ERIM), and Stanford University, has been deployed at Santa Cruz, California. The radar utilizes a phase-coded waveform, two omnidirectional transmitting antennas, and eight broadband loop receiving antennas configured as a phased array with half-wavelength interelement spacing at the highest frequency and spanning a total aperture of 48 m. The signals from the individual loop elements are sampled sequentially and recorded separately for subsequent data processing. While conventional beam-forming techniques provide adequate directional resolution at the higher frequencies, the available array aperture limits the directional resolution at the lower frequencies. In an attempt to improve the directional resolution of the radar, the MUltiple SIgnal Characterization (MUSIC) algorithm (R. O. Schmidt, *IEEE Trans. Antennas & Prop.*, vol AP-34, pp. 276–280 , 1986) was applied to the signals received on the individual loops.

The MUSIC algorithm was applied first to calibration data obtained from a wideband transponder carried on a small boat near the radar site. The transponder was about 300 m from the array and occupied 7 locations over an angular range of 65°. With corrections for only amplitude differences between elements, the RMS error in estimated direction to the transponder over 4 frequencies between 4.8 MHz and 21.77 MHz was less than 8°, with a bias of about 2.3°. Corrections for systematic phase perturbations and mutual coupling between elements should lower both of these values.

The transponder runs represent ideal conditions: a single point target. The ocean targets, however, are distributed in direction and unknown in number. Consequently, the real interest is in the behavior of the MUSIC algorithm for the ocean targets, under various conditions of sea state, wind, and signal-to-noise ratio. Surface buoy measurements, shore-based wind measurements, and radar data from several CODARs in the Monterey Bay area are available for comparison.

The MUSIC algorithm will be summarized briefly and the results of the data processing for both the point transponder targets and the distributed ocean targets will be described.

GeoSAR: A NEW RADAR TERRAIN MAPPING SYSTEM FOR THE NEW MILLENNIUM

Thomas Thompson, Jakob van Zyl, Scott Hensley,
Kevin Wheeler, Randy Bartman
Jet Propulsion Laboratory
California Institute of Technology
Pasadena, California, 91109

Gerald Dildine, Jeff Seib
Calgis, Incorporated
Fresno, California, 93710

John Burton, Robert Yoha, and Mike Gardner
California Department of Conservation
Sacramento, California, 95814

GeoSAR (Geographic Synthetic Aperture Radar) Project is a new 3 year effort to build a unique, dual-frequency, airborne Interferometric SAR for mapping of terrain. This Project, which is funded by the Defense Research Projects Agency (DARPA), will be conducted via a Consortium of the Jet Propulsion Laboratory, Calgis, Inc., and the California Department of Conservation. The airborne portion of this system will operate on a Gulfstream-II aircraft outfitted with P- and X-band Interferometric SARs. The ground portions of this system will be an IFSAR Processor and a Radar-GIS Workstation.

The airborne P-band and X-band radars will be constructed by JPL with the goal of obtaining foliage penetration at the longer P-band wavelengths. The P-band and X-band radar will operate at frequencies of 350 Mhz and 9.71 Mhz with bandwidths of either 80 or 160 Mhz. The airborne radars will be complemented with airborne laser system for measuring antenna positions as well as an aerial camera.

The ground processing will be a two-step step process. First, the raw radar data will be processed into radar images and interferometer derived Digital Elevation Models (DEMs). Second, these radar images and DEMs will be processed with a Radar GIS Workstation which performs processes such as Projection Transformations, Registration, Geometric Adjustment, Mosaicking, Merging, Classification via Interferometric Correlation and Database Management. JPL will construct the IFSAR Processor and Calgis, Inc. will construct the Radar GIS Workstation.

The GeoSAR Project was underway in November 1996 with a goal of having the radars and laser systems fully integrated onto the Gulfstream-II aircraft in November 1998. Then, both Engineering Checkout and User Validation Flights will be conducted from November 1998 through November 1999. The California Department of Conservation will conceive and lead the User Validation Flights. The overall system will be delivered at the end of 1999 and ready for routine operations in the year 2000.

F8.11

Signal processing methods for sub-surface detection

Harold Raemer and Eric Miller
ECE Department and Center for Electromagnetics Research,
Northeastern University, Boston, MA 02115

Sophisticated signal processing methods for the detection and localization of buried objects must be built around a scattering model describing the interaction of the probing energy with the medium parameters of interest (i.e., complex electrical permittivity). These algorithms can assume one of two forms. An imaging-type algorithm would use the forward model as part of an optimization routine to construct a pixel-by-pixel image or volumetric rendering of the subsurface permittivity. Alternatively, in the event that one's primary objective is the localization of known objects such as mines or buried drums of hazardous waste, one would make use of this forward model as part of a more structured object-detection algorithm. This class of algorithms typically employs methods such as template matching, matched filtering, or sequential hypothesis testing and is distinct from an imaging algorithm in that these unknown quantities are the number and spatial locations of the objects rather than a large number of pixel or voxel values.

The forward model to be used in this application is an extension of a simulation program developed by one of the authors, whose purpose was to model radar returns from the terrain surface and discrete objects in the radar's field of view for a wide variety of radar scenarios. The extension, discussed in a paper presented at AP-S/URSI in July 1996 (H.R. Raemer and R. Bilotta, "Simulation of imaging radar returns including underground volume scattering"), adds to the existing capabilities of this software the option of modeling the scattered returns due to a specified volume distribution of complex permittivity deviation from the mean value below the ground surface and spatially resolving these contributions. The simplest option uses the first-order Born approximation for vector fields, accounting for the effects of transmission through the air-earth interface. This can be used to model both subsurface clutter and returns from some buried objects. More advanced options include layered media and hence the effects of reflections from interfaces below the ground surface. Still more advanced options not yet fully implemented involve higher-order vector Born approximations. Some examples of the use of this forward model in the context of the signal processing algorithms referred to above are shown in the presentation. The basis of the simulated scenario is some SAR data on buried objects in desert terrain. The case studies include both buried objects and subsurface clutter due to random spatial variations of complex permittivity.

URSI F Special Session **Session 23** **Salon Gatineau**

Remote Sensing of the Earth's Surface/NASA Scatterometer
Co-chairs: A. Gasiewski, USA and A. Hollinger, Canada

13:10 23.1 **Invited:** Overview of the NSCAT Calibration/Validation Meeting, **W. LINWOOD JONES**, *University of Central Florida, Orlando, FL, USA*

13:30 23.2 NSCAT Sensor Verification and Calibration, **W.-Y. TSAI**, *California Institute of Technology, Pasadena, CA, USA*

13:50 23.3 On-Orbit Calibration of NSCAT Antennas Using Homogeneous Land Targets, **J. ZEC**, W. LINWOOD JONES, *University of Central Florida, Orlando, FL, USA*

14:10 23.4 Testing the NSCAT Model Function, **V. HESANY**, W.J. PLANT, *University of Washington, Seattle, WA, USA*

14:30 23.5 Satellite Scatterometer (NSCAT) Studies of Ocean Surface Stress and SIGMA-O Anomalies in Near Coastal Regions, **D.E. WEISSMAN**, *Hofstra University, Hempstead, NY, USA*

14:50 23.6 Ocean Circulation Simulated with 2-Day and 1-Month Mean NSCAT Wind Velocity Data, **D. HALPERN**, *California Institute of Technology, Pasadena, CA, USA*

15:10 Coffee Break

15:30 23.7 Land and Ice Applications of the NASA Scatterometer, **D.G. LONG**, *Brigham Young University, Provo, UT, USA*

15:50 23.8 Azimuthal Dependence of Interferometric Ocean Surface Velocity Measurements, **D. MOLLER**, S. FRASIER, R.E. McINTOSH, *University of Massachusetts, Amherst, MA, USA*

16:10 23.9 Sea Back Scatter at Low Grazing Angles Including Atmospheric Effects, **R.H. OTT**, *GRCI, Inc., Albuquerque, NM, USA*

16:30 23.10 Combined High-Resolution Active and Passive Imaging of Ocean Surface Winds from Aircraft, **A.J. GASIEWSKI**[1], J.R. PIEPMEIER[1], R.A. McINTOSH[2], C.T. SWIFT[2], J.R. CARSWELL[2], W.J. DONNELLY[2], E. KNAPP[2], E.R. WESTWATER[3], V.I. IRISOV[3], L.S. FEDOR[3], D.C. VANDEMARK[4], [1]*Georgia Institute of Technology, Atlanta, GA,* [2]*University of Massachusetts, Amherst, MA,* [3]*NOAA Environmental Technology Laboratory, Boulder, CO and* [4]*NASA Goddard Space Flight Center, Wallops Island, VA, USA*

16:50 23.11 High-Resolution Multiband Passive Polarimetric Imaging of the Ocean Surface, **A.J. GASIEWSKI**, J.R. PIEPMEIER, *Georgia Institute of Technology, Atlanta, GA, USA*

F23.1

Overview of the NSCAT Calibration/Validation Meeting

W. Linwood Jones

UCF Remote Sensing Laboratory, University of Central Florida, ECE Dept.,
P.O. Box 162450, Orlando, FL 32816, U.S.A.
tel: 407 823-6603
fax: 407 823-5835
email: ljones@pegasus.cc.ucf.edu

On August 17, 1996, the Ku-Band NASA Scatterometer (NSCAT) was launched aboard the Japanese Space Agency Advanced Earth Observation Satellite (ADEOS). The NSCAT Mission, planned for at least three years, is to provide scatterometer data for oceanographic and climatological research in global climate change under NASA's Mission to Planet Earth Program. NSCAT will make accurate measurements of ocean surface wind speed and direction over a wide swath, thus providing a significant expansion and improvement of the current satellite scatterometer data base.

This paper reports on the first NSCAT Calibration/Validation workshop that was held in Honolulu, Hawaii during the week of January 20, 1997. The purpose of this workshop was for the NSCAT project engineering and science team to present their findings of the on-orbit instrument check-out, the preliminary sigma-0 calibration and geophysical validation. This paper presents a summary of the workshop results and conclusions. For the geophysical validation, refinements of the empirical scatterometer geophysical model function will be described; and an assessment of the geophysical measurements accuracy will be given. These wind vector measurement comparisons will be presented using "surface truth" from numerical weather prediction models and in situ wind measurements from buoys and oceanographic research ships.

NSCAT SENSOR VERIFICATION AND CALIBRATION

Wu-Yang Tsai

Jet Propulsion Laboratory, M/S 300-319, California Institute of Technology,
Pasadena, CA 91109-8099, U.S.A.
tel: 818-354-8538
fax: 818 393-5184
email: Wu-Yang.Tsai@jpl.nasa.gov
JPL Sensor Verification and Processor Analysis Team*
NSCAT Science Team#

The NASA Scatterometer (NSCAT) is a Ku-band scatterometer launched on Japan's Advanced Earth Observation Satellite (ADEOS) on August 17, 1996. NSCAT is a specialized microwave radar instrument designed to provide frequent and accurate measurements of near-surface wind velocity over the global oceans. It uses an array of antennas that radiate microwave pulses at a frequency of 14 GHz and measured the echo power. The radar equation is then used to calculate the normalized radar cross-section (sigma-0)of the wind-driven ocean surface at several look angles. A wind retrieval algorithm is used to retrieve the wind speed and direction over the ocean surface using an empirical geophysical model function. The accuracy of sigma-0 measurements and the geophsical model function are key factors in determining the accuracy of the retrieved wind velocity.

The purpose of this paper is to present the process and the results of an intensive effort conducted at JPL to verify and calibrate the NSCAT instrument and processing system. The verification process includes the verification of the instrument functionality and performance, the sigma-0 calculation algorithms, and the expected sigma-0 distribution. The calibration process includes the beam balance using open oceans and uniform natural targets, and beam pointing and sigma-0 calibration using calibration ground station.

*JPL Sensor Verification and Processor Analysis Team member include W. Daffer, S. Dunbar, J. Granger, J. Huddleston, V. Hsiao, S. Lou, C. Morris, G. Neumann, W. Poulsen, M. Spencer, W. Tsai, and S. Yueh

#NSCAT Science Team member supporting this activities include N. Ebuchi, M. Freilich, L. Jones, D. Long, and F. Wentz

F23.3

On-Orbit Calibration of NSCAT Antennas using Homogenous Land Targets

Josko Zec* and W. Linwood Jones

UCF Remote Sensing Laboratory, University of Central Florida
ECE Dept., P.O. Box 162450, Orlando, FL 32816, U.S.A.
tel: 407 823-6603
fax: 407 823-5835
email: ljones@pegasus.cc.ucf.edu

Satellite scatterometers are spaceborne radars designed to measure normalized radar backscatter coefficient (sigma-0). From these direct measurements, wind vectors can be retrieved. Wind retrieval is based on a known relation between sea-surface roughness and wind speed and direction known as the geophysical model function. Multiple antennas, that view the ocean at different azimuths, are needed to resolve wind direction ambiguities. To achieve the desired wind vector accuracy, the antennas must be precisely calibrated. This paper describes a simple relative calibration method applied for the NASA Scatterometer (NSCAT) during post-launch calibration and validation activities at the Jet Propulsion Laboratory. Homogenous large area land targets are used. These targets exhibit uniform and time invariant radar response. Simple polynomial model for incidence angle dependence of the sigma-0 is assumed. Corrections are calculated as differences (in log space) between measurements and the mean response for all beams. This simple model is applied to the Amazon rain forest and Siberian plain. These areas are tested for temporal stability. High resolution masks are applied to filter and extract suitable calibration data sets. Calculated corrections needed to be added to the raw measurements taken at the same incidence angle regardless of the beam. The magnitude of the corrections show the necessity of on-orbit calibration.

Testing the NSCAT Model Function

Vahid Hesany*, William J. Plant

Applied Physics Laboratory, University of Washington, 1013 NE 40th Street,
Seattle, WA 98105-6698
Phone: 206-543-7836
Fax: 206-543-6785
email: plant@crosby.apl.washington.edu

In late August of 1996, NASA successfully launched a Ku band scatterometer, NSCAT, on the Japanese satellite ADEOS. We have utilized both NSCAT data and data from our recent airship experiments to attempt to assess the accuracy of the model function being used to process NSCAT data. One method of carrying out this assessment is to compare model function predictions with in-situ measurements of cross section versus neutral wind speed. We have employed this method utilizing both the simultaneous wind and cross section data obtained in the airship experiments and the collocated buoy winds and NSCAT cross sections tabulated by the Woods Hole Oceanographic Institution and the University of Miami. A second method of assessing model function accuracy which we have employed is that developed for the ERS-1 satellite scatterometer. In this method, three dimensional plots of cross sections from three different scatterometer beams should fall on a surface defined by the model function if this function is correct. This method yields insight into the azimuth-angle dependence predicted by the model function and into the relative levels of HH and VV polarized mean cross sections but is unable to set the absolute wind speed dependence of the model function. Hence the comparison with some surface data set is necessary. We presently have insufficient data at high wind speeds to be able to assess model function performance above 20 m/s. We show, however, that the consistency of the model function both internally and with the surface data is very good at moderate wind speeds. We suggest that at wind speeds below 5 m/s the basic assumption of scatterometry - that cross section depends primarily on wind speed and direction - may not be well satisfied.

F23.5

SATELLITE SCATTEROMETER (NSCAT) STUDIES OF OCEAN SURFACE STRESS AND SIGMA-0 ANOMALIES IN NEAR COASTAL REGIONS

David E. Weissman
Department of Engineering
Hofstra University
Hempstead, New York 11550

This study addresses the consistency of the surface friction velocity derived from the scatterometer normalized radar cross section (NRCS) measurements and the directional properties of the NRCS (SIGMA-0) measurements in near coastal regions. NSCAT data (Level 1.7) colocated with numerous NDBC buoys (within ± 0.5° Lat. and Lon.) is being analyzed to determine the variability of the directional properties of the colocated fore and aft beam measurements. These orthogonal measurements of the NRCS (25 km resolution, and converted to linear power units) by the fore and aft beams are used to calculate the Fourier series coefficients of the azimuthal model: A0 and A2. The spatial variability of A2/A0, as an indication of how the azimuthal modulation varies, is being examined in the vicinity of buoys off the U.S. Atlantic coast, in the Gulf of Mexico and along the coast of California.

Preliminary results show excellent agreement between the satellite derived friction velocity (u*) and buoy measurements. The conversion from the measured NRCS to u* is based on the FASINEX/Weissman Ku-band model function. Other results show some cases in which the A2/A0 term is relatively constant for the 12-to-19 SIGMA-0 cells that lie within the 1° square region centered about each buoy, and other situations in which the A2/A0 values vary randomly and considerably even though the winds appear to be uniform. These latter situations are of strong interest, and are being studied to determine the possible causes of this variability. Under consideration are the long wave systems, atmospheric stability and surface material properties.

Ocean Circulation Simulated With 2-Day and 1-Month Mean NSCAT Wind Velocity Data

David Halpern

Jet Propulsion Laboratory, M/S 300-323, California Institute of Technology,
Pasadena, CA 91109-8099, U.S.A.
tel: 818-354-5327
fax: 818-393-6720
email: halpern@pacific.jpl.nasa.gov

Ocean currents are primarily generated by horizontal variations of surface wind stress, which are related to the near-surface wind field. A goal of biological and physical ocean sciences has been the accurate determination of the surface wind field. A wind-measuring scheme must not only be accurate in regards to the quality of each measurement but also must resolve the rich space and time spectra of wind motions. For many oceanographic applications, the desired accuracy would be 1 m/s for the east-west and north-south wind components (or 1.5 m/s and 4 degrees for speed and direction), 1-day resolution, and 25-km horizontal scale.

In August 1996 the U.S. National Aeronautics and Space Administration (NASA) Scatterometer (NSCAT) was launched on the Japanese Advanced Earth Observing Satellite (ADEOS). NSCAT yields an unprecedented quantity of high-quality, high-resolution 19.5-m height wind velocity vectors. Wind vectors are measured with a 25-km x 25-km footprint every 2 days (sometimes more often) over 98% of the global ocean. An experiment with NSCAT data is described to illustrate differences in wind-driven ocean circulation derived from 2-day and 1-month mean data. A time scale of 1-month has typically been used in oceanography because of the scarcity of data. For this report, data from the Arabian Sea are employed because of an ongoing research project.

Three components of wind-driven circulation of the Arabian Sea were computed: vertical transport of water across the bottom of the Ekman layer north of 8°N, which is related to wind stress curl and zonal component of Ekman transport; north-south component of Ekman transport along the southern boundary at 8.5°N, which is related to zonal wind stress component; Sverdrup transport along 8.5°N, which is related to wind stress curl. Using preliminary NSCAT data for September and October 1996, differences between a ten 2-day data set and a single 20-day data set (same days were used) were 30%, 44%, and 7%, respectively, for vertical transport, Sverdrup transport, and north-south Ekman transport. Differences were large for transports computed from wind stress curl because large wind stress curls occurred for short time intervals. Additional results obtained with reprocessed NSCAT data will be described.

F23.7

LAND AND ICE APPLICATIONS OF THE NASA SCATTEROMETER

David G. Long

Electrical and Computer Engineering Department, 459 Clyde Building, Brigham Young University, Provo, UT 84602
Phone: (801) 378-4383
Fax: (801) 378-6586
email: long@ee.byu.edu

The NASA Scatterometer (NSCAT) launched in August of 1996 is a real aperture Ku-band radar system designed to measure the normalized radar backscatter coefficient (sigma-0) of the earth's surface. NSCAT is a follow-on to the Seasat Scatterometer (SASS) launched in 1978. Scatterometers offer wide-area, frequent coverage and a historical data base dating back to 1978. Due to its low spatial resolution (nominally 25 km), NSCAT, like other scatterometers, has been used primarily for oceanic studies. However, the use of resolution enhancement algorithms such as the Scatterometer Image Reconstruction with Filtering (SIRF) algorithm with NSCAT data can ameliorate this limitation to yield resolutions approaching 4 km. With this resolution NSCAT data can be used in a variety of studies land vegetation and polar ice. Two examples of such studies are presented.

The utility of NSCAT data in studies of polar ice is illustrated through the development of an automated algorithm for detecting the sea ice edge. Polar sea ice is a critical input to global climate and geophysical models. It acts as an insulating layer between the warmer ocean and cooler atmosphere and can radically change the albedo of the Earth's surface. Hence, monitoring the extent of polar sea ice is of great interest to the remote sensing community. An automated algorithm for detecting the polar sea ice edge from NSCAT data has been developed. The new algorithm uses dual polarization resolution enhanced NSCAT imagery. The accuracy of the resulting ice edge is compared to Joint Ice Center (JIC) and SSM/I-derived ice edge maps. A time-series of sea-ice images is presented which reveal the dynamics of the spring retreat of Southern Ocean sea ice.

NSCAT data can also be successfully applied to discrimination and mapping of tropical vegetation in studies of global change. The capability of discriminating various types of tropical vegetation using Ku-band sigma-0 measurements is first demonstrated. Discrimination accuracy is better than 94% over broad classes of vegetation. To illustrate the use of Ku-band data for global change, NSCAT 1996 results over the Amazon rain forest are compared with SASS 1978 results. Regions of significant deforestation are clearly delineated.

Keywords: scatterometry, polar ice, tropical vegetation, NSCAT, global change

Azimuthal Dependence of Interferometric Ocean Surface Velocity Measurements

Delwyn Moller, Stephen Frasier, Robert E. McIntosh
Microwave Remote Sensing Laboratory
University of Massachusetts, Amherst, MA 01003
T: 413.545.0779 / F: 413.545.4652 / moller@alex.ecs.umass.edu

Remote sensing of the ocean surface using interferometric SAR (INSAR) is of significant interest due to it's potential for surface current measurements over large areas. INSARs use the phase difference between colocated SAR images separated by a small time lag to infer surface Doppler velocities, and hence long wave orbital velocities and currents. To date, there have been few studies where interferometric velocity measurements of the ocean surface have been compared with environmental data.

A recent deployment of an X-band, focused phased-array imaging radar (FOPAIR) created an opportunity for such a comparison. In a manner analogous to INSAR, covariances between successive radar images are used to infer surface velocities. In this paper, interferometric velocity measurements from this radar are compared with in situ data. In particular, the dependence of velocity estimates on radar orientation with respect to the wind and the wave field is studied. The data presented was collected at low-grazing angles. Although X-Band INSAR systems capable of near-grazing operation exist, to our knowledge this is the first study of interferometric velocity comparisons with in situ data for these conditions.

In this study, two alternative approaches to estimating the mean surface velocity are evaluated and compared with theoretical expectations. It was found that the velocity estimates differed significantly when a mean velocity was derived from the frequency characteristics of the backscattered returns and not from a power-modulated ensemble average. When the radar boresight was into the the wind and wave field, velocities estimated from the frequency response alone match theory more closely. As a result, some recommendations are made for INSAR processing and interpretation.

F23.9

Sea Back Scatter at Low Grazing Angles Including Atmospheric Effects

R. H. Ott
GRCI, Inc.
3900 Juan Tabo blvd., NE
Suite 12
Albuquerque, NM 87111-3984

Using Helmholtz's formula for the field scattered by a rough sea surface and a propagation factor relating to a dipole close to the sea surface and its image, the geometrical-optics back scatter cross-section from a patch of sea of area A is shown to be given by

$$\sigma(m^2) = \frac{B}{8}\left|1 + R_v\right|^4 A \,,$$

where B is 0.005 (D. E. Barrick, IEEE Trans. Ant. and Prop., Jan., 1972), and R_v is the Fresnel reflection coefficient which is a function of the local grazing angle. The local grazing is determined by a ray-trace through the given refractive index variation with height. The cross-section does not depend upon sea state because, in this model it is assumed the back scatter results from those Fourier components in the water wave spectrum which satisfy the Bragg resonance resonance condition

$$\lambda = 2\lambda_{water} \,.$$

Since the gravity wave spectrum extends down to about 1-2 cm, with shorter lengths representing the capillary waves, the model is valid for radar center frequencies through X-band.

In the figure below, the predicted clutter power is compared with measured data obtained from SPANDAR at Wallops Island, VA (G. D. Dockery, IEE Proc., Vol., 137, Part F, No.2, April, 1990). A ray-trace was performed assuming the measured data was recorded during normal atmospheric conditions (standard atmosphere).

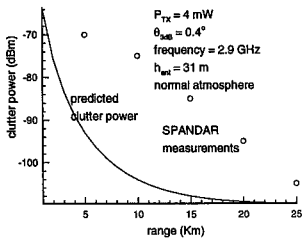

F23.10

Combined High-Resolution Active and Passive Imaging of Ocean Surface Winds from Aircraft

A.J. Gasiewski and J.R. Piepmeier
School of Electrical and Computer Engineering
Georgia Institute of Technology, Atlanta, GA 30332-0250
Ph: (404) 894-2934 FAX: (404) 894-4641
e-mail: ag14@prism.gatech.edu, gt2930b@prism.gatech.edu

R.A. McIntosh, C.T. Swift, J.R. Carswell, W.J. Donnelly, and E. Knapp
Microwave Remote Sensing Laboratory
University of Massachusetts, Amherst, MA 01003
Ph: (413) 545-4858 FAX: (413) 545-4652
mcintosh@ecs.umass.edu, klemyk@ecs.umass.edu, carswell@alex.ecs.umass.edu,
donnelly@alex.ecs.umass.edu, knapp@alex.ecs.umass.edu

E.R. Westwater, V.I. Irisov, and L.S. Fedor
NOAA Environmental Technology Laboratory, Boulder, CO 80303
Ph: (303) 497-6527 FAX: (303) 497-3577
e-mail: ewestwater@etl.noaa.gov, virisov@etl.noaa.gov, lfedor@etl.noaa.gov

D.C. Vandemark
Laboratory for Hydrospheric Processes
NASA Goddard Space Flight Center, Wallops Island, VA 23337
Ph: (804) 824-2038 FAX: (757) 824-1036
e-mail: vandemark@gsfc.nasa.gov

A unique complement of passive and active microwave imaging and sensing instruments with polarimetric capability have been integrated onto the NASA Wallops Flight Facility's Orion P-3B aircraft for the purpose of studying the signature of ocean surface winds. The complement includes: (1) a four-band (X, K, Ka, and W) tri-polarimetric conical- and cross-track scanning radiometer (the Polarimetric Scanning Radiometer, or PSR), (2) a C-band ocean surface scatterometer (C-Scat), (3) a Ka-band conical-scanning polarimetric radiometer (Kaspr), (4) a nadir-viewing Ka-band polarimetric radiometer, (5) a 21- and 31-GHz zenith-viewing cloud and water vapor radiometer, and (6) a radar ocean wave spectrometer (ROWS). The Ocean Winds Imaging (OWI) complement was flown during January, 1997 over the Atlantic Ocean near the Virginia coast in an attempt to provide the first combined high-resolution (<1 km spot size) active and passive images of wind-driven ocean surface wind features. Brightness temperature and backscatter data were observed over open ocean for a variety of wind speeds and cloud conditions. Intercomparisons of data from several of the OWI instruments and implications for ocean surface wind direction sensing from active and passive spaceborne instruments will be discussed.

F23.11

High-resolution Multiband Passive Polarimetric Imaging of the Ocean Surface

A.J. Gasiewski and J.R. Piepmeier
School of Electrical and Computer Engineering
Georgia Institute of Technology, Atlanta, GA 30332-0250
Ph: (404) 894-2934 FAX: (404) 894-4641
e-mail: ag14@prism.gatech.edu

A versatile new airborne microwave imaging radiometer, the Polarimetric Scanning Radiometer (PSR), was recently used to obtain the first high resolution (~0.3-1 km spot size) multiband tri-polarimetric data over the ocean surface. The PSR consists of a set of four tri-polarimetric ($T_v=\langle|E_v|^2\rangle$, $T_h=\langle|E_h|^2\rangle$, and $T_U=2Re\langle E_v E_h^*\rangle$) radiometers housed within a gimbal-mounted scanhead drum. The radiometric bands are X (10.6-10.8 GHz), Ku (18.6-18.8 GHz), Ka (36-38 GHz), and W (86-92 GHz). Each radiometer uses a dual orthogonal-linear polarization receiver with dual-output local oscillator. Preamplification using high electron mobility transistor amplifiers is used prior to single sideband downconversion for the X- and Ku-band radiometers, while direct double sideband downconversion is used for the Ka- and W-band radiometers. Detection is accomplished using custom three level (1.6-bit) digital correlators operating at 1 Gs/sec. The correlators allow detection and cross-correlation of 500 MHz wide intermediate frequency bands. In order to detect the full bandwidths available from the various receivers (up to 2000 MHz), IF subband division is used.

The radiometer antennas are orthogonal linearly-polarized corrugated feedhorns with grooved rexolite lens antennas. A single dual-band antenna is used for the X- and Ka-band channels. Antenna diameters were chosen to provide beamwidths of 8° (X- and K-bands) and 2.3° (Ka- and W-bands). The scanning drum can be positioned to view any angle with 0.1° precision using a computer-controlled stepper motor drive system. Scanning modes include conical (both one- and two-look), cross-track, and spotlight. Minimum scan times of ~3 seconds can be attained in-flight with excellent mechanical stability. Scan patterns include periodic views of
hot and ambient thermal calibration targets.

The PSR was operated on the NASA Wallops Flight Facility P-3B Orion aircraft during January and February of 1997 over the Atlantic Ocean near the eastern U.S. coast. The instrument exhibited excellent aerodynamic, mechanical, and electrical performance. Multiband polarimetric radiometric data from the flights will be presented and discussed.

URSI F

Session 38 Salon Gatineau

Remote Sensing of the Atmosphere
Co-chairs: D. Hudak, Canada and E.R. Westwater, USA

08:10	38.1	**Invited:** Measurement of Clear-Air Gradients and Turbulence Properties with Ground-Based Doppler Radars, **E.E. GOSSARD**[1,2], D.E. WOLFE[2], K.P. MORAN[2], R.A. PAULUS[3], K.D. ANDERSON[3], L.T. ROGERS[3], [1]*Cooperative Institute for Research in Environmental Sciences, University of Colorado,* [2]*NOAA, Environmental Technology Laboratory and* [3]*Naval Command, Control and Ocean Surveillance Center, Boulder, CO, USA*
08:30	38.2	**Invited:** Contributions of MST Radar Measurements to Modern Meteorology and Atmospheric Dynamical Studies, **W.K. HOCKING**[1], *University of Western Ontario, London, ON, Canada*
08:50	38.3	Insects and Birds Observed with a Polarimetric Radar, **A. RYZHKOV**[1], D. ZRNIC[2], [1]*University of Oklahoma and* [2]*National Severe Storms Laboratory, Norman, OK, USA*
09:10	38.4	**Invited:** Remote Sensing of Atmospheric Water Vapor Using a Regional Network of Ground-Based GPS Receivers, **G. ELGERED**, J.M. JOHANSSON, T.R. CARLSSON, L.B. GRADINARSKY, *Chalmers University of Technology, Onsala, Sweden*
09:30	38.5	**Invited:** Remote Sensing of the Troposphere for Global Change Research in the U.S.D.O.E. Atmospheric Radiation Measurement (ARM) Program, **J.C. LILJEGREN**, T.S. CRESS, *Pacific Northwest National Laboratory, Richland, WA, USA*
09:50	38.6	Preliminary Tropospheric Wind and Scattering Observations from the Resolute Bay VHF Radar, **W.O.J. BROWN**[1], W.K. HOCKING[2], [1]*McGill University, Montréal, QC and* [2]*University of Western Ontario, London, ON, Canada*
10:10		Coffee Break
10:30	38.7	Observations of the Planetary Boundary Layer Using 915 MHz Radars, **N. DONALDSON**[1], W.O.J. BROWN[2], R.R. ROGERS[2], [1]*Environment Canada, King City, ON and* [2]*McGill University, Montréal, QC, Canada*
10:50	38.8	Laser Propagation through the Intermittent Atmosphere, **J. GOZANI**, *University of Colorado at Boulder, CO, USA*
11:10	38.9	Zenith Attenuation Statistics Measured by 33 GHz and 95 GHz Atmospheric Radars, **S.M. SEKELSKY**[1], W.L. ECKLUND[2], K.S. GAGE[3], R.E. McINTOSH[1], [1]*University of Massachusetts at Amherst, MA,* [2]*University of Colorado, Boulder, CO and* [3]*National Oceanic and Atmospheric Administration, Boulder, CO, USA*
11:30	38.10	Results of First Round-the-Clock Observations of Absorption and Motions in the Lower Atmosphere Using Spaced-Antenna Reception with Doppler-Filtering of the Ground Wave, E.L. AFRAIMOVICH, **K.S. PALAMARTCHOUK**, *Institute of Solar-Terrestrial Physics, Irkutsk, Russia*
11:50	38.11	**Invited:** Applications of Submillimeter-Wave Passive Channels to Spaceborne Remote Sensing of Atmospheric Clouds, Water Vapor, and Temperature, **A.J. GASIEWSKI**, *Georgia Institute of Technology, Atlanta, GA, USA*

F38.1

MEASUREMENT OF CLEAR-AIR GRADIENTS AND TURBULENCE PROPERTIES WITH GROUND-BASED DOPPLER RADARS

E. E. Gossard
Cooperative Institute for Research in Environmental Sciences, University of Colorado/NOAA, Environmental Technology Laboratory, Boulder, Colorado

D. E. Wolfe and K. P. Moran
NOAA/ERL/Environmental Technology Laboratory, Boulder, Colorado

R. A. Paulus, K. D. Anderson, and L. T. Rogers
Naval Command, Control and Ocean Surveillance Center

An experiment to evaluate the capability of Doppler radar wind profilers to measure other useful meteorological quantities remotely is described. The site chosen was in southern California during a time of year when it offers a natural laboratory for investigating extreme contrasts in temperature and humidity. The adequacy of the standard wind observations obtained by editing the Doppler spectral moments is investigated and found to be very questionable for short-term observations. Here, the data processing is therefore extended to the editing of the raw averaged spectra, and substantial improvement is found. The advantages of the redundancy in five-beam systems are also investigated and found to be very important. A technique of minimizing the variances of the differences (MVD) of opposing radials is described that is found to substantially improve the interagreement of redundant wind profiles. It is also found to have important consequences for radio acoustic sounding systems (RASS) temperature retrievals. We conclude that acquisition of useful wind profiles is possible with spectral editing and with the redundancy of a five-beam system. Otherwise, only average winds from long-term consensusing can be considered to be reliable. Temperatures from RASS are compared with those from balloon soundings under the extreme conditions found at this site. The accuracy of techniques using the spectral width for measuring turbulent dissipation rate when complicated spectra are present is examined, and the importance of correcting the measured second moments for factors such as antenna beamwidth and system dwell time is discussed. Two different techniques for optimizing the calculation of spectral width are examined and the errors assessed. One technique integrates over the uncontaminated range of the chosen spectral peak and then extrapolates a Gaussian function to infinity. The other method uses the slope of the log least-squares best fit of the uncontaminated points to a Gaussian function. Profiles of radar-measured gradients of refractive index are compared with gradients measured by balloon. It is shown how gradients of humidity can be calculated to about the same accuracy as refractive-index gradients by combining the temperature gradients from RASS with the refractive-index gradient observations from the radar.

Contributions of MST Radar Measurements to Modern Meteorology and Atmospheric Dynamical Studies

W.K. Hocking
Dept. of Physics and Astronomy, University of Western Ontario, London, Ontario, N6A 3K7, Canada

MST (Mesosphere-Stratosphere-Troposphere) radars (also known as wind-profiler radars) had their origins in upper atmosphere (mesospheric and ionospheric) work, but they have developed to a stage where they have important applications for tropospheric studies. Moderately powered radars of this type can measure winds and turbulence throughout day and night at altitudes between (typically) 2 and 15 km altitude, whilst higher altitudes (up to 30 km) can be reached with the most powerful systems. Because these instruments utilize scatter from the clear air, they can acquire data on an almost continuous basis, a major advantage for studies of atmospheric dynamics. It is the combination of continuity of data, substantial height coverage, and rapidity of measurement (meassurements at typically one minute intervals and less) which makes these radars so useful.

Applications for these radars in a meteorological sense lie in areas of studies of temporal variability on scales of a few minutes out to seasonal and annual variability, atmospheric wave generation and propagation studies, and studies of turbulence. Other important attributes of these radars are their ability to highlight regions of atmospheric stability (based on the so-called aspect-sensitivity ratio) and also their capability of locating the height of the tropopause to good accuracy. Other, less straight-forward parameters, such as humidity gradients and temperature gradients, can also be found with these instruments under suitable circumstances. The ability of the radars to measure vertical velocities is also an important bonus.

These radars also have excellent potential for helping with aircraft flight planning and safety. By developing a grid of such radars, and applying recent improvements in large scale data assimilation, it is possible that measurements of winds and turbulence along known flight-paths can be made and reported back to a central terminus on a regular basis, thereby giving a good continuous record of data over a large region of the atmosphere. Knowledge of winds and turbulence along such trajectories could be of great value in identifying dangerous small scale weather systems, and may have additional economic benefits in the form of better flight planning.

These various applications, both realized and potential, will be discussed in this talk. Examples will be illustrated throughout. Relationships to studies in other regions of the atmosphere (stratosphere and mesosphere) will also be illustrated where appropriate. The potential scientific and economic advantages of several of these instruments distributed along the Windsor-Montreal corridor will also be discussed.

F38.3

INSECTS AND BIRDS OBSERVED WITH A POLARIMETRIC RADAR

Alexander Ryzhkov[1] and Dusan Zrnic[2]

[1]Cooperative Institute for Mesoscale Meteorological Studies / University of Oklahoma
[2]National Severe Storms Laboratory, Norman, Oklahoma

Observations of clear air echoes with the NSSL's Doppler polarimetric radar reveal two types of characteristics. One has peak intensity during the warm season of the year with the maximum in the afternoon hours; its differential reflectivity Z_{DR} is high (up to 10 dB) but the backscatter differential phase δ has a moderate value of less than 40°. The other type of echo exhibits a much lower Z_{DR} (range between -1 and 3 dB) and has a considerably larger differential phase (sometimes over 100°). Azimuthal dependencies of Z_{DR} and δ are very different for these two classes of echoes. For both types of radar returns the cross-correlation coefficient ρ_{hv} is between 0.3 - 0.5; that is significantly lower than observed in hydrometeors. The first type of echo is attributed to insects whereas the second one is likely caused by migratory birds.

There were no direct in-situ measurements to confirm the identity of reported biological scatterers. Nevertheless, there are compelling arguments linking the second type of clear air echo to migrating birds. These echoes were observed in the fall, during nighttime with favorable northern winds. The scatterers flew with the wind at relative speeds slightly exceeding 10 m s^{-1}. Their size or equivolume diameter inferred from model calculations matches those of birds.

Surprisingly, a simple model of prolate spheroids explains reasonably well the observed polarimetric signatures of both insects and birds. The essential difference between these two classes of radar echo is attributed to the following. At the 10 cm wavelength the insects backscatter predominantly in the Rayleigh regime (D_e < 1 - 2 cm) whereas the birds are mainly in the Mie range of sizes (D_e > 2 - 3 cm).

Both differential reflectivity and backscatter differential phase do not depend on the concentration (N_o) of monodispersed scatterers but are sensitive to their size and shape. Therefore by combining these two measurements it might be possible to roughly estimate the size of scatterers. From the size the type of birds could be inferred. This is an encouraging prospects for applications of dual-polarization radar in the areas of entomology and ornithology.

Remote Sensing of Atmospheric Water Vapor Using a Regional Network of Ground-Based GPS Receivers

G. Elgered*, J.M. Johansson, T.R. Carlsson, and L.B. Gradinarsky
Onsala Space Observatory, Chalmers University of Technology
S-439 92 Onsala, Sweden

The Swedish GPS network has been in continuous operation since August 1993. Today, in January 1997, it includes 21 sites. One major application is the measurement of crustal motions. For example, those associated with the postglacial isostatic adjustment are of importance for studies of mantle rheology as well as for correction of sea level data. The expected land uplift was detected from the first two years of data (Bifrost Project, EOS Trans. AGU. 77, pp. 337,341, 1996). Atmospheric effects are known to have a large impact on the accuracy of the estimated geodetic parameters, end especially the local vertical coordinate. The main part of this error is for most sites caused by the varying amount of water vapor and the corresponding excess propagation path, called the wet delay.

The total excess propagation path is estimated at each GPS site. In order to evaluate this method we use these time series together with interpolated ground pressure data to estimate the wet delay at each site. We evaluate these wet delays by comparisons with independent methods such as microwave radiometry and radiosonde launches. A microwave radiometer has been operated more or less continuously at the Onsala Space Observatory side-by-side with the GPS receiver. The observed sky-brightness temperatures at 21.0 and 31.4 GHz are used to infer the excess propagation path caused by the water vapor in the atmosphere. Radiosonde launches are made at four sites reasonably close (distance <40 km) to GPS receiver sites. The agreement in the wet delays inferred from the different methods is typically just below the one centimeter level. This corresponds to approximately 1 mm in the integrated precipitable water vapor. We present the results from these comparisons in terms of RMS differences and systematic trends for several sites and for different periods of the year.

Finally, we will discuss the application of GPS data for continuous monitoring of the water vapor content when evaluating numerical models used in meteorology and climate studies.

F38.5

Remote Sensing of the Troposphere for Global Change Research in the U.S.D.O.E. Atmospheric Radiation Measurement (ARM) Program

James C. Liljegren and Ted S. Cress
Pacific Northwest National Laboratory[1], Richland, Washington, USA

To progress toward the goal of reliable prediction of the regional effects of global change, climate models have steadily increased resolution. This improvement has not been limited to dimensional resolution (temporal, spatial, wavelength) but has included improved process resolution (e.g. cloud formation processes) as well. Consequently, sophisticated, long-term experimental data are needed to support the development of these process models (e.g. liquid water path, ice water path, CCN, etc.)

In order to provide these sophisticated, comprehensive, long-term measurements of the cloud and radiation processes that control the earth's radiative balance, the ARM Program has acquired/developed and deployed a wide variety of active and passive ground-based remote sensors at its Cloud and Radiation Testbed (CART) in the U. S. Southern Great Plains. Scientifically appropriate subsets of these sensors have been integrated into Atmospheric Radiation and Cloud Systems (ARCS) for deployment in the Tropical Western Pacific and North Slope of Alaska and Adjacent Arctic Ocean in order to address important cloud and radiation processes specific to these regions.

These sensors provide measurements that characterize the dynamics, thermodynamics, and radiative properties of the atmosphere necessary to force the process models. Additional sensors measure the radiative consequences of the atmospheric state with varying spectral and angular resolution for comparison with model predictions. ARM has also developed/acquired algorithms that combine these measurements to derive additional information in order to take advantage of the synergy offered by multiple remote sensors.

This paper will present an overview of the ARM Program's remote sensing capabilities illustrated with representative examples of the measurements.

---

[1]Pacific Northwest National Laboratory is operated for the U.S. Department of Energy by Battelle Memorial Institute under Contract DE-AC06-76RLO 1830.

Preliminary Tropospheric Wind and Scattering Observations from the Resolute Bay VHF Radar

William O.J. Brown*
Department of Atmospheric and Oceanic Sciences,
McGill University, Montreal, Canada.

Wayne K. Hocking
Department of Physics, University of Western Ontario,
London, Ontario, Canada.

A VHF radar is being developed by the University of Western Ontario (in collaboration with Cornell and McGill Universities) at the Early Polar Cap Observatory (operated by the U.S. National Science Foundation and the Canadian Natural Sciences and Engineering Research Council) at Resolute Bay in the Canadian Arctic (75N,95W), (e.g., Hocking et al at this meeting). The radar will operate in MST (Mesospheric, Stratospheric, Tropospheric) mode, and will also carry out meteor and ionospheric experiments. A series of preliminary observations of the troposphere has already been carried out and various aspects of these experiments are reported here.

Nearby the observatory is an Environment Canada meteorological station at which radiosonde soundings are taken every twelve hours. Comparisons between wind measurements made on the radar and those made by the soundings show good agreement, with velocities generally consistent to within about 2 m/s.

Turbulence and scattering aspect sensitivity measurements can also be made with the radar using Doppler spectral width and echo intensity information (e.g., W.K. Hocking, Adv. Space. Res. 17(11), 37-47, 1996). Preliminary analysis also shows agreement between trends in these parameters and indicators of stability (e.g., Richardson number) derived from the radiosonde observations. For example aspect sensitive layers are observed around regions of increased stability and (turbulent) spectral broadening is observed around unstable regions. These and other features of the relationships between turbulence and aspect sensitivity parameters and the sounding observations will be examined in the presentation.

F38.7

Observations of the Planetary Boundary Layer Using 915 MHz Radars

NORMAN DONALDSON, Cloud Physics Research, Environment Canada
14780 Jane St, King City, Ontario, L7B 1A3 *
W.O.J. BROWN and R.R. ROGERS, Dept Atmospheric Sciences,
McGill University, 805 Sherbrooke W, Montreal, Canada, H3A 2K6

The gradients of humidity and temperature at the top of the planetary boundary layer (PBL), usually produce a maximum in the structure constant of refractivity, C_n^2. This signal can be seen by a vertically pointing 915MHz radar, and it provides a means for monitoring the evolution of the boundary layer depth. Understanding the behaviour of the boundary layer top is very important for air pollution studies, since it determines the depth through which pollutants are distributed. Traditional methods for measuring PBL depth had low temporal resolution and the PBL's short term variations produced significant sampling errors. Remote sensing by radar provides a much improved monitoring tool. The figure below shows returned power as a function of time and height on a day with a clearly defined PBL. (Sunrise is at about 11 UTC.)

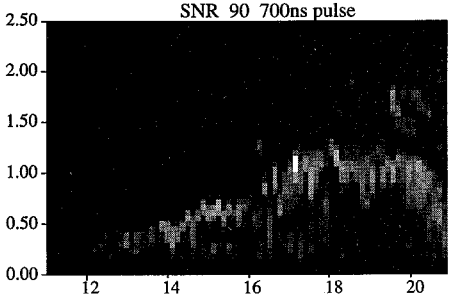

This talk will present some examples of the PBL measured during the Montreal Experiment on Regional Mixing and Ozone (MERMOZ) in June 1996. During this experiment, two Dopplerized 915 MHz radars, owned by Environment Canada and McGill University, were located in the Montreal area. This allowed a comparison of PBL measurements using different sampling strategies and filters, collected in both rural and urban areas. At the downtown site (McGill) the dataset was interspersed with non-meteorological echoes from such things as ground clutter and birds. The differences between the data produced by the two radars lead to different types of algorithms for estimating PBL depth from the time history of radar data.

LASER PROPAGATION THROUGH THE INTERMITTENT ATMOSPHERE

Joseph Gozani
University of Colorado at Boulder
Cooperative Institute of Research in Environmental Sciences
Campus Box 449, Boulder, CO 80309-0449, USA

The theory of propagation of laser through intermittent medium will be discussed from research and application viewpoints. This theory, which is now well established, (J. Gozani, Opt.Lett., 17, 559, 1994; Phys. Rev. E. 53, 6486, 1996) was motivated by measurements conducted recently by the US Air Force in the lower stratosphere. These experiments exhibited randomly irregular statistics in both the in-situ and the optical measurements that could not be predicted by the prevalent theory of propagation through a homogeneously random medium.

The paper will cover recent computations of the second and fourth coherence functions of a wave propagating horizontally in the lower stratosphere. The results, which are obtained by simulations of propagation through global intermittency, show clearly when the effects of these variabilities have a dominant effect on the propagation and when they can practically be ignored.

A dominant effect of the large-scale variability was observed for strong global intermittency at short propagation ranges. These ranges coincide with the ranges that are suitable for optical remote sensing, where the traditional theory is based on the Rytov or Born approximations. When propagation through intermittent media is encountered, special attention is required when interpreting the inverted data collected over these ranges. In particular, the randomization of the Rytov or Born approximations to account for the intermittency are shown to be incorrect, and the complete theory mentioned above is required.

F38.9

Zenith Attenuation Statistics Measured by 33 GHz and 95 GHz Atmospheric Radars

Stephen M. Sekelsky[1], Warner L. Ecklund[2],
Kenneth S. Gage[3], and Robert E. McIntosh[4]

[1] Microwave Remote Sensing Laboratory,
Knowles 209C University of Massachusetts at Amherst, Amherst, MA
tel:(413)545-4217, fax:(413)545-4652, email:sekelskyalex.ecs.umass.edu

[2] Cooperative Institute for Research in Environmental Sciences,
University of Colorado, Boulder, CO
tel:(303)497-5322, fax:(303)497-5373, email:wle@al.noaa.gov

[3] National Oceanic and Atmospheric Administration Aeronomy Laboratory,
Boulder, CO
tel:(303)497-3964, fax:(303)497-5373, email:kgage@al.noaa.gov

[4] Microwave Remote Sensing Laboratory, Knowles 113A,
University of Massachusetts at Amherst, Amherst, MA
tel:(413)545-4858, fax:(413)545-4652, email:mcintosh@ecs.umass.edu

Multi-frequency radar measurements of clouds and precipitation collected at 33.12 GHz and 94.92 GHz using the University of Massachusetts' Cloud Profiling Radar System (CPRS) are compared to simultaneous measurements collected with the NOAA 2.8 GHz cloud profiler to determine zenith attenuation statistics for the higher frequencies under various meteorological conditions, including both convevctive and stratiform precipitation, and non-precipitating clouds. Such information is valuable for predicting the performance of millimeter-wave airborne and proposed space-borne cloud sensors.

The 2.8 GHz radar is essentially non-attenuating over the vertical path considered and its reflectivity measurements are used as a reference such that for clouds having small Rayleigh-sized scatterers at their tops, ice equivalent reflectivity measurements at the three frequencies are equal. A correlation of vertical reflectivity features for the different frequencies is applied over several range gates near cloud top to determine whether or not the particles are sufficiently small. The correlation also produces a quantitative assessment of the quality of the match, which in general is much better for stratiform than convective clouds. Using radiosonde and microwave radiometer data attenuation due to water vapor and oxygen absorption is calculated and then separated from the total extinction. This provides us with the relative contribution to zenith attenuation from atmospheric gases and from hydrometeors. Results are presented for data collected during the Maritime Continent Thunderstorm Experiment (MCTEX), which was held near Darwin Australia in the fall of 1995.

Results of first round-the-clock observations of absorption and motions in the lower atmosphere using spaced-antenna reception with Doppler-filtering of the ground wave

E. L. Afraimovich and K. S. Palamartchouk*

Institute of Solar-Terrestrial Physics, p. o. box 4026, Irkutsk, 664033, Russia
E-mail: kpal@sitmis.irkutsk.su Fax: +7 3952 467 552

Abstract

Spaced-antenna reception of signals from LF-broadcasting stations is a vital technique for experimental research on the lower atmospheric dynamics (E. S. Kazimirovsky, Av. Space Res., 14, 89-96, 1994) because it is rather cheap and simple for operating compared with MST-radar observations. But the reliability of measurements in LF-band can be ensured only at short-range radio paths and full suppression of the ground wave requested. Using usual technique of observations we can only approach these conditions and only at nighttime.

To solve the problem of round-the-clock measurements we proposed Doppler filtering in addition to polarization filtering (E. L. Afraimovich, Interference Methods of Ionospheric Radiosounding, Moscow, Nauka, 198, 1982). The complex signal received at antenna-spaced coherent reception, is subjected to a direct Fourier transform, then the ground wave's spectral line eliminated and spectrum reverse-Fourier-transformed followed by a processing of the signal using existing techniques for measuring the absorption and parameters of motion of the fringe pattern.

Many years spaced-antenna LF facility was being operated by ISTP with traditional scheme of data treatment. Last year was dedicated to improving this facility: it is now fully automated, new antennas and exact time system are installed, procedure of data collecting executed by computer. During November 95 and February and March 96 several weeks of observation were made, then processed by Doppler digital filter and existing techniques for measuring the absorption and parameters of motion of the fringe pattern.

Results (direction and velocity of diffraction pattern motion) obtained using Doppler filtering are compared with latest data of hand-processed records. Insignificant differences of results due to variances of both collecting and processing of data are found. Whole set of results contain round-the-clock values of direction and velocity of wind in D-layer of ionosphere, absorption along ray path, and relative changes of effective height of D-layer.

We present also results of computer modeling of the process of emitting, propagating and spaced-antenna receiving of LF-signal and following data processing. It is of great importance for full and correct understanding of obtained results.

F38.11

Applications of Submillimeter-Wave Passive Channels to Spaceborne Remote Sensing of Atmospheric Clouds, Water Vapor, and Temperature

A.J. Gasiewski
School of Electrical and Computer Engineering
Georgia Institute of Technology, Atlanta, GA 30332-0250
Ph: (404) 894-2934 FAX: (404) 894-4641
e-mail: ag14@prism.gatech.edu

The absorption spectrum of the Earth's atmosphere between 100 and 1000 GHz is characterized by several strong water vapor and oxygen lines useful for tropospheric and stratospheric sounding and imaging from satellites. Specific channels within this range are expected to be useful for satellite meteorology from geosynchronous orbit wherein limitations in antenna size require the use of short wavelengths to obtain acceptable spatial resolution. These most important of these channels are located near the SMMW water vapor absorption lines at 325 and 380 GHz, and the strong oxygen line at 424 GHz. Used in conjunction with MMW channels near the 183 GHz water vapor line and 118 GHz oxygen line and infrared sounding channels, the SMMW channels have the potential to improve (1) the accuracy of water vapor and temperature soundings in cloudy regions, (2) the sounding of water vapor in the upper troposphere and lower stratosphere, and (3) the estimation of ice content of high-altitude clouds, and (4) the mapping of heavy clouds and precipitation. The latter most feature has the potential to improve the tracking of hurricane cores from geosynchronous orbit.

It will be the purpose of this presentation to discuss the limitations and capabilities of SMMW imaging and sounding channels and to review the recent developments in the application of SMMW channels to spaceborne passive remote sensing. Limitations arising from the water vapor continuum absorption effectively restrict direct SMMW probing of low altitudes in the tropics and midlatitudes.

URSI F | Session 54 | Salon Gatineau

Radar/Rain Gauge Measurements of Precipitation
Co-chairs: V. Chandrasekar, USA and I. Zawadzki, Canada

13:10	54.1	Air Motions below Elevated Snow Layers Observed by UHF Radar, **W.O.J. BROWN**, R.R. ROGERS, *McGill University, Montréal, QC, Canada*
13:30	54.2	Radar Observations of Waves, Wind Shear, and Scattering in Snow, **W.O.J. BROWN**, R.R. ROGERS, *McGill University, Montréal, QC, Canada*
13:50	54.3	Studies of the Melting Layer at Three Wavelengths, A. BELLON[1], F. FABRY[1], R. PAPAGEORGES[2], W. SZYRMER[2], **I. ZAWADZKI**[1], [1]*McGill University and* [2]*Université du Québec à Montréal, QC, Canada*
14:10	54.4	Multiparameter Radar and in Situ Observations and Modeling of Winter Storms, **I.A. IBRAHIM**[1], V. CHANDRASEKAR[1], V.N. BRINGI[1], M. SCHOENHUBER[2], H.E. URBAN[2], W.L. RANDEU[2], [1]*Colorado State University, Fort Collins, CO, USA;* [2]*Joanneum Research, Graz, Austria*
14:30	54.5	Multiparameter Radar Study of Convective Storms: Comparison with Insitu Aircraft Observation, **A. ABOU-EL-MAGD**[1], V. CHANDRASEKAR[1], V.N. BRINGI[1], J.W. STRAPP[2], [1]*Colorado State University, Fort Collins, CO, USA;* [2]*Atmospheric Environment Services, Canada*
14:50	54.6	Application of Dual-Frequency Millimeter-Wave Doppler Spectra for the Retrieval of Drop Size Distributions and Vertical Air Motion in Rain, **J.M. FIRDA**, S.M. SEKELSKY, R.E. McINTOSH, *University of Massachusetts at Amherst, MA, USA*
15:10		Coffee Break
15:30	54.7	Drop Size Distributions and Rain Rates Retrieved from Combined UHF and VHF Wind Profiler Measurements, **S.K. AVERY**, R. CIFELLI, D. RAJOPADHYAYA, *University of Colorado, Boulder, CO, USA*
15:50	54.8	Radar Rain Measurement in the Presence of Anomalous Propagation, **A. RYZHKOV**[1], D. ZRNIC[2], [1]*University of Oklahoma and* [2]*National Severe Storms Laboratory, Norman, OK, USA*
16:10	54.9	Proposed Model for the Rain Rate Conversion Factor in Malaysia, J. CHEBIL, **T.A. RAHMAN**, *Universiti Teknologi Malaysia, Bahru, Malaysia*
16:30	54.10	Phase Diversity Processing for Range Ambiguity Resolution, **P. JOE**[1], D. HUDAK[1], J. SCOTT[1], R. PASSARELLI, Jr.[2], A. SIGGIA[2], [1]*Environment Canada, King City, ON, Canada;* [2]*Sigmet Inc., Westford, MA, USA*

F54.1

Air Motions Below Elevated Snow Layers Observed by UHF Radar

William O.J. Brown and R.R. Rogers
Atmospheric and Oceanic Sciences, McGill University, Montreal, Canada

In the air ahead of an approaching warm front, snow produced at high altitudes often fails to reach the ground. To a vertically-pointing radar, the snow appears as an elevated layer, seemingly suspended or descending only slowly over periods of several hours. The inset figure illustrates the appearance of such a layer to a vertically pointing radar. Shown are Doppler spectra from snow at different altitudes. Above 2.5 km the spectra indicate the downwards velocities characteristic of snow. Below that level, the velocities are upwards. We have analyzed many such observations using simultaneous measurements from a UHF wind profiler and a high-resolution, vertically pointing X-band radar. Typically, the UHF data indicate upwards motions in the order of 1 m/s at the lower parts of the echo, as in the example shown. Comparing the observations shows that the base of the UHF echoes is below that of the X-band echoes. In fact, there are no detectable X-band echoes at the altitudes where the upwards motions are observed. We conclude that the upwards motions are in clear air, not snow, and are explained by Bragg scattering by fluctuations in the refractivity of the clear air, and hence preferentially detectable by the radar with the longer wavelength. Inspection of thermodynamic soundings in these conditions shows that the warm front usually overrides a layer of dry air. The base of the snow is thus accounted for partly by evaporation of the snow as it settles into the dry air. The evaporation, in turn, destabilizes the layer by chilling from above, causing turbulence and variability in the humidity field, which may explain the layer of strengthened Bragg scattering below the snow. Not clear, however, is why there should be sustained upwards motions at this level.

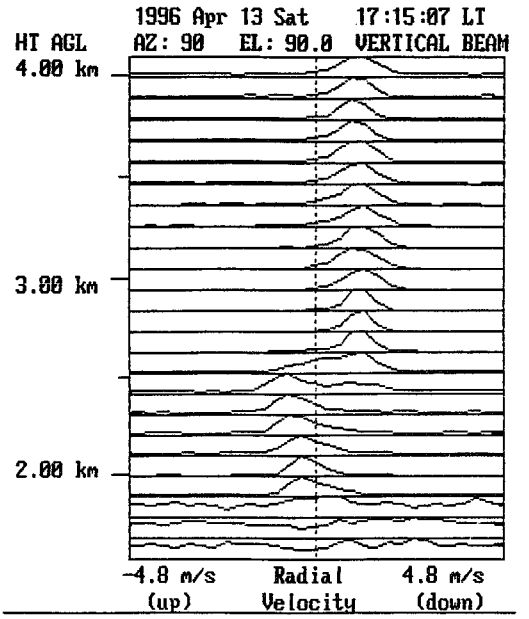

Radar Observations of Waves, Wind Shear, and Scattering in Snow

William O.J. Brown* and R.R. Rogers
Department of Atmospheric & Oceanic Sciences,
McGill University, 805 Sherbrooke St. West,
Montreal, Canada H3A 2K6.

The Atmospheric and Oceanic Sciences Department of McGill University operates a range of equipment including an X band vertically pointing radar (VPR), a UHF wind profiler, a laser ceilometer, and a weather surveillance radar that operates in the S and X bands. (Real-time profiler and other data can be accessed at URL http://grappa.meteo.mcgill.ca/profiler.html). This equipment operates continuously making observations of, among other phenomena, the many snow storms that hit Montreal every winter.

During the snow storms, wave activity is often suggested by bands of increased reflectivity (implying modulation of the snowfall) observed by the radars. These bands can be seen in the spatial domain moving across the area on the weather surveillance radar, or in the time domain on the profiler or the VPR. Wind measurements on the profiler also sometimes show oscillatory behaviour. In many cases, it is difficult to correlate the apparent observations of waves between the different instruments; however occasionally the observations are consistent allowing the period, velocity, and wavelength of the waves to be deduced. Many of the observed waves seem to fall into one of two categories; those with periods of several minutes or less, indicative of shear waves; and those with periods of tens of minutes or more, indicative of gravity waves.

Related phenomena are the sharply defined wind shear layers often observed by the wind profiler in the snow storms. These layers can persist for several hours, sometimes in a stack of regularly spaced layers, and sometimes oscillating slowly up and down. An interesting feature of some of these layers is their aspect sensitivity. For example there may be an apparent increase in reflectivity in directions aligned with the wind shear, suggesting entrainment of snow within shear induced turbulence.

F54.3

Studies of the Melting Layer at Three Wavelengths

A. Bellon[1], F. Fabry[1], R. Papageorges[2], W. Szyrmer[2] and *I. Zawadzki[1]
1. J. S.Marshall Radar Observatory, McGill University
2. University of Quebec in Montreal

The dependency of bright band height and thickness on various parameters is first investigated using hundreds of hours of observations with X-band and UHF vertically pointing radars. Bright band thickness shows a good correlation with precipitation intensity, but is generally larger than measured in previous studies. Furthermore, it is also slightly positively correlated with bright band height. The ratio of the bright band peak reflectivity to the rainfall reflectivity is constant at 8 dB below 0.5 mm/hr and then increases to reach 13 dB at 2.5 mm/hr and 16 dB at 5 mm/hr. The equivalent reflectivity factor of snow just above the melting layer is on average 1 dB below the reflectivity of rain just below the melting layer, independently of precipitation intensity. The bright band statistics are also significantly different for reflectivities in rain above 25 dBZ when observations are made with an X-band radar as opposed to a UHF radar because of the combination of attenuation in the melting layer and the fact that scattering from some of the large hydrometeors above and within the melting layer departs from the Rayleigh approximation usually used to compute reflectivity.

During the second stage of the work the attenuation at X-band caused by the melting layer of stratiform precipitation is derived by comparing long-term average reflectivity profiles from collocated X-band and UHF vertically pointing radars. The total attenuation caused by the bright band is equivalent to the attenuation across approximately 10 km of rain that is present below it. This bright band attenuation is still 3 to 5 times the 'rain equivalent' attenuation, the latter being obtained by integrating the specific attenuation deduced from the entire reflectivity profile across the bright band as if that reflectivity were due to rain. Comparison of X-band and S-band measurements (both at vertical polarization) and at quasi horizontal incidence show an appreciable lower attenuation as compared to the vertical incidence. Polarimetric measurements will be made and preliminary results will be reported.

Finally, the melting layer is modeled within a dynamic framework in which all processes, dynamic, thermodynamic and microphysical, are fully coupled. The microphysical processes are simplified into a "bulk parameterization" in which the of melting snow is characterized by the snow content and its melted fraction. No aggregation of fragmentation of snow flakes is included. Model simulations show that the non uniformity of the snow content creates convective cells within the melting layer. Through condensation in updraft and evaporation in downdraft these cells introduce a modulation in the rate of melting. During melting, the decrease in snow content is very slow at the beginning and it changes rapidly in the lower end of the melting layer. A cross section of the fraction of melted water shows an initially slow change with height followed by a dramatic increase at the bottom of the melting layer. This kind of information is of direct interest to the problem of EM propagation and scattering. Computations of EM properties of the model simulated melting layer show a good agreement with radar observations.

Multiparameter Radar and in Situ Observations and Modeling of Winter Storms

I. A. Ibrahim*, V. Chandrasecar, V. N. Bringi
Colorado State University.
Schoenhuber M, H. E. Urban, W. L. Randeu
Joanneum Research Graz, Austria.

Polarimetric radar is a very useful tool for remote sensing of storm microphysics. Multiparameter radar data have been used extensively in the interpretation of microphysical evolution of convective storms. However, the interpretation of radar polarimetric measurements become complicated in the case of winter storms in which the distributed particles can exist at different heights with varying sizes, shapes, orientations and bulk densities. Colorado State University operates a fully polarimetric, S-band Doppler weather radar which was used to collect coordinated data from winter precipitation. The measurement set include radar reflectivity factor (Z), differential reflectivity (Z_{DR}), specific differential propagation phase (Φ_{DP}), linear depolarization ratio (L_{DR}) and copolar correlation between horizontal and vertical polarizations states (ρ_{hv}).

A 2D-video disdrometer located on the ground was used to obtain two views of each particle of these precipitations entering the sensor area as well as its fallspeed. These data were used to obtain the particle size distribution parameters and evidence of particle type via shape/fallspeed data. A weighing type snow gage located nearby also provided measurements of snow accumulation.

Data from winter precipitation events are presented to provide microphysical interpretation of the radar signatures. A radar model, taking into account particle types (plate/column like ice crystals, dendrities, aggregates, snowflakes and graupel) and mixtures, sizes, orientations and dielectric constant is used to aid in the interpretation process.

F54.5

Multiparameter Radar study of Convective Storms : Comparison with Insitu Aircraft Observation .

A. Abou-El-Magd* , V. Chandrasekar , V. N. Bringi
Colorado State University
J. W. Strapp , Atmospheric Environment Services , Canada .

ABSTRACT

During the summer of 1995 the CSU-CHILL multiparameter radar and an instrumented aircraft (T-28 operated by the South Dakota School of Mines and Technology) were used to collect coordinated measurements over summer-storms in Northern Colorado .

This paper presents comparison of the radar and aircraft data collected on the storm which occurred on 20 June 1995 . The predominant precipitation type for these storm was low-density graupel . The multiparameter radar data consists of the following parameters : a) Reflectivity , b) Differential reflectivity , c) Specific differential propagation phase , d) Copolar correlation between two polarizations , and e) Linear depolarization ratio . The T-28 aircraft was equipped with a High Volume Particle Spectrometer capable of collecting two dimensional images of hydrometeors encountered in the flight path .

On 20 June the T-28 made 12 passes through a storm cell located 15 km east of the radar . The storm had echoes in excess of 40 dBZ associated with conical dry graupel . Aircraft passes were at altitude about 4.0 km above ground level to collect data in the graupel region . Simultaneously , the radar was collecting data in a PPI sector scan mode covering the elevations of the aircraft locations . A comparative study of the multiparameter radar data and the insitu aircraft observation for this storm are presented with the objective of interpreting multiparameter radar signatures .

Application of Dual-Frequency Millimeter-wave Doppler Spectra for the Retrieval of Drop Size Distributions and Vertical Air Motion in Rain

John M. Firda*, Stephen M. Sekelsky, and Robert E. McIntosh
Microwave Remote Sensing Laboratory
University of Massachusetts at Amherst
Amherst, MA 01003
tel:(413)545-4492, fax:(413)545-4652, email:firda@alex.ecs.umass.edu

Knowledge of the drop-size distribution in rain allows one to study the inner processes of rain development and relate this information to the clouds above by quantifying the total amount of liquid flux in the atmosphere. Vertical air motion in rain is a useful parameter as well, because the strength of up drafts and down drafts can be related to the amount of convection in a storm (R.J. Doviak and D.S. Zrnic', Doppler Radar and Weather Observations, 1993). Several researchers have attempted to remotely retrieve drop-size distributions aloft in rain utilizing ground based radar measurements of the Doppler spectrum and an assumed relationship between drop size and terminal velocity. However, accurately determining the drop-size distribution is coupled with vertical air motion as it shifts the entire Doppler spectrum causing errors in the retrieved estimates. Spectral broadening from turbulence also biases the retrieval algorithms.

An improvement to current methods is possible by using dual-frequency millimeter-wave radars. Co-located Doppler spectra were obtained at 33 and 95 GHz with the University of Massachusetts Cloud Profiling Radar System for both precipitating and non-precipitating clouds during the 1995 Ground Based Remote Sensing Intensive Observation Period which was held at the Department of Energy's CART site in Lamont, OK. An algorithm is presented which utilizes co-located millimeter-wave Doppler spectra to retrieve drop-size distributions in rain. Correlation analyses between measured and model rain data are generated from Mie scattering functions and a Marshall-Palmer drop-size distribution to estimate vertical air motion, and turbulent broadening is removed by comparing the two retrieved distributions. Using individual spectra we estimate extinction, vertical air motion, rain-rate and drop-size at a high spatial resolution (60 meter range resolution, 2 second averaging time). The measurements represent the first simultaneous Doppler spectra at these wavelengths.

F54.7

Drop Size Distributions and Rain Rates Retrieved from Combined UHF and VHF Wind Profiler Measurements

S.K. Avery, R. Cifelli, D. Rajopadhyaya
Cooperative Institute for Research in Environmental Sciences
University of Colorado
Boulder, CO 80309-0216

Rain drop size distributions and surface rainfall rates were determined from co-located UHF and VHF wind profiler measurements. The data were collected from several precipitation events during the 1993-1994 wet season near Darwin, Australia and subsequently partitioned into a 4-tier precipitation classification scheme, based on Williams et al (1995). A spectra-fitting algorithm was used to retrieve both the vertical air motions (VHF) and the hydrometeor size distribution parameters (UHF) from the wind profiler data. The model takes advantage of the different scattering sensitivities of VHF and UHF to precipitation and clear air. At VHF, the wind profiler has approximately equal sensitivity to Bragg scatter from gradients in the clear air index of refraction (i.e., turbulence) and Rayleigh scatter from precipitation targets. In contrast, the UHF profiler is dominated by Rayleigh scatter whenever the precipitation exceeds light rain or drizzle.

The model uses the VHF data to extract the clear air vertical velocity information (i.e., mean vertical air velocity and spectral width), and to isolate the portion of the spectra associated with precipitation scatter. The model then examines the UHF data to fit the precipitation component of the spectra with an assumed functional form (i.e., Gaussian, Lognormal, Gamma, Exponential). Because the precipitation backscatter observed with the wind profiler is smeared by the clear air, it is essential to obtain an accurate estimate of clear air parameters for the retrieval of the drop size distribution. Once the drop size distribution parameters have been retrieved, the reflectivity, liquid water content, and rain rate can be calculated in a straightforward manner.

The model-derived rainfall rates were then compared with a tipping bucket rain gauge at the profiler site in order to evaluate the model performance in different types of precipitation events. Preliminary work has shown that the profiler model and gauge rainfall estimates agree well during stratiform rain events; however, the model tends underestimate the gauge-measured rainfall in convective precipitation. In some instances, the discrepancy in rainfall rates can be attributed to poor fitting of the model to the observed spectra. In many instances, though, differences between the profiler and the rain gauge appear to be due to errors in the interpolation of the VHF data to the UHF spectra as well as to a combination of microphysical and kinematic processes occurring between the height of the profiler retrieved rain rate and the ground surface.

An attempt is made to quantify the effect of neglecting the vertical air motions on the rainfall rate retrieval. It is shown that, because of the spectra fitting procedure employed by the model, errors in the measurement of vertical air velocity (VHF) can sometimes produce unexpected errors in the retrieved rainfall rate (UHF).

F54.8

RADAR RAIN MEASUREMENT IN THE PRESENCE OF ANOMALOUS PROPAGATION

Alexander Ryzhkov[1] and Dusan Zrnic[2]

[1]Cooperative Institute for Mesoscale Meteorological Studies / University of Oklahoma
[2]National Severe Storms Laboratory, Norman, Oklahoma

Anomalous propagation (AP) effects pose serious problem for accurate radar rainfall assessment. Traditional use of a high-pass ground clutter filter in all range-azimuth resolution cells would eliminate stationary clutter breakthrough caused by AP. Such filtering may not be desirable, however, since the power removed from the notch around zero radial velocity may result in biases in radar reflectivity or mean Doppler velocity estimates of the weather signal. Here an alternative method for coping with AP is suggested. The method is based on the use of dual-polarization radar that is capable to measure differential phase Φ_{DP} and cross-correlation coefficient ρ_{hv} between horizontally and vertically polarized radar returns.

The areas of ground clutter contamination including those induced by AP at far distances from the radar can be detected by analyzing ρ_{hv} data. For weather echoes ρ_{hv} is usually about 0.8 - 1.0 whereas it is considerably lower in the contaminated areas. The analysis of four Oklahoma storms with AP, observed with the NSSL's S-band polarimetric radar, shows that the threshold of $\rho_{hv} = 0.7$ can be effectively used to discriminate between AP-induced echoes and echoes from rain.

Very often ground clutter returns caused by AP are superimposed on the echoes from precipitation. If the AP contaminated zone is immersed in the precipitation background, it is possible to estimate areal rainfall in this region using Φ_{DP} values outside this zone. Effectiveness of this technique is demonstrated for the storm of June 30, 1994 when precipitation mixed with AP echoes was observed in the test area containing 42 densely located rain gauges. One hour of rain accumulation over the test area was computed using gauge data, conventional radar algorithm based on reflectivity factor Z, and polarimetric algorithm utilizing differential phase data. The polarimetric algorithm is immune to the AP contamination and yields a total rain estimate close to the actual rainfall measured by gauges, whereas conventional R(Z) method produces large positive bias.

F54.9

Proposed Model for the Rain Rate Conversion Factor in Malaysia

Jalel Chebil and Tharek Abd. Rahman*

Faculty of Electrical Engineering, Universiti Teknologi Malaysia
Locked Bag 791, 80990 Johor Bahru, Malaysia
E-mail: jalel@fkeserv.fke.utm.my
Fax: 60-7- 5566272

ABSTRACT

In meeting the rapidly growing demand for radio telecommunications in Malaysia, there is a need to use frequency band above 10 GHz for terrestrial and satellite communication systems. However, at such frequency range, rainfall is a serious cause of attenuation for the radio wave propagation. It is important for any microwave system designer to predict accurately the fading outage due to rain attenuation. The common rain attenuation prediction methods require one-minute rain rate data. However, the availability of such data is generally limited in the tropical regions. Most investigations of rainfall have been carried out for meteorological purposes. the rain data is usually taken for intervals of one hour or longer. In this paper, a model has been proposed to approximate the rain rate conversion factor from one-hour to one-minute integration time in Malaysia.

Two types of data are used in the analysis: hourly and one-minute rain rate data. Hourly rainfall data were obtained from the Malaysian Meteorological Service (MMS) for 35 stations in various location in Malaysia. These data cover a period of almost 12 years for each station. The one-minute rain rate data were collected for few years at the Universiti Teknologi Malaysia-Kuala Lumpur (UTM-KL), at the Universiti Sains Malaysia-Tronoh (USM) and at the Sekolah Menangah Vokesional-Bota (SMV).

The rain rate conversion factor C_f is defined as the ratio of rain rates $R_1(P)$ and $R_{60}(P)$ for a given percentage of time P with an integration time of one-minute and one hour respectively

$$C_f = R_1(P) / R_{60}(P) \qquad (1)$$

C_f is computed at UTM-KL, USM and SMV. It is found that their values are close and their average $C_{f,avg}$ can be considered a good representation of the rain rate conversion factor all over Malaysia. Segal' s model for the rain rate conversion factor does not approximate very well the computed values of $C_{f,avg}$. An extra term was added to Segal's model to obtain a better result. The revised model is expressed as following

$$C_f = a\,P^b + c\exp(d\,P) \qquad (2)$$

where exp( ) denotes the exponential function, and the regression coefficients *a*, *b*, *c* and *d* are obtained from the measured values of C_f with the constraint that $0.001\% \le P \le 1\%$.

Phase Diversity Processing for Range Ambiguity Resolution

Paul Joe, David Hudak, John Scott,

Environment Canada, King Weather Radar Station,
14780 Jane St., King City, Ontario, Canada, L7B 1A3,
Email: paul.joe@ec.gc.ca

Richard Passarelli, Jr. and Alan Siggia

Sigmet Inc.,
2 Park Drive, Unit #1, Westford, MA, USA 01886

Abstract

Doppler weather radars transmit pulses at a repetition frequency at about a thousand pulses per second or more so that the Nyquist velocity range is sufficiently large that accurate estimates of radial velocity can be made. As a result, the unambiguous range of the radar is limited. Phase diversity signal processing can be used to extend the unambiguous range. This involves processing the phase of the return pulse with respect to the current and previously transmitted pulses to provide estimates of radial velocity of first and second trip echoes. The key is the introduction of an adaptive whitening filter to extend the technique from previous formulations. Appropriate partitioning of the returned power provide estimates of the first and second trip echo power. The technique can recover overlaid echoes. Tests on a magnetron radar at the King City Weather Radar Station show that the technique is limited by the radar and not the signal processing algorithms. There is an improvement in the estimate of first trip echo moments. Examples will be presented to show the success and limitations of the technique.

URSI F | Session 69 | Salon Gatineau

Mobile Propagation: Models and Measurements
Co-chairs: R. Bultitude, Canada and R.H. Lang, USA

13:10	69.1	**Invited:** Effect of Terrain on Path Loss in Urban Environments for Wireless Applications, **H.L. BERTONI**, L. PIAZZI, *Polytechnic University, Brooklyn, NY, USA*
13:30	69.2	Effects of Building/Tree Heights on the Propagation Loss for Residential Environments, **S.A. TORRICO**[1], H.L. BERTONI[2], R.H. LANG[3], [1]*Comsearch, Reston, VA,* [2]*Polytechnic University, Brooklyn, NY and* [3]*George Washington University, Washington, DC, USA*
13:50	69.3	Diffraction of Electromagnetic Waves by a Block-Shaped Obstacle, S.V. SAVOV[1], **J.H. WHITTEKER**[2], [1]*Technical University of Varna, Bulgaria;* [2]*Communications Research Centre, Ottawa, ON, Canada*
14:10	69.4	Reflection from Building-Covered Terrain, **J.H. WHITTEKER**, *Communications Research Centre, Ottawa, ON, Canada*
14:30	69.5	A Modified Image Theory with Imaginary Screens and Its Application to Analysis of Wave Propagation in Urban Microcellular Environment, J.K. LEE[1], **J. HUR**[2], [1]*Syracuse University, Syracuse, NY, USA;* [2]*Konkuk University, Seoul, Korea*
14:50	69.6	Highway Propagation Measurement Using Omnidirectional and Directional Antennas at 1840 MHz and its Analysis Using the First Fresnel Break Distance, **S.J. HONG**, K.J. KIM, *LG Information and Communications, Ltd., Anyang, Korea*
15:10		Coffee Break
15:30	69.7	Propagation Loss at 1.8 GHz on Microcellular Mobile Radio Channels, **R.J.C. BULTITUDE**, P.L.C. CHEONG, *Communications Research Centre, Ottawa, ON, Canada*
15:50	69.8	Statistical Modelling of Mobile Multipath Propagation Channels, **A.J. COULSON**[1], A.G. WILLIAMSON[2], R.G. VAUGHAN[1], [1]*Industrial Research Limited, Lower Hutt and* [2]*University of Auckland, New Zealand*
16:10	69.9	Automatic Reconstruction of 3-D Building Dimensions from 2-D Video Data for Urban Propagation Modeling, H. MARTINEZ[1], C. AKTURAN[2], **H. FOLTZ**[1], H. LING[2], W. VOGEL[2], [1]*University of Texas - Pan American, Edinburg and* [2]*University of Texas at Austin, TX, USA*
16:30	69.10	Multipath Simulation of Wireless Communication Systems, **H. RAEMER**, J. PREISIG, D. BRADY, S. MCKNIGHT, *Northeastern University, Boston, MA, USA*
16:50	69.11	A New Approach to 3D Ray Tracing for Site Specific Propagation Prediction, **G. LIANG**, H.L. BERTONI, *Polytechnic University, Brooklyn, NY, USA*

F69.1

Effect of Terrain on Path Loss in Urban Environments for Wireless Applications

H. L. Bertoni, L. Piazzi
Center for Advanced Technology in Telecommunications
Polytechnic University
Brooklyn, NY 11201

The effect of buildings on path loss for elevated base station antennas in the UHF band (300 MHz - 3 GHz)has been modeled a process of multiple forward diffraction past absorbing half-screens. Such modeling has been carried out for buildings of uniform height and of randomly varying height on flat terrain, and is referred to as the Walfisch-Ikegami model. In this paper we report on modeling the effect of buildings of uniform height, but located on terrain with individual hills. Because of the narrow width of the Fresnel zones in the UHF band for propagation out to distances of a few km, the hills can be modeled and being two dimensional. The buildings are assumed to lie in rows that are equally spaced along parallel streets, with the streets running perpendicular to the slope of the hills.

As in the Walfish-Ikegami model, the rows of buildings are represented by a series of absorbing half-screens. Propagation of the fields from the plane of one screen to the next is carried out numerically using the Kirchhoff-Heugens approximation. By successively repeating this process we are able to compute diffraction past 100 or more screens. In this way we have simulated buildings on a sinusoidal terrain and on a cylindrical hill placed on oterwise flat terrain. The signal reaching the tops of successive rows of buildings on the shadowed side of the hills is found to decrease approximately exponentially with distance, in a manner similar to that of the creeping ray fields behind a cylindrical obstacle. The signal reaching the top of a building in the troughs and rising slope of the sinusoidal terrain, or the buildings on the flat plane shadowed by the cylindrical hill can be explained in terms of the initial shadowing of the hill combined with the diffraction effect of the rows immediately before the building in question. We examine how the signal depends on geometric parameters such as hill radius and row separation.

Effects of Building/Tree Heights on the Propagation Loss for Residential Environments

Saúl A. Torrico*
Comsearch, 2002 Edmund Halley Drive, Reston, VA 20191

Henry L. Bertoni
Center for Advanced Technology in Telecommunications, Polytechnic University, Brooklyn, NY 11201

Roger H. Lang
Department of Electrical Engineering and Computer Science, The George Washington University, Washington, DC 20052

The propagation loss between the transmitter and the mobile receiver is an important parameter needed to assess a mobile communication system such as a Cellular System, a Personal Communication System (PCS), or a Wireless Local Loop System (WLL). A theoretical model was proposed by (Saúl A. Torrico, Henry H. Bertoni, and Roger H. Lang, IEEE Vehicular Technology Conf.,854-858,1996), to account for the propagation loss in urban or suburban areas where the effects of trees were considered. Following this approach, results are presented to characterize the effects on the propagation loss of, the height of the buildings vs. the height of the trees above the buildings, or the effects of the mobile receiver location relative to the last building/tree configuration. As in the past model, the rows or blocks of building/houses are viewed as diffracting cylinders lying on the earth, and the canopy of the trees are adjacent to and above the buildings/ houses. The building/houses are represented by absorbing screens and the trees as partially absorbing phase screens. The field at the aperture of the absorbing screen depends on the mean field going through the tree due to a plane wave. Physical optics is then used to evaluate the diffracting fields at the last absorbing/phase screen combination by using the multiple Kirchhoff-Huygens integration for each absorbing/phase half screen configuration. In order to find the properties of the phase screen, trees are represented as a time-invariant ensemble of leaves and branches all having prescribed location and orientation statistics. Leaves are modeled as flat, circular, lossy-dielectric discs; and branches as finitely-long, circular, lossy-dielectric cylinders. The mean field in the canopy is calculated using the discrete scattering theory of Foldy and Lax. By solving the mean wave equation for the mean scattered field propagating through a tree we find the wave propagation constant which has a real and imaginary component. The imaginary part of the propagation constant corresponds to the specific attenuation of the tree.

F69.3

Diffraction of Electromagnetic Waves by a Block-Shaped Obstacle

Sava V. Savov, Dept. Electrical Engineering (TIE),
Technical University of Varna, Varna 9010, Bulgaria

James H. Whitteker, Communications Research Centre, 3701 Carling Ave.,
Box 11490, Station H, Ottawa, Canada K2H 8S2

For planning mobile communications in an urban environment it is essential to have a fast and reasonably accurate method for predicting the transmission loss due to diffraction by buildings. A basic problem to be solved in this context is the diffraction of electromagnetic waves by a three-dimensional block-shaped obstacle.

A physical-optics solution of this problem is presented here. This solution is based on the previous work of one of the authors (S.V. Savov, URSI General Assembly, Lille, 1996) who obtained a solution of the problem of diffraction by two rectangular diffracting screens (cross-hatched in the diagram below) placed one behind the other . The solution of this problem is expressed in terms of Fresnel double integrals. A method of fast calculation of these integrals in Bessel series was suggested by the same author recently (S.V. Savov, J.B. Andersen, *Electronic Letters, 6*, 435-437, 1995). After that a bridged-knife-edges model of the second author is used (J.H. Whitteker, *IEE Proc., pt. H, 2*, 113-116, 1990) to extend this formulation to the case of diffraction by a solid building, represented as two rectangular diffracting screens, with reflecting walls (shaded in the diagram below) joining them.

The solution accommodates both horizontal and vertical wave polarization. The receiver can be placed either in the region illuminated by the transmitter or in the region shadowed by the building. The influence of different parameters of the model is investigated. Some results calculated using this model are compared to known experimental ones and good agreement is found between them.

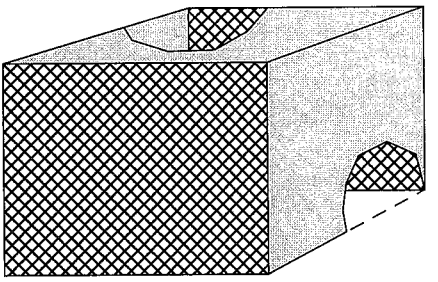

Model Building

Reflection from building-covered terrain

J.H. Whitteker
Communications Research Centre
3701 Carling Ave., Box 11490, Station H
Ottawa, Canada K2H 8S2

In terrestrial propagation problems, it may be required to estimate the radiowave field due to scattering or reflection from ground that may be covered by buildings or trees, on propagation paths of a few kilometres or more. If bare ground is plane but rough on a small scale, the Fresnel reflection coefficient can be used, and the roughness can be accounted for by using a well-known formula of Beckmann and Spizzichino. However, if the ground is covered by buildings or perhaps trees, this formula may not be appropriate, since its derivation neglects shadowing. An alternative for urban areas is to model the buildings as absorbing screens, equally spaced and of the same height, as indicated below:

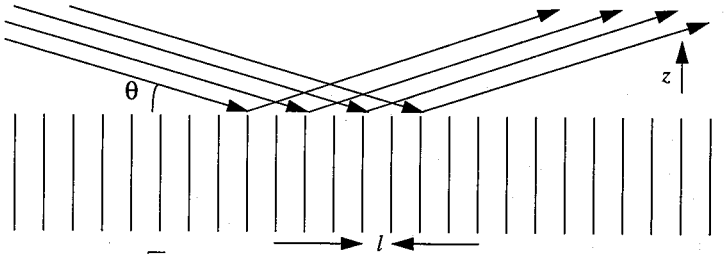

In this model, there is no reflection as ordinarily defined – shadowing is the only effect. Nevertheless, it is possible to define a kind of reflection coefficient. Two approaches were considered, both based on physical optics. One is a generalization of Boersma's integrals, which leads to a formulation similar to that of Xia and Bertoni (*IEEE Trans. Ant. Prop. 40*, 170-177, 1992) for diffraction over buildings. However, with this method, the field cannot be computed very far above the plane of the tops of the diffracting screens. The other approach, and the one finally used, is to perform successive numerical integrations of the field over the diffracting screens. The numerical integration proceeds from one screen to the next until a steady state is reached. In order to minimize the number of screens required, initially the field incident on all the diffracting screens is found, rather than the field in the space above. Then, the field in the space above is found as a function of z, or its scaled analog ζ, by summing contributions from the incident fields found in the first step. The end result is a 'reflection coefficient', a function of α, a dimensionless scaled angle of incidence. This reflection coefficient can be used to replace the Fresnel reflection coefficient in built-up areas.

F69.5

A Modified Image Theory with Imaginary Screens and Its Application to Analysis of Wave Propagation in Urban Microcellular Environment

Jay Kyoon Lee[+] and Jung Hur[*]
[+]Department of Electrical Engineering and Computer Science
Syracuse University
Syracuse, New York 13244-1240 USA

[*]Department of Electronic Engineering
Konkuk University
Kwangjin-gu, Seoul 133-701 KOREA

The cell radius of mobile or personal communication systems proposed for future demand is much shorter than that of the current cellular communication. It will be decreased to several hundred meters or even sub-hundred meters. Such trend of decreasing the cell size will be concentrated especially in urban area, because the demand will increase in that area. This requires much more precise and accurate analysis of wave propagation.

Even though some recent propagation models have overcome disadvantage of the empirical or the statistical approach in classical models, they are not appropriate for *microcellular* environment because the propagation in those models depends mainly on the diffraction over rooftop of buildings. There are three typical wave propagation mechanisms: reflection, diffraction and scattering. Among them reflection is a dominant factor in the microcellular environment. The most efficient tool to deal with the reflection is the image theory. A direct application of the image theory to the building walls and the street surface is not appropriate. With some modification of the image theory, it can still be an efficient tool to analyze the reflection behavior in the urban microcellular environment.

This paper presents a new modified image theory with the concept of *imaginary screens*. We apply it to the imperfect reflectors such as building walls. The useful procedures to generate the equivalent problems for line-of-sight propagation are derived using the modified image theory. Some simulated results are also presented.

The new method makes the geometry of the complex propagation problem much simpler. A zigzag ray path in the original problem is unfolded and changed to a straight path. This simplification of geometry makes any kind of calculation much easier. The reduction of complexity allows the more precise analysis for the same effort. The new method can also handle the propagation problem with walls of different dielectric characteristics.

Highway Propagation Measurement using Omnidirectional and Directional Antennas at 1840 MHz and its Analysis using the First Fresnel Break Distance

Sung Jin Hong* and Kyung Jae Kim
LG Information and Communications, Ltd.
Mobile Communications Research Laboratory
533 Hogye-dong, Anyang-shi, Kyungki-do, 431-080, Korea

ABSTRACT

Choosing the optimal type of the antenna and the transmitting power to be applied to the highways is an important issue in the design of the wireless communications network because the handoff area and the number of base stations to cover a specified service area directly depend on such variables. A comprehensive CW measurements have been performed using both omnidirectional and sector antennas at 1840 MHz on a straight highway in flat terrain, and the measurement data with its analysis using the First Fresnel break distance is presented in this paper. Also, the effects of the vertical antenna pattern on the received signal in the region before the First Fresnel break distance are examined.

The data was collected and analyzed separately for the northern and the southern sides of the highway in reference to the base station location with the main beam of the sector antenna directed toward the southern side. The path loss slopes and the standard deviations calculated by the single regression analysis are summarized in Table 1. The slopes calculated by the multiple regression analysis show clear distinction in their slopes before and beyond 1030 meters which is the First Fresnel break distance computed by the equation, $d_B \cong 4h_t h_r/\lambda$, and significantly lower standard deviations than those obtained by the single regression analysis. The results are summarized in Table 2. with slope 1 corresponding to the region before d_B and slope 2 to the region beyond d_B. (The actual measurement data with the fitted regression lines for the above two cases will be shown in the paper.)

The vertical pattern of the antenna plays an important role in determining the path loss slope particularly in the region near the base station, because the change in the elevation angle is more sensitive to the change in the Tx-Rx separation than it is in the far region beyond the break distance. According to the measured pattern of the antennas used in the measurement (which will be shown in the paper,) the directive gain of the back lobe of the sector antenna varies only 5 dB as the elevation angle changes from 0° to 10°, while the gains of the others -that is, the main lobes of the sector antenna and of the omnidirectional antenna- vary as much as 20 dB with the same change in the elevation angle. Such slow pattern variation of the sector antenna's back lobe is thought to have led to its slope 1 of 3.5, which is higher than those of the other three cases, in the northern side of the base station. The effects of the antenna pattern on the received power in the near region are numerically simulated using the two-ray model, and the results show a good agreement with the measurement data.

Table 1. Single Regression

	Omni (south)	Sector (south)	Omni (north)	Sector (north)
path loss slope	4.5	4.3	4.2	3.8
std. dev. (dB)	7.02	7.37	7.38	7.49

Table 2. Multiple Regression

	Omni (south)	Sector (south)	Omni (north)	Sector (north)
path loss slope 1	1.9	1.6	2.2	3.5
std. dev. 1 (dB)	3.90	4.40	4.09	2.78
path loss slope 2	5.4	5.25	5.2	4.6
std. dev. 2 (dB)	6.36	6.65	7.01	7.62

F69.7

Propagation Loss at 1.8 GHz On Microcellular Mobile Radio Channels

By
R. J. C. Bultitude and P. Lie Chin Cheong
Communications Research Centre, Ottawa

Abstract

It is well known that for mobile radio systems of the future, significant advantages in terms of traffic handling capacity and bit-error performance can be achieved by adopting microcellular system architectures. The concomitant increase in cell densities with such systems, however, could also exacerbate inter-cellular interference problems unless propagation losses on small cells, having base station antennas at street lamp level are better understood and properly modelled.

This paper reports the analysis of data that were measured on 1.8 GHz microcellular-type channels in four Canadian cities, with one of the objectives being the required modelling. Various transmit configurations are considered, including different antenna heights, as well as omnidirectional and directional antenna patterns with both horizontal and vertical polarisation. During the measurements both CW and wideband (impulse response) data were recorded on both line-of-sight (LOS) and non-line-of-sight (NLOS) channels.

The CW results indicate that on about 40% of the streets in an urban area, LOS power loss has a single, continuous slope that is proportional to R^{-n}, where n is close to 2, as for free space. For the other 60% of the streets loss is proportional to R^{-2} only for short ranges. For ranges greater than a breakpoint range, R_b, n takes on greater values. However, the power loss exponent in this region rarely takes on values near 4, nor is R_b often close to the edge of the first Fresnel zone (288 or 144 m for the antenna heights involved), as would be expected from the flat-earth model that is currently proposed for application in microcellular systems. Instead values for "n" can range between 5 and 10 and those for "R_b" can range between 300 and 500 metres.

After more analysis using the wideband data for a closer study of the associated physics, results will be presented as a possible contribution to the development of a new model.

Statistical Modelling of Mobile Multipath Propagation Channels

Alan J Coulson†, Allan G Williamson‡, Rodney G Vaughan†

† Communications Team
Industrial Research Ltd
P O Box 31-310, Lower Hutt
New Zealand

‡ Radio Systems Group
The University of Auckland
Private Bag 92019, Auckland
New Zealand

Phone: +64-4-5690000, Fax: +64-4-5690754, Email: a.coulson@irl.cri.nz

Introduction

Statistical models for *narrowband* multipath propagation, such as Clarke's celebrated "ring of sources", have been proposed by a number of researchers. These models are used to define the bounds of applicability of probability density functions which are used widely in mobile and cellular systems analysis. Models which encompass all facets of multipath propagation - fast fading, shadow fading and time-dispersion - are less common. This paper presents such a model, recently proposed by the authors, and uses it to quantify the statistical origins and bounds of applicability of lognormal shadow fading, Rayleigh fast fading and Suzuki fading.

The Sum-of-Products Models

Figure 1 depicts the model, in which each propagation path between transmitter and receiver is represented as a product of complex random variables with additive time-delays. The paths are summed at the receiver, producing the well-known time-varying pulse train transfer function

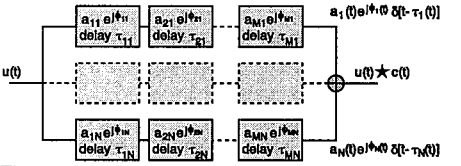

Figure 1 - *A wideband model for examining statistical distributions in multipath propagation.*

$$c(\tau;t) = \sum_{n=1}^{N(t)} a_n(t)e^{j\phi_n(t)}\delta[\tau-\tau_n(t)] = \sum_{n=1}^{N(t)}\left(\prod_{m=1}^{M_n(t)} a_{mn}(t)e^{j\phi_{mn}(t)}\right)\delta\left[t-\sum_{m=1}^{M_n(t)}\tau_{mn}(t)\right].$$

This paper uses the model to examine the rate of convergence of the Central Limit Theorem for the sums and products of complex random variables, and to quantify the influence of correlation both within and between paths on the resulting distribution. It is shown that only three reflections or diffractions are required to produce lognormal variability within a propagation path. The results also define the propagation conditions under which the narrowband envelope of the received sum of paths may be well modelled, at one extreme, as Rayleigh distributed and, at the other extreme, as lognormally distributed. Importantly, it was found that the Suzuki distribution provides an accurate statistical model for both wideband and narrowband multipath fading under most propagation conditions. Finally, sampling requirements are discussed for hypothesis testing statistical distributions of multipath fading channel measurements.

Conclusion

A wideband statistical model of multipath propagation is used to define the limits of applicability of fading distributions used in mobile and cellular systems analysis. In particular, the statistical origins and persistence of lognormal variability are quantified.

F69.9

AUTOMATIC RECONSTRUCTION OF 3-D BUILDING DIMENSIONS FROM 2-D VIDEO DATA FOR URBAN PROPAGATION MODELING

H.Martinez[1], C.Akturan[2], H.Foltz[1], H.Ling[2], and W.Vogel[2]
[1]Engineering Department, Univ. of Texas - Pan American, Edinburg, TX 78539
[2]EERL, Univ. of Texas at Austin, Austin, TX 78758

Accurate modeling of urban propagation requires at a minimum a three-dimensional data base of the major buildings and structures in the area of interest. While this information can sometimes be compiled from architectural data, the process is time-consuming and complete information may not be available in all cases. This presentation will describe a proposed method for automatically deriving three-dimensional model data from video images recorded while driving down city streets. The video images are taken through a fisheye lens, so that each frame captures the entire upper hemispherical view from a given point on the street. A GPS receiver is used to record simultaneously the position from which each image is taken. This equipment, methods for distinguishing buildings from other objects in the images, and applications to predicting satellite communication path blockage were previously described in [R.Akturan and W.J.Vogel, IEEE Trans. Antennas Propagat., to be published].

In the algorithm, building silhouettes are found in each image and the corner points are identified. By tracking the corner points over a number of successive images taken from different positions, the 3-D locations of the corners can be estimated. The connections between corner points are then used to determine the locations of building edges. The ground surface profile is derived from the position and altitude of the data taking vehicle. Algorithms which detect and combine multiple identifications of the same features, remove extraneous or poorly defined features, and fill in unobserved edges and sides of buildings are then executed. The resulting building and ground surfaces are broken down into triangular facets suitable for use as input to electromagnetic simulation software. In particular, the facet files are suitable for use with a shooting and bouncing ray (SBR) technique, similar to that described in [H.Ling et al., IEEE Trans. Antennas Propagat., AP-37, 194-205].

Some advantages of this technique are that (1) the required image data can be obtained rapidly and at low cost, and (2) the images are acquired at street level, so that the structures observed are those most likely to affect urban mobile communications.

Multipath Simulation of Wireless Communication Systems

Harold Raemer, James Preisig, David Brady and Stephen McKnight
Department of Electrical and Computer Engineering and the Center for Electromagnetics Research, Northeastern University, Boston, MA 02115

The effect of multipath propagation on the performance of electromagnetic communication systems is significant. In mobile radio, cellular phone and indoor wireless applications, the multipath arrivals give rise to time-varying fading which can severely distort the signals. The nature of the multipath and resulting fades depends on location of reflecting surfaces, the composition and orientation of the reflecting surfaces, and the location of the transmitter and receiver. Therefore, analytical evaluation of the temporal, spatial, and spectral properties of the multipath fading is difficult. Consequently, most propagation modeling techniques for communications applications (e.g., the Longley-Rice Models) do not explicitly account for the effects of multipath propagation.

The program RS-SIM developed by Harold Raemer for simulation of radar clutter and multipath models return signals in a monostatic or bistatic radar receiver due to scattering from a large swath of terrain and an arbitrary distribution of discrete objects within the radar's field of view. The scattering models for terrain are based on an evaluation of the Stratton-Chu integral by dividing terrain into small patches and accounting for the tilt and rotation of each patch (e.g., Arikan and Raemer, JEWA 1996). The models are based on physical optics supplemented by diffraction. This program is now being applied to the study of one-way radio communication systems operating at frequencies from VHF through the microwave bands. For a wireless link with both transmitter and receiver well above the highest hills in the vertical propagation plane, this is a straightforward application of the existing program to a bistatic radar geometry. Received signals due to scattering constitute "ground clutter" in a bistatic radar and "multipath" in a one-way communication link, but the modeling is the same for both effects. The software is being extended to include the case where the ray-path between transmitter and receiver may be obstructed by hills or buildings. Using a combination of the scattering, shadowing and diffraction code already in the program and new code currently being added, we are constructing a modeling scheme that includes both propagation in the vertical plane and effects due to scattering and diffraction from outside of that plane. In effect, this is a three-dimensional generalization of standard two-dimensional propagation modeling. We are currently simulating a simple scenario involving a ground-based transmitter and receiver with a hill along the vertical propagation plane and another hill or set of discrete objects (e.g., building walls) at a specified horizontal distance from that plane. Some results will be shown to illustrate the sensitivity of the received signal spectrum to variations in heights of transmitter, receiver and the hills and objects and the spacing between these constituents of the scenario.

F69.11

A New Approach to 3D Ray Tracing for Site Specific Propagation Prediction

George Liang* and Henry L. Bertoni
Center for Advanced Technology in Telecommunications
Polytechnic University
Brooklyn, NY 11201

Abstract. A Vertical Plane Launch (VPL) technique for approximating a full 3D site specific ray trace to predict propagation effects in cities for UHF frequencies is described, and its predictions are compared with measurements for Rosslyn VA. The VPL technique employs the standard shoot and bounce method in the horizontal plane while using a deterministic approach to find the displacement in the vertical plane. This approximation is valid since buildings walls are almost always vertical. The VPL method shows significant improvement compared with the Slant Plane/Vertical Plane (SP/VP) method for rooftop antennas. For base station located at street level the VPL method gives better predictions than the 2D method in locations where propagation over buildings is significant.

URSI F

Session 84 — Salon Gatineau

Indoor/Mobile Propagation: Models and Measurements
Co-chairs: M. Fattouche, Canada and D. Sweeney, USA

08:10	84.1	A Study on Signal Penetration into Building, R.-Y. LANE, **H.-J. LI**, *National Taiwan University, Taipei, Taiwan, China*
08:30	84.2	Calculation of Reflection and Transmission Coefficients of Walls for Indoor-Propagation Modelling, **Y. HUANG**, *University of Liverpool, UK*
08:50	84.3	Theory and Experiment for UHF Propagation through Reinforced Concrete, **R. PAKNYS**[1], M.J. NEVE[2], A.G. WILLIAMSON[2], [1]*Concordia University, Montréal, QC, Canada;* [2]*University of Auckland, New Zealand*
09:10	84.4	Modeling of Wave Propagation through a 2-D Inhomogeneous Dry Wall for Cellular and PCS Applications, **G. STRATIS**, D. DEMETRIOU, *ICIG, Motorola, Rolling Meadows, IL, USA*
09:30	84.5	Effects of Antenna Radiation Patterns upon Indoor Radio Channel Operating at 37.2 GHz, **L. TALBI**[1], G.Y. DELISLE[2], [1]*College of Technology, Riyadh, Saudi Arabia;* [2]*INRS-Télécommunications, Verdun, QC, Canada*
09:50	84.6	Analysis of Multipath Characteristics for Indoor Environments, **H.-J. LI**, R.-Y. LANE, C.-W. HSIEH, *National Taiwan University, Taipei, Taiwan, China*
10:10		Coffee Break
10:30	84.7	Frequency-Selectivity in Indoor Propagation Channels, **A.J. COULSON**[1], A.G. WILLIAMSON[2], R.G. VAUGHAN[1], [1]*Industrial Research Limited, Lower Hutt and* [2]*University of Auckland, New Zealand*
10:50	84.8	Transfer Function Estimation in Complex Propagation Environments, **W. WASYLKIWSKYJ**, *George Washington University, Washington, DC, USA*
11:10	84.9	Analytical, FDTD Numerical, and Experimental Studies of Diffraction by a 2-D Inhomogeneous Dielectric Wedge for Cellular and PCS Planning, **V. ANANTHA**[1], G. STRATIS[1], D. DEMETRIOU[1], J.H. GREENE[1], A. TAFLOVE[2], [1]*ICIG, Motorola, Rolling Meadows, IL and* [2]*Northwestern University, Evanston, IL, USA*
11:30	84.10	MMDS Coverage/Propagation Prediction Tool, **A. SCHNEIDER**, *Bell Atlantic Corporation, Arlington, VA, USA*

F84.1

A Study on Signal Penetration Into Building

Rong-Yuan Lane and Hsueh-Jyh Li
Department of Electrical Engineering
National Taiwan University
Taipei, Taiwan, China

Statistical attenuation property about signals penetrating into building is an important parameter for mobile communication system designers. The penetration loss is usually modeled by adding a transmission loss term, which is calculated by using the conventional transmission coefficient expression. However, there may have different types and sizes of windows on building surfaces and penetration losses for glass windows and concrete walls are very different. Fields at the obstruction region are contributed by the penetrating ray as well as those rays which first penetrate through the window and then arrive the receiving antenna after single or multiple reflections.

The penetrating ray will be the dominant contributor to the received field if the wall penetration loss is small compared to the wall reflection loss. On the contrary, the reflected waves will be dominant to the total field if the wall penetration loss is very large (for example, the wall is very lossy or very thick in terms of wavelengths).

In this presentation we will use the ray-tracing technique to numerically study the statistical attenuation property for signals penetrating into buildings. We systematically simulate different penetration environments and theoretically calculate their impulse responses. From which the mechanisms contributed to the total field can be analyzed. Effect of the percentage of windows occupying the wall surface and effect of directions of incident waves on the statistical penetration losses will be numerically studied. Both numerical and experimental results will be demonstrated.

Calculation of Reflection and Transmission Coefficients of Walls for Indoor-Propagation Modelling

Dr Yi Huang (Yi.Huang@liv.ac.uk)
University of Liverpool, Liverpool, L69 3GJ, UK

Indoor radio propagation measurements are well documented for a range of different environments. However, the measured results vary considerably from one site to another. Even for the same type of buildings the path loss and delay spread can be very different, since the thicknesses of walls may not be the same. Thus site-specific modelling approaches, notably ray-tracing methods, have attracted a considerable amount of research interest. How to calculate the reflection coefficient (RC) and transmission coefficient (TC) of walls is a very basic but important issue to the site-specific modelling of indoor communications, because it is necessary to know the RC and TC at each intersection on the wall for each ray considered. The efficiency and accuracy of this calculation is therefore vital for the whole modelling. Unfortunately this problem has not received enough attention and little publication can be found from the open literature.

The calculation of radiowave reflection and transmission coefficients on walls of a building is not a simple problem. At present *intrinsic* reflection and transmission coefficients are used by many authors for the indoor radio modelling. The calculated results are doubtful since they have not taken the thickness of the wall and multiple reflection and transmission within the wall into account. The total reflected and transmitted waves are actually superpositions of infinite number of reflected and transmitted rays on the wall., therefore the total reflected field cannot be obtained simply using the intrinsic RC and TC.

A number of researchers did consider the first few reflections and transmissions (M. C. Lawton and J. P. McGreehan, *IEEE Trans. on Veh Technol.* 1994, 43, pp. 955-968. W. K. Tam and V. N. Tran, *Electronics and Communication Eng Journal*, 1995, 7, pp. 221-228), but the calculation was approximate and complicate, furthermore, it is very inefficient considering this calculation as a fundamental element for the whole channel modelling.

New explicit and compact expressions of the total reflected and transmitted coefficients are derived in this paper. The multiple reflections and transmissions within the wall are taken into account, thus these formulae should offer more efficient and accurate results than any other formulae or methods currently used for indoor radio simulations.

F84.3

Theory and Experiment for UHF Propagation through Reinforced Concrete

Robert Paknys * †, Michael J. Neve ‡, and Allan G. Williamson ‡

† Concordia University, Department of Electrical & Computer Engineering
Montreal, Canada (E-mail: paknys@ece.concordia.ca)

‡ The University of Auckland, Department of Electrical & Electronic Engineering
Auckland, New Zealand (E-mail: mj.neve@auckland.ac.nz)

Future indoor wireless communications systems will require effective planning tools if reliable and efficient services are to be designed. A key component of the planning tools arsenal is the propagation model. These models must account for the interaction of the propagating fields with typical building structures and materials.

The purpose of this work is to gain an understanding of the mechanisms by which UHF signals propagate through reinforced concrete structures. Theoretical investigations are being performed for a 2–D model, consisting of straight wires (representing reinforcing steel), embedded in a lossy dielectric slab of thickness d. The illumination is an electric line source, parallel to the embedded wires. The transmission properties of three cases are being investigated, namely (1) the wire grid in isolation; (2) a homogeneous concrete slab; and (3) the concrete slab with embedded wires.

A moment method model of the wire grid has revealed that the phasefront curvature is hardly affected by the wires, though a substantial amount of signal attenuation can occur, depending on the wire spacing and frequency. Hence, a ray tracing approach using geometrical optics is valid for transmission prediction, using the transmission coefficient for a wire grid. Similar conclusions apply to a lossy dielectric slab, as an examination of the transmission coefficient indicates that the transmitted phasefront emerges as a cylindrical wave. Work is currently underway to modify the moment method wire grid model so that the scattering wires act in the presence of a lossy dielectic slab. The free space Green's function is replaced with with the lossy slab Green's function, and the numerical evaluation of a Sommerfeld integral is needed.

To validate these theoretical formulations, a programme of experimental trials is being undertaken. These trials involve the experimental characterisation of scaled models of typical building structures at appropriately scaled frequencies in an anechoic chamber. This technique has previously been used to investigate propagation in microcellular environments (M. J. Neve, et. al., IEEE Conf. Proc. VTC '96, pp. 615–619), and can provide considerable insight into the mechanisms by which the fields propagate.

Modeling of wave propagation through a 2-D inhomogeneous dry wall for cellular and pcs applications

Glafkos Stratis
ICIG, Motorola
Rolling Meadows
IL 60008

Demetrakis Demetriou
ICIG, Motorola
Rolling Meadows
IL 60008

An inhomogeneous dry wall with metal inhomogeneities presents significant complications in the analysis of electromagnetic wave penetration and reflection. In many scattering problems of practical interest a major inhomogeneity is introduced by equally spaced metallic rebars inside the wall. The periodically spaced metal in the dielectric could cause significant deviations in the reflected and transmitted signals obtained for a pure dielectric using Fresnel's formulae for reflection and transmission.

In this paper we present and compare numerical and experimental results obtained for signals transmitted and reflected from an inhomogeneous dry wall with periodically spaced metal rebars at frequencies appropriate for cellular and personal communication systems. The numerical results are obtained by using a two-dimensional FDTD code. We develop an impulse response model for the wall which allows a post-processing convolutional analysis of signal impulses of practical interest.

First, we use FDTD to obtain the numerical (reflected and transmitted) fields for the homogeneous dielectric wall without any metal for plane wave incidence. This is compared to the theoretical calculation of the fields obtained using the Fresnel's formulae. The correspondence between the two results establishes the validity of the general procedure using FDTD. Next, we model the dielectric wall with periodic metal rebars and obtain results for the reflected and transmitted field at various observation points for an incident plane wave. We present numerical and experimental results for the reflected and transmitted field at various observation angles and frequencies. Both these results are also compared with the results obtained for the pure dielectric wall in order to study the significance of the effect of the metal rebars.

F84.5

Effects of Antenna Radiation Patterns upon Indoor Radio Channel Operating at 37.2 GHz

Larbi Talbi [1*] and Gilles Y. Delisle [2]
1 Electrical Technology Department, College of Technology-Riyadh,
P.O.Box 42826, Riyadh 11551, Saudi Arabia
2 INRS-Télécommunications, 16 Place du Commerce, Verdun,
Québec, Canada, H3E 1H6

Abstract

Various experimental results were conducted at 37.2GHz and aiming the investigation of the influence of antenna directivity on reducing the effects of the multipath of the indoor line of sight (LOS) propagation channel. The received signal envelopes were measured, for three sets of arrangement using two types of antenna, omnidirectional and directional, as the mobile receiver moved away from the fixed transmitter (Fig. 1). In high-speed indoor radio communication systems, delay distorsion due to multipath propagation is a serious cause of channel degradation. One measure of the multipath effect of the channel is the fading of the carrier envelope. Another measure is the width of the received carrier envelope spectral density. In this optic, the cumulative distribution functions for the received signal envelope, as well as the corresponding power spectra are obtained for each set of measurements to determine the influence of antenna directivity on channel characteristics. In addition, NLOS results have been performed using horn antennas to obtain wall reflections as well as corner diffractions. The experimental techniques, results and conclusions will be presented and fully discussed in view of the future system requirements.

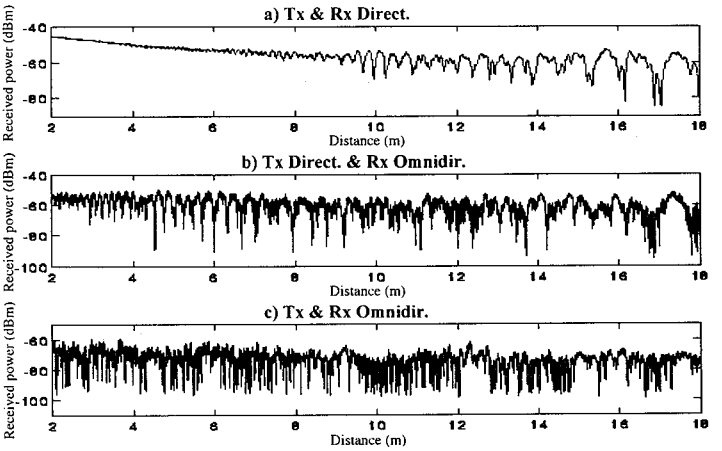

Fig 1. Amplitude variations along the center line of a long narrow corridor.

Analysis of Multipath Characteristics for Indoor Environments

Hsueh-Jyh Li, Rong-Yuan Lane and Chi-Wei Hsieh
Department of Electrical Engineering
National Taiwan University
Taipei, Taiwan, China

Understanding the multipath mechanisms and their statistical properties is helpful for the study of indoor channel characteristics. The shooting and bouncing ray technique is a very useful numerical tool for this understanding, since all parameters such as the amplitude, the time delay, the direction of arrival, and the polarization of multipath components can be obtained with this technique. In this presentation we will use this tool to numerically analyze some statistical channel properties for indoor environments.

It is interesting to analyze the contribution to the total received field for waves after n times of reflections. This information is important because we usually have to set a maximum number of reflections in the numerical simulation so that rays with further times of reflections contribute little and can be neglected. In those regions without line of sight, it is also required to evaluate whether the received field will be greater than the minimum threshold, and this can be evaluated by estimating after how many times of reflections that the wave can arrive the receiver.

The performance of a mobile antenna is dependent on its effective gain in a multipath propagation environment. While the effective gain depends on the distributions of directions of wave arrivals and the cross-polarization coupling. Therefore, information about statistical distributions of the incoming signal directions and its incident polarization vectors after multiple reflections is important for evaluating a mobile antenna's performance.

In this presentation we will demonstrate some numerical results about statistical properties such as the elevation angle distribution of wave arrivals, the effect of depolarization and the average contribution to the resultant field after n times of multiple reflections.

F84.7

Frequency-Selectivity in Indoor Propagation Channels

Alan J Coulson†, Allan G Williamson‡, Rodney G Vaughan†

† Communications Team
Industrial Research Ltd
P O Box 31-310, Lower Hutt
New Zealand

‡ Radio Systems Group
The University of Auckland
Private Bag 92019, Auckland
New Zealand

Phone: +64-4-5690000, Fax: +64-4-5690754, Email: a.coulson@irl.cri.nz

Introduction

Future indoor wireless systems will be required to provide low bit error rate (BER), high bandwidth services which are suitable for both voice traffic and LAN data traffic. Diversity systems are fundamental to providing low BER communications in multipath propagation environments, such as those experienced indoors. This paper compares the BER performance of frequency and space diversity systems in indoor propagation conditions, and quantifies minimum bandwidths required to produce satisfactory BERs.

Diversity from Frequency-Selective Propagation

Figure 1 shows the *number of equivalent frequency diversity branches* available in a multipath propagation channel for a variety of signal bandwidths. For example, a 10 MHz system with RAKE receiver in a channel having an RMS delay spread of 100ns will have a BER performance equivalent to that of a six-branch space diversity narrowband system. Note that where the number of equivalent diversity branches is one, this indicates no diversity. These results demonstrate the differences in frequency-selectivity between indoor and outdoor mobile channels, and indicate the signal bandwidths which must be used to provide effective frequency diversity. To accommodate the high data rates demanded by LAN traffic, signal bandwidths of 100 MHz or more will be required. Figure 1 shows such systems to possess much inherent frequency diversity.

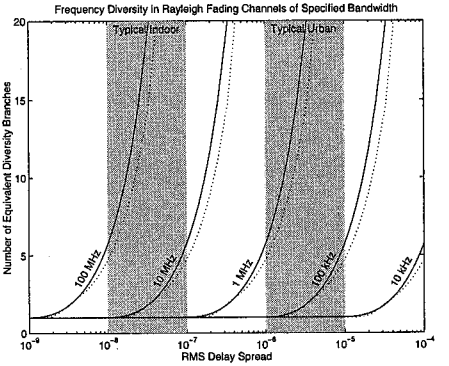

Figure 1 - *The number of equivalent diversity branches available in frequency-selective multipath channels having exponential (solid) and one-sided Gaussian (dotted) mean power delay profiles.*

Conclusion

Multipath propagation provides little inherent frequency diversity to indoor wireless systems having bandwidths of 10 MHz or less have. Such system may be regarded as *narrowband* and will require space diversity to provide satisfactory BERs to all users. Indoor systems with bandwidths of 100 MHz or more have much inherent frequency diversity. The diversity receivers required to equalize the frequency-selective multipath propagation for such systems may utilize this diversity to ensure low BER performance.

Transfer function estimation in complex propagation environments

Wasyl Wasylkiwskyj
The George Washington University
Washington, DC 20052

In characterizing a complex propagation environment it is frequently necessary to measure transfer functions for a large set of receiver/transmitter location pairs. In such cases, in addition to measurement accuracy, consideration must be given to the minimization of the total measurement time (processing and data collection). This is particularly important if the propagation environment in question is not constant but subject to temporal changes. In this paper the problem of total measurement time minimization is considered when the measurement involve a large set transmitter/ receiver pair locations. An algorithm employing pulse compression waveforms is presented that permits the processing of receiver data for near- simultaneous multiple transmitter excitations. Results of numerical simulations are presented that show excellent transfer function reconstruction capabilities in multipath environments.

F84.9

"Analytical, FDTD Numerical, and Experimental Studies of Diffraction by a 2-D Inhomogeneous Dielectric Wedge for Cellular and PCS Planning"

Veeraraghaven Anantha
ICIG,Motorola
Rolling Meadows,
IL 60008

Glafkos Stratis
ICIG, Motorola
Rolling Meadows,
IL 60008

Demetrakis Demetriou
ICIG, Motorola
Rolling Meadows
IL 60008

Jethro H. Greene
ICIG, Motorola,
Rolling Meadows
IL 60008

Allen Taflove
Northwestern University
Evanston, IL 60208

Classical theories such as the Uniform Theory of Diffraction (UTD) have used analytical expressions for diffraction coefficients for canonical scatterers such as the infinite perfectly conducting wedge. Although these theories predict the fields accurately in the far-field region for simple problems, it is difficult if not impossible to extend the analyses to find diffraction coefficients for wedges composed of dielectric and imperfectly conducting materials. In fact, the classical problem of diffraction from an infinite lossless dielectric wedge has not been solved analytically.

Last year, we demonstrated the successful application of the FDTD method to numerically obtain diffraction coefficients for an infinite PEC wedge, and the extension of the approach to infinite homogeneous dielectric wedges. In this paper, we further extend the FDTD approach to analyze the diffracted fields from 2-D inhomogeneous material wedges representing a practical situation, the corners of a building. We present UTD, FDTD, and experimental test results for both vertical and horizontal incident-wave polarizations of illumination of such corners. We conclude by discussing the applicability of UTD in simulation tools for cellular and PCS planning, and the potential for improved simulations by employing diffraction coefficients obtained numerically with FDTD.

MMDS Coverage/Propagation Prediction Tool

Allan Schneider
Bell Atlantic Corporation
Arlington, Virginia 22201

Background:--Among the multiplicity of radiowave propagation models which could stand as possible candidates for inclusion in an MMDS coverage prediction tool, the most likely would surely include: (1) the Longley-Rice Model; and (2) the Terrain Integrated Rough Earth Model, or TIREM. Both of these models are based, more or less, upon the National Bureau of Standards Technical Note 101, "Transmission Loss Predictions for Tropospheric Communication Circuits"

In estimating transmission loss both models require a number of geometric parameters : (a) antenna heights above ground [h_{g1}, h_{g2}]; (b) horizon distances of the antennas [d_{L1}, d_{L2}]; (c) horizon elevation angles [θ_{e1},θ_{e2}]; and (d) for a transhorizon path, the angular distance [θ]. Both the Longley-Rice Model (in the point-to-point mode) and TIREM can calculate these parameters if a terrain profile is specified; only the Longley-Rice Model (in the area-prediction mode) can estimate these parameters from terrain roughness alone.

Both the Longley-Rice and TIREM models then employ complex algorithms to identify the dominant propagation mechanism from the path geometry. For transmission paths within the radio horizon, the transmission loss is based upon geometric optics (ray theory). Fresnel-Kirchhoff diffraction theory (knife-edge or rounded-obstacle) is used for common horizon paths; smooth-earth or multiple-obstacle diffraction theory is used for double horizon paths only slightly longer than the radio horizon. For still longer distances, empirical tropo-scatter models are used.

However, both the Longley-Rice and TIREM models ignore terrain clutter (e.g., buildings and trees) - only terrain irregularity is considered. Since terrain clutter is likely to be especially important in the urban and suburban environs which typify MMDS, the application of either Longley-Rice or TIREM for MMDS coverage prediction seems problematical at best. Consequently, a new radiowave propagation model has been developed to address the impact of terrain clutter on MMDS.

The MMDS Model:--The MMDS propagation model considers, as does Longley-Rice and TIREM, the consequences of earth curvature, atmospheric refraction, and irregular terrain; however, only the MMDS model accounts for trees. The model is predicated upon the hypotheses that (1) the transmitting antenna is well-sited upon a tall tower above any foreground obstructions; (2) the receiving (house-top) antenna may be blocked by trees; (3) the dominant propagation mechanism is either free-space loss (limited by earth curvature) or tree-top diffraction. The principal effect of earth curvature, atmospheric refraction, and terrain irregularity on tree-top diffraction is their impact on the diffraction angle δ. Tree-top/roof-top geometries are modeled stochastically using Monte Carlo techniques which also provide diffraction loss histograms and MMDS coverage probabilities. Diffraction by uncluttered irregular terrain is not considered, since the well-sited transmitting antenna tends to ensure that the potential for irregular terrain diffraction is negligible in comparison to tree-top diffraction, especially above the relatively flat terrain so characteristic of suburban areas in the northeastern United States.

URSI F

Session 101 — **Salon Gatineau**

Satellite-Earth Propagation: Models and Measurements
Co-chairs: N. Golshan, USA and D.V. Rogers, Canada

13:10 101.1 Two Years of Three Site Diversity Measurements at 20 GHz with ACTS, **J. GOLDHIRSH**[1], B.H. MUSIANI[1], A. DISSANAYAKE[2], K.T. LIN[2], [1]*The Johns Hopkins University, Laurel and* [2]*COMSAT Laboratories, Clarksburg, MD, USA*

13:30 101.2 ACTS Ka-Band Propagation Measurements in Florida, **H. HELMKEN**[1], R. HENNING[2], [1]*Florida Atlantic University, Boca Raton, FL and* [2]*University of South Florida, Tampa, FL, USA*

13:50 101.3 Operational Measurements of Ku-Band Path Attenuation during Rainy Months for Toronto and Montréal, A. SHOAMANESH[1], **D.V. ROGERS**[2], [1]*Telesat Canada, Gloucester and* [2]*Communications Research Centre, Ottawa, ON, Canada*

14:10 101.4 Ka-Band Scintillation Observations at the ACTS Propagation Experiment Site in Norman, Oklahoma, **R.K. CRANE**, X. WANG, *University of Oklahoma, Norman, OK, USA*

14:30 101.5 Ka-Band Scintillations on a Low Elevation Angle Link, **C.E. MAYER**, *University of Alaska Fairbanks, AK, USA*

14:50 101.6 Prediction of Clear-Air Fading Distributions on Very-Low-Angle Satellite Links: Summary of Global and Canadian Procedures, **R.L. OLSEN**, *Communications Research Centre, Ottawa, ON, Canada*

15:10 Coffee Break

15:30 101.7 Statistics of Scintillation in Ku-Band for Madrid, Spain, L. GÓMEZ, A. DE LA TORRE, **A. BENARROCH**, J.M. RIERA, *Polytechnic University of Madrid, Spain*

15:50 101.8 Simultaneous Observation of Ku-band Satellite Signal Level Fluctuation and Clear-Air Turbulent Echoes from VHF High-Power Radar, **Y. MAEKAWA**[1], Y. SHIBAGAKI[1], M.D. YAMANAKA[2], S. FUKAO[2], [1]*Osaka Electro-Communication University, Osaka and* [2]*Kyoto University, Kyoto, Japan*

F101.1

Two Years of Three Site Diversity Measurements at 20 GHz with ACTS

Julius Goldhirsh, Bert H. Musiani
The Johns Hopkins University, Applied Physics Laboratory
Johns Hopkins Road, Laurel, Maryland 20723-6099
julius_goldhirsh@jhuapl.edu
Asoka. Dissanayake and K. T. Lin
COMSAT Laboratories
22300 COMSAT Drive, Clarksburg, MD 20871

A three-site rain fade space diversity measurements experiment at 20 GHz has been in near continuous operation since September 1, 1994. Two receiver sites (APL and COMSAT) are located in Central Maryland, and the other is in Virginia. The APL and COMSAT locations are separated by 33 km. The Virginia site is separated 44.5 km from APL and 30.5 km from COMSAT. Receivers at each of the sites measure the 20 GHz CW signal level from the radiating beacon on board the geostationary Advanced Communications Technology Satellite (ACTS). The first year of measurements (September 1, 1994 - August 31, 1995) have shown the following: (1) Fade margins of approximately 3.5 dB and 5 dB will enable continuous communications at the three sites for 99.95% and 99.99% of the time, respectively. These correspond to outages of only 4.32 hours and 52 minutes per year. (2) The diversity gains at the 0.01% probability range between 13 dB (APL) and a value in excess of 30 dB (Virginia). The diversity gains at the 0.05% probability range between 6 dB (COMSAT) and 11 dB (Virginia). (3) The diversity gains versus the single terminal fades relationship for the three site cases are within one dB of each other up to single terminal fades of 18 dB. (4) The joint fade distributions approximately overlap during the spring-summer and fall-winter periods. This result implies that for a given percentage of outage time, the required fade margins are the same for both seasonal periods. (5) The single terminal equal probability fades during the spring-summer period are significantly larger than the fades for the fall-winter period. The larger fades are caused by the greater prevalence of convective rains such as thunderstorms vis-à-vis the stratiform rains which have smaller rain rates associated with them. (6) The diversity gains during the spring-summer period at equal probability levels are significantly larger than those for the fall-winter. The above first year results will be compared and combined with those of the second year (September 1, 1995 - August 31, 1996). A characterization of the year to year variability will be made.

ACTS Ka-BAND PROPAGATION MEASUREMENTS IN FLORIDA

Henry Helmken* and Rudolf Henning**
*Florida Atlantic University
777 West Glades Road
Boca Raton, Florida 33431
**University of South Florida
4202 East Fowler Avenue
Tampa, Florida 33620

The NASA Advanced Communications Technology Satellite (ACTS) Propagation Measurements program has accumulated over three years of continuous propagation data at 20.185 GHz and 27.505 GHz at seven selected sites spanning the North American continent from Alaska to Florida. These frequencies are strongly affected by intense weather phenomena; hence reliable signal transmission system designs in this frequency band have to rely on both measurement data and validated models of channel characterization. The most stressed area in North America, weather-impact-wise, is Florida with its sub-tropical climactic region. As a member of the NASA's ACTS propagation measurements program, beacon and radiometer data have been continuously recorded at the University of South Florida (USF), Tampa, Florida.

NASA's ACTS program was developed to foster the creation and validation of communication technology expansion into the millimeter region. At Ka-band frequencies, reliable signal transmission system design depends heavily on validated channel models and accurate propagation statistics. The Space Communications Technology Center (SCTC) headquartered at Florida Atlantic University (FAU) is a NASA sponsored Center for the Commercial Development of Space and is developing systems for digital satellite communication of voice, data and video via Ka-band and thus is very dependent on accurate propagation information.

An ACTS Propagation terminal (APT) has been established by NASA at the University of South Florida in Tampa, one of the seven sites, supporting both the ACTS program and the SCTC mission. This terminal has been acquiring propagation and related data since December, 1993. Detailed data are routinely processed and data files of calibrated results are sent and archived in the program's central depository at the University of Texas at Austin, TX.

This paper will focus on the measurements of fade statistics and present a summary of the Florida measurements to date. Data have been processed to remove all known artifacts. Weather impact is strongly reflected in such fade statistics as Cumulative Distribution Functions (CDFs), fade duration vs. fade depth and fade slope vs. fade depth. Results will be compared with CCIR and Global Rain Model predictions. Initial results indicate that a two component rain model may be needed for sub-tropical regions like Florida.

URSI Commission: Satellite-Earth Propagation (Models and Measurements)

F101.3

OPERATIONAL MEASUREMENTS OF Ku-BAND PATH ATTENUATION DURING RAINY MONTHS FOR TORONTO AND MONTRÉAL

A. Shoamanesh
Telesat Canada, Gloucester, Ontario, Canada K1B 5P4

D.V. Rogers*
Communications Research Centre, Industry Canada
Ottawa, Ontario, Canada K2H 8S2

Rain attenuation measurements were conducted during the months of May through September for a three-year period at 14.4 GHz on uplink propagation paths from Toronto and Montréal to the ANIK-C2 geostationary satellite at 110°W longitude. The path elevation angles to the satellite were 31° from Toronto and 26.5° from Montréal.

The attenuation measurements were conducted by Telesat Canada by monitoring, via telemetry, the input power to transponders on board the satellite, of the 14.4-GHz signals transmitted to ANIK-C2 from Toronto and Montréal. In order to investigate the operational range of greatest systems interest, this unique method of measuring rain attenuation was used to measure the durations of integer fade levels exceeding 5 through 13 dB, relative to the nominal unfaded signal level. The experiment configuration, along with a description of the operational procedures and data collection/analysis methods, will be presented in the paper.

The telemetry signal from the satellite was recorded continuously throughout the rainy period from May to September. The recorded data were analyzed for each month of the whole measurement period to derive statistics of the number of fades exceeding a given fade threshold for specified 3-hour intervals of the day (i.e., diurnal variation) as well as the total and average durations of fades exceeding each of the specified fade levels. These results are compiled to provide an intercomparison from month to month of the expected time of occurrence and duration of path fading.

To assist in the interpretation of the measurements, the results are also compared to rain rate statistics and additional assorted climatic data for Toronto and Montréal. The implications of the statistical results for Ku-band satellite communication systems will also be addressed.

KA-BAND SCINTILLATION OBSERVATIONS AT THE ACTS PROPAGATION EXPERIMENT SITE IN NORMAN, OKLAHOMA

R. K. Crane and X. Wang
School of Meteorology
University of Oklahoma
Norman, OK 73019

High data rate observations (20 samples per second) of scintillation at 20.2 and 27.5 GHz were made for 10 minute intervals once per hour starting at 11 minutes past the hour over a period of one year. These data were used to generate fluctuation frequency spectra for comparison with the spectra predicted for scintillation produced by atmospheric turbulence. Both the standard sampling rate data (1 sample per second) and the high data rate data were used to compile monthly empirical cumulative distributions of the standard deviations of the beacon level fluctuations calculated for each minute of measurement. The empirical distribution functions (edf's) were generated for comparison with the ITU-R Recommendation P.618-4 model predictions for scintillation intensity for earth-space paths.

The estimated spectra show good agreement with theoretical predictions. The edf's were not in agreement with the ITU-R model predictions. The ITU-R model was based on a statistical curve fitting to a limited number of edf's from a limited number of sites. Based on the ACTS experiment observations at the Norman site, observations at the six other sites in the ACTS Propagation Experiment, and earlier data taken at a mid-latitude site, several of the coefficients used in the current ITU-R prediction model are in error. In general, the ACTS data show that the ITU-R scintillation intensity model predictions are too high.

F101.5

KA-BAND SCINTILLATIONS ON A LOW ELEVATION ANGLE LINK

Charles E. Mayer
University of Alaska Fairbanks
Electrical Engineering Department
PO Box 755900
217 Duckering Building
Fairbanks, AK 99775-5900
(907) 474-6091, Fax (907) 474-6087
E-mail: ffcem@aurora.alaska.edu

The impact of rain-induced attenuation on satellite-earth communication links at frequencies above 10 GHz is predominant. However, for the design of low margin systems, especially those at high frequencies and low elevation angles, scintillation effects must be accounted for to accurately complete a link budget.

Scintillations are rapid fluctuations of signal amplitude and phase, on the scale of a few seconds to tens of seconds, which are associated with fluctuations in the index of refraction produced by turbulence. The measure of the intensity of scintillation used is the standard deviation of the log amplitude of the high pass filtered received signal, that is, the standard deviation of the received signal in decibels. Standard deviations were calculated for both one minute and one hour time periods for the received 20.2 and 27.5 GHz ACTS satellite beacons. Scintillation models by the ITU-R (ITU-R Recommendation P6184) and by Karasawa, et. al. (IEEE Trans. Antennas Propagat., pp. 1608-1614, Nov. 1988) use a mean hourly standard deviation. Scintillation standard deviations in one minute prove very useful in gaining insight into the scintillation process.

Sky temperature thresholds were used to separate wet and dry scintillations. Thresholds were determined for each month by plotting sky temperature against rain rate and calculating the average sky temperature for which the rain rate was zero. Comparisons of new data with models were made by looking at the standard deviation of signal variations due to scintillations on an hour by hour basis. These models make a prediction of standard deviation in a month based on wet refractivity (calculated from the average temperature and relative humidity in a month). This prediction is then scaled to frequency, elevation angle, and aperture size. The models give consistently higher values of standard deviation.

The power spectrum of the received beacons was calculated, and the procedure employed for spectra estimation was to average contiguous spectra. The shapes of the power spectra are consistent with the theoretical predictions.

Prediction of Clear-air Fading Distributions on Very-Low-Angle Satellite Links: Summary of Global and Canadian Procedures

Roderic L. Olsen
Communications Research Centre
P.O. Box 11490, Station H
Ottawa, Canada K2H 8S2

Microwave and millimetre-wave signals transmitted over low-angle satellite links are sometimes subject to severe amplitude fading arising from the refractive structure of the troposphere. The effect can become particularly severe at elevation angles below about 5°, where multipath becomes important in addition to scintillation. The satellite links most affected in the past were geostationary links to locations in the high arctic of Canada and other northern countries. However, there has been renewed interest in using low-angle intercontinental geostationary satellite links from more southerly locations also. The problem is also likely to become important in the future for low-earth-orbit satellite links to locations at high and low latitudes both from link-availability and interference viewpoints.

Although the Radiocommunication Sector of the International Telecommunications Union (ITU-R) has for some time provided a worldwide method for predicting scintillation fading distributions down to 4° elevation angle, there have been no procedures available for estimating the combined effects of scintillation and deep multipath fading. The development of suitable procedures has been hampered by the lack of data. This problem has now been overcome in a set of empirical procedures derived by combining the small data base available with the much more extensive knowledge of the climatology of multipath fading on terrestrial links. This paper summarizes the procedures recently adopted by the ITU-R (Recommendation ITU-R P.618-4, 1996) and the basis on which they were derived (R.L. Olsen, Proc. 7th URSI Commission F Open Symp., 115-118, Amedabad, India, 1995). The paper also summarizes corresponding Canadian procedures employing a high-resolution geoclimatic-factor map for Canada (R.L. Olsen and B. Segal, Can. J. Elec. & Comp. Eng., 17, 1, 11-23, 1992) developed originally for use in predicting multipath-fading distributions on terrestrial links.

F101.7

STATISTICS OF SCINTILLATION IN KU-BAND FOR MADRID, SPAIN

L. Gómez, A. de la Torre, A. Benarroch, J.M. Riera
Polytechnic University of Madrid, Spain

Propagation measurements using the ku-band DBS signal from HISPASAT are being carried out in order to study rain attenuation and scintillation events. A standard commercial receiver is used for this purpose, sampling the AGC signal at 1 Hz so that its level variations can be analysed. The elevation angle is 36°, and the dynamic range of the system allows detecting fades of up to 10 dB, enough to investigate scintillation and also most rain events. The results discussed correspond to data stored from April 1994 until September 1996, having observed scintillation phenomena in 21 months during this period.

The scintillation statistics performed comprise event analysis, including amplitude distributions and spectral characteristics, as well as correlation to meteorological parameters or diurnal and seasonal variability. Moreover, experimental monthly intensity and attenuation are being compared with existing models.

The results obtained for individual event analysis show a behavior similar to scintillation events detected in other experiments (J.V.P. Baptista, P.G. Davies, OPEX Reference Book on Attenuation Measurement and Prediction, ESA ESTEC, Noordwijk, The Netherlands, 1994) in other european countries with relatively high elevation angles, observing gaussian single event distribution, and expected spectral features, that is, a corner frequency of 0.1-0.2 Hz, and a slope of approximately -8/3 .

The investigation of correlation to meteorological parameters shows that scintillation events occur during high temperature intervals, and also coincident with variations in wind speed and humidity. Cumulus clouds were reported in the path in more than half of the cases. Significant seasonal and diurnal variabilities have been observed: more than 80% of the events correspond to June, July and August, and a similar percentage was detected between noon and 20 hours. More frequent tropospheric turbulences, mostly coincident with cumulus clouds, often just before thunderstorms, occur in July. In such cases, the signal may keep fluctuating during nearly 30 minutes, several times during a few hours interval.

The comparison of the experimental monthly average intensity to the ITU-R predicted intensity (Rec. 618-2, ITU-R, Geneva 1992) shows good results, with relative errors below 10%. Somewhat larger errors are derived when comparing experimental attenuation distribution to ITU-R predicted distribution.

Simultaneous Observation of Ku-band Satellite Signal Level Fluctuation and Clear-Air Turbulent Echoes from VHF High-Power Radar

Yasuyuki Maekawa* and Yoshiaki Shibagaki
Osaka Electro-Commun. Univ., Neyagawa, Osaka 572, Japan

Manabu D. Yamanaka and Shoichiro Fukao
Radio Atmospheric Science Center, Kyoto Univ., Uji, Kyoto 611, Japan

In satellite communications, radiowave signals received at earth stations sometimes show a short period fluctuation at time scale of seconds even in clear-air conditions. This phenomenon is referred to as tropospheric scintillation, and often has amplitude of several dBs even in high elevation-angle Ku- or Ka-band paths. Long-term statistical properties of tropospheric scintillation in operational satellite links have been so far investigated, and some practical prediction methods are proposed (Y. Karasawa *et al.*, IEEE Trans., *AP-36*, 11, 1608-1614, 1988). However, detailed mechanisms of scintillation are still poorly understood, and its relation to atmospheric turbulences are not actually investigated by *in situ* measurements.

We conducted simultaneous observations of Japan's broadcasting satellite (BS) signal (Ku-band; 12 GHz, EL=41.4°) and VHF-band atmospheric turbulent back scattering echoes near the propagation path at the MU radar site, shigaraki, shiga, Japan (34° 85'N, 136° 10'E). The fluctuation of the BS signal measured by a 45 cm off-set parabola antenna at 1 sec interval is then compared with the intensity of atmospheric turbulences inferred from the clear-air back scattering echoes of the MU radar. This VHF high-power radar is a monostatic pulse Doppler radar which is composed of an circular array with 475 Yagi antennas in an area with 103 m diameter. The operational frequency is 46.5 MHz with peak output power of 1 MW. For this experiment, the observed height range is 2-22 km with height resolution of 150 m. The antenna beam is pointed to five directions. One is vertical, and others are tilted 10° from the vertical (referred to as "off-vertical") to each of four directions. These beam directions are electrically switched on pulse-to-pulse basis.

Amplitude of the scintillation is here estimated by calculating the standard deviation of the BS signal level fluctuation at 1 min interval. The MU radar echoes are obtained every 2.5 min at 150 m intervals. The two data sets are further averaged over the same time span of 30 min or 1 h. The MU radar echoes are also averaged over the height range of 2-6 km to be compared with the satellite signal scintillation caused by total propagation path effects in the lower troposphere. It is shown that the average amplitude of the scintillation is closely correlated with the height-averaged echo power obtained from the off-vertical beams, but not so well with the echo power obtained from the vertical beam. The off-vertical beam echoes seem to be caused by isotropic turbulences which primarily affects the satellite signal scintillation, whereas the vertical beam echoes also contain partial reflection echoes from stable layered structure of the atmosphere which is not very much concerned with the scintillation.

URSI F Special Session **Session 120** **Salon Gatineau**

Terrestrial Propagation Effects: Models and Measurements
Co-chairs: A.R. Webster, Canada and K. Anderson, USA

08:10	120.1	A Comparison of Worldwide Techniques with Regional Techniques for Predicting the Multipath Fading Distribution on Terrestrial L.O.S. Links, **R.L. OLSEN**[1], T. TJELTA[2], [1]*Communications Research Centre, Ottawa, ON, Canada;* [2]*Telenor Research and Development, Kjeller, Norway*
08:30	120.2	VHF/UHF Propagation over Terrain - Physical-Optics Calculations, R.R. MATSUNAGA, **J.H. WHITTEKER**, *Communications Research Centre, Ottawa, ON, Canada*
08:50	120.3	Fading Mechanisms on Line-of-Sight Microwave Links, **A.R. WEBSTER**, G. HUANG, *University of Western Ontario, London, ON, Canada*
09:10	120.4	Calculating Property Gradients Aloft from Ground-Based Doppler Radar Measurements, **E.E. GOSSARD**[1], B.B. STANKOV[2], D.E. WOLFE[2], [1]*University of Colorado and* [2]*Environmental Technology Laboratory, Boulder, CO, USA*
09:30	120.5	Parabolic Equation Techniques for Wave Propagation, **M.F. LEVY**, *Rutherford Appleton Laboratory, Didcot, UK*
09:50	120.6	Tropospheric Scatter Simulations and Measurements, **R.A. PAULUS**, *NCCOSC, San Diego, CA, USA*
10:10		Coffee Break
10:30	120.7	Rough Sea Effects on Evaporation Duct Propagation, **H.V. HITNEY**, *NCCOSC, San Diego, CA, USA*
10:50	120.8	Description of Signal Level Statistics for an East Coast Over-the-Horizon Coastal Link Operating at C-Band, **J. GOLDHIRSH**, B.H. MUSIANI, *The Johns Hopkins University, Laurel, MD, USA*
11:10	120.9	A Curvilinear Coordinate Based Split Step Parabolic Equation Method for Propagation Predictions over Terrain, **R. JANASWAMY**, *Naval Postgraduate School, Monterey, CA, USA*
11:30	120.10	Amplitude Scintillation on a 36 GHZ Overwater Link, **J. CLAVERIE**, *Ecoles de Coëtquidan (CREC), Guer, France*

F120.1

A Comparison of Worldwide Techniques with Regional Techniques for Predicting the Multipath Fading Distribution on Terrestrial L.O.S. Links

Roderic L. Olsen*
Communications Research Centre
P.O. Box 11490, Station H
Ottawa, Canada K2H 8S2

Terje Tjelta
Telenor Research and Development
P.O. Box 83, N-2007
Kjeller, Norway

Techniques for predicting the deep-fading range of the multipath fading distribution on terrestrial microwave line-of-sight links have been available for several countries for many years. Although these techniques have been used to varying extent in other countries that do no have their own methods, link designers in other countries have been faced with the difficulty of choosing among techniques giving sometimes vastly different results for the same apparent climatic region. Even though the Radiocommunications Sector of the International Telecommunication Union (ITU-R) has provided fully-approved procedures for worldwide application in the UHF to lower-EHF frequency bands since 1990, with a substantial improvement in 1994, the leading regionally-based procedures of Barnett-Vigants for the USA and Morita for Japan still continue to be used for applications worldwide. This is perhaps in large part because detailed results of tests comparing the ITU-R methods with these regionally-based methods on a large climatically-varied data base have not been available.

This paper first summarizes the current ITU-R "Method 1" (Recommendation ITU-R P.530-6), its draft revision, and the methods of Barnett-Vigants (A. Vigants, Bell Syst. Tech. J., 54, 103-142, 1975) and Morita (K. Morita, Rev. Elec. Comm. Lab., 18, 810-821, 1970; T. Ooi and K. Morita, Rev. Elec. Comm. Lab., 29, 51-57, 1981). It then summarizes testing results for ITU-R Method 1 on a 239-link data base from 22 countries around the world in comparison with results for the two regional methods. The ITU-R method is shown to perform significantly better than the regionally-based methods for inland links, and with the use of an improved geoclimatic factor model, for coastal and overwater links also.

VHF/UHF Propagation over Terrain – Physical-Optics Calculations

J.H. Whitteker and R.R. Matsunaga
Communications Research Centre
3701 Carling Ave., Box 11490, Station H
Ottawa, Canada K2H 8S2

The basis of physical optics is Huygens' principle, according to which points in space can be treated as wave sources. It can be derived as an approximation to the Helmholtz integral formula, which is exact, if the wavelength is small enough that (1) locally the wave has the form $A(x, y, z)\exp(\pm ikx)$, where x is in the main propagation direction, and where A varies little in distance $1/k$, and (2) the domain of integration may be limited to the first few unobstructed Fresnel zones closest to a stationary phase point along the free-space line of sight, or on a reflecting surface (J.H. Whitteker, *Radio Sci. 25*, pp. 837-851, 1990). These conditions are not restrictive. The main limitations on accuracy are the detail with which the calculations can be done in a reasonable time, and an imperfect knowledge of the terrain and of things covering it.

A computer program called CRC-Predict performs physical-optics calculations rapidly enough to be used routinely for broadcasting and land-mobile applications (J.H. Whitteker, *Proc. BLOS Conf.*, Austin, Texas, paper 9-6, Aug. 2-4, 1994). Successive integrations are done at increasing distances from the transmitter. In each step, the field is found as a function of height (2D calculation, see diagram below). The field at each point results from two integrations, one for a direct wave and one for a ground-reflected wave. Ideally, steps are short enough that the reflecting terrain between them is well approximated as a plane or very gently curving surface. In practice, longer steps are taken over low terrain, where a simplified terrain model is used for reflections. Apart from this, the terrain profile is used as it comes from the terrain data base. Trees and buildings add to the height of the obstructing terrain. When a receiver is among trees or buildings, a small clearing is assumed. Predictions have been verified with measurements at various frequencies, most recently at 1.5 GHz.

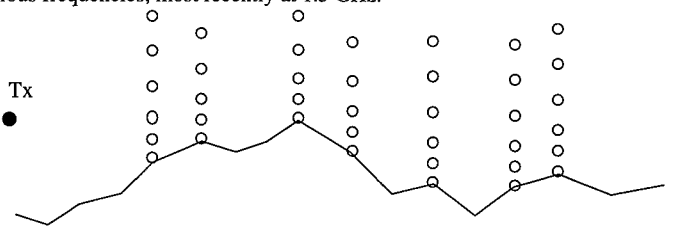

Schematic drawing of a terrain profile, and points (open circles) where the field is calculated by CRC-Predict

F120.3

Fading Mechanisms on Line-of-Sight Microwave Links.

Alan R. Webster* and George Huang,
Department of Electrical and Computer Engineering,
The University of Western Ontario,
London, ONT. N6A 5B9
Canada.

Experimental results are presented relating to signal fading on a 51km terrestrial microwave link situated in southern Ontario. Two separate, though related, systems have been operated simultaneously on this link for a number of consecutive fading seasons (May to October each year). The main experimental technique involves a vertical wide-aperture receiving array designed to measure the complex amplitude of the arriving signal which is readily transformed into an angle-of-arrival (AOA) spectrum in the vertical plane. Operating at a frequency of 16.65GHz, the system is capable of resolving individual incoming rays with a resolution approaching 0.1^0 in AOA over an unambiguous range of $\pm 0.7^0$; the dynamic range of 65dB allows for 45dB fades and 20dB enhancements. The second experiment uses vertical acoustic sounding to probe the lowest few hundred metres of the atmosphere for the presence of large temperature gradients associated with the presence of atmospheric layers, the prime cause of microwave fading. The microwave link itself traverses somewhat rolling terrain with approximately the same ground level and antenna height at each end, a fairly typical link in this part of the world.

Much of the fading on such microwave links occurs during the night-time hours with anomalous conditions developing once the sun has set. Ground cooling after a warm day often results in a developing temperature inversion resulting in a ground based layer. This in turn results in broad signal fading due to defocussing on top of which deep fades are superimposed due to interaction with weak ground reflected rays. Later, elevated layers sometimes develop leading to true atmospheric multipath in which interaction between rays of comparable, and near normal, amplitude produces deep fades alternating with considerable enhancements. Examples are presented confirming this general scenario.

These two fading mechanisms seem to produce somewhat different fading statistics with the first mentioned more likely to produce deep fades, at least in the range quoted above. Additionally, due to the elevated AOA of the strongest ray, which is almost always a feature of such fading, differing success may be experienced with diversity arrangements. Some ray-tracing examples are presented to illustrate this point.

CALCULATING PROPERTY GRADIENTS ALOFT FROM GROUND-BASED DOPPLER RADAR MEASURMENTS

Earl E. Gossard
Cooperative Institute for Research in the Environmental Sciences
University of Colorado/NOAA
Boulder, Colorado 80309

Boba B. Stankov and Daniel E. Wolfe
Environmental Technology Laboratory
Systems Demonstration and Integration Division/NOAA
Boulder, Colorado, 80309

A technique is described for using ground-based wind profiler measurements to calculate gradients of potential refractive index above the radar. The technique depends on accurate measurements of the 0-, 1st-, and 2nd moments of the Doppler spectrum recorded by the profiler. It therefore requires a calibrated system to measure backscattered power (0- moment). If the system includes a Radio Acoustic Sounding System (RASS), the humidity gradients can also calculated using the refractive index equation. The sign of the gradient is lost in this method, and information from supporting systems such as GPS, ACARS and models into which the radar information is assimilated may be necessary to obtain complete profiles. The errors in the method are discussed and modifications in the current data editing and processing techniques are proposed.

F120.5

Parabolic equation techniques for wave propagation

M.F. Levy
Rutherford Appleton Laboratory
Chilton, Didcot, Oxon OX11 0QX, UK

Parabolic equation (PE) techniques have become the preferred method for solving long-range radiowave propagation problems. They are based on an approximate factorisation of the wave equation into forward and back propagating terms, with only a small loss of accuracy when backscattering can be neglected. The resulting partial differential equation for the forward propagating wave can be marched in range, providing accurate full-wave solutions without requiring large computing resources. There is no difficulty including range and height variations of the refractive index of the propagation medium, provided these remain slow on the scale of a wavelength. For tropospheric propagation, terrain effects are modelled by introducing suitable boundary conditions at the air/ground interface.

The basic PE derivations are recalled and implementation options using either spectral methods or finite-difference schemes are described. Recent work has focused on boundary conditions. The non-local framework has led to the formulation of generalized impedance boundary conditions which can be used to truncate the integration domain in a perfectly transparent fashion or to develop accurate models for propagation over rough surfaces. Matching spectral methods provide an efficient numerical implementation. A survey of non-local techniques is given, with particular emphasis on application to microwave propagation over the rough sea surface. Finally we give an overview of the current state-of-the-art in PE methods for radiowave propagation applications, listing the problems now satisfactorily solved and the outstanding questions.

Tropospheric Scatter Simulations and Measurements

Richard A. Paulus
Propagation Division
NCCOSC RDTE DIV D883
49170 PROPAGATION PATH
SAN DIEGO CA 92152-7385

The capability of a parabolic equation propagation model to predict the mean and distribution of troposcatter signals in the upper VHF and UHF is examined. A simple method to account for tropospheric scatter in parabolic equation (PE) modeling of radio and microwave propagation has been proposed (H.V. Hitney, *IEEE Trans. Antennas Propagat., 41*, 905-909, 1993). The atmospheric refractivity profile is represented in the PE model at equally spaced vertical points separated by a height interval, δz, which varies between approximately 0.5 and 18 m depending upon frequency and the refractivity profile. The troposcatter model adds a random fluctuation to the mean refractivity at each vertical point in the PE model based upon the one-dimensional spectrum of refractive index fluctuations,

$$S_n(k) = 0.249 C_n^2 k^{-5/3}$$

using an effective refractive index structure parameter profile

$$C_{ne}^2 \cong 3.9 \times 10^{-15} e^{-z/2000}$$

(Doviak *et al., IEEE Trans. Geosci, Remote Sens., 21*, 25-33, 1983). This model was shown by Hitney to yield single realization results comparable to Yeh's empirical model and measured data.

Using Hitney's model, the statistics of the output of the model generated from numerous model runs using a standard atmosphere refractivity profile are compared with signal distributions measured in the southern California Bight (Rogers, *IEEE Trans. Antennas Propagat., 44*, 460-465, 1996). Signal levels were measured at 143.09, 262.85, and 374.95 MHz on a 127.2 km path between San Clemente Island and Point Loma in San Diego. The data from which the distributions were calculated were limited to periods when standard atmosphere propagation conditions prevailed.

F120.7

ROUGH SEA EFFECTS ON EVAPORATION DUCT PROPAGATION

Herbert V. Hitney
Propagation Division, Tropospheric Branch
NCCOSC RDTE DIV D883
49170 PROPAGATION PATH
SAN DIEGO CA 92152-7385

The evaporation duct is an important propagation mechanism for over-the-horizon over-sea paths at frequencies above several GHz. Various models and some limited experimental data indicate that wind-driven sea-surface roughness counteracts the effectiveness of the evaporation duct when both the duct height and the wind speed are high. Several methods have been proposed to model the effects of surface roughness under these ducting conditions, but these models are not all in agreement. A summary of existing waveguide, parabolic equation (PE), hybrid, and ray optics models will be presented along with results from one previous measurement program. All of these models use the same rough surface reflection coefficient reduction factor proposed by Miller and Brown (A.R. Miller, *et al.*, *IEE Proc.*, 131, 2, pp. 114-116, 1984), which was developed for optical region paths but may not be appropriate to over-the-horizon ducting conditions. Some of the differences between the PE and other models may be explained by approximations of grazing angle made by the PE models, which do not explicitly compute grazing angle. However one new PE model requires no approximations of grazing angle, but it also shows some differences to the other models.

This paper reviews current propagation models applicable to rough surface evaporation ducting conditions. Also a new Rough Evaporation Duct (RED) propagation experiment will be described that is specifically designed to address these effects. The proposed propagation path for RED is a 45 km over water link between the islands of Oahu and Molokai, Hawaii, which should be subject to both high wind speeds and high evaporation duct heights much of the time. Low terminal heights of about 5 meters and frequencies of 3, 10, and 18 GHz are planned. Propagation loss will be measured versus time simultaneously for all three frequencies.

Description of Signal Level Statistics for an East Coast Over-the-Horizon Coastal Link Operating at C-Band

Julius Goldhirsh, Bert H. Musiani
The Johns Hopkins University, Applied Physics Laboratory
Johns Hopkins Road, Laurel, MD 20723-6099
email: julius_goldhirsh@jhuapl.edu

Since July 1, 1997 an 128 km experimental propagation link which skirts the mid-Atlantic coast from approximately Dam Neck, Virginia (near Virginia Beach) to Wallops Island, Virginia has been operational. The transmitter located at Dam Neck radiates a CW signal at C-Band which is received at a site on Wallops Island and sampled and recorded at a rate of 50 Hz. The receiver/data acquisition system has a dynamic range of approximately 70 dB. The objectives of the experiment are to establish statistics associated with signal connectivity for the given geometric configuration. In particular, it is the objective to arrive at cumulative distributions of signal levels and their durations. The mode of propagation at different time intervals is complicated as it may encompass forward scatter from turbulent irregularities of the refractive index in the common volume as well as propagation via the mechanism of coastal evaporation ducts and/or surface ducts. Preliminary measurements and estimates of the structure constant show that scatter via the mechanism of turbulent irregularities in the common volume is, in general, always present. There are however extended periods of time in which propagation via the mechanism of ducting produces enhanced signals approaching levels greater than those obtained for clear line of sight cases (i.e., positive propagation factor). Signal level signatures associated with scatter from turbulent irregularities of the refractive index (e.g., propagation factors are smaller than -40 dB and estimated structure constants are smaller than $4X10^{-13} cm^{-2/3}$) are observed to be noisy requiring sampling at .02 second intervals. The changes of signal level over this sampling interval is generally within 10 dB. On the other hand, propagation factor levels above -35 dB are found to give sample to sample signal level variations smaller than 1 dB. Preliminary statistics of the type mentioned above covering the summer period will be presented.

F120.9

A Curvilinear Coordinate Based Split Step Parabolic Equation Method for Propagation Predictions Over Terrain

Ramakrishna Janaswamy
Code EC/Js, Department of Electrical & Computer Engineering
Naval Postgraduate School
Monterey, CA 93943, USA
email: janaswam@ece.nps.navy.mil

The Parabolic Equation (PE) method has emerged as an extremely valuable method for assessing radiowave propagation in the lower atmosphere in the presence of ducts and terrain features. Propagation loss can be easily estimated over very long ranges of the order of a few hundred kilometers for frequencies through SHF band, and for antenna heights extending up to several kilometers. Modeling over terrain irregularities poses particular challenges in an otherwise straight-forward numerical solution procedure. The PE can be solved either by using the implicit finite difference approach (S. W. Marcus, *IEEE Trans. Antennas Propagat.*, 40, 12, pp. 1451-1458, 1991) or by the split-step algorithm (A. E. Barrios, *IEEE Trans. Antennas Propagat.*, 42, 1, pp. 90-98, 1994). The first author uses a rectangular mesh and employs interpolation/extrapolation in going over upslope/downslope terrain. The second author uses a transformation where the coordinate lines are shifted parallel to the terrain in the vertical direction and remain distorted at large heights. This produces in a corrective term in the modified refractive index that increases with height. This is sometimes undesirable.

In the present approach, we solve the PE over terrain by using a a curvilinear coordinate system that is conformal to the terrain at the lower boundary and gradually degenerates into a Cartesian mesh away from it. The coordinate system is generated by the specification of the terrain elevation at discrete points. This coordinate system has the advantage of preserving the number of points on any vertical line regardless of the terrain slope and produces a corrective term in the refractive index that diminishes at the maximum height. We will show formulation and results for both the horizontal and vertical polarizations and compare with other models or measured results.

AMPLITUDE SCINTILLATION ON A 36 GHZ OVERWATER LINK

Jacques CLAVERIE - Ecoles de Coëtquidan (CREC) - 56381 GUER CEDEX - FRANCE

INTRODUCTION

Amplitude scintillation is an important phenomena when dealing with millimetric propagation within the Marine Boundary Layer (MBL). In the present paper, new experimental scintillation data are presented and analyzed in terms of C_n^2.

EXPERIMENTAL SETUP

The LORIENT (South coast of Brittany - France) 1993 campaign was organized by several NATO countries (AC 243/RSG 8-21/Comission 3) during the autumn of 1993. Among the various types of equipment, a completely overwater 36 GHz link was installed between the shore and a little island, 9.7 km distant. The antennas heights were 15.4 m and 8.05 m above the mean sea level at the emission and reception sites, respectively. Twice a day and for 30 minutes periods, the received signal was sampled at a 40 Hz frequency in order to compute the propagation path losses and particularly the amplitude scintillation power density spectra. An instrumented buoy also measured the "bulk" meteorological parameters.

THEORETICAL BACKGROUND AND MODELING

For millimetric line-of-sight links operating within the MBL, the observed scintillation is due to the sea movement (swell) and to the atmospheric turbulence. The agitation of the sea mainly affect the low frequency part of the amplitude scintillation spectrum. If the atmospheric turbulence follows the Kolmogorov's hypotheses, it should be responsible for a $f^{-8/3}$ decrease with a cut-off frequency related to the transverse wind speed.

For propagation studies, the atmospheric turbulence is described by the means of C_n^2, the refractive index structure constant which value can be deduced from the scintillation spectrum. C_n^2 is also computable from the bulk meteorological parameters values, using the PIRAM software that we developed for MBL propagation modeling and which is based upon the Monin-Obukhov similarity theory.

EXPERIMENTAL RESULTS AND FIRST CONCLUSIONS

In order to stay within stationary conditions for the propagation channel, the scintillation data are analyzed for each 5 minutes period. It is worth noting that the scintillation amplitude exceed sometimes 10 dB. The corresponding power density spectra are computed by averaging 11 consecutive spectra consisting of 1024 points FFT. The figure below shows a representative example of an experimental spectrum.

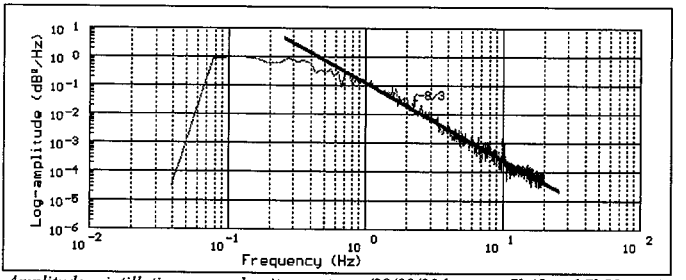

Amplitude scintillation power density spectrum (29/09/93 between 7h45 and 7h50 a.m.) The y axis corresponds to the normalized log-amplitude (maximum value set equal to 1)

For all the available data, the $f^{-8/3}$ decrease is verified. Except in the cases of low wind speed, the values of C_n^2 deduced from the scintillation data agree quite well with the ones provided by the PIRAM model. A more precise comparison is actually being undertaken in order to identify the meteorological situations that could probably explain the major discrepancies.

URSI G | Session 16 | Salon Jolliet

Propagation and Telecommunication - Part I
Co-chairs: B. Reinisch, USA and J.W. McDougall, Canada

13:10 16.1 FDTD Analysis of HF Propagation in the Ionosphere, **L.J. NICKISCH**[1], P. FRANKE[2], [1]*Mission Research Corporation, Monterey, CA and* [2]*Colorado Research Associates, Boulder, CO, USA*

13:30 16.2 The Performance of Several Pulsed and CW Spread-Spectrum Signals over HF Skywave, D.M. HAINES, **B.W. REINISCH**, *University of Massachusetts-Lowell, MA, USA*

13:50 16.3 Automatic Scaling of Digisonde Ionograms from Oblique Sounding, X. HUANG[1], **B.W. REINISCH**[1], A. FINN[2], R. BARNES[2], S. BRAENDLER[2], [1]*University of Massachusetts-Lowell, MA, USA;* [2]*Defense Science and Technology Organization, Salisbury, Australia*

14:10 16.4 Generalized Digisonde Drift Analysis (GDDA): Measuring the Full Velocity Field, J.L. SCALI[1], **B.W. REINISCH**[1], T.W. BULLETT[2], J.-S. GUO[3], [1]*University of Massachusetts-Lowell and* [2]*Phillips Laboratories, Hanscom AFB, MA, USA;* [3]*Center for Space Science and Applied Research, CAS, Beijing, China*

14:30 16.5 High Frequency Communications and Ionospheric Event Impacts, **D.P. ROESLER**, *Collins Avionics and Communications Division, Cedar Rapids, IA, USA*

14:50 16.6 Comparison of Observed Ionospheric Total Electron Contents with the Parametrized Ionospheric Model, R.O. CONKRIGHT[1], **K. DAVIES**[2], [1]*NGDC/NOAA and* [2]*SEC/NOAA, Boulder, CO, USA*

15:10 Coffee Break

15:30 16.7 High Latitude Ionospheric Observations during Winter Darkness, Using Ionosonde, Radar, and Sampled-Aperture HF Array Data, **J.W. MacDOUGALL**[1], D.J. DUMAS[2], H.G. JAMES[2], R.W. JENKINS[2], P. PRIKRYL[2], [1]*University of Western Ontario, London and* [2]*Communications Research Centre, Ottawa, ON, Canada*

15:50 16.8 Numerical Simulation of Nonlinear Effects in Ionospheric Propagation, **P.M. FRANKE**[1], L.J. NICKISCH[2], [1]*Colorado Research Associates/NWRA, Boulder, CO and* [2]*Mission Research Corporation, Monterey, CA, USA*

16:10 16.9 The Distance Determination in the Radiowaves Propagation by the Ionosphere, **S. KOSTIĆ**, Z. ŽIVKOVIĆ-DŽUNJA, *University of Novi Sad, Yugoslavia*

16:30 16.10 Nonparaxial Propagation of Localized Wave Packets in Ionospheric Waveguide, **N.I. PETROV**, *All-Russian Electrotechnical Institute, Istra, Russia*

G16.1

FDTD ANALYSIS OF HF PROPAGATION IN THE IONOSPHERE

L. J. Nickisch
Mission Research Corporation
10 Ragsdale Drive, Suite 201
Monterey, CA 93940-5776

Patricia Franke
Colorado Research Associates
3380 Mitchell Drive
Boulder, CO 80304

The Finite Difference - Time Domain (FDTD) technique is a powerful method for obtaining numerical solutions to electromagnetic propagation problems. The FDTD method solves the Maxwell equations directly in the time domain by temporal integration. No approximations beyond that of finite differencing are necessary. We have successfully removed certain restrictions which had formerly limited use of the FDTD method to frequency-independent media; the FDTD method can now be applied to propagation in the ionosphere. First we report on an interesting mechanism for the transfer of HF energy to the medium when an HF pulse transits a region of plasma containing structures which have a scale size near the HF wavelength. The mechanism is the result of polarization coupling and is not predicted by scalar wave analysis. Yet its effect can be quite pronounced for HF waves transiting regions of structured ionization. Secondly, we compare FDTD computations of HF backscatter from Field Aligned Irregularities to the predictions of Born Theory. We show that the usual Born scattering cross section formula requires modification (or at least a modified interpretation) for HF ionospheric propagation.

The Performance of Several Pulsed and CW Spread-Spectrum Signals Over HF Skywave

D. M. Haines and B. W. Reinisch
University of Massachusetts Lowell
Center for Atmospheric Research

It has been the desire of many serious users of the HF radio band (e.g. ground-to-air, ship-to-shore, mobile military units, and routine ground-to-ground services) to embed a channel evaluation signal, or even better, an entire oblique sounder capability into their communications equipment. With the development of digital signal generation by arbitrary waveform generators and direct digital synthesizers, the capability now exists to bundle the functionality of an oblique sounder into HF communications equipment using conventional analog AM, FM, or SSB, or newer digital modulation techniques. The selection of the communications signal is often dictated by the need for compatibility with conventional systems, however, the choice for the oblique sounding signal is still open.

The Digisonde Portable Sounder, or DPS, is capable of generating a large set of different waveforms with the additional flexibility of varying many of the waveform parameters under program control. With the recent addition of an FM/CW (chirp) waveform, the DPS is a unique testbed for analyzing the relative merits of various sounder waveforms. The DPS has been operated using phase coded and frequency modulated spread-spectrum radio signals during on-the-air bistatic testing. The waveforms evaluated are a simple rectangular pulse, a pulsed 8 or 16-chip PSK waveform, an FM/CW (chirp) waveform, a 127-chip PSK/CW, and a new method of pulse compression for PSK/CW which totally eliminates time-domain sidelobes. All of the DPS waveforms provide a measure of the time domain impulse response of the HF skywave channel which, if repeated at many frequency steps, produces an oblique ionogram. In addition to the time domain response, a Doppler spectrum is also formed at each frequency step, thus providing a three dimensional scattering function for the channel.

G16.3

Automatic Scaling of Digisonde Ionograms From Oblique Sounding

Xueqin Huang and Bodo W. Reinisch
University of Massachusetts Lowell
Center for Atmospheric Research

Anthony Finn, Rodney Barnes, and Shane Braendler
Defense Science & Technology Organization
Salisbury, Australia

Reliable automatic real-time scaling algorithm for vertical ionograms are in operation for a number of years, for example the ARTIST program in the Digisondes. This presentation describes a simple technique for the autoscaling of bistatic oblique ionograms that takes advantage of the existing ARTIST algorithm. All recent Digisondes are synchronized with GPS timing signals and pairs of Digisondes can and have been used for oblique sounding. When the distance is shorter than 900 km, the crossed-loop antenna array used for Digisonde receiving makes it possible to distinguish between ordinary and extraordinary waves. With the assumption that the ionosphere curvature can be omitted an oblique ionogram can be converted into the equivalent vertical ionogram at the mid point. Since a digital ionogram is a two-dimensional array of radar range versus frequency, tagged with echo amplitude and polarization, the equivalent vertical ionogram can be constructed by changing the frequency axis, f, from f to $f\cos\phi$, and the range axis, P', from P' to $P'\cos\phi$ - $R(1-\cos(D/2R))$, where R is the earth radius, ϕ the ionospheric incidence angle and D the surface distance. The resulting vertical ionogram is then scaled with ARTIST which determines the h'(f) traces, the ionospheric characteristics and the electron density profile representing the mid-point ionosphere.

This technique has applied to oblique ionograms from USA and Australia and it shows very good performance of the technique. The electron density profiles inversed from the equivalent vertical ionograms are compared with those obtained from oblique ionograms.

Generalized Digisonde Drift Analysis (GDDA): Measuring the full velocity field

J.L. Scali, B.W. Reinisch
University of Massachusetts Lowell
Center for Atmospheric Research

T. W. Bullett
Phillips Laboratories, Hanscom AFB.

Jian-Shan Guo
Center for Space Science and Applied Research
Chinese Academy of Sciences

Most single station techniques which calculate vector velocities from Doppler line of sight measurements, make the assumption of spatial and temporal uniformity in the plasma motion within the sampled volume. While the current Digisonde drift analysis (DDA) method does not need to assume temporal uniformity, the technique does rely on the assumption of spatial uniformity.

Since the Digisonde drift method obtains a large number of reflection sources within a relatively short time, combination analysis is used to develop a velocity field distribution. Given a set of N sources, and selecting r at a time to calculate a velocity, ${}^{N}C_{r}$ velocities are calculated. Combinations of sources from a dominant plasma motion would produce similar velocities, while combinations of sources from different plasma motions result in random velocities. The resultant distribution maps out a velocity field, where all main velocity components are identified.

In this paper the GDDA technique is applied to high latitude stations, where changes in the velocity structure have been shown to occur within 10 second periods as observed at Sondrestrom and Qaanaaq (Greenland). Temporal uniformity in general is not maintained at these high latitude regions, and without a proper measure of the magnitude of the vector velocities, the uncertainties in E-field measurements deduced from these velocities are large and may not reflect the true nature of the high latitude dynamics. The GDDA method when properly used, has enormous application to any system(s) where complex velocities are observed within the instrument's field of view.

G16.5

High Frequency Communications and Ionospheric Event Impacts

Daniel P. Roesler (Collins Avionics & Communications Division, Rockwell, Cedar Rapids, IA, 52498; Ph. 319-295-1551; e-mail: droesler@collins.rockwell.com)

High Frequency (2- to 30-MHz) radios operate in an area of the electromagnetic spectrum that supports ionospheric propagation. Signals being transmitted within the HF portion of the spectrum can be reflected by the layers of the earth's ionosphere allowing HF communications to be conducted over very long distances (100s to 10,000 kilometers). However, the densities of the reflective layers are variable and thus the ability of these layers to reflect HF signals changes from hour to hour. Sunspot cycle, season, and time of day are the major factors influencing benign diurnal propagation. Recent technological advances in the form of ALE (Automatic Link Establishment) have solved the diurnal frequency selection problem with appropriate network and frequency management support. However, the dynamically varying ionosphere under disturbed conditions (magnetospheric, auroral oval, and solar flare shock waves) can disrupt HF communications. Recent developments in ionospheric event monitoring and ionospheric storm tracking may be utilized to support global HF communications systems. The impacts and consequences to the C^4I infrastructure that HF communications supports will be discussed.

Comparison of Observed Ionospheric Total Electron Contents With the Parametrized Ionospheric Model

by R.O. Conkright [1] and K. Davies* [2]

[1] NGDC/NOAA, 325 Broadway, Boulder, CO 80303
[2] SEC/NOAA, 325 Broadway, Boulder, CO 80303

Abstract

We compare Faraday measurements of ionospheric total electron content (TEC) with corresponding TECs from the PIM which is a global ionospheric model based on first principles models. PIM covers the E and F layers (up to 1600 km) for all latitudes, longitudes, and times. The user-selected outputs include profile parameters (e.g., foF2, TEC), electron density profiles, and ion composition. The user can select one of two options in which the maximum electron density is obtained: (1) from PIM or (2) from the URSI numerical model. We compare TECs measured at Hamilton, MA over two sunspot cycles (1968 - 1990) with the TECs from the model. In general, the night PIM-TECs are in good agreement with the observed TECs especially in winter whereas, for high sunspot numbers, the noon PIM-TECs are less than the noon values at Hamilton.

G16.7

High Latitude Ionospheric Observations during Winter Darkness, Using Ionosonde, Radar, and Sampled-Aperture HF Array Data.

J.W. MacDougall , Department of Electrical Engineering,
University of Western Ontario, London, Ont., Canada, N6A 5B9
and
D. J. Dumas, H.G. James, R.W. Jenkins, and P. Prikryl
Communications Research Centre, P.O. Box 11490, Station H, Ottawa, Ont., Canada, K2H 8S2

Ionospheric data gathered by CADI ionosondes in the polar cap are examined together with signal-direction observations obtained from a sampled-aperture HF receiving array located in the high arctic observing signals over a polar cap path. Most of the examples are from a two-day period in January 1996. Information from the SuperDARN radars is also examined, to help establish the ionospheric conditions within the polar cap during this time interval.

For a portion of each of the two days, between 0500 and 1300 UT, the sampled-aperture results show changing directions indicative of irregular F-region ionospheric features moving in an approximately antisunward direction. Locations and velocities are inferred from the data. During these times, the CADI ionosondes show strong E-layer returns, not always overhead. F-layer returns are rarely seen at these times, but when seen, indicate relatively low electron densities. The visibility of E layer- propagated signals in the sampled-aperture data is examined. Moving features are observed in the ionosonde data at other times during the day.

The data from these portions as well as the remainder of the two days are discussed within the context of models for the high-latitude ionosphere which include moving large-scale ionospheric irregularities. The general features of the signal-direction observations, and also those seen in the CADI ionograms, can be reproduced by the modelling, which thus provides a conceptual basis for interpreting both types of data.

Some of the issues involved in doing radio propagation radio studies in the polar cap regions, and the required measurements for polar cap propagation studies will be discussed.

Numerical Simulation of Nonlinear Effects in Ionospheric Propagation

P M Franke
Colorado Research Associates/NWRA, Boulder CO 80304

L J Nickisch
Mission Research Corporation, Monterey, CA 93940

A direct numerical simulation of Maxwell's equations, including the effects of the plasma motion and heating, is used to characterize the nonlinear behavior associated with the ionospheric propagation of high-powered electromagnetic waves. These nonlinearities have been studied extensively through experiments at ionospheric heating facilities. Motivated by the possibility of exploiting the nonlinear properties to mitigate phenomena such as the blocking of HF signals by sporadic e-layers, numerical experiments were designed to investigate the behavior of different nonlinear terms, testing their sensitivity to system parameters, e. g. field strength, and electron concentration and profile.

Nonlinearities arise in this context through the modification of the plasma distribution by the incoming field itself, either through the motion imparted to the plasma or through heating. These effects are included in a finite-difference time-domain implementation of the Maxwell's equations through the constitutive relations. A conservation of momentum equation is used to calculate the motion of the plasma, this motion can then be related to the dipole moment of the plasma By including a continuity equation for the particles, the signal, if sufficient in strength, can move the particles around. The nonlinearities are introduced through the advective terms, which are usually ignored, in these two equations. Heating of the ionosphere can also introduce nonlinear effects by modifying both the collision frequency and the electron density of the surrounding plasma. All of these effects alter the medium in a manner proportional to the incoming electric field strength thereby modifying the propagation conditions for subsequent signals.

Results will be presented which show the propagation history of signals at HF frequencies through a variety of electron density profiles, and different field strengths. The effects of the nonlinearities can be illustrated by following the evolution of the frequency spectrum as the signal propagates. Nonlinearities will spread the energy from the forced frequency into other related frequencies. The conditions under which various phenomena such as "self-trapping" of the signal (soliton formation), cross- and inter- modulation of different signals, and scattering will be investigated.

G16.9

THE DISTANCE DETERMINATION IN THE RADIOWAVES PROPAGATION BY THE IONOSPHERE

Srdjan Kostić, B.S.
Zdenka Živković-Džunja, Ph.D.

University of Novi Sad
Faculty of Technical Sciences,
Institute for Power and Electronic Engineering
Fruškogorska 11
21 000 Novi Sad, Yugoslavia

Abstract

The ionosphere is defined as the part of the upper atmosphere in which free electrons are sufficiently numerous to influence the propagation of the radio waves. This paper examines the propagation path determination using the ray tracing technique for the radio waves reflected from the ionosphere. Ray tracing is the process of determining the path of an electromagnetic signal by the successive application of ray theory over series of thin homogenous slabs of medium. The ray tracing algorithm used in this paper is applied on the concentric model ionosphere with no magnetic field and for the HF band of the radio waves. Bouger's low may be applied to trace rays via a succession of thin concentric slabs of ionosphere. The most common application of the ray tracing is to find the position at which a ray launched into the ionosphere returns to earth.

The expressions of the distance determination in the radiowaves propagation are applied using corresponding literature. The application program "MATLAB" is used for solving these expressions. Same program shows the graphical 3D presentation of the influence of variations for the elevation angle of the radio wave and the height of the reflection layer into the ionosphere on the distance radio propagation. Also, it is significant to say that the paper observes the influence of the radiowaves frequency, the layer height and other more important factors on the refractive index of the reflection layer. According to this 3D figure, some conclusions are noted in this paper. As consequence, these conclusions give possibility for the correct choice of parameters for obtaining desired distance of the radio communication by the ionosphere.

Nonparaxial propagation of localized wave packets in ionospheric waveguide

N.I.Petrov
All-Russian Electrotechnical Institute,
19-39, Lenina str, Istra,
Moscow region, Russia
Phone: (096) 3153258; Fax: (095) 5603134; E-mail: alex@rdiees.msk.ru

It is known that an expansion of radiation field on the Gaussian beams is an effective method for the analysis of propagation of radiation in the ionospheric waveguides. Such approach speeds up analysis of field structure and estimation of wave effects. However the Gaussian beams keep their parameters during the propagation only in paraxial approximation.

In this paper the coherent states formalism is used for investigation of the nonparaxial propagation of wave packets in ionospheric waveguide with parabolic distribution of dielectric permittivity. Exact analitical expressions for the trajectory and width of nonparaxial wave packets are obtained. The length of the mode structure formation in ionospheric waveguide is determined.

It is shown, that the nonaxial wave beam diverges at the propagation in ionospheric waveguide and the trajectory of wave beam relaxes on the axis of the waveguide. The width of the beam increases only up to value determining by the axis displacement or incidence angle of the beam at initial plane. The length of mode structure formation decreases at the increasing of axis displacement or incidence angle of the beam, wavelength of radiation and gradient parameter of the waveguide. Note, that the mode structure formation length is more sensitive to the change of gradient parameter of medium.

URSI G **Session 31** Salon Jolliet

Radio Studies at High to Very High Latitude - Part I
Co-chairs: J.-P. St-Maurice, Canada and R. Behnke, USA

08:10 31.1 SuperDARN Observations of High-Latitude Ionospheric Perturbations Produced by Gravity Waves: A Case Study, **C.S. HUANG**, D.A. ANDRE, G.J. SOFKO, *University of Saskatchewan, Saskatoon, SK, Canada*

08:30 31.2 Observations of Plasma Structuring at Svalbard, **S. BASU**[1], E.J. WEBER[1], Su. BASU[2], E. MacKENZIE[3], P. DOHERTY[3], [1]*Phillips Laboratory, Hanscom AFB, MA,* [2]*National Science Foundation, Arlington, VA and* [3]*Institute for Space Research, Boston College, Newton, MA, USA*

08:50 31.3 A SuperDARN Study of Field-Aligned Current Structures near Magnetic Local Noon, **K.A. McWILLIAMS**[1], G.J. SOFKO[1], R.A. GREENWALD[2], W. BRISTOW[2], [1]*University of Saskatchewan, Saskatoon, SK, Canada;* [2]*The Johns Hopkins University, Laurel, MD, USA*

09:10 31.4 Are Cusp-Related, Double-Peaked Doppler Spectra Measurements with the SuperDARN HF Radar Mapping the LLBL?, **A. SCHIFFLER**, G. SOFKO, *University of Saskatchewan, Saskatoon, SK, Canada*

09:30 31.5 Small Versus Large Aspect Angle Effects on Farley-Buneman Turbulence in the Auroral E-Region, **A.M. HAMZA**, *University of New Brunswick, Fredericton, NB, Canada*

09:50 31.6 Auroral Scintillations: E or F Layer Dominated?, **J. AARONS**[1], B. LIN[1], M. MENDILLO[1], M. COLERICO[1], J. SCALI[2], B. REINISCH[2], T. BULLETT[3], A.S. RODGER[4], [1]*Boston University, Boston,* [2]*University of Massachusetts, Lowell and* [3]*Phillips Laboratory, Hanscom AFB, MA, USA;* [4]*British Antarctic Survey, Cambridge, UK*

10:10 Coffee Break

G31.1

SuperDARN Observations of High-Latitude Ionospheric Perturbations Produced by Gravity Waves: A Case Study

C. S. Huang, D. A. Andre, and G. J. Sofko
Institute of Space and Atmospheric Studies, University of Saskatchewan, 116 Science Place, Saskatoon, SK. S7N 5E2, Canada

We have used the Saskatoon HF radar to observe ionospheric perturbations produced by gravity waves. The main features of the perturbations are as follows. 1. There are two distinct range intervals from which strong radar scattered echoes are received. The near range interval is from 1000 to 1500 km, and the far range interval is from 2000 to 3000 km. The radar echoes in the two range intervals appear as periodic enhancements in the range-time-intensity (RTI) plots and have the same frequency spectra, implying that they have the same source mechanism. It is shown that the periodic radar echoes are caused by gravity wave modulation of ionosphere. 2. Ground scattered returns are from the near range interval. The velocity and width of the Doppler spectra are very small over this interval. In contrast, velocities and widths typical of ionospheric scatter are received from the far range interval. Accordingly, the echoes from the far range interval are due to ionospheric F region scattering. The periodic ionospheric echoes imply that small scale plasma wave perturbations, which cause the scattering, are generated in large scale ionospheric structures produced by gravity waves. 3. The ground scattered return exists from 15 UT to 24 UT. However, the ionospheric echoes become very weak around local noon (from 17 UT to 20 UT). The intensity of the ionospheric echoes decreases from high latitude to low latitude.

A theoretical model has been constructed to explain the observations. The gravity wave source is assumed to be in the cusp-cleft region near magnetic local noon. Gravity waves propagate to the F region and produce large-scale periodic density structures. The density gradient of the ionospheric structures close to the wave source is large enough for plasma instabilities to be generated, so that ionospheric scattering occurs. When gravity waves propagate to regions far from the wave source, the wave-induced ionospheric structures are weak since the wave amplitude is smaller. Consequently, no small scale plasma instability is excited and only ground scatter is observed. We have calculated numerically both the ionospheric density perturbations produced by gravity waves at the high latitudes and the resulting HF ray paths in the perturbed ionosphere. It is shown that for reasonable parameters of gravity waves, the amplitude of relative fluctuations in the ionospheric electron density may reach 50% or higher. Small scale perturbations may be generated by plasma instabilities in the steep gradient regions of the large scale structures. It is found that some HF rays may be "trapped" in the periodically perturbed ionosphere and travel large distances to the scattering region. Thus, HF radars may receive simultaneously both ground-scattered signals associated with large-scale gravity wave-induced perturbations and ionospheric echoes from the resulting small scale electron density irregularities. The simulation results provide a good explanation of the Saskatoon HF radar observations.

OBSERVATIONS OF PLASMA STRUCTURING AT SVALBARD

S. Basu* and E.J. Weber (Phillips Laboratory, PL/GPIA, 29 Randolph Road, Hanscom AFB, MA 01731), Su. Basu (National Science Foundation, Arlington, VA 22230), E. MacKenzie and P. Doherty (Institute for Space Research, Boston College, Newton, MA 02159)

The occurrence and distribution of structured plasma in the F-region of the ionosphere near the the cusp/cleft region is reported. This study is performed by measuring the effects of these irregularities on the amplitude scintillation of 250 MHz signals from quasi-stationary polar beacon satellites which are recorded by the Phillips Laboratory at Ny Alesund, Svalbard (78.9° N, 11.8° E; 75.7° CGMLAT). These measurements are augmented by the use of the dual frequency (1.2/1.6 GHz) GPS carrier phase data obtained from the International GPS Geodynamic Service (IGS) managed by the Jet Propulsion Laboratory (JPL) at the same station. The 250 MHz amplitude scintillation data recorded at 50 Hz yielded information on irregularities with scalelengths ranging from a few km to 100 m. On the other hand, the GPS carrier phase data obtained at one minute intervals provided information on phase fluctuations caused by the irregularities with typical scalelengths greater than 10 km. Under magnetically quiet conditions, the GPS satellite constellation data indicated the presence of weak irregularities around magnetic noon at Ny Alesund primarily poleward of the station. Under magnetically active conditions, strong irregularities with the time rate of change of the total electron content (TEC) exceeding $2x10^{16}$ m^{-2} min^{-1} were obtained and the band of irregularities extended equatorward and poleward of Ny Alesund to cover the magnetic latitude interval of 71° - 78° around magnetic noon. The 250 MHz measurements indicated, in general, a moderate enhancement of amplitude scintillation on active days for several hours at similar local times. The ground-based optical and satellite in-situ data associated with the above irregularity structures detected by the GPS and polar beacon satellite observations are interpreted in the context of current theories of irregularity generation at high latitudes.

G31.3

A SuperDARN Study of Field-Aligned Current Structures near Magnetic Local Noon

K. A. McWilliams* and G. J. Sofko, Institute of Space and Atmospheric Studies, University of Saskatchewan, 116 Science Place, Saskatoon, SK, Canada S7N 5E2, ph. 306-966-6444, fax 306-966-6400, e-mail: mcwilliams@dansas.usask.ca.

R. A. Greenwald and W. Bristow, The Johns Hopkins University Applied Physics Laboratory, Johns Hopkins Road, Laurel, MD, USA 20707, ph. 301-953-5408, fax 301-953-6670, e-mail: ray_greenwald@jhuapl.edu

The magnetospheric component of the field-aligned current (FAC) profiles in the high-latitude *F*-region can be determined from the vorticity of the ionospheric plasma convection velocities measured by SuperDARN. The implementation of an ionospheric conductivity models makes it possible to estimate the total FAC within the radar field of view. On the dayside, several hours away from noon, there is evidence of three "normal" current systems - Region 2, Region 1, and Region 0. In the vicinity of magnetic local noon, however, the systems are more complex. The validity of the latitudinal ionospheric Pedersen FAC closure of the Region 1 current through the Region 2 and Region 0 currents was tested. The negative results of the current closure analysis, in addition to the general trends seen in the morphology of these dayside FAC structures, led to the postulation of a magnetospheric-ionospheric noon current system, when there was frontside reconnection of the interplanetary magnetic field and the magnetosphere, with a considerable degree of longitudinal closure in the ionosphere. The ionospheric segment involves a Pedersen closure current which flows eastward across the throat joining the morning and afternoon convection reversal regions. The current then flows out of the ionosphere as a postnoon Region 1 system to the inner edge of the low-latitude boundary layer (LLBL) in the magnetosphere, westward across noon in the LLBL and then into the ionosphere as morning-side Region 1 current. The LLBL portion of this current and the eastward magnetopause current across noon combine to generate magnetic flux which counteracts the flux erosion caused by frontside reconnection.

Are Cusp-related, double-peaked Doppler spectra measurements with the SuperDARN HF radar mapping the LLBL?

Andreas Schiffler
Institute of Space and Atmospheric Studies, University of Saskatchewan, Saskatoon, Canada

George Sofko
Institute of Space and Atmospheric Studies, University of Saskatchewan, Saskatoon, Canada

Abstract. The Saskatoon SuperDARN HF radar has been used to measure Doppler velocity spectra of backscatter from the F-layer. Parametric spectral estimators and a special multipulse sequence improved the resolution of the spectra. A distinct double-peaked (D-P) spectral signature was found in spatially localized regions. A statistical analysis of the features reveals a pattern that maps the northward edge of the auroral oval and concentrates around the cusp. A comparison with DMSP SSJ/4 particle data suggests a strong spatial correlation between the D-P spectra and spatially structured (10–70 km) regions of soft-electron precipitation (several hundred eV) in which the fluxes are high 2–5 $ergs/cm^2/s$. Several generating mechanisms for the D-P spectra are presented, including vortical plasma flows. The comparison with DMSP particle-data classification in the pre-noon sector, shows that the location of the D-P spectral features corresponds to the region just inside the magnetopause, in the outer portion of the low latitude boundary layer (LLBL). The results suggest that the radar can be used to monitor this important region, in which the direct interaction between the shocked solar wind and the magnetosphere is occuring, over a large area in real-time.

G31.5

Small Versus Large Aspect Angle Effects On Farley-Buneman Turbulence in the Auroral E-region .
A. M. Hamza , *University of New Brunswick* —
The nonlinear coupling of three Farley-Buneman waves with finite $k_{\parallel}$, is investigated using a low-order dynamical system model. In the present calculation we return to the conventional three-wave approximation but refine the physics included. Indeed, we keep the parallel currents associated with the three Farley-Buneman waves as dynamical variables. The finite $k_{\uparrow} \parallel$ effects are of two types. On one hand, the waves become dispersive and the nonlinear coupling does not neccessarily satisfy the frequency matching condition. On the other hand a new nonlinearity comes into play, leading to lower effective turbulence levels. Both effects are included in our analysis, and it is shown that large aspect angle echoes can indeed be excited and maintained at an observable level. We also evaluate the parallel ohmic heating $J_{\parallel}E_{\parallel}$ and show that there is significant ohmic heating associated with large aspect angle echoes as compared to small aspect angle cases. The low-dimensional dynamical system has even more potential than just suggesting a possibility for the excitation of large aspect angle echoes. It is also possible to investigate the route to full turbulence, namely study the transition to turbulence. Does it occur through period doubling or through a Ruelle-Takens picture: steady state $\rightarrow$ periodic solution $\rightarrow$ doubly periodic solution $\rightarrow$ turbulence. We should also point out that we the conventional zero aspect angle results by taking the limit of very small $k_{\parallel}$.

AURORAL SCINTILLATIONS: E OR F LAYER DOMINATED?

J. Aarons, B. Lin, M. Mendillo, M. Colerico
Boston University, Boston, MA

J. Scali, B. Reinisch,
Univerasity of Massachusetts, Lowell, MA

T. Bullett, Phillips Laboratory, Hanscom AFB, MA

A. S. Rodger, British Antarctic Survey, Cambridge,England

In case studies of magnetic storms which produced auroral region phase fluctuations on GPS signals, the question was asked of sounder observations whether E or F layer irregularities dominated at specific times in the evolution of the storm effects. For one storm, March 3-5, 1995 allsky-imager data from Millstone Hill, Massachussetts and Goose Bay, Labrador showed SAR arcs and aurora. Sounder data from Millstone Hill and Goose Bay and GPS phase fluctuations from Greenbelt, Maryland, Millstone Hill and St. Johns were available for this period. Other storms were also studied. In addition Halley Bay sounder data were analyzed for these periods. When phase fluctuations appeared on the GPS data during magnetically quiet periods before the storm, foF2 was considerably higher than foEs. When phase fluctuations on GPS appeared early in the development of the storms studied, foF2 was again considerably higher than the critical frequency of the observed auroral E layer, foE. A period of time followed when the two were equal and short bursts of time when foE or foEs was larger than foF2. A thick auroral E layer develops during some periods of storms. However there were times when auroral absorption made sounder data unavailable.

Irregularity intensities are controlled by instability parameters operating on the electron density in various regions. Recent observations of energetic particle precipitation have established that several different regimes operate in various sectors of the auroral region during a storm. Particle data have shown a variety of flux levels of soft and hard particles. The thickness of the E and F layers must be estimated to assess their individual contributions to the amplitude and phase scintillation.

Studies of irregularity intensities have found mechanisms for both E and F layer instabilities including shears, high velocity plasma, precipitation, and electron density gradients. The questions remain only partially answered but the use of multi-sensors appears to point to several instability sources, each dominating in the different areas and in different phases of magnetic storms.

URSI G — Session 48 — Salon Jolliet

Radio Studies at High to Very High Latitude - Part II
Co-chairs: J.-P. St-Maurice, Canada and R. Behnke, USA

13:10	48.1	The Role of a Polar Cap Observatory in Radio Studies of the Very High Latitude Ionosphere, **J.D. KELLY**, *SRI International, Menlo Park, CA, USA*
13:30	48.2	The Auroral *E*-Region during a Highly Disturbed Day, **J-P ST-MAURICE**[1], W. KOFMAN[2], C. CUSSENOT[2], [1]*University of Western Ontario, London, ON, Canada;* [2]*CEPHAG, St. Martin d'Heres, France*
13:50	48.3	Electron Heating Effects in the Sunlit Polar E Layer as Measured with the Sondrestrom Incoherent-Scatter Radar, **R.T. TSUNODA**, *SRI International, Menlo Park, CA, USA*
14:10	48.4	The Effect of Electron-Neutral Energy Exchange on the Fluid Farley-Buneman Instability Threshold, **R.S. KISSACK**, J-P ST-MAURICE, D.R. MOORCROFT, *University of Western Ontario, London, ON, Canada*
14:30	48.5	Determination of F-Region Gravity Wave Sources with the SuperDARN Radars, **G.E. HALL**, J.W. MacDOUGALL, J.P. ST-MAURICE, D.R. MOORCROFT, *University of Western Ontario, London, ON, Canada*
14:50	48.6	Radio-Optical Characteristics of Polar F-Layer Patches, **D.J. McEWEN**[1], J.W. MacDOUGALL[2], [1]*University of Saskatchewan, Saskatoon, SK and* [2]*University of Western Ontario, London, ON, Canada*
15:10		Coffee Break
15:30	48.7	Observations of 50-MHz Broad and Highly Shifted Coherent Echoes at Large Magnetic Aspect Angles, **A.V. KUSTOV**, G.J. SOFKO, *University of Saskatchewan, Saskatoon, SK, Canada*
15:50	48.8	Theoretical and Experimental Investigations of Radio Wave Scattering from High-Latitude Irregularities, **N.B. MYERS**, S.P. YUKON, T.J. TANIGAWA, S.L. MATTHEWS, J. ERNSTMEYER, *Rome Laboratory, Hanscom AFB, MA, USA*
16:10	48.9	Dual-Radar Natural Plasma Line Observations at EISCAT, **B. ISHAM**[1], C. LA HOZ[2], [1]*Arecibo Observatory, Arecibo, Puerto Rico;* [2]*The Auroral Observatory, Tromsø, Norway*
16:30	48.10	Determination of Electron Density Profiles Using the SuperDARN Radars, **D. ANDRE**[1], G.J. SOFKO[1], M.J. McKIBBEN[1], K.B. BAKER[2], [1]*University of Saskatchewan, Saskatoon, SK, Canada;* [2]*JHU/Applied Physics Laboratory, Laurel, MD, USA*

G48.1

The Role of a Polar Cap Observatory in Radio Studies of the Very High Latitude Ionosphere

John D. Kelly
Geoscience and Engineering Center
SRI International
Menlo Park, CA 94025 USA

An incoherent-scatter radar located in the northern polar cap is essential for continued progress in understanding the Sun's influence on the structure and dynamics of the upper atmosphere. The anticipated Polar Cap Observatory (PCO), to be located at Resolute Bay, NWT, will be able to probe the very high latitudes of the ionospheric region that is often exposed to the interplanetary medium. These unique measurements are essential to understanding the fundamental processes that are critical to the CEDAR Polar Aeronomy Initiative and the Space Weather Program. For example, measurements of the polar cap convection and cross cap potential are an indication of direct coupling of the solar wind and the terrestrial ionosphere. These measurements will allow the determination of the response time to establish a new convection pattern following a change in IMF. These experiments will be complemented by coordinating with other major observatories including Sondrestrom, Svalbard, EISCAT, Millstone Hill, and SuperDARN. For example, the combined observations with these facilities will allow much of the auroral oval and polar cap ionosphere to be examined simultaneously under a variety of solar wind conditions. These multipoint measurements will greatly assist with the studies such as substorm evolution and should therefore contribute to the ultimate space weather goal of prediction.

Other research goals for the PCO include polar cap ionospheric response to magnetic storms, polar cap patches, ionospheric current systems, auroral emissions, and neutral and ion composition. Although whenever possible data from multiple sensors will be used to provide a "collective, multi-dimensional view of the polar upper atmosphere", the incoherent scatter radar by itself should contribute substantially to these research goals.

THE AURORAL *E*-REGION DURING A HIGHLY DISTURBED DAY

J-P St-Maurice
Department of Physics and Astronomy
U. of Western Ontario, London, Ontario N6A 3K7, Canada
W. Kofman, and C. Cussenot
CEPHAG, BP 46, 38402 St. Martin d'Heres, France

We have studied EISCAT *E*- and *F*-region data from a particularly disturbed day recorded in April 1990. During a 30-hour time interval, the electric field stayed stronger than 25 mV/m. For a brief period of time a value in excess of 200 mV/m could even be inferred from the *F*-region ion temperatures and from unusually large line-of-sight ion drifts even at 100 km altitude. The largest values were reached in the middle of a 4-hour time interval during which the electric field was almost always equal to or greater than 75 mV/m.

We studied the connection between observed *E*-region electron and ion temperatures and the ambient dc electric fields. The electric fields were inferred directly (but infrequently) using ion drift measurements from multiple radar receivers. The fields were also inferred much more frequently from a study of the ion temperature profile. We found that the bulk of the electron *E*-region temperatures depended on the electric field in a way that was reasonably close to that which has become expected from the empirical description proposed in (T.R. Robinson, J. Atm. Terr. Phys., 48, 417, 1987). However, there were also anomalies with much larger electron temperatures than expected from earlier studies. Often, the anomalies coincided with *F*-region ion temperatures that were smaller than expected. In these cases the culprit seemed to be a low altitude *F*-region neutral wind of the order of 300 m/s. Indeed, the field-aligned ion velocities differed systematically between normal and anomalous events. The difference could be explained with the notion of a drag from the inferred neutral wind.

A different set of *E*-region temperature anomalies was also found in regions with very low *E*-region densities just prior to large and sudden jumps in the *E*-region electron density. In those cases both the *E*-region ion and electron temperatures were much higher than anticipated from *F*-region ion temperatures or electric field measurements. This raised the possibility of strong gradients in the electric fields in regions of large *E*-region conductivity depletions.

We also looked for evidence for ion heating by unstable plasma waves in the unstable *E*-region. However, since the ion and neutral masses are comparable, the expected temperatures increases should be of the order of 100 K, 200 K at best (under similar conditions electrons undergo 1000 K types of changes). The small ion temperature increases made a detection of the theoretically expected much more tentative. Nevertheless, our preliminary results do indicate that the ions are heated by the waves at a rate comparable to theoretical expectations.

G48.3

Electron Heating Effects in the Sunlit Polar E Layer as Measured with the Sondrestrom Incoherent-Scatter Radar

Roland T. Tsunoda
Geoscience and Engineering Center
SRI International
Menlo Park, CA 94025 USA

It is well known that the electron temperature in the E region of the ionosphere, around 110 km, can become greatly elevated when the ionospheric electric field strength is large. Heating is believed to be produced by a modified two-stream instability that becomes operative under these conditions. While the source mechanism for electron heating appears to have been identified, little is yet known about the heating characteristics. For example, we do not know how the electron temperature varies with either the strength of the electric field or the background plasma density, or both. A reason for this difficulty in characterizing the heating is that incoherent-scatter radar measurements of electron temperature are made in the auroral region where the electric field and plasma density tend to be anticorrelated, a situation which makes it difficult to separate the dependence on either parameter. Another reason is that the extraction of electron temperature from incoherent scatter data becomes difficult because the signal-to-noise ratio decreases as the electron-to-ion temperature ratio is raised.

In this paper, we present a new method of estimating the electron temperature in a sunlit E layer under large electric-field conditions. Because the electron density and raw power are related through the temperature ratio, we show that the electron-to-ion temperature ratio can be estimated directly from the raw power measurements if we know the plasma-density profile of the E layer under magnetically quiet conditions. By using this method, we show that we are able to obtain estimates of electron temperature with good altitude and time resolution. Results from a case study are presented. This technique is applied to measurements made with the Sondrestrom incoherent-scatter radar on a day (3 October 1994) when the electric field strength exceeded 150 mV/m. The characteristics of the electron temperature profile as a function of time are presented and discussed with reference to the modified two-stream instability.

THE EFFECT OF ELECTRON-NEUTRAL ENERGY EXCHANGE ON THE FLUID FARLEY-BUNEMAN INSTABILITY THRESHOLD

R. S. Kissack, J-P St-Maurice and D. R. Moorcroft
Department of Physics and Astronomy
U. of Western Ontario, London, Ontario N6A 3K7, Canada

The traditional equation for the linear instability threshold phase speed v_{ph} of Farley-Buneman waves in terms of electron and ion temperatures is $v_{ph}^2=(\gamma_e T_{e0}+\gamma_i T_{i0})/m_i$, with γ_e and/or γ_i taken to be identically unity or 5/3, depending on whether the electrons/ions are assumed to behave isothermally or adiabatically. A generalized fluid treatment of Farley-Buneman waves has allowed us to study modifications to the threshold phase speed through the inclusion of electron thermal effects associated with the electron temperature dependence of the electron-neutral collision frequency, as well as electron collisional energy exchange with the neutral background. The results are presented in a form which makes manifest their consistency with earlier, less general treatments. Out of this generalized v_{ph}^2 equation, an equation for an "effective γ_e" is presented. Our analysis of its behavior leads to simple criteria to indicate when electron-neutral collisional energy exchange is important, and at what wavelength departures from isothermality become significant. Our principal results are that (1) in general, γ_e depends on wavelength, aspect angle, electron and ion temperatures, and the form of the electron-neutral interaction; (2) perturbed heat flow effects can at times be important for wavelengths down to 1 to 2 meters; (3) collisional energy exchange is important at smaller aspect angles and for longer wavelengths, as well as at higher temperatures and lower altitudes; (4) the electrons can never behave adiabatically; (5) the maximum value of γ_e under normal experimental conditions is approximately 1.2; (6) while $\gamma_e \simeq 1$ when $T_{e0} \simeq T_n$, for elevated electron temperatures γ_e can even become negative. The negative values can apparently only be reached at small aspect angles and at long wavelengths, and only under certain circumstances. Nevertheless, it is even possible to have $(\gamma_e T_{e0}+T_{i0})/m_i<0$. This indicates that thermal effects can trigger a different kind of instability at long wavelengths.

G48.5

Determination of F-region Gravity Wave Sources with the SuperDARN Radars.

G. E. Hall, J. W. MacDougall, J. P. St.-Maurice, and D. R. Moorcroft,
Department of Physics, University of Western Ontario, London, Ont., N6A 5B9

For this study, we examined data from the SuperDARN radars at Saskatoon and Kapuskasing in Canada and from the Canadian Advanced Digital Ionosconde (CADI). The SuperDARN system is a worldwide set of HF radars designed for study of high-latitude convection, with radars in both the northern and southern high-latitude regions. Each of these radars yield maps of backscattered power over 16 beams 3.2° wide and for ranges from 180 to 3000 km.

It has been found that sometimes the signal is totally deflected by the ionosphere and then back-scattered by the ground (ground-scatter). It has been shown by Samson et al (J. Geophys. Res., 95, 7693-7709, 1990) that this ground-scatter is modulated by F-region gravity waves causing focusing of the reflected power. Hence an analysis of the ground scatter provides a means to obtain the gravity wave phase velocities.

We present a new method for obtaining F-region gravity wave source positions and times using the SuperDARN radars. For this method, we find the lines of power maxima on range-time plots, which gives the line-of-site gravity wave phase fronts, for each of the 16 beams. The line-of-site of all of the beams yields the propagation direction and velocity for the gravity wave package. In principle, the source location should be given by the curvature of these phase fronts. However, as this was usually not sufficiently accurate, the source positions and times were determined from the dispersion of these wave packets. Once the source position was determined with the Saskatoon SuperDARN, the same process was used to find the source position and time from the Kapuskasing SuperDARN, in order to check consistency.

The gravity wave features are observed to agree with those observed with the Canadian Advanced Digital Ionosconde (CADI) radars which make spot measurements of gravity wave direction and velocity. We found that the gravity wave source positions occurred in the auroral region during periods of weak, localized magnetic fluctuations as observed by magnetometer.

RADIO-OPTICAL CHARACTERISTICS OF POLAR F-LAYER PATCHES

D. J. McEwen,
Dept. of Physics, University of Saskatchewan, Saskatoon, Sk., S7N 5E2
J. W. MacDougall,
Dept. of Electrical Eng., University of Western Ontario, London, Ont., N6A 5B9

One of the dynamic features of the polar ionosphere is the appearance of large plasma patches drifting across the polar cap in an antisunward direction. They are regularly seen over Eureka, Canada (80N, 86W) during the winter (dark) months optically from their 630 nm. emission (McEwen, D. J., and D. P. Harris, Radio Science 31,619-628, 1996) and with a digital ionosonde (Grant et al., Radio Sci., 30, 1537-1549, 1995) due to their enhanced electron density. They appear typically as ionized blobs from 100 to > 1000 km in diameter, with intensities of 50-500 R above airglow background and with electron densities a few times higher than ambient. Previous studies have demonstrated that they appear only when the Interplanetary Magnetic Field (IMF) Bz component is Southward and that they originate in the dayside ionosphere. The mechanism for their entry into the polar cap is as yet not well established. From our vantage point at Eureka, near the north magnetic pole, they are seen at all UT hours, but with frequency and brightness diminished now at solar sunspot minimum.

A study was made of the relationships between the heights, electron densities and optical parameters of some 75 patches observed with the two instruments during the winter solstice months of 1993 and 1994. This showed the patch brightnesses to be proportional to their electron density (over brightnesses ranging from 50 to 500 R). The lower threshold of detectability in both instruments was similar (about 50R brightness and 5×10^{10} el/m^3 density. There was no pronounced correlation between patch height and emission brightness. Patch virtual reflection heights ranged from 220 to 350 km. The brightest patches were all below 300 km. in virtual height.

These results will be discussed in relation to patch morphology and lifetimes, and to their characteristics as determined by spacecraft observations.

References

G48.7

Observations of 50-MHz broad and highly shifted coherent echoes at large magnetic aspect angles

A. V. Kustov and G. J. Sofko
Institute of Space and Atmospheric Studies
University of Saskatchewan, Saskatoon, Canada

Recent observations of 50-MHz auroral coherent echoes by the SAPPHIRE radar system at large geometrical aspect angles of 8-17^0 revealed that broad echoes (with Type 2-like spectral width) frequently occurred at large mean Doppler shifts, sometimes exceeding even the ion-acoustic speed. These echoes were observed along the electrojet direction and, because of this, were associated with large off-perpendicular nonlinear Farley-Buneman modes. In this paper, several individual events were considered when the broad highly shifted echoes were observed in a significant portion of the SAPPHIRE radar field of view. A threshold effect was found in which the echo onset required a magnetic disturbance of at least 400 nT. A very weak decrease of echo power with aspect angle (1 dB per degree) was noticed. Typically, the highly shifted echoes from along the electrojet were broader than simultaneous echoes perpendicular to the electrojet direction. For some events, a spectral width increase with aspect angle was inferred. The width increase appeared to saturate at large mean Doppler shifts. The mean Doppler shift of these echoes was found to vary significantly across the SAPPHIRE field of view, indicating the possible importance of aspect and flow angle effects. Broad and highly shifted echoes were typically skewed positively for positive mean Doppler shift, in contrast to the negative skewness of simultaneous echoes observed perpendicular to the electrojet direction. No definitive aspect angle variation of this spectral asymmetry was found. Presented results suggest that large off-perpendicular Farley-Buneman modes do not exhibit resonant peaks at the ion-acoustic speed (as known for modes propagating across the magnetic field) but rather spread in their velocities around this value.

Theoretical And Experimental Investigations Of Radio Wave Scattering From High-Latitude Irregularities

*N.B. Myers, S.P. Yukon, T.J. Tanigawa, S.L. Matthews, James Ernstmeyer
Rome Laboratory, 31 Grenier St, Hanscom AFB, MA 01731-3010

An experiment designed to measure the frequency coherence of signals that have been scattered from large scale field-aligned irregularities was performed in September, 1995. The experiment was planned to take advantage of naturally occurring ionospheric irregularities in the auroral oval in Alaska, as well as artificial ionospheric irregularities created by the High Power Auroral Stimulation (HIPAS) ionospheric heater located near Fairbanks, Alaska. A 1-kW steerable log periodic transmitter was located in southeastern Alaska. Three receivers were placed in separate locations in Alaska to provide various scattering angles for probe signals scattered from ionospheric irregularities. An FM/CW waveform was used by the channel probe system to provide range/Doppler information in order to identify propagation modes and to determine the ionospheric effect on each mode by measuring the doppler spreading of the probe signal. The channel probe system was capable of operating between the frequencies of 6 and 30 MHz. Theoretical calculations showed that frequencies larger than 10 MHz would have little chance of being measured on the ground. This is due to the inclination angle of the Earth's magnetic field and the requirement of near-specular scattering to produce large enough amplitudes of the scattered signals to be above the natural background noise level. For the geometry of the experiment, significant refraction of the probe signal was necessary in order to place the specular scattering cone on the Earth's surface. Thus, with the typical magnitude of the nighttime ionospheric density, only the lower frequencies could be expected to be refracted significantly and subsequently measured. Support diagnostics were available that included a digisonde near Fairbanks, and the auroral backscatter measurements of the High Latitude Monitoring Station, located at Elmendorf AFB, Alaska. While no measurements were made that could be identified with signals scattered from the irregularities generated from the HIPAS ionospheric heater, measurements were obtained of signals scattered from the auroral oval.

G48.9

Dual-Radar Natural Plasma Line Observations at EISCAT

B. Isham *
Arecibo Observatory, P.O. Box 995, Arecibo PR 00613, Puerto Rico (USA)
phone +1-809-878-2612, fax +1-809-878-1861, e-mail isham@naic.edu

C. La Hoz
The Auroral Observatory, N-9037 Tromsø, Norway
phone +47-77-64-51-61, fax +47-77-64-55-80, e-mail cesar@phys.uit.no

In recent years there has been renewed interest in making use of the natural incoherent scatter plasma line as an aeronomical diagnostic tool. While frequency and intensity measurements provide accurate information on the electron density and energetic particle spectrum, the reliable use of two plasma lines (up and downshifted, bistatic, or dual radar) to measure electron temperature and field-aligned current has proved elusive. As a result, various authors have noted that the standard Langmuir dispersion equation appears to be inadequate for use in interpreting incoherent scatter data from the ionosphere, and it has been suggested that an additional term or terms in the equation may be required.

EISCAT observations have recently been made of the natural photoelectron-enhanced plasma line using the UHF (931 MHz) and VHF (224 MHz) incoherent scatter radars. These radars have k vectors of 19.5 m^{-1} and 4.69 m^{-1}, respectively, and thus probe the plasma at two significantly different scale sizes. During the measurements an HF pulse was transmitted for 0.2 s every 10 s, and the resulting HF-enhanced plasma line was used as a marker for the desired electron density. The chirped plasma line technique was then used to obtain the natural plasma line spectrum. To our knowledge these are the only plasma line data to have been taken with two radars simultaneously. The data can be used to investigate the Langmuir wave dispersion relation in the ionospheric plasma.

G48.10

Determination of electron density profiles using the SuperDARN radars.

D. Andre*, G.J. Sofko, M.J. McKibben
Institute of Space and Atmospheric Studies
University of Saskatchewan
116 Science Place
Saskatoon, Canada S7N 2E5

K.B. Baker
JHU/Applied Physics Laboratory
Johns-Hopkins Road
Laurel, MD 20723

The main purpose of the SuperDARN radars is the monitoring of the ionospheric electric field over a wide area. They do this via measuring the autocorrelation function of ionospheric instabilities in the HF wavelength range. In order to determine the heights of backscatter occurrence an interferometer array has been installed so that the radars can also measure the angle of arrival of the backscattered radiation. The calibration of the interferometer is facilitated by meteor echoes which occur in abundance at short ranges. We have been using the angle of arrival measurements in conjunction with groundscatter to determine electron density profiles in the E and the F region. Ground scatter occurs when the radar rays are refracted back to the Earth by the ionosphere, where part of it is scattered back to the radar due to the surface roughness. For a spatially uniform ionosphere the relation beween angle of arrival and slant range starts at low angles of arrival and great slant ranges and varies to high angles of arrival and small slant ranges in a roughly parabolic shape up to a cutoff angle, above which the radar rays penetrate the ionosphere. The exact location of this curve depends predominantly on the maximum electron density in the ionosphere and the height of the maximum, and to a lesser degree on the layer width. Electron density profiles can be determined for each radar beam with a time resolution of 10 minutes or better at all times, when there is a band of ground scatter around 1000km slant range (E-region) or 2000km slant range (F-region).

URSI G **Session 62** **Salon Jolliet**

Ionospheric Modeling and Lower Latitude Irregularities - Part I
Co-chairs: C. Fesen, USA and E. Kudeki, USA

13:10 62.1 **Invited:** Simultaneous Meteor Observations by Powerful UHF and VHF Radars, **Q.H. ZHOU**[1], P. PERILLAT[1], J.Y.N. CHO[1], J.D. MATHEWS[2], M.C. KELLEY[3], [1]*Arecibo Observatory/NAIC, Arecibo, Puerto Rico;* [2]*Pennsylvania State University, PA and* [3]*Cornell University, Ithaca, NY, USA*

13:30 62.2 **Invited:** Coherent Scatter Radar Imaging Experiments at Jicamarca, **D.L. HYSELL**, *Clemson University, Clemson, SC, USA*

13:50 62.3 **Invited:** The Intermediate Tidal Ion Layer, Ion Rain, and F-Region Instabilities, **J.D. MATHEWS**[1], D.W. MACHUGA[1], M.P. SULZER[2], [1]*Penn State University, University Park, PA, USA;* [2]*Arecibo Observatory, Arecibo, Puerto Rico*

14:10 62.4 **Invited:** Two-Stream Waves in the E-Region Ionosphere Nonlinearly Drive Large-Scale D.C. Currents, **M. OPPENHEIM**, *University of Colorado, Boulder, CO, USA*

14:30 62.5 **Invited:** F-Region Incoherent Scatter Electric Field Measurements at Jicamarca, **E. KUDEKI**[1], S. BHATTACHARYYA[1], R.F. WOODMAN[2], [1]*University of Illinois at Urbana-Champaign, Urbana, IL, USA;* [2]*Jicamarca Radio Observatory, Lima, Peru*

14:50 62.6 Critical-Frequency Variations in the Midlatitude Ionospheric F2-Region and Prediction of Them, **I.G. ZAKHAROV**, O.F. TYRNOV, *Kharkiv State University, Kharkiv, Ukraine*

G62.1

Simultaneous meteor observations by powerful UHF and VHF radars

Qihou H. Zhou, Phil Perillat, and John Y. N. Cho
Arecibo Observatory, NAIC, Arecibo, Puerto Rico
John D. Mathews
CSSL, The Pennsylvania State University, State College, PA, USA
Michael C. Kelley
School of Electrical Engineering, Cornell University, Ithaca, NY, USA

We have used the Arecibo 430 MHz incoherent scatter radar and the 47 MHz radar to study meteor echoes. The two antennae are colinearly mounted so that the two beams share the same center. Both radars operate monostatically using the same 300 meter in diameter dish. For the simultaneous UHF/VHF observations made in the early morning of September 29, 1994, the 430 MHz transmitter and the 47 MHz transmitter were operated at a peak power of about 1.5 MW and 20 KW respectively. The transmitted pulses, identical for the two systems, had a width of 2 μs and were separated by 5 ms. Complex data samples were collected without any integration. Using the same selection criteria, 1868 meteors were found in the 430 MHz beam while 367 were found in the 47 MHz beam in the 6 hr of observation. 145 meteors were detected in both systems.

The characteristics of the UHF meteors are essentially the same as those reported in Zhou and Kelley (J. Atmo. Terr. Phys., *in press*) and Mathews et al. (ICARUS, *in press*). Those UHF echoes typically have an effective radar cross-section of the order of 3×10^{-8} m^2, and an electron line density of the order of 4×10^9/m. The visual magnitude is estimated to be approximately +16 and the typical mass of the meteoroids is of order of 10^{-6} g. Unlike smaller UHF/VHF radars, the powerful Arecibo 430 MHz radar is more sensitive to head-on meteors than to those arriving at an oblique angle. Practically all of the UHF echoes are head-echoes, i.e., the scattering volume is closely behind the meteor head. The VHF echoes are estimated to have a visual magnitude of +10 or fainter. Most of the VHF echoes are also head-echoes although several long lasting echoes have also been observed. We also discuss the results from those meteors that appeared in both beams.

COHERENT SCATTER RADAR IMAGING EXPERIMENTS AT JICAMARCA

D. L. Hysell
Department of Physics and Astronomy
Clemson University
Clemson, SC 29634

This presentation reports on additional radar imaging experiments performed at the Jicamarca Radio Observatory. The imaging technique is similar to the one used in radio astronomy to infer the arrival angle distribution of a radio target from multiple-baseline interferometry data. The problem for radar observations of geophysical targets differs in that 1) the brightness distribution for a radar experiment is limited by the transmitter radiation pattern, 2) the geophysical target is not static, and 3) radar images can be computed at multiple Doppler frequencies for added information about the dynamics in the scattering volume. In addition, the fact that the radar experiments are generally conducted with high signal-to-noise ratios actually complicates the optimal signal processing.

Two imaging experiments have been carried out at recently Jicamarca. The first involved observations of a bottomside spread F layer. Animated sequences of high-resolution radar images of the layer showed it to be composed of horizontally periodic, quasi-sinusoidal waveforms that emerged, grew, and dissipated, apparently under the influence of a vertical shear in the zonal plasma flow. The period, growth time, and lifetime of the quasi-sinusoidal modes could be measured.

Additional imaging radar observations were made of a topside spread F radar plume. The resulting images clearly depict a large-scale depletion bubble or wedge moving eastward through the radar beam. The dynamics of the plasma in and around the depletion was consistent with the "chimney" picture outlined by several authors, with regions of depleted plasma rising rapidly into the base and upward through the depletion. The images also illustrated the emergence of secondary instabilities on the westward wall of the depletions. Animated images from both experiments may be viewed on the Clemson Atmospheric Science web site (http://landau.phys.clemson.edu).

G62.3

The Intermediate Tidal Ion Layer, Ion Rain, and F-Region Instabilities.

J. D. Mathews, D. W. Machuga
Communications and Space Sciences Laboratory
316 EE East, Penn State University, University Park, PA 16802

M. P. Sulzer
Arecibo Observatory, Box 995
Arecibo, Puerto Rico, 00613.

High resolution ISR observations of the evening E and F regions at Arecibo have revealed the presence of layers and associated processes in unprecedented detail. In particular, these observations revealed "streaks" of ionization-termed "ion rain" [Mathews et al., GRL, submitted, 1997]-apparently descending from the base of the F-region onto the descending intermediate tidal ion layer which correspondly oscillates in altitude with an amplitude of 3-5 km. Further examination of the data reveals that the ion rain structures continue up through the F-region to at least 270 km altitude. In the F-region, the normalized amplitudes of these structures is 1-3wavelengths in excess of 50 km. We suggest that these structures are a manifestation of polarization electric fields of about 1 mV/m generated in a "field" of self-organizing linear Perkins instabilities of relatively small horizontal-scales but occurring over large horizontal-scales in the bottom-side of the nighttime F region. Also revealed was evidence that these instability-generated E-fields map down the highly conducting geomagnetic field lines to 100 km altitude or somewhat lower and where the associated horizontal-scales are found to be no more than 10-100 km [Mathews, J. Atmosph. Terr. Phys., in press, 1997]. In addition, we present numerical simulations of 3-dimensional ion trajectories in wind and electric field structures similar to those implied by these observations. These simulations give insight into formation of the ion rain structures.

Two-stream waves in the E-region ionosphere nonlinearly drive large-scale D.C. currents

M. Oppenheim
University of Colorado
Boulder, CO 80309

Ionospheric two-stream waves nonlinearly drive D.C. currents in the *E*-region ionosphere. These currents flow parallel to, and with a comparable magnitude as, the fundamental Pederson current, acting to discharge the electrojet. The fundamental mechanism of this nonlinear current is quite simple. *E*-region plasma waves generate oscillating electric fields causing electrons to $\vec{E} \times \vec{B}$ drift perpendicular to the wave propagation direction on the density maxima and minima of the waves. On the maxima these electrons drift with the same velocity but in the opposite direction as they do on the minima. Since more electrons exist at the maxima than the minima, a net D.C. current results. This wave-driven current will modify the large scale dynamics of the *E*-region during highly active periods and may be responsible for a number of observed features of *E*-region waves, including the oft-repeated radar observation that equatorial Farley-Buneman waves travel at the acoustic velocity as well as the squaring-off of gradient-drift waves observed by rockets.

G62.5

F-region incoherent scatter electric field measurements at Jicamarca

Erhan Kudeki, and Santanu Bhattacharyya
University of Illinois at Urbana-Champaign, IL 61801

Ronald F. Woodman
Jicamarca Radio Observatory, Aptd 13-0207, Lima, Peru

Low latitude ionospheric electric fields in the American longitude sector have been routinely monitored at the Jicamarca Radio Observatory over the past two decades. Electric field data are obtained from incoherent scatter measurements of $\vec{E} \times \vec{B}$ plasma drift velocities at F-region heights using a pair of antenna beams directed perpendicular to $\vec{B}$. Relatively long decorrelation times of incoherent scatter returns from nearly field aligned plasma density fluctuations permit the use of pulse-to-pulse signal processing techniques in extracting drifts information from radar phase data. As a consequence drifts estimates are free from "chirp errors" that often contaminate measurements based on double or multiple pulse methods. Furthermore the effect of phase noise on drifts estimates is reduced as a result of long time delays involved in differential phase measurements. The single-time-delay pulse-to-pulse correlation processing method used until very recently at Jicamarca provides F-region height averaged vertical drifts estimates with a few m/s uncertainties. We will describe a new processing method recently adopted at Jicamarca that takes advantage of the additional informations available in signal correlations at even longer time delays. The method is based on power spectrum estimation and least squares fitting a spectral model that includes a Doppler shifted cusp associated with the long tail of the incoherent scatter autocorrelation function for the decribed radar beam geometry. The new method provides maximum-likelihood line of sight drift velocity estimates with uncertainties of less than a m/s and 15 km height resolution throughout F-region heights. Improved resolution and statistical accuracy opens up the possibility of more detailed studies of equatorial electrodynamics at Jicamarca including altitudinal variations and short time scale wavelike fluctuations in F-region drifts. Results obtained with the new method will be presented.

G62.6

Critical-frequency variations in the midlatitude ionospheric F2-region and prediction of them

Zakharov I.G., Tyrnov O.F.

Kharkiv State University, Svobody Sq.4, Kharkiv 310077, Ukraine

1. There were investigated short-time critical-frequency variations in the midlatitude ionosphere *F2*-region ($\delta f_0 F2$), caused by the solar and geomagnetic activities. It is shown that in order to predict these variations, one should use the $\delta f_0 F2$-values for 03.00, 09.00, 15.00 and 21.00 LT showing the assymmetry of diurnal $\delta f_0 F2$-variations with respect to midday and midnight, and also particular variations of this parameter during morning and evening hours. There were found seasonal- diurnal features of energy coming from the auroral into the midlatitude ionosphere. On this basis, it has been substantiatid that it is necessary to use-instead of the standart averadge- diurnal and three-hour geomagnetic-activity indices - that index which characterizes a middle activity level over time-intervals not smaller than 9 hours, which - as a rule - refer to evening and night hours.

2. Methods of a short-time prediction of the midlatitude ionosphere $\delta f_0 F2$-value were developed using indices of the solar and geomagnetic activities; the prediction accuraty of our methods under arbitrary heliogeophysical conditions is about 1.4 times higher than that when using the methods of the ionospheric-magnetic sevice of the FSU.

URSI G

Session 78 — **Salon Jolliet**

D-Region Radio Studies
Co-chairs: W. Hocking, Canada and M. Kelley, USA

08:10	78.1	Middle Atmosphere Temperatures and Tides Using a VHF Meteor Radar, **W.K. HOCKING**, T. THAYAPARAN, *University of Western Ontario, London, ON, Canada*
08:30	78.2	Comparison of Turbulence Parameters Measured by EISCAT VHF and Tromsø MF Radars, **C. MEEK**[1], C. HALL[2], [1]*University of Saskatchewan, Saskatoon, SK, Canada;* [2]*University of Tromsø, Norway*
08:50	78.3	A Study of PMSE Aspect Sensitivity and Its Use as a Measure of Layer Tilt and Criterion for Turbulent Parameter Extraction, **J.Y.N. CHO**[1], W. SINGER[2], P. CZECHOWSKY[3], [1]*NAIC/Arecibo Observatory, Arecibo, Puerto Rico;* [2]*Institut für Atmosphärenphysik, Kühlungsborn, Germany;* [3]*Max-Planck-Institut für Aeronomie, Katlenburg-Lindau, Germany*
09:10	78.4	Intercomparisons of Multiple-Receiver Techniques for Wind Measurements at MF and VHF Frequencies,-**J.L. CHAU**, B.B. BALSLEY, *University of Colorado, Boulder, CO, USA*
09:30	78.5	Inter-Hemispheric Mesopause Temperature Differences as a Cause of PMSE Occurrence in the Northern and Southern Hemispheres, **M. HUAMAN**, B.B. BALSLEY, *University of Colorado, Boulder, CO, USA*
09:50	78.6	Detection of a Meteor Contrail and Meteoric Dust in the Earth's Upper Mesosphere, **M.C. KELLEY**[1], C.M. ALCALA[2], J.Y.N. CHO[3], [1]*Cornell University, Ithaca, NY and* [2]*Mission Research Corporation, Monterey, CA, USA;* [3]*NAIC/Arecibo Observatory, Arecibo, Puerto Rico*
10:10		Coffee Break
10:30	78.7	First Measurements of Polar Summer Mesosphere Echoes Using a 24.5 MHz Radar Located at Resolute Bay, **R.T. TSUNODA**, R.C. LIVINGSTON, J.D. KELLY, *SRI International, Menlo Park, CA, USA*
10:50	78.8	Preliminary Results Obtained with the New Resolute Bay VHF Atmospheric Radar, **W.K. HOCKING**[1], J.-P. ST.-MAURICE[1], D. MOORCROFT[1], M.C. KELLEY[2], R.R. ROGERS[3], W.O. BROWN[3], [1]*University of Western Ontario, London, ON, Canada;* [2]*Cornell University, Ithaca, NY, USA;* [3]*McGill University, Montréal, QC, Canada*
11:10	78.9	A New Approach to MF Radar Interferometry for Estimating Mean Winds and Momentum Flux, **D. THORSEN**, S.J. FRANKE, [1]*University of Colorado, Boulder, CO and* [2]*University of Illinois, Urbana, IL, USA*
11:30	78.10	Experimental Investigations of Frequency Variations of Electron/Neutral Collisions in the Ionospheric D-Region, **A.M. GOKOV**, O.F. TYRNOV, *Kharkiv State University, Kharkiv, Ukraine*
11:50	78.11	Ionospheric Electric Fields and Remote Rocket Launch, **O.F. TYRNOV**, S.I. MARTYNENKO, Yu.B. MILOVANOV, V.T. ROZUMENKO, A.M. TSYMBAL, *Kharkiv State University, Kharkiv, Ukraine*

G78.1

Middle atmosphere temperatures and tides using a VHF meteor radar

W. K. Hocking and T. Thayaparan
Department of Physics, University of Western Ontario
London, Ontario, Canada

Abstract

Various techniques have been used to observe temperatures in the mesosphere and lower thermosphere. At present the most common procedures are based on optical procedures, but these are limited in their coverage by clouds, daylight and even moonlight. Therefore a good radar method for determining mesospheric and lower thermospheric temperatures could be a powerful tool.

In this paper, we will show an efficient method to extract temperatures with a meteor radar. The method relies on the exponential decay of underdense meteor trails. Whilst not a new idea in principle, the technique has never been implemented satisfactorily due to various pragmatic difficulties. However, by imporving the angular and height resolutions of our system, and invoking some new data fitting procedures, we have been able to refine our procedures to the extent that reliable measurements have become possible.

In this paper, monthly mean temperatures measured with the VHF meteor radar located at London, Ontario, Canada (43 N, 81 W) will be presented. Using a one-year set of data, the monthly mean temperatures are compared with lidar measurements and the CIRA empirical model. Our monthly mean temperatures in general show very good agreement with these other data.

We can also use our data to determine amplitudes and phases of the diurnal and semi-diurnal temperature tides in the 85 to 94 km altitude range, something hitherto rarely done by any technique. The results of these determinations will be presented.

Comparison of turbulence parameters measured by EISCAT VHF and Tromsø MF radars

G78.2

Chris Meek[1] and Chris Hall[2]
[1]Institute of Space and Atmospheric Studies, University of Saskatchewan, Canada
[2]Institute of Mathematical and Physical Sciences, University of Tromsø, Norway.

Abstract

The measured parameter for Eiscat VHF is the RMS 1 Km 5m vertical velocity (V_Z) perturbations from incoherent scatter observations (Chris Hall, Radio Science, 1997, in press). This is a measure of the energy which must be later dissipated, not a measure of the dissipation rate itself. Some gravity wave (GW) contamination is possible through record length and sample spacing.

Several turbulence-related parameters which may be measured on an MF radar are spectral width of fading, *the characteristic time of fading* (Manson and Meek, J. Atmos. Sci., **44**, 3661, 1987), and pattern scale (with the spaced antenna system). Turbulence is usually estimated from spectral width, but this must be corrected for beam-broadening (viz. the background horizontal wind contributes to spectral width because of the difference in apparent radial velocity across the beam). The characteristic time parameter, available from the *Full Correlation Analysis* of spaced antenna data (FCA, e.g. Briggs, MAP Handbook, vol. 13, 1984), is the fading rate in the pattern with background velocity effect removed. However again contributions from GW with wavelengths or periods within the potential scattering volume and time: $\sim$ 3Km x 50Km x 5min can occur (e.g. Vanderpeer and Hocking, Geophys. Res. Lett., **20**, 17, 1993). A third parameter, the pattern scale, is an estimator of the angular spread of the echoes. Turbulence is one possible cause of such distributed scattering.

It is found that Eiscat RMS V_Z perturbation (mean over several years) and Tromsø MF radar characteristic-time-based (1 year) climatologies agree in gross features: both have minimum turbulence in summer and maximum in winter. In summer, the MF data show a clear diurnal variation, with a minimum near noon, and although the VHF is plagued with spurious values, a 24hr component fit shows phase agreement with the MF. [In contrast, Saskatoon MF radar data for 1994 show a large summer maximum, a smaller winter maximum, and equinoctial minima; but in agreement, the summer data show a diurnal oscillation with a minimum near noon.] In magnitude, the MF values are some 50-100 times greater than the VHF. An attempt is also made to compare individual values – although there is only one day in common.

G78.3

A Study of PMSE Aspect Sensitivity and its use as a Measure of Layer Tilt and Criterion for Turbulent Parameter Extraction

J. Y. N. CHO
NAIC/Arecibo Observatory, Arecibo, Puerto Rico
W. SINGER
Institut für Atmosphärenphysik, Kühlungsborn, Germany
P. CZECHOWSKY
Max-Planck-Institut für Aeronomie, Katlenburg-Lindau, Germany

Polar mesosphere summer echoes (PMSEs) are known to be highly aspect sensitive with respect to the vertical much of the time. The narrowness of the Doppler spectra observed at the same time imply that strong turbulence is not the driving force behind PMSE generation. However, there are also clear instances, especially in the higher altitude region of PMSE occurrence, in which bursts of energetic turbulence widen the spectra and eliminate the aspect sensitivity. PMSEs also have a tendency to occur in horizontally extended layers that are often tilted with downward phase motion, which appear to be related to wave activities.

Thus a careful analysis of the radar aspect sensitivity and spectral width (with nonturbulent broadening subtracted) with respect to height and time can reveal where and when strong turbulence is likely to occur. Given multiple-beam data we can also obtain statistics for the preferred direction of layer tilt, which can then be related to the ambient winds and waves. Finally, the condition of very weak or no aspect sensitivity can be used as a criterion for the extraction of turbulent velocity fluctuation strength from the Doppler spectral width.

We present the results of the study outlined above using data from the 50-MHz Arctic Lidar Observatory for Middle Atmospheric Research Sounding System (ALOMAR-SOUSY) radar located in Andoya, Norway. The data set covers the summer seasons of 1994 and 1995. To calculate the aspect sensitivity we compensated for the vertical "smearing" effect of the oblique beams by performing a weighted averaging of the vertical beam data using the oblique beam pattern, a necessary operation for wider-beam radars.

G78.4

Intercomparisons of Multiple-receiver techniques for wind measurements at MF and VHF frequencies.

J. L Chau and B. B. Balsley
CIRES, University of Colorado, Boulder. CO-USA

Time domain (Correlation analysis) and frequency domain (Cross-spectral Analysis) multiple-receiver techniques for wind measurements are compared for short-term data sets (i.e. < 1 day). Data from the Urbana MF radar and from the Jicamarca VHF radar are used for these comparisons. The effects of using antennas situated in right-triangles and square configurations are investigated. Scattering mechanisms are also studied, with angle-of-arrival diagrams, spectrograms and with velocity intercomparisons. The latter uses a simple approach to a full-correlation-analysis when isotropic scattering is expected (R. F. Woodman, Radio Sci., 30, 1459-1465, 1995). Differences in the velocity estimates are related to statistical (e.g. variances of parameters), atmospheric (e.g. scattering processes) and processing factors (e.g. bias corrections).

G78.5

Inter-Hemispheric Mesopause Temperature Differences as a Cause of PMSE Occurrence in the Northern and Southern Hemispheres

Mercedes Huaman and Ben B. Balsley
Cooperative Institute for Research in the Environmental Sciences (CIRES)
University of Colorado, Boulder, CO 80309

Archived satellite data provide a few reliable long-term measurements of global mesospheric temperatures. Careful analyses of these data can enable a reasonable estimate to be made of possible differences in summer mesopause temperatures at high northern and southern latitudes. It is commonly assumed that PMSE, which are found at high latitudes during summer, require very low temperatures. Thus, a measurable difference in summer mesopause temperatures in the two hemispheres determined from satellite data could explain the observed difference in PMSE occurrence in the two regions. In this case, the observed reduced occurrence of PMSE in the southern hemisphere would be associated with a slightly warmer mesopause in the south.

In this contribution we present the results of our analysis of summer high-latitude mesopause temperatures from satellite data. These results support our earlier speculations that the southern high-latitude summer mesopause temperatures are, indeed, at least a few degrees warmer than their northern counterpart during the entire local summer season. Such a difference could well account for the observed weaker southern-hemispheric PMSE occurrence.

Detection of a Meteor Contrail and Meteoric Dust in the Earth's Upper Mesosphere

M. C. KELLEY
School of Electrical Engineering, Cornell University, Ithaca, New York 14853
C. M. ALCALA
Mission Research Corporation, Monterey, California 93940
J. Y. N. CHO
NAIC/Arecibo Observatory, Arecibo, Puerto Rico 00613

In 1983 a series of small rockets were launched from the Poker Flat Rocket Range near Fairbanks, Alaska to study what has come to be called polar mesospheric summer echoes (PMSE). Very intense VHF radar returns from the region had been discovered using the Poker Flat Radar (W. L. Ecklund and B. B. Balsley, *J. Geophys. Res.*, *86*, 7775–7780, 1981). The purpose of the experiment was to understand the scattering mechanisms and to this end simple nosetip Langmuir probes were flown on Super Arcas rockets. We report here on a fortuitous simultaneous radar and rocket detection of what seems to be a meteor trail produced over the Poker Flat Rocket Range. The two data sets are mutually consistent and taken together suggest some very interesting properties for the trails of large meteors. Most notable is the evidence that the ablated material has coagulated into particles the order of 50 nm in radius. This estimate is based primarily on the fall speed deduced from both the Doppler shift of the VHF radar signal and the time rate of change of the target as it fell through the beam. In addition the very existence of the radar target, the extremely sharp edges of the trail, and the existence of electron density structures inside the trail more than an order of magnitude smaller than the Kolmogorov microscale, all require large charged aerosols and a very high Schmidt number. Curiously the environment leading to PMSE is very similar to the properties of a large meteor trail some minutes after it is formed. In the former case ice particles grow and become charged by the plasma and, when more than half the charge is tied up on the ice, the plasma diffusion coefficient becomes so small that structure can be supported at VHF scattering scales. In the late-time meteor case large aerosols coagulate and tie up both natural charge in the plasma and the original meteor trail electrons. Following earlier modeling results (J. Rosinski and R. H. Snow, *J. Meteor.*, *18*, 736–745, 1961; D. M. Hunten et al., *J. Atmos. Sci.*, *37*, 1342–1357, 1980) we conclude that the incident meteor was the order of 50–100 g and would have had a visual magnitude of about -4. Such a meteor is not uncommon but it is remarkable indeed to have had the opportunity to study its evolution with radar and particularly with rocket instrumentation. Two experimental techniques are discussed which could be used to test the conclusions of this report and, if verified, to further study large charged mesospheric aerosols.

G78.7

First Measurements of Polar Summer Mesosphere Echoes Using a 24.5MHz Radar Located at Resolute Bay

Roland T. Tsunoda, Robert C. Livingston, and John D. Kelly
Geoscience and Engineering Center
SRI International
Menlo Park, CA 94025 USA

Thus far, polar summer mesosphere echoes (PMSE) have been detected only with radars that operate at frequencies above 50 MHz. Given that the inner scale for atmospheric turbulence at D-region altitudes would be associated with Bragg backscatter at a radar frequency around 6 MHz, we recognized that important information regarding the source mechanism for PMSE could probably be extracted from frequency dependence studies in the range of 6 to 50 MHz. With this premise in mind, we set up an SRI frequency-agile radar (FAR) to operate at 24.5 MHz from Resolute Bay, Canada. The FAR was configured with a Hermes final amplifier to provide 30kW peak power, which was transmitted through four four-element Yagi antennas. The transmitted signal was a seven-baud Barker-coded waveform with a 20μs baud length, providing 3km altitude resolution. The backscattered signals were received on a separate set of four Yagi antennas and recorded for post processing. The system sensitivity was modest in comparison to other radars that have been used for PMSE studies.

The measurements were made over a two-week period in August 1996 and again in October. Data reduction, to date, has consisted of computing Doppler spectra as a function of altitude and integrating the spectra over one-minute periods. Examining the power profiles plotted in a range-time-intensity (RTI) format, we have found what appears to be the first measurements of PMSE at 24.5 MHz. The echoes were found to occur at altitudes between 83 and 95 km, with characteristics that appear to resemble those of PMSE obtained at higher radar frequencies. Some of the more interesting features included slow altitude variations with corresponding variations in backscatter power. These features will be described and discussed in light of earlier PMSE measurements and theories.

Preliminary Results Obtained with the new Resolute Bay VHF Atmospheric Radar

W.K. Hocking, J.-P. St. Maurice, D. Moorcroft,
Dept. of Physics and Astronomy, University of Western Ontario, London, Ontario, N6A 3K7, Canada

M.C. Kelley,
School of Electrical Engineering, Cornell University, Ithaca, New York, 14853, USA.

R.R. Rogers and W.O. Brown
Dept. of Atmospheric and Oceanic Sciences, McGill University, Montreal, Quebec, H3A 2K6, Canada

In recent years it has become clear that the polar regions of the Earth's atmosphere hold keys to understanding of a variety of important processes. These include aurorae, polar mesosphere summer echoes (PMSE), the ozone hole, and global warming. Because of these issues, a renewed effort has been developed to establish polar atmospheric observatories, and the so-called "Polar Cap Observatory" is one of these facilities. This facility is being established at Resolute Bay, in the Canadian North-West Territories (75°N, 95°W), which also happens to be quite close to the North magnetic pole. As part of it's early development by the U.S. National Science Foundation (NSF) and the Canadian Natural Sciences and Engineering Research Council (NSERC), several instruments have been deployed at the site of the PCO, and these are collectively called the "Early Polar Cap Observatory". One of the instruments developed as part of this exercise is a new VHF atmospheric radar.

This radar is capable of tropospheric meteorological wind measurements, middle atmosphere studies, meteor studies and ionospheric work, and is operated in a variety of modes. These different modes will be discussed, and preliminary results from the radar will be reported. These results include validation of the beam-pointing function of the radar, demonstration of its capability for meteorological studies in the troposphere and lower stratosphere, as well as the results of our first searches for PMSE. Future plans for the instrument will also be outlined.

G78.9

A new approach to MF radar interferometry for estimating mean winds and momentum flux

Denise Thorsen*
Cooperative Institute for Research in Environmental Sciences,
University of Colorado, Boulder

Steven J. Franke
Department of Electrical and Computer Engineering,
University of Illinois, Urbana

Recently concerns have been raised over potential biases in spaced antenna full correlation analysis (SA-FCA) estimates of the horizontal wind vector. Numerical simulations (Holdsworth and Reid, *Radio Sci.*, **30**, 1263–1280, 1995) suggest that non-optimum system parameters can lead to small-to-moderate biases in the estimated wind speeds and directions. It has not yet been shown how much influence these effects have on actual MF radar derived winds. In fact, the cause and extent of any biases are probably different at each radar site. Nevertheless, the remaining uncertainties provide motivation for the development and study of complementary wind estimation methods which are based on different assumptions, or use different aspects of the radar signals. Furthermore, there is also a need for the development and refinement of techniques which can provide estimates of geophysically important parameters such as the vertical fluxes of horizontal momentum carried by gravity waves.

To this end, new techniques are applied to measured Doppler velocity and angle of arrival to estimate horizontal wind vectors, variances, and momentum fluxes, from MF radar data. The approach used to estimate mean winds was first introduced as "time domain interferometry" (TDI) by Vandepeer and Reid (*Radio Sci.*, **30**, 1191–1203, 1995), which they used along with the beam steering capabilities of the Buckland Park MF radar, located near Adelaide, Australia. The algorithm is refined and used with data from the Urbana MF radar, which employs a single vertical antenna beam, to obtain a monthly mean wind climatology which is compared with the results from the conventional SA-FCA. The comparison validates the scattering model used in the development of the TDI technique and highlights instrumental and processing biases that differ between the two techniques. An extension of the TDI method that can provide estimates of the Reynolds stress tensor associated with propagating gravity waves is also proposed, and some preliminary results are presented.

G78.10

Experimental investigations of frequency variations of electron/neutral collisions in the ionospheric D-region

Gokov A.M., Tyrnov O.F.

Kharkiv State University, Svobody Sq.4, Kharkiv 310077, Ukraine

In the paper some experimental investigations of frequency variations of electron/molecule collisions, $\nu(z)$, in the ionospheric D-region at middle latitudes are presented. The investigations were made by a partial reflection thechnique in the vicinity of Kharkiv under different heliogeographical conditions ($\nu(z)$-changes for periods of ionospheric disturbances having different natures are not considered here) during 10 years. The main parameters of our partial reflection facility are as follows: the operation frequency f= 1.8-4 MHz; the duration of sounding pulses, $\tau = 25\,\mu$s, having the tact frequency, F= 1-10 Hz and the effective pulse power, P_1G_1~ 1-10 Mw. Variations of $\nu(z)$ at z< 70 km and z> 70 km were investigated separately. In the first case, there was used the known methods of obtaining of $\nu(z)$ (J.S.Belrose, M. J.Burke, J.Geophys. Res., 1, 2799 - 2818, 1964), when at z < 70 km the differential absorption for the "x" and "o" magnetoionic components of partial reflection signals was small, and the ratio of their averages over a series of measurements (~10-12 min) of intensities was related to ν by $a(z) = \langle A^2_x(z)\rangle / \langle A^2_o(z)\rangle \sim R(\nu)$. Here $R(\nu)$ is the ratio of reflection coefficients for these components. The total number of $a(z)$-records (whith the signal/noise ratio being > 5) was about 300. In the second case (z > 70 km), $\nu(z)$-values were calculated by the methods (Benediktov E.A., Grishkevich L.V., Ivanov V.A., Izvestija vuzov. Radiophyzika, 15, 695-701, 1972, in russian) using simultaneous measurements of $a(z)$ and correlation coefficient $\rho_{A_oA_x}(z)$ of A_o and A_x, (the total number of records in this case was more than 100). The errors of obtaining $\nu(z)$ do not exceed 30% in both cases.

The following main features in the $\nu(z)$- behaviour were found:

1. Variations of $\nu(z)$ in the middle latitude D-region over a daylight period do not exceed ~30%;

2. Within the whole D-region, $\nu(z)$-values differ seasonally (winter-summer) 1.5-2.5 times.

On the basis of the experimental data obtained and the results taken from other authors, there was constructed an empirical model for $\nu(z)$-variations in the middle latitude ionospheric D-region, which agrees rather good to the observed $\nu(z)$-changes.

G78.11

Ionospheric electric fields and remote rocket launch

Tyrnov, O.F., S.I. Martynenko, Yu.B. Milovanov, V.T. Rozumenko, and A.M. Tsymbal

Kharkiv State University, Svobody Sq.4,Kharkiv 310077, Ukraine

The observations have been made at the Radiophysical Observatory of Kharkiv State University at low geomagnetic (L=2.0) and middle geographic latitudes, about 10,000 km from the space shuttle launching site at Florida, the U.S.A. The perturbations observed with a partial reflection facility may roughly be grouped into two subsets: those occupying a limited altitude range of only about or less than 10 km and those occupying the whole D region.

The data consist of the extraordinary and ordinary mode noise and signal plus noise measured concurrently with a height resolution of 3 km within an altitude range of 60 to 105 km and with a radar interpulse period of 1 s for each of the magnetoionic modes. They are band-pass filtered and spectra of time-series of partial reflection data are commonly computed; in case of the long periods of the oscillations under study, 10-s decimated data were used.

Some of the spectra for partial reflection data show both the magnetic field line eigenfrequency period and its harmonics. The peaks are not sharp, but rather have fractional width of about 10 % that can be explained by the nonstationary of the perturbation.

The temporal variation of resonance structure was obtained by calculating successive spectra to give a plot of frequency and time.

To estimate an effect of the variations in electric field intensity on changes in lower -ionosphere parameters, we use the system of the energy balance and continuity equations in the electron density, electron temperature, and the positive-ion density in a stratified inhomogeneous weakly-ionized plasma. The initial system of the equations is considerably simplified with the help of the multiple time scale analysis.

URSI G **Session 86** **Salon Peribonca**

Ionospheric Modeling and Low Latitude Irregularities - Part II
Co-chairs: C. Fesen, USA and E. Kudeki, USA

08:10 86.1 Comparison of Experimental and Modelled Ionospheric Propagation Data at Sunspot Maximum and Minimum, C.J. COLEMAN, **G.F. EARL**, B.D. WARD, *Defence Science and Technology Organisation, Salisbury, South Australia*

08:30 86.2 A Simulation of the High-Latitude Ionosphere and the Interpretation of HF Direction Finding Results, **D.J. DUMAS**, *Communications Research Centre, Ottawa, ON, Canada*

08:50 86.3 A Comparison of Ionosphere/Plasmasphere Model and Experimental Corrections to GPS Signals, P. WEBB, I. HORVATH, R. BARKER, **E.A. ESSEX**, *La Trobe University, Bundoora, Australia*

09:10 86.4 Tidal Effects on the Ionosphere, **C.G. FESEN**[1], R.G. ROBLE[2], [1]*University of Texas at Dallas, Richardson, TX and* [2]*High Altitude Observatory, NCAR, Boulder, CO, USA*

09:30 86.5 Measurements of Equatorial Spread *F* Effects on an HF Path, **T.J. FITZGERALD**, P.E. ARGO, R.C. CARLOS, *Los Alamos National Laboratory, Los Alamos, NM, USA*

09:50 86.6 Analysis of the Structure and Motion of Equatorial Depletion Bands Using Radio Sounding and Optical All-Sky Images, **G.S. SALES**, R. PICKETT, A. GEE, *University of Massachusetts Lowell, MA, USA*

G86.1

COMPARISON OF EXPERIMENTAL AND MODELLED IONOSPHERIC PROPAGATION DATA AT SUNSPOT MAXIMUM AND MINIMUM

C.J.Coleman, G.F.Earl* and B.D.Ward
High Frequency Radar Division, Defence Science & Technology Organisation, Salisbury, South Australia

OTH radar systems are critically dependent on the characteristics of oblique ionospheric propagation. To support real time operations, such radars are typically equipped with a frequency management system (FMS) which is required to monitor variations in propagation conditions. For system development, reliance must be placed on propagation prediction codes which are similar to those used for telecommunication planning.

The JINDALEE FMS has been used to acquire a very large data base of backscatter sounder measurements. The data base is most complete at periods of sunspot maximum (1991) and minimum (!986), and has been used to evaluate the performance of a range of prediction codes and related ionospheric models over one year's data centred on each period.

A typical prediction code involves several elements, all of which contribute to their overall accuracy. These components include some form of ionospheric model, a propagation/ray-tracing computation, together with a model of the system and ionospheric losses.

For this study, which is a systematic extension of the preliminary findings presented at the 1996 URSI General Assembly, ionospheric prediction codes were used to synthesize backscatter ionograms for direct comparison with measured data. The ray path calculations were performed using IONCAP, and numerical ray tracing together with a variety of ionospheric models.

Our philosophy in handling the inherent difficulties in comparing monthly median predictions with ionograms featuring considerable day-to-day variability will be discussed. The paper will also review the adequacy of existing models for propagation predictions in both mid and low latitude regions.

A Simulation of the High-Latitude Ionosphère and the Interpretation of HF Direction Finding Results

Denis J. Dumas
Communications Research Centre, Ottawa, Ontario, Canada

The high-latitude ionosphere is known to have an irregular electron density profile, often with large-scale enhancements in ionization (patches) convecting across the polar cap in an anti-sunward direction. These patches and accompanying smaller-scale structures pose a problem for HF direction finding (DF) systems at these latitudes since they allow signals to propagate at large angular deviations from the great-circle path, therefore causing false bearing estimates of the transmitter location. We have developed a computer simulation of the high-latitude ionosphere and have used it to interpret HF direction finding results and to determine which DF algorithms are more reliable under these conditions.

The simulation uses a spherical earth model with multiple ionospheric layers, a dipole magnetic field, and ray tracing based on the Haselgrove equations. Patches are specified as ionization enhancements with ellipsoidal shapes superimposed on the background ionosphere, and travel through the ionosphere at speeds consistent with observed ionospheric motions. Field-aligned scattering centres travel with the patches and are confined within them.

The results of the simulation are used to interpret HF direction finding measurements obtained from a sampled-aperture antenna array located in Northern Canada. Several DF algorithms have been used and their relative performance under high-latitude conditions has been studied using both measured and simulated data. The capacity of the simulation to reproduce the measured data and the strengths and weaknesses of the DF algorithms are discussed.

G86.3

A COMPARISON OF IONOSPHERE/PLASMASPHERE MODEL AND EXPERIMENTAL CORRECTIONS TO GPS SIGNALS

P. Webb, I. Horvath, R. Barker and E. A. Essex*
School of Physics
La Trobe University
Bundoora, Victoria 3083, Australia
p.webb@latrobe.edu.au

The plasmasphere is a generally toroidal-shaped region of 'cold' plasma centred around the magnetic equator and which extends out to an altitude of 20,000 km to 30,000 km. Consequently its effects on signals from the Global Positioning Satellites (GPS), which orbit at an altitude of around 20,000 km, need to be considered. The first steps at producing a model of the ionosphere/plasmasphere region will be discussed. The aim is to produce a program that can be run on a desktop PC which calculates electron density at specified altitudes and hence allows the determination of Total Electron Content (TEC) to be made. To put these effects into perspective for GPS, during the daytime the TEC contribution due to the plasmasphere is ~ 10% of the total, and at night time it can be up to 50%. From these TEC values, signal propagation delays introduced by travelling through the ionosphere/plasmasphere can be calculated and used to correct data obtained from the GPS satellites. This is especially useful for single frequency GPS receivers, which have no other way of determining this delay. An existing ionospheric model is combined with a purpose designed plasmaspheric model representing the electron density at higher altitudes. Additions, to more accurately model various features, such as the plasmapause, have also been included. Experimental results from various sources are compared to those obtained from the model. These will include observations from GPS satellites, as well as the TOPEX/POSEIDON satellite which orbits at an altitude of 1335 km. In the Southern Hemisphere, at present, there are major discrepancies between existing models such as PIM and the IRI, and the experimental results obtained. Limitations relating to the model at present, and future improvements will also be considered.

G86.4

Tidal effects on the ionosphere

C G Fesen*, Center for Space Sciences, U. Texas, Dallas, Richardson, TX
R G Roble, High Altitude Observatory, NCAR, Boulder, CO

The effects of waves from the lower atmosphere on the ionosphere are investigated using simulations from the National Center for Atmospheric Research thermosphere-ionosphere-electrodynamic general circulation model. Calculations were performed for equinox and solstice conditions during solar cycle minimum when the effects of the waves are expected to be larger than at solar cycle maximum. The model predictions of n_{max} and h_{max} for low and middle latitudes are examined and compared with data. Of particular interest is examination of the role of lower atmosphere waves in the observed daily variability in the ionosphere and in the generation of the atmospheric dynamo.

G86.5

Measurements of equatorial spread *F* effects on an HF path

T. Joseph Fitzgerald*, Paul E. Argo, and Robert C. Carlos
Los Alamos National Laboratory, Los Alamos, New Mexico 87545

The ionospheric phenomenon called equatorial spread *F* encompasses a variety of effects associated with plasma irregularities occurring in the post-sunset and nighttime ionosphere near the magnetic equator. These irregularities can seriously degrade the performance of high frequency (HF) radio systems such as Over-the-Horizon (OTH) radars which reflect off the equatorial ionosphere. The presence of irregularities leads to Doppler and delay spread on the HF propagation path; in addition, the irregularities degrade angle-of-arrival estimates. In August, 1990, we participated in the NASA-sponsored EQUIS sounding-rocket campaign near Kwajalein Atoll in the equatorial Pacific Ocean. The campaign included in-situ measurements of plasma density and coherent and incoherent scatter radar measurements. During the campaign we fielded a 700 km bistatic path between Maloelap Atoll and Bikini Atoll in the Marshall Islands. The one-hop reflection region for this path was 10.18°N, 168.40°E near the magnetic equator. We obtained three types of measurements: Doppler spread and spatial correlation for a single frequency CW path; frequency coherence of multiple CW paths; and Doppler spread and time-delay spread for a 60 kHz bandwidth path. Data was collected on average for about 2 hours in the post-sunset time period (1830-2030 LT) over a period of two weeks. On all but one evening significant spread *F* effects were observed. In this paper we discuss our measurements using phase stable continuous wave (CW) transmissions at multiple frequencies over an array of receive antennas. We employed four CW transmissions with the lowest frequency at 10.224 MHz and other frequencies offset higher by 0.5, 1.5, and 4.0 kHz. The receive antenna separations varied from a minimum of 25 to 450 m in the transverse direction, and 50 to 150 m along the path. We describe the diagnostic experiments that we carried out and summarize the statistics of Doppler spread, spatial coherence, and frequency coherence.

Analysis of the Structure and Motion of Equatorial Depletion Bands Using Radio Sounding and Optical All-sky Images

G.S. Sales, R. Pickett and A. Gee
University of Massachusetts Lowell

In Chile, beginning after sunset, a series of relatively narrow bands of electron density depletion oriented north-south in the F-region of the ionosphere are detected at the western horizon and drift eastward. These depletions are directly associated with the formation of equatorial bubbles that rise over the magnetic equator and extending north and south along the magnetic field lines passing through the rising bubble. These electron depleted bands represent the upwelling of low density, low altitude plasma into the upper, higher density F-region.

We address the need for improved understanding of the structure and motion of these depletion regions, which appear as dark bands when observed by an all-sky photometer system against the background of normal 630.0 nm airglow that has an intensity of about 40 Rayleighs at these latitudes. These depletions appear as dark bands, typically 100 to 200 km in width extending southward away from the magnetic equator. In this investigation, these emission depletion bands were observed at Agua Verde, Chile which lies some 1500 km south of the magnetic equator.

Using HF sounding and satellite measurements, it is demonstrated that these depletion regions appear highly irregular on the scales of meters to kilometers and often result in the severe disturbance of satellite navigation and communications systems when their signals pass through these bands. Extensive 630.0 nm optical measurements of these depletions have been made using an all-sky imaging photometer along with Digisonde vertical soundings at the same site. These radio and optical images have provided a basis for measuring the width of these depletions and the speed with which they move.

The problem of describing the three dimensional structure of these depletion bands is addressed using a combination of the optical and radio data in conjunction with modeling techniques. A quantitative comparison is made of the simulated emission intensity calculated using the depletion model with a smoothed version the measured optical data with the goal of deriving the structure of the depletion band. The end product is a description of the 3-D geometry of the depletion in terms of empirical and model parameters.

URSI G

Session 128 **Salon Jolliet**

Ionospheric Tomography
Co-chairs: H. Na, USA and P.A. Bernhardt, USA

13:10	128.1	**Invited:** Comparison and Analysis of Multiple Sensor Ionospheric Reconstructions, **G.S. BUST**, *University of Texas at Austin, TX, USA*
13:30	128.2	Recent Progress in Ionospheric Tomography at High Latitudes, **L. KERSLEY**, S.E. PRYSE, I.K. WALKER, P.S.J. SPENCER, C.N. MITCHELL, M.J. WILLIAMS, C.A. WILLSON, S.T. BERRY, *University of Wales, Aberystwyth, UK*
13:50	128.3	Southern Hemisphere Computerized Ionospheric Tomography Campaign, A. VILLANI, **E.A. ESSEX**, *La Trobe University, Bundoora, Australia*
14:10	128.4	Enhanced CIT Using Four New Satellites with Radio Beacons, Limb Scanning, and Various Inclinations, **P.A. BERNHARDT**[1], K.F. DYMOND[1], D.M. COTTON[2], P.R. STRAUS[3], [1]*Naval Research Laboratory, Washington, DC,* [2]*Boston University, Boston, MA and* [3]*The Aerospace Corporation, Los Angeles, CA, USA*
14:30	128.5	Combining CIT and GPS-TEC Measurements to Investigate Protonospheric TEC, **D.S. COCO**, C. COKER, T.L. GAUSSIRAN, II, *University of Texas at Austin, TX, USA*
14:50	128.6	Real-Time Four-Dimensional Tomography: Current Status, **G.R. KRONSCHNABL**, T.L. GAUSSIRAN, II, G.S. BUST, D.S. COCO, *University of Texas at Austin, TX, USA*
15:10		Coffee Break
15:30	128.7	TID Investigation Utilizing CIT and GPS-TEC, **T.L. GAUSSIRAN, II**, D.S. COCO, *University of Texas at Austin, TX, USA*
15:50	128.8	A Volumetric Guide to ART Based CIT Image Reconstruction, **C. BISWAS**, H.R. NA, *University of California, Los Angeles, CA, USA*

G128.1

Comparison and Analysis of Multiple Sensor Ionospheric Reconstructions

Gary S. Bust
Applied Research Labs
The University of Texas at Austin

The recent focus of research and development in computerized ionospheric tomography (CIT) at the Applied Research Laboratories, the University of Texas at Austin (ARL:UT) has been to combine separate data sources (Transit, GPS, GPS MET, UV sensors, etc.) into a single time varying estimation of a regional (and/or global) 3D ionosphere. The differing type of data sources, combined with the many reconstruction algorithms developed by the community, leads to a large number of estimation schemes. Since there are very few measurements of ionospheric profiles over extended regions, it is difficult to compare and contrast the different estimation schemes. What is required is a single open architecture, interactive tool that allows the merging of different data sources with different reconstruction schemes. In addition, the ability to incorporate realistic ionospheric simulations as well as independent measurements of the ionosphere allows comparisons between different estimation schemes.

Such an interactive ionospheric tomography reconstruction and analysis tool is under development at ARL:UT. The ultimate design goal of the tool is to have several user selectable module to perform such tasks as: a general data input module, providing as many different reconstruction schemes as possible, include ionospheric simulation modules, inputs of independent ionospheric measurements, and a suite of analysis tools. Currently the tool allows input of Transit, GPS and GPS MET data.

This paper will examine data taken during three multi-array, multi-data source CIT campaigns in the USA, and a long term two array net currently operating in the western half of the country. Results from these campaigns, combined with GPS MET data are analyzed with the tool described above, and compared with ionosonde and DMSP data. The results are also be compared with simulations for the same period.

RECENT PROGRESS IN IONOSPHERIC TOMOGRAPHY AT HIGH LATITUDES

L Kersley*, S E Pryse, I K Walker, P S J Spencer, C N Mitchell, M J Williams, C A Willson and S T Berry

Department of Physics, University of Wales, Aberystwyth SY23 3BZ, UK

Abstract

The recent work in the field of ionospheric tomography undertaken by the group at UWA is reviewed.

The experimental activities described involve a chain of four receiving systems for investigation of the high-latitude ionosphere, a key region of importance to many radiowave propagation applications. The stations at Tromsø in continental Norway and Bjornoya, Longyearbyen and Ny Ålesund in the Svalbard archipelago yield observations that cover the main regions of the ionosphere at high latitudes. Around magnetic noon, tomographic images can be formed extending from the cusp in the north to an ionosphere characteristic of daytime midlatitudes in the south. Post-noon, the images show the development of a trough in a region of counterstreaming of flux tubes at the boundary between the return flow of the polar cap afternoon cell and the corotation at lower latitudes. During the night the images span the polar cap and auroral zone and reveal structures in the former that are characteristic of the density enhancements associated with patches convecting in the anti-sunward flow. The unique ability of the tomographic method to reveal the spatial distribution of such features has importance to the understanding of the dominant mechanisms responsible for patch formation, one of the unsolved problems of the polar ionosphere. At auroral latitudes, the changes in layer height in regions spanning both auroral-E and F-region ionisation present a particular challenge to tomographic imaging. Progress in this area is described. After magnetic midnight the images cover the dawn cell with, in winter, the depleted densities of the polar hole.

The paper discusses the role of ionospheric tomography in addressing areas of current interest to the geophysics of the ionosphere at high latitudes. In addition, by revealing the spatial structuring in this region, where steep density gradients affect the propagation of radio signals, it is shown that ionospheric tomography has considerable potential to monitoring and modelling of the high-latitude plasma for applications purposes.

G128.3

SOUTHERN HEMISPHERE COMPUTERIZED IONOSPHERIC TOMOGRAPHY CAMPAIGN

A. Villani and E.A. Essex*
School of Physics
La Trobe University
Bundoora, Victoria 3083, Australia
e.essex@latrobe.edu.au

The structure of the ionosphere may be investigated using the technique of computerized ionospheric tomography (CIT). The CIT technique uses the total electron content (TEC), to derive the vertical ionospheric profile. This is accomplished by setting up an array of receiving stations to collect differential phase data from satellites such as the polar orbiting satellites from the United States Navy Navigation Satellite System (NNSS). The differential phase equipment used is a JMR satellite receiver system. Four receiving stations have been installed along the eastern coast of Australia, spanning across geographic latitudes 44 degrees S and 27 degrees S at the locations : Kingston, Melbourne, Newcastle and Brisbane. The data collected is relative TEC. A baseline for the TEC values can be obtained with the aid of GPS and critical frequency data. When this data is unavailable the technique of combining the differential phase measurements from the receiving stations is used. The TEC measurements are then transformed into a two-dimensional tomographic image via various algorithms. The resulting ionospheric profile is compared with that obtained from ionosondes. The results of the application of different tomography algorithms to processing satellite passes from a five months observation campaign will be discussed.

Enhanced CIT Using Four New Satellites with Radio Beacons, Limb Scanning, and Various Inclinations

P.A. Bernhardt[1] and K.F. Dymond[2]
[1]Beam Physics Branch, Plasma Physics Division
[2]E.O. Hulbert Center for Space Research
Naval Research Laboratory
Washington, DC 20375-5320

D.M. Cotton
Center for Space Physics, Boston University
Boston, MA 02215

P. R. Straus
The Aerospace Corporation
Los Angeles, CA 90009

Computerized ionospheric tomography (CIT) is based on beacon transmitters located on low earth orbiting (LEO) satellites such as TRANSIT and COSMOS. Two problems with this type of CIT are (1) the lack of horizontal integration paths for total electron content and (2) the restriction of current beacon satellites to polar (i.e., north-south) orbits. Reconstructions based on only vertical and oblique measurements of total electron content (TEC) are not unique. The problem with this type of reconstruction uncertainty in the vertical density profiles. Polar orbiting do not provide zonal images of ionospheric densities using only one chain of receivers. To alleviate these weaknesses, four new satellites are scheduled for launch in 1997 through 1999 that have both multi-frequency radio beacon transmitters and instruments designed to provide horizontal integrations with optical and radio techniques. These satellites will carry radio beacons that radiate at 150.012, 400.032, and possibly 1066.752 MHz. These frequency transmissions can be used with existing "TRANSIT" receivers to obtain total electron content (TEC) between the satellite and the ground. Three of the satellites, TERRIERS, ARGOS, and STRV-1d, will also carry optical instruments that measure extreme ultraviolet radiation resulting from radiative recombination [i.e., $O^+ + e^- \rightarrow O + h\nu$ (91.1 nm)] at night or photoionization [i.e. $O + h\nu$ (sun) $\rightarrow O^+ + e^- + h\nu$ (83.4 nm)] during the day. As the optical sensors scan the earth's limb, the measurements provide horizontal, line-of-sight integrations for functions of the oxygen ion and electron densities in the F-layer. The fourth satellite, P97-1, will use an orbiting GPS receiver to determine the TEC from the satellite to GPS satellites along paths the occult the earth's ionosphere. Model simulations of CIT show significant improvements using the limb scanning data. The P97-1 satellite will also be in a 20 to 60 degree inclination circular orbit. The STRV-1d satellite will be in a 7 degree geosynchronous transfer orbit. This two orbits will permit focusing ionospheric research on imaging mid- and low-lighted structures, respectively.

G128.5

Combining CIT and GPS-TEC Measurements to Investigate Protonospheric TEC

David S. Coco*, Clayton Coker, Thomas L. Gaussiran II
Applied Research Laboritories
The University of Texas at Austin

The total electron content (TEC) in the protonosphere can be investigated by combining the two-dimensional (2D) computerized ionospheric tomography (CIT) reconstructions and TEC data from the Global Positioning Satellite (GPS) system. This technique allows one to produce protonospheric TEC estimates over large ionospheric regions when data from CIT and GPS networks are both available. Since GPS coverage from existing networks is continuous and almost global now, this means that this technique can be used for practically all CIT networks whenever they are operational. This technique is especially useful for monitoring the latitudinal variations in the protonospheric TEC, and the changes in these variations over time.

This paper will discuss the algorithms used to create the GPS TEC maps and also combine the CIT and GPS TEC data. Recent results from the application of this technique will be presented. For this study, the CIT data was collected from an ARL:UT dual chain CIT network operating in the western part of the US over the past year and the GPS data was collected from the National Geodetic Surveys Continuously Operating Reference Station (CORS) network. The protonospheric TEC derived from measurements from these networks is compared to measurements from other ionospheric sensors and with model predictions. Latitudinal and diurnal variations in TEC are presented along with examples from quiet and disturbed ionospheric conditions. Preliminary results indicate that the protonospheric TEC from this technique is often significantly larger than the TEC from model predictions. Error sources are discussed along with the potential for accuracy improvements for this technique.

REAL-TIME FOUR-DIMENSIONAL TOMOGRAPHY: CURRENT STATUS

Glenn R. Kronschnabl*, Thomas L. Gaussiran II, Gary S. Bust, David S. Coco
Applied Research Labs
The University of Texas at Austin

The Applied Research Laboratories, The University of Texas at Austin (ARL:UT), is currently developing a real-time four-dimensional (4D) (latitude, longitude, height, time) multiple ionospheric sensor tomography reconstruction (MISTR) processor. The goal of the MISTR processor is to provide "on-demand" volumetric ionospheric specifications based on real-time ionospheric measurements.

The need for such a capability has become increasingly pronounced as many radio-frequency (RF) applications, such as over-the-horizon (OTH) radars and single site location (SSL) systems, strive to improve system performance. For RF applications such as these, system performance is limited by insufficient and/or inaccurate modeling of the ionosphere. MISTR aims to improve system performance by providing "on-demand" volumetric ionospheric specifications based on real-time ionospheric measurements. RF applications that incorporate MISTR products instead of simple parameterized or climatological inospheric models should realize a substantial improvement.

The ionospheric measurements that are currently being incorporated are two-dimensional (2D) computerized ionospheric tomography (CIT) reconstructions and total electron content (TEC) data from the Global Positioning Satellite (GPS) System. The algorithms are to be designed such that other ionospheric data of opportunity, such as optical ultra-violet (UV) measurements, or scaled vertical incidence ionosonde profiles, can be combined into the processor fairly easily.

The goal of this paper is to provide an overview of the MISTR processor and the algorithms ARL:UT developed to fuse the different ionospheric measurement types. The strengths and weaknesses of the current algorithms will also be discussed. Finally, some preliminary results will be presented from the MISTR processor. The test data are taken from the ARL:UT semi-permanent CIT network, a dual-chain network of eight Transit satellite receivers in approximately two parallel lines in the western half of the U.S, where the two chains were roughly centered at longitudes of 105 and 118 degrees W and spanned over 1000 km, respectively.

G128.7

TID investigation utilizing CIT and GPS-TEC

Thomas L. Gaussiran II*, David S. Coco
Applied Research Laboritories
The University of Texas at Austin

Traveling ionospheric disturbances (TIDs) are non-linear wave phenomena which affect communication and play an important role in the global atmospheric energy budget. There exists three different saturated spectra theories which describe the development of propagating TIDs. These theories differ in how they approximate the non-linear behavior of the TIDs and, as a result, provide significantly different predictions of TID charateristics. To identify which theory is most correct a complete characterization of the TID is required.

Applied Research Laboritories at the University of Texas at Austin (ARL:UT) has developed and collected data from experimental resources to characterize TID wave parameters. These resources provide a collection of data with unique complementary spatial and temporal resolution. In 1996 a study was undertaken which involved 3 chains of CIT receivers along with a dense collections of GPS receivers which are part of the Continuously Operating Reference Station (CORS) network managed by the National Geodetic Survey (NGS). This campaign occured over the Eastern half of the US and lasted for slightly more than two weeks. By combining this data in the multiple ionospheric sensor tomography reconstruction (MISTR) processor three dimensional reconstructions were performed and allowed to evolve in time.

This paper will present the experimental observations which were made during an April 1996 campaign. We will examine how the TID wave characteristic parameters can be extracted from the reconstructions. The wave parameters from the observed TIDs should allow us to identify which of the three different saturated spectra theories is most correct. This information should assist modelers to more accurately include the effects of TIDs in their models.

G128.8

A volumetric guide to ART based CIT image reconstruction

Chaitali Biswas* and Helen R. Na
Department of Electrical Engineering
University of California, Los Angeles CA 90095–1594, USA.

This paper presents a new a priori guided reconstruction algorithm for the standard computerized ionospheric tomography imaging system. Images of ionospheric electron density reconstructed from satellite TEC measurements lack substantial information in the vertical direction due to geometric limitations of the CIT system. Hence, most current CIT reconstruction algorithms use a priori information such as values of electron density from model ionospheres to drive the reconstruction process towards a feasible solution. The new approach, however, uses prominent structural and behavioral parameters derived from analysis of available ionospheric models, instead of raw electron density values to guide the reconstruction algorithm. The paper describes methods for enhanced CIT reconstruction by efficient combination of satellite TEC information with additional measurements of electron density from oblique ionosondes and incoherent backscatter radars. Additionally, a normalized shape matrix is defined based on the structures of the apriori images. The a priori images are derived from the IRI-90 model. The simulation involves reconstructions for the equatorial ionosphere above the Caribbean region for various times of the day and year and for different levels of solar activity. The algorithm centers around the fundamental SIRT recontruction process with a vector of error based weights that feeds a priori information into the system. There are two instances of error calculation in each iteration, once in the projection domain for the selection of the optimal profile for distribution of residual TEC data along each ray path, and subsequently during the shape correction phase when the shape matrix of the current reconstruction is compared with the shape matrices of the a priori images. The weights are re-evaluated in a manner allowing the reconstruction to achieve maximal conformity with measured TEC data while preserving volumetric or shape information Thus, the algorithm uses parameters based on the shape of a priori models as opposed to direct a priori values, avoiding significant degradation or divergence that could arise in situations where the a priori model values are not representative of the measured ionospheric distribution.

URSI H **Session 87** Salon Peribonca

In-situ Studies of Artificial Waves - Part I
Co-chairs: W.J. Burke, USA and R.F. Benson, USA

10:10 87.1 **Invited:** A Review of Sounding Results of the Oedipus-C Experiment, **H.G. JAMES**, *Communications Research Centre, Ottawa, ON, Canada*

10:30 87.2 An Explanation of Proton-Cyclotron Echoes on Topside Ionograms, **D.B. MULDREW**, *Industry Canada, Ottawa, ON, Canada*

10:50 87.3 Experimental Application of an Electron Beam Antenna in Space, **N.B. MYERS**[1], J. ERNSTMEYER[1], W.J. RAITT[2], [1]*Rome Laboratory, Hanscom AFB, MA and* [2]*Utah State University, Logan, UT, USA*

11:10 87.4 OEDIPUS C Sounder-Accelerated Electrons at Frequencies below the Plasma Frequency, **R.F. BENSON**[1], W.J. BURKE[2], D.A. HARDY[2], H.G. JAMES[3], [1]*NASA/Goddard Space Flight Center, Greenbelt, MD and* [2]*Phillips Laboratory/GPSG, Hanscom AFB, MA, USA;* [3]*Communications Research Centre, Ottawa, ON, Canada*

11:30 87.5 Radio-Frequency Sounders in Space, **R.F. BENSON**, *NASA/Goddard Space Flight Center, Greenbelt, MD, USA*

11:50 87.6 Plasma Response of Insulated and Uninsulated Conductors in Ionospheric Plasma Due to High Negative Voltage Pulsing, **S.G. BILÉN**, B.E. GILCHRIST, *University of Michigan, Ann Arbor, MI, USA*

H87.1

A REVIEW OF SOUNDING RESULTS OF THE OEDIPUS-C EXPERIMENT

H.G. James
Communications Research Centre,
Ottawa, Ontario K2H 8S2, Canada

The OEDIPUS-C tethered payload was launched on 7 November 1995 from the Poker Flat Research Range, Alaska on a Black Brant XII sounding rocket. The 255-kg payload reached an apogee of 824 km on its 16-min flight. Approximately 13 minutes of data were recorded starting at the subpayload separation 174 s after launch. The two spinning subpayloads were connected, for the first half of the experiment phase, by a 24-gauge wire serving as a conducting tether. A final tether length of 1.17 km was achieved at about 278 s after subpayload separation. The tether was cut at both subpayloads 449 s after separation. The subpayload separation vector stayed within 6° of the local magnetic field **B** throughout the flight. All-sky imagers and meridian scanning photometers on the ground beneath the trajectory showed that auroral arcs of 5-10 kR intensity occurred in the region of apogee around the north coast of Alaska.

OEDIPUS C carried a 10-W transmitter High-frequency EXciter (HEX) on its forward subpayload and a synchronized Receiver for EXciter (REX) on the aft subpayload. The HEX and REX had three different frequency modes: a 0.1-8.0 MHz sweep, a 0.5 - 2.1 MHz sweep and fixed frequency operation at 4.5 MHz. Throughout the flight, HEX and REX were connected cyclically to quadrupole antennas configured as V dipoles. The 320-s post-tether-cut part of the flight, most of the downleg, produced a number of new topside sounding observations. First, the series of about 420 swept-frequency ionograms reveal an ionosphere with a dense peak at about 100 km altitude, with $foE \approx 8$ MHz. The complete absence of any F layer is consistent with the observations by both onboard particle detectors and ground optical equipment of sustained auroral-particle precipitation in the region. When the payload was within 200 km of the E-region peak, "bumpy" and double-valued swept-frequency ionogram traces gave evidence of localized density structures.

The separated transmitter and receiver produced novel bistatic propagation results. Several series of fringes in various cold-plasma modes can be explained with reference to Faraday rotation or to interference between two waves propagating in the same mode. The amplitudes of different cold-plasma modes transmitted across the link can be analyzed for checks on the plasma antenna theory. Because the transmitter is always above the receiver, direct measurements of the reflection coefficient of the ionosphere were obtained. During the latter part of the downleg, a few instances of whistler-mode reflection traces were obtained.

AN EXPLANATION OF PROTON-CYCLOTRON ECHOES ON TOPSIDE IONOGRAMS

D. B. Muldrew
Communications Research Centre, Industry Canada,
P. O. Box 11490, Ottawa, Ontario, Canada, K2H 8S2

Proton-cyclotron echoes appear on topside ionograms as thin traces at delay times approximately equal to multiples of the proton-cyclotron period t_p. At frequencies below the electron-cyclotron frequency f_H, the proton echo delay is almost an exact multiple of t_p. At frequencies above f_H, there can be an additional delay to t_p depending on two factors: (1) the antenna orientation, and (2) the closeness of the proton-echo frequency f to f_H. Protons passing within a few centimeters of the antenna during an RF pulse are energized by an amount depending on the RF phase at the time of closest approach. At multiples of t_p later, these protons return to almost the same field line they were on at the time of energization by the RF transmitter pulse although they may have moved some tens of meters along the field line. At multiples of t_p, nt_p (where n=1, sometimes 2, and rarely 3) the protons are thus located in a plane containing the linear dipole antenna (73 m tip-to-tip) at the time of the pulse and the direction of the magnetic field. At nt_p the protons, which were energized with the time variation of the sounder pulse frequency, produce a field which simulates the original field of the RF pulse and if wave propagation in the plasma is possible at the pulse frequency, a wave may be produced which propagates to the new position of the antenna which has moved in the plasma at the satellite velocity $\mathbf{V}_s$. For $f > f_H$, perpendicularly-propagating electron Bernstein waves are responsible for the propagation. No such Bernstein waves exist for $f < f_H$ and proton echoes are observed if $\mathbf{V}_s$ is approximately in the plane of the energized protons at nt_p so that wave propagation is not necessary to receive an echo.

There may be two effects responsible for factor (2) mentioned above. As the wave frequency approaches f_H, the group velocity of the Bernstein waves approaches zero and consequently the propagation time to the antenna increases. A secondary effect may be that the energy density of the Bernstein waves, and to some extent of the energized electrons, is so large that the local energy density of the Earth's magnetic field is reduced. This would result since the total energy density (i.e. pressure) remains constant. These effects could explain the observed increase in proton echo delay which can be as much as a few percent.

H87.3

Experimental Application of an Electron Beam Antenna in Space

*Neil B. Myers and James Ernstmeyer, Rome Laboratory, 31 Grenier St, Hanscom AFB, MA 01731-3010
W. John Raitt, Utah State University, Center for Atmospheric and Space Sciences, Logan, UT 84322-4405

An electron beam was modulated at VLF frequencies during a sounding rocket experiment in order to produce electromagnetic radiation in space at the fundamental modulation frequency. This experiment, CHARGE-2B, was launched in March 1992 from Poker Flats Research Range, Alaska, and represents the first time that a space experiment was launched with the principal objective of using a modulated electron beam as a virtual antenna to generate electromagnetic radiation. A deployable free flying payload was incorporated in the nosecone and configured to separate from the beam-emitting payload during the flight to measure both electric and magnetic field fluctuations in three dimensions due to operation of the electron gun. The tail section of the rocket was also separated from the beam-emitting payload and remained in electrical contact by use of a 426 m conducting tether that was insulated from the surrounding plasma. This provided an important reference to determine the vehicle potential of the beam-emitting payload during operation of the electron gun. The electron gun consisted of two 3-keV, 1-A modules that were operated synchronously to provide a total beam current of 2 A. The beam current was modulated with a sinusoidal waveform to maximize the power in the fundamental frequency and minimize harmonic generation. A neutral gas release system using a modified thruster nozzle provided periodic control of the vehicle potential during beam emission. Electromagnetic waves generated by the modulated electron beam were observed at the free flying payload throughout the flight to the maximum separation distance of 2 km. Three ground-based VLF receive sites were deployed near the footprint of the rocket trajectory traced down to Earth along magnetic field lines. No evidence of electromagnetic waves due to the electron beam were observed at the ground sites.

OEDIPUS C Sounder-Accelerated Electrons at Frequencies Below the Plasma Frequency

Robert. F. Benson*
Laboratory for Extraterrestrial Physics
NASA/Goddard Space Flight Center, Greenbelt, MD 20771, USA
Phone: (301) 286-4037, Fax: (301) 286-1683
e.mail: u2rfb@lepvax.gsfc.nasa.gov

William J. Burke and David A. Hardy
Phillips Laboratory/GPSG, Hanscom AFB, MA 01731

H. Gordon James
Communications Research Centre
3701 Carling Ave., Box 11490, Station H, Ottawa, Ontario K2H 8S2

The radio pulses from ionospheric topside sounders have been shown to accelerate the ambient ionospheric electrons and ions (e.g., Galperin et al., Cosmic Res., 19, 22-29, 1981; James, J. Geophys. Res., 88, 4027-4040, 1983). It has also been shown that the electron heating can be correlated to specific sounder-operating frequencies relative to the ambient plasma frequency and electron gyrofrequency. In particular, electron heating is observed corresponding to plasma resonances stimulated by the sounder pulses, including a class of plasma emissions (known as diffuse plasma resonances) stimulated at frequencies below the plasma frequency (Serov et al., Cosmic Res., 23, 361-372, 1985; Shuiskaya et al., Planet. Space Sci., 38, 173-180, 1990). The above results were based on wave-injection experiments performed during ionospheric topside sounding where the sounder transmitter and receiver were located on the same spacecraft. Here we report observations of such electron heating by sounder pulses from the OEDIPUS C rocket bistatic wave propagation experiment (transmitter and receiver separated by as much as 1 km). Each payload contained identical particle detectors operating in synchronism with the sounder and each of these detectors contained wave/particle correlators. The electron heating was found to correspond to sounder operation at the electron gyrofrequency over most of the flight, the second harmonic of the electron gyrofrequency over part of the flight, and to a broad frequency region below the electron plasma frequency when the plasma/gyro frequency ratio was sufficiently large and precipitating auroral electrons were present.

H87.5

Radio-Frequency Sounders in Space

Robert. F. Benson
Laboratory for Extraterrestrial Physics
NASA/Goddard Space Flight Center
Greenbelt, MD 20771, USA
Phone: (301) 286-4037, Fax: (301) 286-1683
e.mail: u2rfb@lepvax.gsfc.nasa.gov

Radio-frequency sounders in space are most often referred to as topside sounders because their original purpose was to investigate the global distribution of electron density in the ionosphere at altitudes above the F layer peak density. They have been used predominately for four types of investigations: (1) local and remote topside electron densities and electron density gradients, (2) plasma wave propagation, (3) natural emissions and (4) stimulated plasma emissions. This paper will give a brief overview of some of the results that have been obtained in these areas from investigations of ionograms as recorded on 35 mm film from the Alouette/ISIS program (International Satellites for Ionospheric Studies). Topics will include (1) electron density contours and spread F, (2) electrostatic plasma waves near resonant frequencies in the ambient plasma, (3) auroral kilometric radiation (AKR) and (4) stimulated emissions at frequencies below the electron plasma frequency (known as diffuse resonances).

The lifetimes of the Alouette/ISIS satellites span approximately 60 satellite-years of pole-to-pole operation. Unfortunately, not all of the sounder data have been extracted from the original telemetry tapes. In particular, only about 15% of the ISIS 1 and 2 tapes have been processed to produce topside-sounder ionograms on 35 mm film. This paper will briefly describe an effort underway at the Goddard Space Flight Center to transform selected samples of several decades of ISIS 1 and 2 ionospheric topside sounder data to digital ionograms. The digital ionograms are being archived at the National Space Science Data Center (NSSDC) at Goddard for computer-retrieval via the internet (see the NSSDC ISIS WWW home page at http://nssdc.gsfc.nasa.gov/space/isis/isis-status.html).

Some results from the recent OEDIPUS C rocket bistatic wave propagation experiment will be discussed along with plans to orbit a radio sounder called the Radio Plasma Imager (RPI) on the Imager for Magnetopause-to-Aurora Global Exploration (IMAGE) which was selected as NASA's first Medium Class Explorer (MIDEX) satellite. IMAGE is scheduled for launch in January, 2000.

Plasma Response of Insulated and Uninsulated Conductors in Ionospheric Plasma Due to High Negative Voltage Pulsing

Sven G. Bilén* and Brian E. Gilchrist
Radiation Laboratory
Electrical Engineering and Computer Science Dept., University of Michigan
1301 Beal Avenue, Ann Arbor, MI 48109-2122, USA

Recently, much work has been performed toward understanding the transient response of a conductor-plasma system in which the conductor is quickly biased to high (both negative and positive) voltages. To date, however, not much work has examined the case of quickly biasing insulated conductors. In addition, there is currently little understanding of the transient response of a distributed system, such as a long conductor immersed in a plasma, to the application of high voltages. This work begins by examining in 1d and 2d the transient response of both conductor-plasma and conductor-insulator-plasma geometries. Extension to distributed systems, *i.e.*, long conductors, is then made.

Our research is aimed at understanding the propagation characteristics of electromagnetic pulses along long conductors in plasma with specific application to electrodynamic tethers in the ionosphere. Electrodynamic tethers are, in general conducting wires that join two separated spacecraft as they orbit the Earth or other planetary body having a magnetic field. A complete understanding of the electrical response of an electrodynamic tether system requires knowledge of both its steady-state and its transient response. Because of the physical separation of the system's two ends, a perturbation (*e.g.*, a switch closure) on one end takes a finite amount of time to propagate along the tether to the other end. How this pulse front affects the surrounding ionospheric plasma and how that interaction affects the tether's transmission line characteristics are questions which are examined.

The transient response of a plasma immersed conductor to the initial pulse front is examined numerically using the particle-in-cell (PIC) plasma simulation method. The evolution of the sheath dynamics is examined as the pulse front travels past a given section of the tether and disturbs the steady-state sheath. This models the transition of a tether/plasma system from open- to closed-circuit states (*i.e.*, no current to current flowing states).

Understanding the transient and pulse propagation behavior of an electrodynamic tether system is of special importance to systems detecting natural electric field transient signatures and those utilizing tether current pulses or modulation, such as for low frequency wave generation.

URSI H | Session 94 | Salon Jolliet

In-situ Studies of Artificial Waves - Part II
Co-chairs: B. Gilchrist, USA and H.G James, Canada

13:10 94.1 **Invited:** A New Method for Estimating Electromagnetic Fields Produced by Distributed Current Sources in a Cold Magnetized Plasma, **G.P. GINET**, *USAF Phillips Laboratory, Hanscom AFB, MA, USA*

13:30 94.2 Relationships between MHz Modulations of Electron Beams Detected during TSS 1R and Whistler Waves Observed during Spacelab 2, C.Y. HUANG[1], **W.J. BURKE**[2], M.P. GOUGH[3], L.C. GENTILE[1], D.A. HARDY[2], D.G. OLSON[2], [1]*Boston College Institute for Scientific Research, Newton, MA and* [2]*USAF Phillips Laboratory, Hanscom AFB, MA, USA;* [3]*University of Sussex, UK*

13:50 94.3 Electron Acceleration and Trapping during the OEDIPUS C Sounding Rocket Experiment, **W.J. BURKE**[1], D.A. HARDY[1], M.P. GOUGH[2], C.Y. HUANG[3], L.C. GENTILE[3], D.G. OLSON[1], [1]*USAF Phillips Laboratory, Hanscom AFB, MA, USA;* [2]*University of Sussex, UK;* [3]*Boston College Institute for Scientific Research, Newton, MA, USA*

14:10 94.4 Enhancing Tethered Multipoint Measurements of Ionospheric Plasma Using Simultaneous Radiowave Measurements of Total Electron Content, **D.P. MORRIS**, B.E. GILCHRIST, *University of Michigan, Ann Arbor, MI, USA*

14:30 94.5 Predictions for the Radar Spectra for Ionospheric-Plasma Interactions in Space Shuttle OMS Plumes, **P.A. BERNHARDT**, J.D. HUBA, *Naval Research Laboratory, Washington, DC, USA*

14:50 94.6 RF Discharges Generated by Crossed-Dipole Antennas, **A.A.E. LÜTTGEN**[1], K.G. BALMAIN[1], H.G. JAMES[2], [1]*University of Toronto and* [2]*Communications Research Centre, Ottawa, ON, Canada*

15:10 94.7 Whistler Wave Ducting in the Ionosphere and Laboratory Experiments, M.J. ROWLANDS, **M.C. LEE**, R.J. RIDDOLLS, N.E. DALRYMPLE, *Massachusetts Institute of Technology, Cambridge, MA, USA*

15:30 94.8 RF-Enhanced Langmuir Waves in the Ionosphere and in the Laboratory, **M.C. LEE**[1], R.J. RIDDOLLS[1], N.E. DALRYMPLE[1], K.D. VILECE[1], M.J. ROWLANDS[1], D.T. MORIARTY[1], K.M. GROVES[2], M.P. SULZER[3], S.P. KUO[4], [1]*Massachusetts Institute of Technology, Cambridge, MA,* [2]*Air Force Phillips Laboratory, Hanscom AFB, MA,* [3]*Arecibo Observatory, Arecibo, Puerto Rico and* [4]*Polytechnic University, Farmingdale, NY, USA*

15:50 94.9 Sheath Waves Observed on Oedipus C, **H.G. JAMES**[1], K.G. BALMAIN[2], [1]*Communications Research Centre, Ottawa and* [2]*University of Toronto, ON, Canada*

16:10 94.10 RF Effects Seen on the OEDIPUS-C Tether Current Monitor, **J.G. LAFRAMBOISE**[1], D.D. WALLIS[2], H.G. JAMES[3], [1]*York University, North York,* [2]*Herzberg Institute of Astrophysics/NRC, Ottawa and* [3]*Communications Research Centre, Ottawa, ON, Canada*

16:30 94.11 **Invited:** Control of Radiation Belts Using Tethers, **K. PAPADOPOULOS**[1], A. DROBOT[2], C.L. CHANG[2], [1]*University of Maryland, College Park, MD and* [2]*SAIC, McLean, VA, USA*

16:50 94.12 The Three Levels Active Experiment in the Magnetosphere, **S.I. KLIMOV**[1], O.V. LAPSHINOVA[2], S.A. ROMANOV[1], W.W.L. TAYLOR[3], N.N. ANTROPOV[4], V.A. GRUSHIN[1], F.L. DUDKIN[5], V.E. KOREPANOV[5], M.M. MOGILEVSKY[1], M.N. NOZDRACHEV[1], W.E. PINE[6],, P. TRISKA[7], [1]*Space Res Inst (IKI) and* [2]*RKK ENERGIYA, Moscow, Russia;* [3]*Hughes STX and INSPIRE, Washington, DC, USA;* [4]*RIAM, Moscow, Russia;* [5]*LCISR, Lviv, Ukraine;* [6]*Chaffey High School and INSPIRE, CA, USA;* [7]*IFA, Prague, Czechia*

H94.1

A New Method for Estimating Electromagnetic Fields Produced by Distributed Current Sources in a Cold Magnetized Plasma

Gregory P. Ginet, USAF Phillips Laboratory, Hanscom AFB, MA 01731

A theory of the production of electromagnetic fields by a distributed current source in a magnetized plasma is useful in interpreting active space experiments involving pulsed-electron beams or actively radiating antennas. Previous calculations of the electric fields expected in pulsed electron beam experiments suffer from non-convergent integrals and discontinuities which stem from an inconsistent application of the boundary conditions at infinity. To circumvent these problems we have developed a new formulation of the linear response in terms Green's functions for the scalar and vector potentials from which the electromagnetic fields can be obtained in the usual manner. We present the Green's functions as expansions in spherical Bessel functions and Legendre polynomials containing a single, well-defined integral over azimuth in wave-vector space that must be done numerically. Application of the theory to a simple current source will be shown.

Relationships between MHz Modulations of Electron Beams Detected during TSS 1R and Whistler Waves Observed during Spacelab 2

Cheryl Y. Huang[1], William J. Burke[2], M. Paul Gough[3],
Louise C. Gentile[1], David A. Hardy[2], and David G.Olson[2]

Systematic experiments were conducted during the latter part of the Tethered Satellite System Reflight (TSS 1R) in which a 1 keV, 100 mA electron beam was emitted from the shuttle for extended intervals at pitch angles near 90°. Rapid plasma responses to these emissions were measured within the beam flux tube by the Shuttle Potential and Return Electron Experiment (SPREE). The SPREE particle correlator identified the energies/angles of time-modulated electron fluxes. Observed modulations at megahertz frequencies fall into two classes: (1) narrow bands that are close in frequency to harmonics of the electron gyrofrequency f_{ce} and (2) broad bands that are at interharmonic frequencies. In the latter case, electrons with different energies were modulated at different frequencies. Whenever SPREE intercepted beam electrons they were found to be modulated at harmonic or interharmonic frequencies after a single gyroturn. These data suggest that beam electrons were modulated by strong beam-plasma interactions very near to the emission aperture. They in turn generated the time-varying electric fields that modulated lower-energy electrons within or near the beam cylinder. During the Spacelab 2 mission, intense whistler waves were detected when the University of Iowa's Plasma Diagnostic Package flew close to the field lines along which electron beams were emitted from the shuttle. Observed whistler intensities and dispersions were consistent with requirements of coherent Cerenkov radiation sources, suggesting that the beam was modulated close to its emission aperture. The detection of modulated beam electrons by SPREE provides strong experimental confirmation of this hypothesis.

1. Boston College Institute for Scientific Research, Newton, MA
2. USAF Phillips Laboratory, Hanscom AFB, MA
3. University of Sussex, Sussex, UK

H94.3

Electron Acceleration and Trapping during the OEDIPUS C Sounding Rocket Experiment

William J. Burke[1], David A. Hardy[1], M. Paul Gough[2],
Cheryl Y. Huang[3], Louise C. Gentile[3], and David G. Olson[1]

The OEDIPUS C sounding rocket was launched from the Poker Flat rocket range on November 7, 1995 at 0638:17 UT. OEDIPUS C was a tethered mother-son payload with a 50 kHz to 8.0 Mhz stepped frequency transmitter on the forward payload and an HF receiver on the aft payload. In the course of the upleg of the flight, the tether was deployed to a distance of ~1.2 km. At apogee the tether was cut. As part of the complement of environmental sensors, multiangular electrostatic analyzers (ESAs) were flown on both the forward and aft payloads. These detectors compiled electron spectra from 20 eV to 20 keV in energy over a detection fan of 140° by 8°. The HF transmitter normally swept through 165 frequency steps every 0.5 seconds. During each 3 ms step, the transmitter was turned on for only the first 300 μs. The stepping of the ESA was synchronized with the transmitter so that the analyzer sampled all electron energies at each frequency step. The output pulses of the ESAs were also processed by an onboard particle correlator to detect bunching of electron fluxes produced by coherent wave-particle interactions and time delays between the initiation of waves by the transmitter and the observation of enhanced fluxes by the ESAs.

Throughout the flight the analyzer in the forward payload measured large increases in the electron flux at energies up to several keV whenever the transmitter was emitting at approximately the local electron gyrofrequency f_{ce}. Similar effects were observed on the aft payload for separations up to several hundred meters. At low altitudes, weak electron acceleration responses were detected in association with emissions both below f_{ce} and at its harmonics. The correlator measured clear Mhz modulations of accelerated electrons at the harmonics of the f_{ce}, indicating strong particle trapping of accelerated electrons by the emitted waves. There were significant time delays between the initiation of wave transmissions and the detection of particle enhancements by the aft payload ESA. This presentation relates ESA observations to the theory of electron cyclotron interactions and discusses potential applications of wave emission technologies in the magnetosphere.

1. USAF Phillips Laboratory, Hanscom AFB, MA
2. University of Sussex, Sussex, UK
3. Boston College Institute for Scientific Research, Newton, MA

Enhancing Tethered Multipoint Measurements of Ionospheric Plasma Using Simultaneous Radiowave Measurements of Total Electron Content

Dave P. Morris* and Brian E. Gilchrist
Radiation Laboratory
Electrical Engineering and Computer Science Dept., University of Michigan
1301 Beal Avenue, Ann Arbor, MI 48109-2122, USA

In order to significantly advance our understanding of ionosphere-thermosphere-magnetosphere coupling processes, improved spatial and temporal resolution measurements are needed. To address this need, numerous next generation mission concepts are now being developed which specify wide separation of several to even a hundred or more *in-situ* satellite/sensor systems. Nonetheless, adequate spatial resolution and coverage remain concerns where the feasible number of multipoint sites must be limited primarily due to cost considerations.

We are evaluating the use of radiowave signal propagation between satellite/sensor platforms as one method of increasing the knowledge of spatial variation and character of the plasma between platforms. The simplest information which can be obtained via this method is a measure of total electron content (TEC) and its time variability along the signal ray path between the satellites as they move together through their orbit. Two-frequency techniques, similar to those used by the Global Positioning System (GPS), represent one possible approach to providing this information. It is also possible that this radiowave transmission system could be part of an existing telemetry system.

By way of example, we have considered and will discuss two specific missions using multiple tethered satellites for vertical gradient measurements in the equatorial ionosphere in order to more accurately investigate the causes and sources of Spread-F or formation of ionospheric layers. One mission concept is based on a satellite which is deployed to a distance of 100 km below the space shuttle and reaches down to 130 km. The orbit is nearly circular. The second is a free-flyer mission in a highly elliptical orbit with a more modest separation distance of 4 to 6 km, but using three tethered sensor locations. A radiowave signal between platforms augments *in-situ* plasma measurements by providing a measure of vertical dimensions to layers differentiating between "sheet-like" and "blob-like" layers.

H94.5

Predictions for the Radar Spectra for Ionospheric-Plasma Interactions in Space Shuttle OMS Plumes

P.A. Bernhardt*, J.D. Huba
Beam Physics Branch, Naval Research Laboratory
Washington, DC 20375-5320

A theoretical model is presented to explain the enhanced backscatter from the 430-MHz radar at Arecibo during burns of the Space Shuttle orbital maneuver system (OMS) engines near 317 km altitude as reported by Bernhardt, Ganguli, Kelley, and Swartz [*JGR*, **100**, 23811, 1995]. Similar radar signatures were obtained by the Millstone Hill radar observing the plume of an Atlas Centaur burning in the ionosphere [Wand and Mendillo, *JGR*, **89**, 233, 1984]. Molecular ion beams can be generated in the exhaust plume because of charge exchange between the ambient O^+ ions and the high speed exhaust molecules (primarily H_20). Cooling of the exhaust vapors in the exhaust plume yield an ion beam is much colder than the ambient plasma. These cold ions also move in gyro orbits around the magnetic field. The electrons have a field aligned drift necessary to neutralize the parallel ion motion. These electrons retain their ambient temperature which is well above the plume ion temperature. Thus, the plasma in the exhaust plume consists of three components: (1) field aligned beam of hot electrons, (2) a stationary background component of hot ions, and (3) a spiraling beam of cold ions. The incoherent scatter spectra is calculated for this plasma with three distribution components. The results show Doppler shifts from the electron beam component and broadening of the spectra from the gyro motion the produces a ring velocity distribution. An enhancement in the backscatter is not seen, however, when just considering scattering from thermal velocity fluctuations.

One cause of the enhanced backscatter could be plasma turbulence generated by the by the pick-up ion motion in the presence of the earth's ambient magnetic field. After examining several plasma turbulence mechanisms, it is shown that the turbulence is likely caused by an ion ring instability from the gyro motion of the pick-up ions. The plasma turbulence influences the frequency spectra of the radar echoes by producing narrow upshifted and downshifted ion-ring lines. Analysis of these coherent backscatter lines can yield characteristics of the exhaust plume such as vector flow velocity, temperature and composition. Experimental observations of the radar backscatter spectra in side Space Shuttle plumes can provide validation of the use of ISR for monitoring natural, high-speed ion beams. The predictions of our radar scatter calculations will be tested in future experiments using the Space Shuttle OMS engines over incoherent scatter radars located at Arecibo, Puerto Rico, Jicamarca, Peru, and Kwajalein, Marshall Islands.

RF Discharges Generated by Crossed-Dipole Antennas

Andrea A.E. Lüttgen* and Keith G. Balmain
Department of Electrical and Computer Engineering, University of Toronto
10 King's College Rd., Toronto, Ontario M5S 3G4, Canada

H. Gordon James
Communications Research Centre, Ottawa, Ontario K2H 8S2, Canada

Early during the OEDIPUS-C tethered sounding rocket experiment, the payload was separated into two parts connected by a conducting wire that was used for double-probe and sheath-wave experiments. In a separate set of experiments, signals were sent from a 10 watt transmitter in the forward sub-payload connected to a crossed-dipole antenna and were received by a similar antenna connected to a receiver in the aft sub-payload. To drive the separation, argon thrusters on the forward sub-payload were used. A video camera on the aft sub-payload recorded the view of the forward sub-payload and its antenna. While the thrusters were operating, the transmitter was turned on and RF discharges were observed, i.e. the high electric fields near the dipole accelerated the ambient electrons which then caused light emission on collision with the argon gas. The light pattern consisted of a glow around the antennas as well as between the monopoles, and it changed as a function of the frequency.

In order to study these RF discharges, a laboratory experiment has been carried out in which a crossed-dipole antenna transmitting an amplified signal is placed in the center of a magnetized laboratory plasma generated by a high-voltage dc discharge. The antenna is in the form of two v-shaped monopoles. Each monopole consists of two orthogonal 6.5 cm wires perpendicular to the axial magnetic field. The complete, balanced dipole antenna is fed via a pair of coaxial cables connected to a 180 degree hybrid. Frequencies range from well below to well above the electron cyclotron frequency. For diagnostic purposes, three cylindrical probes parallel to the magnetic field are located on the anode plate at different positions relative to the dipole, i.e. under an antenna wire, between the monopoles and between the wires of the same monopole. Luminous bands are observed extending from the antenna wires along the magnetic field for the entire length of the plasma chamber. Also observed are luminous bands between the monopoles. These effects are associated with increases of the probe floating potentials to positive values. At a certain frequency above the cyclotron frequency, the glow abruptly vanishes while the probe potentials drop to negative values. Strong similarities are noted, comparing the glow distributions in the laboratory with those in space, and comparisons are made with calculations of the antenna near-field magnitudes.

H94.7

WHISTLER WAVE DUCTING IN THE IONOSPHERE AND LABORATORY EXPERIMENTS

M.J. Rowlands, M.C. Lee, R.J. Riddolls, N.E. Dalrymple
MIT Plasma Science and Fusion Center
Cambridge, MA 02139

The Versatile Toroidal Facility (VTF) is a torus of 1 m major radius used to simulate ionospheric plasmas. Hydrogen plasmas are formed in the chamber at a base pressure on the order of 10^{-7} torr. Currently, plasmas can be generated by electron emission from four LaB_6 cathodes, spaced around the bottom of the chamber, and by electron cyclotron resonance heating (ECRH) with microwaves injected radially into the chamber from a 3 kilowatt magnetron. Eighteen Large toroidal field coils, spaced equally around the chamber, produce a toroidal magnetic field of .08 Tesla. A .01 Tesla uniform vertical field is added to the toroidal field to yield a helical magnetic field that guides the electron beams along their path. In the ionosphere, whistler waves, usually excited by lightning, are ducted in areas of increased plasma density along the earth's magnetic field. However, according to Helliwell's theory, they are only ducted up to half the electron cyclotron frequency. Rocket experiments in the atmosphere have confirmed this theory. In VTF, the electron beams excite whistler waves along the helical magnetic field in the chamber, much like lightning in the atmosphere. Under certain plasma conditions, like lower plasma density, high magnetic field, the measured cutoff under other conditions in the chamber, whistler waves are ducted up to 3/4 of the electron cyclotron frequency. A ray tracing computer program has been created to analyze wave ducting for various plasma conditions and an adapted theory has been applied to help explain whistler waves ducting in the VTF chamber. Experimental results from VTF will be examined as well as results from the ray tracing simulation in order to better explain the discrepancy between atmospheric and laboratory data.

RF-ENHANCED LANGMUIR WAVES IN THE IONOSPHERE AND IN THE LABORATORY

M.C.Lee, R.J. Riddolls, N.E. Dalrymple, K.D. Vilece, M.J. Rowlands, and D.T. Moriarty
MIT Plasma Science and Fusion Center
Cambridge, MA 02139
K.M. Groves
Air Force Phillips Laboratory, Hanscom AFB, Massachusetts 01731
M.P. Sulzer
Arecibo Observatory, Arecibo, Peurto Rico 00613
S.P. Kuo
Polytechnic University, Farmingdale, New York 11735

Laboratory experiments, carried out at MIT Plasma Science & Fusion Center with the Versatile Toroidal Facility, have been conducted to simulate ionospheric plasma heating caused by High Frequency (HF) radio waves. The Versatile Toroidal Facility (VTF) is a student-built large toroidal plasma machine having a helical magnetic field, that guides electrons emitted from heated LaB_6 filaments to flow from the bottom side to the topside of the plasma chamber. These upward flowing electrons serve two purposes: (1) creating a backgound plasma through electron collisions with neutral gases (e.g., H_2, Ar, O_2), and (2) forming a field-aligned electric current. The VTF plasma machine is ideal for the study of ionospheric plasma heating [Lee et al., 1997 IEEE ICOPS] and space plasma processes, in a plasma environment characterized by: $\omega_{pe}/\omega_{ce} \geq 3$ and $T_e \sim T_i \sim 5ev$ where ω_{pe}, ω_{ce}, T_e, and T_i represent the electron plasma frequency, the electron gyrofrequency, the electron temperature, and the ion temperature in the VTF, respectively. Recent VTF laboratory experiments have successfully reproduced "cascading " and "frequency-upshifted" spectra of HF wave-enhanced Langmuir waves resembling the spectra observed in Arecibo experiments. The VTF experimental results are well-explained using the source mechanism proposed by Kuo and Lee [Geophys. Res. Lett, 19, 249, 1992] to interpret observed Langmuir wave spectra at Arecibo, Puerto Rico. This mechanism is referred to as a nonlinear scattering of parametric decay instability (PDI)-excited Langmuir waves by pre-existing lower hybrid waves to preferentially produce anti-Stokes (i.e., frequency-upshifted) Langmuir waves. Recent radar spectral observations of anti-Stokes Langmuir waves at Arecibo with improved range and time resolution [Sulzer and Fejer, J. Geophys. Res., 99, 15,035, 1994] can be reasonably understood in terms of this nonlinear scattering process.

H94.9

SHEATH WAVES OBSERVED ON OEDIPUS C

H. G. James
Communications Research Centre
Ottawa, Ontario K2H 8S2, Canada

K. G. Balmain
University of Toronto
Department of Electrical and Computer Engineering
10 King's College Road
Toronto, Ontario M5S 3G4, Canada

The OEDIPUS-C (OC) sounding rocket payload deployed a conducting tether to a total length of 1174 m during the upleg part of its trajectory. Up to the time of tether cutting a little after apogee, the double payload carried out experiments on sheath waves, which are electromagnetic waves that are guided along a conductor in a plasma. The transmitter, HEX, on one end of the payload applied a swept-frequency rf signal between the tether and the rocket body. At the other end, a synchronized receiver, REX, measured the resulting signal between the wire and the body. The electron plasma frequency f_p fell monotonically from 0.6 to 0.1 MHz throughout the upleg, while the gyrofrequency f_c went from 1.3 to 1.1 MHz. The f_p values were considerably lower than those obtained on the 1989 OEDIPUS-A (OA) flight, on which essentially the same experiment was carried out. On OC, the transmissions produced strong received signals throughout the 0.1-8.0 MHz frequency sweep range except for stop bands. The first stop band lies in the narrow range from f_c to the upper hybrid resonance frequency. Although the details of the OC transmitted spectrum are distinctly different, its shape has the same physical interpretation as the OA sheath-wave spectrum: because the sheath-wave stop bands occur precisely in the frequency intervals tied to harmonics of f_c where electron cyclotron (Bernstein) waves propagate (James et al., Radio Sci., 30, 57-73, 1995), it is inferred that Bernstein waves damp sheath waves. Additional OC evidence for electrostatic waves is obtained in dispersed delayed signals near the stop bands. The OC data reproduce the phenomenon of tether-length resonances observed on OA. The implied index of refraction of the sheath waves is generally close to 1.

RF EFFECTS SEEN ON THE OEDIPUS-C TETHER CURRENT MONITOR

H94.10

J.G. Laframboise*
Physics and Astronomy Department, York University
4700 Keele Street, North York, Ontario M3J 1P3 Canada

D.D. Wallis
Herzberg Institute of Astrophysics,
National Research Council Canada,
100 Sussex Drive, Ottawa, Ontario K1A 0R6, Canada

H.G. James
Communications Research Centre, Ottawa, Ontario K2H 8S2, Canada

The OEDIPUS-C tethered payload was launched on 7 November 1995 from the Poker Flat Research Range, Alaska. The Tether Current Monitor (TCM) instrument operated the two subpayloads and the conducting tether as a double electrostatic probe. During the part of the experiment discussed here, the flight upleg, the angle between the tether and the geomagnetic-field direction was less than 5°. The TCM configured the payload cyclically as a high-impedance voltage probe and as a low-impedance current probe.

OEDIPUS C also carried a high-frequency exciter (HEX) on its forward subpayload. With the HEX connected to the forward subpayload dipoles and with the frequency swept from 25 kHz to 8.0 MHz, the transient response of the TCM voltage showed a number of reproducible features. At the lowest frequencies of the sweep, the RF pulses drove the forward subpayload potential negative with respect to the aft subpayload by several tens of volts. The time-constant of relaxation of the payload's potential between the HEX pulses increased as background density decreased.

The TCM voltmeter data showed a steady rise in the time-averaged floating voltage of the forward subpayload as the HEX transmitter was swept from lower to higher frequencies. This is as expected when ponderomotive effects become relatively more important relative to rectification. Superposed on this was another feature in which the forward subpayload was driven increasingly negative as the frequency approached the electron gyrofrequency from below, and increasingly positive as it approached it from above. This suggests that RF forcing of the electrons counteracted geomagnetic restriction of the electron collection below the gyrofrequency, but enhanced it above the gyrofrequency.

In order to verify this explanation, we have performed a perturbation analysis of the electron motion in the combined RF near-field and steady geomagnetic field in the neighbourhood of an antenna element, assumed to be an infinite cylinder perpendicular to the geomagnetic field.

H94.11

Control of Radiation Belts Using Tethers

K. Papadopoulos, Univ. of Maryland, Physics Department, College Park, MD
A. Drobot and C. L. Chang, SAIC, McLean, VA

The presence and dynamic injection of energetic particles in the Radiation Belts (RB) limits the lifetime and often prevents the placement of satellites in particular locations because it degrades their electronic components. A new concept in active control of the RB fluxes is presented. The concept relies on the following:

- The lifetime of the energetic particles in the RB decreases in the presence of low frequency waves in cyclotron resonance with the particles.
- The relevant low frequency modes are often Field Line Resonance (FLR) Eigenmodes of the L-shells with high values of Q.
- Operating a long ($\sim$ 5–10 km) tether as a capacitive antenna powered by solar panels at the FLR frequency, leads to enhanced wave amplitude and decrease of the lifetime of the energetic particles.

Following the presentation of the basic physics processes controlling the concept, the paper discusses the power requirements, operation and flux levels of a tether system operating at L=6 and L=4, for reduction of the energetic electron and ion flux correspondingly.

THE THREE LEVELS ACTIVE EXPERIMENT IN THE MAGNETOSPHERE.

Klimov,S.I.,*{1}, O.V.Lapshinova {2}, S.A.Romanov {1}, W.W.L.Taylor {3}, N.N.Antropov {4}, V.A.Grushin {1}, F.L.Dudkin {5}, V.E.Korepanov {5}, M.M.Mogilevsky {1}, M.N.Nozdrachev {1}, W.E.Pine{6}, and P.Triska{7}.
{1}Space Research Institute (IKI), Profsoyuznaja 84/32, 117810, Moscow, Russia, Fax (095) 310-7023; e-mail SKLIMOV@ESOC1.IKI.RSSI.RU, {2}RKK ENERGIYA (Moscow region, Russia), {3}Hughes STX (GSFC, and MD, US), and INSPIRE (Washington,DC, US), {4}RIAM (Moscow, Russia), {5}LCISR (Lviv, Ukraine), {6}Chaffey High School (Ontario, CA, US), and INSPIRE (Upland, CA, US), {7}IFA (Prague, Czechia).

The INTERBALL Project is devoted to the detailed study of the energy, momentum and mass transfer in the critical regions of the solar wind / magnetosphere system. The INTERBALL-1 spacecraft which also carries the small subsatellite MAGION-4 was launched on August 3, 1995 into an eccentric elliptical orbit with the inclination of 62,9 degrees and apogee of about 191 000 km. The INTERBALL-2 spacecraft was launched on August 29, 1996 at the same inclination, but with an apogee of about 20 000 km above the Northern auroral zone and polar cap. These spacecraft are part of the international project INTMINS (INTerball-Mir-INSpire).

For INTMINS, plasma and electron beams are injected from the space station MIR into the surrounding plasma. The plasma-wave phenomena resulting from the injection are observed with scientific instruments flown onboard the INTERBALL Project spacecraft. The simultaneous ground-based observations of waves caused by electron and plasma injections are carried out by the INSPIRE network (Interactive NASA Space Physics Ionosphere Radio Experiments). During the first phase of the INTMINS project, from 1 to 10 August 1995, electron and plasma injections were performed when MIR was above the sites of the INSPIRE network. During the second phase on 17 September and 6 October 1995, electron and plasma injections from the MIR are made when MIR and INTERBALL were on the same magnetic field line. The major objectives was to work out the most efficient way of the collaboration between all participants of the INTMINS project. The current plan for MIR-INSPIRE is to have two major operations periods per year in November and April. INTMINS operation over other countries and the special periods when INTERBALL, MIR and an INSPIRE station is on or near the same field line as well are planed.

The first observations from INTERBALL-1, the result of INSPIRE network observations during major operations periods, and results of theoretical calculations of the propagation of electromagnetic waves connected with electron beam injection will be presented.

URSI H **Session 111** Salon St-Charles

Auroral Phenomena
Co-chairs: D.J. Knudsen, Canada and J. Labelle, USA

13:10 111.1 **Invited:** Wave Observations from the FAST Satellite: Solitary Waves and AKR, **R.E. ERGUN**[1], C.W. CARLSON[1], J.P. McFADDEN[1], W. PERIA[1], C. CHASTON[1], G.T. DELORY[1], F.S. MOZER[1], M. TEMERIN[1], R. ELPHIC[2], R. STRANGEWAY[3], D.M. KLUMPAR[4], E.G. SHELLEY[4],, W.K. PETERSON[4], E. MOEBIUS[5], L. KISTLER[5], C. CATTELL[6], R. PFAFF[7], [1]*Univ of California, Berkeley,* [2]*Los Alamos Nat'l Lab,* [3]*Univ of California, Los Angeles,* [4]*Lockheed Martin Palo Alto Res Lab,* [5]*Univ of New Hampshire,* [6]*Univ of Minnesota and* [7]*Goddard Space Flight Ctr, Greenbelt, MD, USA*

13:30 111.2 Polar Observations of ELF/VLF Chorus Emissions, **U.S. INAN**, C. CHEN, D. LAUBEN, T.F. BELL, *Stanford University, Stanford, CA, USA*

13:50 111.3 Excitation of Ion-Acoustic Turbulence and its Role in Auroral Processes at Freja Altitude, **M. PRAKASH**, *State University of New York at Stony Brook, NY, USA*

14:10 111.4 Ground-Level Observations of Auroral Radio Emissions, **J. LABELLE**, *Dartmouth College, Hanover, NH, USA*

14:30 111.5 Formation of Small-Scale Discrete, Auroral Arcs when the Ionospheric Conductivity is Finite, **A. STRELTSOV**, W. LOTKO, *Dartmouth College, Hanover, NH, USA*

14:50 111.6 Magnetospheric Radio Imaging, **J.L. GREEN**, S.F. FUNG, *NASA/Goddard Space Flight Center, Greenbelt, MD, USA*

15:10 Coffee Break

15:30 111.7 The Auroral Particle and Plasma Wave Environment Encountered by OEDIPUS-C, **D.J. KNUDSEN**[1], H.G. JAMES[2], D. HARDY[3], D.D. WALLIS[4], [1]*University of Calgary, AB and* [2]*Communications Research Centre, Ottawa, ON, Canada;* [3]*Phillips Laboratory, Hanscom AFB, MA, USA;* [4]*Magnametrics, Ottawa, ON, Canada*

H111.1

Wave Observations from the FAST Satellite: Solitary Waves and AKR

R. E. Ergun[1]*, C. W. Carlson[1], J. P. McFadden[1], W. Peria[1], C. Chaston[1], G. T. Delory[1], F. S. Mozer[1], M. Temerin[1], R. Elphic[2], R. Strangeway[3], D.M. Klumpar[4], E.G. Shelley[4], W.K. Peterson[4], E. Moebius[5], L. Kistler[5], C. Cattell[6], and R. Pfaff[7]

[1]Space Sciences Laboratory, University of California, Berkeley, CA
[2]Los Alamos National Laboratory, Los Alamos, NM
[3]University of California, Los Angeles, CA
[4]Lockheed Martin Palo Alto Research Laboratory, Palo Alto, CA
[5]University of New Hampshire, Durham, NH
[6]University of Minnesota, Minneapolis, MN
[7]Goddard Space Flight Center, Greenbelt, MD

The FAST (Fast Auroral SnapshoT) satellite was recently launched into a high inclination, 4200 km apogee orbit. The mission was designed to make detailed studies of auroral plasma processes with high spatial and temporal resolution observations of electromagnetic fields and particles. We present observations of plasma waves and turbulence, VLF emissions, auroral kilometric radiation (AKR), and the accompanying particle distributions in or near the auroral density cavity. The focus will be on recently discovered large-amplitude, 100 microsecond duration solitary waves and on digital waveform captures of AKR source crossings. The solitary waves appear to have a substantial (~10%) component parallel to the magnetic field and are frequently observed near, but generally not in, the auroral density cavity. These structures are often accompanies by strong modulations in both anti-earthward and earthward traveling energetic, field-aligned electrons. The estimated size of the structures is such that the electron transit time is on the order of their duration. These observations strongly suggest that the nonlinear solitary waves play a substantial role in acceleration of the field-aligned auroral electrons. The FAST satellite has also made several, 0.5 microsecond resolution, digital AKR waveform captures of three components of E and one component of B in the auroral density cavity. Analysis of these wave form captures shows power in both the Z-mode and X-mode, and occasional bursts of electrostatic emissions. Wave amplitudes are typically ~40 mV/m, but are occasionally observed at substantially higher amplitudes. The electron distributions are depleted below ~1 keV (typical) in energy, creating both a perpendicular and parallel instability.

POLAR OBSERVATIONS OF ELF/VLF CHORUS EMISSIONS

U. S. Inan, C. Chen, D. Lauben, and T. F. Bell
Space, Telecommunications and Radioscience Laboratory
Stanford University, Stanford, CA 94305

The POLAR spacecraft is equipped with a plasma wave instrument (PWI) with a number of unique properties, including wideband snapshot measurements of all six components (three electric and three magnetic) of the wave fields. Outside the plasmasphere on closed field lines (L-shells of ~4 to 10) one of the most intense plasma wave emission is the discrete ELF/VLF chorus, which is omnipresent especially in the morning sector, and is often the strongest emission in the entire band measured by the PWI instrument (few Hz to 800 kHz). Chorus emissions are important because they are believed to drive pulsating aurora and possibly the diffuse aurora, yet the generation mechanism of these waves is still not well understood. The availability of 6-channel measurements of chorus on POLAR provides an opportunity for measurement of the wave progataion directions, which should in turn help identify the source regions of the emissions. In this paper, we review the POLAR observations of chorus emissions, including their omnipresent occurrence outside the plasmapause, measurement of their intensities, spectra and wave-normal angles.

H111.3

Excitation of ion-acoustic Turbulence and its Role in Auroral Processes at Freja Altitude

Manju Prakash
Physics Department, SUNY at Stony Brook, Stony Brook, New York 11794, USA.

Freja spacecraft wave experiment provides data on solitary kinetic Alfven Wave (SKAW) structures co-located with ion-acoustic turbulence observed in the auroral zone. These structures are electromagnetic in nature with transverse scale size nearly 1 km. length scale is of the order of the electron inertial length in the auroral zone. The typical $\frac{E_x}{B_y}$ ratio associated with the wave events is of the order of inertial Alfvén speed. The SKAW events are associated with broadband emissions identified as H^+ ion-acoustic waves. Following Vlasov-Maxwell formalism, I examine the mechanism of the excitation of the ion-acoustic turbulence by the auroral electrons. These electrons are accelerated by the parallel electric field associated with the SKAW structures. Conditions for the unstable growth of the ion acoustic mode is calculated. It is further shown that, the conditions favourable to the unstable growth of these waves do exist in the auroral plasma. I also study auroral plasma heating rate due to the anomalous resistivity effects resulting from ion-acoustic turbulence.

Wahlund, J. -E., Louarn, P., Chust, T., Feraudy, H. dem Roux, A., Holback, B., Cabrit, B., Eriksson, A. I., Kintner, P. M., Kelley, M. C., Bonnell, , J., and Chesney, S., Observations of ion-acoustic fluctuations in the auroral topside ionosphere by the Freja spacecraft. Geophys. Res. Lett, 21 1835-1838,1994.

Ground-Level Observations of Auroral Radio Emissions

J. LaBelle*
Department of Physics and Astronomy, Dartmouth College, Hanover, NH 03755, USA
ph: (603) 646-2973; fax: (603) 646-1446; e-mail: jlabelle@einstein.dartmouth.edu

Radio emissions from aurorae provide a means of remotely sensing ionospheric plasma processes. At frequencies 50-5000 kHz, at least three distinct types of auroral radio emissions occur: impulsive auroral hiss, a broadband emission below the electron cyclotron freqency (f_{ce}); auroral roar, a relatively narrow band emission observed near $2f_{ce}$ and $3f_{ce}$; and auroral medium-frequency bursts, a broadband emission at frequencies above f_{ce} which is correlated with auroral hiss. Auroral roar occurs shortly before the substorm onset and becomes intermittent during the expansion phase. MF-bursts and impulsive auroral hiss occur primarily during the expansion phase of substorms. Recent waveform observations show that auroral roar is characterized by fine structure and that MF-bursts have time scales the order of 0.1–0.3 ms. Two competing models of auroral roar have been developed: one involves direct generation of EM waves by the cyclotron maser instability, and the other involves electrostatic upper hybrid wave generation followed by mode conversion. Theories of MF-burst generation are not well-developed, but two mechanisms have been proposed, exploiting the parallel energy and perpendicular energy in the auroral electrons, respectively. Several experiments are underway to test these theories. For example, at Sondrestromfjord, Greenland, simultaneous ground-based wave and incoherent scatter measurements will identify the ionospheric structure associated with auroral radio emissions. The FAST satellite, combined with ground-based wave observations in Canada and Antarctica, will provide *in situ* wave and particle measurements at times when radio emissions are observed at ground level.

H111.5

Formation of Small-Scale Discrete, Auroral Arcs When the Ionospheric Conductivity is Finite

A. Streltsov* and W. Lotko
Thayer School of Engineering, Dartmouth College, Hanover, NH 03755, USA
ph: (603) 646-2723; fax: (603) 646-3856; e-mail: as@exos.dartmouth.edu

Results from a study of the formation and temporal evolution of small-scale (sub-kilometer scale-size in the North-South direction), discrete auroral arcs, when the ionospheric conductivity is finite and depends on the intensity of the current flowing into the ionosphere are presented. In this study auroral arcs are associated with a parallel electric field (parallel potential drop) of the small-scale, dispersive, ultra-low-frequency (ULF) Alfvén waves, standing between southern and northern ionospheres along auroral magnetic field lines. These waves form in a localized transverse gradient of the background plasma density via coupling between a field line resonance (FLR) and an externally driven surface wave propagating along the gradient. FLRs for the first three odd harmonics are investigated in the dipolar magnetic field geometry by using a 2D, magnetically incompressible, two-fluid MHD model. The model includes a dispersion of the small-scale Alfvén waves due to the finite electron inertia (at low altitude), as well as the dispersion due to the finite electron temperature (at high altitude). Plasma parameters are chosen so that the refraction by the parallel inhomogeneities of the background plasma and magnetic field cause the dispersive Alfvén wave to become trapped in the resonance layer.

Computations show that even very low ionospheric conductivity ($\Sigma_P = 2$ mho) is not sufficient to prevent the formation of dispersive FLRs with strong parallel electric fields when the transverse inhomogeneity of the background plasma is strong enough. The fundamental FLR is more strongly affected by a state of low conductivity than higher-harmonic (third and higher) FLRs. The difference in conductivities of northern and southern ionospheres does not produce significant asymmetry in the distribution of electric and magnetic fields along the resonant field line. The transverse gradient of the background Alfvén speed plays an important role in structure of the FLR when the ionospheric conductivity is finite. In cases when the transverse inhomogeneity of the plasma is not strong enough, the low ionospheric conductivity can prevent even higher-harmonic FLRs from the contracting to the scales where dispersive effects (leading to a parallel electric field) are important, and hence, it can prevent the formation of associated small-scale, discrete auroral arcs. The nonlinear ionization of the ionosphere by an intense parallel current of dispersive FLR increases the ionospheric conductivity and makes conditions for developing a strong parallel electric field more favorable. The dependence of the last effect on the mode number is discussed.

MAGNETOSPHERIC RADIO IMAGING

James L. Green and Shing F. Fung, Space Science Data Operations Office, Code 630 NASA/Goddard Space Flight Center Greenbelt, MD 20771

NASA has recently selected a new mission called the Imager for Magnetopause-to-Aurora Global Exploration (IMAGE) as the first mid-sized explorer in magnetospheric physics to be launched in January 2000. The IMAGE mission will have an impressive array of remote sensing instruments which will image a number of important phenomena such as the auroral zone, the geocorona, the ring current, the plasmasphere, auroral ion fountain, and the magnetopause on a time scale of minutes. IMAGE will be placed in a polar orbit with apogee altitude of 7 Earth radii (R_E) where it will be well situated to observe the structure and dynamics of the magnetospheric boundaries during geomagnetic storms.

One of the key instruments on IMAGE is the Radio Plasma Imager or RPI. This instrument utilizes many of the recent advances in radio transmitter and receiver design, and modern digital processing techniques that have been perfected for ionospheric sounding. Like ionospheric sounding, free-space electromagnetic waves, launched within a lower density region will reflect at the plasma cutoffs. The location and characteristics of the plasma at a remote reflection point can then be derived from measurements of the delay time, frequency, and direction of an echo. The characteristic of large scale ionospheric disturbances can be displayed in skymaps, Doppler maps, and other useful images from the hundreds of echoes which are detected by this technique. In an analogous way, similar images of the magnetosphere at radio frequencies could be obtained RPI. The RPI will be operating at frequencies between 3 kHz to 3 MHz and will provide quantitative electron density profiles simultaneously in several different directions on a time scale of minutes or less. The IMAGE orbit is well situated in the magnetopheric density cavity, providing an excellent opportunity for RPI to observe the structure and dynamics of many different magnetospheric boundaries at the same time. Simulations of these observations have been done utilizing RPI characteristics and extensive ray tracing calculations within a three-dimensional magnetospheric model. This paper will review the techniques used in magnetospheric radio imaging as will be flown on the IMAGE spacecraft . In addition, a variety of simulations will also be presented to illustrate many of the expected radio imaging results. For more information on the IMAGE mission and on the RPI via the world wide web see: http://image.gsfc.nasa.gov/.

H111.7

The Auroral Particle and Plasma Wave Environment Encountered by OEDIPUS-C

D. J. Knudsen[1]*, H. G. James[2], D. Hardy[3], and D. D. Wallis[4]

[1]Dept. of Physics and Astronomy, University of Calgary, Alberta
[2]Communications Research Centre, Ottawa, Ontario
[3]Phillips Laboratory, Hanscom AFB, Massachusetts
[4]Magnametrics, Ottawa, Ontario

Auroral plasma wave emissions extend from DC to several MHz. Waves at VLF and below can be divided into two distinct types, namely auroral hiss with a cutoff near the lower hybrid frequency, and ULF/ELF emissions which extend from DC up to the proton cyclotron frequency and above. Hiss is often associated with energetic "inverted-V" auroral precipitation, while ULF/ELF waves are often associated with broad-band, field-aligned electron precipitation sometimes referred to as "suprathermal electron bursts". From the Freja satellite and from sounding rockets such as SCIFER and AMICIST, the latter ELF/suprathermal burst environment is characterized by strong energization of the ambient auroral plasma; inverted-V precipitation and associated VLF waves also couple energy to the ambient plasma, but not as strongly on average (Lynch et al., Geophys. Res. Lett., 23, 3293-3296, 1996). The OEDIPUS-C sounding rocket, launched in November 1995, traversed regions containing inverted-V precipitation and also field-aligned electron bursts. The experiment consisted of two tethered sub-payloads, one of which carried an RF receiver "REX" which sampled intermittently the natural auroral wave background, interleaved with measurements of active emissions from the "HEX" transmitter on the forward sub-payload. In addition to instruments for measuring energetic electrons and waves, OEDIPUS-C carried low-energy ion detectors, a fluxgate magnetometer, Langmuir probes, and a tether current and voltage monitor which allowed the entire system to be operated as a large double probe with up to 1.2 km separation between the two sub-payloads. We compare the OEDIPUS-C observations of the nightside auroral plasma and ULF/ELF/VLF plasma wave environment with recent observations made by Freja and other spacecraft, with the aim of identifying the conditions most conducive to strong coupling between auroral energy sources and the ambient auroral plasma.

URSI GH | Session 2 | Salon Jolliet

HF Ionospheric Modification
Co-chairs: F. Djuth, USA and M. Sulzer, USA

08:10 2.1 **Invited:** Measurements of Artificial Periodic Inhomogeneities at HIPAS, **F.T. DJUTH**[1], J.H. ELDER[1], K.M. GROVES[2], E.R. SHINN[2], J.M. QUINN[2], J. VILLASENOR[3], A.Y. WONG[3], [1]*Geospace Research, Inc., El Segundo, CA,* [2]*Phillips Laboratory, Hansom Air Force Base, MA,* [3]*University of California, Los Angeles, CA and HIPAS Observatory, Fairbanks, AK, USA*

08:30 2.2 **Invited:** Energy Balance Studies Using the Arecibo ISR and Heating Facility, **M.P. SULZER**, S. GONZALES, *Arecibo Observatory, Arecibo, Puerto Rico*

08:50 2.3 Nonlinearities for the Excitation of Low Frequency Decay Modes of Parametric Instabilities in Collisional Magnetoplasmas, **S.P. KUO**, *Polytechnic University, Farmingdale, NY, USA*

09:10 2.4 A Generation Mechanism for the Frequency Up-Shifted Plasma Lines Observed in the Tromsq's HF Heating Experiments, **S.P. KUO**[1], S.C. KUO[2], M.C. LEE[3], [1]*Polytechnic University, Farmingdale,* [2]*Brookhaven National Laboratory, Upton, NY and* [3]*Massachusetts Institute of Technology, Cambridge, MA, USA*

09:30 2.5 Study of ELF/VLF Wave Generation by HF Heater-Modulated Electrojet, **S.P. KUO**[1], M.C. LEE[2], P. KOSSEY[3], [1]*Polytechnic University, Farmingdale, NY,* [2]*Massachusetts Institute of Technology, Cambridge and* [3]*Air Force Phillips Laboratory, Hanscom AFB, MA, USA*

09:50 2.6 Ducting of VLF Transmissions by HF-Enhanced Ionospheric Ducts: Conjugate-Point Experiments, M.J. STARKS, **M-C LEE**, *Massachusetts Institute of Technology, Cambridge, MA, USA*

10:10 Coffee Break

10:30 2.7 First Diagnostic Experiment of an Artificial Ionospheric Lens in the E-Layer with the WIND Spacecraft, L.M. ERUKHIMOV[1], G.P. KOMRAKOV[1], N.A. MITYAKOV[1], Yu.V. TOKAREV[1], M.L. KAISER[2], **P. RODRIGUEZ**[3], [1]*Radiophysical Research Institute, Nizhny Novgorod, Russia;* [2]*NASA, Greenbelt, MD and* [3]*Naval Research Laboratory, Washington, DC, USA*

GH2.1

Measurements of Artificial Periodic Inhomogeneities at HIPAS

Frank T. Djuth* and John H. Elder
Geospace Research, Inc., 550 N. Continental Blvd., El Segundo, CA 90245

K. M. Groves, E. R. Shinn, and J. M. Quinn
Ionospheric Effects Division, Phillips Laboratory,
Hanscom Air Force Base, MA 01731

J. Villasenor and A. Y. Wong
Department of Physics, University of California, Los Angeles, CA 90024, and
HIPAS Observatory, Fairbanks, AK 99701

Results from recent experiments exploring the use of high-powered, high-frequency (HF) radio waves to probe the altitude region from the lower mesosphere to the lower thermosphere are presented. The measurements were made at the High-Power Auroral Stimulation (HIPAS) Observatory located near Fairbanks, Alaska. The principal objective was to assess the feasibility of using artificial electron density perturbations created in the auroral environment to determine the properties of the background neutral gas between ~50 km to 150 km altitude. The measurement technique relies on the production of so-called "artificial plasma inhomogeneities" (API) in the altitude region(s) of interest. These induced irregularities are believed to be horizontally stratified and conform to the standing wave pattern produced by the reflection of the powerful HF wave in the ionosphere. Information about the neutral atmosphere in the auroral region is obtained by measuring the relaxation time of the induced irregularities and the Doppler shift of the backscatter. The relaxation characteristics of the API backscatter at altitudes $\gtrsim 80$ km are indicative of ambipolar diffusion. At lower altitudes, the echo decay constant is controlled by electron attachment, principally to O_2. It is believed that the phase velocities of API echoes are related to vertical neutral wind velocities at altitudes below ~95 km. In general, the observations confirm that API can be an effective diagnostic of neutral gas motion, neutral density, and/or neutral temperature. However, additional validation tests are required to establish direct relationships between measured API parameters and atmospheric properties. The location of HIPAS in the auroral region makes such observations extremely interesting from a geophysical perspective. Initial tests indicate that the dependence of API backscatter power on the power of the modification transmissions is linear. However, several fundamental questions remain unanswered concerning the exact nature of the API source process, the observed variability in API backscatter, and the relationship between API and regions of natural partial reflection.

Energy Balance Studies Using the Arecibo ISR and Heating Facility

Michael P. Sulzer* and Sixto Gonzales
Arecibo Observatory

The Arecibo incoherent scatter radar is located in Puerto Rico (18.35 N 66,75 W). The radar operates at a frequency of 430 MHz and has a nominal power rating of 2.5 MW. The antenna has the form of hemispherical reflector with a diameter at the aperture of 305 m. The electron and ion temperatures, ion composition and electron density of the ionosphere are determined from the returned spectra using a nonlinear least squares fit. We have recently developed the capabilities to include independent temperatures for the O^+ and H^+ ions in the lower topside ionosphere in the NLLS fit [Sulzer and González, Geophysical Research Letters, p. 3235, 1996]. We will describe the measurement technique and show how the the goodness of the fits improves with the addition of this new degree of fredoom. We will also show the measurements. The general behaviour of the proton temperatures during the day is that they are several hundred degrees higher than the oxygen ion temperatures, and at night the three temperatures are equal. Finally we will describe an application of this new capability in which we will use the Arecibo HF facility to heat the ionosphere and then observe the cooling of T_e, T_{H+} and T_{O+}. We will use these observations to solve the energy balance equations. One of the parameters we expect to study in this manner is the $O - O^+$ collision cross section.

Akn.: The Arecibo observatory is operated by Cornell University under a cooperative agreement with NSF.

GH2.3

Nonlinearities for the Excitation of Low Frequency Decay Modes of Parametric Instabilities in Collisional Magnetoplasmas

S.P. Kuo
Department of Electrical Engineering
Polytechnic University, Route 110, Farmingdale, NY 11735

A general coupled mode equation for the low-frequency decay modes of parametric instabilities in collisional magnetoplasmas is derived. This is an extension of the previous work [S.P. Kuo, Phys. Plasmas 3 (11), 3857, 1996] in the collisionless case. The relative importance of the nonlinear contributions from the ponderomotive force, differential ohmic heating force, nonlinear beating current, and anisotropic effect to the parametric coupling can then be compared through the coupling terms of the equation. The results show that the ponderomotive force is the dominant nonlinearity if the low frequency decay modes are not quite field-aligned. However, the ground backscatter radar and the in-situ rocket probe measurements all show that the density irregularities presented in the HF heating experiments are field-aligned in nature. They have low threshold condition of excitation and relatively long live, thus, play an essential role to the ionospheric modification. Therefore, those nonlinearities have to be compared in this situation to be relevant to the heating experiments. It is found that the relative importance among them becomes scale-length dependent. In general, as increasing the scale length from submeters to tens of meters, the dominant nonlinearity is shifting from ponderomotive force, to nonlinear beating current and then to differential ohmic heating force. The nonlinearities depend also on the mode types of the high frequency source waves. Different source waves including EM wave, electron plasma wave, and upper hybrid wave, will be considered to exemplify the importance of different nonlinearity in different scale-length range.

A Generation Mechanism for the Frequency Up-Shifted Plasma Lines Observed in the Tromsq's HF Heating Experiments

S.P. Kuo[1], S.C. Kuo[2], and M.C. Lee[3]

[1]Department of Electrical Engineering, Polytechnic Univ., Farmingdale, NY 11735
[2]Department of Applied Science, Brookhaven National Lab., Upton, NY 11973
[3]Plasma Fusion Center, MIT, Cambridge, MA 02138

A new spectral feature in the backscattering spectrum of EIS CAT 933 MHz radar was observed throughout most of the observing period of the heating experiments performed with 0-mode heater transmitting near Tromsq, Norway on August 16-18, 1986. The radar returns were enhanced at frequencies offset from the radar frequency by a frequency a few hundred KHz more than the heater frequency of 4.04 MHz [Isham et al, 1990]. Moreover, running alternately with the radar in the chirped and in the unchirped mode it was shown that the enhanced plasma lines seemed to emanate from very local regions [Birkmayer et al, 1986]. It is noted that a similar phenomenon of recording frequency upshifted HF-enhanced plasma lines (HFPLs) has also been observed in the Arecibo heating experiments, except the amount of frequency upshift is in the range of a few tens of KHz [Sulzer and Fejer, 1984]. A physical mechanism [Kuo and Lee, 1992] based on a nonlinear scattering process by which the parallelly propagating Langmuir waves generated by the parametric decay instability of the HF pump scatter off the background lower hybrid density fluctuations to produce the observed frequency upshifted plasma lines has successfully explained the Arecibo's observations and has even been verified recently by a laboratory experiment [Lee et al, 1997]. However, the amount of frequency shift observed in the Tromsq's experiments well exceeds the lower hybrid wave frequency. Thus, a different physical mechanism is considered in the present work for explaining the Tromsq's observations. It is the parametric decay of a right handed circularly polarized pump wave (0-mode) into a Whistler wave (decay mode) and a frequency upshifted Langmuir wave (sideband). Since the frequency of Whistler wave extends to the range of a few hundred KHz, the frequency of the excited Langmuir wave agrees with that of the experimental observation.

GH2.5

Study of ELF/VLF Wave Generation by HF Heater-Modulated Electrojet

S.P. Kuo[1], M.C. Lee[2], and Paul Kossey[3]

[1]Department of Electrical Engineering, Polytechnic Univ., Farmingdale, NY 11735
[2]Plasma Fusion Center, MIT, Cambridge, MA 02138
[3]Air Force Phillips Lab, Hanscom AFB, MA 01731

Generation of ELF/VLF waves by the modulation of the electrojet by the powerful HF heater is of current interest. It is done by applying an amplitude modulated HF heater to modify the electron temperature of the electrojet in time. This in turn causes the modulation of the conductivity and thus, the electrojet current. Emissions are then produced at the modulation frequency and its harmonics. The present work extends the previous one [S.P. Kuo and M.C. Lee, Geophys. Res. Lett., 20, 189, 1993; S.P. Kuo, Radio Sci., 28, 1019, 1993] of thermal instability to the nonlinear saturation regime. Two heater-modulation schemes are considered. One, corresponding to the one adopted in the Tromsq heating experiments [P. Stubbe, H. Kopka, and R.L. Dowen, J. Geophys. Res., 86, 9073, 1981], modulated the heater by a rectangular periodic pulse. The other one needs two overlapping heater waves (beat wave) having a frequency difference equal to the desired modulation frequency. It is essential a sinusoidal amplitude modulation and is the approach adopted in the Arecibo heating experiments. The nonlinear evolutions of the generated ELF/VLF waves are determined numerically. Their spectra are also evaluated. The results show that the signal quality of the beat wave scheme is better (i.e., harmonic components have relatively lower intensities than that of the fundamental line). The field intensity of the emission at the fundamental modulation frequency is found to increase with the modulation frequency, consistent with the Tromsq results.

Ducting of VLF Transmissions by HF-enhanced Ionospheric Ducts: Conjugate-Point Experiments

M.J. Starks and M-C Lee
Plasma Science and Fusion Center
Massachusetts Institute of Technology
Cambridge, MA 02139

The ducting of man-made VLF emissions by magneto-ionic density perturbations has been well-recognized since early observations by Helliwell, *et al.* (*Proc. IRE*, *46*, 785, 1958). Years of VLF monitoring in Antarctica have produced many recordings of VLF transmissions ducted from man-made sources (*e.g.* Clilverd, *et al.*, *Planet. Space Sci.*, *39*, 1059, 1991). These natural waveguides are often detected by the observation of large-scale spread F events that may produce ducts extending to the magnetic conjugate point. Experiments at the Arecibo Observatory carried out in 1992 by MIT's Ionospheric Research Group indicate a connection between large-scale spread F and heating of the ionospheric plasma by intense HF waves. The incident radio waves may trigger, amplify, and even maintain the resulting density perturbations, thus permitting whistler-mode ducting of VLF broadcasts from a nearby Navy transmitter at 28.5 kHz. In an experiment postponed from September 1996, we plan to conduct an extensive night-time HF heating campaign at Arecibo. Plasma conditions will be continuously monitored for the triggering of large-scale spread F events. A specially-designed broadband VLF receiver and a large loop antenna will be deployed at the magnetic conjugate point near Trelew, Argentina to monitor any VLF emissions exiting trans-hemispheric ducts. An additional receiver will be placed near the transmitter in Puerto Rico to facilitate later processing of the recorded signal, including the removal of the earth-ionosphere waveguide contribution. Theoretical computations of signal strengths and subsequent simulation of the required post-processing indicate promising results when the Arecibo heating facility is finally available for experiments.

GH2.7

First Diagnostic Experiment of an Artificial Ionospheric Lens in the E-layer with the WIND Spacecraft

L. M. Erukhimov[1], *G. P. Komrakov*[1], *N. A. Mityakov*[1],
Yu. V. Tokarev[1], *M. L. Kaiser*[2], and *P. Rodriguez*[3]*
RadiophysicalResearchInstitute, NizhnyNovgorod, Russia[1].
NASA, GoddardSpaceFlightCenter, Greenbelt, MD, USA,[2]
NavalResearchLaboratory, Washington, D.C., USA[3]

Recently, a special antenna configuration for the heating facility "Sura" to create in the ionosphere an artificial focusing lens has been proposed and realized (L.M.Erukhimov, N.A.Mityakov and Yu.V.Tokarev, Radiophysics and Quantum Electronics, 1996, n12, in press). The focusing lens is based on the enhancement of electron density in the heated volume of the ionospheric E-region due to the dependence of recombination on electron temperature. Since the dense plasma plays the role of a defocusing lens, the "Sura" array was phased so that the antenna pattern would have its minimum in the scanning beam plane. In the heated ionospheric E-region (100–170 km) this two-peak beam pattern would give a horizontal profile of the electron density fluctuation like $\triangle N \propto \rho^2/\rho_0^2$, where ρ is the coordinate, and the subcript 0 refers to the lens dimension. This density profile could be used as a more stable focusing lens than a thermodiffusion one in the ionospheric F-region. The first diagnostic experiment of an artificial ionospheric lens has been sponsored by the Russian Fund of Fundamental Investigations and by the Civilian Research and Development Foundation. The artificial focusing lens was tested on November 17, 1996, with the help of a "Sura" probe signal which was observed by the WIND receivers. In this experiment, the artificial lens was prepared using two sections of "Sura" to form the two peak beam pattern. These sections were operated at 9.075 MHz with the effective power 45 MW. A third antenna section was used for the emission of probe signals at the same frequency. The modulation cycle for the heating transmitter was 2 min on – 1 min off, with an oppositely-phased modulation for probe signal. The WIND receiver operated in a high rate sampling mode at the frequency of 9.075 MHz.

Here we present the results of our observations. We demonstrate the appearance of the focusing structure in the ionospheric E-layer and effects induced in the ionosphere by this structure. We also show that this focusing system can be used for enhancement of ionospheric heating effects and for ground based decametric radio astronomy observations.

URSI GH | Session 113 | Salon Jolliet

Electrodynamic Coupling Between Atmospheric Regions
Co-chairs: U.S. Inan, USA and E.M. Westcott, USA

08:10	113.1	**Invited:** Lightning-Ionosphere Interactions, **U.S. INAN**, *Stanford University, Stanford, CA, USA*
08:30	113.2	Analysis of Blue Jets: Optical Emissions, Ionization and Possible Relation to VHF Radar Echoes, **E.M. WESCOTT**, D.D. SENTMAN, M.J. HEAVNER, *University of Alaska Fairbanks, AK, USA*
08:50	113.3	Mesospheric Gravity Waves Generated by Thunderstorms and Small Scale Structure of Sprites, **V.P. PASKO**, U.S. INAN, T.F. BELL, *Stanford University, Stanford, CA, USA*
09:10	113.4	Model of Red Sprites due to Intracloud Fractal Lightning, J.A. VALDIVIA, **G.M. MILIKH**, K. PAPADOPOULOS, *University of Maryland, College Park, MD, USA*
09:30	113.5	Model of Infrared Emission from Sprites, **G.M. MILIKH**, D.A. USIKOV, J.A. VALDIVIA, *University of Maryland, College Park, MD, USA*
09:50	113.6	Nighttime D and E Region Electron Density Measurements Determined from ELF/VLF Radio Atmospheric Waveforms, **S.A. CUMMER**, U.S. INAN, *Stanford University, Stanford, CA, USA*
10:10		Coffee Break
10:30	113.7	A Two-Dimensional Model of Runaway Electron Beams Driven by Quasi-Electrostatic Thundercloud Fields, **N.G. LEHTINEN**, *Stanford University, Stanford, CA, USA*
10:50	113.8	Laboratory Study of Ionospheric Plasma Effects Caused by Whistler Waves, R.J. RIDDOLLS, **M.C. LEE**, *Massachusetts Institute of Technology, Cambridge, MA, USA*
11:10	113.9	Multistation Observations of ELF/VLF Waveforms of Lightning Flashes Leading to the Production of Sprites and Elves, **S.C. REISING**, U.S. INAN, T.F. BELL, *Stanford University, Stanford, CA, USA*
11:30	113.10	Measurement of Total Charge Transfer in Sprite-Producing Lightning Using ELF Radio Atmospherics, **S.A. CUMMER**, *Stanford University, Stanford, CA, USA*
11:50	113.11	Whistle VLF-Waves Generated in the Ionospheric E-Region by Infra-acoustic Waves, **A.M. GOKOV**, *Kharkiv State University, Kharkiv, Ukraine*

GH113.1

LIGHTNING-IONOSPHERE INTERACTIONS

Umran S. Inan
Space, Telecommunications and Radioscience Laboratory
Stanford University, Stanford, CA 94305

Recent experimental and theoretical results indicate that thunderstorms and lightning discharges interact with the overlying mesosphere and ionosphere over time scales ranging from sub-millisecond to many hours. Spectacular high altitude optical emissions, referred to as sprites, blue-jets and elves, as well as radio frequency measurements of electrical conductivity changes, provide evidence of the electrodynamic coupling between the largely neutral troposphere and the ionized upper atmosphere. Although observations of high altitude optical emissions have been achieved at relatively few locations around the world, all evidence indicates that thunderstorms at other locations around the globe should similarly interact with their overlying ionospheres. In this paper, we review the most recent experimental evidence for these coupling processes, and discuss theoretical paradigms that should guide the design of new measurements.

ANALYSIS OF BLUE JETS: OPTICAL EMISSIONS, IONIZATION AND POSSIBLE RELATION TO VHF RADAR ECHOES

E. M. Wescott*, D.D. Sentman and M.J. Heavner
Geophysical Institute
University of Alaska Fairbanks
P.O. Box 757320
Fairbanks, Alaska 99775-7320

Blue jets are narrow cones of blue light that appear to propagate upward from the cloud tops at about 120 km/s to terminal altitudes of about 40 km. We have refined our previous analysis of 56 examples that occurred over an intense thunderstorm over Arkansas on July 1, 1994. About half of the blue jets were associated with a storm cell near Texarkana Arkansas/Texas and the rest were observed over a cell near Foreman Arkansas. Both cells produced very large hail (5 - 7 cm diameter) indicating updrafts of the order of 80 m/s. Comparison to cloud-to ground lightning flashes revealed: 1. Blue jets were not coincident with either positive or negative CG flashes, but they do occur in the same general area as negative CG flashes and very large hail; 2. Cumulative distributions of the negative CG flashes in $\pm$ 10 s before and after the jet and within a radius of 15 km show a significant reduction for 2 s following the event.

The blue jets were recorded on both monochromatic TV systems from two aircraft, and with a low light level color TV on one of the aircraft. The corrected output signals from the red, green and blue TV tubes have been analyzed and compared with the nitrogen emission bands of auroras. Unless the blue jets are ionized, there would not be enough blue nitrogen emissions to match the observed signal levels. We examine the VHF radar observations of Rumi (*J. Geophysical Res., 62(4),* 547-564, 1957) in the context of our conclusions that blue jets are partially ionized, and might have a radar crossection. Rumi reported radar echoes that seemed to propagate upward from cloud top altitudes at about 100 km/s to about 50 km altitude. We will discuss several theories of blue jets and compared predictions with our analyzed observations.

GH113.3

MESOSPHERIC GRAVITY WAVES GENERATED BY THUNDERSTORMS AND SMALL SCALE STRUCTURE OF SPRITES

Victor P. Pasko*, Umran S. Inan, and Timothy F. Bell
Space, Telecommunications and Radioscience Laboratory
Stanford University, Stanford, CA 94305

Sprites are vertically oriented clusters of luminous glows lasting several milliseconds at ~50 to 90 km altitudes above large mesoscale thunderstorms [e.g., Sentman et al., GRL, 22, 1205, 1995]. They are believed to be produced by quasi-electrostatic thundercloud fields [e.g., Pasko et al., GRL, 23, 649,1996], and typically appear several hours after the onset of a storm, even in extremely active (high flash rate) storms [e.g., Lyons, JGR, 101, 29641, 1996].

We propose that the occurrence of sprites may be facilitated by vertical gravity wave (GW) structures supported by mesoscale storm systems. The oscillations of air due to penetrative convection at thundercloud tops can lead to the upward launching of GW with periods near the local Brunt-Väisälä period at the source altitude and with a vertical oscillation velocity as high as ~30 m/s extended over an area ~10 km by 10 km [Pierce and Coroniti, Nature, 210, 1209,1966; Stull, J. Atmos. Sci., 33, 1279, 1976]. These GW arise mainly from mechanical forcing by vertical displacements associated with oscillatory updrafts and down drafts rather than thermal effects [Fowell et al., J. Atmos. Sci., 49, 1427, 1992].

Sprites are believed to be due to the electrical breakdown of the neutral atmosphere by large mesospheric electric field transients following intense cloud-to-ground discharges [e.g, Pasko et al., GRL, 23, 649,1996]. Since the optical emission excitation rates are sensitive functions of atmospheric neutral density and may be enhanced several orders of magnitude in response to only several percent density depletion, the appearance and spatial structure of sprites may be related to GW formations. In this work we employ a modified quasi-electrostatic model of mesospheric heating and ionization [Pasko et al., GRL, 23, 649,1996] to quantitatively investigate the effects of GW generated density fluctuations on optical emissions associated with sprites.

We show that cylindrical GWs generated by penetrative convection in large area Mesoscale Convective Complexes with periods comparable to the local Brunt-Väisälä period (~5-8 min) and horizontal wavelengths ~20-25 km can form mesospheric cylindrical structures closely resembling those observed in optical emissions associated with sprites. Diffraction effects of GW produced by large area sources can lead to focusing of the wave energy in localized regions of space, with significant associated enhancements of atmospheric perturbations. In this model the observed several hours delay between the onset of a thunderstorm and the appearance of sprites is a consequence of the time required for the GW to reach mesospheric altitudes. We discuss sprite development involving formation of small scale (lateral extent <100 m at ~70 km altitude) streamers (transient filamentary plasmas controlled by nonlinear space charge waves) with upward and downward motion.

Model of Red Sprites due to Intracloud Fractal Lightning

J. A. Valdivia, G. M. Milikh* and K. Papadopoulos
University of Maryland, Departments of Physics and Astronomy,
College Park, MD 20742, USA

Among the most puzzling aspects of the observations of "red sprites" is the presence of fine structure in the emissions (J.R. Winckler et al., J. Geophys. Res., 101, 6997, 1996). Vertical striations with horizontal size of 1 km or smaller, often limited by the instrumental resolution, are apparent in the red sprite emission. The first published theoretical model of the red sprites (G.M. Milikh et al., Geophys. Res. Lett., 22, 85, 1995) associated their generation with transient electric fields induced by large intracloud lightning discharges modeled as a horizontal electric dipole. The model demonstrated that energization of the ionospheric electrons by the transient fields could account for several of the observed features. Two subsequent publications (V.P. Pasko et al., Geophys. Res. Lett., 22, 365, 1995; H.L. Rowland et al., Geophys. Res. Lett., 22, 361, 1995) reached the same conclusions using the similar methodology, but emphasizing different sources for the lightning generated electric fields. All of the above models while successful in explaining some observed characteristics of the red sprites, such as the color and the generation altitude of the emissions, suffer from two important drawbacks. First, dipole or monopole distributions generate electric fields smoothly distributed at ionospheric heights, thereby failing to account for the persistent fine structure of the red sprites. Second, the threshold charge and dipole moment requirements of all three models have been considered as unrealistically large.

The objective of this paper is to extend the results of (G.M. Milikh et al., Geophys. Res. Lett., 22, 85, 1995) by incorporating in the calculation of the transient field the dendritic fine structure of the lightning channel (E.R. Williams, Scientific American, November 1988, and by W.A. Lyons, Geophys. Res. Lett., 21, 875, 1994). The presented model consists of some elements. The first is a computer model of the intracloud fractal discharge structure that produces the spatio-temporal distribution of the amplitude and phase of the electromagnetic field. The next element of the model includes the self-consistent computation of the propagation of the lightning induced fields in the lower ionosphere. The fields interact and energize the ambient electrons. The collision of energetic electrons with neutral particles results in the observed emissions. The structuring of the emissions is attributed to the highly inhomogeneous fields projected in the lower ionosphere, when the internal structure of the discharge is included in the model. The model not only accounts for the structure, but simultaneously reduces the required charge for the lightning discharge driving the red sprites to levels more consistent with observational requirements.

GH113.5

Model of Infrared Emission from Sprites

G. M. Milikh*, D. A. Usikov and J. A. Valdivia
University of Maryland, Departments of Physics and Astronomy,
College Park, MD 20742, USA

Recently, discovered is the sprite phenomena which manifests itself as optical flashes sparkling above the top of giant thunderstorms at heights of 50–95 km (D.D. Sentman et al., Geophys. Res. Lett. 22, 1205, 1995; D.J. Bossipio et al., Science, 269, 1088, 1995; J.R. Winckler et al., J. Geophys. Res., 101, 6997, 1996). This phenomena occurs due to the electromagnetic pulse or quasistatic field from the lightning which energizes the ambient electrons. The electrons collide then with the air molecules exciting their electronic levels followed by the optical emissions. However, only less than 1% of the total absorbed electromagnetic energy of lightning is released through the optical emissions, while most of this energy is pumped into the nitrogen vibrational levels having long lifetimes. This energy then is transferred through resonant molecular collisions into the $CO_2(001)$ vibrational level with much shorter lifetime τ = 2.5 ms, leading to the radiation of the infrared photons of wavelength λ = 4.26 μm. The radiated IR photons propagate through the optically thick atmosphere, therefore this emission is almost totally absorbed in the atmosphere beneath the sprite, but could be detected from the space.

A model of the 4.26 μm infrared emission due to red sprites is presented. The model discusses generation of nitrogen vibrons due to the collisions of the nitrogen molecules with the electrons energized by the electric field from lightning, followed by a transition of the nitrogen vibrons to the $CO_2(001)$ vibrational level, which then radiates infrared photons. The intensity of the IR source based on the lightning parameters is evaluated. The propagation of IR photons from sprites through the optically thick atmosphere is considered, and the sprite radiance is computed. Then the amount of the IR energy collected by a satellite detector overflying the sprite is obtained, and the signal-to-noise ratio at the detector is estimated. The model reveals that for some satellite locations the IR signal from the sprite could be observed by a state-of-the-art space infrared detector if the sprite is caused by a sufficiently strong electric field. Based on the model of sprite caused by the low altitude lightning, minimum electric field required to produce the IR emission which could be observed by the state-of-the-art space detector is estimated. Such observations could help to estimate the energetics and frequency of sprite appearances. They could be specially helpful if combined with optical observations in the visible range. In fact a short (msec) optical pulse from the sprite could help to direct the IR detector toward the sprite and distinguish the beginning of the sprite. Finally a sufficient input to the IR emission could come from the bright "elves".

Nighttime D and E Region Electron Density Measurements Determined from ELF/VLF Radio Atmospheric Waveforms

Steven A. Cummer and Umran S. Inan
Space, Telecommunications and Radioscience Laboratory, Stanford University, Stanford, CA 94305

Electron densities in certain regions of the ionosphere are extremely difficult to measure, particularly in the nighttime *D* region and *E* region. Propagation of very low frequency (VLF, defined here as 1-20 kHz) waves in the earth-ionosphere waveguide is known to be strongly dependent on *D* region electron densities. Extremely low frequency (ELF, defined here as ~10-1000 Hz) wave propagation is strongly dependent on both *D* and *E* region parameters due to the long wavelengths involved. Both VLF and ELF propagation are quantitatively well-understood, but the difficulty in employing them for ionospheric diagnostics lies in finding a suitable source.

Lightning discharges launch intense signals with frequency content throughout the VLF/ELF bands. These waveforms, commonly referred to as radio atmospherics or sferics, contain a great deal of information about the *D* and *E* region ionosphere along the propagation path from the source discharge to the receiver because the propagation effects depend so strongly on the ionosphere. We compare continuous broadband magnetic field observations with results from a very general ELF/VLF propagation model in an effort to extract characteristics of the *D* and *E* region electron densities along the sferic propagation paths. This technique can provide measurements over a number of spatially distributed regions simultaneously (depending on the location of lightning discharges) and can detect temporal variations on time scales as short as 15 minutes. Initial results indicate that the nighttime *D* region height can be determined to an accuracy of 0.5 km using VLF sferics.

GH113.7

A Two-Dimensional Model of Runaway Electron Beams Driven by Quasi-Electrostatic Thundercloud Fields

N. G. Lehtinen,
STAR Laboratory, Stanford University, Stanford, CA 94305

Intense, transient quasi-electrostatic (QE) fields, which exist above the thunderclouds following a positive cloud-to-ground lightning discharge, can produce an upward travelling runaway electron (REL) beam. In the present work we develop a new two-dimensional REL-QE model which expands the previously reported one-dimensional model [*Bell et al.*, 1995] and incorporates the recently developed electrostatic heating (ESH) [*Pasko et al.*, 1997b] and QE models [*Pasko et al.*, 1997a]. The new model provides information on the lateral electron distribution in the beam and allows us to determine the ionospheric effects and the optical luminosities resulting from the simultaneous action of the QE fields on the ambient electrons and the runaway electrons. The REL beam radius changes with altitude, attaining its maximum value of 10--15 km at altitudes of 70--90 km. The model is self-consistent and includes the changes in space charge and conductivity due to the REL. Optical emissions [*Bell et al.*, 1995] and γ-ray emissions [*Lehtinen et al.*, 1996] are calculated and compared to experimental observations. It is shown that the structure of the electric field and the optical emissions can be significantly affected by the runaway electrons.

References

Bell, T. F., V. P. Pasko, and U. S. Inan, Runaway electrons as a source of red sprites in the mesosphere, *Geophys. Res. Lett., 22*, 2127, 1995.

Lehtinen, N. G., M. Walt, U. S. Inan, T. F. Bell and V. P. Pasko, γ-ray emission produced by a relativistic beam of runaway electrons accelerated by quasi-electrostatic thundercloud fields, *Geophys. Res. Lett., 23*, 2645, 1996.

Pasko, V. P., U. S. Inan, T. F. Bell and Yu. N. Taranenko, Sprites Produced by Quasi-Electrostatic Heating and Ionization in the Lower Atmosphere, *J. Geophys. Res., in press*, 1997a.

Pasko, V. P., U. S. Inan and T. F. Bell, Ionospheric Effects due to Electrostatic Thundercloud Fields, *to be submitted to JATP*, 1997b.

LABORATORY STUDY OF IONOSPHERIC PLASMA EFFECTS CAUSED BY WHISTLER WAVES

R.J. Riddolls and M.C. Lee
MIT Plasma Science and Fusion Center
Cambridge, MA 02139

Laboratory experiments have been conducted with the Versatile Toroidal Facility (VTF) to simulate ionospheric plasma effects caused by whistler waves. Lightning is a primary source of whistler waves, producing waves with a broad range of frequencies. However, measurements made in rocket and balloon experiments [Kelley et al., 1985] led to some speculation about how whistler waves can be generated by lightning. We have chosen to investigate a mechanism producing ionospheric whistler wave radiation associated with atmospheric lightning discharges. It has been proposed that a transient electric field caused by the discharge propagates upward into the ionosphere and accelerates electrons until they are in the runaway state. In ionospheric experiments, these proposed runaways have been observed to emit whistler radiation with maximum intensity in the vicinity of the lower hybrid resonance frequency. In our VTF experiments, a background ECRH plasma is created, to which we add an electron beam plasma. The runaway electrons associated with the electron beam plasma excite a broad spectrum of whistler wave radiation. The VTF whistler spectrum is discussed and compared to the spectrum observed in ionospheric experiments. Intense whistler waves can interact with ionospheric plasmas to excite lower hybrid waves [Lee and Kuo, 1984]. Density fluctuations associated with the lower hybrid waves can nonlinearly scatter high-frequency plasma waves and change the frequency spectra of these waves. For example, photoelectron-produced Langmuir waves can be scattered by the lower hybrid waves to create frequency-upshifted and -downshifted Langmuir waves. VTF experiments can simulate this lightning-induced ionospheric plasma process well. The limitations of simulating lightning-induced ionospheric plasma effects in VTF experiments will be discussed.

GH113.9

Multistation Observations of ELF/VLF Waveforms of Lightning Flashes Leading to the Production of Sprites and Elves

Steven C. Reising*, Umran S. Inan and Timothy F. Bell
Space, Telecommunications and Radioscience Laboratory
Stanford University, Stanford, CA 94305

Recent measurements have shown that radio atmospherics ('sferics') launched by sprite-producing positive cloud-to-ground (+CG) lightning flashes exhibit large ELF slow tails, indicating the presence of continuing currents in the source lightning flashes [Reising et al., *GRL, 23,* 3639, 1996]. In addition, data from the Sprites '95 campaign indicated that sferics from elve-producing lightning have large VLF peaks relative to their ELF slow-tail magnitudes, consistent with the production of elves via heating by the electromagnetic pulse (EMP) from lightning [Inan et al., *GRL, 23*, 133, 1996].

A new ELF/VLF broadband (10 Hz to 22 kHz) sferic receiver was operated at Yucca Ridge, Colorado (40°40' N, 104°56' W), in coordination with sprite and elve measurements during July and August of 1996. Simultaneous measurements at Stanford, California, and at Palmer Station, Antarctica (64°46' S, 64°03' W), allowed the observation of sferics at different distances from the source. Arrival azimuth of the sferics is determined using wideband VLF direction finding, with an accuracy of ±1° at ~12,000 km from the source. Triangulation of sferics received at two or more locations provides unambiguous identification of source lightning flashes originating in the storm of interest.

In the present work we perform quantitative analysis of sferics launched by large positive CG flashes during optical measurement periods in order to determine the characteristics of sprite-producing and elve-producing lightning flashes. Characteristics of ELF and VLF radio atmospherics from three separate mesoscale convective systems on separate days are analyzed in relation to optical measurements of mesospheric phenomena.

Measurement of Total Charge Transfer in Sprite-Producing Lightning using ELF Radio Atmospherics

Steven A. Cummer
Space, Telecommunications and Radioscience Laboratory, Stanford University, Stanford, CA 94305

Existing models of the transient high altitude optical emissions called sprites require large amounts of charge (~100-300 C) to be moved from cloud altitudes of 5-10 km to the ground in order to produce the observed levels of optical emissions. Experimental evidence for such large charge transfer in sprite-producing cloud-to-ground lightning comes from radio atmospherics containing large ELF (defined here as <2 kHz) "slow tails", which indicate substantial slowly varying (≤1 msec) lightning current components.

To quantitatively assess the theoretical models of sprite production, it is critical to measure the temporal charge variation in these sprite-creating lightning discharges. The omnipresent electromagnetic radiation from the return stroke (termed a radio atmospheric, or sferic) is easily measurable and can, in principle, be used to deduce the lightning return stroke current waveform at large distances from the discharge, provided that the propagation effects are known or can be suitably modeled. Using a general subionospheric ELF propagation model, we quantitatively interpret magnetic field waveforms of ELF radio atmospherics observed at Stanford, California (~1800 km from the source lightning) to determine the temporal variation of the lightning current and thereby measure the total charge transfer during the stroke. For sprite-producing lightning current waveforms observed in July, 1996, we find that 25-300 coulombs of charge is transferred during the first 5 ms of the discharge, assuming a 10 km altitude for the initial charge.

The larger discharges (>100 C) are large enough to produce optical emissions through both the quasi-electrostatic heating (QE) and runaway electron mechanisms. The fact that relatively weak but nevertheless detectable sprites were produced by the removal of <50 C of charge indicates that other factors not considered in the present QE and runaway electron models may also be involved in the generation of optical emissions at mesospheric altitudes.

GH113.11

Whistle VLF-waves generated in the ionospheric E-region by infra-acoustic waves

Gokov A.M.

Kharkiv State University, Svobody Sq. 4, Kharkiv 310077, Ukraine

It is known that during earthquakes (before and at the time of a seismic shock), explosions, strong thunderstorms and other phenomena, infra-acoustic waves are generated. Usually, the frequencies of infra-acoustic oscillations are about 0.01-0.05 Hz. Such waves having sufficiently small absorptions may penetrate into the ionosphere ap to 200 km, causing plasma disturbances at the heights of the ionospheric E-region; the waves being transformed into electromagnetic radiation.

In the paper there is discussed one of the possible mechanism of transforming an infra-acoustic wave into electromagnetic radiation at the heights of the ionospheric E-region. It is shown that at these heights infra-acoustic waves may generate whistle VLF-waves, for such waves a dispersion equation being obtained $n^2(\omega) = \omega_p^2 / \omega\,\omega_B \cos\theta$ (ω_p, ω_B are the plasma and cyclotron electron frequency, respectively; θ is the angle between a propagation direction and magnetic field), from which there is obtained a relatioship between the frequencies of VLF-whistlers, fs , and an infra-acoustic wave, f_i . On the basis of this relationship there has been calculated a height interval in which generation of electromagnetic radiation of the type of whistle VLF-waves $f_s \sim$ 100 Hz - 100 kHz is possible, a corresponding frequency interval of the infra-acoustic waves causing them being found (0.05 Hz < f_i < 2 Hz). It is shown that intensity of the VLF-waves generated strongly depends on a magnitude of the electron density, N, in the ionosphere and considerably increases with N.

In practice the mechanism considered allows to establish a relationship between the frequency Doppler shift of a radio wave when high frequency sounding the ionosphere and a lower frequency electromagnetic radiation during explosions, strong earthquakes, thunderstorms and other phenomena.

URSI J | Session 14 | Salon Matapedia

Very Long Baseline Interferometry: On the Ground and in Space
Co-chairs: P. Dewdney, Canada and J.S. Ulvestad, USA

08:10	14.1	The VSOP Mission: In-Orbit Status and First Results, **H. HIRABAYASHI**, *Institute of Space and Astronautical Science, Kanagawa, Japan*
08:50	14.2	U.S. Space VLBI: VSOP Mission Ground Support System, **R. WIETFELDT**, D. MURPHY, J. SMITH, D. TRAUB, *Jet Propulsion Laboratory, Pasadena, CA, USA*
09:10	14.3	A Correlator/Signal Processing System for Space VLBI, **B. CARLSON**[1], B. PETRACHENKO[2], P. DEWDNEY[3], T. BURGESS[3], D. WELLBORN[3], R. CASORSO[3], [1]*University of Calgary, AB,* [2]*NRCan,* [3]*NRC, Canada*
09:30	14.4	Early VLBA Correlator Experience with VSOP Observations, **J.D. ROMNEY**, *National Radio Astronomy Observatory, Socorro, NM, USA*
09:50	14.5	The Mark IV VLBI Correlator System, **A.R. WHITNEY**, *MIT Haystack Observatory, Westford, MA, USA*
10:10		Coffee Break
10:30	14.6	Position Angle of the Orbiting VLBI Antenna Feed, **L. KOGAN**, *National Radio Astronomy Observatory, Socorro, NM, USA*
10:50	14.7	Space VLBI in the 21st Century, **J.S. ULVESTAD**[1], R.P. LINFIELD[2], [1]*National Radio Astronomy Observatory, Socorro, NM and* [2]*California Institute of Technology, Pasadena, CA, USA*

J14.1

The VSOP Mission: in-orbit status and first results

Hisashi Hirabayashi et al.
Institute of Space and Astronautical Science
3-1-1 Yoshinodai, Sagamihara, Kanagawa, 229 Japan

The VSOP (VLBI Space Observatory Programme) satellite, MUSES-B, will place an 8 meter diameter radio-telescope in an elliptical, ~6 hour, Earth orbit to make the first dedicated space-VLBI observations on baselines up to 30,000 km. The main reflector of the satellite is a deployable parabola composed of a gold-coated molybdenum mesh, and a 0.5 mm rms surface accuracy expected. The multi-waveband feed horn is located at the Cassegrain focus with left-hand circular polarization receivers. The observing bands — 1.6 GHz, 5 GHz and 22 GHz — include standard VLBI continuum frequencies and the main OH (1.6 GHz band) and H_2O (22 GHz band) maser lines. The reference time signals are uplinked in real-time, and data down-loaded in real-time, on a 128 Mbps link supported by a dedicated five station international telemetry network.

Muses-B is scheduled for launch on the 7th of February, 1997, and will be the payload of the first launch of ISAS's new M-V rocket. The main antenna is planned for deployment within 14 days after launch. The first three or four months after launch will be devoted to an in-orbit checkout of the satellite, tracking station system checks, fringe detection tests and test imaging experiments. Following these in-orbit checkouts, routine observing will commence. By the middle of July, some first results can be presented, together with engineering results.

The VSOP mission is being led by the Institute of Space and Astronautical Science (ISAS), in close collaboration with the National Astronomical Observatory (NAO) of Japan. NASA/JPL and NRAO of the USA are key collaborating institutions, and most radio-telescopes world-wide will participate in VSOP observations. The in-orbit checkout activities will be done by the VSOP Science Operations Group in Japan and international in-orbit checkout partners.

The VSOP World Wide Web site (http://www.vsop.isas.ac.jp/) contains additional information and pictures of mission activities.

U.S. Space VLBI: VSOP Mission Ground Support System

R. Wietfeldt, D. Murphy, J. Smith, D. Traub

Space Very Long Baseline Interferometry (VLBI) is a scientifically and technologically exciting extension to the technique of ground-based VLBI, in practice since its first development in 1967. In this paper we describe the design and implementation at the Jet Propulsion Laboratory of the JPL/DSN ground support system that enables observations of the first generation of Space VLBI satellites, the VLBI Space Observatory Programme (VSOP) satellite of Japan's Institute of Space and Astronautical Science (ISAS) and the Radioastron satellite of Russia's Astro Space Center (ASC), launched in 1997 and 1999, respectively.

J14.3

A Correlator/Signal Processing System for Space VLBI

Brent Carlson (U of Calgary), Bill Petrachenko (NRCan),
Peter Dewdney (NRC), Tom Burgess, Dale Wellborn,
Ron Casorso (NRC)

A new S2 VLBI correlator is on-line at the Dominion Radio Astrophysical Observatory (DRAO) in Penticton, B.C., Canada. It will be primarily used for processing about 25% to 30% of VSOP (VLBI Space Observatory Program -- ISAS, NAO -- Japan) data from up to 8 S2s at various ground radio telescopes as well as 3 DSN tracking stations. It will also be used for processing Canadian geodetic data acquired from ARO and two mobile antennas.

The correlator is an XF correlator that is modular in design allowing essentially unlimited expansion. The correlator constructed for the VSOP mission has 10 station capacity and is equipped with, at present, 6 S2 VLBI playback terminals (S2-PT). The S2-PT uses 8 VHS transports to provide 128 Mbit/sec recording capacity for 6 hours (upgradable to 8.5 hours). A 6 hour tape set costs CAN $80 and weighs about 2 kg.

The correlator at DRAO has the following basic capabilities:
-8 one or two bit data channels at up to 32 Msample/sec/channel.
-8 256-level tone extractors per station.
-Quantizer statistics acquisition on each channel of each station.
-Up to 4000 frequency points "synthetic autocorrelator" for each station.
-2 independent programmable pulsar timers that can gate one or more of each of the 8 channels on each station.
-High speed delay and Doppler compensation beyond the limits of practicality for high velocity and acceleration tracking.
-48 correlator modules -- each one contains 8, 32 complex lag chainable correlators or up to 512 complex lags per module. Multiple modules can be chained together for up to 16384 complex lags (8192 frequency points).
-On-the-fly continuum and spectral line correlator configuration.
-Multiple simultaneous job processing capability.

The correlator uses a unique approach for fringe stopping whereby the fringe phase is calculated and quantized to 16 phase steps on a station basis and then carried through the lag chain on the correlator module. The station phases are then subtracted at the lag to form the final baseline phase. This approach eliminates post correlation corrections required to compensate for station velocity and smearing due to station acceleration. This talk will discuss this unique approach as well as the hardware and software architecture and implementation of the system.

Early VLBA Correlator Experience with VSOP Observations

Jonathan D. Romney
National Radio Astronomy Observatory
Post Office Box O
Socorro, New Mexico 87801-0387

As part of NRAO's participation in the international Space VLBI missions VSOP and Radioastron, the VLBA correlator has been enhanced to accommodate observations with an orbiting interferometer element. Although not designed specifically to support Space VLBI observations, the correlator's design anticipated this possibility, so that only relatively minor modifications were required.

Some enhancements were essential new features specific to an orbiting element — incorporation of software predicting the spacecraft position and velocity — or were necessitated by aspects of the current missions — applying timing corrections measured as part of the ground-to-space phase transfer process. Others involved extending the range of one parameter in the correlator's wavefront model, and accommodating a large residual fringe rate window required by the limited accuracy of orbit reconstruction. Some enhancements were also required to maintain compatibility with upgraded ground radio telescope equipment. Finally, a variety of new operational procedures had to be developed to cope with the recording of data from a single orbiting element at a number of different ground telemetry stations, and to obtain and manage the many files that must be exchanged among mission elements.

These developments are all complete, and have been tested as extensively as could be done in the absence of true Space VLBI observations. Final validation will have to await the VSOP mission, scheduled to be launched on 1997 February 7. In-orbit checkout is expected to last about six months, with the first interferometric tests planned to occur in late March or early April 1997, and scientific observations ramping up starting in May 1997.

This paper will review briefly the scientific requirements for the several correlator enhancements, and the implementation of each, but will concentrate on surveying their performance in the correlation of these early observations.

J14.5

The Mark IV VLBI Correlator System

Alan R. Whitney, *MIT Haystack Observatory, Westford, MA USA*

The Mark IV VLBI correlator system is being developed by an international consortium, dubbed IACC (for International Advanced Correlator Consortium) including Haystack Observatory, NFRA/JIVE (Netherlands) and Jodrell Bank (UK), with support in the U.S. from NASA, USNO and Smithsonian, and in Europe from JIVE. Target correlators for this development effort include four large VLBI correlators in the U.S. and Europe, as well as the Westerbork array in The Netherlands and the Smithsonian Submillimeter Array on Mauna Kea. The key technical developments and capabilities will be discussed, particularly with respect to VLBI.

The primary characteristics of the Mark IV VLBI correlator system are as follows:

- 1 Gbit/sec/station, expandable to 2 Gbits/sec/station
- Expandable to 32 simultaneous stations
- Fully station-based, using X-F correlation algorithm
- Flexibility to optimize for both continuum and spectral-line processing
- Compatible with Mark IIIA, Mark IV and VLBA recordings
- Compatible with space-VLBI
- 4X playback-speedup factor compared to Mark IIIA correlator

The heart of the Mark IV correlator system is a new full-custom VLSI correlator chip developed at Haystack Observatory. This chip contains all necessary phase-rotation, delay-management and correlation functions so as to allow station-based playback data to be applied directly to the chip; that is to say, all baseline-based operations are performed within the chip with no redundancy of operations as in some earlier X-F correlator designs. Furthermore, station-based processing parameters are intermixed into each station-data-stream so that baseline-based processing parameters are calculated by simple arithmetic operations in a local microprocessor.

All hardware subsystems of the Mark IV correlator are nearing completion, with the expectation of first fringes in the first half of 1997. Fully operational systems are expected to be complete in 1998.

Position Angle of The Orbiting VLBI Antenna Feed.

L. Kogan

National Radio Astronomy Observatory, PO Box 0, Socorro, NM 87801, USA

The knowledge of the position angle of an antenna's feed is very important for polarization observations. The position angle change during tracking of the source depends on mounting device of the antenna. The issue has been developed for ground based antennas and has not been investigated for an orbiting antenna. The analysis of the position angle behavior has been provided for Japanese satellite VSOP antenna which is planned to be used in the orbiting VLBI experiment. The projection of the Sun on the aperture is used as a referencing direction. The analytic expression for the position angle has been obtained. The plots of the position angle for wide range of right ascensions and declinations of sources as a function of time are demonstrated. As expected the most typical rate of position angle change is close to 1 degree/day. But at the same time this rate can be as high as 30 degrees/day at some specific times. There is no any change of the position angle for the sources located at the ecliptic plane.

J14.7

Space VLBI in the 21st Century

J. S. Ulvestad*
National Radio Astronomy Observatory
P.O. Box O
Socorro, NM 87801

R. P. Linfield
Jet Propulsion Laboratory
California Institute of Technology
Pasadena, CA 91109

The first dedicated space VLBI mission, VSOP, is being launched in 1997. Along with its scientific goals, this mission will be exploratory in nature, leading to scientific questions that can be addressed with more advanced missions in the 21st century. Several mission concepts are under discussion in the international community; they have in common the push to much higher sensitivity and to higher observing frequencies. Key scientific goals for advanced space VLBI missions in the early part of the 21st century include

- High-frequency imaging, in the optically thin regime, of cores and jets in compact gamma-ray blazars and other active galactic nuclei
- Studies of the physics of extragalactic water megamasers
- Cosmological studies of the scale of the universe using techniques such as geometrical measurements of distances to water masers, imaging of gravitationally lensed radio sources, and measurements of proper motions in high redshift objects

In the U.S., we have been studying a future space VLBI mission named ARISE (Advanced Radio Interferometry between Space and Earth). ARISE has been approved as a mission-concept study in a competitive NASA proposal process. It currently is under consideration as part of the Structure and Evolution of the Universe theme in NASA.

ARISE would consist of an orbiting 25-m radio telescope, operating in conjunction with ground arrays at observing frequencies ranging from 5 GHz to 86 GHz. The current concept is that the radio telescope will be based on an inflatable antenna structure. Ground tests are now being conducted to assess the surface accuracy as a function of antenna diameter for such antennas, and to investigate the causes of the dominant error terms. A study of the possibility of enabling the high-frequency performance by means of array feeds is also under way. It is expected that a flight demonstration of a 25-m inflatable antenna, although not yet with surface quality good enough for 86 GHz, will take place around the year 2000.

URSI J

Session 29

Salon Matapedia

Instrumentation and Signal Processing Techniques
Co-chairs: D. Backer, USA and K. Tapping, Canada

13:10	29.1	The Princeton Mark IV Pulsar Observing System, **I.H. STAIRS**, S.E. THORSETT, J.H. TAYLOR, *Princeton University, Princeton, NJ, USA*
13:30	29.2	High Speed Baseband Recording with 2-Bits, **F.A. JENET**, S.B. ANDERSON, W.R. COOK, T.A. PRINCE, S.C. UNWIN, *California Institute of Technology, Pasadena, CA, USA*
13:50	29.3	S2 Pulsar Baseband Processing System, **R. WIETFELDT**[1], N. BARTEL[2], D. DEL RIZZO[2], W. VAN STRATEN[2], W. CANNON[3], S. NOVIKOV[3], M. BAILES[4], D. STINEBRING[5], [1]*Jet Propulsion Laboratory, Pasadena, CA, USA;* [2]*York University, North York, ON, Canada;* [3]*ISTS;* [4]*University of Melbourne, Parkville, Australia;* [5]*Oberlin College, Oberlin, OH, USA*
14:10	29.4	Berkeley Pulsar Processors: Signal Analysis, **D.C. BACKER**, *University of California, Berkeley, CA, USA*
14:30	29.5	The Performance of Digital Correlators with Large Dynamic Range, **G. HOVEY**[1], M.R. ITO[2], [1]*Dominion Radio Astrophysical Observatory/NRC, Penticton and* [2]*University of British Columbia, Vancouver, BC, Canada*
14:50	29.6	Correction for the Digital Representation of the Signals at VLBA Correlator, **L. KOGAN**, *National Radio Astronomy Observatory, Socorro, NM, USA*
15:10		Coffee Break
15:30	29.7	Noise Balls and the Orthogonal Modes of Polarization in Pulsar Radio Emission, **M.M. McKINNON**[1], D.R. STINEBRING[2], [1]*National Radio Astronomy Observatory, Green Bank, WV and* [2]*Oberlin College, Oberlin, OH, USA*
15:50	29.8	Real-Time Interference Cancellation Using the Adaptive Filter, **R.F. BRADLEY**[1], R. ESCOFFIER[1], S.G. WILSON[2], C. BARNBAUM[3], [1]*National Radio Astronomy Observatory and* [2]*University of Virginia, Charlottesville, VA and* [3]*Space Telescope Science Institute, Baltimore, MD, USA*
16:10	29.9	Holographic Antenna Measurements at DRAO, **A.D. GRAY**, *Herzberg Institute of Astrophysics/NRC, Penticton, BC, Canada*
16:30	29.10	Progress on the Evaluation of a Phased Array Feed, **J.R. FISHER**[1], R.F. BRADLEY[2], K.S. SAINI[3], [1]*National Radio Astronomy Observatory, Green Bank, WV,* [2]*National Radio Astronomy Observatory, Charlottesville and* [3]*University of Virginia, Charlottesville, VA, USA*
16:50	29.11	Upgrading the 10.7cm. Radio Flux Programme, **K.F. TAPPING**, *Dominion Radio Astrophysical Observatory/NRC, Penticton, BC, Canada*

J29.1

The Princeton Mark IV Pulsar Observing System

I.H. Stairs, S.E. Thorsett and J.H. Taylor
Joseph Henry Laboratories and Physics Department,
Princeton University, Princeton, NJ 08544

Highly accurate timing of radio millisecond pulsars has applications not only in the study of the pulsars themselves, but also in areas such as astrometry, time-keeping, and experimental tests of cosmology and general relativity. Observations forming the basis of the general relativity tests have measured the phases of pulsar "clocks" with typical uncertainties of 2–20 μs, averaged over a few minutes. These tests could be considerably strengthened and improved with higher timing precision. The chief obstacle to improved time resolution is dispersion of the pulses during their propagation through the ionized interstellar medium. This phenomenon results in delays of lower-frequency radiation components relative to the higher frequencies, and across a typical observing bandwidth can amount to many (often hundreds or more) times the intrinsic pulse widths. With a traditional filter bank system, which removes the dispersion between channels after the pulse is detected, residual smearing remains within the individual channels. A superior approach is pre-detection or "coherent" dedispersion, in which the raw signal voltage is convolved with the inverse of the transfer function of the interstellar medium. This technique was first used more than two decades ago, but only recently have computer speeds and the cost of data storage approached levels allowing its widespread use over bandwidths of several MHz or more.

The Princeton Mark IV system was designed to implement this coherent dedispersion technique. A fast analog-to-digital converter samples quadrature components of the signals in two orthogonal polarization channels, allowing 10 MHz bandwidth with 2-bit sampling or 5 MHz bandwidth with 4-bit sampling, and producing a 10 MB/s continuous throughput. The resulting data are fed to a SPARC 20 computer and then onto DLT 7000 tape drives and/or a 108 GB disk array. Data analysis is performed by a fast (1.25 Gflop) processor made by Texas Memory Systems, which is well optimized for FFTs and related signal processing tasks. It yields a compute-to-observe ratio of approximately ten for our 10 MHz bandwidth data. As a side benefit of the technique, we obtain the full Stokes parameters of the received signal. We find that narrow-band radio-frequency interference can be effectively excised as part of the coherent signal-processing task.

High Speed Baseband Recording with 2-Bits

Fredrick A. Jenet, Stuart B. Anderson, W. Rick Cook, Thomas A. Prince, and Steven C. Unwin

California Institute of Technology, Pasadena, CA 91125, USA

Abstract

The study of radio pulsars at the highest time resolution is currently limited by the capability of the signal detection system to accept a wide-bandwidth signal, and to sample the data rapidly enough. We describe a new instrument for pulsar research which utilizes baseband recording at 400 Mbit/s to achieve both a high bandwidth and a high sustained data rate. We are capable of quadrature sampling dual polarizations with 50 MHz bandwidth and 2-bit voltage resolution (2 X 2 X 50 X 2 = 400 Mbit/s). The Wide Bandwidth Digital Recording (WBDR) system is based on a custom VLSI analog/digital VLSI converter operating at 50 MHz, and a commercial digital cassette tape recorder. Signal analysis is performed entirely in software, using a massively parallel computer. In order to achieve a sample rate of 50MHz, the data is digitized with 2-bits. Such digitizing adds unwanted non-linear artifacts into the data by both underestimating the total power in the signal and scattering power across the entire bandpass. We will describe a treatment that removes these effects.

J29.3

S2 Pulsar Baseband Processing System

R. Wietfeldt (JPL), N. Bartel, D. Del Rizzo, W. Van Straten (York U.), W. Cannon, S. Novikov (ISTS), M. Bailes (U. of Melbourne), D. Stinebring (Oberlin College)

The S2 baseband processing system for pulsars is designed for a variety of pulsar measurements such as ultrafast signal fluctuations and pulse timing. Its key features are: the S2 recorder; the efficient mechanism for high data volume, high data rate transfer from S2 tapes to computer/workstation via the S2 'tape-to-computer interface'; and the tightly coupled control interface to the computer which enables automated data transfer and processing. Developed originally for Very Long Baseline Interferometry (VLBI) applications, the S2 recorder is based on the use of commercial VHS tape transports (VCR's) modified for use in digital high density, high data rate applications. A single S2 recorder provides up to 500 GBytes storage and an unattended operating time of up to 8.5 hours at the maximum data rate of 128 Mbits/s (16 MBytes/s) or about 1 GByte/minute. For more challenging applications, multiple S2's may be used. In this paper, we present an overview of the S2 baseband processing system. In particular, we discuss plans to direct S2 data into super-computers to maximize throughput of the data-intensive pulsar processing problems, best served by super-computing parallel-processing methodologies. We present first scientific results of pulsar recordings of August 1995 and results from more recent investigations.

Berkeley Pulsar Processors: Signal Analysis

D. C. Backer
Astronomy Department and Radio Astronomy Laboratory
University of California
Berkeley, CA 94720
dbacker@astro.berkeley.edu

Three Berkeley Pulsar Processors have been constructed and placed into use at Green Bank, Effelsberg and Arecibo. The scientific uses of these signal processors include precision timing and polarimetric studies. The maximum bandwidth that can be used is 112 MHz. Dispersion within each of 32 narrow bandwidth channels is removed 'coherently' (in the volage domain) by complex convolution in a low-bit quantization, full custom VLSI chip. The processors feature agility to observe at a wide range of radio frequencies and a wide range of dispersions. Remote operation is routine. A fourth system, with modified design and maximum bandwidth of 168 MHz, has been constructed at the Naval Research Laboratory and placed into operation for a galactic plane pulsar search at Nançay. Description of Berkeley Pulsar Processors may be found on http::/astro.berkeley.edu/~mpulsar.

Following an introduction to the design of this system and description of some results, I will focus on analysis of the effects of quantization on the signals. The first stages of this analysis have been published in 97 January issue of PASP. The A/D quantizes the signal to 4-bits. After mixing, filtering and decimation of samples is done, the signal is further quantized to 2-bits/4-levels. The deconvolution for dispersion removal is then done with 3-bit/15-level coefficients. Restoration of power to a linear scale is not as simple as the conventional Van Vleck correction of digital correlators. Our solution to this will be described.

J29.5

The Performance of Digital Correlators With Large Dynamic Range

G. J. Hovey
Dominion Radio Astrophysical Observatory
National Research Council
P.O. Box 248 Penticton
B.C., V2A 6K3, Canada

M. R. Ito
Department of Electrical Engineering
University of British Columbia
Vancouver, B.C.

It is well known that the sensitivity and linearity of any digital correlator are degraded when a small number of quantization levels are used. While the digital correlator's sensitivity is irretrievably reduced, its non-linear input-output characteristic can be corrected, i.e. linearized. These effects have been analyzed by many authors and methods have been developed for linearizing the response of correlators with less than five levels of quantization.

One way in which sensitivity can be improved is to increase the number of quantization levels. Advances in integrated circuit technology have made possible the development of such correlators for application in radio astronomy.

In this paper we discuss the benefits of multi-level quantization and present as an example the sensitivity and non-linear response of a 14-level correlator. We compare the effectiveness of approximation methods using a Padé and Taylor series inversion for linearizing the input-output response of that correlator.

Correction for the digital representation of the signals at VLBA correlator

L. Kogan

National Radio Astronomy Observatory, PO Box 0, Socorro, NM 87801, USA

Two types of correlators are used in radio astronomy: XF and FX. XF correlator has a correlation of the digitized signals at the output. FX correlator measures (in some sense) Fourier transform of the correlation function which is a cross-power spectrum of the input signals. If the conversion function for the correlation is linear then the spectrum measured by a FX correlator is identical of the spectrum of input analog signal with accuracy of a constant factor. VLBA uses FX correlator with TWO and FOUR level digitizing of the input signals. So three combinations are possible: TWO-TWO, FOUR-FOUR, and TWO-FOUR. It is clear that the last two are more linear. Conversion functions for the homogeneous digitizers were well known. Conversion functions for the mix case (TWO-FOUR) has been calculated by us. The all three conversion functions are linear for a small correlation and has a rise for high correlation. At VLBI the final estimation of the correlation is made after fringe stopper procedure. This procedure suppresses the output for a large correlation and therefore has to linearize the conversion function. The final more linear conversion function has been calculated for the all three digitizing combinations. In the case of auto correlation the fringe stopper procedure is absent. So *different conversion functions have to be used for auto and cross correlation.* Conversion function of FX correlator (b-factor) has been estimated for the all three digitizing combinations. The correction is implemented at AIPS - the software package used for post correlator data reduction.

J29.7

NOISE BALLS AND THE ORTHOGONAL MODES OF POLARIZATION IN PULSAR RADIO EMISSION

Mark M. McKinnon*
National Radio Astronomy Observatory
Green Bank, WV 24944

Daniel R. Stinebring
Department of Physics
Oberlin College
Oberlin, OH 44074

One of the most fascinating and common features of pulsar radio emission are the orthogonal modes of polarization. The modes are most obvious in observations of individual pulse polarization where they appear as abrupt, 90-degree transitions in polarization position angle. A combination of superposed orthogonal modes and instrumental noise can describe the rich variety in the observed distributions of position angle. The simultaneous interaction of the orthogonal modes causes the pulsar radio emission to depolarize. When the amplitudes of the polarization vector for each mode are comparable, a large fraction of emission subpulses will have very little linear polarization. In this case, the statistics of the linear polarization may be dominated by instrumental noise. Since the position angle of instrumental noise is distributed uniformly, one would expect a uniform component of position angle to accompany the orthogonal modes in a position angle histogram. However, when the amplitudes of the polarization vectors are quite different, the position angle histogram will reflect the position angle of the stronger mode. We derive the theoretical distributions of position angle for the combination of superposed orthogonal modes and instrumental noise. The theoretical distributions compare favorably with the position angle histograms that are observed in PSR B2020+28.

The depolarization of pulsar radio emission at high radio frequency has been attributed to the orthogonal modes or to the randomization of position angle. Based upon our analysis, we conclude that the randomization of the position angle is an artifact of superposed orthogonal modes and that the modes are the principal depolarization mechanism.

REAL-TIME INTERFERENCE CANCELLATION USING THE ADAPTIVE FILTER

Richard F. Bradley*
National Radio Astronomy Observatory†
Charlottesville, VA 22903

Stephen. G. Wilson
EE Department
University of Virginia
Charlottesville, VA 22903

Raymond Escoffier
National Radio Astronomy Observatory
Charlottesville, VA 22903

Cecilia Barnbaum
Space Telescope Science Institute
Baltimore, MD 21218

The concept of adaptive interference cancellation was first introduced in the mid-1970's as a way to greatly reduce unwanted noise in low frequency (audio) systems. Recently, high-speed digital filter chips make adaptive filtering practical in a bandwidth of a few megahertz. Such a system is worthy of consideration for radio astronomy applications. The fundamental system consists of two receivers - the "primary" channel receives the desired signal that is corrupted by interference, and the "reference" channel receives only the interference. The reference channel is processed using a digital adaptive filter and then subtracted from the primary channel thus producing the system output. The weights of the digital filter are adjusted by way of an algorithm that minimizes, in a least-squares sense, the power output of the system. Through an adaptive-iterative process, the interference canceler will lock onto the interference and the filter will adjust itself to minimize the effect of the interference at the system output. Our current research effort is toward a *proof-of-principle system* for radio astronomy.

The *proof-of-principle system* will consist of one primary channel and one reference channel. The primary channel will be the combined output from a pair of crossed-dipole feeds tuned for 90-100 MHz operation and located at the Green Bank 140-foot prime focus. The reference channel will be the output of a combined pair of orthogonal, five-element yagi antennas, also tuned for the 90-100 MHz band, and mounted on a remotely-controlled, rotatable mast located at the apex of the 140-foot prime focus mount. The front-end box will house the two ambient temperature receivers. Each receiver will consist of a low-noise amplifier, RF filter, and a downconverter module that contains additional amplifiers and a mixer to produce a 25 MHz IF. In the control room, the primary and reference channels are mixed down to 5 MHz where they are digitized and processed. The reference channel is processed by the adaptive filter and then subtracted from the primary channel to form the system output which is then converted back to analog form and sent to the spectral processor. Initial evaluation of proof-of-principle system is scheduled for early '97. Technical issues to be investigated include the interference coherence bandwidth, multiple source cancellation, and the noise spectrum characteristics of the canceling circuits. Results of the initial evaluation will be presented.

---

†The National Radio Astronomy Observatory is a facility of the National Science Foundation operated under cooperative agreement by Associated Universities, Inc.

J29.9

Holographic Antenna Measurements at DRAO

Andrew D. Gray
National Research Council Canada
Herzberg Institute of Astrophysics

The Dominion Radio Astrophysical Observatory (DRAO), located near Penticton, BC, operates a seven element, interferometric, earth-rotation aperture synthesis radio telescope (hereafter referred to as the ST) used for astronomical observations at 408 and 1420 MHz. During summer '95 and summer '96 a series of measurements were made with this instrument in order to construct holographic surface plots of the seven antennas at 1420 MHz, performed as part of an on-going effort to assess and, where necessary, improve the performance of this instrument.

Holography at DRAO presented some challenges. Since the ST operates only in protected radioastronomy bands it was not possible to use ground- or satellite-based beacons as a reference signal, and few astronomical sources are sufficiently strong that they dominate the incoming signal even when outside the main lobe of the antennas. Cygnus A was finally chosen as most suitable since it is sufficiently compact that, some source structure aside, there was adequate signal even on the longest baselines. The effect of the source structure on the data then had to be modelled and removed before the data could be used.

The observing technique adopted was to track Cygnus A continuously (i.e., while it was above the horizon) with one antenna as a reference, while the other six antennas were moved simultaneously to various offset positions until sufficient data had been gathered. The offset signals were correlated with the reference signal using the existing ST digital complex cross-correlator. For the two measurement sessions different antennas were used as reference to ensure that holographic data were available for all antennas.

Once recorded, the data were corrected for source structure then assembled and transformed to the aperture plane. For antennas measured in both the '95 and '96 sessions the results compared well, verifying the validity of the technique. Random surface errors of up to approximately 2.5 cm (roughly $\lambda/8$) were detected on various antennas. One antenna showed evidence of significant phase curvature, corresponding to a focus error of about 2.5 cm. Efforts are now being made to use the results of these measurements to improve image fidelity. Further holography experiments will be undertaken in summer '97.

Progress on the Evaluation of a Phased Array Feed

J. Richard Fisher *
National Radio Astronomy Observatory†
Green Bank, WV 24944

Richard F. Bradley
National Radio Astronomy Observatory
Charlottesville, VA 22903

Kamaljeet S. Saini
Department of Electrical Engineering
University of Virginia
Charlottesville, VA 22903

We have developed a prototype receiver for the evaluation of a phased array as a reflector antenna feed. Our first attempt was a 19 element ambient-temperature system located at the prime focus of the 140-foot telescope in Green Bank. Each element included a 1.0-2.0 GHz sinuous antenna fed by a tapered balun to a low-noise MMIC-type amplifier, a bandpass filter, a second MMIC amplifier, and a mixer. The noise temperature of the element was approximately 300 K. A FET-based switch matrix, functioning as a commutator, successively connected pairs of signals from the 19 amplifiers to a FFT spectrometer cross-correlator. Full array correlation was done, two pairs at a time, in 86 seconds with one second of integration on each pair. This provides adequate sensitivity to measure the array response to a few strong celestial radio sources.

Our first telescope measurements in October 1996 emphasized a number of measurement details that are particularly acute with an phased array. 1) Making a reference measurement in the absence of a point source in the beam requires a large telescope move because of the large array field of view. Because there is a lot of correlated noise from spillover, the reference must be taken at the same azimuth/elevation as the source measurement. This puts a stiff stability requirement on the receiver because it takes at least 20 minutes for the source to move out of the field of view. 2) Establishing a phase and amplitude reference for the array is difficult. Both the reflector focal plane field and the array response are unknown so there is no way to calibrate with a celestial source. We tried illuminating the array with a simple antenna near the vertex of the reflector, but reflections from feed support structure and the reflector itself made the wavefront complex and apparently unstable. 3) Measurements of array element self-products using one spectrometer channel were difficult to calibrate with respect to element pair cross-products using two channels.

In our first observations, we saw the expected focal plane field pattern as it was scanned across the array. As always happens with an early abstract deadline, we hope to have better calibrated data from another run before this meeting. Enhancements to the array receiver are under way to improve stability and calibration. Element self-products will be measured as cross-products with a correlation receiver design. Thermal, mechanical, and electrical stability of the amplifier chain are being improved. A calibration signal will be weakly coupled into each receiver just ahead of the low-noise amplifier, and this distributed signal will be phase-calibrated with respect to a plane wavefront on the antenna range. The correlation receiver design will permit a simpler and faster RF commutator switch with improved isolation.

---

†The National Radio Astronomy Observatory is a facility of the National Science Foundation operated under cooperative agreement by Associated Universities, Inc.

J29.11

Upgrading the 10.7cm Radio Flux Programme

K. F. Tapping
Dominion Radio Astrophysical Observatory
National Research Council
P.O. Box 248, Penticton
BC, V2A 6K3, Canada

The 10.7cm solar radio flux density provided daily for almost 50 years by the National Research Council is currently the best index of solar activity we have. It is easy to measure objectively and consistently, and is tightly correlated with the magnetic activity which is the underlying process driving the observed manifestations of solar activity.

The expanding usage of the data led in 1985 to a complete upgrade of the programme. We would develop new receivers and data logging systems, overhaul the measurement and calibration processes, and automate data distribution to the maximum degree possible.

New receivers were developed which use no downconversion. All amplification and filtering are done at the observing frequency of 2800MHz. They are simple, total-power receivers, designed for linearity and dynamic range. To provide the required gain stability the receivers are embedded in aluminum slabs which are 60cm square and 7.5cm thick. The components and cables are in milled slots and holes, so that they are effectively mounted in a waveguide which is well below cutoff. The low feedback and good thermal stability are more than adequate for our solar observations. Special efforts were made to avoid signal and ground loops.

Ground radiation can be a significant contributor to the receiver output, depending upon the elevation of the Sun and the ground temperature. A flux determination procedure has been developed which makes measurements of the ground radiation so that they can be largely removed from the measured flux densities.

Two independent flux monitors are used to make the measurements. In general, the two series of measurements track to within one solar flux unit (10^{-22} $W.m^{-2}.Hz^{-1}$). The consistency of these measurements provide a rough check of system accuracy. However, the measurements are periodically checked against a dual-horn calibration system.

Routine data distribution and archiving are now largely automatic. We are now also putting the data on the World Wide Web.

URSI J **Session 46** **Salon Matapedia**

Aperture Synthesis: Instrumentation and Techniques
Co-chairs: L. Higgs, Canada and T.J. Cornwell, USA

08:10	46.1	Mapping the Sun Using a Sparse Antenna Array, **K.F. TAPPING**, *Dominion Radio Astrophysical Observatory/NRC, Penticton, BC, Canada*
08:30	46.2	Wide-Field Imaging Techniques Used in the NRAO VLA Sky Survey, **J.J. CONDON**, W.D. COTTON, *National Radio Astronomy Observatory, Charlottesville, VA, USA*
08:50	46.3	Low-Radio-Frequency Wide-Field Imaging and Supernova Remnant W49B, **D.S. BRIGGS**, N.E. KASSIM, R.S. FOSTER, *Naval Research Laboratory, Washington, DC, USA*
09:10	46.4	The DRAO Galactic Plane Survey: Panoramic Spectral Imaging of the Milky Way, **T.L. LANDECKER**[1], A.R. TAYLOR[2], [1]*Herzberg Institute of Astrophysics/NRC, Penticton, BC and* [2]*University of Calgary, AB, Canada*
09:30	46.5	Mosaicing with the BIMA Array, **M. WRIGHT**, *University of California, Berkeley, CA, USA*
09:50	46.6	Aperture Synthesis with Imperfect and Time-Varying Antennas, **A.G. WILLIS**, *Dominion Radio Astrophysical Observatory/NRC, Penticton, BC, Canada*
10:10		Coffee Break
10:30	46.7	Determination of an Hour Angle Correction of a Point Radio Source by a Radio Interferometer with Connected Elements, **N.A. DUGIN**, *Radiophysical Research Institute, Nizhny Novgorod, Russia*
10:50	46.8	Formation of Phase-Coherent Signals from Interferometer Antenna Sites Using Very High Intermediate Frequency, A.A. ROMANYCHEV, **N.A. DUGIN**, *Radiophysical Research Institute, Nizhny Novgorod, Russia*
11:10	46.9	The Hamaker-Bregman-Sault Measurement Equation for Synthesis Radio Telescopes, as Used in AIPS++ Processing, **T.J. CORNWELL**[1], M.H. WIERINGA[2], [1]*National Radio Astronomy Observatory, Socorro, NM, USA;* [2]*Australia Telescope National Facility, Narrabri, Australia*

J46.1

Mapping the Sun Using a Sparse Antenna Array

K.F. Tapping
Dominion Radio Astrophysical Observatory
National Research Council
P.O. Box 248, Penticton
BC, V2A 6K3, Canada

Mapping the solar disc is a problem for most synthesis radio telescopes in that the mapping fields are smaller than the Solar Disc. Even when mosaicing is employed to build the maps by combining multiple fields, it is difficult to maintain a realistic balance between spatial information at large and small scales.

The Synthesis Telescope at the Dominion Radio Astrophysical Observatory consists of seven 9m antennas in a 600m linear array. Three of the antennas are movable. At 21cm wavelength the DRAO ST achieves arc-minute resolution over a mapping field 2.5° across. The u,v plane coverage in a single 12-hour synthesis observation is sparse. Full coverage is achieved by observing for about 12 days, using a different set of movable antenna spacings for each day.

The large field makes the DRAO Synthesis Radio Telescope attractive for solar mapping. However, the Sun's rotation and the rapid evolution of centres of activity restrict the observing time to one 12-hour synthesis per map. Only one set of antenna spacings can be used per image, making the u,v plane coverage very sparse.

A useful property of the Sun in a 2.5° mapping field is that we can know in advance that the map will be dominated by a bright, roughly-circular object surrounded by black sky. Accordingly, the antenna spacings for the observations were chosen by deriving the visibility function for uniformly bright solar disc, and then selecting the antenna spacings to unamibiguously sample this function. These spacings were used for the observations.

The process worked surprisingly well. Usable maps were obtained without any subsequent image improvement. However, the CLEAN algorithm, together with an assumption that no bright, isolated structures were present beyond the solar limb made the images significantly better, well showing the disc and bright active region sources.

WIDE-FIELD IMAGING TECHNIQUES USED IN THE NRAO VLA SKY SURVEY

J. J. Condon* and W. D. Cotton
National Radio Astronomy Observatory
520 Edgemont Road, Charlottesville, VA 22903 USA

The NRAO VLA Sky Survey (NVSS) is an aperture-synthesis survey covering 82% of the sky with a grid of 217,446 "snapshot" observations of partially overlapping primary-beam areas. The grid geometry and integration times were chosen to ensure nearly uniform sensitivity over the sky.

The low-resolution, wideband, widefield snapshot images cannot be made without stretching or violating the assumptions behind normal imaging algorithms. We made several first-order corrections to minimize the resulting errors: (1) A two-dimensional Fourier transform can be used since the VLA is instantaneously coplanar, but the image coordinates must be corrected geometrically by amounts depending on the zenith and parallactic angles of the phase center. (2) We significantly reduced bandwidth smearing by correcting the fringe visibilities associated with CLEAN components for the calculated smearing losses. (3) The (u, v) coordinates must be scaled to correct for the nonuniform IF passband. (4) The signal-weighted centroid frequency varies across the primary beam, whose width is proportional to wavelength. This shrinks the image. (5) The synthesized beamwidth is a finite fraction of the primary beamwidth, so correcting for primary-beam attenuation moves sources outward. The last two radial distortions were removed from the images geometrically.

The instrumental polarization pattern is fixed to the alt-azimuth mounted antennas. We corrected individual snapshots (fixed parallactic angle) using the observed instrumental polarization maps. The residual polarization is only 0.3% rms.

The poor (u, v)-plane coverage of a single VLA snapshot results in high dirty-beam sidelobes which must be CLEANed carefully. We found that CLEAN systematically reduces the flux densities of all sources on a deeply CLEANed image. This CLEAN bias was minimized by restrictions on the size of the CLEANed area and rejecting weak, isolated CLEAN components.

J46.3

LOW-RADIO-FREQUENCY WIDE-FIELD IMAGING AND SUPERNOVA REMNANT W49B

D.S. Briggs*, N.E. Kassim and R.S. Foster
Remote Sensing Division (Code 7213)
Naval Research Laboratory
Washington, DC 20375-5351

Radio synchrotron emission studies of supernova remnants (SNRs) relate to questions on the shock acceleration of high energy particles and the origin of cosmic rays. Addressing these questions requires delicate comparisons of the radio surface brightness across extended sources and between different frequencies. Unfortunately, production of the sensitive, high-resolution, meter-wavelength image required to anchor such an analysis is substantially more complicated at low radio frequencies than at conventional centimeter frequencies. The NRAO Very Large Array (VLA), for instance, can easily image such SNRs at 1.4 GHz (20 cm) and 5 GHz (6 cm), while imaging at 330 MHz (90 cm) remains challenging. This latter frequency is critical, as it provides a long frequency baseline for spectral variation studies and is required for indications of spectral curvature. We present the first scientific analysis of full-resolution 330 MHz VLA data of the SNR W49B, which properly compensates for the effects peculiar to wide-field, low-frequency imaging with a non-coplanar array.

The unique problems at low frequencies arise from the larger field of view which must be imaged due to the increased size of the array element primary beam. The intrinsic number of confusing background sources also rises with decreasing frequency. Finally, 3-dimensional imaging arrays such as the VLA suffer from geometric distortion due to the large field of view – the simple 2-dimensional Fourier inversion commonly employed at higher frequencies is not adequate. Solutions to these problems extend beyond the VLA and are also relevant to similar challenges which face future planned ground and space-based very-low-frequency (< 100 MHz) arrays.

The program dragon was written by Tim Cornwell of NRAO for the solution of the wide-field problem but is very slow. In the usual "contiguous faceting" mode of operation, it completely tessellates the curved sky with small tangent planes. We have ported dragon to the parallel architecture SGI Power Challenge Array and can now produce VLA B-configuration images in a few hours. For high-resolution A-configuration images, required for the shock acceleration studies and still extremely computationally challenging, we have implemented a "targeted faceting" approach to sidelobe removal. A low-resolution image is used to automatically tabulate all sources in the primary beam. A large but tractable region of the sky is tessellated with normal contiguous facets, and the remaining sources are addressed with small targeted facets. For a complete deconvolution to thermal noise, several hundred or more targeted facets may be required. The resulting high-resolution image may be greater than a degree in size, while reducing the computational load by an order of magnitude. This approach, plus enhancements to the parallization of the code and the fast computer have allowed us to explore the problem's complicated parameter space in a tractable time.

The DRAO Galactic Plane Survey - Panoramic Spectral Imaging of the Milky Way

T.L. Landecker (Dominion Radio Astrophysical Observatory, Herzberg Institute of Astrophysics, National Research Council of Canada) and A.R. Taylor (Department of Physics and Astronomy, University of Calgary)

The Synthesis Telescope at the Dominion Radio Astrophysical Observatory (DRAO) is now largely dedicated to the Galactic Plane Survey. This project, carried out by a consortium of 33 scientists from Canada and other countries, is producing detailed images of a large section of the plane of our galaxy in a number of wavebands chosen to reveal the principal constituents of the Interstellar Medium (ISM), the neutral atomic gas, the ionized gas, the dust, and the relativistic plasma. The DRAO Synthesis Telescope is unique in its ability to image the interstellar atomic hydrogen with arcminute resolution, and this is its principal contribution. In addition, images of the continuum emission at 408 and 1420 MHz, the latter including polarimetric data, are made. The area covered will be galactic longitudes 75° to 145° , between latitudes of $-3.5°$ and $+4.5°$.

Other partners are contibuting images of CO molecular emission (FCRAO, Massachusetts), high-resolution reprocessed IRAS infrared data (IPAC, Caltech), continuum radio data at 151 MHz (Cambridge Uinversity), and continuum radio data at 232 and 327 MHz (Beijing Astronomical Observatory). Much of the data will achieve an improvement in angular resolution of an order of magnitude compared to earlier surveys with wide coverage.

The DRAO data are being collected on a mosaic of field centres spaced to give complete coverage at 1420 MHz, where the telescope field of view is $\sim 2°$. Special image processing techniques have been developed to remove the effects of strong sources, particularly Cyg A and Cas A. Data corresponding to the broadest structures is incorporated in the final images from single-antenna measurements.

Techniques developed to improve the quality of the data from the DRAO Telescope will be discussed, and the first scientific results from this survey will be presented.

J46.5

MOSAICING WITH THE BIMA ARRAY

Melvyn Wright, Radio Astronomy Laboratory,
University of California, Berkeley, CA 94720
Tel: 510-642-0420
E-mail: wright@creek2.berkeley.edu

We discuss the mosiacing algorithms in the MIRIAD software and their use at millimeter wavelengths at BIMA in making spectral and polarization images. The importance of complete sampling on image fidelity in forming astrophysically important ratios such as spectral indices and molecular abundance ratios is emphasised. We discuss recent mosaiced images at 3mm wavelength which combine single dish and interferometer data from different observatories. The dynamic range and image fidelity of mosaiced observations may be limited by pointing errors, sampling and calibration rather than by thermal noise. A mosaiced image of CO in IC342 combined observations from 3 observatories to obtain the CO isotopic ratio. These images used a model fitting technique to find a consistent calibration. Observations of Cas A combined single dish and interferometer observations at 19 pointing centers in a Maximum Entropy deconvolution. The flux density in this image is determined almost completely by the single dish data. Polarization observations of Cygnus A required time multiplex of both pointing centers and polarization. The calibration, sensitivity and errors for these images are discussed.

For larger sources faster observations are required to provide adequate sampling of pointing centers and visibility data with reasonable observing efficiency. Faster sampling leads to high data rates.

Aperture Synthesis with Imperfect and Time-Varying Antennas

A.G. Willis

Dominion Radio Astrophysical Observatory, P.O. Box 248, Penticton, BC, Canada V2A 6K3, Email: twillis@drao.nrc.ca

Abstract. The designers of most successful aperture synthesis arrays, such as the VLA and WSRT, have been careful to specify that all the dishes in the array are the same in terms of size, surface accuracy etc. This requirement ensures that each dish has a similar field of view, a feature that is particularly desirable if one is going to do wide-field mapping, and that at a particular wavelength each dish performs like all the other dishes.

Unfortunately the Synthesis Telescope at the Dominion Radio Astrophysical Observatory fails to meet this requirement. The reason for this is quite simple; the telescope was built on a shoe-string budget over a twenty-year period. Consequently, some of the components are rather dissimilar. In particular, two of the seven dishes in the array have a diameter, 9m, that is different from that of the remaining dishes, 8 m. Correspondingly, these two dishes have a field of view that is slightly different to those of the remaining antennas. The antennas are also used for observations at wavelengths as short as 21cm. Consequently the dishes should have an rms surface accuracy of about a cm or better. However, there is some evidence (A. Gray - these proceedings) that some of the dishes have irregularities of this order or worse.

We believe that these telescope characteristics are responsible for some of the aberrations seen in SST wide field images. We discuss the modelling procedures that were used to simulate telescope imperfections and compare synthetic images derived from the modelling techniques with images obtained from actual observations. The strategies that have been implemented at DRAO to improve images affected by these imperfections are discussed.

Finally we look ahead to some of the imaging problems that may be anticipated if the Square Kilometer Array Interferometer (SKAI) is built. Potential designs of this array incorporate receiving elements whose shape, and thus field of view, are likely to continually change during the course of an observation. We examine the imaging and computational requirements that will be necessary for such an array.

J46.7

Determination of an hour angle correction of a point radio source by a radio interferometer with connected elements.

Dugin N. A.
Radiophysical Research Institute (NIRFI)
Nizhny Novgorod, Russia.

It is proposed a method to record and process the signals of a radio interferometer with quadrature output when receiving the radiation of a point cosmic radio source near fixed hour angles $t = 0, \pm\pi/2$ or π (Dugin N.A. A method to determine a cosmic source hour angle correction. Patent A SU N 1827032, 13.10.92). As a result a correction to an hour angle (site longitude, source coordinate) is denermined with an error depending on instrument parameters. The desired result can be obtained in a single experiment while it is usually required long-term observations at a large scatter of radio source hour angles (A.R.Thompson, J.M.Moran, G.W.Swenson. Interferometry and Synthesis in Radioastronomy. New York. Wiley-Interscience Publication, 1986).

The experiment procedure consists in a short- term (few minutes) measurement of a radio source signal including moments of culmination $t = 0$, π or $t = \pm\pi/2$ and processing by "interference lobe stopping" method for two or more values of one of interferometer baseline projections which orientation can be arbitrary. The correction is calculated from the relation

$$\Delta t = \frac{\lambda\,(\varphi_2 - \varphi_1)}{2\,\pi \cos\delta\,(N_2 - N_1)}$$

where λ is the operating wavelength, δ is the source declination, $N_{1,2}$ are the given values of East- West baseline projection (at $t=0$ and π), $\varphi_{1,2}$ are the observation period averaged values of measured and calculated phase differences for $N_{1,2}$. A strict symmetry of the record relative moments $t = 0, \pm\pi/2, \pi$ makes the resulting value of phase difference φ independent of the value of one of the baseline projections. The method approbation on interferometers with baseline 417 m at frequency 540 MHz and with baseline 60 m at frequency 152 MHz showed its efficiency even for instruments with moderate parameters: the error of the hour angle correction determination was close to a limiting error attained in observations of six most powerful radio sources.

One of the advantages of this method is the possibility to use non-stearable antennas with large effective areas (for example, RATAN-600) as interferometer elements that makes it possible to improve the accuracy of single measurements and to carry out observations of a great number of sources including those with small declinations.

Formation of phase-coherent signals from interferometer antenna sites using very high intermediate frequency.

Romanychev A.A., * Dugin N.A.
Radiophisical Research Institute, Nizhny Novgorod, Russia.

One of the main problem in design of the aperture synthesis systems is the problem of getting phase-coherent signals from antenna sites which is solved differently according to the parameters of the instruments involved (A.R.Thompson, J.M.Moran, G.W.Swenson. Interferometry and Synthesis in Radioastronomy. New York,Wiley-Interscience Publication,1986). In most cases for interferometers with connected elements and baselines up to severel kilometers operating in cm-dm wavelength band they use systems which form phase-coherent signals of a local oscillator at the antenna sites and transfer the signal to the center at the low intermediate frequency (IF~30--60 MHz) over a separate channel.

In this work it is proposed to incorporate IF channel into procedure of the interferometer antenna sites signal synchronization, the IF value becoming close to the VHF value of the local oscillator. One of possible versions of the scheme is the use of a double frequency transformation with a single local oscillator (ω_{LO}) at the central station (see Figure) and $\omega_{IF1} \sim \omega_{LO} \sim \omega_S$ /2, where ω_S is the interferometer operating frequency. The second intermediate frequency $\Omega_{IF2}=\omega_{LO}-\omega_{IF1}$.; in principle, it can be reduced to zero that completely eliminates signal phase fluctuations independent of transmitting channel lengths. If $L_1=L_2$, $L_3=L_4$, the attenuation factor of receving signal phase fluctuations is defined by the ratio ω_{LO} / Ω_{IF2}. A similar scheme with one antenna transmitting channel and signal frequency separation has been tested in laboratory conditions at ω_S=1140 MHz, ω_{LO}= 600 MHz, ω_{IF1}= 540 MHz, Ω_{IF2}= 60 MHz , phase changes of the channel being suppressed by approximately 10 times. Due to strict requirements to the quality of directional filters the scheme with one channel is most effective at frequences < 1,5 GHz.

The advantages of the scheme proposed are: 1) the decrease of ω_{LO} by 2 times as compared with the traditional approach and, therefore, the reduction in requirements to the attenuation of transmitting channels; 2) the reduction in a number of transmitting channels up to one; 3) the absence of antenna local oscillators, synchronized by reference generators.

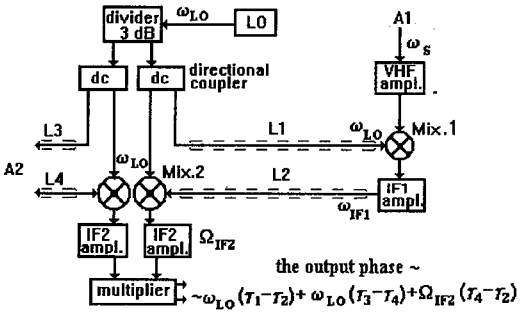

J46.9

The Hamaker-Bregman-Sault Measurement Equation for Synthesis Radio Telescopes, as used in AIPS++ Processing

T.J. Cornwell*
National Radio Astronomy Observatory
Socorro, NM, USA

M.H. Wieringa
Australia Telescope National Facility
Narrabri, NSW, Australia

Abstract

The Hamaker-Bregman-Sault Measurement Equation is a new formulation of the radio interferometry that describes the behavior of a telescope in measuring polarized radiation. It also allows description of a wide range of instrumental effects. Thus the HBS measurement equation unifies the description of many different types of radio interferometric array. This means that processing of data from different arrays can also be unified with considerable practical advantages ranging from simplicity of software development to the advent of entirely new algorithms. The HBS equation is the basis of synthesis processing in a new object-oriented software package, AIPS++, being developed by a consortium of radio observatories. We will describe our experience implementing the HBS equation in AIPS++, and show some of the results obtained using it.

URSI J **Session 108** **Salon Matapedia**

Radio Telescopes for the 21st Century
Co-chairs: P. Dewdney, Canada and C.D. Wilson, Canada

13:10 108.1 A Large Adaptive Antenna for Radio Astronomy, **B. VEIDT**, P. DEWDNEY, *Herzberg Institute of Astrophysics/NRC, Penticton, BC, Canada*

13:30 108.2 The Very Large Array Upgrade Project, **R.A. PERLEY**, *National Radio Astronomy Observatory, Socorro, NM, USA*

13:50 108.3 The Arecibo Upgrade: Measured Performance with the New Gregorian Feed System, L.A. BAKER, D.B. CAMPBELL, **M.M. DAVIS**, P.F. GOLDSMITH, *Cornell University, Ithaca, NY, USA*

14:10 108.4 Prospects for Ground-Based Solar Radar Observations in the International Solar-Terrestrial Program Era, **B. ISHAM**, *Arecibo Observatory, Arecibo, Puerto Rico*

14:30 108.5 Ionospheric Corrections in Radio Astronomy Using GPS Data, **W.C. ERICKSON**[1], R.A. PERLEY[2], C. FLATTERS[2], N.E. KASSIM[3], J.A. PAYNE[4], [1]*University of Maryland, College Park, MD,* [2]*National Radio Astronomy Observatory, Socorro, NM,* [3]*Naval Research Laboratory, Washington, DC and* [4]*Los Alamos National Laboratory, Los Alamos, NM, USA*

14:50 108.6 Water Vapor Measurements Using the 183 GHz Line, **C.D. WILSON**[1], M. WIEDNER[2], R.E. HILLS[2], O. LAY[3], J. CARLSTROM[4], [1]*McMaster University, Hamilton, ON, Canada;* [2]*Cambridge University, Cambridge, UK;* [3]*NASA, Ames and* [4]*University of Chicago, IL, USA*

15:10 Coffee Break

J108.1

A Large Adaptive Antenna for Radio Astronomy

Bruce Veidt and Peter Dewdney
Dominion Radio Astrophysical Observatory
Herzberg Institute of Astrophysics
National Research Council
Penticton, BC

Astronomers in Canada and internationally have have expressed a need for a new decime tre and centimetre wavelength radio telescope with a sensitivity about two orders of mag nitude better than that of the Very Large Array (VLA). This telescope will be a tool fo observing the early universe and should be capable of detecting highly red-shifted spectra lines of atomic hydrogen (HI), hydroxyl (OH), and carbon monoxide (CO). To achieve thi will require a collecting area of one square kilometre, a tuning range from 200 MHz t 20 GHz, and be arranged as an aperture synthesis array with the longest baselines on th order of several hundred kilometres. Thus it is called the Square Kilometre Array (SKA).

The great challenge of this project is to do it at a reasonable cost. A total cost of severa hundred million dollars (US) has been set as a target, and this eliminates conventiona designs such as the VLA or even the Green Bank Telescope. Designs under study elsewher include a huge phased array which samples the electromagnetic field across the aperture an forms a beam electronically, and an array consisting of a large number of spherical reflector with special feed antennas which permit efficient operation at large angles off axis.

This paper will describe work in Canada on a novel reflector antenna concept that uses reflecting surface mounted on linear actuators and placed near to the ground, greatly reducin the cost of a backup structure. The greatest challenge for this design is the elevated receive package, which will be the main emphasis of this paper.

The Very Large Array Upgrade Project

R.A. Perley
National Radio Astronomy Observatory

The VLA was formally dedicated in October, 1980, and has remained since that time the world's premier radio astronomical facility. However, the VLA was designed and built with the technology of the 1970s, and major improvements in its sensitivity, frequency coverage, and resolution can now be realized at relatively small cost by implementation of modern technologies. The National Radio Astronomy Observatory (NRAO) has formally organized the VLA Upgrade Project, with the immediate goal of producing, by mid-1997, a design study of upgrading the VLA to a state-of-the-art instrument.

The purpose of the design study is to put the observatory in a good position to compete for any special funding opportunities that may arise, and to have a well-defined project to present to the next decadal review committee. The design study will examine in detail a wide range of suggested improvements to the VLA's capability, including (but not limited to):

1. Retrofitting existing receivers with improved low-noise devices, while increasing the instantaneous bandwidth available for correlation to at least 2 GHz.
2. Adding new frequency bands, centered near 2.7 and 33 GHz. All new and retrofitted horn/polarizers will have a bandwidth ratio of 1.5:1 or greater.
3. Extending the 21-cm band to below 1200 MHz with maximum sensitivity.
4. Replacing the current low-frequency system with a wide-band prime focus system capable of continuous frequency coverage from approximately 250 MHz through 1000 MHz.
5. Replacing the current LO/IF waveguide transmission system with a fiber-optic system, capable of at least 2 GHz bandwidth.
6. A new correlator, providing up to 8192 spectral channels from at least 33 antennas.
7. A super-compact **'E'** configuration, giving improved low surface brightness imaging capability, with special emphasis on mosaicing.
8. Addition of at least four new, fixed antennas. These, and at least two nearby VLBA stations will be connected by fiber to the new correlator.

Implementation of these improvements would give astronomers a radio telescope capable of high fidelity imaging over a resolution range of 2500, with nearly continuous frequency coverage between 250 MHz to 50 GHz, to a sensitivity (between 2 and 30 GHz) of better than 3μJy in 12 hours. The new correlator will provide unprecedented spectral resolution and flexibility. The new antennas, plus the inner VLBA stations, would define a new, high resolution **'A+'** configuration with 8 times the current maximum resolution. When the VLA is in its contracted configurations, the new antennas would be part of the VLBA, vastly increasing its imaging capability, and eliminating the 'VLA-VLBA' resolution gap.

A summary of anticipated research is given in 'The VLA Development Plan', available on the WWW at URL http://info.aoc.nrao.edu/vla/upgrade/jan1995.html

J108.3

The Arecibo Upgrade: Measured Performance with the New Gregorian Feed System

L. A. Baker, D. B. Campbell, M. M. Davis, and P. F. Goldsmith
National Astronomy and Ionosphere Center,
Cornell University, Ithaca, NY 14853-6801
Phone: 1-607-255-3735, Fax: 1-607-255-8803, e-mail:campbell@astrosun.tn.cornell.edu

The Arecibo 305-m telescope upgrading will be completed in the first half of 1997. The sensitivity and frequency coverage will be greatly increased (P-S. Kildal, L.A. Baker and T. Hagfors, Proc. IEEE, 82(5), 714, 1994). These improvements result primarily from the replacement of the line feeds used to correct the spherical aberration with a dual reflector Gregorian feed system. The secondary and tertiary subreflectors bring the incident plane wave to a point focus. The 213 m by 237 m illuminated area on the primary reflector is offset downhill to prevent spillover for zenith angles up to 15 degrees. A recently installed 16 m high ground screen around the perimeter of the primary reflector shields against ground radiation up to approximately 18 degrees. At the maximum tracking zenith angle of 20 degrees the gain loss from spillover is about 1 dB, and the system noise will increase about 3K.

The table below gives the expected performance of the new system. Performance will be optimum near 1 GHz. Below this frequency diffraction effects degrade the performance, while at higher frequencies the primary reflector limits performance because of the current 2.3 mm r.m.s. error of its surface. The primary reflector panels will be reset in the future to allow improved operation at higher frequencies.

Expected Performance

	Frequency [MHz]	ZA≤15 [K/Jy]	ZA = 20 [K/Jy]
Effective Aperture	300	9	7
	430	10	8
	1,400	11	9
	2,380	11	9
	5,000	8	6
	8,000	5	4
Sidelobe Level	250	-12.2 dB	
	500	-13.5 dB	
	1,000	-15.2 dB	
	5,000	-16.0 dB	
Cross Polarization	< -28 dB		

Prospects for Ground-Based Solar Radar Observations in the International Solar-Terrestrial Program Era

B. Isham
Arecibo Observatory, P.O. Box 995, Arecibo PR 00613, Puerto Rico (USA)
phone +1-809-878-2612, fax +1-809-878-1861, e-mail isham@naic.edu

It has been more than thirty years since solar radar was first shown to be a viable and interesting technique for the study of the sun (J. C. James, *Astrophys. J.*, **146**, 356-366, 1966). Solar radar frequencies lie in the 10 to 100 MHz range, and scatter from the coronal plasma occurs at or near the corresponding plasma resonance level, generally between one and five solar radii from the center of the sun. Because of this, solar radar is an ideal technique for the study of coronal structure and dynamics, including wave activity and turbulance. What is new today is the opportunity to participate in multi-instrument solar observing campaigns in which the collective database provides enhanced possibilities for understanding the observations. We review past observations and their theoretical interpretations, survey past and potential solar radar systems, discuss the advantages of renewed solar radar observations, and identify the facilities most favorable for performing such observations.

J108.5

IONOSPHERIC CORRECTIONS IN RADIO ASTRONOMY USING GPS DATA

W.C. Erickson
Astronomy Department
University of Maryland
College Park, MD 20742

R.A. Perley and C. Flatters
National Radio Astronomy Observatory
Socorro, NM 87801

N.E. Kassim
Remote Sensing Division (Code 7213)
Naval Research Laboratory
Washington, DC 20375-5351

J.A. Payne
Los Alamos National Laboratory
Los Alamos, NM 87545

We have conducted an experiment to evaluate the usefulness of GPS ionospheric data for making Faraday rotation and interferometer phase corrections to VLA data. Four GPS receivers were first installed at the VLA site in the summer of 1995, one at the array center and one at the end of each arm. Data from the center receiver, which has since remained at the VLA site, have been used to estimate ionospheric Faraday rotation.

An ionospheric model was developed and fitted to the GPS Total Electron Content (TEC) data and allows us to predict the TEC in any direction to an accuracy of a few percent. This simple model is parameterized only by TEC overhead magnitude, gradient, and gradient azimuth. Such a model is required since the GPS data pertain only to the directions of the visible GPS satellites. Ionospheric Faraday rotation during observations of the ~80% linearly polarized radio pulsar PSR 1932+109 in October of 1996 were estimated and compared with the predictions from these data. While ionospheric conditions were unfortunately calm during the pulsar observations, the predicted Faraday rotation of the source appeared to track the observed values quite well. The model was also used to estimate the interferometer phase variations caused by large scale (1000 km) ionospheric structures. We measured these refractive effects by observations of radio point sources in the summer of 1995, and the model predictions followed the slow variations reasonably well, reducing the rms scatter by 20-50%.

Data from all four receivers were used to estimate the phase gradients along each arm of the VLA caused by smaller scale (100 km) ionospheric structures. This prediction is accurate, but only when the direction of observation is within a few degrees of one of the satellites.

Water Vapor Measurements using the 183 GHz line

C. D. Wilson, McMaster University
M. Wiedner, R. E. Hills, Cambridge University
O. Lay, NASA Ames
J. Carlstrom, University of Chicago

Correcting for phase fluctuations produced by the atmosphere will be critical in order for the planned millimeter and submillimeter arrays to achieve sub-arcsecond resolution. Although several different techniques are currently under investigation, the JCMT-CSO single baseline interferometer are currently the only possible test site at frequencies above 300 GHz. We have built two 183 GHz radiometers which will be used to measure the difference in the water vapor content of the atmosphere above the two telescopes and thus correct the phase. The goal is to obtain the path difference to better than 30 microns on timescales of 1 second.

The major advantage of using the 183 GHz line is that the emission is relatively strong: at an offset of 1.2 GHz from the line center, we expect to see about 15 K of emission for each millimeter of additional path. For comparison, the equivalent numbers are about 2 K per mm at 225 GHz and 0.4 K at 22 GHz. The disadvantage is that the center of the line becomes optically thick at relatively low values of total water vapor. It is for this reason that we use three IF channels offset by 1.2, 4.2, and 7.8 GHz from the line center. The highest frequency channel serves mainly to monitor the emission from clouds. We record both the absolute sky brightness in these channels and the short term fluctuations. Preliminary results from observing runs in November 1996 and spring 1997 will be presented.

URSI J **Session 109** **Salon Matapedia**

Natural and Man-Made Disturbances and Effects on Radio Telescopes
Co-chairs: T. Gergely, USA and M.M. McKinnon, USA

15:30 109.1 Radio Astronomy and the 1997 World Radiocommunication Conference (WRC-97), **T.E. GERGELY**, *National Science Foundation, Arlington, VA, USA*

15:50 109.2 Coordination of Arecibo Observatory and Iridium, **M.M. DAVIS**, *National Astronomy and Ionosphere Center, Arecibo, Puerto Rico*

16:10 109.3 Test Observations of the Iridium Satellites with the NRAO 140-Foot Telescope, **M.M. McKINNON**, *National Radio Astronomy Observatory, Green Bank, WV, USA*

16:30 109.4 Commercial Developments in the Millimeter Wave Band and Their Impact on Radio Astronomy, **A.W. CLEGG**, *Millimeter Wave Report, Arlington, VA, USA*

17:10 109.5 The Effect of a Proposed 94.5 GHz Space Based, Cloud-Profiling Radar on Millimeter-Wave Radio Astronomy, **A.R. THOMPSON**[1], J.E.B. PONSONBY[2], [1]*National Radio Astronomy, Charlottesville, VA, USA;* [2]*Nuffield Radio Astronomy Laboratories, Macclesfield, UK*

J109.1

Radio Astronomy and the 1997 World Radiocommunication Conference (WRC-97)

Tomas E. Gergely
Division of Astronomical Sciences
National Science Foundation
Arlington, VA
22230
USA

In 1992, the International Telecommunication Union decided to hold WRCs on a regular, two year basis. While WRCs require extensive preparations and are costly, it was thought that a two year schedule would accelerate the introduction of new technologies. WRC-95 was the first WRC held under this schedule, and preparations are now in full swing for the next one, to be held in October-November, 1997.

Some items of interest to radio astronomers WRC-97 is expected to deal with are the following: 1. Increasing the amount of spectrum allocated to mobile satellites operating at frequencies below or near 1 GHz. 2. Allocating the spectrum in the 50 to 64 GHz range, approximately, to the passive services, to allow remote sensing in the oxygen absorption bands. 3. Allocations to facilitate the introduction of new services in the mm-wave range. 4. Adopting new limits for spurious emissions. I discuss the status of known US and foreign proposals, and their possible impact on radio astronomy.

Each WRC also elaborates Agendas for the forthcoming ones, and astronomers need to think about what issues may need to be dealt with. For example, as commercial exploitation of the millimeter wave spectral range intensifies, alternative and additional allocations to the currently allocated bands to radio astronomy could be identified.

Coordination of Arecibo Observatory and Iridium

Michael M. Davis, National Astronomy and Ionosphere Center,
Post Office Box 995, Arecibo, PR 00613
mdavis@naic.edu

The US Federal Communications Commission has issued the following directives for coordination of the Mobile Satellite Service with the Radio Astronomy Service:

47 CFR 25.213 (a) (2) :

> "Mobile-Satellite Service space stations transmitting in the 1613.8 - 1626.5 MHz band shall take whatever steps necessary to avoid causing harmful interference to [the Arecibo Observatory, among others] during periods of observation."

47 CFR 25.213 (a) (4):

> "The Radio Astronomy Service shall avoid scheduling radio astronomy observations during peak MSS/RDSS traffic periods to the greatest extent practicable."

Discussion is ongoing between Cornell University, which operates Arecibo Observatory under a Cooperative Agreement with the National Science Foundation, and Motorola, which holds the FCC license for Iridium. One aspect of these discussions has to do with the approach to scheduling the telescope to avoid peak traffic periods in so far as practicable.

Data for 249 observing sessions in 1988 which used the OH line feed have been used to identify possibly viable scheduling methods. These sessions occupied 15% of the time in 1988, and are typically 4 to 5 hours in length. They are heavily concentrated to those sidereal times when the Galaxy is overhead at Arecibo.

Various procedures have been followed to reorganize the observing into periods of expected minimum MSS use. Scheduling in the early morning hours alone is not adequate, as it cannot provide enough Galactic observing time. Adding one or two weekend days provides much more flexibility. One approach under consideration would have the MSS operators provide the profile of maximum to minimum use as a ranking of each of the 168 hours of the week. This profile would serve to permit the OH observations at 1612 MHz to be scheduled from minimum to maximum MSS traffic, in so far as practicable. The profile could be updated as necessary, and provides more flexibility than a fixed scheduling mask.

J109.3

TEST OBSERVATIONS OF THE IRIDIUM SATELLITES WITH THE NRAO 140-FOOT TELESCOPE

Mark M. McKinnon
National Radio Astronomy Observatory
Green Bank, WV 24944

Test observations of the Iridium satellites will be made with the NRAO 140-foot telescope in early 1997. The objective of the test is to insure that the spectral power flux density of the satellite's spurious emissions in the 1610.6 - 1613.8 MHz radio astronomy band does not exceed harmful levels of interference. Since radio telescopes are not designed to observe the strong signals from satellites in low-Earth orbit, the test observations require unconventional observing techniques in addition to modifications of the telescope receiver. Observations of a satellite will be made at a fixed telescope position because the angular rate of satellite motion is generally larger than the tracking rate of the telescope. The RF signal path will bypass the low noise amplifiers of the telescope's L-band receiver to avoid amplifier saturation. There is no need to cryogenically cool the receiver because the modified system will have sufficient sensitivity for the observation. One particularly stringent requirement upon the observing technique and subsequent data analysis is the removal of spurious emissions from other sources of interference such as the Glonass satellites. The unwanted signals can be removed by synchronizing data collection with the temporal modulation of the Iridium downlink signal. The synchronous detection scheme will work provided that the strength of the unwanted signal is constant over the timescale of the downlink modulation. I will discuss these preparations of the 140-foot telescope for the tests and, perhaps, some preliminary results of the tests.

Commercial Developments in the Millimeter Wave Band and Their Impact on Radio Astronomy

Andrew W. Clegg
Millimeter Wave Report
PO Box 4749, Arlington VA 22204-0749
mmwr@msn.com

Increased commercial use of the millimeter wave radio band is occurring as lower frequency bands become congested and the demand for large bandwidth wireless transmission capacity increases. The increased demand is due in part to: (1) the advent of Personal Communications Services, which use the mmW band for cell-site interconnect; (2) the growing popularity of the internet; and (3) substantial changes in U.S. telecommunication laws.

A number of emerging commercial uses of the mmW band, and their impact on the radio astronomy service, will be reviewed. These uses include:

- Canadian Local Multipoint Communications Services (LMCS) and U.S. Local Multipoint Distribution Services (LMDS)
- The first commercial mmW satellite system, recently proposed by Motorola.
- The "Stratospheric Telecommunications Service."
- Collision avoidance radars for motor vehicles.
- Wideband, fixed point-to-point links for PCS backhaul and interconnect.
- Feeder links for the Mobile Satellite Service.
- New mmW allocations for Part 15 (unlicensed) devices.
- Passive imaging systems for navigation in inclement weather.

In the first half of 1997, the U.S. FCC is also scheduled to complete its proceedings on wireless communications above 40 GHz. The Commission's proposal calls for the creation of the Licensed Millimeter Wave Service (LMWS) and the subsequent allocation of several LMWS frequency bands above 40 GHz. LMWS is a catch-all service which will incorporate virtually all new licensed radio technologies in the mmW band. The possible impact of LMWS on radio astronomy will be discussed.

J109.5

The Effect of a Proposed 94.5 GHz Space Based, Cloud-Profiling Radar on Millimeter-Wave Radio Astronomy

A. R. Thompson*, National Radio Astronomy Observatory,
520 Edgemont Rd., Charlottesville, VA, 22903 USA
and
J. E. B. Ponsonby, Nuffield Radio Astronomy Laboratories,
Jodrell Bank, Macclesfield, Cheshire, SK11 9DL, England

An allocation for a downward-looking, satellite-borne radar at a frequency of approximately 94.5 GHz is being sought for studies of the albedo and radiation balance of the Earth, as determined by clouds. Radio astronomers are interested in possible effects on radio telescopes operating in nearby bands, in particular the bands 86-92 GHz, 97.88-98.08 GHz, and 105-116 GHz. Radio astronomy receivers in these bands commonly use SIS (superconductor-insulator-superconductor) mixers cooled to 4K as the input stages, and to avoid noise resulting from lossy elements there is usually no filtering to restrict the input bandwidth.

The satellite would operate in a polar orbit of nominal height 450 km and period approximately 95 min. The radar beam would point towards the nadir and the width of the beam footprint at the ground would be approximately 1 km. Three levels of interaction between the radar and the radio telescope must be considered: coupling between the main beams of both systems, coupling between the main beam of one system and the sidelobes of the other, and coupling between the sidelobes of both systems. If coupling involving a main beams occurs, it persists for a few tenths of a second only, because of the high directivity of the beams and the speed of the satellite. However, the power level of the radar required to measure Rayleigh scattering from cloud particles would, with coupling between both main beams, produce a peak level of approximately 0.7 W at the radio astronomy receiver, and damage to an SIS mixer would result. The probability of occurrence of such coupling is low and there are several practical ways to guard against it. Coupling between a main beam and sidelobes could cause overloading of the receiver and loss of data for a period of about one second during a satellite pass. In the case of coupling between sidelobes at the 0 dBi level, there would be no overloading and interference would occur only if the radio astronomy receiver were tuned to cover the frequency of the radar transmission. With some care in the design and operation of both systems, it should be possible for the two scientific activities to work simultaneously.

URSI J **Session 126** **Salon Chaudière**

Millimeter/Sub-Millimeter Radio Telescopes and Instrumentation
Co-chairs: R. Blundell, USA and S. Weinreb, USA

08:10	126.1	The Submillimeter Wavelength Array, **J.M. MORAN**, *Harvard-Smithsonian Center for Astrophysics, Cambridge, MA, USA*
08:30	126.2	The Millimeter Array, **P.J. NAPIER**, *National Radio Astronomy Observatory, Socorro, NM, USA*
08:50	126.3	Submillimeter-Wave Telescopes on the Antarctic Plateau, **A.A. STARK**, *Smithsonian Astrophysical Observatory, Cambridge, MA, USA*
09:10	126.4	Antarctic Submillimeter Telescope and Remote Observatory, **T.M. BANIA**, *Boston University, Boston, MA, USA*
09:30	126.5	Pointing and Optics Alignment Requirements and Solutions for the Large Millimeter Telescope, **C. READ PREDMORE**, *University of Massachusetts, Amherst, MA, USA*
09:50	126.6	Description and Performance of a Heterodyne SIS Receiver at 425/441 GHz for the PIROG Balloon-Borne Experiment, **P. FEBVRE**[1], S. GEORGE[1], A. DESCHAMPS[1], B. LECOMTE[1], G. OLOFSSON[2], [1]*DEMIRM - Observatoire de Paris, France;* [2]*Stockholm Observatory, Saltsjöbaden, Sweden*
10:10		Coffee Break
10:30	126.7	VHF Pilot-Signal Stabilized Monolithic Integrated Circuit Millimeter-Wave Radiometers, **S. WEINREB**, *University of Massachusetts, Amherst, MA, USA*
10:50	126.8	A Cryogenic Focal Plane Array for 85-115 GHz Using MMIC Preamplifiers, **N.R. ERICKSON**, R.M. GROSSLEIN, R.B. ERICKSON, S. WEINREB, *University of Massachusetts, Amherst, MA, USA*
11:10	126.9	Characteristics of Broad-Band InP Millimeter-Wave Amplifiers for Radiometry, **E.J. WOLLACK**, M.W. POSPIESZALSKI, *National Radio Astronomy Observatory, Charlottesville, VA, USA*
11:30	126.10	Fixed Tuned SIS Receiver Development for the Sub-Millimeter Array, **C.-Y.E. TONG**, R. BLUNDELL, D. COSMO PAPA, *Harvard-Smithsonian Center for Astrophysics, Cambridge, MA, USA*

J126.1

THE SUBMILLIMETER WAVELENGTH ARRAY

James M. Moran
Harvard-Smithsonian Center for Astrophysics
60 Garden St.
Cambridge, MA 02138

The Submillimeter Wavelength Array (SMA) is under construction and is expected to begin operations in 1998 on Mauna Kea, near the CSO and JCMT facilities. The array will consist initially of six 6-meter diameter antennas arranged on the sides of Reuleaux triangles. Four configurations will be available with diameters of approximately 24, 64, 171 and 470 m. Each antenna will be equipped with a cryostat at its Nasymth focus and will accept eight receivers covering all usable bands from 230 to 850 GHz. The maximum angular resolution will vary from 0.1" to 0.4" over the frequency range. Signal processing will be performed on a special purpose XF correlator, which is based on a chip developed at the Haystack Observatory and the NASA/SERC for VLSI Design. The correlator will accept two channels (for either dual polarization or dual frequency operation) from each antenna of 2 GHz bandwidth each. The subchannel bandwidth is 104 MHz. Spectral resolutions as fine as 0.6 km/s will be available with full processing capacity.

The Smithsonian Astrophysical Observatory is the general contractor for the project. The mechanical assembly of the first antenna was completed in August, 1996. The antennas have reflector backup structures constructed of carbon fiber tubes and steel nodes. Each primary reflector consists of 72 machined aluminum panels, which have rms accuracies of about 5 microns. The overall reflector surface is expected to have an rms accuracy of 12 microns. Holographic measurements are being conducted at 90 GHz with a tower-mounted transmitter. In the laboratory, receiver temperatures of 24, 30 and 65 K(DSB) have been achieved at 230, 346 and 460 GHz, respectively, for SIS mixer receivers with junctions fabricated at JPL. Initial interferometric tests on celestial sources are planned for 1997 at the assembly site at Haystack Observatory in Westford, MA.

An agreement for collaboration has been reached between SAO and the Institute of Astronomy and Astrophysics of the Academy of Science (Taiwan). ASIAA will initially provide two additional antennas to the array. Preparations are also being made to include the 15-m JCMT and 10-m CSO telescope in the array on a part time basis.

THE MILLIMETER ARRAY

Peter J. Napier, NRAO, Socorro, NM
Phone: 505 8357000, email: pnapier@nrao.edu

The Millimeter Array (MMA) is a synthesis array proposed to the US National Science Foundation as the next major NRAO initiative in millimeter and submillimeter ground-based astronomy. The MMA consists of forty 8 m diameter antennas designed and equipped to operate throughout the millimeter/submillimeter atmospheric windows that are accessible from a high altitude site. The antennas will be transportable into a number of array configurations having maximum baselines varying in length from 80 m to 3 km.

The MMA is being designed as a highly flexible instrument with capabilities for high quality observations in astronomical fields as varied as cosmology, primordial galaxies, galactic structure, astrochemistry, the sun and stars, star formation and molecular clouds, evolved stars and circumstellar shells, and planetary science. It is expected that observations will be possible in bands with center frequencies of 40, 85, 110, 160, 235, 340, 475 and 665 Ghz. To allow observations at the shortest wavelengths a high altitude site is required in order to reduce the amount of signal attenuation and noise emission caused by atmospheric water vapor. Sites at 3800 m altitude on Mauna Kea in Hawaii and at 5000 m altitude in the Andes Mountains in Northern Chile are being studied. The Chilean site offers significant advantages in atmospheric opacity and in the amount of space available for large arrays, but a final site selection has not yet been made. Medical and physiological effects must be considered for sites at this altitude, but a study of the problems shows that there is a feasible operating scenario.

The antennas and wide bandwidth signal processing systems represent significant technical challenges. The principal antenna requirements include low antenna noise, a surface accuracy of 25 μm rms, a pointing accuracy of 1 arcsec. rms and an ability to switch rapidly, in 1 second of time, between sources separated by 2 degrees in the sky. This latter capability is needed to allow frequent observations of phase calibration sources. The signal transmission system and correlator are currently required to provide 16 GHz of continuum bandwidth for each antenna.

The MMA technical design is being carried out as a partnership between the NRAO, OVRO and BIMA called the MMA Development Consortium (MDC). It is anticipated that the MMA will have substantial involvement from international partners and the MDC will expand to accommodate that growth of the project. Full information about the MMA can be found on the WWW at http://www.tuc.nrao.edu/mma/mma.html. This talk will provide a progress report on the current state of the MMA Project.

J126.3

Submillimeter-wave Telescopes on the Antarctic Plateau

Antony A. Stark
Smithsonian Astrophysical Observatory
60 Garden Street, Cambridge, Massachusetts 02138
aas@cfa.harvard.edu

The Antarctic Submillimeter Telescope and Remote Observatory (AST/RO) has been operational at the South Pole since January 1995. Preliminary results include site testing and observations of atomic carbon in PDR regions, high-latitude translucent clouds, the galactic center and the Magellanic Clouds. A off-axis 10-meter telescope will be proposed to the Office of Polar Programs as a user-facility instrument for wavelengths between 200 microns and 6 millimeters. Given the climatic conditions at Pole, this instrument will have a data acquisition rate approximately two orders of magnitude faster than comparable instruments at Mauna Kea. Prospects for the observation of protogalaxies and arcminute-scale CMBR anisotropies will be discussed.

Antarctic Submillimeter Telescope and Remote Observatory

T. M. Bania, Department of Astronomy, Boston University, USA

The cold, clear, dry atmosphere above the South Pole makes it a superb site for making ground based astronomical measurements at submillimeter wavelengths. AST/RO, a 1.7 m diameter telescope for research in astronomy and aeronomy at wavelengths between 200 and 2,000 μm, was installed at the South Pole during the 1994-95 austral summer. The immediate scientific goals of this instrument are heterodyne spectroscopy of atomic and molecular lines in the interstellar medium and the earth's stratosphere at wavelengths near 600 μm; however, AST/RO is a general-purpose telescope for the millimeter, submillimeter, and far-infrared. AST/RO has four heterodyne receivers mounted on an optical table suspended from the telescope structure in a warm Coudé room: (1) *230 GHz SIS receiver*; (2) *460-500 GHz Schottky-barrier diode receiver* (This receiver will work without a liquid helium supply.); (3) *492 GHz SIS waveguide receiver*; and (4) *492 GHz SIS quasi-optical receiver.* The spectrometers are two 1.1-GHz bandwidth AOSs, each with 2048 channels, and one 63-MHz bandwidth 2048 channel high-resolution AOS. The entire system is highly automated to reduce to a minimum the need for human intervention; we have successfully operated AST/RO from Boston over the Internet. Nonetheless an astronomer will always be wintering over with AST/RO in order to provide the support needed to conduct successful observations.

Since installation AST/RO has been in continuous operation, exploiting the consistently clear submillimeter sky above the Antarctic Plateau. Direct measurements show that at 492 GHz the zenith opacity remains below unity for most of the winter. AST/RO is being used to study the physical properties of the atomic and molecular interstellar medium in the Milky Way and in the Large and Small Clouds of Magellan. At present our focus is on determining the properties of the neutral atomic carbon gas using its spectral line at 609 μm wavelength ([C I] $^3P_1 - {}^3P_0$) as our observational probe of photodissociation regions (PDRs). The sensitivity of AST/RO's spectrometers, its $\sim 100''$ beamsize, and the sky conditions at South Pole together allow us to conduct extremely sensitive surveys of large areas of sky. To assess the influence on PDR structure and composition of UV fields, metallicity, and dust opacity, we have focussed initially on (1) specific astrophysical laboratories in order to isolate particular physical conditions, and (2) objects with substantial amounts of information about the other important PDR tracers, namely C^+ and CO.

J126.5

Pointing and Optics Alignment Requirements and Solutions for the Large Millimeter Telescope

C. Read Predmore
Five College Radio Astronomy Observatory
University of Massachusetts
Amherst, Massachusetts 01003

The Large Millimeter Telescope (LMT) is a joint project between the University of Massachusetts and the Instituto Nacional de Astrofisica, Optica y Electronica (INAOE) near Puebla, Mexico. The 50 meter diameter telescope will primarily operate at 230 GHz or a wavelength of 1300 microns. The required surface accuracy is $\lambda/20$ or 65 microns.

The primary surface consists of 126 hexagonal segments. Each segment is 5 m across and is actively controlled to maintain the desired parabolic surface as a function of elevation and under differing thermal effects. This is similar to the active surface control system for the Keck 10 m diameter optical telescope. A set of four laser absolute distance measurement systems on the subreflector support legs near the primary focus can be used to measure the overall figure of the primary and the position of the secondary with respect to the primary.

Another stringent requirement for the LMT is pointing to $1/10^{th}$ of the 6 arcsecond beamwidth at 230 Ghz. Some of the terms in the elevation error pointing budget are:

Pointing model errors:	0.15 arcsec
Error in calculation of static refraction:	0.15 arcsec
Primary pointing error:	0.40 arcsec
Error in lateral position of the secondary:	0.15 arcsec
Error in secondary tilt:	0.15 arcsec
Error in feed location:	0.15 arcsec
Total Elevation Pointing Error:	**0.52 arcsec**

The above specifications require that the position of the secondary with respect the primary be known and stable with a tolerance of 10-20 microns. Likewise the feed horn location needs to be stable to ~0.3 mm. The main uncertainty in positioning the primary with respect to the ground will be thermal effects. Most of the thermal effects will be accounted for by measuring the temperature of each structural member of the telescope and using a Finite Element Analysis to predict the thermal distortion of the LMT and the resulting pointing error. In addition, commercial and other laser distance measuring systems are being considered to measure the telescope structure from reference points on the ground.

Description and performance of a heterodyne SIS receiver at 425/441 GHz for the PIROG balloon-borne experiment

P. Febvre[1], S. George[1], A. Deschamps[1], B. Lecomte[1] and G. Olofsson[2]

[1] DEMIRM - Observatoire de PARIS - 75014 PARIS - France

[2] STOCKHOLM Observatory - S-133 36 Saltsjöbaden, Sweden

Abstract. The balloon-borne experiment PIROG 8 developped under a joint swedish/french collaboration is scheduled to fly from the south of France during spring 1997. It will carry a fully remote-controlled submillimeter heterodyne receiver based on the technology of superconductor-insulator-superconductor (SIS) tunnel junctions. The scientific goal is to try to detect the weak O_2 line at 425 GHz in the interstellar medium, which has never been observed so far. The receiver will operate in a double side-band mode in order to observe simultaneously the ^{13}CO line at 441 GHz to verify the correct operation of the receiver and to do the pointing of the telescope. First, a general overview of the receiver will be given, including a description of the front-end design and some considerations associated to the fact that the receiver will be fully remote-controlled, which is new for a submillimeter SIS receiver. The design of the submillimeter waveguide mixer based on a SIS junction cooled at liquid helium temperature will be presented. The role of the superconducting integrated tuning circuit used to match the SIS junction with its microwave environment will be emphasized. The performance and miscellaneous measurements done on the receiver to prepare the flight campaign will be presented. Best achieved DSB receiver noise temperature is 180 K at 4.2 K physical temperature and 130 K at 1.5 K physical temperature. A breakdown of the contribution of the different receiver components to the noise of the receiver will be presented. A full analysis of the theoretical performance planned for such a receiver will be made and compared with the experimental results. It will be used to diagnos the receiver behaviour and its intrinsic limitations. Some very helpful means to predict the potential improvement of a SIS mixer in the general case will be deduced. On the other hand, some considerations about the presence of the Josephson currents in the SIS junction and their consequences on the stability and sensitivity of the receiver will be presented in the context of an embarked experiment.

J126.7

VHF Pilot-Signal Stabilized Monolithic Integrated Circuit Millimeter-Wave Radiometers

Sander Weinreb
Department of Physics and Astronomy
University of Massachusetts
Amherst, MA 01003

Gain fluctuations often limit the sensitivity of radiometers used for measurements of broadband continuum radiation. For bandwidths of the order of 10 GHz a gain stability of the order of 10^{-5} is required in a 1 second period. It has been found that the inherent statistical fluctuations in GaAs and InP field-effect transistors (both FET's and HEMT's) are typically larger than this requirement and the radiometer sensitivity will be degraded unless the radiometer is Dicke-switched at a rapid rate between the antenna and a reference termination with noise temperature close to the antenna temperature.

Monolithic integrated circuit (MMIC) low noise amplifiers for frequencies as high as 140 GHz have been developed in the semiconductor research facilities of Lockheed Martin and TRW. These MMIC amplifiers have been cascaded to form very compact tuned-radio frequency (TRF) receivers with no local oscillator. In many cases where the radiometer is mechanically switched at a slow rate or if the radiometer unbalance is to large, the transistor gain fluctuations will limit the sensitivity.

This paper describes MMIC amplifiers which have an additional pilot signal channel which is used to stabilize the gain. The MMIC's are 4-stage GaAs HEMT amplifiers, were fabricated at Martin Marietta Laboratories , and have of the order of 20 dB gain in the frequency range of 85 to 115 GHz. The pilot signal channel is accessible through separate terminal pads on the MMIC and a loss of the order of 0 to 10 dB in the frequency range of 200 to 500 MHz. The important assumption for the gain stabilization is that the gain of the pilot signal is proportional to the product of the transconductances of the four transistors in the MMIC and stabilizing this transconductance product will stabilize the millimeter wave gain. Measurements have been made which show that the transconductance fluctuation is the dominate source of gain fluctuation in millimeter-wave transistors. The pilot signal gain can be very precisely determined by a bridge-technique which provides a gain measurement independent of the pilot signal source power or detector sensitivity.

At the conference the pilot signal MMICs will be described along with the stabilization circuitry now under construction. Test data on the transconductance fluctuations of millimeter-wave transistors and measurements of pilot-signal MMIC's will be presented along with examples of miniature TRF radiometers.

A Cryogenic Focal Plane Array for 85-115 GHz Using MMIC Preamplifiers

Neal R. Erickson,* Ronald M. Grosslein, Ronna B. Erickson and Sander Weinreb
Department of Physics and Astronomy
University of Massachusetts
Amherst, MA 01003

A new focal plane array, designed for radio astronomy use in the 85-115 GHz range, is in the final stages of assembly. This array has 16 pixels, and uses GaAs MMIC preamplifiers operated at a temperature of 20 K. Following the preamp is a subharmonic mixer having an IF band of 5-20 GHz. With this wide IF, the entire signal band may be covered with single sideband response using just two LO's, at 40 and 60 GHz.

The input amplifiers are among the best wideband MMIC low noise devices made to date and were fabricated using GaAs technology at Martin-Marietta Labs. At 20 K their typical noise is 110-140 K from 90-115 GHz, increasing to 200 K at 85 GHz. These chips can deliver a wideband gain (cold) of $\sim$ 25 dB, although the best low noise bias yields 5 dB less. They are housed in a compact block with WR10 waveguide ports. Two MMIC's are used to produce >40 dB gain. A low loss isolator has been developed for use between these two MMIC stages to ensure stability. This isolator is based upon a commercial full band Faraday rotation isolator, but is modified to achieve lower loss, much smaller size, and a partially shielded magnetic field to permit close packing without interactions.

The input feeds are square corrugated horns which pack well in an array, and achieve symmetric low side-lobe patterns. The aperture and most of the horn are at room temperature, while toward the waveguide end there is a 0.2 mm gap in the wall, and the remainder of the horn is at 20 K. The gap is a very effective thermal insulator and the effective aperture for thermal radiation is reduced to just that of the cold part of the horn.

The subharmonic mixer uses a commercial beam-lead antiparallel-pair diode, and has a conversion loss of 10-15 dB across the band with an LO power of only 8 mW. The mixer is integrated with a 5-20 GHz low noise MMIC amplifier. The mixer operates single sideband through the combination of an integrated 80 GHz high pass filter, and the rapid gain roll-off of the preamplifiers above 115 GHz. LO is provided by a pair of 220 mW injection-locked Gunn oscillators, which are split 16 ways using a waveguide splitter.

The array will be expanded to include a second set of 16 elements in the opposite polarization during the next year. The array is still under construction but the initial 16 pixels are expected to be ready for use by April 1997.

J126.9

Characteristics of Broad-Band InP Millimeter-Wave Amplifiers for Radiometry

E.J. Wollack* and M.W. Pospieszalski
NRAO [1] , Charlottesville, VA
October 4, 1996

ABSTRACT

The performance of InP HEMT (High-Electron Mobility Transistor) amplifiers is characterized in a direct detection 3.8 mm receiver over a temperature range of 50 to 300 K. The effects of low frequency noise up-conversion are observed in the total power response. The measured spectrum of gain fluctuations at room temperature is characterized by $\delta g_n^2(f) \simeq (1\,\mathrm{Hz}/f)^\alpha\, \delta g_o^2$, with an index $\alpha \simeq 0.9$ and $\delta g_o^2 \simeq 6 \times 10^{-9}\,\mathrm{Hz}^{-1}$ per device used in the amplification chain. When the devices are cooled to 50 K, δg_o^2 increases by a factor of ~ 5. The measured receiver sensitivity is 3 mK $\mathrm{Hz}^{-1/2}$ at an ambient temperature of 300 K and 0.8 mK $\mathrm{Hz}^{-1/2}$ at 50 K (video frequency $\gg$ 10 KHz, rf bandwidth $\sim$ 20 GHz). The measured sensitivity is the best reported for a HEMT direct detection receiver in the 3 mm atmospheric window. At 50 K the observed receiver sensitivity is competitive with the performance of sub-Kelvin bolometric detectors or SIS junctions used for direct detection. Implications of the observed stability for radio astronomy instrumentation will be discussed.

Subject headings: low noise receivers — millimeter radiometry — gain stability

---

[1]The National Radio Astronomy Observatory is a facility of the National Science Foundation operated under cooperative agreement by Associated Universities, Inc.

FIXED TUNED SIS RECEIVER DEVELOPMENT FOR THE SUB-MILLIMETER ARRAY

J126.10

C.-Y. Edward Tong*, Raymond Blundell and D. Cosmo Papa
Harvard-Smithsonian Center for Astrophysics,
60 Garden St., Cambridge, MA 02138.

Fixed tuned receivers incorporating superconductor-insulator-superconductor (SIS) mixers are being developed at the Smithsonian Astrophysical Observatory for the Sub-Millimeter Array (SMA). The target frequency bands include all the atmospheric windows between 200 and 900 GHz. Since the array will function as a fully automated interferometer, fixed tuned receivers are needed to ensure ease of operation.

Waveguide receivers have been designed to provide an impedance bandwidth of about 35% without any movable mechanical parts. Sub-millimeter radiation is coupled to the SIS junction through an integrated superconducting thin film network that tunes out the capacitance of the junction. At the lower frequency windows (below 400 GHz), this type of receiver has low-noise performance over the entire 35% bandwidth of the waveguide circuitry. Quantum limited receiver noise temperatures (~3hf/k) are achieved.

At higher frequencies, traditional lumped element SIS mixers become more and more difficult to fabricate. Most SIS mixers operating above 400 GHz require small area, high critical current density devices. We have developed a novel distributed mixing approach that employs non-linear superconducting transmission lines. These mixer elements are in fact long and narrow SIS junctions. Local oscillator power and signal are coupled into the non-linear transmission line from one end of the line. Mixing occurs along the line as they propagate down the long junction. The design constraints on the critical current density of the device and that of the integrated tunning network are greatly reduced in this type of distributed mixer. Quantum limited receiver noise performance has been obtained up to about 600 GHz. Further work is being carried out to extend the frequency of operation towards 900 GHz.

URSI K | Session 13 | Salon Chaudière

Hazard Evaluation and Prevention
Co-chairs: O.P. Gandhi, USA and A. Thansandote, Canada

08:10	13.1	A System for Calibration of Microwave Antennae and Radiation Survey Meters, A. THANSANDOTE, S. WASOONTARAJAROEN, **G. GAJDA**, D. LECUYER, *Radiation Protection Bureau, Ottawa, ON, Canada*
08:30	13.2	Radio Frequency Fields from Cellular Transmitter Towers and Roof-Top Antennas, A. THANSANDOTE, **G. GAJDA**, D. LECUYER, *Radiation Protection Bureau, Ottawa, ON, Canada*
08:50	13.3	Microwave Fields as Control of Complex Formation Time in Hemoglobin Binding Site, **M. ZAGO**, A. PALOMBO, G. D'INZEO, *University "La Sapienza", Rome, Italy*
09:10	13.4	Voltage-Gated Membrane Channels under GSM and DECT Exposure: A Global Analysis, **F. APOLLONIO**[1], G. D'INZEO[1], L. TARRICONE[2], [1]*University "La Sapienza", Rome and* [2]*University of Perugia, Italy*
09:30	13.5	Simulation of Radio Frequency Coils for Super High Field Magnetic Resonance Imaging, **T.S. IBRAHIM**, R. LEE, *Ohio State University, Columbus, OH, USA*
09:50	13.6	Molecular Simulation to Study Thermal Variations at Microscopic Scale in Bioelectromagnetics, M. ZAGO[1], L. TARRICONE[2], **A. PALOMBO**[1], G. D'INZEO[1], [1]*University "La Sapienza", Rome and* [2]*University of Perugia, Italy*
10:10		Coffee Break
10:30	13.7	Compact, Low Coupling, Higher Efficiency, Broadband Stacked-Patch Antennas for Cellular Telephones, S.S. PATTNAIK, G. LAZZI, **O.P. GANDHI**, *University of Utah, Salt Lake City, UT, USA*
10:50	13.8	Potential Effects of 60 Hz Magnetic Fields on Cell-Cell Communications *In Vitro*, **E.J. ROTHWELL**, K.M. CHEN, G.S. WALLINGA, F. NAN, C.C. CHANG, J.E. TROSKO, B.L. UPHAM, *Michigan State University, East Lansing, MI, USA*
11:10	13.9	Frequency Response of Transmembrane Potential in Gap Junction Connected Biological Cells, **E.C. FEAR**, *University of Victoria, BC, Canada*
11:30	13.10	Comparison of Calculated and Measured Near-Fields, Radiation Patterns, and SAR Distributions for Model of the Human Head for Some Typical Cellular Telephone Antennas, **G. LAZZI**, O.P. GANDHI, *University of Utah, Salt Lake City, UT, USA*
11:50	13.11	Investigation of Action of the Unheat Millimeterwave Radiation on Animal, V.V. MURAV'EV[1], **A.A. TAMELO**[1], J.N. VISHNYAKOVA[1], U.M. BYAHUN[1], N.H. FEDOSOVA[2], [1]*Belarusian State University of Informatics and Radioelectronics, Minsk and* [2]*Belarusian Agricultural Academy, Gorky, Belarus*

K13.1

A SYSTEM FOR CALIBRATION OF MICROWAVE ANTENNAE AND RADIATION SURVEY METERS

Art Thansandote, Siriwat Wasoontarajaroen, Greg Gajda* and Dave Lecuyer
Radiation Protection Bureau, Health Canada
Ottawa, Ontario K1A 1C1, Canada

In measuring environmental radiofrequency (RF) fields, one may use radiation survey meters or antennae coupled with a receiver (such as a spectrum analyzer) which can operate in the desired frequency band. Periodic verification of the calibration of such survey meters or antennae is required in order to obtain valid measurements. As the responsible organization for RF radiation safety, the Radiation Protection Bureau (RPB) of Health Canada is mandated to develop and maintain a facility for calibration verification. Also, considering the large number of RF surveys conducted annually by RPB and other Canadian federal and provincial agencies, the establishment of such a facility is essential.

The system, which can be used for antenna gain measurement as well as for calibration verification, is located in the RPB's microwave anechoic chamber (14 m x 8 m x 5 m). This system consists of two pedestals (2 m high), one stationary and the other mounted on a set of plastic rails and capable of motion up to 3.5 m. An electromechanical linear slide is mounted on each pedestal with the axis of motion parallel to the bore sight of the antennae under test. A 2.4 m boom is attached to the platform of each slide and is moveable along the bore sight axis under computer control. The receiving and transmitting antennae are mounted on the ends of the booms between the pedestals. In front of each pedestal is a screen of microwave absorbers, behind which a rack of transmitting or receiving equipment is mounted. In order to minimize the effect of multipath propagation in the chamber, the two slides are used to move the antennae or survey meter relative to their surroundings while maintaining their spacing. This effect produces variations in the received power which can be later averaged out in order to obtain a reading free of multipath interference. The equipment is interconnected by GPIB bus and is controlled remotely in a shielded control room adjacent to the chamber. Gain measurements and calibration verifications can be carried out rapidly and completely under computer control.

The system was tested with several commercial antenna models. The gain of an EMCO 3115 double-ridged horn was measured at 2.5 GHz and was found to be 8.7 dB compared to the manufacturer's gain specification of 8.1 ± 2.0 dB. More data will be presented and discussed.

RADIOFREQUENCY FIELDS FROM CELLULAR TRANSMITTER TOWERS AND ROOF-TOP ANTENNAS

Art Thansandote, Greg Gajda* and Dave Lecuyer
Radiation Protection Bureau, Ottawa, Ontario K1A 1C1, Canada

Following the introduction of cellular radio systems in the mid 1980's, there has been a rapid growth in the number of cellular telephone users, transmitter towers and antennas on roofs of buildings. While the cellular telephone industry expands their services by increasing the area of coverage, they face public opposition in the siting and installation of transmission facilities. This opposition is mainly due to a public perception of health risks from exposure to radiofrequency (RF) fields from the roof-top and tower antennas. As the responsible organization for RF radiation safety, the Radiation Protection Bureau of Health Canada is mandated to address this concern and has carried out the measurement of RF fields in the vicinity of typical cellular radio towers and roof-top antennas. This type of measurement presents a challenge since the levels of RF fields from such facilities are too low to detect using a commercial radiation survey meter.

In response to the challenge, a system comprised of a probe antenna, spectrum analyzer, laptop computer, and a computer-controlled vertical positioner has been assembled. This system is portable, battery operated, light weight and suitable for field operation or can be run from a mobile unit. The probe antenna is a half-wave folded dipole, fabricated on a printed circuit board, and tuned to a cellular band. The probe is mounted on a fibreglass boom, approximately 1 m long, which is attached to the vertical positioner and can be raised or lowered by computer control. The spectrum analyzer is used to tune to each of the active channels and measure and record the power density for later analysis. The vertical positioner is used to adjust the height of the probe antenna to compensate for multipath interference. All operations are under full computer control and require no operator input. The system allows averaging of the data for 6 min. as specified in the Canadian RF exposure limits and can also monitor exposure levels for long periods of time, unattended.

Several transmission facilities have been surveyed at locations accessible to the general public. At each one, the total, time-averaged power density from all the channels acquired has been found to be at least hundreds of times below the Canadian exposure limit of 5.9 W/m^2 for the 800-900 MHz cellular band.

K13.3

MICROWAVE FIELDS AS CONTROL OF COMPLEX FORMATION TIME IN HEMOGLOBIN BINDING SITE

M. Zago, A. Palombo, G. D'Inzeo, Department of Electronic Engineering, "La Sapienza" University of Rome, Via Eudossiana 18, 00184 Rome, Italy.

Introduction: An interesting research area in biophysics and organic chemistry is the one related on searching efficient ways to stimulate biochemical reactions. The objective of controlling the molecular dynamics actively is reachable by varying the global thermodynamic parameters such as temperature and pressure or by adding reagents to obtain the desired final products. Other possible way to partially or fully control the evolution of complex systems is the excitation of biomolecules by means of an external physical agent such as an electromagnetic field.

Matherial and Methods: A primary objective of chemists and physicists is the determination, once and for all, of appropriate temperature and pressure conditions or electromagnetic field intensities and frequencies to be assessed on molecular systems for reaching the desired product. One of our research objectives in bioelectromagnetism is instead the evaluation of the effects of environmental fields on biological matter. We have focused our attention in the evaluation of the effects of microwaves electromagnetic fields in the formation time of site-ligand complexes of biological significance. In particular we considered the hemoglobin binding site, protoporphyrin IX and analyzed the binding time with metals.
By means of a molecular simulation study we analyzed the dynamics of Zn^{++} complexation with protoporphyrin IX in presence and in absence of a microwave field. With our study we predicted an inhibitory effect of a 2.45 GHz electromagnetic field (SAR = 5 W/kg) on the binding time of Zn^{++} with protoporphyrin IX. This result was confirmed experimentally [D'Inzeo et al. "Electromagnetic field and molecular dynamics of Zn-protoporphyrin host-guest system"; Abstract Book of the 3rd EBEA Congress, Nancy, 1996].

Results and Conclusions: In this theoretical work using molecular simulations we consider different SAR values produced by the fields. We are exploring the SAR range from 2 W/kg up to 10 W/kg, limit values typically considered in the international safety standards for 2.45 GHz exposure. Our simulations put in evidence that an electromagnetic field acts as a control element of the temporal evolution of the binding of Zn-protoporphyrin.

Voltage-Gated Membrane Channels under GSM and DECT Exposure: A Global Analysis

F. Apollonio[1], G. D'Inzeo[1], L. Tarricone[2]

[1]Department of Electronic Engineering, University "La Sapienza" of Roma, Italy.
[2] Institute of Electronics, University of Perugia, Italy

In the recent past an increasing attention has been focused on environmental problems: a typical example is the evaluation of possible risks in the use of wireless communication systems due to effects of electromagnetic (EM) fields on human beings [K.Mann, J.Roschke, Neuropsychobiology , vol. 33, 41-47, 1996].
Bioelectromagnetic effects can be studied both at macroscopic and at microscopic level. Researchers interested in the biological effects of EM fields, at microscopic level, are focusing their attention on the behaviour of transmembrane ionic channels and on their kinetic properties: ionic channels, in fact, act as a gate regulating current fluxes through cell membrane. Theoretical studies of the biochemical dynamic properties of the channels have suggested the development of a modelistic approach considering the membrane channel as a non-deterministic state machine [G. D'Inzeo, S.Pisa, L.Tarricone, Bioel. & Bioen. Journ., 29, 290-304, 1993].
In this work the response of these theoretical models, for voltage-dependent channels such as Potassium, Calcium, Sodium channels, is analyzed for the electromagnetic fields used in GSM and DECT cellular phones, typical examples of wireless communication devices.
"Pulsed" signals, as GSM and DECT can be considered, usually consist of a single frequency carrier (900 MHz for GSM and 1900 MHz for DECT), modulated by a digital waveform of lower frequency, generally in the range of ELF frequencies.
Two different techniques have been followed in order to consider the low-frequency contribution and the high-frequency contribution of the external signal. In the former case a serial implementation resulted a good way to describe the effects of the low-frequency contribution of GSM and DECT signals on the channel behaviour; in the latter case a parallel implementation has been required in order to simulate the effects of the single frequency carrier of GSM and DECT.
In the parallel implementation a master-slave methodology is used: a master process activates a fixed number of slave processes. Each slave process takes care of generating a fragment of current signal. After a certain number of time steps, the master collects all the signal fragments from the slaves and links them.
In this way the sensitivity of the channel to "pulsed" signals is fully considered, taking into account both the low-frequency and the high-frequency signal contributions.

K13.5

SIMULATION OF RADIO FREQUENCY COILS FOR SUPER HIGH FIELD MAGNETIC RESONANCE IMAGING

T. S. Ibrahim*, and R. Lee

ElectroScience Laboratory
Department of Electrical Engineering
The Ohio State University
1320 Kinnear Rd.
Columbus, Ohio 43212-1191

Magnetic resonance imaging (MRI) was introduced in the late 1970's as a tool for imaging slices through the human body. Since its start, the magnets used in MRI had a field strength which varied between 0.5 to 2.0 Tesla (T). A typical MRI system, such as the one at the Ohio State University Hospital, uses a 1.5 Tesla magnet. Currently, an 8 T MRI system is in the process of being built at the same hospital. Being twice as powerful as the largest MRI systems in the world, it will be possible to obtain images with much greater details. This would help many diagnostic applications including early detection of small tumors.

The current MRI system uses quadrature radio frequency (RF) coils for high field and whole body imaging. The resonance frequency for the 1.5 T system is approximately 64 MHz. The goal of the RF coil design at this frequency is to produce a uniform magnetic field distribution and low values of specific absorption ratio (SAR) in the human body. It is expected that the resonance frequency for the new magnet will rise to approximately 340 MHz which will affect the distribution of the magnetic field and the values of the SAR in the human body. In order to retain to nice properties of a uniform magnetic field and a low SAR, we must redesign the RF coils. A simulation tool would be a great aid to the redesign of the coil.

In this paper, the finite-difference time-domain (FDTD) technique will be used to present some numerical simulation models of some of the RF coils used for the existing MRI system. The results of the magnetic field and SAR calculations will be presented at 64 and 340 MHz for an empty coil, one filled with a homogeneous medium, and one containing a human head model RF. At 340 MHz, the values of the SAR calculations and the distribution of the magnetic field will be discussed and compared to those at 64 MHz for all the above 3 mentioned cases.

MOLECULAR SIMULATION TO STUDY THERMAL VARIATIONS AT MICROSCOPIC SCALE IN BIOELECTOMAGNETICS

M. Zago[1], L. Tarricone[2], A. Palombo[1], G. D'Inzeo[1], [1]Department of Electronic Engineering, "La Sapienza" University of Rome, Via Eudossiana 18, 00184 Rome, [2]Institute of Electronics, University of Perugia, Via G. Duranti 1/A, 06131, Perugia, Italy.

Introduction: An important issue in the investigation of bioelectromagnetic (BEM) problems is the exact evaluation of the energy transferred in short intervals of time from the electromagnetic field (EM) to small regions of the target system. This typical dosimetric problem is generally rather complex in most BEM situations, especially when a possible non-thermal effect is studied (Om P. Gandhi, Biological Effects and Medical Applications of Electromagnetic Energy, Prentice Hall, 1990). In fact, even if in that case the field level can be very low, a long debate has been carried on the possibility to have local thermal variation both on time and spatial microscale (S. F. Cleary, "Biophysical Mechanisms of interaction", Review of Radio Science 1990-1992, Oxford University Press, 1993). We propose a theoretical approach to micro-dosimetry, based on Molecular Dynamics (MD). We shortly describe MD tools to analyze dosimetric aspects at microscopic level, and discuss their advantages and promising perspectives.

Materials and Methods: In the recent past, dielectric properties of fluids have been investigated with MD packages by the authors, demonstrating the usefulness of the approach (D'Inzeo et al., "Evaluation on water response to electrostatic fields via molecular simulation", Abstract Book of the BEMS XVIII Annual Meeting, 1996). GROMOS has been chosen as the reference package and customized for BEM purposes. Its force field has been modified so that external EM exposure is taken into account.
This allows the local evaluation of EM effects on target bodies, such as changes in the bond energies and conformational variations. As simulations are time-marching, the time variation of local energies inside a body can be monitored at interatomic level, with very small time resolutions (such as femtoseconds). GROMOS has been used to investigate electrostatic effects on a water box. Debye's and Langevin's theories have been accurately verified and extended, extrapolating some analytical relationships among the field amplitude E, the local body temperature T and the molecular relaxation time τ.

Results and Conclusions: This methodology is now used to study the thermal variations at microscopic scale induced by continuous wave microwave fields and pulsed wave microwave fields with small amplitudes such as GSM and DECT signals. The amount of local energy can be evaluated as the coupling is due to dipole orientation.

K13.7

COMPACT, LOW COUPLING, HIGHER EFFICIENCY, BROADBAND STACKED-PATCH ANTENNAS FOR CELLULAR TELEPHONES

SHYAM S. PATTNAIK, GIANLUCA LAZZI and OM P. GANDHI
Department of Electrical Engineering, University of Utah,
Salt Lake City, UT, 84112, E-Mail: pattnaik@ee.utah.edu

ABSTRACT: Public concern and increasing federal regulation have spawned extreme interest of the wireless industry in design of low coupling (lower rates of energy absorption by the human body) antennas that are additionally very compact and have high gain. We have designed a lower coupling (specific absorption rates or SARs) microstrip antenna for cellular telephone applications. To overcome the inherent narrow bandwidth of a microstrip antenna and to cover both the transmitting band (825MHz-850MHz) and receiving band (870MHz-895MHz) of the present day cellular telephone, a stacked microstrip antenna is designed by stacking two patches one above the other. Using the FDTD simulation code, the radiation patterns of this designed antenna are calculated for X-Y, Y-Z and X-Z planes over the entire range of frequencies of interest. The antenna maintains a fairly high gain (2-2.9 dBi) over the entire range of frequencies even with a finite ground plane. In the absence of the head, the calculated radiation patterns are almost omni-directional with a somewhat lower radiation (3 to 4 dB lower) towards the side of the ground plane. This makes it possible to mount the antenna both on the side and on the top of the cellular telephone. We have used the anatomically-based model of the head and neck to show that this stacked microstrip antenna gives a considerably reduced coupling of the EM energy to the human body.

Experimental radiation pattern measurements have been performed in our laboratory by using a computer-controlled automated set up. In all of the considered situations, the co- and cross-polarized components have been measured by mounting the antenna on a cellular telephone. The experimental measurements are in good agreement with the calculated results using the FDTD method, both with and without the tissue-simulant model of the head.

Such reduced size, high gain, broadband microstrip patch antennas will go a long way in fulfilling the requirements of low SAR antennas for personal wireless devices.

Potential Effects of 60 Hz Magnetic Fields on Cell-Cell Communications in Vitro

E.J. Rothwell*, K.M. Chen, G.S. Wallinga, and F. Nan
Department of Electrical Engineering

C.C. Chang, J.E. Trosko, and B.L. Upham
Department of Pediatrics and Human Development

Michigan State University
East Lansing, MI 48824

While a link between exposure to low-frequency electromagnetic fields and various types of cancer has been suggested by several epidemiological studies, a causal relationship has not yet been established. It must be remembered that carcinogenesis is a multi-step, multi-mechanism process, consisting of an initiation, a promotion and a progression phase. Evidence seems to rule out a connection between EM fields and cancer initiation where DNA damage leads to gene or chromosome mutations. This leaves the possibility that exposure to EM fields affects the promotion phase, during which an initiated cell is clonally multiplied by a mitogenic process.

Much recent evidence suggests that an alteration of gap junctional intercellular communications (GJIC) is closely linked to the promotional stage of carcinogenesis. Many growth factors associated with tumor promotion have been shown to down-regulate GJIC, while several anti-tumor promoters have been shown to be associated with the up-regulation of GJIC. This suggests that if EM fields are involved in the cancer promotion phase, they may either directly down-regulate GJIC, or may modulate existing tumor promoters or suppressors.

This paper will discuss several experiments performed at Michigan State University to investigate the potential effect of EM fields on GJIC. Normal rat liver epithelial cells have been exposed to a 60 Hz magnetic field at various field strengths and for various time periods. Scrape loading and photobleaching techniques will be used to measure the effect of field exposure on GJIC, and the results reported.

In establishing a mechanistic connection between tumor promotion and magnetic field exposure, it is necessary to accurately determine the intracellular exposure level, as well as the nature and strength of the currents induced within each cell. To this end, numerical techniques such as the quasistatic (Faraday's law) and finite element methods have been employed to solve Maxwell's equations within simple models of biological cells. Results from these studies will also be presented.

K13.9

Frequency Response of Transmembrane Potential in Gap Junction Connected Biological Cells

E.C. Fear, Department of Electrical and Computer Engineering,
University of Victoria, Victoria, British Columbia, Canada

INTRODUCTION and OBJECTIVE: The mechanisms for biological interactions of weak electromagnetic (EM) fields remain unknown. To gain insight into these interactions, the behaviour of biological cells exposed to EM fields can be modeled. Some cells are connected by gap junctions which provide intercellular communication. In this work, the frequency responses of various configurations of gap-connected cells are examined.

METHODS: The finite element method (FEM) is used to model cell configurations, as FEM is well-suited to these geometrically complex models. At lower frequencies, quasi-static approximations apply. A commercial FEM solver, EMAS (Ansoft), is used to perform computations. An equivalent circuit model is developed and used to further examine cell behaviour.

RESULTS: The transmembrane potential (TMP) as a function of frequency was computed. With an applied electric field parallel to the long axis, FEM results indicate that cell chain and cluster relaxation frequencies are much smaller than those of similarly shaped elongated cells. Additionally, the relaxation curve shape changes (Figure 1). Using the ECM model, the relaxation curve can be decomposed into a low-pass filter component (single cell with overall shape of the chain) and a band-stop component (gap junctions). The width of the band-stop region decreases with increasing gap area and decreasing gap conductivity. The two method approach facilitates both insight into the cell behaviour, and quantitative evaluation of the TMP for large gap-connected cell chains and clusters.

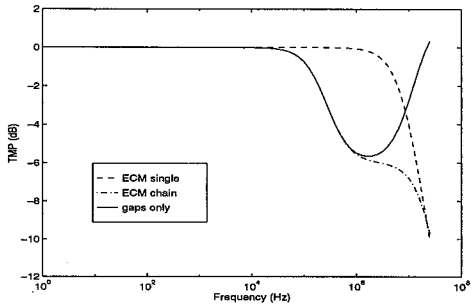

FIGURE 1. Decomposition of relaxation curves derived from ECM for a 2 cell chain.

K13.10

COMPARISON OF CALCULATED AND MEASURED NEAR-FIELDS, RADIATION PATTERNS, AND SAR DISTRIBUTIONS FOR MODEL OF THE HUMAN HEAD FOR SOME TYPICAL CELLULAR TELEPHONE ANTENNAS

Gianluca Lazzi and Om P. Gandhi
Department of Electrical Engineering
3280 MEB, University of Utah
Salt Lake City, UT 84112, USA

We have used the Finite-Difference Time-Domain (FDTD) method to compare the numerically-computed near- and far-fields generated by various cellular telephones with measurements. Different antenna configurations have been considered, and a novel technique to model helical antennas working in the normal mode, as well as helix-monopole antennas, is presented in order to avoid both the stair-casing approximation in the FDTD code and the subgridding technique. By observing that a helix working in the normal mode is equivalent to a sequence of loops and dipoles, it is possible to model the helix as a stack of electric and magnetic sources with relative weights calculated using information obtained from analytical expression for the far-fields.

Three typical cellular telephones have been used, one with monopole antenna, one with helix antenna, and one with helix-monopole antenna, and measurements of the far-fields as well as the near-fields show the reliability of the FDTD code. These telephones have also been tested against the ANSI/IEEE safety guidelines that prescribe a maximum Specific Absorption Rate (SAR) of 1.6 W/kg as averaged over any 1 g of tissue. A 1.974 $\times$ 1.974 $\times$ 3 mm resolution model of the human head based on MRI scans of a male volunteer has been used in the FDTD code, and results compared with those measured by using the Utah heterogeneous -- four tissue -- experimental model. Even though peak 1-g SARs from 0.13 to 5.41 W/kg are obtained, agreement between the measured and the calculated data is very good and generally within $\pm$ 25 percent.

K13.11

Investigation of Action of the Unheat Millimeterwave Radiation on Animal

Murav'ev V.V.[1], Tamelo A.A.[1], Vishnyakova J.N.[1], Byahun U.M.[1], Fedosova N.H.[2]

[1]Belarusian State University of Informatics and Radioelectronics
6,P.Brouki vul., Minsk 220027 Republic of Belarus
tel.398-095, fax (017) 231-0914, E-mail: cit@micro.rei.minsk.by
[2]Belarusian Agricultural Academy
10, International ave., Gorky, 213410 Republic of Belarus, tel./fax (02233) 25-907

Introduction- Experimental results of the unheat millimeterwave influence at transplatation cows embryos are described. Results of the treatment of cows mastitis and endometritis are described also. The authors hypothesis about parametric millimeterwave influence are discused.

Results of Experiments and its Discution- The receach work for elaborating the method and the apparatus for informational influence by the electromagnetic fields (П<10 mW/cm2) have been carry out since that very important for make cattle more productive including profilaxis and treatment such diseases as mastitis, endometritis and others. Results of practical application of the informational electromagnetic wave processes at purposeful rearing of high productive animal, prophilaxis and undrugs treatment are being considered. New method of treatment of mastitis without contra-indications by the microwave unheat doses have been suggested. Effectiveness of cows mastitis treatment methods are being corroborated by laboratory investigations of milk gland sekret. At 4 days we have good quality milk according to the standarts. Dinamics of harmful microflora icreasing in the potions of the milk and increasing number of blood leucocytes have been described. At treatment, the level of the harmonys have stable phisiologicaly standart character. The conception of rapid selection of high productive scattles stocks using unheat microwave doses, infrared and low frequency oscillations was develop by the authors. Record number of settle down cows embryos is 71.43 per cent. That is 24.4 per cent higher than test group. Increasing of settle down of the microorganisms contominated embryos at the microwave radiation influence is 20 per cent. The authors hypothesis about parametric influence are discused. The experimental results corroboted the hypothesis of electromagnetic influence phenomenon. The authors considered that the method are providing adaptation processes effective control of organism at restoring of homeostathis through neirohumoral system.

Conclusion - At influence unheat millimeterwave number of settle down cows embryos is 71.43 per cent. Using the method at 4 days we have good quality milk according to the standarts. The authors hypothesis about parametric millimeterwave influence are confirmed.

References

1. Muraviev V.V., Tamelo A.A., Fedosova N.H. Vesczi Academii Agrarnih Navuk Belarusy.-1994, N2,-p.73-78.
2. SU A1 No 1782488, 1990.

URSI K

Session 88 Salon Richelieu

Electromagnetic Engineering in Medicine and Biology
Co-chairs: M. Stuchly, Canada and T.J.F. Pavlasek, Canada

08:10 88.1 Flexible Microwave Array Applicator for Superficial Heating of Large Contoured Surfaces, **P.R. STAUFFER**[1], D. DEARDORF[1], F. ROSSETTO[1], G.B. GENTILI[2], M. LEONCINI[2], [1]*University of California, San Francisco, CA, USA;* [2]*University of Florence, Italy*

08:30 88.2 EM Analysis of the Feeding Network of DCC Planar Applicators for Superficial Microwave Hyperthermia, G. BIFFI GENTILI[1], C. SALVADOR[1], **M. LEONCINI**[1], P. STAUFFER[2], F. ROSSETTO[2], [1]*University of Florence, Italy;* [2]*University of California, San Francisco, CA, USA*

08:50 88.3 The Input Impedance of Inhomogeneous Cylindrical Tissue Layers Excited with Axial and Circumferential Polarization Waves, **R.M. NAJAFABADI**[1], A.F. PETERSON[2], [1]*Atlanta, GA and* [2]*Georgia Institute of Technology, Atlanta, GA, USA*

09:10 88.4 Temperature Imaging by Non-Contacting Microwave Radiometry, **E. DI GIAMPAOLO**[1], F. BARDATI[2], [1]*University of Aquila and* [2]*University of Rome, Italy*

09:30 88.5 Calculation of the Power Absorbed by the Head Using a Non Uniform FDTD, **J. WIART**, S. CHAILLOU, S. DRAGO, *France Telecom CNET, Issy Moulineaux, France*

09:50 88.6 Comparison of 60-Hz Uniform Electric and Magnetic Induction in Human Organs Using High-Resolution Modelling, **T.W. DAWSON**, M.A. STUCHLY, K. CAPUTA, *University of Victoria, BC, Canada*

10:10 Coffee Break

10:30 88.7 A Small Sensor to Measure the Electric and the Magnetic Field Component Simultaneously in Biological Material, **A. GILLE**, J.L. TER HASEBORG, *Technical University of Hamburg-Harburg, Hamburg, Germany*

10:50 88.8 Biological-Tissue-Equivalent Phantom Material for EM Modeling of Human Body at Microwave Frequency, **L. HAMADA**[1], R. WANG[1], K. ITO[2], [1]*Graduate School of Science and Technology and* [2]*Chiba University, Chiba, Japan*

11:10 88.9 EM Interaction between a Head and Antennas: Exact Scattering Solution of a Double-Layered Lossy Spherical Head, K.W. KIM, **Y. RAHMAT-SAMII**, *University of California, Los Angeles, CA, USA*

11:30 88.10 EM-Energy Absorption in Human Heads Depending on Age, Size and Shape, **M. BURKHARDT**, F. SCHÖNBORN, N. KUSTER, *Swiss Federal Institute of Technology (ETH), Zürich, Switzerland*

11:50 88.11 Decontamination of Milk Contaminated by Some Stable and Pathogenetic Microorganisms (with Mycobacteria as Specific Instances) by Means of Low-Temperature U.H.F. Irradiation, **B.I. KHAIKIN**[1], I.D. ZOLOTAREV[2], [1]*All-Russian Institute for Scientific Research in Brucellosis and Tuberculosis of Animal and* [2]*Omsk State Engineering University, Omsk, Russia*

K88.1

FLEXIBLE MICROWAVE ARRAY APPLICATOR FOR SUPERFICIAL HEATING OF LARGE CONTOURED SURFACES

Paul R. Stauffer*, Dana Deardorf, and Francesca Rossetto
Radiation Oncology Dept., University of California, San Francisco CA
Guido Biffi Gentili and Marco Leoncini
Electronics Engineering Dept., University of Florence, Florence Italy

This effort describes the design and radiation characteristics of a multiaperture microwave array applicator intended for use in heating large superficial tumors for the treatment of cancer. Previous microwave applicators have tended to be bulky and awkward to couple to human tumors, with centrally peaked radiation patterns that fall below 50% of maximum heating rate well inside the aperture periphery, preventing the combination of applicators for treating large areas. A new Conformal Microwave Array (CMA) applicator has been designed to meet the following specifications:

- Easily adjustable radiation pattern for uniform heating of large tumors overlying contoured anatomy,
- Thin and lightweight so it can be secured comfortably to the patient to allow movements during therapy for improved patient tolerance,
- Transparent to external beam radiation to allow delivery of heat and x-irradiation therapies simultaneously for maximum synergism of biological effects,
- Simple low cost construction easily customized to meet patient requirements.

CMA applicators were constructed from very flexible (0.15 mm thick) copper-plated polyamide substrate by etching a series of 0.1-10 mm wide annular gaps from the front copper surface producing an array of isolated square patches surrounded by a continuous rim of copper foil (P.R.Stauffer et al. IEEE MTT-S Intl Microwave Symp. Digest 1:531-4, 1994). The isolated patches were coupled to independently controlled 915 MHz generators via microstrip feedlines etched on the back side of the substrate. The rest of the contiguous front copper surface served as a co-planar ground plane surrounding all radiating slots. Applicator performance characteristics were investigated with: i) theoretical electromagnetic modeling, ii) empirical measurements of radiated patterns in layered tissue loads, and iii) thermal dosimetry during clinical treatments. Finite Difference Time Domain (FDTD) analysis was used to calculate radiation patterns in layered tissue models from single patch apertures (P.R. Stauffer et al. *IEICE Trans. Communications*, E78-B: 826-35, 1995) and from multiaperture arrays for optimization of antenna design parameters such as aperture and gap size, thickness of water bolus coupling medium, and microstrip feedline excitation.

Both theoretical simulations and empirical measurements demonstrate that individual square slot radiators produce $\geq$ 50% of maximum power deposition out to the periphery of apertures ranging from 1.5-5 cm square, making them effective building block elements of larger arrays. When driven with independent generators to minimize field interaction between elements, the array applicators demonstrate effective heating out to the perimeter of the array. Clinical results demonstrate the ability to maintain therapeutic temperatures of 41.5-44.0°C comfortably, both on the skin surface and interstitially in target tissue 1 cm beneath diffuse disease.

Our results confirm the usefulness of electromagnetic simulation programs for both prediction of radiation patterns and applicator design optimization. Furthermore, we have demonstrated that CMA applicators can effectively heat arbitrarily large contoured tissue regions $\leq$ 1.5 cm deep with improved patient comfort, facilitating new treatment protocols involving simultaneous heat and radiation, and longer duration heat treatments for accumulation of higher thermal dose or local activation of systemic chemotherapy agents.

EM ANALYSIS OF THE FEEDING NETWORK OF DCC PLANAR APPLICATORS FOR SUPERFICIAL MICROWAVE HYPERTHERMIA

G. Biffi Gentili, C. Salvador, M. Leoncini*
Electronics Engineering Department, University of Florence, Florence - Italy
P. Stauffer, F. Rossetto
Radiation Oncology Department, University of California, San Francisco - USA

A planar Dual Concentric Conductor (DCC) radiator for superficial microwave hyperthermia was recently proposed which, when used in array configuration, would allow the treatment of large contoured surfaces (P. Stauffer et al., IEEE MTT-S Int. Microwave Symposium Digest, 531-534, 1994), (P. Stauffer et al., IEICE Trans. Comm., E78-B, 826-835). The radiating aperture consists of a squared radiating slot 0.1-10 mm wide, etched from the front surface copper layer of a very thin dielectric substrate (Fig. 1). This applicator provides a good field uniformity to the periphery of each aperture and is lightweight and flexible for reliable fixation over the tumor. Because the applicator is very thin (0.15 mm) it is transparent to external beam radiation thus facilitating simultaneous radiotherapy applied directly through the applicator.

In order to fully exploit its capability in actual clinical applications, its planar characteristics must be maintained by also using a planar feeding network rather than cumbersome coaxial cable connections from the back plane. This would indeed enhance the conformability and lightness of the applicator with the possibility of simultaneous radiotherapy becoming a true reality. A possible way to feed each radiating element by using planar microstrip transmission lines is that depicted in Fig. 2 where microstrips, printed on the back side of the thin dielectric substrate, are used to feed energy to the front surface radiating slots. Power from the microwave source is electromagnetically coupled to each aperture at the microstrip-slot crossing point. This very simple construction produces planar applicators that can be implemented easily by properly defining suitable layouts on double-sided flexible PCB material.

In this work, a moment method approach was used to design appropriate microstrip feed network for DCC applicators operating at 915 and 432 MHz. Simulations were run by modeling the feed transmission line, the radiating aperture, the layered tissue load (i.e. skin/fat/muscle). The presence of a water bolus coupling medium between the radiating elements and tissue load was also considered. Results indicate that in order to obtain a good matching, the slot width at the crossing points must be approximately equal to the thickness of the dielectric substrate.

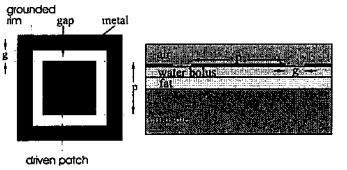

Fig. 1: The DCC applicator.

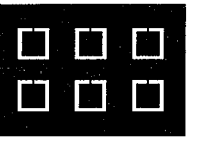

Fig. 2: Microstrip feeding of DCC apertures.

K88.3

The Input Impedance of Inhomogeneous Cylindrical Tissue Layers Excited with Axial and Circumferential Polarization Waves

Reza M. Najafabadi
Bolton Dr. N.W.
Atlanta, GA 30318

Andrew F. Peterson
School of Electrical and Computer Engineering
Georgia Institute of Technology
Atlanta, GA 30332

For efficient power deposition in hyperthermia treatment of cancerous tumors, the information about the input impedance of tissue layers is necessary. In this paper, inhomogenous cylindrical tissues will be excited with two polarizations, axial and circumferential, with a single rectangular waveguide aperture on its surface. We formulate the problem using the Helmholtz equations to find the electric field within the cylinder and incorporate a Fourier transformation to cast the electric field into the Fourier domain. From the two-dimensional Fourier transforms of the aperture excitation field, we determine the unknown coefficients associated with a cylindrical wave expansion. At a rectangular aperture, the input impedance of tissues will be calculated at 915 MHz for various thicknesses and tissue properties. An optimal bolus layer thickness will be found for both axial and circumferential polarizations in order to maximize the power deposition to the tumor.

TEMPERATURE IMAGING BY NON-CONTACTING MICROWAVE RADIOMETRY

Emidio Di Giampaolo[1]* and Fernando Bardati[2]
[1]Dept. of Electrical Engineering, University of Aquila, 67040 L'Aquila, Italy
[2]DISP, University of Rome "Tor Vergata", 00133 Rome - Italy
bardati@disp.utovrm.it

Microwave radiometry is based on the measurement of spontaneous temperature-dependent electromagnetic emission from lossy bodies. Maps of sub superficial temperatures can be obtained by inversion of data measured by a radiometer operating at various microwave frequencies. In terms of free-space wavelength λ, a typical range is between 6 and 30 cm. The mathematical problem can be formulated as the solution of the following Fredholm integral equation of first kind in the temperature T with discrete data g

$$g(\lambda_n) = \int_{\Omega} W(\underline{r},\lambda_n) T(\underline{r})\, d\underline{r}$$

where Ω is the emitting body and W is a weighting function depending on the antenna in use. Because reciprocity in antenna theory, W can be obtained by power loss distribution at the points of Ω when the antenna radiates onto the body (Bardati et al., in *Non-Invasive Thermometry of the Human Body*, M. Miyakawa and C. Bolomey Eds., CRC Press, Boca Raton, FL, 1995, pp. 225-253).

In most radiometric systems the antenna contacts the body. Since a contacting antenna has some disadvantages, we are considering the feasibility of a non-contacting device. Due to clinical application, easy-handling is a prerequisite. Therefore the non-contacting antenna should be relatively small, i.e. not exceeding a few wavelengths at the lowest frequency. Moreover it should focus to a small area of the body to achieve transversal resolution.

We assume a layered cylindrical model for Ω, the physical parameters being those of skin, fat, muscle and bone in this order. The cross-section (on a plane, α, tangent to Ω) of the antenna beam is assumed to be a gaussian pulse, the waist of which is comparable with the body external radius (10 cm). The weighting functions for the above geometry and eight wavelengths have been computed analytically and the retrieval of a hot-spot embedded in the muscle region of Ω has been performed.

The antenna is required to radiate a beam whose cross-section on α is the gaussian pulse already used for the temperature retrieval. For the sake of simplicity, also the antenna has cylindrical symmetry, being composed of two reflectors and a TEM horn. The reflectors are shaped to comply with the above requirements. A method, originally developped by Kildal, is used for the synthesis. The method is based on geometrical optics and power conservation inside ray tubes. It maps biunivocally points on two given wavefronts and has been exploited in a preliminary paper (Bardati and Di Giampaolo, 1996 USNC/URSI Radio Science Meeting, Baltimore, MD, p.131). The solution of the synthesis problem is not unique, since it depends on the initial ray-path passing through an edge of each wavefront and reflector. Different solutions are compared on the basis of size reduction and easy access to allow simultaneous operations in a clinical environment. Then the weighting functions are obtained for the antenna-body system. The FDTD method has been used for the analysis, since it works efficiently in the presence of dielectric inhomogeneities. Finally the hot-spot retrieval has been repeated by means of these weighting functions for a comparison with previous results.

K88.5

Calculation of the power absorbed by the head using a Non Uniform FDTD.

Joe Wiart, Stéphane Chaillou, Stéphane Drago
France Telecom C.N.E.T DMR/RMC
38-40 ave Général Leclerc 92794 Issy Moulineaux Cedex 9 FRANCE
wiart@issy.cent.fr

Recent years have seen an explosive growth in the area of wireless. According to the European Community (IBC meeting, London, Nov 1996), in 2010 more than 200 M users will use wireless. Questions have arisen about power absorbed by the head, and the reduction of this absorbed power is a new challenge. On the one hand it allows to increase the energy used for the communication, and on the other hand, it insures, from the health point of view, the use of handsets. When an antenna is close to the head, a large part of the emitted power is absorbed by the tissues, moreover the antenna pattern is modified. Standards have been established (ANSI/IEEE, CENELEC) for the absorbed power by the tissues, which must be below the limits. In the future, mobile phones will have to be in compliance with these standards.

To compute the local absorbed power, numerical techniques are necessary, and the Finite Difference in Time Domain (F.D.T.D) method has been more and more used for this purpose. The numerical model of the head has been built from Magnetic Resonance Image (M.R.I) with a segmentation process. Previous studies have shown that power is mainly absorbed by tissues close to the antenna. To improve the knowledge of the power deposition in these tissues finer mesh is required. The decrease of the mesh size in a uniform FDTD code is impractical due to memory and CPU time limitations. To refine the mesh at the tissues close to the antenna with only a moderate increase of memory size, two avenues can be considered : sub-gridding and non uniform mesh. The second approach has been adopted in this work, with a Non Uniform FDTD code (J.A Svigely «Efficient solution of Maxwell equations using the non uniform orthogonal finite difference time domain method» PhD thesis, University of Illinois,1995).

The non uniform model of the head has been generated from a fine uniform M.R.I model (voxels a 1x1x1.5 mm^3) trough a non uniform sampling. At regions close to the antenna, e.g., the inner ear, a fine mesh from the original M.R.I data is used, whereas on the other side of the head and close to the neck, the mesh has been enlarged to about 3x3x3mm^3. Two kinds of antenna have been modeled. The first one is a $\lambda/2$ dipole, and the second one is a handset comprising of a $\lambda/4$ monopole on top of a metal box surrounded by a plastic layer. The monopole has been meshed with small cells (1x1x1mm^3) near the excitation gap and larger cells (1x1x3 mm^3) far away from this gap. In both cases the antenna is located at a distance of 1.5 cm away from the head, few millimeters from the ear. The dipole and the handset are oriented to be lined up with the ear and the mouth. The well known « PML » absorbing boundary conditions have been used.

The numerical results for the real parts of the impedance of the dipole and handset antenna in free space are 98Ω and 44Ω respectively, and in the presence of the head 79Ω and 50Ω respectively. When the dipole antenna is used the head absorbs 50 % of the emitted power (E.P), and the skin absorbs 14% of this E.P . When the handset is used, the head absorbs 45 % of the E.P, the skin absorbs 14%. Next, we have considered the power deposition in a small volume including the inner ear. Numerical simulations show that for the case of a 5x5x5 cm^3 cube, about 60% of the power is absorbed in this volume. The skin of this area absorbs 70% of the power absorbed by all the skin.

Comparison of 60-Hz Uniform Electric and Magnetic Induction in Human Organs Using High-Resolution Modelling

Trevor W. Dawson, Maria A. Stuchly, and Kris Caputa

Department of Electrical and Computer Engineering
University of Victoria, P.O. Box # 3055
Victoria, British Columbia
Canada V8W 3P6

Abstract

Accurate and verified modelling of the induced internal fields is an important element in the understanding of any possible low-frequency (particularly 50/60 Hz) electric and magnetic health effects in humans. Calculations using the Impedance, Finite-Difference Time-Domain, and Finite Element Methods have been reported for both isolated and combined electric and magnetic induction in both anatomically-derived and synthetic human models.

At the low frequencies under consideration, the time-harmonic induced internal electric field can be represented in terms of a scalar potential as $E=-j\omega(A+\nabla\psi)$, where A is a vector potential for any external magnetic field. The electric field must satisfy the differential equation $\nabla\bullet(\sigma E)=0$, and is subject to the boundary condition $\sigma\mathbf{n}\cdot E=j\omega\rho_S$, where ρ_S is the surface charge density induced by any external electric field. In our implementation of this Scalar-Potential Finite-Difference (SPFD), the finite-difference equations are arranged as a sparse symmetrically-preconditioned matrix system, which is reliably solvable using the conjugate gradient method. This code requires substantially less memory than vector methods. It permits full-body induction calculations on a workstation, for an anatomically-based whole-body model composed of cubic voxels with 3.6-mm edges. For magnetic excitation the code can be in isolation. For electric excitation, the code is run in a two-stage hybrid mode, in which the surface charge density is taken from earlier low-resolution quasi-static FDTD calculations. This surface charge density is interpolated onto the 3.6-mm model, for use in the boundary conditions for high-resolution SPFD runs.

The 3.6-mm resolution is sufficient to incorporate representations of some of the smaller body structures, such as larger blood vessels and glands. The calculations provide detailed dosimetric data for a wide variety of tissues and organs. In this paper, the effects of magnetic and electric excitation of the whole body, will be compared in terms of their effects on certain organs. In particular, the source levels needed to produce threshold maximum or average current densities in these organs will be described. The work is of relevance in the development and interpretation of any necessary protection standards.

K88.7

A SMALL SENSOR TO MEASURE THE ELECTRIC AND THE MAGNETIC FIELD COMPONENT SIMULTANOUSLY IN BIOLOGICAL MATERIAL

A. Gille, J. L. ter Haseborg, Technical University Hamburg-Harburg, Department of Measurement Engineering / EMC, Harburger Schlosstr.20, 21071 Hamburg, Germany, Phone: +49 40 7718-2873, -3013, Fax: -2382
Email: Gille@tu-harburg.d400.de, terHaseborg@tu-harburg.d400.de

In this paper a sensor is presented, which is able to measure the electric and the magnetic field component simultanously in the frequency-range 100MHz up to 1GHz. Of special interest is the measurement of the electromagnetic field in or on the surface of biological tissues, so that the sensor is adapted for this case. The sensor consists of a double loaded electrically small loop as shown in **figure 1**. The magnetic field induces a current circulating in the loop, which results in the voltages V_m at the two loads. The electric field component in z-direction induces the voltages V_e as shown in **figure 1**. In fact there is a superposition of the two voltages V_m and V_e at the loads. Assumed, that $R_1 = R_2$, it is possible to receive voltages proportional to the electric or magnetic field respectively by addition and substraction of the two voltages V_1 and V_2 (R.W.P.King and Ch.W.Harrison: "Antennas and Waves: A Modern Approach", The M.I.T. Press, Massachusetts Inst. of Techn., Cambridge, Massachusetts and London, England, 1969).

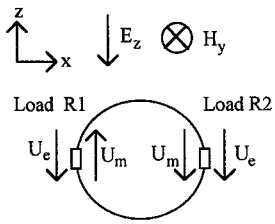

Figure 1: Double loaded loop

$$V_1 = V_e - V_m \qquad V_2 + V_1 = 2\,V_e \sim E_z$$

$$V_2 = V_e + V_m \qquad V_2 - V_1 = 2\,V_m \sim H_y$$

If the loop is constructed with microcoaxial cable (semi-rigid-cable), the (outer surface) of the shield is part of the sensor and the signal can be transmitted through the coaxial cable. A small gap in the coaxial shield represents the load. The realized loop has a diameter of 1cm, so that it is electrically small up to 1GHz.

For measurements in biological tissues it must be payed attention to the electrical properties of the tissues, they have a conductivity and a permittivity, depending on the tissue and the frequency. To decrease the influence of the surrounding medium on the sensor and to avoid a direct contact with it, the sensor has to be insulated. A suitable insulation for a dipole is described by Smith (G.Smith, IEEE Trans. on Biomed. Eng., V.22-6, p.477-482, 11/75). It is modified for a double loaded loop.

Measurement values in different media will be presented in comparison with analytically and numerically determined values. The results will be discussed.

Biological-Tissue-Equivalent Phantom Material for EM Modeling of Human Body at Microwave Frequency

Lira HAMADA †, Rong WANG † and Koichi ITO ‡

† Graduate School of Science & Technology
‡ Department of Electrical & Electronics, Faculty of Engineering
Chiba University
1-33 Yayoi-cho, Inage-ku, Chiba-shi, 263 Japan

In the past few years, the phantom materials simulating various biological tissues have been developed for experimental evaluation of the interaction between the human body and the incident electromagnetic fields. Each phantom has different features and characteristics to meet the purpose of experiments. As medical application acquires popularity, a low cost and easily-made phantom is required not only in laboratories but also in hospitals, for the purpose of checking the devices and instruments.

The saline-solution-based phantoms are widely used from its availability, although its permittivity is not the same as actual biological tissues. Therefore, we have developed a semi-solid phantom material which realizes the same complex permittivity as the tissues for the purpose of SAR (Specific Absorption Rate) estimation by thermographic method to develop hyperthermic instruments.

This static phantom basically consists of easily-available materials; polyethylene powder, TX-151(©OIL CENTER RESEARCH INC. USA), sodium azide, sodium chloride, agar and deionized water. This phantom can be fabricated manually requiring no special equipment, be formed in arbitrary shape and be preserved for months at room temperature wrapped by thin plastic film.

Figure 1 shows the frequency dispersion of measured relative complex permittivity of actual muscle tissue (Johnson and Guy, Proc. IEEE,60,6,692-718,1972) and this phantom set to be muscle-equivalent (measured with HP 85070M dielectric probe kit). These data are showing good correspondence in the wide range of microwave frequency from 200 MHz to 3 GHz. The permittivity also can be controlled with varying the mix ratio of the ingredients and can simulate those of high-water content tissues; such as muscle or brain.

The phantom has been used for EMC measurements and microwave hyperthermia. Some experimental examples have been compared with the saline-solution-based phantoms. The results show the difference of the complex permittivity has not negligible effect in both case, therefore this tissue-equivalent phantom is effective as human model.

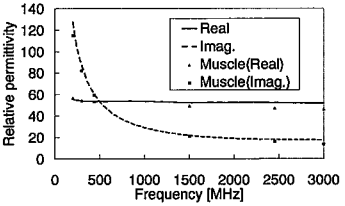

Fig.1. Complex permittivity of the muscle-equivalent phantom

K88.9

EM Interaction between a Head and Antennas: Exact Scattering Solution of a Double-Layered Lossy Spherical Head

Kang W. Kim and Yahya Rahmat-Samii
Department of Electrical Engineering
University of California, Los Angeles
Los Angeles, CA 90095-1594

A powerful computational model has been developed for a systematic and parametric study of electromagnetic (EM) interaction between a human head and various types of antennas used in personal communication systems. In contrast to commonly used, purely numerical techniques, the model solves an exact EM scattering problem for a number of infinitesimal dipoles in presence of a double-layered lossy dielectric sphere. The model calculates the radiation pattern and power absorption with dipoles of any orientation and location, and uses a double-layered head (skin/skull layer and homogeneous brain) model that can produce important data for antenna interactions with biological tissues in personal communications. Also, the results of this canonical problem can be used to validate other numerical schemes that treat more realistic head models.

The model utilizes free-space dyadic Green's functions so that the exact EM field of an infinitesimal dipole with arbitrary orientation and location, scattered from a double-layered lossy dielectric sphere, is expressed as an infinite sum of the spherical vector wave functions. In this calculation, however, the number of terms in summation is adaptively determined by ensuring that the magnitude of the last term is less than 5×10^{-7} times total sum of the previous terms. Also, an actual dipole antenna of any type is modeled as finite array of infinitesimal dipoles with varying amplitude and phase. For example, the near and far field of an array of infinitesimal dipoles ($\geq$ 50 infinitesimal dipoles) which simulates a half-wavelength dipole antenna agrees well with the analytical formula. Since multiple loops of calculations are required to determine a field value at a desired point, computational time can be significantly reduced using parallel processing algorithm.

In the paper, results of parametric study of EM interactions between a lossy dielectric head model and various antennas will be presented. Calculations of power absorption in the lossy dielectric head model will be determined by varying parameters such as: 1) distance between a spherical head model and antennas, 2) size of the head model (adult and child head), 3) input frequency, 4) electrical parameters of the head model (permittivity and conductivity), 5) type of antennas, 6) effect of skin, etc. Averaged and local specific absorption rate (SAR), and SAR distribution will be presented for a range of parameters. Finally, a possible design of directional antennas which reduce the radiation toward the head, thus absorption into the head, will be explored.

EM-Energy Absorption in Human Heads Depending on Age, Size and Shape

Michael Burkhardt*, Frank Schönborn and Niels Kuster
Swiss Federal Institute of Technology (ETH)
8092 Zurich, Switzerland
Phone:+41-1 632 2151, Fax:+41-1 632 1057, e.mail: burkhardt@ifh.ee.ethz.ch

Introduction

Several studies have recently been performed to assess the absorption of EM-energy in human heads induced by handheld mobile communications equipment (MTE). These studies have mainly been based on MRI data of human heads and conducted using volume techniques such as the Finite-Difference-Time-Domain (FDTD) method. The results, which greatly differ in their details and even in their conclusions, have proven to be difficult to compare, since the complexity of the problems involves too many parameters. For example, (O.P. Gandhi et al., IEEE MTT-44, 1884-1897, 1996) reported increased absorption in heads of children compared to adults, which contradicts other findings.

Objectives

The objective of this study was to investigate possible differences in the energy absorption in human heads in the close vicinity of RF transmitters depending on anatomy, shape, size and age. In addition, the requirements for a generic phantom representing an entire user group was to be derived.

Methods

The study was conducted on the basis of different numerical head phantoms derived from MRI data: Two newly discretized adult heads and two children's heads with voxel sizes of approximately $1 \times 2 \times 2\,\mathrm{mm}^3$, as well as the three head phantoms of adults described in (V. Hombach, IEEE MTT-44, 1865-1873, 1996). The phantoms varied in age, size, shape, resolution of the discretization and number of distinguished tissues. Additionally, one head model was scaled down to the size of those of children, corresponding to a small baby, a 3 year old and a 7 year old child. The child heads based on MRI data were those of a 3 year old and a 7 year old child. The human head data originates from Europe, USA and Asia. Since the objective was to evaluate the differences of the absorption between child and adult heads, it was important to have a well defined source at a well defined distance from the head. A $0.45\,\lambda$ dipole was chosen and oriented parallel to the body's axis. The selected frequencies were those of the major mobile communications bands, i.e., 900 MHz and 1.8 GHz. The numerical simulations were performed with two FDTD based codes. In addition, the results were validated by layered spherical phantoms computed by FDTD and the Generalized-Multipole-Technique (GMT), as well as with the results obtained by the near field scanner DASY2 (T. Schmid, IEEE MTT-44, 105-113, 1996).

Results and Discussion

The spatial peak SAR values averaged over 1 g and 10 g of tissue were computed for the different heads exposed by the two dipole sources operating at 900 MHz and 1.8 GHz and at different distances. For the same exposure conditions, the spatial peak SAR values averaged over 1 g varied less than $\pm 20\%$ and those averaged over 10 g less than $\pm 15\%$. In conclusion, there is no significant difference between adults and children in the absorption of electromagnetic fields at both frequencies for a defined source at a given distance. However, if the position of MTE is defined in absolute angles with respect to the line connecting both auditory canals, the spatial peak SAR significantly depends on the shape of the head, which defines the distance between the RF currents on the device and the skin (N. Kuster et al., Mobile Communications Safety, Chapman&Hall, 13-64, 1996). Therefore, the maximum absorption occurring among a group of users including children can reliably and efficiently be simulated by using a homogeneous phantom of worst-case shape.

K88.11

Decomination of milk contaminated by some stable and pategenetic microorganisms (with mycobacteria as specific instances) by means of low-temperature U.H.F. irradiation.

B.I.Khaikin, Doctor of veterinary medicine, Proffesor, All-Russian Institute for Scientific Reseach in Brucellosis and Tuberculosis of Animal. Russia, Omsk, 644048, Pr.Marksa, 38, flat # 264, phone: (381-2) 41-99-38, E-mail: vsv@voskr.omsk.su

I.D.Zolotarev, Doctor of science (Engineering), Omsk State Engineering University. Russia, Omsk, 644050, Pr.Mira, 11, tel: (381-2) 63-04-39.

Unavailability of a realiable and easily controllable method of decontaminating milk, with pathogenic microorganisms as contaminants, results in frequent cases when people and animals, who take milk contact such diseases as tuberculosis, brucellosis and the like. At the same time, the decontamination procedures that have been in use are based on setting certain heat conditions (85° C for 30 minutes or boiling). The installations employed to this effect are cumbersome, their mode of operation is hard to control, they decrease the biological value of milk (with protein denatured andvitamins and ferments inactivated), moreover, they consumemuch electric power.

Microwaves to sterilize, various objects in fast volume heating conditi, with positive results achieved, have been applied in many countries, russia included.
/ F.Borodina, S.G.Kuznetsova, 1991 and others /. Howere most of the research dealt with the effect of heat conditions on microorganisms in matters other than milk.

Our research to theeffect of U.H.F. irradiation was carried out by means of an experimental plant that contained of a SHF oscillator, a wave guide line, an exposure chamber and a power unit. The subject of inguiry were samples of milk (20 ml) conta-
minated by potentially pathogenic mycobacteria (m.Perfingins close to virulentstocks from the point of thier stability.

The results of the multiple duplication showed that the optimum conditions in which 100% ofthe test objects were destroyed were the following: pulse length - 2.5 mcsec, pulse recurrence / repetition / frequency - 600 hertz and exposure - 10 sec. or 300 hertz fnd 17 sec. at a temperature of not more than 62° C. During the study of the qualities of the treated milk it was established that in compliance with the GOST 70-x standart requirement,they had not in the least become worse, some of them had ever improved, to mention just one point - pyroxidase test proved positive which testifies that the vitamins and ferments remained intact as well as possibly carbohydrates, and there was no bacteria contamination and the like. The main qualities appeared unchanged.

Conclusion.

The research testifies that the procedure of decontaminating milk, contaminated by some stable and pathogenic microorganisms / mycobacteria / by means of selective U.H.F. irradiation, which results in considerable power consumption decrease, shows promise and may serve to get environmentally pure biological produce of high value.

APS/URSI B — Session 12 — Salon Harricana

RCS Analysis and Measurements
Co-chairs: R. Burkholder, USA and S. Kashyap, Canada

08:10	12.1	Scattering from a Cylinder with Two Sets of Rotating Blades, **K.K. CHAN**[1], R. MARTIN[2], F. TREMBLAY[2], [1]*Chan Technologies Inc., Kirkland, QC and* [2]*Defence Research Establishment, Ottawa, ON, Canada (APS)*
08:30	12.2	Target Identification in the Time-Frequency Domain, **I. JOUNY**[1], P. KARUNARATNE[1], M. AMIN[2], [1]*Lafayette College, Easton and* [2]*Villanova University, Villanova, PA, USA (APS)*
08:50	12.3	Electromagnetic Excitation of a Thin Wire: A Traveling-Wave Approach, **J.C. BOGERD**[1], A.G. TIJHUIS[2], J.J.A. KLAASEN[1], [1]*TNO Physics and Electronics Laboratory, Gravenhage and* [2]*Eindhoven University of Technology, Eindhoven, The Netherlands (APS)*
09:10	12.4	PO Analysis of Depolarizing Trihedral Corners, C. GENNARELLI[1], **G. RICCIO**[1], G. PELOSI[2], [1]*Università di Salerno, Fisciano and* [2]*Università di Firenze, Florence, Italy (APS)*
09:30	12.5	Scattering Analysis of Bodies of Revolution by MEI, J. CHEN, **W. HONG**, *Southeast University, Nanjing, China (APS)*
09:50	12.6	Backscattering Characteristics of Finite Narrow Rectangular Loop Array, **T.M AU**, Y.W.M. CHIA, M.-S. LEONG, *National University of Singapore, Singapore Park, Singapore (APS)*
10:10	12.7	Electromagnetic Scattering by Finite Periodic Strip Grating on a Grounded Dielectric Slab, **J.I. LEE**, Y.K. CHO, *Kyungpook National University, Taegu, Korea (APS)*
10:30	12.8	Analysis of a Parallel-Plates Open Resonator, K. ADAM, **D.I. KAKLAMANI**, K. UZUNOGLU, *National Technical University of Athens, Greece (APS)*
10:50	12.9	Sources for OTH Radar Array Calibration, **I.S.D. SOLOMON**[1,2,3], D.A. GRAY[2,3], Yu.I. ABRAMOVICH[2,4], [1]*Defence Science and Technology Organisation, Salisbury,* [2]*CRC for Sensor Signal and Information Processing (CSSIP),* [3]*University of Adelaide and* [4]*University of South Australia, Adelaide, Australia (APS)*
11:10	12.10	Scattering Analysis of 3-D Body by MEI, J. CHEN, **W. HONG**, *Southeast University, Nanjing, China (APS)*
11:30	12.11	UHF Periscope Detection and Discrimination, **I.H.H. ZABEL**, P.K.W. PHU, *Massachusetts Institute of Technology, Lexington, MA, USA (URSI)*
11:50	12.12	RCS and Radar Detection of Submarine Masts, **S. KASHYAP**, A. LOUIE, A. DROSOPOULOS, *Defence Research Establishment, Ottawa, ON, Canada (URSI)*

JOINT-12.11

UHF Periscope Detection and Discrimination

Ingrid H. H. Zabel and Phillip K. W. Phu
Massachusetts Institute of Technology
Lincoln Laboratory

UHF airborne early warning systems may offer potential for both periscope detection and discrimination at long range. We present UHF doppler and time domain scattering signatures of periscopes and discuss detection performance as a function of periscope height and type, sea state, and dwell time from measurements made with Lincoln Laboratory's Radar Surveillance Technology Experimental Radar (RSTER). We find that for long dwell times, the periscope return dominates over the surrounding sea clutter. The periscope return is narrow in doppler space, whereas the sea clutter is broad-band and centered slightly off of zero doppler. The periscope scattering signature is modulated in the time domain by a function with a period on the order of 10 seconds; other observations suggest that this modulation is due to fluctuating multipath from the sea surface. We can detect periscopes in relatively high sea states given sufficient dwell time. We are unable to discriminate the periscope types investigated; this is expected at UHF, where the wavelength is longer than the discriminating structural features on the masts. Measurements were made at low grazing angles; we extend these measurements to higher grazing angles using method of moments RCS modeling. This modeling suggests an operational mode for periscope detection that is practical for airborne early warning systems. To begin to address the discrimination problem, we compare doppler signatures of periscopes and a small boat, both moving and under power. The boat's doppler signature typically has a larger spread than the periscope's. We find that bulk filtering, based possibly on doppler signature, target RCS, or length may go a long way toward improving periscope discrimination capabilities of early warning radar.

This work was sponsored by DARPA under Air Force contract F19628-95-C-0002. Opinions, interpretations, conclusions, and recommendations are those of the author and are not necessarily endorsed by the United States Air Force.

RCS and Radar Detection of Submarine Masts

S. Kashyap, A. Louie and A. Drosopoulos
Defence Research Establishment Ottawa
Ottawa, Ontario, Canada

A submarine depends upon its masts for its operation. Figure 1 shows a typical mast configuration of a submarine. These masts include periscopes, communication masts, electronic counter-measures (ECM) masts, among others. The radar cross-section (RCS) of these masts must be minimized to avoid detection by enemy radar. The RCS varies with the number of masts, the size and shape of the masts, and whether they are coated with an appropriate radar absorbing material (RAM). The RCS is also a function of the sea state, because of the induced rocking motion, and because of the blockage of the microwaves by the sea surface. In addition to these factors, the detection of the masts by an airborne radar depends also upon radar parameters and effects of the sea clutter.

This paper concerns the computation of the RCS of submarine masts, and includes an investigation into various aspects of airborne radar detection of submarine masts under different mast states and sea states. We use the physical theory of diffraction (PTD) to compute the RCS of the masts, with their axes leaning at various angles to the sea surface, to represent fluctuation due to the rocking motion under different sea states. We also find the probability of mast detection by an airborne radar for the noise-limited and the sea-clutter-limited cases.

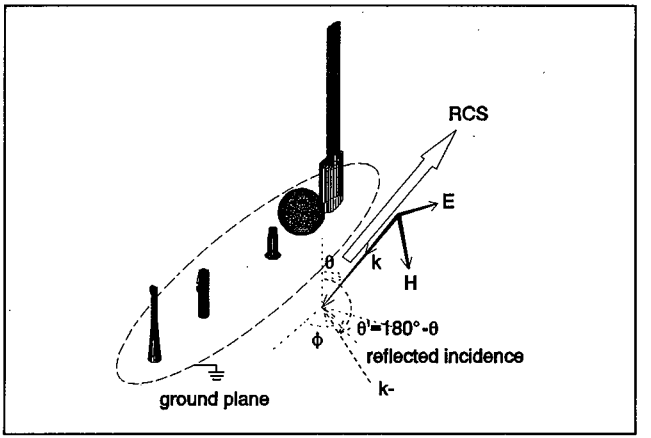

Figure 1 A submarine mast configuration used for analysis.

APS/URSI D **Session 26** **Salon Richelieu**

Microwave, MM-Wave and Optical Devices and Circuits
Co-chairs: G. Rebeiz, USA and G. Haussmann, USA

13:10 26.1 Microwave and Millimeter-Wave Propagation in Photonic Band-Gap Structures, **J.D. SHUMPERT**, T. ELLIS, G. REBEIZ, L.P.B. KATEHI, *University of Michigan, Ann Arbor, MI, USA (URSI)*

13:30 26.2 A Study of a Grid Amplifier Circuit Using a Two Dimensional Array of Slots, **N. BAILEY**[1], R.M. WEIKLE, II[2], [1]*National Radio Astronomy Observatory and* [2]*University of Virginia, Charlottesville, VA, USA (URSI)*

13:50 26.3 Effects of the Variations of the Doping Densities on the Performance of High Efficiency LHL InP IMPATT Diodes, **E.-S.A. EL-BADAWY**[1], S.H. IBRAHIM[2], H.A. EL-MOTAAFY[3], [1]*International Islamic University Malaysia (IIUM), Kuala Lumpur, Malaysia;* [2]*EED, MTC and* [3]*High Technology Institute (HTI), Cairo, Egypt (URSI)*

14:10 26.4 Modeling of IMPATT Diode and High Power Operation of IMPATT Oscillator, **S. KAR**, *Institute of Radiophysics and Electronics, Calcutta, India (URSI)*

14:30 26.5 Inter-Computer Free-Space Data Link, **S. AKBAR**, *PAF Academy, Risalpur, Pakistan (URSI)*

14:50 26.6 A Ka-Band GaInP/GaAs HBT Double Balanced Downconvert Mixer Using Lumped Element Balun, **A.P. FREUNDORFER**, *Queen's University, Kingston, ON, Canada (APS)*

15:10 Coffee Break

15:30 26.7 A Ka-Band GaInP/GaAs HBT Receiver, **A.P. FREUNDORFER**, Y. JAMANI, *Queen's University, Kingston, ON, Canada (APS)*

15:50 26.8 Computer Simulation for Optical Manipulator Using Fiber-Probe by GMEIE's, **M. TANAKA**, K. TANAKA, *Gifu University, Gifu, Japan (URSI)*

16:10 26.9 New Boundary Integral Equations of Photon Scanning Tunneling Microscope, K. TANAKA, **M. TANAKA**, *Gifu University, Gifu, Japan (URSI)*

16:30 26.10 Inexpensive Submillimeter Wavelength Receiver Components, **T.W. CROWE**[1], C.M. MANN[2], W.L. BISHOP[1], P.J. KOH[1], J.L. HESLER[1], R.M. WEIKLE, II[1], [1]*University of Virginia, Charlottesville, VA, USA;* [2]*Rutherford Appleton Laboratory, Didcot, UK (URSI)*

JOINT-26.1

Microwave and Millimeter-wave Propagation in Photonic Band-Gap Structures

J. D. SHUMPERT*, T. ELLIS, GABRIEL REBEIZ, AND LINDA P. B. KATEHI
RADIATION LABORATORY
DEPARTMENT OF ELECTRICAL ENGINEERING AND COMPUTER SCIENCE
THE UNIVERSITY OF MICHIGAN, ANN ARBOR, MI 48109-2122 USA

Electromagnetic wave propagation in periodic dielectric media is analogous to electron-wave propagation in crystals. From solid-state theory, we know that semiconductors allow electron conduction without scattering only in certain "band-gaps". Early work at optical frequencies successfully demonstrated that light propagation could be inhibited in certain frequency gaps in special photonic crystals [E. Yablonovitch, Phys. Rev. Lett., 58 (20), 2059-62, 1987]. Carrying this idea into the macroscopic world, preliminary results suggest that microwave and millimeter-wave frequencies could be also be manipulated by carefully designing and fabricating photonic structures composed of regions of differing dielectric constants. This inhibition of electromagnetic wave propagation in periodic dielectric media is due to interference effects between the alternating regions of high and low dielectric constants. Although the term *photonic band-gap* is used extensively in the literature, the reality of extending this property to infrared and other frequencies suggests that the former term be replaced by *electromagnetic band-gap*. Photonic band-gap structures are found to have unique properties that are advantageous in applications involving semiconductor integrated circuits. Such structures offer the advantage of changing the physical properties of substrates used in fabricating planar circuits. A number of applications for such a structure can be imagined including dielectric mirrors, resonant cavities, filters, isolators, and waveguides.

For simple structures, one can theoretically determine the eigenvalues and subsequently the band-gap regions of the system. In order to determine the frequencies of interest for a complex structure, a moment method code has been developed to determine the eigenvalues of a two-dimensional, inhomogeneous dielectric region. This region is then used as a unit cell of a three-dimensional structure. By using the periodicity of the unit cell, one can model the photonic structure and determine the desired band-gaps. Future work should include metallizing the cover layer to include antennas and other more interesting circuit components.

In parallel to the theoretical modeling, experimental studies with micro-machined dielectrics are under way to corroborate the theoretical values for the band-gaps. A one-dimensional periodic dielectric substrate has been fabricated and tested to see if the band-gap predicted by coupled-mode theory exists for microstrip excitation. After establishing the existence of this band-gap in one-dimensional structures at microwave frequencies, many different two-dimensional lattice structures including the square, hexagonal, and rectangular lattices, have been fabricated and tested. Results from these experiments will be presented and compared to theoretical predictions at the conference.

A Study of a Grid Amplifier Circuit using a Two Dimensional Array of Slots

Nancyjane Bailey* and Robert M. Weikle, II

School of Engineering and Applied Science
University of Virginia, Charlottesville, VA 22903

* National Radio Astronomy Observatory
2015 Ivy Road, Charlottesville, VA 22903

All grid amplifiers reported to date have used a two-dimensional array of dipoles as the radiating elements. Transistors are placed at the intersections of the dipoles, so the only grid parameters a designer can adjust are the width and length of the dipoles. External polarizers and tuning slabs are often required.

This work examines a new grid amplifier circuit that uses a two-dimensional array of slot radiators. The slots are fed by coplanar waveguide feedlines. Transistors are embedded in the feedlines, which act as part of a matching network. The input and output slots are orthogonally polarized, providing isolation between the amplifier input and output.

Two circuits were built and tested. The first was a 5×5 array. This circuit proved to be unstable at the design frequency. The second circuit consisted of a single unit cell (see figure 1 below). This circuit also exhibited instabilities, but was stable when only one device in the cell was biased. With a single device biased, the amplifier circuit had 11.4 dB of gain at 5.1 GHz. With both devices biased, the circuit could be stabilized by adding a diagonal metal sheet that split the unit cell in half. Coupling between the orthogonal input and output slots is believed to be the cause of the instability. At present, it is not clear if the instability is inherent to this array architecture or is a feature of the specific geometry of the unit cell. Currently, a full-wave analysis of the cell is being conducted and the results will be reported at this conference.

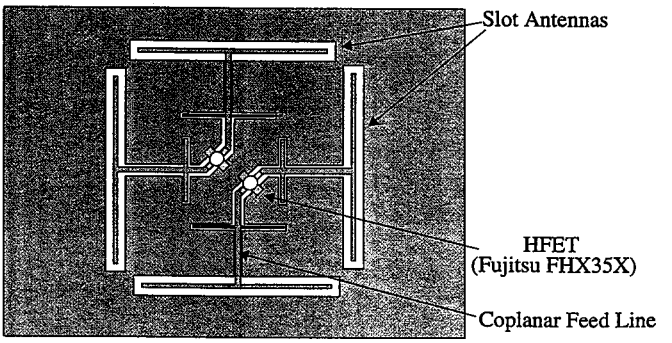

Figure 1. Diagram of the single-cell quasi-optical amplifier.

JOINT-26.3

Effects of the Variations of the Doping Densities on the Performance of High Efficiency LHL InP IMPATT Diodes

El-S. A. El-Badawy[1], S. H. Ibrahim[2], and H. A. El-Motaafy[3]

[1] ECED, Fac. of Engineering, International Islamic University Malaysia(IIUM), Jalan Gombak, 53100 Kuala Lumpur, Malaysia, e-m: sayed@iiu.my, Fax: 603-6867566. Senior Member IEEE, Member of OSA.
[2] EED, MTC, Cairo, Egypt.
[3] EED, High Technology Institute(HTI), Ramadan-Tenth City, Cairo, Egypt.

Abstract

The purpose of this paper is to shed further light on the effects of the variations of the doping densities of the drift and avalanche regions and the size of the doping clump on the performance of n-type LOW-HIGH-LOW (LHL) IMPATT diodes with wide range of structural parameters. This has been achieved by studying the performance of a properly-chosen set of such devices employing an IMPATT diode full-scale computer simulation program (H. A. El-Motaafy "Full-scale Computer Simulation of TRAPATT Diodes", The Third National Radio Science Conference, Cairo, Egypt, 1985).

It is found that if the doping density in the drift region, N_d, is too low, the diode will operate according to the regular IMPATT mode. If N_d is increased, the diode will be capable of supporting high-efficiency modes where the avalanche generated pulse (AGP) is bunched and accelerated and may be prematurely collected by the undepleted region. If N_d is too high, the depletion layer width modulation (DLMW) effect degrades the performance. Furthermore, the bunching and acceleration of the AGP will be less significant. It is found that by increasing N_d, optimum values of the dc-bias current and the operating frequency increase, but the optimum RF voltage level decreases; this is attributed to the fact that an increase in N_d makes the DLWM effect more significant. It is also shown that for a given set of operating conditions there is an optimum value of N_d below which the high efficiency operation may be suppressed and the diode operates according to the regular IMPATT mode.

The effects of the variation of the avalanche region doping density, N_a, and the size of the doping clump, Q_c, are also investigated. It is found that: the variation of N_a has no significant effect on the performance , the optimum RF level is slightly reduced with increasing N_a, the efficiency increases with Q_c, and, in the regular IMPATT mode, the optimum RF level increases with Q_c.

Modeling of IMPATT diode and High Power Operation of IMPATT Oscillator

Subal Kar

Institute of Radio Physics & Electronics,
92, A. P. C. Road, Calcutta : 700 009, INDIA

A large-signal analytical model for IMPATT diode has been developed. With practical approximations near the oscillation threshold the model equations are :

$$G_D = -3\frac{\alpha'}{\theta}(1-\cos\theta)\ I_{d.c}\left(1-\frac{9}{8}\frac{\alpha'^2}{\theta^2}\ v_{r.f}^2\right)$$

$$I_{th} = \theta^2\,\omega_0^2\,C_d^2\ R_s / 3\alpha'(1-\cos\theta)$$

$$v_{r.f}^2 = 4\theta^2\,(I_{d.c} - I_{th}) / 9\alpha'^2\,I_{th}$$

$$P_0 = \frac{1}{2}\left|G_D\right| v_{r.f}^2$$

The analysis and also the experiment used SDR (p^+nn^+) Silicon IMPATT diode (Type No: HP 5082-0432) in X-band (8-12 GHz)
[With $\alpha' = 0.176V^{-1}$, $\theta = 0.74\pi$, $C_d = 0.5$ pF, $R_s = 1.6$ ohms].

Numerical results show that smaller values of the parasitic series resistance (R_s) can produce higher power output (P_o), thus diamond heat-sink with very small R_s will be suitable for the design of high power microwave and millimeter-wave sources. The nature of variation of the power output (P_o) with d.c bias current($I_{d.c}$) obtained from the model and also from the experiment are in good agreement and the power saturation at higher current levels observed in both the curves may be explained on the basis of the model in which $v_{r.f}$ saturates at large $I_{d.c}$. The optimum threshold current for oscillation to yield maximum power output has been observed experimentally to be one third of the typical d.c. operating current as specified by the manufacturers and this is in agreement with the I_{th} calculated from the model for maximum power output.

Further work on modeling is in progress to investigate the effect of harmonic frequency circuits on the improvement of the power output of IMPATT oscillator which will help to account for the experimentally observed (S. Kar and S. K. Roy, Int. J. of Elect., 75, 941-950, 1993) increase of the power output of an IMPATT oscillator with the device embedded in a modified resonant-cap cavity (a double-resonant circuit) with optimally chosen resonant frequencies.

JOINT-26.5

INTER-COMPUTER FREE-SPACE DATA LINK

Dr. Salim Akbar, Department of Avionics Engineering,
College of Aeronautical Engineering, PAF Academy, Risalpur, Pakistan

This paper describes electronic circuits and software of semiconductor-laser based free-space digital link for inter-computer data communications. Block diagrams and schematics of designed and tested circuitry are presented.

The free-space inter-computer data link operates between two personal-computers in half-duplex handshake-mode, without the use of standard modems (modulators/demodulators). The computers' serial ports, compatible with the RS-232C protocol, have been employed for data transmission and reception and a parallel port on each computer has been used for handshake signals. The handshake signals and transmitted/received data have been converted to one-line serial transmission/reception with the help of simple transmitter/receiver interface circuits featuring voltage-level translations and tri-state buffers. The serial-data handshake signals in the transmitters, at each end, are fed to an electrical laser-drive circuitry which, in turn, feeds an aluminum gallium arsenide semiconductor laser. Three different schemes for electrical modulation of semiconductor lasers are also discussed and detailed circuits are presented. The received optical data at the other ends is converted back to electrical signals using a large-area silicon photovoltaic photodiode detector and a transresistance amplifier circuit. From the received signals, the data and handshake information are recovered using the mentioned interface circuitry before feeding to computers' serial and parallel ports, respectively. Based on data exchange, the two computers undertake necessary processing and may, consequently, feed data to external peripheral devices such as remote optical search and tracking systems based on quadrant photodiodes, and remote antenna positioning systems. Electronic circuit implementation for interfacing the above two applications with the personal computers are also described in detail.

Computer Simulation for Optical Manipulator using fiber-probe by GMEIE's

Masahiro Tanaka and Kazuo Tanaka
Department of Electronics and Computer Engineering Gifu University
1-1 Yanagido, Gifu city, Gifu 501-11, Japan
Tel. 81-58-293-2779 Fax 81-58-230-1895
e-mail: masahiro@tnk.info.gifu-u.ac.jp and tanaka@tnk.info.gifu-u.ac.jp

An optical manipulator is a technology to trap and manipulate a very small particle using laser-light force. In this presentation the fiber-probe which has a tip is used to trap and manipulate a very small particle (D.W.Pohl and D.Courjon ed., "Near Field Optics," Kluwer Academic Publishers, 1993). Since it can occur to trap and manipulate only spatial condition, it is very difficult to understand intuitively. So we have to calculate the force on the particle, for we know whether it is possible or impossible. There are few papers to report the force on the particle by the light emitted from the fiber-probe. However most of them are calculated by using geometrical theory. It is necessary to simulate using by more accurate method.

We have already reported a new method of the optical manipulator using uncoated fiber-probe (M.Tanaka and K.Tanaka, Trans. IEICE Japan, **J79-CI**, 101-108, 1996 (Japanese), M.Tanaka and K.Tanaka, submitted to J. Opt. Soc. Am. A). In this presentation we show a method and results of computer simulation for the 2 dimensional optical manipulator using the optical-fiber coated with perfect conductor.

The method is based on Guided Mode Extracted Integral Equations (GMEIE's) which have developed in Gifu University, Japan (K.Tanaka and M.Kojima, J. Opt. Soc. Am. A, 6, 667-674, 1989). GMEIE's can be solved by using only conventional boundary element method or moment method without mode expansion technique etc.. And the force exerting on the particle can be calculated by Maxwell's stress tensor and/or Lorentz's force. We can check the results of GMEIE's by using the energy conservation law and the forces by using equality between above two different expressions of the forces. Computer simulation results satisfies the energy conservation law within an accuracy of 0.1% and satisfy the equality between two different expressions of the force within an accuracy of a few percents. We can compare physical properties of two types of fiber-probe which are not coated and coated with perfect conductor.

JOINT-26.9

New Boundary Integral Equations of Photon Scanning Tunneling Microscope

Kazuo Tanaka and Masahiro Tanaka
Department of Electronics and Computer Engineering of Gifu University,
Yanagido Japan 501-11,

Recent development of near-field optics (NFO) anticipates promising and fantastic applications such as an ultra high-resolution optical scanning microscope called photon scanning tunneling microscope (PSTM) and optical manipulator for small particles [D.W.Pohl and D.Courjon ed., "Near Field Optics", Kluwer Academic (1993), M. Ohtsu, Oyo Buturi **65**, 2(1996)]. Since it is difficult to apply conventional optical theory to NFO, it is important subject to find accurate and efficient method in developing software of computer-aided design (CAD) and simulations of NFO equipment. Especially, the basic and effective simulator of PSTM is strongly expected.

So far, many researchers have tried to use various techniques. Integral equation method are most popular among them, because we can apply various techniques in solving integral equations. However, most of these works presented so far employed some kind of approximation in the formulation and/or in numerical calculations.

We have developed a boundary-element method based on new integral equations called Guided-Mode Extracted Integral Equations (GMEIE's) for CAD of optical waveguide circuits [K.Tanaka and M.Tanaka, J. Opt. Soc. of Am. A, **13**, 1362 (1996)]. In this paper, we apply GMEIE's to simulations of the two-dimensional NFO problems and show the validity of our new method in analyzing NFO problems. We have applied GMEIE's to the optical manipulator [M.Tanaka and K.Tanaka, Trans. of IEICE Japan **J79-C-I**, 101(1996), M.Tanaka and K.Tanaka, submitted to J. Opt. Soc. Am. A (1996)] previously. So, a PSTM is analyzed by using GMEIE's in this paper. Rigorous boundary integral equations for PSTM are derived and they are solved by the conventional boundary-element method. A strong point of our new method is that numerical results can be verified by several universal laws. For the problem treated in this paper, we can derive three universal laws, i.e., optical theorem for collection-mode, energy conservation law for illumination-mode and reciprocity relation between collection-mode and illumination-mode. Results of numerical simulations by this method are verified by using these universal laws. Many important physical properties are investigated in detail by the numerical simulations.

INEXPENSIVE SUBMILLIMETER WAVELENGTH RECEIVER COMPONENTS

Thomas W. Crowe, Chris M. Mann†, William L. Bishop, Philip J. Koh, Jeffrey L. Hesler, Robert M. Weikle, II

Applied Electrophysics Laboratories
University of Virginia
Charlottesville, VA 22901

† Space Science Department
Rutherford Appleton Laboratory
CHILTON, DIDCOT, OXON
OX1 1OQx, United Kingdom

Abstract

The submillimeter wavelength portion of the electromagnetic spectrum has been primarily exploited only for scientific applications, such as radio astronomy, studies of the composition of the upper atmosphere, chemical spectroscopy and plasma diagnostics. The most significant impediment to potential commercial applications is the overwhelming cost of building standard receiver components, such as sources and mixers. Although many groups have demonstrated quasi-optical components which in principal can be manufactured at low cost, the best receivers† and sources continue to rely on waveguide technology and whisker contacted GaAs Schottky barrier diodes. However, three relatively recent developments promise to make the manufacture of submillimeter components much more cost efficient. These are the fabrication of excellent planar (whiskerless) GaAs Schottky diodes, the availability of advanced computer aided design tools suitable for this wavelength range, and the demonstration of inexpensive techniques for fabricating large numbers of waveguide components.

This talk will begin with a review the status of all-solid-state heterodyne receivers and sources based on planar GaAs Schottky mixers and multipliers. Next the design of a 585 GHz fundamentally pumped mixer with Hewlett Packard's Microwave Design System software will be reviewed. This mixer has yielded results comparable to the best whisker contacted mixer in this frequency range, but has the benefit of using planar diodes and achieves wide RF bandwidth with no physical tuning elements. Finally, the potential fabrication of large quantities of high quality submillimeter wavelength waveguide assemblies by micromachining and molding techniques will be presented.

† *Excluding superconductive mixers which require cooling to cryogenic temperatures and are thus not practical for commercial applications.*

APS/URSI G **Session 32** **Salon Jolliet**

Propagation and Telecommunication - Part II
Co-chairs: B. Reinisch, USA and J.W. McDougall, Canada

10:30 32.1 Ionospheric Effects on Synthetic Aperture Radar at VHF, **T.J. FITZGERALD**, *Los Alamos National Laboratory, Los Alamos, NM, USA (URSI)*

10:50 32.2 Ionospheric Frequency-Dispersion Effects in Polarimetric Spaceborne-Radar Applications, **Y. LE HELLOCO**, B. UGUEN, G. CHASSAY, *Laboratoire Composants et Systèmes pour Télécommunications, Rennes, France (URSI)*

11:10 32.3 Effects of Ionosphere 3D-Disturbance on Waveguide Propagation, **T.I. BICHUTSKAYA**[1], G.I. MAKAROV[2], *St. Petersburg University, St. Petersburg, Russia (URSI)*

11:30 32.4 Antenna and Ionospheric Propagation Analysis of Marconi's Experiment in Newfoundland, **S.A. SAOUDY**, A. SINHA, B. YAN, B.P. SINHA, *Memorial University of Newfoundland, St. John's, NF, Canada (APS)*

11:50 32.5 Temporal Variations of the Wideband Indoor Wireless Millimeter-Wave Channel, **P. MARINIER**, G.Y. DELISLE, C.L. DESPINS, *INRS-Télécommunications, Verdun, QC, Canada (APS)*

JOINT-32.1

Ionospheric effects on synthetic aperture radar at VHF

T. Joseph Fitzgerald
Los Alamos National Laboratory, Los Alamos, New Mexico 87545

Synthetic aperture radars (SAR) operated from airplanes have been used at VHF because of their enhanced foliage and ground penetration compared to radars operated at UHF. A satellite-borne VHF SAR would have considerable utility but in order to operate with high resolution it would have to use both a large relative bandwidth and a large aperture. The presence of the ionosphere in the propagation path of the radar will cause a deterioration of the imaging because of dispersion over the bandwidth. The range resolution of a SAR is given by $\rho_r \approx c/2B$ where B is the bandwidth and c is the speed of light. Therefore, as the center frequency, f_c, is reduced, a larger relative bandwidth, B/f_c, is necessary to attain the same resolution. The azimuth resolution of a SAR, ρ_a, is given by

$$\rho a \approx \frac{c/f_c}{4\sin\frac{\Delta\theta}{2}} \tag{1}$$

where $\Delta\theta$ is the synthesized angular aperture. As the frequency is reduced the size of the aperture, $\Delta\theta$, must be increased to retain the same resolution. The first effect of the ionosphere on a SAR pulse is to produce a group path change; that is, the target will appear to be displaced in range, Δr. This effect depends upon the operating frequency, f_c, and the integrated electron column density (total electron content or TEC) along the ray path and is $\Delta r \approx 81$ TEC/f_c^2 meters if f_c is given in Hz and TEC in m^{-2}. Values of TEC of 10^{17} m^{-2} give $\Delta r \approx 130$ m at $f_c = 250$ MHz. The displacement will also be affected by refractive effects as the radar pulse traverses the ionosphere. The second effect of the ionosphere on the radar pulse is that of dispersion; that is, higher frequencies will return sooner than lower frequencies from the same target. The amount of spreading, $\Delta\rho r$ depends upon the bandwidth of the pulse and is given by

$$\Delta pr \approx \Delta r\left[\frac{1}{\left(1-B/2f_c\right)^2}-\frac{1}{\left(1+B/2f_c\right)^2}\right]. \tag{2}$$

In this paper we present calculations of the effects of a deterministic slab ionosphere on SAR imaging for a radar operated with a 100 MHz bandwidth centered at 250 MHz and over an angular aperture of 23° at a look angle of 26°. An ionosphere with vertical TEC of $10^{17}m^{-2}$ induces a point spread function with an approximate halfwidth of 150 m in the slant-range direction compared to the nominal resolution of 1.5 m.

Ionospheric frequency-dispersion effects in polarimetric spaceborne-radar applications

Y. Le Helloco, B. Uguen and G. Chassay

Laboratoire Composants et Systèmes pour Télécommunications (LCST)
URA CNRS 834 - INSA
20, avenue des buttes de Coësmes, 35043 Rennes cedex, France

Introduction

Over the past few years, progress in polarimetric treatment and SAR imaging has led to a wider use of polarimetric tools in the study of high resolution radar data. We analyze here the Ionosphere frequency-dispersion effects on the quality of these polarization-diversity images.

Ionosphere dispersion effects on the wideband SAR images quality

The Ionosphere is a frequency-dependent medium which leads to a frequency-dependent value of the refraction index. Furthermore, the Ionosphere is anisotropic. This leads to the well-known Faraday effect. Therefore, the transmitted electromagnetic wave undergoes frequency-dependent phase shift and attenuation, which lead to an alteration of the wideband signals and the image resolution [ENERT P., International Conference on Radar, 512-517, 1994]. Consideration is given in this presentation to the polarization-diversity linear-frequency modulated gaussian and rectangular shaped pulses. In particular, a novel wideband polarimetric formalism is investigated.

Ionosphere dispersion effects on the SAR images polarimetric information

In full polarimetric SAR applications, we have to deal not only with resolution alterations, but also with polarimetric information lost. The first point we take into account is the non-reciprocal Faraday rotation influence on some widely-used polarimetric tools such as the covariance matrix or the Huynen parameters. This is performed by introducing a suitable methodology and deriving the measured parameters as a function of the target ideal parameters. We also show that the polarization degree of the propagated electromagnetic wave is less than unity, because of the frequency-dependent nature of the Faraday rotation. This so-called depolarization effect is quantitatively analyzed from a radar system point of view (up and down propagation), through a Stokes vector and wave coherency matrix formalism.

Conclusion

To conclude, the Ionosphere-dispersion effects on the wideband signals and SAR images are studied in the case of polarization-diversity systems, which emit short pulses. These different aspects are investigated in a radar situation and are shown to be significant in the case of wideband low-frequency (P,L band) applications.

JOINT-32.3

Effects of Ionosphere 3D-Disturbance on Waveguide Propagation

T.I.Bichutskaya, G.I.Makarov
St.Petersburg University,
Institute of Radiophysics,
St.Petersburg, Russia

Introduction

The presence of a border 3D-irregularity in the waveguide leads ,among other effects, both to vertical and to horizontal polarization of the scattered electromagnetic field whatever the polarization of transmitted field. It has usually been suggested (E.C.Field et al.,Radio Sci. 21, 511-517, 1986) this depolarization is negligible that gives rise to the simplified scalar problem. In the present paper the problem is considered as vector and the above mentioned effects are studied and estimated.

Discussion

The strong problem of propagation of electromagnetic waves of point vertical electric dipole in the 3d-irregular earth-ionosphere waveguide is 6-vector one. The solution of Maxwell's equations is constructed as the sum of vertical vector modes with coefficients containing the lateral dependence. The vertical problem is formulated in each cross-section of irregular waveguide. The result of integrating of differential equations in the ionosphere determines the effective reflection height and the ionosphere impedance - the parameters that are needed to resolve the vertical problem . The local both TE and TM modes are characterized by complex eigenvalues and by vector eigenfunctions of the transverse operator and are utilized as the basis vector functions to resolve a lateral problem. The system of dependent lateral equations in partial derivatives is solved by both numerically integrating and geometrical optics method . In the last case the phase and amplitude of lateral distribution of field in zero aproximation are determined of the eikonal equation and the transfer equation. In this problem the real part of lateral wave number is analogous to a refractive index and its imaginary part determines the field absorption. The differential equation for a beam divergence added to the equations in ray variables describing the ray trace are integrated numerically. As result the focusing effects of 3d-irregularity were obtained. The numerically integrating of lateral equations system gives rise to the estimation of depolarizating effect of a border 3d-irregularity.

Conclusion

It is presented the theoretical computations which evaluate the both depolarizating and focusing effects of ionosphere 3d disturbance on VLF propagation in the earth-ionosphere waveguide. The evaluation of these effects shows that its magnitude is strongly dependent on irregularity position relatively the propagation path.

APS/URSI B

Session 34

Salon MacKenzie

Advances in Finite Element Techniques
Co-chairs: M. Salazar-Palma, Spain and S. Kubina, Canada

08:10 34.1 Hybrid MoM/SBR and FEM/SBR Methods for Scattering by Large Bodies with Inhomogeneous Protrusions, **J.M. JIN**, F. LING, X.Q. SHENG, *University of Illinois at Urbana-Champaign, Urbana, IL, USA (APS)*

08:30 34.2 A 2-D Edge-Based Singular Element for the Full-Wave Finite-Element Analysis, **Z. PANTIC-TANNER**[1], J.S. SAVAGE[2], D.R. TANNER[3], A.F. PETERSON[2], [1]*San Francisco State University, San Francisco, CA,* [2]*Georgia Institute of Technology, Atlanta, GA and* [3]*Lockheed Martin, Sunnyvale, CA, USA (URSI)*

08:50 34.3 A Novel Class of Hierarchical Higher Order Tangential Vector Finite Elements for Electromagnetics, **L.S. ANDERSEN**, J.L. VOLAKIS, *University of Michigan, Ann Arbor, MI, USA (APS)*

09:10 34.4 Analysis of Ferrite Loaded Cavity Backed Slot Antennas Using a Hybrid FEM/MoM Approach, **A.C. POLYCARPOU**, C.A. BALANIS, *Arizona State University, Tempe, AZ, USA (APS)*

09:30 34.5 Analysis of Large Cavity Field Problems Using a Finite Element Formulation of the Connection Scheme, J. LOUKOTA[1], **S. CASTILLO**[2], J.B. MILLARD[2], R. JEDLICKA[2], [1]*Motorola Space and Systems Technology Group, Scottsdale, AZ and* [2]*New Mexico State University, Las Cruces, NM, USA (APS)*

09:50 34.6 A PVM Based Parallel Sparse Matrix Equation Solver to Speed up Computation of MEI Method, **R.M.M. CHEN**, G.F. NIU, Y.W. LIU, K.K. MEI, *City University of Hong Kong, Kowloon, Hong Kong (APS)*

10:10 Coffee Break

10:30 34.7 Error Estimation and h-Adaptivity for Optimal Finite Element Analysis, **T. CWIK**, J. LOU, *California Institute of Technology, Pasadena, CA, USA (APS)*

10:50 34.8 Analysis of Microwave Integrated Circuits Using the Finite Element Method, **A.C. POLYCARPOU**, C.A. BALANIS, *Arizona State University, Tempe, AZ, USA (APS)*

11:10 34.9 Analysis of Arbitrary Shaped Cross-Sectional Discontinuity in Rectangular Waveguides Using FEM-BIM with Triangular Prism Elements, **J. PARK**, S. NAM, *Seoul National University, Seoul, Korea (APS)*

11:30 34.10 Application of High-Order Finite Element in Grid Truncation Scheme for Open Region Electromagnetic Problems, Y. ZHAO, **Y.-Y. WANG**, *Southeast University, Nanjing, China (APS)*

11:50 34.11 An Anisotropic Perfectly Matched Layer-Absorbing Medium in Finite Element Time Domain Method for Maxwell's Equations, **V. MATHIS**, *Dassault Electronique, Saint Cloud, France (APS)*

JOINT-34.2

A 2-D EDGE-BASED SINGULAR ELEMENT FOR THE FULL-WAVE FINITE-ELEMENT ANALYSIS

*Z. Pantic-Tanner**
San Francisco State University
San Francisco, CA 94132

J. S. Savage
Georgia Institute of Technology
Atlanta, GA 30332-0250

D. R. Tanner
Lockheed Martin
Sunnyvale, CA 94088-3504

A. F. Peterson
Georgia Institute of Technology
Atlanta, GA 30332-0250

The finite element method (FEM) based on edge elements is a powerful numerical technique for solving a variety of waveguide and cavity problems. However, many of these structures contain conducting or dielectric edges embedded in an inhomogeneous isotropic or anisotropic medium, and the field behavior can be singular in the vicinity of these edges [J. Meixner, AP-20, 442, 1972], [J. Van Bladel, Oxford: Clarendon Press, 1991]. If polynomial edge-elements are used to model these rapidly varying fields, it becomes necessary to use a fine mesh in the vicinity of the edge [P. Daly in J. R. Whiteman Ed, London: Academic Press, 337, 1973]. The increase in the number of unknowns in the mesh has the effect of increasing the computational time as well as memory requirements. One way of coping with the singular field behavior is to augment the trial functions with appropriate singular functions associated with a nodeless (unknown) variable [J. P. Webb, MTT-36, 1819, 1988] which leads to an increase of the bandwidth of the global FEM matrix. A more efficient approach is to use singular elements. In this case the ordinary elements touching the singular node are replaced with singular elements whose trial functions properly model singular field behavior. Scalar singular elements have been used in various FEM formulations resulting in faster convergence of the numerical solution [Z. Pantic and R. Mittra, MTT-34, 1096, 1986], [J. M. Gill and J. Zapata, MTT-42, 92, 1994], [Z. Pantic-Tanner, C. H. Chan, and R. Mittra, URSI Symp. Dig., 336, 1988]].

In this paper a new edge-based singular element similar to one presented in [Z. Pantic-Tanner, D. R. Tanner, S. A. Savage, and A. F. Peterson, URSI Symp. Dig., 90, 1995] is proposed. This new vector singular element is used in the H-field FEM formulation and is compatible with edge elements, specifically the linear-tangential/quadratic-normal edge element. Two edge-based basis functions associated with the singular node are modified to mimic the analytically predictable singular behavior, while the rest (four edge-based and two face-based) are the same as in [A. F. Peterson, AP-43, 357, 1994]. This element can cope with any order of singularity. Basis functions are expressed in a triangular polar coordinate system and all the necessary integrations are performed in closed form. The sparsity of the FEM equations is preserved, and spurious modes are eliminated. The number of unknown parameters needed to model the fields is significantly reduced by employing singular elements, as the numerical data show. Results also suggest that for the same number of unknown parameters needed to model the fields, the field distribution produced by the singular elements is much smoother in the vicinity of the singular point.

Numerical results for the circular cavity with septum, L-shaped cavity and similar structures are presented in the paper.

APS/URSI B Special Session **Session 41** **Salon Peribonca**

Radar Polarimetry
Co-chairs: E. Pottier, France and M. El-Shenawee, USA

10:30 41.1 Characterization of Fracture Surface by Polarimetric Borehole Radar, **T. MIWA**, M. SATO, H. NIITSUMA, *Tohoku University, Sendai, Japan (APS)*

10:50 41.2 **Invited:** Statistics for the Determination of Propagation Parameters from Polarimetric Radar Data, V. SANTALLA DEL RIO[1], **Y.M.M. ANTAR**[2], [1]*Universidad de Vigo, Spain;* [2]*Royal Military College of Canada, Kingston, ON, Canada (APS)*

11:10 41.3 **Invited:** Polarimetric Responses of Underground Targets Using an Hybrid Transfer Function FDTD Method, **P. LUNEAU**[1], G.Y. DELISLE[2], [1]*Comlab Télécommunications Inc. and* [2]*INRS-Télécommunications, Verdun, QC, Canada (APS)*

11:30 41.4 Calibration of Polarimetric Radar Systems[1], **L.A. MUTH**, R.C. WITTMANN, *National Institute of Standards and Technology, Boulder, CO, USA (APS)*

11:50 41.5 A Spectral-Polarization Method for Analyzing the Radio Signal Interference Pattern, E.L. AFRAIMOVICH, **K.S. PALAMARTCHOUK**, *Institute of Solar-Terrestrial Physics, Irkutsk, Russia (URSI)*

JOINT-41.5

A Spectral-Polarization Method for Analyzing the Radio Signal Interference Pattern

E. L. Afraimovich and K. S. Palamartchouk*

Institute of Solar-Terrestrial Physics, p. o. box 4026, Irkutsk, 664033, Russia
E-mail: kpal@sitmis.irkutsk.su Fax: +7 3952 467 552

Abstract

The preponderance of the data on ionosphere irregularities dynamics and structure was obtained from ground-level measurements of spatio-temporal characteristics of the radio signal interference pattern (IP). Such measurements were always made with spatially separated receiving antennas, beginning with he simplest version of three antennas in a pioneer paper of S. N. Mitra (Proc. Inst. Electr. Engrs., 3, 441-482, 1949) and ending with radio astronomical interferometers (C. Mercier J. Atmos. Terr. Phys., 48, 605-624, 1986).

The objective of this paper is to demonstrate that it is in principle possible to reconstruct the some characteristics of the shape of IP and to measure IP velocity characteristics at the terrestrial surface level without recourse to a conventional spaced-antenna method, but by analyzing three mutually orthogonal projections of the radio signal field vector using a single receiving antenna. The proposed technique can also improve spatial resolution when carrying out remote sounding operations from moving platforms such as satellites and aircrafts. This idea seems to have been pioneered in a monograph (Afraimovich E. L. Interference Methods of ionospheric Radio Sounding. Moscow: Nauka, 198 p., 1982) but has not yet received an appropriate development.

As early as 1951 Morgan and Evans (Proc IRE, 39, pp. 552-556) showed that the complex amplitudes of three mutually orthogonal projections of the one-mode regular signal field determine parameters of the ellipse of polarization and the direction rotation of the polarization vector, as well as the angles of arrival. The above-listed parameters constitute a description of a full field vector of a plane radio wave and are related to complex amplitudes of the field projections by a system of equations. However, this method can be used directly in a data treatment only for a strictly regular one-mode signal. External noise and signal scattering contribute to an increase of the error of measurement, and the multimode approach with similar values of mode amplitudes causes irreversible interference distortions, which imposes a drastic limitation on the use of this method in research and applied radio engineering.

This problem is resolved in large part by a spectral-polarization method for analyzing a full field vector of the radio wave based on integrated Doppler filtering of modes (E. L. Afraimovich et al., A method to measure the full vector of field. USSR Inventor's Certificate No. 650026, 1979). The method, in essence, implies that all algorithms for calculating parameters of a full field vector using a system of equations with respect to mutually orthogonal projections utilize, instead of complex amplitudes of projections, complex amplitudes of the components of a complex Doppler spectrum of these projections.

So the initial stage of analysis involves calculating complex Doppler spectra of time variations of these projections. Thereupon, for each spectrum component, these data are used to determine angle-of-arrival spectra. In conjunction with data on Doppler frequency shifts, this procedure makes it possible to reconstruct some characteristics of the IP shape and parameters such as direction and velocity of its motion.

APS/URSI D | Session 42 | Salon Richelieu

Space Antennas
Co-chairs: R. Murphy, Canada and P. Wood, Canada

08:10 42.1 Focal Plane Beam Synthesis Method for Dielectric Lens Antennas, K.K. CHAN[1], **M. GIMERSKY**[2], R. POKULS[2], [1]*Chan Technologies Inc., Kirkland and* [2]*Spar Aerospace Ltd., Ste-Anne-de-Bellevue, QC, Canada (APS)*

08:30 42.2 Multibeam Antenna Using a Phased Array Fed Reflector, **K. UENO**, *NTT Wireless Communication Systems Laboratories, Yokosuka, Japan (APS)*

08:50 42.3 Pattern Correction in Large Deployable Reflector Antennas with Phased Array Feed, **K. HARIU**[1], H. TSUNODA[1], Y. KAWAKAMI[1], T. NOGUCHI[2], [1]*Advanced Space Communications Research Laboratory, Tokyo and* [2]*Mitsubishi Electric Corporation, Kanagawa, Japan (APS)*

09:10 42.4 Weight Optimization Method for Array-Fed Reflector Antennas Used for Multibeam Satellite Communications, **H. SHOKI**[1], Y. SUZUKI[1], K. TOKUNAGA[2], H. TSUNODA[2], [1]*Toshiba Research and Development Center, Kawasaki and* [2]*Advanced Space Communications Research Laboratory, Tokyo, Japan (APS)*

09:30 42.5 Design and Near-Field Measurement Performance Evaluation of the Sea Winds Dual-Beam Reflector Antenna, **Z. HUSSEIN**[1,2], Y. RAHMAT-SAMII[2], K. KELLOGG[1], [1]*California Institute of Technology, Pasadena and* [2]*University of California at Los Angeles, CA, USA (APS)*

09:50 42.6 An Inflatable Parabolic Torus Antenna Design for the Soil Moisture Radiation Mission, R.A. HOFERER, **Y. RAHMAT-SAMII**, *University of California, Los Angeles, CA, USA (APS)*

10:10 Coffee Break

10:30 42.7 The Lunar Prospector Helix Antenna, **J.T. LOANE**, D.R. TANNER, *Lockheed Martin Missiles and Space, Sunnyvale, CA, USA (APS)*

10:50 42.8 Luneberg Lenses Performance Limitations Due to Fabrication Process, **P.G. INGERSON**, *TRW Antenna Products Center, Redondo Beach, CA, USA (APS)*

11:10 42.9 Interaction of Multipactor Discharge and RF Structures, **R.A. KISHEK**[1], Y.Y. LAU[1], R.M. GILGENBACH[1], D. CHERNIN[2], [1]*University of Michigan, Ann Arbor, MI and* [2]*Science Applications International Corporation, McLean, VA, USA (URSI)*

11:30 42.10 Antenna System for Ariane 5 Booster, **O.A. SHUNIN**, V.S. TENSIN, *Research Institute of Measuring Systems, Nizhny Novgorod, Russia (APS)*

11:50 42.11 An Electrically Small Compact Minimum Scattering Shaped Reflector for a Large Beam, P. WERNTZ, **P. RAMANUJAM**, *Hughes Space and Communications Company, Los Angeles, CA, USA (APS)*

JOINT-42.9

INTERACTION OF MULTIPACTOR DISCHARGE AND RF STRUCTURES

R. A. Kishek, Y. Y. Lau, and R. M. Gilgenbach,
University of Michigan, Ann Arbor, MI, and
D. Chernin, Science Applications International Corp., McLean, VA

Multipactor is a resonant, low-to-medium rf voltage breakdown phenomenon in microwave cavities, windows, and accelerator structures. A simple model is used to study the temporal evolution of a first-order, two-surface multipactor discharge and its interaction with the surrounding rf structure. The model assumes an infinitesimally thin sheet of electrons released with monoenergetic velocities in a parallel plate geometry.

The loading of the structure by the changing multipactor current, a combination of de-tuning and of reducing the quality factor of the resonant structure, is found to cause saturation. The steady state multipactor current has been derived analytically, and compares favorably with the computational results of the model. Transiently, the behavior of the multipactor depends on the quality factor of the rf structure. Non-resonant structures experience a fairly steady growth of the discharge towards the steady state level predicted by the theory. Highly-resonant structures, on the other hand, experience large oscillatory transients in the level of the discharge before it settles to the steady state. During these oscillations, the discharge feeds from the significant energy stored in the structure, and can be very damaging to the structure itself.

Simulations performed with two electron sheets instead of one reveal a novel phase-focusing mechanism in which one sheet grows at the expense of the other. This "cannibalism" results from the different impact energies, hence different yields, encountered by the different sheets (parts of the bunch). This mechanism may result in the multipactor electrons being very tightly bunched. A multipactor discharge can take place during the "fill-time" of an rf structure, even if the operating voltage is above the multipactor region, if the rise time of the voltage is long enough. The conventional susceptibility diagram is modified to include the effects of surface materials. This is the first attempt where the dynamics of a multipactor discharge are linked to the material properties. Comparison with published experimental data is given.

APS/URSI B **Session 53** **Salon St-Maurice**

Wavelets

Co-chairs: T.K. Sarkar, USA and R. Nevels, USA

13:10 53.1 Numerical Performance of Wavelet-Like Transforms for the Solution of Large Complex Matrix Equations, **T.K. SARKAR**[1], M. SALAZAR-PALMA[2], [1]*Syracuse University, Syracuse, NY, USA;* [2]*Universidad Politécnica de Madrid, Spain (URSI)*

13:30 53.2 Application of Discrete Wavelet-Like Transforms for Solution of Large Matrix Equations, **T.K. SARKAR**[1], M. SALAZAR-PALMA[2], [1]*Syracuse University, Syracuse, NY, USA;* [2]*Universidad Politécnica de Madrid, Spain (URSI)*

13:50 53.3 A Comparison of Moment Impedance Matrices Obtained by Direct and Transform Matrix Methods Using Wavelet Basis Functions, **R. NEVELS**, R. MILLER, *Texas A&M University, College Station, TX, USA (URSI)*

14:10 53.4 A Wavelet Approach to Effective Modal Analysis of Complex Lamination, **B.Z. STEINBERG**[1], J.J. McCOY[2], M. MIROTZNIK[2], [1]*Tel-Aviv University, Tel-Aviv, Israel;* [2]*Catholic University of America, Washington, DC, USA (APS)*

14:30 53.5 Unified Analysis of Finite-Size Printed Antenna Arrays and their Feed Circuits Using a Wavelet-Based Sparse Moment Method Approach, **K.F. SABET**[1], J.-C. CHENG[2], L.P.B. KATEHI[2], K. SARABANDI[2], [1]*EMAG Technologies, Inc. and University of Michigan, Ann Arbor, MI, USA (URSI)*

14:50 53.6 Analysis of Scattering by Surfaces Using a Wavelet-Transformed Triangular Patch Model, Z. BAHARAV[1], **Y. LEVIATAN**[2], [1]*Hewlett Packard-Israel Science Center and* [2]*Technion-Israel Institute of Technology, Haifa, Israel (URSI)*

15:10 Coffee Break

15:30 53.7 Numerical Simulation of Scattering from Rough Surfaces: A Wavelet-Based Approach, D. ZAHN, K.F. SABET, **K. SARABANDI**, *University of Michigan, Ann Arbor, MI, USA (APS)*

15:50 53.8 Combining the Wavelet Transform Technique with the Hybrid FEM/BEM Approach for Solutions of Large Scattering Problems, **Z. XIANG**, Y. LU, *Nanyang Technological University, Singapore (URSI)*

16:10 53.9 Determination of Method of Moments Impedance Matrix Using Wavelet Expansions, **I. PASSAIS**, B. UGUEN, G. CHASSAY, *URA CNRS 834, Rennes, France (URSI)*

16:30 53.10 An Adaptive Wavelet Transform for Solutions of Electromagnetic Integral Equations, **Z. XIANG**, Y. LU, *Nanyang Technological University, Singapore (APS)*

JOINT-53.1

Numerical Performance of Wavelet like Transforms for the Solution of Large Complex Matrix Equations

Tapan K. Sarkar
Department of Electrical Engineering and Computer Science
121 Link Hall
Syracuse University
Syracuse, New York 13244-1240
Tel: 315-443-3775; Fax: 315-443-4441
Email: tksarkar@mailbox.syr.edu

Magdalena Salazar-Palma
ETSI de Telecommunicacion
Universidad Politecnica de Madrid
Cindad Universitaria
28040 Madrid

Abstract: The numerical performance of the wavelet-like transforms (It is important to note that these orthogonal transforms are not wavelet transforms in the true sense!!) is illustrated through the solution of a large (4096 × 4096) complex matrix equation arising in the solution of electromagnetic scattering from a collection of wire structures arbitrarily situated in free space. The objective is to illustrate that for these class of problems there may be some advantages in compressing the large matrix by a wavelet-like transform. However, it is rather inconclusive as to what the appropriate parameters are that achieves the best results. This is because, the various mathematical properties of monotonic convergence of the wavelet coefficients and so on that are associated with the classical wavelet transform does not translate directly to the wavelet like transforms. For example, it will be shown that increasing the order of the filter does not necessarily provide a better compression for the matrix - in fact, in some cases it becomes worse. Secondly increasing the order of the filter does not also provide a better accuracy in the reconstruction of the original matrix form its wavelet coefficients. The reasons for lack of such monotonic convergence results are due to the fact that these are wavelet-like transformations and since they are not true wavelet transforms, the theorems associated with such transforms therefore are not applicable.

However, an advantage with these type of transformations are that they are orthogonal transformations and they provide a sparse matrix. Therefore the application of an iterative method like the conjugate gradient for the solution of these sparse systems would be computationally efficient but the number of iterations for the conjugate gradient to field the final result is the same whether it is applied to the dense complex matrix or to the wavelet - compressed sparse matrix.

Application of Discrete Wavelet-like Transforms for Solution of Large Matrix Equations

Tapan K. Sarkar
Department of Electrical Engineering and Computer Science
121 Link Hall
Syracuse University
Syracuse, New York 13244-1240
Tel: 315-443-3775; Fax: 315-443-4441
Email: tksarkar@mailbox.syr.edu

Magdalena Salazar-Palma
ETSI de Telecommunicacion
Universidad Politecnica de Madrid
Cindad Universitaria
28040 Madrid

Abstract: The objective of this presentation is to present the discrete wavelet transform from a filter theory perspective. This provides a physical insight into the mathematical aspects of the wavelet transforms. For DWT one need not worry about the scaling and the wavelet functions at all but basically has to construct some finite impulse response filters. The objective is to illustrate how such constructs are done and how to carry out the DWT. The DWT had much success in the compression of images and other matrix like structures. However the DWT cannot be directly applied to the solution of large matrix equations. DWT has to be modified and it is shown how the wavelet-like transforms can be utilized in the solution of large matrix equations. Because these are wavelet-like transforms, the various mathematical properties of monotonic convergence and increased accuracy do not scale in a straight forward function. In addition increasing the order of the filters also does not provide more accurate solutions. The strengths and the weaknesses of the wavelet like transforms in the solution of large matrix equations will be illustrated.

Also it is interesting to note that these wavelet-like transforms are orthogonal transforms and hence do not change the condition number of the matrix. This is in direct contrast to the choice of wavelet bases in the solution of an operator equation where the resulting system of the equations are often ill-conditioned. Unless the wavelet bases are properly decimated, in the solution of the operator equation, the condition number of the resultant matrix deteriorates in a very rapid fashion.

JOINT-53.3

A Comparison of Moment Impedance Matrices Obtained by Direct and Transform Matrix Methods Using Wavelet Basis Functions

Robert Nevels* and Richard Miller
Department of Electrical Engineering
Texas A&M University
College Station, TX 77843-3128

It has now become clear that for a wide variety of applications, a method of moments impedance matrix obtained with a wavelet basis function can be much more sparse than one obtained using a classical basis. This is because the impedance matrix elements computed using a classical basis function, such as a pulse or triangle, contain components that convey only amplitude and phase information while each wavelet matrix element is constructed as a product of the amplitude/phase and the frequency information. The mechanism through which frequency information is imparted on the matrix elements can be attributed to the orthogonality, vanishing moments and localization properties of the wavelet basis.

In this presentation we will compare the two competing methods for computing the impedance matrix, the direct method and the transform matrix method. The direct (or traditional) method is to formulate the integral equation, expand the unknown current in a wavelet basis, and test with the same wavelets used in the basis. This Galerkin procedure produces individual matrix elements that require double integration over a product of two wavelets or a wavelet and a scaling function. With this method, actually evaluating impedance matrix elements becomes complicated, not only because wavelets are complicated functions, but also because the multi-resolution aspect of the formulation results in singularities in both the diagonal and off-diagonal terms in the impedance matrix. Even with a semi-orthogonal wavelet, where singularities can be evaluated analytically, identification and evaluation of these singularities is tedious. With an orthogonal wavelet, singularities are often more numerous and can only be evaluated numerically.

A alternative to the direct method is to instead compute the impedance matrix ($\boldsymbol{Z}$) and the excitation vector ($\boldsymbol{V}$) using a classical basis function ($\boldsymbol{I}$) and then obtain the wavelet basis equation, $[\underline{Z}]\,[\underline{I}] = [\underline{V}]$, by the change of basis operations: $[\underline{V}] = [W]\,[V]$, $[\underline{I}] = [W]\,[I]$, $[\underline{Z}] = [\underline{W}][Z][W]^T$ where $[W]$ is a basis transformation matrix.

Wavelet impedance matrices obtained by these two methods will be compared in terms of computation time, and accuracy using plane wave excitation of a thin finite length wire and a two-dimensional finite width flat plate as examples.

UNIFIED ANALYSIS OF FINITE-SIZE PRINTED ATNENNA ARRAYS AND THEIR FEED CIRCUITS USING A WAVELET-BASED SPARSE MOMENT METHOD APPROACH

Kazem F. Sabet†, Jui-Ching Cheng‡, Linda P.B. Katehi‡, and Kamal Sarabandi‡

† EMAG Technologies, Inc., 2901 Hubbard Rd., Suite E-116, Ann Arbor, MI 48106
‡ Department of Electrical Engineering and Computer Science, The University of Michigan, Ann Arbor, MI 48109-2122

Abstract. The accurate near-field characterization of printed antenna arrays, and in particular, the calculation of their input impedance, require a rigorous full-wave modeling of the entire array structure. With the size of the array or complexity of the feed circuit growing, the numerical modeling of the overall structure turns into a large-scale computational problem. The recent developments in the application of wavelet techniques to the numerical solution of integral equations has made it possible to utilize the method of moments (MoM) for the full-wave modeling of this type of complex open-environment structures in a very effective manner.

The use of multiresolution expansions in conjunction with the method of moments can generate highly sparse linear systems due to the cancellation property of wavelet basis functions. Using rooftop multiresolution expansions eliminates the difficulties related to the correct enforcement of the PEC boundary conditions. The resulting sparse linear system is stored with minimal memory usage and is inverted very efficiently using a sparse-based iterative solver like the biconjugate gradient (BiCG) method. A major advantage of using a wavelet-based MoM implementation is a notable improvement in the condition number of the linear system. This improvement directly contributes to a very fast convergence of the BiCG iterative process. A dramatic acceleration of the matrix fill process can be accomplished by invoking the fast wavelet transform (FWT). Using this algorithm enables us to limit the tedious task of numerical integration of the Green's function to only scaling functions at the highest resolution level. The moment matrix is then generated recursively for all lower resolution levels. Taking advantage of improved condition numbers, it is possible to identify in advance all interactions which eventually lead through the FWT to negligible matrix elements. The numerical evaluation of such interactions is thus skipped during the matrix fill process.

In this paper we apply the approach described above to the modeling of finite-size arrays of printed microstrip patch antennas with a corporate feed circuit as shown in the figure below. A non-uniform high-resolution mesh is initially utilized to discretize the geometry. This mesh is subsequently transformed into a coarser multiresolution grid using the FWT. The input feed line of the array is excited using a voltage gap generator. After computing the current distribution on the structure, the input impedance is calculated within a very high degree of accuracy using a least-squares Prony's method.

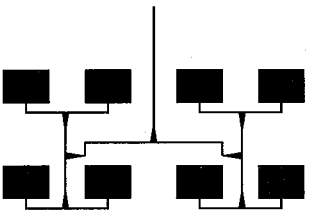

JOINT-53.6

Analysis of Scattering by Surfaces Using a Wavelet-Transformed Triangular Patch Model

Z. Baharav
Hewlett-Packard -Israel Science Center
Technion, Haifa 32000, Israel
E-mail: zachi@hp.technion.ac.il

Y. Leviatan
Department of Electrical Engineering
Technion - Israel Institute of Technology
Haifa 32000, Israel
E-mail: leviatan@ee.technion.ac.il

A new approach to incorporating wavelet transforms in the solution of three-dimensional scattering by surfaces is presented. The problem is formulated by the EFIE and reduced to matrix form via a moment procedure using triangular patch basis functions (S.M. Rao, D.R. Wilton, and A.W. Glisson, *IEEE Trans. Antennas Propagat.*, vol. AP-30, pp. 409–418, May 1982). The matrix equation is then wavelet-transformed, yielding new expansion functions. These expansion functions themselves are not wavelets, but rather "wavelet combinations" of the initial triangular patch basis functions. The solution of the transformed matrix equation is subsequently effected by an iterative impedance matrix compression (IMC) scheme. The underlying idea behind the IMC approach (Z. Baharav and Y. Leviatan, *Microwave and Optical Technology Letters*, vol. 12, pp. 268–272, August 1996; Z. Baharav and Y. Leviatan, *IEEE Trans. Antennas Propagat.* vol. AP-44, pp. 1231–1238, September 1996) is that only a few of the new expansion functions may be needed for an accurate representation of the current on the scatterer. The iterative procedure (Z. Baharav and Y. Leviatan, *Microwave and Optical Technology Letters*, vol. 12, pp. 145–150, June 1996) provides the means to determine these dominant expansion functions in a systematic manner. Taking only the dominant functions into consideration, the matrix equation is readily compressed into a much smaller one, which can therefore be solved with much less computational effort. It also facilitates an effective way to refine the resolution locally. Numerical results for the problem of scattering by a conducting patch will be given to illustrate the salient features of the proposed approach.

Combining the Wavelet Transform Technique with the Hybrid FEM/BEM Approach for Solutions of Large Scattering Problems

Zhonggui Xiang and Yilong Lu
School of Electrical and Electronic Engineering
Nanyang Technological University, Singapore

Several different approaches are available for the analysis of scattering from arbitrarily shaped, inhomogeneous and lossy bodies. Some finite methods such as the finite element method (FEM) are suitable for the so-called interior problems while some other methods such as the boundary element method (BEM) are preferred for the so-called exterior problems. Some hybrid methods [Gong and Glisson, *IEEE Trans. Antennas Propag.*, 1990; Jin, Volakis and Collins, *IEEE AP Magazine*, 1991] combining the advantages of the above-mentioned methods are able to efficiently solve a more general class of problems. As well known, the use of the FEM results in a sparse matrix. However, a dense matrix will be encountered when solving the boundary integral equations by using the traditional basis and weighting functions in the method of moments (MoM), unless some other techniques are co-operated [Collins, Jin and Volakis, *Electromagnetics*, 1990]. Recently, wavelet transform method (WTM) is applied to solve electromagnetic (EM) problems because the use of wavelets as the basis and weighting functions in the MoM results in a sparse matrix equation. In this paper, a hybrid technique uniting advantages of the WTM, FEM and BEM is proposed. The FEM is used to formulate the fields within a fictitious boundary Γ enclosing the considered structure and establish a relationship with those at the opening. The fields outside the fictitious boundary Γ are formulated by the BEM involving an integral expression of the fields over Γ. A system is then

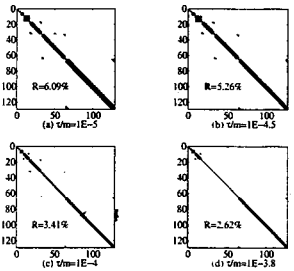

Fig. 1. The sparse patterns of A by the NCSW transform

derived by enforcing field continuity across Γ as follows: .

$$[K]\{u\} + [C]\{\Psi\} = \{0\}, \quad (1)$$

$$[C]^T\{u\} - [P]\{u\} - [Q]\{\Psi\} = \{B\}, \quad (2)$$

where u and Ψ are electric or magnetic field and its normal derivative on Γ, respectively. K is a sparse matrix from the FEM and C is a diagonal matrix. B stands the incident matrix and T denotes the transpose of a matrix. The use of conventional basis and weighting functions in the MoM always results in dense matrices P and Q. The cost to directly solve the combined system equation of (1) and (1) is expensive, especially for large-size EM problems. Here, we factorize sparse matrix K once to solve u in (1) and substitute u into (2) to obtain a matrix equation in the form of $A\Psi = B$. A is the combination of P and Q, and therefore, is a dense matrix. Here, we use an effective wavelet matrix transform method by which the so-called "edge effect" problem and the exhaustive wavelet integrations are overcome. The numerical results for the scattering by TM excitation from a four-layered dielectric cylinder with circular cross section are given to demonstrate the validity and capability of the method. Note that the singularity of A is completely determined by P and Q. To obtain a satisfactory compression rate and solution accuracy we choose non-orthonormal cardinal spline wavelet (NCSW) transform with 8-order vanishing moments [Xiang and Lu, *IEEE Trans. Antennas Propag.*, 1997]. Fig. 1 shows the sparsity of A by the NCSW transform with different threshold values. The off-diagonal elements are nearly equal to zeros only if the chosen fictitious boundary Γ is smooth enough. Fig. 2 shows the accuracy of the approximate solution by the proposed technique, compared with the one by the FEM/BEM method. Even with so sparse a matrix ($R = 2.62\%$, ratio of the number of remaining elements after thresholding to the total elements) one can obtain a good accurate solution by a sparse solver. The proposed technique can handle other more complicated scattering problems. It is more effective than the traditional approaches for large EM problems.

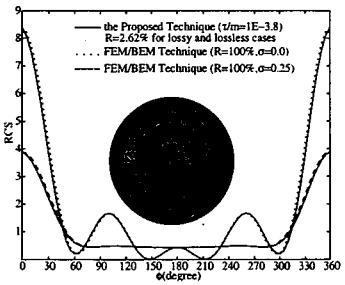

Fig. 2. RCSs of a four-layered circular homogeneous cylinder ($a = 0.15\lambda$, $b = 0.20\lambda$,$c = 0.25\lambda$, $d = 0.30\lambda$, $\epsilon_{r1} = 8.0$, $\epsilon_{r2} = 6.0$, $\epsilon_{r3} = 4.0$, $\epsilon_{r4} = 2.0$, $\mu_r = 1.0$, $f = 300MHz$, $\varphi_i = \pi$, and σ is the same in all layers) under TM plane wave incidence.

JOINT-53.9

Determination of Method of Moments Impedance Matrix Using Wavelet Expansions.

I. Passais, B. Uguen, G. Chassay
Laboratoire Composants et Systèmes pour Télécommunications (LCST)
URA CNRS 834 - INSA
20, avenue des buttes de Coësmes, 35043 Rennes cedex, France

Introduction

A technique of computation of the Method of Moments impedance matrix elements is proposed, using wavelet as bases and testing functions in order to decrease matrix element computation time and obtain a sparse matrix equation.

The analysis of electromagnetic scattering by objects which contain a large number of length scales is a typical problem. The Method of Moments is based on projection of the unknowns on expansion and testing functions. But this method is limited when the size of the matrix equation increases.

Recently, the electromagnetic community employed wavelets in the Method of Moments, allowing a reduction in the number of unknowns of the problem. A reduction in computation time was also made possible.

The method which consists in applying a fast wavelet transform on the impedance matrix, obtained using a standard pulses bases-point matching procedure, has been used. It leads to a sparse impedance matrix after application of a thresholding operation. Sparse matrix algorithms can then be used to solve the matrix equation (conjugate gradient method associated with appropriate storage procedure). It has been shown that matrix inversion time is then considerably reduced without damaging the accuracy of the solution. However, this method does not allow a reduction in the time of computation of the original impedance matrix elements.

Our aim is therefore to improve the matrix element computation time. The matrix equation obtained is sparse and will then be solved by the method described above. We use the wavelets as expansion and testing functions in the Method of Moments. Thanks to the properties of these functions, we compute the matrix elements efficiently. At each resolution, an adaptive mesh is proposed and, according to the scatterer shape under study, the computation of all the matrix components may not be needed.

To illustrate the method, it is applied to structures containing several different lengthscales.

Conclusion

In order to predict the scattering of objects which contain different dimensional lengthscales (in comparaison with the wavelength), the calculation of impedance matrix elements is presented using the Method of Moments using wavelet functions is presented. The perspective of the study is to apply the method to 3D problems.

APS/URSI D **Session 61** **Salon Matapedia**

Opto-Electronics, Techniques, Devices and Materials
Co-chairs: A.P. Freundorfer, Canada and A.Q. Martin, USA

13:10 61.1 A Method-of-Lines Based Efficient Method for Optical Waveguide Discontinuity Problems, **Y.-P. CHIOU**, H. CHANG, *National Taiwan University, Taipei, Taiwan, China (APS)*

13:30 61.2 Optically Controlled Scanning Antennas Comprising a Plasma Grating, **V.A. MANASSON**, L.S. SADOVNIK, V.A. YEPISHIN, *WaveBand Corporation, Torrance, CA, USA (APS)*

13:50 61.3 An Active Transversal Filter MMIC for Very High Speed Lightwave Systems, Y. JAMANI, **A.P. FREUNDORFER**, *Queen's University, Kingston, ON, Canada (APS)*

14:10 61.4 High-Q Microcavity Ring and Disk Resonators: FDTD Analysis of Resonance and Coupling Characteristics, **S.C. HAGNESS**, D. RAFIZADEH, S.-T. HO, A. TAFLOVE, *Northwestern University, Evanston, IL, USA (APS)*

14:30 61.5 Fields and Currents Due to a Modulated Laser Beam Exciting an Array of Narrow Slots, **A. KUSTEPELI**, A.Q. MARTIN, *Clemson University, Clemson, SC, USA (APS)*

14:50 61.6 Boundary Integral Analysis of Fused Biconical Optical Fiber Coupling Devices with Asymmetrical Structure, J.-H. LI, **H. CHANG**, *National Taiwan University, Taipei, Taiwan, China (URSI)*

JOINT-61.6

BOUNDARY INTEGRAL ANALYSIS OF FUSED BICONICAL OPTICAL FIBER COUPLING DEVICES WITH ASYMMETRICAL STRUCTURE

Jia-Han Li and Hung-chun Chang*

Department of Electrical Engineering, National Taiwan University
Taipei, Taiwan 106-17, China

*also with the Graduate Institute of Electro-Optical Engineering, National Taiwan University

This paper concerns numerical modeling of fused optical fiber couplers composed of fibers with different sizes made with biconical tapering technology. Such coupler structure can be designed for wavelength-flattened couplers and Brewster-window-type all-fiber devices. One feature of the fused coupler is that in the neck region of the coupler the light is guided by the boundary between the (reduced) fiber cladding and the external medium which is air in our case, so that the fused structure becomes a strongly guiding composite waveguide. The cross-sectional structure in the coupling region has the (asymmetrical) dumbbell shape under strongly fused condition. Because the tapered structure is slowly varying, it is an appropriate assumption that only the lowest-order even-like and odd-like modes are excited. The coupling coefficient which is defined as half the difference between the even-like and odd-like supermode propagation constants depends on the polarization state. The difference in the coupling coefficient between orthogonal polarization states is usually called the form birefringence. The form birefringence is thus an important parameter that determines the polarization-dependent performance of the coupler. However, the form birefringence is small, and accurate determination of such small quantity requires careful numerical calculation. We have reported such accurate calculation of the small form birefringence for fused couplers composed of identical fibers at PIERS 1997, Hong Kong. In this paper we present and discuss our results for the asymmetrical coupler structure.

The boundary integral method is again employed, which is a suitable technique for solving the modes on the coupler since the reduced fiber cladding, which is now the waveguiding region of the coupler, is essentially a homogeneous medium. We have also established a three-dimensional computer model, based on the vectorial modal calculation and by properly modeling the tapered structure, which can simulate the power transfer characteristics of the fused coupler during the tapering process. The coupled power versus the drawn length at different wavelengths and the dependence on the polarization of the input wave can then be predicted. In summary, we have performed detailed analysis of the coupling characteristics, including the form birefringence, of fused biconical 2×2 optical fiber coupling devices with asymmetrical structure based on full-wave boundary integral method. A 3-D vectorial model has also been established to simulate the polarization-dependent device function of realistic coupler structure.

APS/URSI B | Session 65 | Salon MacKenzie

Special Session in Memory of Peter P. Silvester
Co-chairs: G. Pelosi, Italy and A. Konrad, Canada

13:00 Remembering Peter P. Silvester

13:10 65.1 **Invited:** Finite Element Analysis of Out-of-Plane Propagation in Two-Dimensional Photonic Crystals, **R. COCCIOLI**[1], T. ITOH[1], G. PELOSI[2], [1]*University of California, Los Angeles, CA, USA;* [2]*University of Florence, Italy (APS)*

13:30 65.2 **Invited:** A Review of Some Recent Advances in Perfectly-Matched Absorbers for Mesh Truncation in FEM, **R. MITTRA**[1], M. KUZUOGLU[2], [1]*Pennsylvania State University, University Park, PA, USA;* [2]*Middle East Technical University, Ankara, Turkey (APS)*

13:50 65.3 **Invited:** High Precision Differentiation of FEM Approximate Solutions, **D. OMERAGIĆ**, *McMaster University, Hamilton, ON, Canada (APS)*

14:10 65.4 **Invited:** Hierarchal Triangular Edge Elements Using Orthogonal Polynomials, C. CARRIÉ, **J.P. WEBB**, *McGill University, Montréal, QC, Canada (APS)*

14:30 65.5 **Invited:** Some Thoughts on the Relationship Between Finite Elements, Finite Differences and TLM, **W.J.R. HOEFER**, *University of Victoria, BC, Canada (APS)*

14:50 65.6 **Invited:** Full Wave Analysis of Geometrically Complex Anisotropic MMIC Waveguiding Structures, **M. SALAZAR-PALMA**, L.-E. GARCIA-CASTILLO, *Universidad Politécnica de Madrid, Spain (URSI)*

15:10 Coffee Break

15:30 65.7 **Invited:** Hybrid Finite Element Methods for Conformal Antenna Simulations, **J.L. VOLAKIS**, *University of Michigan, Ann Arbor, MI, USA (APS)*

15:50 65.8 **Invited:** A Guided Tour of Interpolatory Vector Basis Functions, **A.F. PETERSON**[1], R.D. GRAGLIA[2], D.R. WILTON[3], [1]*Georgia Institute of Technology, Atlanta, GA, USA;* [2]*Politecnico di Torino, Italy;* [3]*University of Houston, TX, USA (APS)*

16:10 65.9 **Invited:** Tree-Cotree Decompositions for Higher Order Tangential Vector Elements, J.B. MANGES, **Z.J. CENDES**, *Ansoft Corporation, Pittsburgh, PA, USA (URSI)*

16:30 65.10 **Invited:** 2D and 3D Finite Element Modeling of Electrical Machines, J.-C. SABONNADIERE, **A. FOGGIA**, *E.N.S.I.E.G., Saint Martin d'Heres, France (APS)*

JOINT-65.6

FULL WAVE ANALYSIS OF GEOMETRICALLY COMPLEX ANISOTROPIC MMIC WAVEGUIDING STRUCTURES

Magdalena Salazar-Palma, Luis-Emilio García-Castillo*
E.T.S.I. Telecomunicación, Universidad Politécnica de Madrid, Spain
Email: salazar@gmr.ssr.upm.es, Tel.: 34-1-336-7358, Fax: 34-1-336-7362

Accurate computation of the propagation characteristics of waveguiding structures is of paramount importance in the design of monolithic microwave integrated circuits (MMICs). In many cases such structures exhibit rather complex geometries. To start with, the fabrication process generally involves undercutting or overcutting effects in the metallizations. It has also been proposed the use of conducting strips with V cross sections and other peculiar shapes showing given advantages over the ordinary rectangular ones. Dielectric ridges, proximity between conductors and dielectric corners, mutual couplings, and so on, are other typical configurations and effects in high density packaged MMICs. Furthermore, MMICs are also physically complex structures, due to the use of multilayer techniques, with materials exhibiting dielectric and magnetic anisotropies.

Since the early work of P.P. Silvester (Alta Freq., vol. 38, May 1969, pp.313-317; IEEE Trans. Microwave Theory Tech., vol. MTT-17, Apr. 1969, pp.204-210; etc.) up to date, the Finite Element Method (FEM) has demonstrated to be a powerful and flexible tool, able to deal with a wide variety of configurations and arbitrary shaped geometries. The FEM is very well suited to handel problems involving inhomogeneities and anisotropies. In fact the FEM formulation of such problems may be done in a straightforward way. The historical drawback of the FEM full-wave analysis of such structures, namely the appearance of spurious modes, that was also addressed by P.P. Silvester, together with Z. Cendes, already in 1970 (IEEE Trans. Microwave Theory Tech., vol. MTT-18, Dec. 1970, pp. 1124-1131), may be easily solved nowadays by means of discretizations based in edge elements. The accuracy of the FEM solutions may be enhanced by using higher order elements and curved elements, if curved boundaries are present (see F. Blanc-Castillo, M. Salazar-Palma, L.E. García-Castillo, 25th European Microwave Conf. Proc., Sept. 1995, pp. 444-448).

Nevertheless, the accuracy of the FEM greatly depends on a proper discretization of the domain of definition of the problem, namely on the number and the size of the elements in which the domain is subdivided and, as a consequence, on the number and the distribution of the nodes where the degrees of freedom are defined. In general, the method is used in an iterative way applying it to a sequence of meshes, with an increasing number of degrees of freedom, until a convergent solution is obtained. In fact, once a FEM code is available the user's most cumbersome task is to create an adequate mesh. The authors have recently published (see Ch. 16, in *Finite Element Software for Microwave Engineering*, John Wiley & Sons, 1996) a self adaptive mesh technique that provides numerical results to a prespecified degree of accuracy. The procedure automatically generates meshes well adapted to the electromagnetic field behavior, with local errors of the same order of magnitude. The achievement of these type of meshes, called equilibrated or optimal, ensures the maximum rate of convergence of the finite element method, minimizing the overall computational time required to obtain the final result. Thus, the self adaptive mesh technique is most adequate for the analysis of the complex MMIC waveguiding structures described previously. This paper will present its application to the full wave analysis of a number of such structures: anisotropic coplanar waveguides, multiconductor and multilayer structures with overcutting and undercutting effects, dielectric ridges, etc. Comparisons with results by other authors will be provided.

TREE-COTREE DECOMPOSITIONS FOR HIGHER ORDER TANGENTIAL VECTOR ELEMENTS

J. B. Manges and Zoltan J. Cendes
Ansoft Corporation
Four Station Square, Suite 660
Pittsburgh, PA 15219

Edge-based finite elements have important applications in modeling both quasi-static and high frequency electromagnetic problems. Because they model the curl nullspace well, discretization of the curl-curl operator by all orders of tangential vector elements results in singular matrices. It was first demonstrated in 1988 that in the case of edge elements, this singularity is intimately related to the graph structure of the finite element mesh (R. Albanese and G. Rubinacci, "Integral Formulation for 3D Eddy-current Computation Using Edge Elements," IEE Proceedings, 135, Pt. A, pp. 457-462, 1988).

Specifically, a tree-cotree decomposition of the edges of the finite element mesh was shown to sort edge variables into dependent and independent degrees of freedom for the curl operator. In approaching the matrix singularity issue in the high-order element case, the question therefore naturally arises whether this tree-cotree decomposition methodology can be generalized. This was accomplished in (J. Webb and B. Forghani, "A T-Omega method using heirarchal edge elements," IEE Proceedings, Sci. Meas. Technol., 142, No. 2, pp. 131-141, 1995).

In the current work we wish to take a more fundamental look at how this generalization takes place, especially in regard to the properties of the underlying finite element space itself. We begin by presenting a unifying framework for the construction of 2D tangential elements that includes the familiar zero order and first order complete elements. A second order complete element is then constructed and its convergence rate is verified. Finally, the high order element tree-cotree decomposition is presented as an extension of the edge element (zero order) case and the theory is illustrated with examples from 2D electromagnetics.

APS/URSI B Special Session **Session 73** **Salon Harricana**

Novel Trends in Electromagnetics
Co-chairs: N. Engheta, USA and P.L.E. Uslenghi, USA

13:10 73.1 **Invited:** Complementary Structures in Two Dimensions, **C.E. BAUM**, *Phillips Laboratory WSQW, Kirtland AFB, NM, USA (URSI)*

13:30 73.2 **Invited:** Knots and Unknots: Scattering and Perceived Symmetry, O. MANUAR, **D.L. JAGGARD**, *University of Pennsylvania, Philadelphia, PA, USA (APS)*

13:50 73.3 **Invited:** The Electrodynamics of Torus Knots, **D.H. WERNER**, *Pennsylvania State University, State College, PA, USA (APS)*

14:10 73.4 **Invited:** Radiation and Scattering by Isorefractive Structures, **P.L.E. USLENGHI**, *University of Illinois at Chicago, IL, USA (URSI)*

14:30 73.5 **Invited:** Phase Retrieval Antenna Diagnostics for Bi-Polar Planar Near-Field Antenna Measurements, R.G. YACCARINO, **Y. RAHMAT-SAMII**, *University of California, Los Angeles, CA, USA (APS)*

14:50 73.6 **Invited:** Topological and Geometrical Considerations for Maxwell's Equations on Unstructured Meshes, **C. KAUS**, R.W. ZIOLKOWSKI, *University of Arizona, Tucson, AZ, USA (URSI)*

15:10 Coffee Break

15:30 73.7 **Invited:** Coherent Scattering and Propagation Model for Coniferous and Deciduous Tree Canopies, **Y.-C. LIN**, K. SARABANDI, *University of Michigan, Ann Arbor, MI, USA (URSI)*

15:50 73.8 **Invited:** Heaviside Operational Calculus and the Theory of Images, **I.V. LINDELL**, *Helsinki University of Technology, Espoo, Finland (URSI)*

16:10 73.9 **Invited:** Time Adaptive Time-Domain Techniques for the Design of Microwave Circuits, **E. TENTZERIS**[1], J. HARVEY[2], L.P.B. KATEHI[1], [1]*University of Michigan and* [2]*Army Research Office, Ann Arbor, MI, USA (APS)*

16:30 73.10 **Invited:** Fractionalization of the Curl Operator and Its Electromagnetic Application, **N. ENGHETA**, *University of Pennsylvania, Philadelphia, PA, USA (APS)*

JOINT-73.1

Complementary Structures in Two Dimensions

Carl E. Baum
Phillips Laboratory WSQW
3550 Aberdeen Avenue SE
Kirtland AFB, New Mexico 87117-5776

Self-complementary antennas are based on the Babinet principle in which electric and magnetic fields are interchanged (duality) with the structure invariant to this transformation. This paper develops self-complementary structures from the electric and magnetic parts of a complex potential as used in conformal transformation. This leads to various geometries of electrically small impedance sheets with relatively simply calculable admittance properties. However, the results are the same as those derived from the Babinet principle for more general electromagnetic scattering and antennas involving planar structures (not in general electrically small).

This interchange of electric and magnetic potential functions for defining self-complementary leads to some generalization of the concept of self-complementary structures. Starting from some self-complementary structure involving geometrical symmetry, (e.g., rotation, reflection, etc.), the original geometry can be changed to a generally non-symmetrical one via a conformal transformation. The values of the electric and magnetic potentials are unchanged by the transformation, thereby leaving the terminal impedance properties unchanged. So one can think of any single-port device (two terminals) with $f_g = 1$ (or $\Delta u = \Delta v$) as self-complementary, and similarly for N-terminals devices with an admittance matrix.

By including both $R_s^{(in)}$ and $R_s^{(out)}$ to fill the entire plane, and invoking reciprocation symmetry so as to make the electric and magnetic boundaries all lie on a common circle, one has a self-complementary geometry applicable to a special cylindrical TEM transmission line (plane wave). The N terminals occupy equal arcs, equally spaced around the circle. By a stereographic transformation (plane to sphere) a conical TEM transmission line (spherical wave) is defined. However, there are various possible stereographic projections depending on the selected radius of the sphere, and point of tangency of the sphere to the plane (i.e., not necessarily in the center of the circle). This gives various possible conical transmission lines, all with the same admittance properties. If desired, one can apply the stereographic projection back to a different plane to obtain yet other geometries for a cylindrical transmission line. All of these can be considered self-complementary in the generalized sense discussed above.

RADIATION AND SCATTERING BY ISOREFRACTIVE STRUCTURES

Piergiorgio L. E. Uslenghi
Department of Electrical Engineering and Computer Science (M/C 154)
University of Illinois at Chicago
851 South Morgan Street, Chicago, Illinois 60607-7053, USA

An isorefractive body is made of a linear, isotropic and homogeneous material whose refractive index is equal to the refractive index of the medium surrounding the body, although the intrinsic impedances of the two media have different values. If a planar surface separates two semiinfinite media isorefractive to each other, an incident plane wave produces a reflected wave, and a transmitted wave which propagates in the same direction of the incident wave; both reflection and transmission coefficients are independent of angle of incidence and polarization of the primary wave. The fact that lateral waves on either side of a planar isorefractive boundary propagate with the same phase velocity has been utilized in obtaining an exact solution to plane wave scattering from a class of wedge structures (P. L. E. Uslenghi, *IEEE Trans. Antennas Propagat.*, vol. 45, no. 1, Jan. 1997).

If the surface which separates two isorefractive media is a coordinate surface in a system of orthogonal curvilinear coordinates for which the wave equation is separable, then the boundary conditions at the interface between the two media can be satisfied by mode matching and an exact, canonical solution to the boundary - value problem is obtained. This exact solution is possible because the eigenfunction expansions of the electromagnetic field on either side of the interface contain the wavenumber as a parameter (and this has the same value in both media), but not the intrinsic impedance.

Exact solutions are presented for plane-wave scattering by isorefractive elliptic and parabolic cylinders. The radiation from electric or magnetic dipoles located on the symmetry axis of an isorefractive prolate or oblate spheroid, or of an isorefractive paraboloid, is exactly determined. All these new canonical solutions are important not only per se, but also because they constitute limiting cases of more general solutions which may be developed in the future.

JOINT-73.6

TOPOLOGICAL AND GEOMETRICAL CONSIDERATIONS FOR MAXWELL'S EQUATIONS ON UNSTRUCTURED MESHES

*Cynthia Kaus**, Department of Mathematics, and
Richard W. Ziolkowski, Department of Electrical and Computer Engineering

The University of Arizona, Tucson, AZ 85721
Tel: (520) 621-6173, Fax: (520) 621-8076, E-mail: ziolkowski@ece.arizona.edu

There is a great deal of interest in computational electromagnetics (CEM) to develop numerical methods based upon unstructured grids in three dimensions. Original attempts to achieve this have not been completely successful. Unusual late time instabilities occur which are directly connected to grid elements with some form of severe skewing. The actual cause of these instabilities and their late time appearance are not well understood. We believe that problems exist in the geometrical representation of the differential calculus on these unstructured grids and that the resolution to these numerical problems may be found with a systematic approach based upon connections between the associated global and discrete (local) mathematics.

Maxwell's equations have a very natural representation in differential form notation. The exterior derivative, d, takes the place of the usual curl, gradiant and divergence operations and is independent of a change in coordinate systems. Maxwell's equations can be written in terms of the exterior derivative as $dF = 0$ and $d \star F = J$ where $F = B + Edt$ is the field two-form and $J = \rho - jdt$ is the current 3-form. The Hodge star operator, $\star$, which is dependent on the choice of metric, connects the basic field quantities through the constitutive relations $B = \mu \star H$ and $D = \epsilon \star E$.

These differential form representations naturally lead to integral relations that can be localized to topological objects - the simplices, s_k, of the space. The integral relations are as follows: $dE|s_k = -\partial_t B|s_k$ and $dH|s_k^* = \partial_t D|s_k^*$, where s_k is the primary grid (simplices) and s_k^* is the complementary grid. Using Stokes' theorem on each equation we obtain: $E|\partial s_k = -\partial_t B|s_k$ and $H|\partial s_k^* = \partial_t D|s_k^*$. The boundary operator, ∂, is a map which takes $k-$simplices into $(k-1)-$simplices. Its adjoint, ∂^*, the coboundary operator, takes $(k-1)-$simplices into $k-$simplices. Using the definition of the adjoint of a linear operator, we can determine the coboundary operator in terms of the boundary operator and a star operation which is analogous to the Hodge star operator. The integral relations can then be interpreted as follows:

$$\left(\frac{1}{\epsilon} \star \partial_t D\right)|s_k = H|(\partial \star s_k) \qquad \text{and} \qquad \left(\frac{1}{\mu} \star \partial_t B\right)|s_k^* = E|(\partial \star s_k^*)$$

We believe that this form of Maxwell's equations will lead to the desired discretization scheme if the underlying topology is properly preserved. For instance, this representation leads to the combinatorial Laplacian $\Delta_k = \partial_k^* \partial_k + \partial_{k+1} \partial_{k+1}^*$ which can be used to show that the space of chains satisfies a Hodge decomposition: $C_k = B_k \oplus Im\partial_k^* \oplus H_k$, where B_k is the image of ∂_{q+1} and H_k is the kernel of the combinatorial Laplacian. The corresponding discretization scheme should then preserve the divergence properties of the original Maxwell system. The question still arises about which types of unstructured grids can be used such that this mathematical theory will still hold. The mathematical literature assumes tetrahedral elements are used for the primary grid, but we believe that the theory will hold with quadrilateral and parallelpiped elements as well.

Our progress to date on these topological and geometrical considerations for Maxwell's equations on unstructured meshes will be discussed in detail in the presentation.

Coherent Scattering and Propagation Model for Coniferous and Deciduous Tree Canopies

*Yi-Cheng Lin and Kamal Sarabandi

Radiation Laboratory
Department of Electrical Engineering and Computer Science
The University of Michigan
Ann Arbor, MI 48109-2122
Phone: (313) 763-8162 FAX: (313) 747-2106
Email: yclin@eecs.umich.edu

ABSTRACT

In this paper a coherent scattering and propagation model for coniferous and deciduous tree canopies is developed and tested. In contrast to the traditional incoherent approaches such as radiative transfer theory, the present model preserves the phase information of the scattered field, takes into account the coherent effects due to the tree structure and incorporates the inhomogeneous extinction profile within the tree canopies in the scattering formulation. This study has a number of important practical applications including remote sensing of vegetation using polarimetric and interferometric SARs, performance evaluation of wireless communication systems near trees, and simulation of GPS measurements under vegetation canopies.

The model comprises three major components: 1) accurate generation of tree structures, 2) modeling the interaction of electromagnetic wave with vegetation particles, and 3) the Monte Carlo simulation. Generation of tree architectures is implemented by a stochastic fractal-based Lindenmayer systems. The electromagnetic problem is formulated by considering the tree structure as a cluster of scatterers composed of dielectric cylinders (trunks and branches), disks (broad leaves), and needles (needle leaves). The total scattered field is obtained from the coherent addition of the individual scattering of each scatterer which is illuminated by a mean field. The mean field at a given point within the tree structure accounts for the accumulated attenuation and phase change caused by vegetation particles. Finally, the desired statistics of the scattered field is obtained using a Monte Carlo simulation. The model is successfully validated using the measured data acquired by SIR-C and JPL TOPSAR over the selected coniferous and deciduous stands in Raco, Michigan.

JOINT-73.8

HEAVISIDE OPERATIONAL CALCULUS AND THE THEORY OF IMAGES

Ismo V. Lindell
Electromagnetics Laboratory
Helsinki University of Technology
Otakaari 5A, Espoo FIN-02150 FINLAND
ismo.lindell@hut.fi

The operational calculus originally introduced by Heaviside is shown to be directly applicable to forming image principles for various electromagnetic structures. The image expression is reduced to the compact form of a pseudo-differential operator applied to the original source function The final step is an interpretation of this result in terms of computable functions. For complicated operators an approximation can be done at the last stage. The Heaviside method replaces previously applied, often heuristic, identification processes by a simple logical procedure.

The method is demonstrated though some examples by finding image solutions to selected electromagnetic problems. The general idea is shown first in terms of transmission-line concepts. As a first example the time-harmonic problem of electromagnetic source in front of a planar interface of another medium is considered. The image solution has been worked some time ago by this author and colleagues under the label Exact Image Theory (*IEEE Trans. AP* **32**(2)126-133,(8)841-847,(10)1027-1032), to improve various approximate image methods. The original derivation was loaded by rather complicated turns of algebra, which made it hard to digest. It is shown that, by applying the Heaviside method, the image expressions can be derived in the form of an operational expression through a few universal steps. As a second example, the electrostatic Neumann image for a dielectric sphere, previously obtained through more or less heuristic reasoning, is arrived at in a logical fashion. Novel image principles for the anisotropic half space and the rough interface are discussed at the end of the paper.

APS/URSI B **Session 77** **Salon Marquette**

High Frequency Techniques
Co-chairs: A. Taflove, USA and J. Volakis, USA

08:10 77.1 A Ray Tracing Technique for Predicting the Steady State Performance of Arbitrarily Shaped Reverberation Chambers, D.-H. KWON, **R.J. BURKHOLDER**, P.H. PATHAK, *Ohio State University, Columbus, OH, USA (URSI)*

08:30 77.2 Comparative Study of UTD and PTD Codes for Airborne Antenna Applications, **J.J. KIM**, O.B. KESLER, *Texas Instruments Incorporated, McKinney, TX, USA (URSI)*

08:50 77.3 Modification of the UTD Solution: Additional Transition Region Terms, **M. LUMHOLT**, *TICRA, Copenhagen K and Technical University of Denmark, Lyngby, Denmark (APS)*

09:10 77.4 UTD Analysis of Inter-Antenna EMC on Fully Realistic Aircraft Models, V. OLIKER[1], **P. HUSSAR**[2], [1]*Matis, Inc., Atlanta, GA and* [2]*IIT Research Institute, Annapolis, MD, USA (URSI)*

09:30 77.5 Scattering by the Unidirectionally Conducting Strip - Comparison of Different Techniques, **O. BREINBJERG**, M.V. JENSEN, M. LUMHOLT, *Technical University of Denmark, Lyngby, Denmark (URSI)*

09:50 77.6 High-Frequency Diffraction by a Strip on an Infinite Material Slab, S. SAPMAZ, **K. KOBAYASHI**, *Chuo University, Tokyo, Japan (URSI)*

10:10 Coffee Break

10:30 77.7 High-Frequency Analysis of Electromagnetic Fields Scattered by the Edges of Cylindrically Curved Conducting Surfaces, **T. ISHIHARA**, T. YAMAKI, *National Defense Academy, Yokosuka, Japan (URSI)*

10:50 77.8 On Radar Invisibility of an Impedance Wedge, **A.V. OSIPOV**, *St. Petersburg State University, St. Petersburg, Russia (URSI)*

JOINT-77.1

A Ray Tracing Technique for Predicting the Steady State Performance of Arbitrarily Shaped Reverberation Chambers

D.-H. Kwon, R.J. Burkholder*, and P.H. Pathak
The Ohio State University ElectroScience Laboratory
1320 Kinnear Road, Columbus, Ohio 43212

A useful high-frequency asymptotic ray technique is presented for the efficient computational analysis of electrically large and arbitrarily shaped reverberation chambers. Such chambers are being considered as an attractive alternative to the usual anechoic chambers for the purpose of testing the effect of high strength electromagnetic (EM) fields, with relatively arbitrary polarization, on objects containing vulnerable electronic components. The test object is placed within the chamber, and the chamber is excited by a source antenna or a waveguide fed aperture. The fields excited by the source build up to a high value via multiple wave interactions between the metallic walls of the chamber: hence the name reverberation chamber. A rotating "mode stirrer" may also be placed inside the chamber so as to try and produce a nearly uniform field distribution within the chamber much like in a conventional microwave oven. As a result, the test object can be subjected to an almost uniform high EM field with a relatively arbitrary polarization, thereby allowing a rapid testing procedure. While rectangular cavity shapes are of interest in the design of such reverberation chambers, other shapes are also being considered.

To date, it appears that the analysis of such large metallic enclosures has been performed largely by using statistical power balance techniques which provide average field values rather than a detailed field structure, or by perturbational local plane wave procedures that may require the computation of a perturbational series. While a modal analysis of such cavities has also been presented previously for rectangular enclosures, this procedure is rather inefficient due to a very large number of modes present in the large cavity, and it is restricted to a handful of cavity shapes for which the wave equation is separable such that the modes can be found in closed form. A purely numerical solution may be used at lower frequencies of operation for which the chamber may not be electrically large, but would quickly become intractable at higher frequencies.

Recently, a time domain ray tracing approach was proposed for analyzing the transient field build-up in a chamber, using a stepped input modulated at the steady-state frequency of interest (ω). While this approach can be applied to arbitrarily shaped chambers and can predict the early-time field build-up, it was found that an unrealistically large number of ray reflections would have to be included to predict the steady-state fields because very little energy is lost when a ray reflects from the highly conductive metallic walls used in practice. (Although it was shown that the ray fields in lossier chambers do indeed converge to steady-state after a manageable number of reflections). The early-time transient field in a realistic chamber due to a stepped input is highly erratic, and there is very little evidence of the expected $1-e^{-t/\tau}$ energy build-up, where τ is the time constant of the chamber related to the quality (Q) factor by $\tau = Q/\omega$ (D.A. Hill, et. al., *IEEE Trans. Electromag. Compat.*, 36, 169-178, 1994). However, it has now been found that a non-coherent summation of the power in each ray arriving at a point as a function of time is smoothly monotonic and has the expected $1-e^{-t/\tau}$ behavior. Furthermore, the time constant τ extracted from this function using curve-fitting closely agrees with the time constant of reference chambers, and is relatively independent of the observation point in the chamber (although the steady-state level of the function may change with position). This strongly supports the supposition that the steady-state performance of a reverberation chamber may be predicted from the early-time transient behavior which is obtainable using ray methods. The ray tracing and τ extraction technique will be presented along with computed results for a rectangular chamber and compared with a reference solution.

Comparative Study of UTD and PTD Codes for Airborne Antenna Applications

Jacob J. Kim* and Oren B. Kesler

Texas Instruments Incorporated
2501 West University Drive, MS 8019
McKinney, Texas 75070

If modern antenna systems are to function properly, the antenna radiation pattern must meet certain specifications. In fact, the antenna system performance is very much dependent upon the resulting antenna radiation patterns. For this reason, the design of airborne antenna systems requires radiation analysis of antennas on an aircraft structure. In recent years, many computer codes based on low frequency numerical techniques (e.g., MoM, FEM, FDTD, etc.) have been developed to predict the radiation characteristics of various antenna types. However, the global modeling of the large electrical size of realistic aircrafts is not usually included in the full-wave analysis. Thus airborne antenna radiation analysis techniques in the literature generally employ high-frequency approximations such as uniform geometrical theory of diffraction (UTD) and physical theory of diffraction (PTD).

Although there is a general understanding of the difference between UTD and PTD techniques, the capabilities of computer codes based on these techniques are not well known for airborne antenna applications. Thus we need a more accurate understanding of these techniques and the detailed capabilities of the computer codes to apply the prediction codes for optimum airborne antenna design. Currently there are three typical computer codes available for airborne antenna radiation analysis. The Ohio State University Aircraft code and NEC/Basic Scattering Code (NEC/BSC) are based on the UTD technique, and the DEMACO Apatch code is based on the PTD and Shooting & Bouncing Rays (SBR) technique.

This paper compares the accuracy, compuational efficiency, and geometry modeling capabilities of the above analysis codes when the antennas are mounted on a large airframe such as an aircraft fuselage or wing. A systematic investigation of various assumptions and their limitations in such techniques has been undertaken. The results were compared with measurements.

JOINT-77.4

UTD ANALYSIS OF INTER-ANTENNA EMC ON FULLY REALISTIC AIRCRAFT MODELS

Vladimir Oliker
Matis, Inc.
1565 Adelia Place
Atlanta, GA 30329

Paul Hussar*
IIT Research Institute
185 Admiral Cochrane Drive
Annapolis, MD 21401

Previously, implementation of the Uniform Geometrical Theory of Diffraction (UTD) to solve antenna radiation and coupling problems in platform environments has relied on simplified platform geometry representation as an assortment of simple shapes such as cylinders, ellipsoids, plates, etc. In contrast, solution of scattering problems via the Physical Theory of Diffraction commonly relies on highly realistic flat-faceted platform CAD models. The availability and faithfulness of flat-faceted models of numerous military aircraft makes it attractive to consider whether the utility range of these models can be extended to include support of analyses of radiation and coupling problems via the UTD. Here, the applicability of flat-faceted models to the computation of aircraft inter-antenna coupling will be demonstrated. A general procedure, known as the Propagation Path Finder (PPF) has been developed to permit identification of UTD propagation paths linking points (representing antenna terminals) located in the vicinity of a single flat-faceted geometrical object of general shape. The employment of the PPF-computed paths in the analysis of inter-antenna coupling in terms of UTD wedge-diffraction and surface-diffraction mechanisms will be described. In particular, it will be shown that realistic values for curved-surface geometrical parameters required by the UTD can be directly obtained from suitable flat-faceted aircraft representations.

SCATTERING BY THE UNIDIRECTIONALLY CONDUCTING STRIP - COMPARISON OF DIFFERENT TECHNIQUES

Olav Breinbjerg*, Morten Vogh Jensen, Michael Lumholt
Department of Electromagnetic Systems
Technical University of Denmark
DK-2800 Lyngby, Denmark

The plane wave scattering from a unidirectionally conducting (UEC) strip is analysed employing different approximate techniques. These are based on the exact analytical solution for the UEC half-plane problem and account for different scattering mechanisms such as first-order edge diffraction, second-order edge diffraction and surface wave diffraction. The accuracy of the different approximate techniques is determined through comparisons with integral equation (IE) results.

The UEC strip ($-w \le x \le w, y = 0, -\infty < z < \infty$) is illuminated by a plane wave incident from the direction (θ^i, ϕ^i). The direction of infinite conductivity is $\hat{u} = \hat{x}\cos\alpha - \hat{z}\sin\alpha$. The UEC strip is modelled by two partly overlapping UEC half-planes occupying $(x \ge -w, y = 0, -\infty < z < \infty)$ and $(x \le w, y = 0, -\infty < z < \infty)$, respectively. For the surface current density, the following three approximate techniques are investigated: PO being the physical optics current for the infinite UEC plane, PO+FW being the superposition of the PO current and the fringe wave currents on the two half-planes, PO+FW+SW being the superposition of the PO+FW current and the surface wave currents on the two half-planes. For the scattered far-field, three approximations are calculated as the fields radiated by the aforementioned three sets of currents. A fourth approximation is based on edge diffraction coefficients extracted from the exact UEC half-plane solution. The techniques based on currents constitute a Physical Theory of Diffraction formulation while the technique based on diffraction coefficients constitutes a Geometrical Theory of Diffraction formulation.

Results for the surface current density are shown below for one specific configuration. The accuracy of the different techniques and the importance of the SW current are apparent.

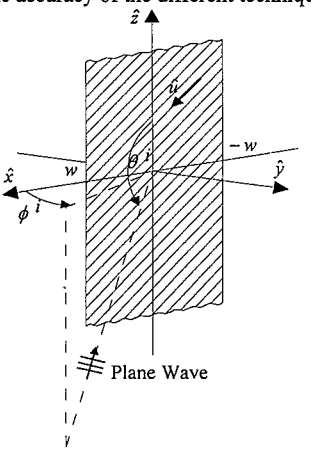

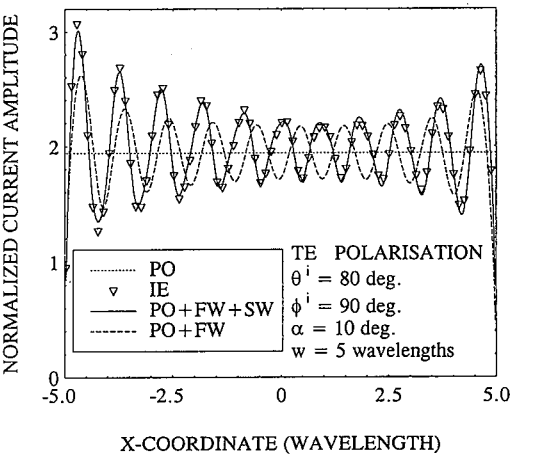

JOINT-77.6

HIGH-FREQUENCY DIFFRACTION BY A STRIP ON AN INFINITE MATERIAL SLAB

Sevtap Sapmaz and Kazuya Kobayashi*
Department of Electrical and Electronic Engineering, Chuo University
1-13-27 Kasuga, Bunkyo-ku, Tokyo 112, Japan

The problem of diffraction by strips in the proximity of medium discontinuities is an important subject in diffraction theory, and it is relevant to several engineering applications. Regarding the diffraction by strips in a homogeneous medium, a number of papers were published and various significant results have been obtained. However, there are only a few contributions related to the diffraction problem where the strips are located between two media (J. M. van Splunter and P. M. van den Berg, *Can. J. Phys.*, 57, 1148–1156, 1979; A. Büyükaksoy and G. Uzgören, *Radio Sci.*, 22, 183–191, 1987). In our recent paper, we have analyzed the high-frequency diffraction by a perfectly conducting strip located at the plane interface between two semi-infinite media using the Wiener–Hopf technique to derive lateral wave contributions and uniform asymptotic expressions for the diffracted field, which are not known in the previous works (S. Sapmaz, K. Kobayashi, A. Büyükaksoy and G. Uzgören, *IEICE Trans. Electron.*, E79-C, 709–719, 1996). As an important generalization to the problem treated in our previous paper, we shall investigate in this paper the plane wave diffraction by a strip located on an infinite material slab for both E and H polarizations by the Wiener–Hopf technique.

The geometry of the problem is illustrated in Fig. 1, where u^i is the incident plane wave of E or H polarization, and the regions $y > 0$, $y < -d$ and the region $-d < y < 0$ are characterized by the relative permittivity/permeability (ε_1, μ_1) and (ε_2, μ_2), respectively. In the figure, the perfectly conducting strip of zero thickness occupies the region $\{(x, y, z) |\ 0 < x < l,\ y = 0,\ z \in (-\infty, \infty)\}$. Applying boundary conditions to the Fourier integral representations for the unknown scattered field, the problem is formulated in terms of the modified Wiener–Hopf equation, which is reduced to a pair of simultaneous integral equations via the factorization and decomposition procedure. The method of successive approximations is then applied, and the first, second and third order asymptotic solutions of the integral equations are derived explicitly for the strip width large compared with the wavelength. Taking the inverse Fourier transform and applying the saddle point method, the high-frequency scattered far field expression is derived. It is shown that the first order solution leads to the geometrical optics field, the singly diffracted field and the surface waves, while the second and third order solutions correspond to the doubly and triply diffracted fields, respectively. Numerical examples of the radar cross section are presented and the far field scattering characteristics of the strip are discussed.

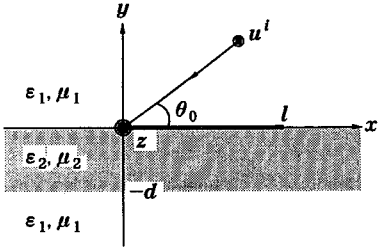

Fig. 1. Geometry of the problem.

HIGH-FREQUENCY ANALYSIS OF ELECTROMAGNETIC FIELDS SCATTERED BY THE EDGES OF CYLINDRICALLY CURVED CONDUCTING SURFACES

T. Ishihara* and T. Yamaki
Dept. of Electrical Engineering
National Defense Academy
Hashirimizu, Yokosuka, 239, Japan

High-frequency solutions for the diffraction of an electromagnetic wave incident on the edges of cylindrically curved perfectly conducting surfaces are examined in the present study. When the creeping wave or the geometrical ray is incident on one of the edges of the cylindrically curved surface, the edge diffracted rays, the surface diffracted rays, and the whispering gallery modes are excited in the respective regions. These waves again become the incident waves on the other edge of the cylindrically curved surface. Between the regions for the edge diffracted rays and the surface diffracted rays, the transition region surrounding the tangent to the surface at the edge of the cylindrically curved surface is appeared in the convex side. Also, the field points in the concave side are divided into two regions by the existence of the edges of the cylindrically curved surface; the creeping waves (or the surface diffracted rays) are observed in one of the regions, while those waves disappear in the other region.

We have derived analytically the uniform asymptotic representations for the radiated field from the concave surface exited by the incident whispering gallery modes by applying the asymptotic techniques in evaluating the integral representation of the scattered field. We have also derived the asymptotic representation for the scattered field in the transition region between the surface diffracted rays and the edge diffracted rays. In order to obtain the smooth variation of the scattered field in the transition region in the concave side, we have derived the pseudo creeping wave representation.

The asymptotic field representations proposed here are compared numerically with the results calculated from the moment method. Numerical comparisons with the reference solution reveal the validity and the utility of the various asymptotic representations and the pseudo creeping wave representation. Also shown are the transient electromagnetic scattered fields excited by the incident pulse with truncated Gaussian time variation.

JOINT-77.8

ON RADAR INVISIBILITY OF AN IMPEDANCE WEDGE

Andrey V. OSIPOV
Institute of Radio Physics, St. Petersburg State University
Uljanovskaja 1, Petrodvorets, 198904 RUSSIA

This paper presents the far-field analysis of the electromagnetic scattering from a wedge of exterior angle 2Φ with impedance faces. It starts with Malyuzhinets' solution (G.D.Malyuzhinets, Sov. Phys. Dokl., **3**, 752-755, 1958) for diffraction of a plane wave in a wedge-shaped domain defined in the polar co-ordinate system by $0 \le r < +\infty$ and $-\Phi < \phi < \Phi$ with $\Phi \ge \pi / 2$, while the material properties of the wedge faces are described by an associated Brewster angle θ that relates to the normalised surface impedance through the relation $\eta = \sin\theta$ if the field is H polarised, or through $\eta^{-1} = \sin\theta$ for E-polarised field. At large distances from the edge of the wedge where $r >> \lambda$ and λ is the wavelength, the Malyuzhinets solution is evaluated asymptotically and a simple expression for the backscattering diffraction coefficient of an impedance wedge is derived. It is demonstrated that the monostatic tip diffraction from a wedge of arbitrary angle can be made to vanish by appropriate choice of the surface impedance. The unique value of impedance is always real, and explicit formula is given for its evaluation. The figure shows the monostatic backscattering echowidth σ / λ (in *dB*) of a wedge with $\Phi = 7\pi / 8$ as a function of the observation angle ϕ for several values of the face impedances : $\theta = \pi / 2$ - curve 1, $\theta = \pi / 5$ - curve 2, $\theta = \pi / 8$ - curve 3, $\theta = \pi / 10$ - curve 4, $\theta = 0$ - curve 5, and $\theta = i\infty$ - curve 6. Curves 2 and 3 demonstrate the phenomenon of the "invisibility" of an impedance wedge at $\phi \approx \pm 37^{o}$ and $\phi = 0^{o}$, respectively, because in these directions the backscattering diffraction coefficient nullifies. Also in a notable vicinity of those observation angles, the RCS level remains rather low, lower than that of the so-called absorbing wedge with normalised surface impedance unity (curve 1).

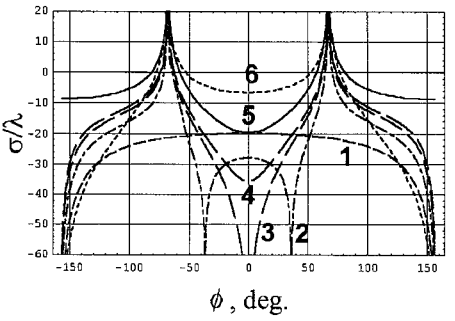

APS/URSI B Special Session **Session 100** **Salon St-Maurice**

Frontiers of Mathematical Methods in Electromagnetics
Co-chairs: D.H. Werner, USA and R. Mittra, USA

13:10 100.1 **Invited:** In Search of a Physically Realizable Perfectly Matched Absorber, R. MITTRA, **D.H. WERNER**, *Pennsylvania State University, University Park, PA, USA (URSI)*

13:30 100.2 **Invited:** Fractal Constructions of Linear and Planar Arrays, **D.H. WERNER**[1], R.L. HAUPT[2], [1]*Pennsylvania State University, State College, PA and* [2]*HQ USAFA/DFEE, USAF Academy, CO, USA (APS)*

13:50 100.3 **Invited:** Fractal Superlattices and Scattering: Lacunarity, Fractal Dimension and Stage of Growth, A.D. JAGGARD[1,2], **D.L. JAGGARD**[2], [1]*Wheaton College, Wheaton, IL and* [2]*University of Pennsylvania, Philadelphia, PA, USA (URSI)*

14:10 100.4 **Invited:** Fractal Apertures: The Effect of Lacunarity, **D.L. JAGGARD**[1], A.D. JAGGARD[1,2], [1]*University of Pennsylvania, Philadelphia, PA and* [2]*Wheaton College, Wheaton, IL, USA (URSI)*

14:30 100.5 **Invited:** Extension of the Electrostatic Fractional Image Method to the Case of Electrostatic Dielectric Wedge, **N. ENGHETA**, *University of Pennsylvania, Philadelphia, PA, USA (URSI)*

14:50 100.6 **Invited:** Spherical-Multipole Analysis of Scattering by Finite and Semi-Infinite Elliptic Cones, S. BLUME, **L. KLINKENBUSCH**, *Ruhr-Universität Bochum, Germany (APS)*

15:10 100.7 **Invited:** Scattering Dyadic for Self-Dual Target, **C.E. BAUM**, *Phillips Laboratory WSQW, Kirtland AFB, NM, USA (URSI)*

15:30 100.8 **Invited:** Genetic Algorithm Optimization of Stacked Vertical Dipoles above a Ground Plane, **P.L. WERNER**[1], Z. ALTMAN[2], R. MITTRA[1], D.H. WERNER[1], A.J. FERRARO[1], [1]*Pennsylvania State University, University Park, PA, USA;* [2]*Issy-Les-Moulineaux, France (APS)*

15:50 100.9 **Invited:** A Discussion and Survey of Model-Based Parameter Estimation in Computational Electromagnetics, **E.K. MILLER**, *Sante Fe, NM, USA (APS)*

16:10 100.10 **Invited:** Adaptive Decomposition in Electromagnetics, **J.W. BURNS**, N.S. SUBOTIC, D. PANDELIS, *Environmental Research Institute of Michigan, Ann Arbor, MI, USA (APS)*

16:30 100.11 **Invited:** Resolution of a Neural Network Direction Finding Array, **H.L. SOUTHALL**, *USAF Rome Laboratory, Hanscom AFB, MA, USA (APS)*

16:50 100.12 Multipath Mitigation in Compact RCS Ranges Using the Network Model and 2-D PML Spectral Estimation Techniques, J.F. STACH, **I.J. LAHAIE**, E.I. LEBARON, *Environmental Research Institute of Michigan, Ann Arbor, MI, USA (URSI)*

17:10 100.13 **Invited:** A Fourth-Order Compact Difference Scheme for Maxwell's Equations, **J.L. YOUNG**[1], D. GAITONDE[2], J.S. SHANG[2], [1]*University of Idaho, Moscow, ID and* [2]*WL/FIMC, Wright-Patterson AFB, OH, USA (APS)*

JOINT-100.1

In Search of a Physically Realizable Perfectly Matched Absorber

Raj Mittra & Douglas H. Werner
EE Department & Applied Research Laboratory
Pennsylvania State University, University Park, PA

The quest for an efficient absorber for microwave frequencies has had a very long history because of its potential application in the reduction of reflection from radar targets. One promising candidate that has been extensively researched in recent years is the chiral medium which has been shown to absorb microwave energy, though for a limited range of frequencies and incident angles. Since it is desirable for the absorber to perform over a relatively wide band of frequencies as well as range of incident angles, and since none of the available candidates satisfy these criteria sufficiently well, a vigorous search for such an absorber still continues unabated today.

Recently, Berenger introduced the concept of a Perfectly Matched Layer (PML), and demonstrated that a half-space of such a medium is indeed non-reflecting, regardless of the frequency, angle of incidence and polarization of the incidence wave. Subsequently, a whole host of authors have found alternate descriptions of such a medium, using, for example, a stretched coordinate system (Rappaport, *IEEE Microwave Guided Wave Lett.*, **5,** 90-92, 1995), anisotropic constitutive parameters (Sacks et al., *IEEE Trans. Antennas Propagat.*, **43,** 1460-1463, 1995; Gedney, *IEEE Trans. Antennas Propagat.*, **44**(12), 1630-1639, 1996), and an unsplit representation (Mittra and Pekel, *IEEE Microwave Guided Wave Lett.*, **5,** 84-87, 1995; Veihl, Ph.D. Dissertation, 1996). It has been adequately and unquestionably verified that the PML indeed possesses the kind of remarkable non-reflecting characteristics claimed by Berenger in his original paper. However, while the PML concept has been extensively applied for mesh truncation in Finite Difference Time Domain (FDTD) and Finite Element (FE) codes, neither the split-field representation of Berenger, nor the stretched-coordinates or anisotropic medium representations have, as yet, been translated into a physically-realizable absorbing medium that can actually be fabricated. There are several obvious reasons for this: Berenger's equations contain split, non-physical E and H-field components; the coordinate streching cannot be accomplished in practice as it can be on paper; and, the anisotropic ε and μ tensors have negative real conductivities in one of their elements. More recently, at the 1996 AP-S/URSI symposium, Zilkowski has provided an insight into the fundamental differences between the chiral and PML-type media, and has gone on to propose the concept of a time-dependent Lorentz medium that also possesses absorbing characteristics similar to PML. However, to date, the development of a physically realizable version of this medium is still pending.

The objective of this paper is to develop a version of the PML equations, derived from their unsplit forms originally introduced by Mittra and Pekel, that has the potential for systematic translation into an artificial (but physical) dielectric/magnetic medium with the desirable absorption characteristics over a broad band of frequencies and a wide range of incident angles. Unlike a chiral medium, the proposed PML neither relies upon the resonance characteristics of the inclusions, nor on the absorption characteristics of the background medium in which they are embedded. The geometrical characters of the inclusions themselves are very different than those of the helices and loop-dipole combinations employed in the chiral medium, and are comprised, instead, of periodic arrays of discs, knots, and variants of these configurations.

Fractal Superlattices and Scattering: Lacunarity, Fractal Dimension and Stage of Growth

Aaron D. Jaggard*† and Dwight L. Jaggard†

*Department of Mathematics
Wheaton College
Wheaton, IL 60187
adj@pender.ee.upenn.edu

†Moore School of Electrical Engineering
Complex Media Lab., Univ. of Pennsylvania
Philadelphia, PA 19104-6390
jaggard@pender.ee.upenn.edu

Introduction

Reflection and transmission properties of finely divided fractal layers (superlattices) are formulated, solved analytically, and characterized for variations in lacunarity (texture or "gappiness"), fractal dimension, and stage of growth. The scattering coefficients are found for different stages of fractal growth using a *doubly recursive method.* This computational technique efficiently provides the reflection and transmission coefficients for a large number of interfaces. This is a continuation of the initial research [D. L. Jaggard and A. D. Jaggard, *Optics Lett. 22,* 145-147 (Feb. 1, 1997)] on the effect of lacunarity on fractals and waves.

Reflection from Superlattices

Fractals are characterized by their self-similarity and are invariant under change of scale. The research reported here is concerned with the reflection and transmission of electromagnetic waves from polyadic superlattices. We characterize wave interactions with these structures and relate scattering properties to geometrical *fractal descriptors* such as lacunarity, fractal dimension, and stage of growth. The results for valid for arbitrary angle of incidence.

The analytical solution developed here displays the functional form of the solution of a family of fractal structures which are formed through iteration. In this way, the iterative nature of the geometry is directly related to the iterative nature of the solution and the physics of the problem is linked to its mathematics.

Reflection from stage one and stage two of a three-gap fractal superlattice is shown as a function of *kL* (normalized superlattice length) and a measure of lacunarity (epsilon). Light regions denote large reflection and dark regions denote nulls. Note the fine structure of second stage of growth (lower plot) when compared to its first stage of growth counterpart (upper plot).

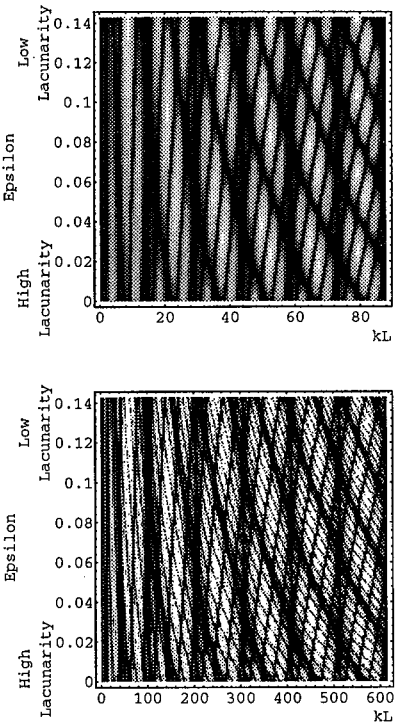

JOINT-100.4

Fractal Apertures: The Effect of Lacunarity

Dwight L. Jaggard† and Aaron D. Jaggard*†

†Moore School of Electrical Engineering
Complex Media Lab., Univ. of Pennsylvania
Philadelphia, PA 19104-6390
jaggard@pender.ee.upenn.edu

*Department of Mathematics
Wheaton College
Wheaton, IL 60187
adj@pender.ee.upenn.edu

Introduction

Electromagnetic waves can be used to remotely extract information on the fractal nature of a structure through observation of the scattered fields. Here, the wavelength of the incident fields is used as a variable length electromagnetic yardstick to interrogate the multi-scale nature of a family of fractal apertures. The goal is to investigate the effect of fractal type, fractal dimension, lacunarity, and stage of growth on the diffracted fields.

This work has applications to the synthesis of new arrays and apertures based on fractal geometry. The first work in this area considered the fractal distribution of array elements for robust, sparse linear arrays [Y. Kim and D. L. Jaggard, *Proc. IEEE 74,* 1278-1280 (1986)]. More recent work has investigated fractal antenna elements as well as self-similar apertures. The latter forms the basis for the research reported here.

Diffraction from Fractals

Fractals are characterized by their self-similarity and are invariant under change of scale. This dilation symmetry can be used to calculate the diffracted fields through iteration. The amount of space a fractal occupies is measured by its *fractal dimension.* The texture or "gappiness" of a fractal is measure by its *lacunarity.* Of particular interest here is the effect of lacunarity on diffraction.

This research builds on previous investigations of triadic Cantor targets [D. L. Jaggard and T. Spielman, *Microwave and Optical Tech. Lett. 5,* 460-466 (August 1992)] and two-dimensional generalized Cantor apertures [D. L. Jaggard, T. Spielman, and M. Dempsey, IEEE AP-S/URSI Meeting, Ann Arbor (1993)].

Fractal Apertures

Examples of fractal apertures are shown below. On the left is the triadic cantor target while on the right is a Cantor square. The iterative process used to generate these apertures allows one to find closed-form solutions for the diffracted fields.

Here we find the self-similarity of the apertures below and others is evident in their diffraction patterns.

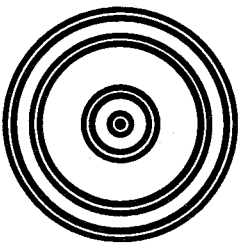

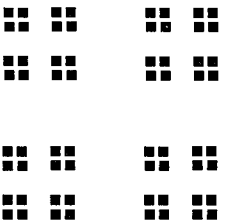

EXTENSION OF THE ELECTROSTATIC FRACTIONAL IMAGE METHOD TO THE CASE OF ELECTROSTATIC DIELECTRIC WEDGE

Nader Engheta

Moore School of Electrical Engineering
University of Pennsylvania
Philadelphia, Pennsylvania 19104, U.S.A.
Tel: (215) 898-9777, Fax: (215) 573-2068
E-mail: engheta@pender.ee.upenn.edu

Recently, we introduced and studied the idea of electrostatic fractional image methods for perfectly conducting wedges and cones using the tool of fractional calculus [N. Engheta, "Electrostatic "Fractional" Image Methods for Perfectly Conducting Wedges and Cones" *IEEE Trans. on Antennas and Propagation*, Vol. 44, No. 12, pp. 1565-1574, Dec. 1996]. This idea was based on our earlier work on the concept of fractional multipoles in electromagnetism [N. Engheta, "On Fractional Calculus and Fractional Multipoles in Electromagnetism" *IEEE Trans. Antennas & Propagation*, Vol. 44, No. 4, pp. 554-566, April 1996]. In that image method, we have shown that for the two-dimensional (2-D) electrostatic potential distributions in front of a perfectly conducting wedge with arbitrary wedge angles, and for the three-dimensional (3-D) potential in front of a perfectly conducting cone with arbitrary cone angles, electric potentials can be described equivalently as the electrostatic potentials of sets of equivalent "image" charge distributions that effectively behave as "fractional-order" multipoles, hence the name "fractional" image methods. The fractional orders of these so-called fractional images depend on the wedge angle (for the wedge problem) and on the cone angle (for the cone problem).

In the present work, we have been able to extend this fractional image method to the case of 2-D electrostatic potential of a *dielectric* wedge with arbitrary wedge angle. It is well known that the electrostatic potential due to a 2-D static uniform line charge in the presence of a 2-D dielectric wedge can be solved using Poisson's equation [see, e.g., R. W. Scharstein, "Mellin Transform Solution for the Static Line-Source Excitation of a Dielectric Wedge", *IEEE Trans. on Antennas and Propagation*, Vol. 41, No. 12, pp. 1675-1679, Dec. 1993, and K. I. Nikoskinen and I. V. Lindell, "Image Solution for Poisson's Equation in Wedge Geometry," *IEEE Trans. on Antennas and Propagation*, Vol. 43, No. 2, pp. 179-187, Feb. 1995]. In our fractional image method for the dielectric wedge, which uses the concept of fractional derivatives/integrals, we show that the potential distribution can be expressed in terms of electrostatic potentials of several "fractional-order images" that are situated at various locations. We also demonstrate that the magnitudes and fractional orders of these fractional images depend on parameters such as the relative dielectric constant of the wedge and the wedge angle. As expected, in the limit of infinite relative permittivity these results approach those of the fractional images for the perfectly conducting wedges. In this talk, we present some of our recent results of this study and discuss physical insights and justifications into these findings.

JOINT-100.7

Scattering Dyadic for Self-Dual Target

Carl E. Baum
Phillips Laboratory WSQW
3550 Aberdeen Avenue SE
Kirtland AFB, New Mexico 87117-5776

One of the symmetries one can impose on a target is that of self-duality, i.e., invariance to interchange of electric and magnetic parameters (including dyadic constitutive parameters). With this symmetry, the scattering dyadic describing the scattering of electromagnetic waves attains special properties. A result valid for general incidence and scattering directions in that rotation of the incident field about the direction of incidence is matched by an equal rotation of the scattered field about the direction of scattering. For forward scattering the two rotation directions are the same, but for backscattering, they are opposite. The temporal waveforms are invariant to this transformation. In backscattering, this makes the scattering dyadic symmetric without having yet assumed reciprocity. Various point symmetries of the target also introduce simplifications (symmetries) in the scattering dyadic. In backscattering, if there is a reflection plane through the observer, the scattering dyadic becomes diagonal (with only one independent element) when referred to appropriate transverse (h,v) axes. If there is an N-fold rotation axis passing through the observer, the backscattering is zero for $N \geq 3$.

In forward scattering, the scattering dyadic is a combination of the transverse identity and a rotation (only two independent components). For a target with inversion symmetry, the scattering dyadic is invariant to reversal of the direction of incidence (and scattering). This also applies to special cases of rotation and/or reflection symmetry with an axis or normal to the reflection plane parallel to the direction of incidence. If inversion symmetry is combined with reciprocity, the scattering dyadic is proportional to the transverse dyadic (no depolarization).

For low frequencies (wavelengths large compared to the target) the scattering is dominated by the induced electric-and magnetic-dipole moments. For self-dual targets, the two polarizabilities are equal. This gives an invariance to combined reversal of directions of incidence and scattering. For the special symmetries of tetrahedral (T), octahedral (O), icosahedral (Y), and spherical (O_3) (including reciprocity), the forward scattering is polarization independent for all target orientations.

Multipath Mitigation in Compact RCS Ranges Using the Network Model and 2-D PML Spectral Estimation Techniques

John F. Stach, Ivan J. LaHaie*, and Edward I. LeBaron
Environmental Research Institute of Michigan
P.O. Box 134001, Ann Arbor, MI 48113-4001
stach@erim.org, lahaie@erim.org, lebaron@erim.org

Recent studies on error budgets for compact RCS ranges have indicated that nonuniform illumination of the target can be a significant source of measurement error, particularly if the target RCS is characterized by large dynamic range variations (specular flashes, etc.). These deviations from an ideal plane wave illumination can arise from both the finite aperture of the collimator (either a reflector or an array) as well as from multipath reflections off the chamber walls/structures, and become most significant at the lower frequency limits of the range, where the reduced size (in wavelengths) of both the aperture and the absorber treatment makes it more difficult to confine the energy in a well-collimated beam. While there has been recent work on accurately characterizing the range illumination imperfections using 2-D (planar) field probes and/or flat plate scanning, little research has been done on using this information to mitigate the resulting RCS measurement errors (which we will refer to in general as "multipath").

We will present a technique for multipath error mitigation based on the network model (NM) algorithm (J.F. Stach, Proc. AMTA, 178-181, 1995). The NM algorithm uses the knowledge of the range illumination to perturb a moment method model of the target so that it is consistent with the contaminated RCS measurements. It then uses the perturbed model to predict the RCS under ideal plane wave illumination. The perturbation is performed in a minimum norm sense, and the accuracy of the prediction is dependent on the accuracy of the underlying MoM target and illumination models, as well as on the diversity and signal-to-noise ratio of the measured RCS data. A key aspect of the NM technique is the need to predict the target RCS under the (known) nonideal illumination. Because most available MoM codes are restricted to plane wave illumination, it is desirable to represent the range illumination as a discrete spectrum of plane waves. Conventional Fourier analysis of 2-D field probes will yield such a representation, but because of its poor resolution at lower frequencies, an extremely large number of plane waves (on the order of the number of probe samples) are needed to accurately represent the field. This in turn leads to an excessively large burden in the MoM computations. We will demonstrate the use of a coherent, 2-D nonlinear spectral estimation algorithm called 2-D Parametric Maximum Likelihood (PML) (S.R. DeGraaf, Proc. ASSP Workshop Spectrum Est. and Mod., 391-396, 1988) to provide an accurate representation of the field in terms of a small number (10-20) of plane waves, thereby significantly reducing the computational burden.

We will present numerically-simulated results of multipath mitigation using a simple, generic model for the compact range illumination. The tradeoff between target/illumination model accuracy, data diversity, and measurement noise will be illustrated. We will show that the multipath contamination can be reduced to the level of the residual measurement errors using a relatively simple MoM model for the target.

APS/URSI Special Session **Session 105** **Salon Richelieu**

Radiation Physics
Co-chairs: E.K. Miller, USA and R.C. Hansen, USA

13:10 105.1 Duality in Antennas, **R.C. HANSEN**, *R.C. Hansen, Inc., Tarzana, CA, USA (URSI)*

13:30 105.2 UTD Perspective on Where Objects Radiate, **R.J. MARHEFKA**, *Ohio State University, Columbus, OH, USA (URSI)*

13:50 105.3 The Interpretation of Body Current Distributions in Designing Low-RCS Scatterers, **S. CASTILLO**, *New Mexico State University, Las Cruces, NM, USA (URSI)*

14:10 105.4 Numerical and Physical Characterization of Radiation from Discontinuities in Electromagnetic Systems, **T.K. SARKAR**[1], M. SALAZAR-PALMA[2], [1]*Syracuse University, Syracuse, NY, USA;* [2]*Universidad Politécnica de Madrid, Spain (URSI)*

14:30 105.5 The Differential Radiated Power of a Sinusoidal Filament of Electric Current, **J.R. MAUTZ**, E. ARVAS, *Syracuse University, Syracuse, NY, USA (APS)*

14:50 105.6 An Analytical Investigation of the Loaded V-Dipole as a Transient Radiator, **S.M. BOOKER**[1], P.D. SMITH[2], [1]*New Jersey Institute of Technology, Newark, NJ, USA;* [2]*University of Dundee, UK (URSI)*

15:10 Coffee Break

15:30 105.7 On the Origin of the Radiation Field, R. GÓMEZ MARTIN, **A. RUBIO BRETONES**, I. SÁNCHEZ GARCIA, *Universidad de Granada, Spain (URSI)*

15:50 105.8 Power Radiated by Accelerating Charge, **J.R. MAUTZ**, E. ARVAS, *Syracuse University, Syracuse, NY, USA (APS)*

16:10 105.9 Radiation Center Identification by Normalized Pattern Function Imaging, **J.S. GWYNNE**, J.D. YOUNG, *Ohio State University, Columbus, OH, USA (URSI)*

16:30 105.10 An Exploration of Radiation Physics in Electromagnetics, **E.K. MILLER**, *Santa Fe, NM, USA (APS)*

JOINT-105.1

DUALITY IN ANTENNAS

R. C. Hansen
Consulting Engineer
Tarzana, CA 91357

Duality in physics between waves and particles is well known. There is also a duality in antenna theory between current distributions and discontinuities which is less well known. Accelerated charges, or varying currents, radiate (Jackson), whereas uniform currents do not radiate. Nonetheless all of us calculate antenna patterns as the Fourier transform of a current distribution and from this one readily calculates radiated power and radiation resistance. An example is the thin dipole with a sinusoidal current distribution. A more complete integral transform, performed in 1932 by Carter, yields the exact near-fields of the thin dipole, and of course radiation resistance and reactance. It is the shape (and phase) of the current distribution that leads to exact near-fields.

Examination of Carters result leads to the dual model; the near-fields consist of three spherical waves in cylindrical coordinates. A spherical wave radiates from each end of the dipole, and a third spherical wave emanates from the center, if the dipole length is different from half-wavelength. The standing wave of current might be considered to be comprised of two oppositely directed travelling waves, and in fact probably all non-constant current distributions are composed of some combination of travelling waves, leaky waves, and surface waves. Thus the dual approach to a dipole assumes the sinusoidal current distribution to be produced by two travelling waves. These travelling waves do not radiate along their length, but radiation occurs at the discontinuities: the ends and center of the dipole. The complete dual calculation was made possible when Chang computed the reflection coefficient for a wire using the Weiner-Hopf technique. New insight into the behavior of antennas might be provided from the consideration of reflection coefficients experienced by uniform currents at various types of discontinuities.

UTD Perspective on Where Objects Radiate

Ronald J. Marhefka
The Ohio State University
ElectroScience Laboratory
1320 Kinnear Road
Columbus, OH 43212-1191

The Uniform Geometrical Theory of Diffraction (UTD) has been used successfully for a long time in the analysis of antennas in the presence of large scattering structures. One of the features that has made it useful is that it represents the scattering and radiation from an object as discrete localized centers. This concept came from asymptotic mathematical theory (stationary phase, end points, etc.) as well as physical insight into how light interacts with bodies. At frequencies pertinent to communication and radar systems, we more or less took the concept on faith. Modern visualization tools allow us to view the scattering centers and make one to one correlation of them to our previously hypothesized UTD ray paths. The measurement and theory compare, so we are confident in the validation of both concepts.

The process of correlating high resolution measurements with UTD can be very useful in many ways. To illustrate this point, an example of scattering from plates will be discussed. From a UTD point of view, first order far zone scattering from plates can be modeled by radiation from their vertices only. On comparing calculated with measured patterns, it is discovered that classical asymptotic theories (UTD, PTD, etc.) that include first order and even edge to edge diffractions do not predict all the lobes measured. A technique to define a new additional vertex component that accounts for these missing lobes has been developed. In order to determine the proper interpretation and to validate the results, plates were measured over sufficient angle increments and frequency bandwidths. The data is processed into the image domain, the returns from everything but a localized vertex region is gated out and the data is transformed back to the pattern domain. This leaves a result presumably scattering from just the chosen vertex. Comparing the new vertex diffraction coefficient comprised of the original first order plus the newly developed vertex component with the localized measurements shows excellent agreement validating both results.

These same scattering centers can apply to antenna radiation as well. Data for ultra-wide band rhombic type antennas used in SAR applications measured by Young and Gwynne indicate that along with the feed point, vertex locations are points of radiation.

JOINT-105.3

THE INTERPRETATION OF BODY CURRENT DISTRIBUTIONS IN DESIGNING LOW-RCS SCATTERERS

Steven Castillo
The Klipsch School of Electrical and Computer Engineering
New Mexico State University
Dept. 3-O, Box 30001
Las Cruces, NM 88003

The design of a low Radar Cross-Section (RCS) body is an optimization process. However, the number of variables affecting the RCS is overwhelming. Typically, the design procedure is performed using physical intuition together with a high-frequency analysis of the scatterer. In such a case, coupling between various parts of the body is small so that the total RCS can be considered to be the sum of the individual, independently calculated RCS contributions.

As the frequency is decreased, the coupling between the various parts of the body increases so that each part can no longer be analyzed seperately. Thus, a full-wave solution of the scattering problem must be used. Once the RCS is calculated for the scatterer at a given frequency, the question arises as to what is contributing to the calculated (or measured for that matter) RCS? Considering only the relative magnitude of the currents on the body can lead to erroneous conclusions since the phase relationships between the fields produced by the currents are being neglected. Standard imaging techniques that rely on artificially added bandwidth that are robust in the high-frequency regime also fail at lower frequencies since the strong coupling between various regions on the scatterer as a function of frequency is neglected.

Examining the coherent, contributions of each of the current elements (a single patch for a moment-method solution) to the far field is an accurate method of determining the contribution of the currents to the total RCS. Coherent, far-field contribution data is easily extracted from an existing method-of-moments (MoM) code without adding any computational complexity. In this paper, we examine the use of coherent, far-field contribution data for several different scatterers over moderately wide frequency bands. Conclusions will be given concerning the affects that changes in a given geometry as well as a change in frequency can have on the RCS of some relatively simple shapes.

Numerical and Physical Characterization of Radiation From Discontinuities in Electromagnetic Systems

Tapan K. Sarkar
Department of Electrical Engineering and Computer Science
121 Link Hall
Syracuse University
Syracuse, New York 13244-1240
Tel: 315-443-3775; Fax: 315-443-4441
Email: tksarkar@mailbox.syr.edu

Magdalena Salazar-Palma
ETSI de Telecommunicacion
Universidad Politecnica de Madrid
Cindad Universitaria
28040 Madrid

Abstract: Radiation is claimed to be energy emanated from structures when there is acceleration or deceleration of charges flowing in that system. In an approximate fashion, the radiation fields are given by the time domain by $\partial A/\partial t$ or in the frequency domain by $-j\omega A$. The objective of this presentation is how to characterize radiation from transmission lines and discontinuities in transmission structures. A unified methodology is presented to illustrate why a dynamic solution procedure is required to extract radiation characteristics. Based on the unitary properties of the s-parameters for lossless networks it is possible to predict the power leakage from a discontinuity and thereby localize the area of energy loss. The presentation will illustrate the details of the analysis of open line transmission structures including the dynamic analysis which is used to solve for the current distribution on the entire structure. Once the current distribution is known, two planes are selected at which the current distribution is decomposed into forward and backward travelling waves and other higher order evanescent and propagating modes. Based on the dominant mode the s-parameters can be computed and since the multiport s-parameters form a unitary matrix for lossless structures, the amount of power that is radiated. Numerical examples will be presented to illustrate the application of the methodology.

The objective of this presentation is to illustrate that it is possible to localize regions where the power loss has occurred. Since one is analyzing lossless devices, the power loss from a region can be directly related to radiation as there is no other mechanism through which powerloss can occur in a lossless circuit.

JOINT-105.6

An analytical investigation of the loaded V-dipole as a transient radiator

S.M. Booker*
Department of Mathematics
New Jersey Institute of Technology, Newark, NJ, U.S.A.

P.D. Smith
Department of Mathematics and Computer Science
University of Dundee, Dundee, Scotland, U.K.

In recent years there has been considerable and growing interest in the potential of transient electromagnetics for a wide variety of applications. The development of such applications depends, in part, on a better understanding of the physical processes underlying transient radiation.

A direct time domain analysis of a V-dipole antenna loaded with an arbitrary impedance profile is presented. The V-dipole is assumed to support initially a transient current pulse which propagates outwards along the antenna arms; the form of this pulse is directly related to the voltage applied to the antenna feed point. The far field radiated by the loaded V-dipole is determined from this ansatz yielding an approximation for the early-time radiation in a simple integral form. The integral obtained is trivial to evaluate, and in many cases a closed form solution may be obtained.

Two examples are presented of a V-dipole antenna excited by a gaussian voltage source: the perfectly conducting V-dipole, and a V-dipole antenna loaded with a Wu-King impedance profile. Closed form solutions may be obtained for these two examples and these are shown to be in excellent qualitative agreement with published theoretical and experimental results.

The approach presented here has significant practical value since it provides an early-time approximation of the far field radiated by a loaded wire antenna, without recourse to numerical computation. In addition, the method provides a clear physical insight into the temporal processes involved in transient radiation from such a structure. The role of direct time domain analysis in describing the physical behaviour of transient radiators is thoroughly examined.

On the the origin of the radiation field

Authors: Rafael Gómez Martín, Amelia Rubio Bretones *, Ignacio Sánchez García

GRUPO DE ELECTROMAGNETISMO
DEPTO. FISICA APLICADA
FACULTAD DE CIENCIAS
UNIVERSIDAD DE GRANADA
18071 GRANADA (SPAIN)
FAX: 34-58-243214, E-mail RGOMEZ@GOLIAT.UGR.ES

It is well known from the basic principles of Electrodynamics that the origin of the radiation field lies in acelerated charges (Panofsky and Phillips, Addison Wesley, 1962). This explains why from a macroscopic point of view the origin of this field is related to the time derivative of the current. Based on this concept, in this paper we study the local variation with time of the effective velocity of the charges defined as $v(t,s) = I(t,s)/Q(t,s)$ along several wire structures, such as curved wires and antennas with concentrated or distributed loadings. The goal is to identify where the charges are accelerated and to relate the local variations of the velocity to the places where the radiation originates. Besides the interest of this study as a fundamental problem in electromagnetism, these results could find a practical application in the control of the the radiation of antennas and RCS.

The study is carried out by feeding the thin wire structures with a Gaussian pulse and computing $v(t,s)$ along the wire using the code DOTIG1 (A. Rubio Bretones, R. Gómez Martín and A. Salinas, COMPEL, 1989). This code is based on the solution of the thin-wire Time-Domain Electric Field Integral Equation (TD-EFIE) by the method of moments (MM), using a marching-on-in-time procedure. In this procedure, the TD-EFIE is discretized in space and time, and the unknown distribution of induced current at a time step is expressed in terms of previously-calculated current values, and in terms of the known incident field. The charge is then calculated using the continuity equation.

JOINT-105.9

Radiation Center Identification by Normalized Pattern Function Imaging

J.S. Gwynne* and J.D. Young
The Ohio State University ElectroScience Laboratory
Department of Electrical Engineering
Columbus, Ohio 43212

A technique that is applicable to ultra wide bandwidth (UWB) and ultra wide angle (UWA) antennas is presented that isolates and characterizes the radiation centers from either measured or theoretical complex pattern data. The approach is very well suited for those involved with UWB/UWA SAR imaging. It provides a means for characterizing the radiation from the antenna at all angles in terms of attenuation and dispersion relative to the boresight response. Evaluating the antenna effects on the overall SAR image quality is much more intuitive with data presented in this form.

By viewing the antenna as a transducer with a set of complex transfer functions describing the transmit and receive properties, this approach simplifies the analysis by normalizing to the boresight response. The normalized boresight receive and transmit transfer functions are equal and are referred to as the normalized pattern function. Viewing these data in the time and frequency domains has proven to be very useful where, as an example, a waterfall plot showing the normalized pattern function as time versus angle reveals the antenna's radiation centers. By carrying this one step farther, images can be created that focus the radiation centers into a two dimensional spatial domain.

Results of several common antennas will be presented in the frequency, time, and image domains. In each, radiation centers will be located and off boresight performance will be described. This includes data from a horn, log periodic, slotline bowtie hybrid, and sinuous antenna.

APS/URSI A — Session 106 — Salon Harricana

Measurement Techniques and Material Characterization
Co-chairs: C.M. Weil, USA and S. Riad, USA

13:10	106.1	Complex Permittivity Measurement from Coaxial Cable Mutual Coupling, **T.S. BIRD**, D.B. HAYMAN, *CSIRO, Epping, Australia (URSI)*
13:30	106.2	Calibration and Modeling of a Large Broadband Coaxial Nearfield Sensor for Dielectric Measurements, **W.H. WEEDON**[1], W. SHI[2], [1]*Applied Radar Analysis, Watertown and* [2]*Northeastern University, Boston, MA, USA (URSI)*
13:50	106.3	Radio Frequency Characterization of Ferrite Materials, **Q. YU**[1], T.W. HOLMES[1], K. NAISHADHAM[2], [1]*ITT Automotive, Inc. and* [2]*Wright State University, Dayton, OH, USA (URSI)*
14:10	106.4	Establishment of a NIST Service in Dielectric Standard Reference Materials, **C.M. WEIL**, M.D. JANEZIC, *National Institute of Standards and Technology, Boulder, CO, USA (URSI)*
14:30	106.5	Use of Gaussian Beams Techniques for Dielectric Permittivity Measurement in Free Space, **M.G. SERBAN**, D.D. SANDU, O. RUSU, P. GASNER, *"Al.I. Cuza" University, Iasi, Romania (URSI)*
14:50	106.6	Determination of Volumetric Water Content in Lossy Geophysical Media Using Time Domain Reflectometry, **B. OSWALD**[1], H.R. BENEDICKTER[1], W. BÄCHTOLD[1], H. FLÜHLER[2], P. MARSCHALL[3], [1]*Swiss Federal Institute of Technology, Zürich,* [2]*Swiss Federal Institute of Technology, Schlieren and* [3]*National Cooperation for the Disposal of Radioactive Waste, Wettingen, Switzerland (APS)*
15:10		Coffee Break
15:30	106.7	Coated Spheres as Constituents of a Novel Artificial Dielectric and as Scatterers in a Photonic Band Gap Material, **S.A. KYRIAZIDOU**[1], N.G. ALEXOPOULOS[2], R.E. DIAZ[3], [1]*University of California, Los Angeles, CA* [2]*University of California, Irvine, CA and* [3]*Northrop Grumman Company, Pico Rivera, CA, USA (URSI)*
15:50	106.8	Observation of Dielectric Temperature Coefficient Image Using Photothermal Dielectric Microscope, **Y. CHO**, T. KASAHARA, *Yamaguchi University, Ube, Japan (URSI)*
16:10	106.9	Antenna Effects in Reverberation Chamber Measurements, **D.A. HILL**, J.M. LADBURY, G.H. KOEPKE, *National Institute of Standards and Technology, Boulder, CO, USA (URSI)*
16:30	106.10	Electromagnetic Field Sensors Close to Scattering Structures, **G. MONIEN**, H. SINGER, *Technical University of Hamburg-Harburg, Hamburg, Germany (URSI)*
16:50	106.11	Measurement of Extremely Low Nonlinear Distortions, **K. BORGEEST**, J.L. TER HASEBORG, *Technical University of Hamburg-Harburg, Hamburg, Germany (URSI)*

JOINT-106.1

COMPLEX PERMITTIVITY MEASUREMENT FROM COAXIAL CABLE MUTUAL COUPLING

T.S. Bird & D.B. Hayman
CSIRO Telecommunications & Industrial Physics
PO Box 76 Epping NSW 2121 AUSTRALIA

A number of techniques is available for non-invasive measurement of the complex permittivity of dielectric materials. Two common methods involve one- or two-port measurement in either a closed structure, such as a coaxial-transmission line or waveguide, or in an open environment, such as for single or two-in-line apertures radiating into the material under test. Another possible two-port approach, which has received relatively little attention to date, uses mutual coupling between a pair of co-planar apertures. Two examples of this arrangement for coaxial cables are shown in Fig. 1. Coaxial cables are usually preferred for material measurement because they can be calibrated over a wide, continuous band of frequencies. Providing there is an accurate solution for the cross-coupling between the apertures, then the solution can be used to determine the complex permittivity of the material. The solution for scattering parameters of both coaxial structures in Fig. 1 is available (Bird, *IEE Proc. - Microw. Ant. Propag.*, **143**, 265-271, 1996). For the case of separate apertures (Fig. 1b), S_{21} was shown to be significantly dependent on the permittivity. An explanation for this is that S_{21} is approximately proportional to the factor $\exp(-jk_e s)$, where s is the centre-to-centre spacing of the cables and k_e is the wave-number in the material under test.

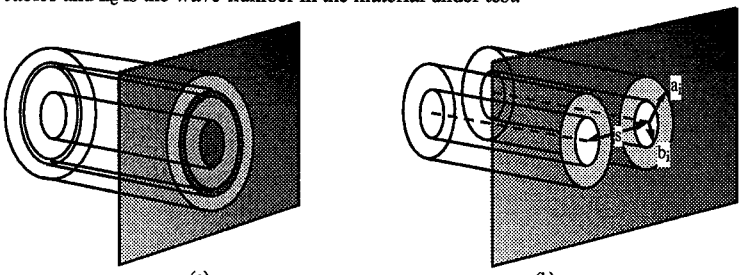

(a) (b)

Fig. 1: Dual coaxial cables

This paper describes the use of the solution for cross-coupling between coaxial cables (Fig. 1b) to determine the complex permittivity of materials. The approach with dual-coaxial cables is similar to a one-port coaxial probe measurement, except that now four complex parameters are involved. Care should be taken in preparing the dual-coaxial cable mount to ensure that the cables finish flush with a large, smooth ground plane. The mount is placed in contact with the material under test and the two-port scattering parameters are measured using a network analyser. The measured data is then matched to the theoretical solution by adjusting the real and imaginary parts of the complex permittivity using a least-squares cost function in an optimization loop. Weighting parameters in the cost function allow the emphasis of the four scattering parameters to be adjusted from a simple one-port evaluation to a full two-port one. Examples of the use of the method will be presented for several materials, including polyethylene and distilled water.

Calibration and Modeling of a Large Broadband Coaxial Nearfield Sensor for Dielectric Measurements

William H. Weedon*
Applied Radar Analysis
14 Union Street, Suite 2, Watertown, MA 02172

Wei Shi
Department of Electrical and Computer Engineering
Northeastern University, Boston, MA 02115

Nearfield coaxial sensors have been used many times in the past for the measurement of the dielectric constant and loss factor of materials including liquids, rocks, and biological media, to name a few. Many sensors, including commercially-available sensors, have an aperture that is small compared to the smallest wavelength in the "unknown" medium. This allows quasi-static analysis techniques (N. Marcuvitz, *Waveguide Handbook*, New York: MIT Radiation Laboratory, 1951; D. K. Misra, *IEEE Trans. Microwave Theor. Techniq.*, Vol. MTT-35, 1987) to be utilized to develop expressions for the sensor input admittance. Recently, a large open-ended coaxial probe (G. P. Otto and W. C. Chew, *IEEE Trans. Instrumen. and Measurement*, Vol. 40, 1991) was developed for measuring materials with large-grain heterogeneities, such as rocks and concrete, in order to average out the variations in complex permittivity due to the irregularities. Quasi-static based methods cannot be used for this sensor at high frequencies (~ 1 GHz) since the aperture is not smaller than a wavelength in the medium.

In this work, two numerical models are used in place of the quasi-static analysis procedure to compute the input admittance of the probe for various complex dielectric media as a function of frequency. The first numerical model is a mode-matching solution that was developed by Otto and Chew. The second numerical model is a finite-difference time-domain solution computed in cylindrical coordinates. The two numerical models are compared with each other and with measurements for certain known media, such as water and methanol, and are shown to give good agreement.

The numerical models are then used to compute the probe's input admittance versus a range of real and imaginary dielectric constant values and frequency. A multi-term polynomial approximation to the input admittance, including various combinations of powers of real and imaginary dielectric constant, is then generated for each measurement frequency. The polynomial model is then used as the basis for a least-squares conjugate gradient inversion scheme for computing the complex dielectric constant from the measurements. In this manner, an accurate physical model is utilized for the sensor, while retaining a fast numerical scheme for inverting the measurements.

JOINT-106.3

Radio Frequency Characterization of Ferrite Materials

Qin Yu* and Thomas W. Holmes
ITT Automotive, Inc.
Body and Electrical Systems MS–F43
2040 Forrer Blvd., P.O. Box 1804
Dayton, OH 45401-1804

Krishna Naishadham
Department of Electrical Engineering
Wright State University
Dayton, OH 45435

Miniature ferrite core inductors (also known as chokes), consisting of a thin wire wound on a high–permeability magnetic material, find useful application in the suppression of electromagnetic interference (EMI) in electronic systems. In addition to the designed inductance of the choke, the parasitic self–capacitance and winding resistance play an important role in its useful operating frequency range, defined to be the frequency span below the first self–resonance. The resonant frequency and the quality factor (Q) depend on several parameters, including the distributed capacitance and the magnetic material properties. In some applications, such as automotive electronic systems, it is required to design chokes with useful frequency range extended into the RF range (100 MHz to 1 GHz), implying shifting up the self–resonant frequency by reducing the parasitic capacitance. At high frequencies, it is imperative that the field confinement in the underlying magnetic material be understood in order to minimize the parasitics. In this paper, we discuss a novel method to measure the frequency–dependent magnetic characteristics of ferrites at RF.

At RF, parasitic resistance resulting from winding and core losses, and stray capacitance, preclude direct measurement of the impedance. These parameters are strongly influenced by the helix curvature, geometry of the winding and the core material characteristics. Therefore, we develop a measurement technique for estimating the material characteristics and the equivalent impedance of both toroidal and slug–type chokes, using a Vector Network Analyzer (HP 8753) with a specially designed coaxial test fixture, which minimizes the impedance mismatch in the measurement path. The proposed method is considerably more accurate than existing methods of measuring the impedance of ferrite core inductors using LCR bridges [Bartoli et al., *J. Circuits, Sys. and Comp.*, pp. 607–626, 1995], because it eliminates the assumption that the inductance may be approximated by its quasi–static value. This assumption is valid only for low self–resonant frequencies (about 10 MHz), and severely breaks down for RF chokes. The measurement method consists of two steps: (a) determining the shift in the resonant frequency of a given choke by connecting, in turn, two precisely known capacitors in shunt with the choke, and (b) comparing the change in impedance between ferrite core and air core inductors with no external capacitors connected. In each case, the frequency is swept around the resonant frequency to obtain measurements over a fairly wide band. The former measurement yields the parasitic capacitance and the inductance, while the latter provides a method to compute the complex permeability of the material. With slug–type cores, one obtains only the "effective permeability", which is significantly different from the actual material permeability because of a large air gap. The toroidal choke, on the other hand, directly results in fairly accurate material permeability, because the field is well–confined to the core. The measured results for toroidal chokes compare within 20-25% of manufacturer's specifications at low frequencies, but, more importantly, show that the useful operating frequency range of certain Mn-Zn chokes can be extended into the RF regime. For one such choke, the self–resonant frequency was close to 200 MHz, and the magnetic loss was quite small up to 700 MHz.

ESTABLISHMENT OF A NIST SERVICE IN DIELECTRIC STANDARD REFERENCE MATERIALS

Claude M. Weil* and Michael D. Janezic
Electromagnetic Fields Division (813.08)
National Institute of Standards and Technology
Boulder, CO 80303-3328, USA

There exist increasing needs in industry and elsewhere for dielectric and magnetic standard reference materials (SRMs) that have been well-characterized in the RF/microwave frequency spectrum. These enable industry to assess the accuracy of their own measurement systems and to help establish some degree of traceability in dielectric and magnetic characterization measurements back to NIST. The latter issue is of importance to industry for such purposes as quality assurance, vendor qualification, etc..

This talk will describe efforts currently underway to establish a certified NIST service in dielectric SRMs. The basic criteria used for selecting candidate materials for use as dielectric SRMs will be discussed, as will details of how this service is expected to work. Five different low-loss polymers, glasses and ceramics have been tentatively selected for use as dielectric SRMs:

Polytetrafluroethylene (DuPont FEP),	$\epsilon_R' = 2.05$
Cross-linked Polystyrene (Rexolite),	$\epsilon_R' = 2.53$
Fused Silica Glass (Corning 7940),	$\epsilon_R' = 3.82$
Alumino-Silicate Glass (Corning 1723),	$\epsilon_R' = 6.15$
Alumina (Coors Vistal),	$\epsilon_R' = 9.97$

The SRM selected for use by the customer will be initially machined into a 60-mm diameter sample and subsequently characterized at 10 GHz in the NIST TE_{01n} mode cylindrical cavity resonator to expected accuracies of ±0.5% in ϵ' and ±0.00005 in ϵ''. In the final step of this process, a smaller sample of this material is machined to the customers specifications.

The talk will also review the uncertainty estimates developed for the cavity resonator, which have enabled NIST to specify the anticipated SRM accuracies quoted above. We will also review data on measurement repeatability using multiple samples of the same SRM. This provides data on the sample-to-sample variability and material homogeneity. We will also discuss the anticipated long-term stability of these materials.

JOINT-106.5

USE OF GAUSSIAN BEAMS TECHNIQUES FOR DIELECTRIC PERMITTIVITY MEASUREMENT IN FREE SPACE

Mihai Gabriel SERBAN, *Dumitru* D. SANDU, *Octavian* RUSU, *Paul* GASNER
"Al.I.Cuza" University, Faculty of Physics
Blvd. Copou, no. 11, Iasi, RO-6600, ROMANIA
E-mail: mgserban@uaic.ro

Free space methods are contactless and nondestructive, this making them adequate for on-line quality control in industry and agriculture. Unfortunately the errors' level is high, because the relations that describe the interaction of microwaves with the sample are based on the classical "plane electromagnetic wave" approach. In a real experiment the antenna radiated field has a beam shape and depends on position and the "plane electromagnetic wave" condition cannot be realized even if are used focalized microwave beams obtained with lens corrected antennas.

We have developed a new approach of free space, reflection type methods, using a Gauss-Laguerre beam mode decomposition of the field radiated by the antenna used in our experimental setup. This technique allows a good description of the radiated field in the near, medium and far zones. We use a scalar horn for which almost 98% of the power is carried by the fundamental Gaussian beam mode, that permittiing us to consider only the fundamental Gaussian beam mode in our analysis.

The reflection coefficient for the fundamental beam mode is deduced using a plane wave spectrum representation of the incident Gaussian beam. The reflected field is a superposition of Gauss-Laguerre beam mode. The characteristics of the reflected beams are obtained as a function of plate thickness and permittivity. If the permittivity and thickness of the sample are in usual limits almost 99.5% of the energy is transferred in the fundamental Gaussian beam mode and we may consider only this mode in the reflected field.

The reflected field is received by the same antenna. The received signal is obtained evaluating the integral of the product between the function that describes the structure of antenna radiated field and the incident field, in a normal plane extending to infinity. Using only the Gaussian beam modes the deduced relations are simple.

This approach eliminates the need of considering the errors arising in usual free space meausurements because the real structure of the fields are considered. The only error that must be modelled is due to the multiple reflections between sample and antenna. We modelled the multiple reflections considering that at the aperture plane the unabsorbed energy is reflected also like a Gaussian beam.

Using this model we obtained the expression for the received signal as a function of antenna-dielectric plate distance and dielectric plate characteristics.

The real and imaginary parts of the relative complex permittivity were found from the obtained expression of the received signal using a conjugate gradient method technique using an initial guess for ε_r.

Experimental results show a good agreement with results obtained using other methods.

Coated spheres as constituents of a novel artificial dielectric and as scatterers in a Photonic Band Gap material

Sissy A. Kyriazidou* [a]
Nicolaos G. Alexopoulos[b]
Rodolfo E. Diaz[c]
[a] Electrical Engineering Department
University of California, Los Angeles 90095
[b] Electrical and Computer Engineering Department
University of California, Irvine 92697
[c] Northrop Grumman Co.

Abstract

The model for a novel artificial dielectric is presented, motivated by the explanation of the optical transparency of water by Diaz (Nicolaos G. Alexopoulos, Rodolfo E. Diaz, to appear in IEEE Trans. Ant. and Prop. 1997). The proposed material consists of coated spheres. The parameter space of the system is thoroughly analyzed and, for specific choice of the electrical properties of the core and shell, it exhibits a transparency window over a small band of frequencies. The frequency selective properties are exhibited in the bulk without relying on antenna-mode resonances of elements, thus bypassing the usual drawbacks of Frequency Selective Surfaces used today. Radomes, reflectors and filters constructed of such a material would have no inherent limitation on their topology, nor would they exhibit unwanted passbands.

Moreover, the model of the coated sphere is studied as a periodically embedded scatterer within a dielectric for the formation of a three-dimensional Photonic Band Gap (PBG) material. In analogy to a semiconductor crystal that exhibits electron band gaps, a PBG crystal is characterized by photonic band gaps which prevent the propagation of electromagnetic waves of specific energies in certain directions. Such a control over the electromagnetic wave propagation may have a wide range of applications for instance in novel antenna structures, Frequency Selective Surfaces and integrated circuits (modulation of electron-hole recombination rate) among others. In this paper, the particular crystal resulting from the periodic implantation of coated spheres is examined as a function of the dimension and electrical properties of the coating. Emphasis is given on the structures that promote the existence of a photonic band gap. Analytical results are presented within the dipole approximation (Bethe small-aperture theory) and further extensions are discussed.

JOINT-106.8

Observation of Dielectric Temperature Coefficient Image Using Photothermal Dielectric Microscope

Yasuo Cho and Teruaki Kasahara
Dept. of Electrical and Electronics Eng., Yamaguchi University
Tokiwadai, Ube-shi 755, Japan

Introduction Numerous dielectric materials have been developed with the progress of microwave telecommunication and satellite broadcasting, and they have various dielectric properties according to the respective microwave application. Among such properties to be considered when we design a dielectric material, one of the most important and general properties is temperature characteristics of dielectric constant. Normally, temperature coefficients of dielectric constant have been determined from the temperature response of the resonant frequency using the resonant cavity method, so that the obtained coefficient by this method is macroscopic average value of the coefficients distributing in the dielectric material. However it is easily understood that microscopic measurement for the distribution of the temperature coefficients of dielectric constant provides more precise information for designing the material than that obtained by the macroscopic measurement. In this article, two dimensional image of the distribution of the temperature coefficient of the dielectric constant of a two phases composite ceramics composed of TiO_2 and $Bi_2Ti_4O_{11}$ is observed using scanning photothermal dielectric microscope.

Observation of dielectric temperature coefficient image A schematic diagram of the a scanning photothermal dielectric microscope system is shown in Fig.1. The coaxial resonator probe with a capacitor specimen, combined with a translation stage, is the basis of the microscope system. It measures the microscopic area distribution of temperature coefficient of materials. The probe is connected to the oscillator tuned to the resonance frequency of the probe. The localized alternating temperature change due to the absorption of the focused chopped light causes the localized alternating variation of the capacitance because of its temperature characteristics, so that the oscillating frequency is modulated by the change of capacitance. By detecting this FM signal using FM demodulator and lock-in amplifier, we obtain a voltage signal proportional to the capacitance variation. Using this system, we measured a two dimensional image of the distribution of the temperature coefficient of dielectric constant of the ceramics for microwave application which is composed of only two phases, TiO_2 and $Bi_2Ti_4O_{11}$. TiO_2 has a large negative temperature coefficient of dielectric constant of τ_ϵ=-876ppm/°C whereas $Bi_2Ti_4O_{11}$ has a large positive coefficient of τ_ϵ=+1034ppm/°C. The result is shown in Fig.2. The clear temperature coefficient image corresponding to the two different grains was obtained.

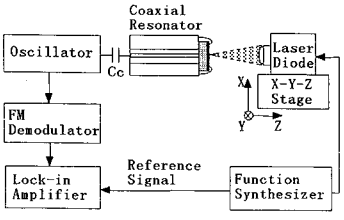

Fig. 1 Schematic diagram.

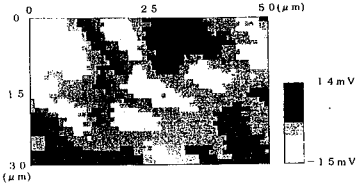

Fig. 2 Dielectric temperature coefficinet image.

Antenna Effects in Reverberation Chamber Measurements

David A. Hill*, John M. Ladbury, and Galen H. Koepke
Electromagnetic Fields Division
National Institute of Standards and Technology
Boulder, CO 80303
USA

Reverberation chambers (also called mode-stirred chambers) are finding increased use for EMC measurements (radiated emissions or immunity). A reference antenna measurement is generally used to determine the power density or field strength in the chamber. The effective area of a reference antenna in a well-stirred chamber is usually assumed to be $\lambda^2/8\pi$ which can be interpreted as the effective area of an isotropic antenna ($\lambda^2/4\pi$) times a polarization mismatch factor (1/2). In practice the effective area of the reference antenna can be reduced by impedance mismatch or dissipative loss, but these factors have usually been neglected because they are difficult to evaluate.

Impedance mismatch can be analyzed as a free-space term plus a term which depends on the chamber volume and quality factor (Q). Chamber Q can be calculated or measured (D.A. Hill, M.T. Ma, A.R. Ondrejka, B.F. Riddle, M.L. Crawford, and R.T. Johnk, *IEEE Trans. Electromag. Compat. 36*, 169-178, 1994). We have recently used a network analyzer to perform S-parameter measurements for a variety of antenna/chamber configurations. These measurements yield the impedance mismatch of both the transmitting and receiving antennas and allow a comparison with the theory. Antenna efficiency reduction (due to dissipative loss) is more difficult to analyze or measure, but some estimates can be made from measured data.

Small electric or magnetic field probes are also used to measure chamber field strength. They present a special case of receiving antenna, but are not impedance matched because of their capacitive (for electric field probes) or inductive (for magnetic field probes) impedance. Instead, they are normally calibrated in a different facility (such as an anechoic chamber or a TEM cell) and respond to a linear component of the electric or magnetic field at a point. We have taken extensive 3-axis, electric-field probe data, and the measured electric field magnitude is consistent with power density measurements taken with a reference antenna.

JOINT-106.10

ELECTROMAGNETIC FIELD SENSORS CLOSE TO SCATTERING STRUCTURES

G. Monien **H. Singer**

Department of Theoretical Electrical Engineering
TU Hamburg-Harburg - 21071 Hamburg - Germany

The measurement of electromagnetic field components and their uncertainty is influenced by numerous parameters, which have to be considered when analyzing the measurement results. Furthermore, the influence of the sensor on the surrounding environment has to be taken into account. Until now the different sensor structures were optimized under the aspect of reducing the deviation, but only a few investigations were dealing with the measurement of the field components close to scattering structures. This problem is investigated by a computer program for numerical field calculation (CONCEPT) with the aim to describe specific limitations using different sensor types.

The sensor properties may be evaluated by the comparison of the measured field value with the undistorted field. The resulting deviation is influenced on one hand by the nonlinear frequency response and on the other hand by the field inhomogeneity and coupling to adjacent structures.

The field inhomogeneity can be considered as the mean value of the field over the sensor surface or the cross section in comparison with the field value at the measuring point. A strong correlation to the measuring deviation was found. For electrical field sensors this connection may be realized with the help of the reaction theorem. The open-circuit voltage is calculated by

$$u_L = \frac{1}{I} \int_A J_A E_i \, dA$$

using the surface current J_A and the electric field strength E_i of the incident undistorted field (*A Reaction Theorem and Its Application to Antenna Impedance Calculations*, J.H.Richmond, IRE AP, vol. AP-9 no. 6, Nov. 1961). Considering the surface current to be uniform and equal to one yields a resulting value corresponding to the mean value of the field. For magnetic field sensors it is possible to obtain a similar dependency upon the sensor voltage from the surface integral over the time derivation of the magnetic field strength.

The coupling of field sensors to neighboring structures consists of a capacitive or inductive part as well as a part of radiation. The dominating one depends on the geometry of the sensor, the structure and the field sources. The coupling corresponds to the variation ΔZ of the complex antenna impedance

$$\Delta Z = Z - \frac{1}{I^2} \int_S J_S E_i \, dS = Re\{\Delta Z\} + j * Im\{\Delta Z\}$$

S is the surface of the scattering structure, J_S the surface current, E_i the undistorted incident field and I the source current of the sensor. The imaginary part is rapidly decreasing and is equal to zero at distances large compared with the sensor size. The radiation coupling exists also for higher distances but has less influence on the measurement deviation.

After the presentation of the different parts yielding a deviation in the vicinity of scattering structures, limiting values are given for the specific sensor types which may help to avoid uncertain measurement results. These limits are illustrated by typical examples, which will be compared with analytical and measured data.

Measurement of Extremely Low Nonlinear Distortions

K. Borgeest, J.L. ter Haseborg
Technical University of Hamburg-Harburg, Dept. of Measurement Engineering/EMC
Harburger Schloss-Strasse 20, 21071 Hamburg, Germany,
Tel +49/40/7718-2240, Fax -2382, Emails borgeest@tu-harburg.d400.de

The measurement of low nonlinear distortions requires a measurement setup which is distortion free in the used dynamic range. The analysis of protection circuits for radio direction finder antennas are a typical application. The types of nonlinear distortions are harmonics and intermodulations. Harmonics are multiples of the base frequency. Intermodulations are undesired modulation products between signal frequencies in case of a multiple frequency input. For measurement purposes a dual frequency input is assumed. In practice the intermodulation products are more important, because partially they come very close to the signal frequencies, so they cannot be removed by filters.

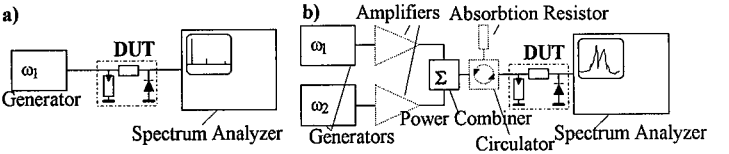

Fig. 1: Setups for the measurement of harmonics (left) and intermodulations (right)

The measurement of harmonics (Fig. 1a) requires a signal generator with little harmonics. The signal passes the DUT, e.g. the antenna protector, the spectrum consisting of the base frequency and its harmonics is displayed on the spectrum analyzer.

The measurement of intermodulation products is more complicated (Fig. 1b). Two signals are summed in a power combiner. The dual frequency signal is fed into the DUT and displayed with close intermodulation products on a network analyzer. A particular problem in the setup are intermodulation products generated in the generator outputs, because the combiner does not isolate the two signals perfectly from each other, a small amount of the signal from one generator reaches the output of the other generator. Combiners based on transformers (hybrid combiners) isolate better than combiners which simply consist of a three-resistor star. Hybrid combiners can reach isolations of 30 dB. If the DUT does not match perfectly with the line impedance, reflections impair isolation, because in reverse direction the combiner divides the signal. In this case an isolator between the combiner and the DUT suppresses reflections. An isolator can be realized with a circulator of which one port is terminated with the characteristic impedance. So the signal from the combiner is fed into the DUT, but the reflected signal will be absorbed by the resistor at the third port. For VHF applications circulators are realized with active circuits which will be discussed in detail.

If the generator drivers are not linear, additional linear amplifiers can be used. The lowest harmonics and intermodulations are obtained with MOSFETs. Some circuit concepts will be discussed. Concerning the harmonics only, the design of the oscillators is also an issue. To generate stable oscillations the loop amplification must be greater than one, so the amplitude would grow until the active element clamps without an active amplitude control. The quality of the feedback also determines the spectral purity.

APS/URSI B | Session 118 | Salon St-Maurice

Applications of Neural Networks
Co-chairs: P.M. Goggans, USA and M. Ney, France

08:10 118.1 Sectorial Direction Finding Antenna Array with a MLP Beamformer, **E. CHARPENTIER**, J.-J. LAURIN, *École Polytechnique de Montréal, QC, Canada (APS)*

08:30 118.2 Antenna Array Signal Processing with Neural Networks for Direction of Arrival Estimation, **A.H. EL ZOOGHBY**, C.G. CHRISTODOULOU, M. GEORGIOPOULOS, *University of Central Florida, Orlando, FL, USA (APS)*

08:50 118.3 Inverse Scattering by Dielectric Circular Cylindrical Scatterers Using a Neural Network Approach, **A-K. HAMID**, M. ALSUNAIDI, A. ALSUNAIDI, *King Fahd University of Petroleum and Minerals, Dhahran, Saudi Arabia (APS)*

09:10 118.4 Analysis and Design of Microstrip Circuits Using Neural Networks, **E.A.F. ABDALLAH**[1], M.A. ABOU EL-SOUD[2], A. ABO ZAID[2], A.E.M. ELCHIATY[1], [1]*Electronics Research Institute, Cairo and* [2]*Mansoura University, Mansoura, Egypt (URSI)*

JOINT-118.4

Analysis and Design of Microstrip Circuits Using Neural Networks

Esmat A.F. Abdallah*, M.A. Abou El-Soud**
Ali Abo Zaid**, and Abd El-Halim M. Elchiaty*
* Electronics Research Institute, El-Tahrir st., Dokki, Cairo, Egypt.
** Fac. of Eng., Mansoura Univ., Egypt.

In this paper the artificial neural network technique (ANN) is used as a mapping algorithm in order to produce a new method for microwave device models. This method is used since it is a robust and good in correcting the error or interpolating a certain pattern using the interpolation generalized property.

A visual software package was designed for analog and digital networks using the backpropagation training algorithm. The package was optimized to overcome some problems in other packages and has the following global characteristics:

- Three kinds of learning protocols; batch mode learning (off line), switched pattern learning (on line), and pattern to pattern learning.
- Fast backpropagation using transformed cost function which follows the fast error correction .
- Over 120 neurons per layer can be learned.
- Editing and writing patterns inside the program.

This software package was applied to fit the characteristic curves of the microstrip transmission line that were used in Presser Graphical Technique. The results were found to be satisfactory in calculating the effective dielectric constant. It was also applied to calculate the dispersion G-factor of Owens. More accurate results were obtained by using only two layers containing three neurons for the first hidden layer and one neuron for the output layer.

Finally, the neural network technique was used to design a small signal narrow band amplifier operating at 3.5 GHz using gallium arsinide FET transistor ATF-25735. First, the S-parameters were interpolated from the discrete values given in the data sheet of the transistor. This technique is used in this case as a single interpolation machine for the eight parameters (magnitude and phase) at each frequency and the results were compared with the spline interpolation of the eight parameters. It should be noted that our model has the advantage of only having one neural network to interpolate eight different curves over the whole frequency range of the transistor. So, it can be used in CAD programs without using the dedicated programming technique. Second, the ANN was used to interpolate the noise parameters of the transistor over the frequency range given in the data sheet.

Another visual software package has been designed to facilitate the microwave amplifier design using microstrip circuits making advantage of the neural network interpolation for the transistor S-parameters. An amplifier was designed using the aforementioned technique and fabricated using thin film technology and tested. Good results were obtained.

APS/URSI A **Session 125** **Salon Harricana**

Random Media and EM Properties of Materials
Co-chairs: R.G. Mazzolin, Canada and I.R. Ciric, Canada

08:10	125.1	Microwave Characterization of High Temperature Superconductor Films Using Dielectric Resonator Measurements, **K. NAISHADHAM**[1], E.K. MOSER[2], [1]*Wright State University, Dayton and* [2]*Wright Laboratory, WL/MLPO, Wright-Patterson AFB, OH, USA (URSI)*
08:30	125.2	Ferroelectric Materials for Phased Array Applications, **J.B.L. RAO**[1], D.P. PATEL[1], L.C. SENGUPTA[2], J. SYNOWCZYNSKI[2], L.H. CHIU[2], E. NGO[2], S. SENGUPTA[2], [1]*U.S. Naval Research Laboratory, Washington, DC and* [2]*U.S. Army Research Laboratory, APG, MD, USA (APS)*
08:50	125.3	Isoimpedance Inhomogeneous Magnetodielectrics - Wave Materials for Unusual Applications, **Ar. KNYAZ**, An. KNYAZ, *Ukrainian Telecommunication Academy, Odessa, Ukraine (APS)*
09:10	125.4	Effective Electromagnetic Material Properties for Alternating Wedges and Hollow Pyramidal Absorbers, **C.L. HOLLOWAY**[1], M. JOHANSSON[2], [1]*Institute for Telecommunication Sciences, U.S. Department of Commerce, Boulder, CO, USA;* [2]*Chalmers University of Technology, Gothenburg, Sweden (APS)*
09:30	125.5	Optimum Design of N Sheet Capactive Jaumann Absorber Using Genetic Algorithm, **A. CHELDAVI**, M. KAMAREI, *University of Tehran, Iran (APS)*
09:50	125.6	Experimental Investigation of the Effects of Rough Surface Criterion and Surface Conductivity on Radio Links, **R.G. MAZZOLIN**[1], J.S. DAHELE[2], [1]*79 Communication Regiment, Kingston, ON, Canada;* [2]*Royal Military College of Science (Cranfield), Swindon, UK (APS)*
10:10		Coffee Break
10:30	125.7	A Comparison of the Point Spread Functions for Polarization-Difference and Intensity-Only Imaging in Scattering Media, **J.S. TYO**, *University of Pennsylvania, Philadelphia, PA, USA (APS)*
10:50	125.8	A Combined Steepest Descent-Fast Multipole Algorithm for the Analysis of Three-Dimensional Scattering by Rough Surfaces, V. JANDHYALA, B. SHANKER, **E. MICHIELSSEN**, W.C. CHEW, *University of Illinois at Urbana-Champaign, Urbana, IL, USA (APS)*
11:10	125.9	Broadband, High-Temperature Dielectric Properties Measurements of Thin Substrates Using Open-Ended Probes, S. BRINGHURST, M.F. ISKANDER, **M.J. WHITE**, *University of Utah, Salt Lake City, UT, USA (APS)*
11:30	125.10	A Resonant Technique to Measure the Dielectric Properties of Planar Materials, **W.R. HUMBERT**, W.R. SCOTT, Jr., *Georgia Institute of Technology, Atlanta, GA, USA (APS)*
11:50	125.11	Analytical Investigation of Reflections from Single GaAs-GaA1As Multiple Quantum Well (MQW), J.-G. MA, **Z. CHEN**, *Technical University of Nova Scotia, Halifax, NS, Canada (APS)*

JOINT-125.1

Microwave Characterization of High Temperature Superconductor Films Using Dielectric Resonator Measurements

Krishna Naishadham*
Department of Electrical Engineering
Wright State University
Dayton, OH 45435

Eric K. Moser
Materials Directorate
Wright Laboratory, WL/MLPO
Wright-Patterson AFB, OH 45433

Dielectric resonators (DRs), formed by sandwiching a cylindrical piece of polished dielectric material (sapphire) between two planar high temperature superconducting (HTS) thin–films, offer an attractive platform for microwave testing of HTS materials. They also find dual use as components in low–noise microwave receivers and satellite communications systems. In this paper, we report measured results on the surface resistance of polished niobium and YBCO films using miniaturized *open* DRs (i.e., the DR is not packaged in a metallic cylindrical cavity as is usually done in practice [Z. Y. Shen, *High Temperature Superconducting Microwave Circuits*, Artech House, 1994]). Packaging the DR in a metallic cavity introduces the cumbersome process of de–embedding the case modes, and the associated decrease in accuracy if the sample is not concentrically placed in the cavity. The open DR is tested in our experiments as a two-port system using a vector network analyzer configuration, by exciting and detecting the modal fields with loop–terminated coaxial cables. The observed Q factor of the resonator is a gauge of the surface resistance of the endplates, an important property for the microwave characterization of HTS thin films.

In HTS DR measurements, because of the extremely high Q's (of the order of 10^6) resulting from very low dissipation, the measured parameters are very sensitive to the background "noise" contributed by the coupling mechanism, fixture parasitic modes, temperature–dependent cable losses, radiation, etc. Our objective of testing superconducting samples adds the complication of cooling the resonator to cryogenic temperatures. Because the resonant frequency shifts substantially as the temperature is varied, and because the properties of the test cables and coupling loops vary with temperature, maintaining accurate calibration is difficult. The loop coupling fixture is inherently difficult to compensate, because multiple measurements such as thru–reflect–load (TRL), routinely used for the calibration of room temperature measurements, cannot be accomplished at cryogenic temperatures within reasonable *repeatable* accuracy. In this paper, we report an accurate calibration and parameter extraction procedure based on non-linear least squares minimization using the Marquardt algorithm. In this model, transmission line theory is applied to effectively filter out the background noise contributed by cable losses and fixture parasitics, and the geometrical attributes of Q-circles traced out by the measured data in the complex impedance space [D. Kajfez, *Q Factor*, Vector Fields, 1994] are determined, from which one calculates the unloaded Q of the DR. We discuss the utilization of this method in the characterization of HTS DRs with small area thin–films (about 10 mm^2), at frequencies in the 20 – 40 GHz range, and at temperatures below the transition value (T_c) for the films. It is believed that the cryogenic measurements reported in this paper for frequencies in the Ka band are the first of their kind for HTS materials.

AUTHOR INDEX

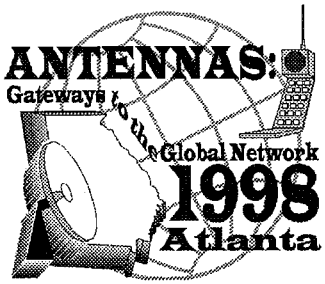

Antennas and Propagation Society International Symposium
&
National Radio Science Meeting

Atlanta, Georgia
June 21-26, 1998
Renaissance Waverly Hotel
http://seal.gatech.edu/eeed/ap-ursi98/

Paper Submission

Paper processing in this meeting will depart radically from long-standing practices associated with the joint meeting. All papers will be handled electronically during the review and organization process. Electronic submission of papers is strongly encouraged, but not required. Detailed submission instructions are available through the following vehicles:

http://apsursi98tpc.ces.clemson.edu

ftp://apsursi98tpc.ces.clemson.edu

apsursi98tpc.info@ces.clemson.edu
(use "Submission" as the subject of your e-mail message)

Papers will undergo a review process. It is expected that the technical program will accommodate no more than 950 papers, including both podium and Interactive Forum formats.

Interactive Forum

An Interactive Forum will be held daily during the first three days of the Symposium and Meeting. It is expected that many authors will take advantage of the opportunity to present papers that involve substantial quantities of data, interactive computer demonstrations, or perhaps hardware display. The best use of the Interactive Forum will be recognized at the Awards Banquet.

Deadlines

Mail submission (paper manuscripts and floppy disks): January 5, 1998
Electronic submission (e-mail attachment or FTP): January 12, 1998

Organizers

General Chair: Andrew F. Peterson, School of Elec. & Comp. Engr., Georgia Tech
ap16@prism.gatech.edu, (404)894-4697

General Co-Chair: James C. Wiltse, Georgia Tech Research Institute

Technical Program Chair: L. Wilson Pearson, Clemson University
Wilson.Pearson@ces.clemson.edu(864)656-3946

Technical Program Co-Chair: Anthony Q. Martin, Clemson University